True reality: of this there is no academic proof in the world; for it is hidden, and hidden, and hidden.

Jalaludin Rumi

THERMODYNAMICS AND KINETICS OF THE CHLORINATION-VOLATILISATION OF MIXED METAL OXIDES

by

DAMIAN THOMAS CUMMINS

October 1974

A thesis submitted for the
degree of Doctor of Philosophy
of the University of London

John Percy Research Group in
Process Metallurgy,
Royal School of Mines,
Imperial College of Science and Technology,
Prince Consort Road,
London SW7

A B S T R A C T

Chloride-volatilisation processing of ores and raw materials, thermodynamic aspects of chlorination-volatilisation and the kinetics of chlorination-volatilisation reactions are reviewed. An apparatus consisting of a gas metering train, a multi-zone furnace, a packed bed reactor and a downstream condenser was constructed for the purpose of studying the chlorination (Cl_2)-volatilisation of mixtures of metal oxides. By performing equilibrium experiments on CdO/ZnO, Co_3O_4/ZnO and CoO/ZnO mixtures the standard free energy changes of the following reactions were determined:

$ZnCl_{2(g)} + CdO_{(s)} = CdCl_{2(g)} + ZnO_{(s)}$ (702-1072°C)

$CoCl_{2(g)} + ZnO_{(s)} + 1/6\ O_{2(g)} = ZnCl_{2(g)} + 1/3\ Co_3O_{4(s)}$ (853-955°C)

$CoCl_{2(g)} + ZnO_{(s)} = ZnCl_{2(g)} + CoO_{(s)}$ (895-1066°C)

These data, in combination with data obtained from the literature, have enabled the standard free energy changes of the Cl_2 + CdO, Cl_2 + 1/3 Co_3O_4 and Cl_2 + CoO reactions to be calculated. Non-equilibrium experiments were performed on packed beds of ZnO granules (705-873°C) and packed beds of CdO/ZnO pellets (750-950°C). The ZnO results showed that: a) the reaction was chemically controlled at 705°C, b) at 873°C boundary layer mass transport appeared to have been at least partly influencing the overall reaction rate, and c) packed beds and granular oxide-compacts are not particularly satisfactory for studying the kinetics of chlorination of single oxides. With the CdO/ZnO experiments the best separation that could be obtained was the equilibrium separation. As each experiment proceeded the rate of $CdCl_2$ production decreased whilst that of $ZnCl_2$ increased. These respective decreased and increased rates became more pronounced with increasing reaction temperature. Extensive examinations of the structures of unreacted and reacted pellets were performed. These showed that the CdO reaction rate was transport controlled, and that the decrease in CdO reaction rate with increasing termperature was due to pellet sintering and densification. A mass transfer control reaction model has been developed. Predictions made by this model are consistent with the reaction behaviour observed at 850 and 950°C.

L I S T O F C O N T E N T S

Page

Page

LIST OF TABLES

LIST OF GRAPHS

LIST OF FIGURES

LIST OF PLATES

INTRODUCTION

The comparatively high volatilities exhibited by most metal chlorides have long attracted the attention and ingenuity of metallurgical engineers in their pursuit of suitable processes for metals extraction and refinement. Historical accounts[1] trace the first recorded use of chlorides to the Patio process which operated during the sixteenth century in Mexico. It is difficult, however, to be certain when chloride volatilisation first became a significant feature of any process. Chloridising-roasting, first introduced for silver ores in late eighteenth century Europe, was often accompanied by a considerable loss of metal values due to vapourisation. In 1854 Saint-Claire Deville isolated aluminium metal by heating aluminium oxide, carbon and chlorine in a retort and then reducing the condensate with metallic sodium; this method, however, was never adopted on a large scale due to its considerable expense. Plattner was the first investigator to suggest the use of chlorine gas in a hydrometallurgical process, he was also the first person to study chloride vapourisation, the results of his work being published in 1856. The use of chlorine gas in pyrometallurgy was initiated by Swinburne and Ashcroft who developed a process for treating complex sulphide ore, their technique achieved commercial prominence in Australia in 1897. However, it was not dependent upon chloride vapourisation. Perhaps the first use of chloride volatilisation by design was at the turn of the century when Pohle and Croasdale chloridised-roasted at 1050°C, a higher temperature than had hitherto been used, and recovered the vapourised metal values from the fume. Since then, various other processes have appeared, some of which have been surpassed by better developments, others by historical events; the Caveat tin process in Thailand did not attain full production before becoming a victim of the second world war. The undeniable difficulties encountered in the field of chloride vapourisation have on occasions stopped development of successful plants and techniques, the Arvida plant of Alcan being one expensive example. Complexities of operations, handling problems, high costs and many process design difficulties have, however, been overcome in many instances.

There are in operation at the present time several important metallurgical applications of chloride volatilisation. The largest individual chlorination process is the production of titanium tetrachloride, most of which is used for the manufacture of white paint pigment. This process generally consists of packed or fluidised bed chlorination of rutile-coke mixtures at temperatures of about 1000°C, the gaseous titanium chloride formed in the reactor is collected in a condenser and subsequently fractionally distilled as part of its purification treatment. This production route is cheaper and more efficient than the sulphate route, but relies upon rapidly dwindling rutile deposits. As a result of this latter situation, considerable research efforts[12,13] are currently centred on selective chlorination of illmenite.

Iron pyrite cinder contains small quantities of many different non ferrous metals, this, apart from their value, prevents direct usage of the cinder in iron production. Several chloride routes, some of which involve volatilisation, are employed for extracting and recovering these impurities. Each year Duisberger Kupferhutte treat about 2 million tons of pyrite cinder; their current process involves chloridising-roasting at about 600°C followed by percolation leaching. This company has recently developed[9] to pilot plant scale an integrated process for removing the non-ferrous impurities from pyrite cinder pellets by chlorination-volatilisation at 1200°C in a vertical shaft furnace. Economic reasons have so far prevented its full scale commercial implementation. In Japan the Kowa Seiko company operate a high temperature (1250°C) chloridising-roasting process[11] during which volatilisation of the non-ferrous values occurs; the hardened iron oxide pellets produced by this integrated process are ideal for charging direct to the blast furnace with no further treatment. The treatment of pyrite cinder is, however, becoming less economically viable for two main reasons: firstly, supplies of sulphur for sulphuric acid production are currently being generated in increasing quantities by oil refineries; secondly, installation and maintenance costs in sulphur dioxide producing industries are rising as a result of the tighter environmental controls that are being introduced.

The mechanism of segregation as currently exploited in the Torco[25,64] process was inadvertently discovered in 1923 when a Chilean copper ore being given a pre-treatment roasting accidently contained what might be termed the "right ingredients", namely common salt and carbon. The rather unexpected behaviour of copper segregation was quickly exploited with plants appearing in Rhodesia in 1929 and shortly afterwards in the Belgian Congo; an unpredictable and sudden slump in copper prices was, however, responsible for their rapid closure. Despite this initial setback, interest was maintained and the mechanism was gradually understood in terms of a local volatilisation-reduction process. After much laboratory and pilot plant investigation, commercial exploitation has once again been achieved. In 1965 the Anglo American Corporation set up a 500 ton per day plant at Rhokana to treat low grade refractory copper ores; this proved to be successful and therefore led to plans for more plants along the Zambian copper belt. The segregation process seems likely to be restricted to low grade refractory ores and dumped tailings due to the increased complexity as compared with other processes; attempts at applying the technique to nickel ores have so far been unsuccessful.

Smaller scale applications of chloride vapourisation techniques may be found associated with the extraction and purification of tantalum[22,23], niobium,[22,23,24] vanadium, hafnium, zirconium, thorium, and beryllium. In the new and expanding field of vapour deposition gaseous chlorides have found interesting and exciting applications; these are however of a specialised and highly technical nature.

General economic trends, the greater availability and lower price of certain raw materials and advances in materials technology have jointly produced more favourable conditions for the introduction of new and improved vapourisation processes. Increased attention is now being focussed on more complex and lower grade ores as easily treated high grade deposits become scarce. Large amounts of industrial wastes and recycled scrap, together with demands for higher purities have also produced incentives for new extraction and separation techniques. The high chlorine consumption of synthetics producers has done much to help reduce costs;

chlorine is now available in larger amounts at lower comparative prices than at any time previously. More chemically resistant refractories and other materials of construction have been developed together with improved handling techniques, advances in plant design and recycling routes. These and other similar factors will greatly influence the choice and success of any new process.

The ultimate success of a new process will, however, depend upon the degree of scientific skill and understanding available both when evaluating possibilities and during the design of the eventual process. Of this understanding the first and most important part must certainly be accurate quantitative knowledge of relevant thermo-chemical equilibria. For chloride systems significant quantitative data are available[3,4,29,30] but in many instances this is not as accurate as is desired; estimates are therefore necessary. Equilibria involving several components in different phases have often not, for reasons of low priority, and experimental difficulty, been determined directly. Such equilibria may thus only be quantified by the compilation of several sets of data, this leads to the compounding of errors and in cases of sensitive equilibria, produces considerable uncertainty. Once the positions of the chemical equilibria of interest have been satisfactorily established, it is then necessary to determine the rates and mechanisms of the chemical reactions which lead towards these equilibria. In order to be economic a process must operate at an acceptable rate of production. Chemical processes are usually made up of many individual consecutive and concurrent sub-processes; these can be chemical or transport in nature. Under different circumstances, a given overall process may be controlled by either a chemical sub-process, a transport sub-process or a combination of sub-processes. When studying reaction kinetics it is these rate controlling steps, or combinations of steps, that are of greatest importance. Chemical rates are very temperature and mechanism sensitive, transport rates on the other hand are most influenced by physical properties and configurations on both a microscopic and macroscopic level. The theoretical understanding of gas-solid pyrometallurgical reactions is becoming well advanced,[54,56,57,58,59,60] the similarities between many a system enables useful comparisons to be made. The elucidation of a rate

controlling step, or series of steps, is a difficult procedure as only critical experimental data will survive detailed analysis. In the past many workers have advanced various theories on the basis of inconclusive evidence; this has in many cases been due to a lack of appreciation of the importance of transport phenomena. Laboratory studies are rarely capable of being scaled up to plant operating levels unless reactor performances and characteristics are known. The complexity of fluid motion in packed and fluidised beds greatly influences heat and mass transfer in almost all such reactors; the understanding of these interplays is of paramount importance in gas-solid reactor design. This brief mention of important factors to be considered when evaluating and designing proposed processes for chloride volatilisation sets a general perspective against which the present work on mixed oxide chlorination may be viewed.

Separation of metals from mixtures of oxides by chlorination-volatilisation is an attractive concept which has received appreciable attention during the last ten to fifteen years. Work has generally tended to concentrate, for obvious reasons, on fairly complex mixed oxide ores in the hope that commercial processes would emerge. Few thermochemical or kinetic studies have been performed.

As previously explained, thermodynamic data are in certain instances unreliable and therefore suitable for making only semi-quantitative predictions. As a first part of this study, equilibrium separations for the zinc oxide/cadmium oxide and cobalt oxide(s)/zinc oxide systems were measured by a direct experimental method. Having established accurate thermodynamic data it was then possible to carry out a limited number of packed bed non-equilibrium studies, firstly on ZnO and then on ZnO/CdO mixtures.

The results of the equilibrium experiments performed during this study make a useful data contribution to the field of chlorination thermodynamics. The non-equilibrium separation experiments on the CdO/ZnO mixtures elucidated the rate controlling step and demonstrated various other important kinetic phenomena. Fundamental investigations of this type are an essential part of the development of applications of chlorination-volatilisation processes.

CHAPTER ONE

LITERATURE REVIEW

1A INTRODUCTION

The study of chlorination* as a potential route for the extraction and separation of metals from their ores has a long history[1]. However, the first really significant paper on chlorination was published in 1957 by Hohn, Jangg, Putz and Schmiedl[2]. Their work brought together the best currently available free energy data on the chlorination of metal oxides and sulphides, and thus showed that there are a large number of theoretically feasible chlorination reactions. Also presented were the results of a series of experiments on the chlorination of a complex pyrite, together with proposals for an industrial process. In this process an iron-copper-nickel sulphide was exothermically reacted (in a fluidised bed reactor at 450°C) with chlorine to give solid metal chlorides and gaseous sulphur. Although this extraction route was not primarily dependent upon chloride-volatilisation, several important points still central to the study of chlorination-volatilisation processes were demonstrated: a) complex low grade ores can often be reacted with chlorine to produce more easily processed metal chlorides, thus avoiding smelting operations; b) selective extraction may be possible; and c) the chlorine can sometimes be recycled. The majority of the chloride-volatilisation studies reported since 1957 have been similar to the investigation of Hohn et al. Each typically consists of a basic thermodynamic analysis of the proposed process, followed by experimental results on the chlorination/chloridisation of the metal ore or metal containing raw material under study. In addition to these process-studies there have been a number of thermodynamic determinations, kinetic studies and thermodynamic data reviews.

---

* In this thesis: a) the word 'chlorination' refers to a process in which one or more metal chloride is formed from either chlorine (Cl_2) or a chlorine containing gas (eg HCl, CCl_4); b) the word 'chloridisation' refers to a process in which either a solid or liquid chloride (eg NaCl, $CaCl_2$) is used to form the metal chloride(s); and c) the word 'chloride/chloridisation/chlorination-volatilisation' refers to a process in which the product metal chloride(s) are gaseous.

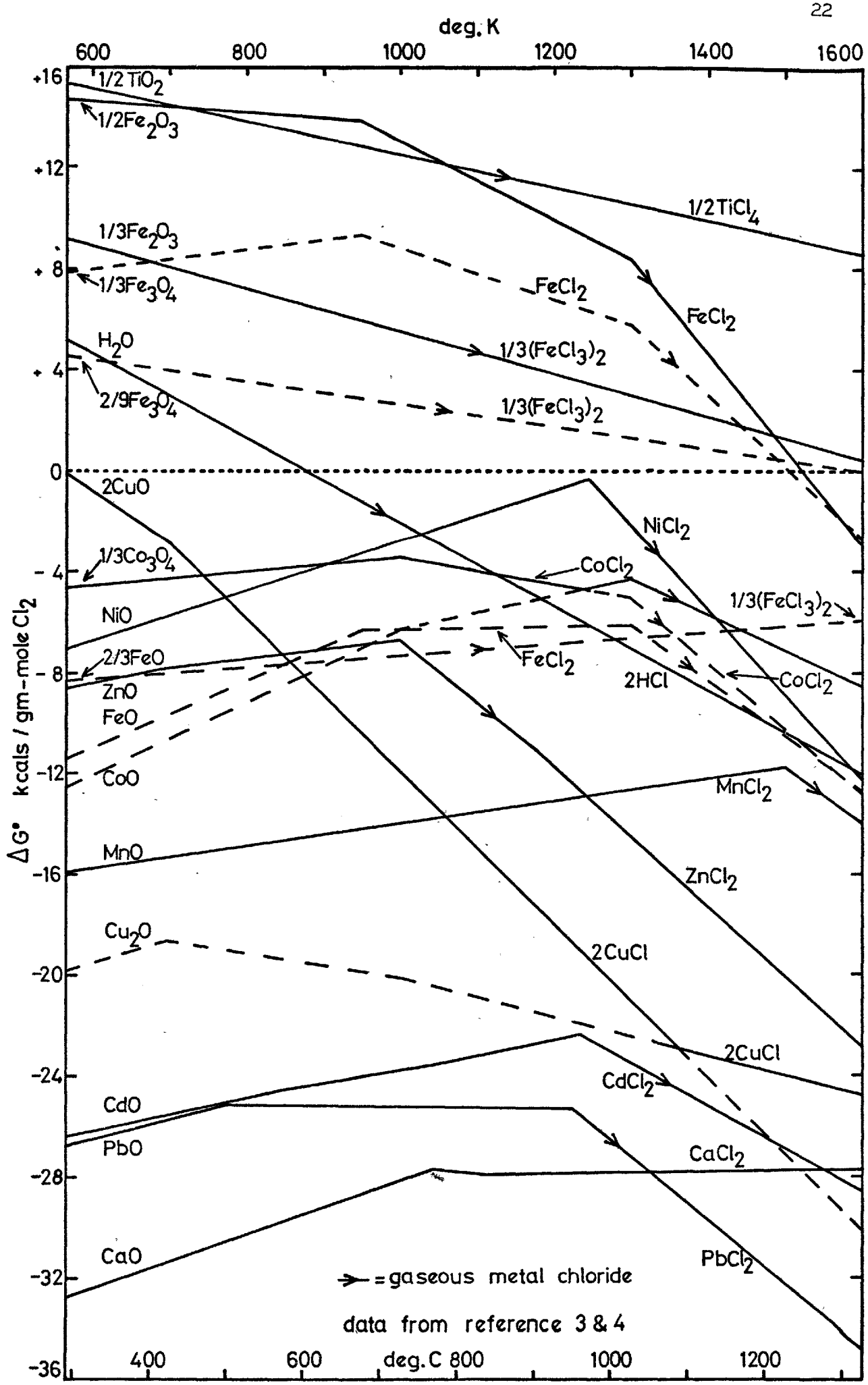

GRAPH 1A: METAL OXIDE + CHLORINE STANDARD FREE ENERGY OF REACTION

Of all the various chloride-volatilisation studies reported in the literature, few are directly comparable with the work being presented in this thesis. Rather than describing just these few specific studies, it has been decided to present a review on the following three aspects of chloride-volatilisation:

a) chloride-volatilisation of ores and raw materials
b) thermodynamic studies and determinations
c) chlorination kinetics

Plotted on graph 1A are standard free energy change[3,4] lines for reaction of 1 gm-mole of $Cl_{2(g)}$ with the oxides of Ti, Fe, H, Cu, Co, Ni, Zn, Mn, Cd, Pb and Ca. With metals that form two or more oxides, full lines are drawn for reactions involving their most stable oxide, broken lines for their less stable oxide(s). The lines account for phase changes at the 1 atmosphere-transformation temperatures.

1B CHLORIDE-VOLATILISATION OF ORES AND RAW MATERIALS

Most of the process-orientated chlorination/chloridisation-volatilisation studies reported in the literature have been performed on low grade complex oxides. Of foremost interest has been the wish to obtain effective extraction of one or more metals, whilst suppressing the transport of undesirable elements. To help obtain high overall reaction rates, experimental investigations have normally employed comparatively finely divided solids. Fluidised beds have thus frequently been used. With some oxide systems, high oxygen potentials and low chlorinating gas (eg Cl_2, HCl, CCl_4) partial pressures have enhanced separation efficiencies. Low oxygen potentials, necessary when forming chlorides from relatively stable oxides, have been obtained either by adding solid carbon to the charge, or by using reducing gases (eg CO, H_2). The usual variables that have been investigated are: a) the source of the ore or raw material, its size fraction and its pre-treatment, b) the reaction temperature and heating rate, c) the reactant concentration (eg P_{Cl_2}, Wt % NaCl, P_{CO}), and d) the addition of various gases (eg CO_2, SO_2, H_2O, O_2). Few structural examinations of either unreacted, part-reacted or fully reacted solids have been reported.

1B1 Purification of pyrite cinder by chloride-volatilisation processes

Chloride-volatilisation studies on pyrite cinder have almost always employed either gaseous chlorine or calcium chloride (m.pt. 772°C, b.pt 2000°C)[3]. Papers have appeared in the literature on laboratory scale studies[5,6,7,8,10],

large scale pilot plant work[9] and fully developed industrial processes[11].

1B1a Fulidised bed chlorination: Okajima and co-workers[5], Orlov and Piskunov[6,7], and Orlov[8] have reported on the fluidised bed chlorination (using Cl_2) of pyrite cinders containing various combinations and concentrations of the impurity metals Cu, Zn, Ni and Co. The results presented in these four different papers are in good general agreement. They show that the process is most efficient using comparatively high temperatures (eg 950°C), together with low chlorine concentrations (about 1%) in carrier gases of high oxygen potentials. At the start of reaction the measured Cu, Ni, Zn and Co volatilisation rates were relatively high, however, as the beds became depleted rates decreased by very large amounts; thus high extractions were only achieved after long reaction times. Neither a decrease in particle size (0.25-0.05 mm) nor an increase in chlorine content, above about 1%, significantly raised the non-ferrous extraction rates. Large increases in rates only occurred by increasing the reaction temperature. (Orlov investigated the extraction of cobalt in some detail and calculated that its volatilisation rate had an apparent* activation energy of 32.5 K cals/mole). Using practicable reaction times, typical percentage extractions (at 950°C) were Cu-95%, Zn-85%, Co-85% and Ni-75%. These values were only slightly improved by using high chlorine concentrations (up to 50%) however, at high P_{Cl_2}'s iron volatilisation became a major problem. The effects produced by adding up to either 30%-CO_2, 4%-SO_2, 4%-H_2O or 4%-O_2 to the chlorinating gas were studied by Orlov and Piskunov. CO_2 and SO_2 did not markedly influence the extraction process. However, both O_2 and H_2O caused a significant decrease in Co extraction together with a very large reduction in iron volatilisation. The various papers conclude that fluidised bed chlorination of pyrite cinder is technically feasible if operated under carefully controlled reaction conditions.

1B1b Packed bed chlorination:- A 100 ton/day pyrite-cinder-chlorination pilot plant, developed in West Germany, has been described by Lippert, Pietsch, Roeder and Walden[9]. This process, which exhibits a number of

---

* Since this value was calculated from overall rate data, without the identification of any individual process(es), it is not a true activation energy.

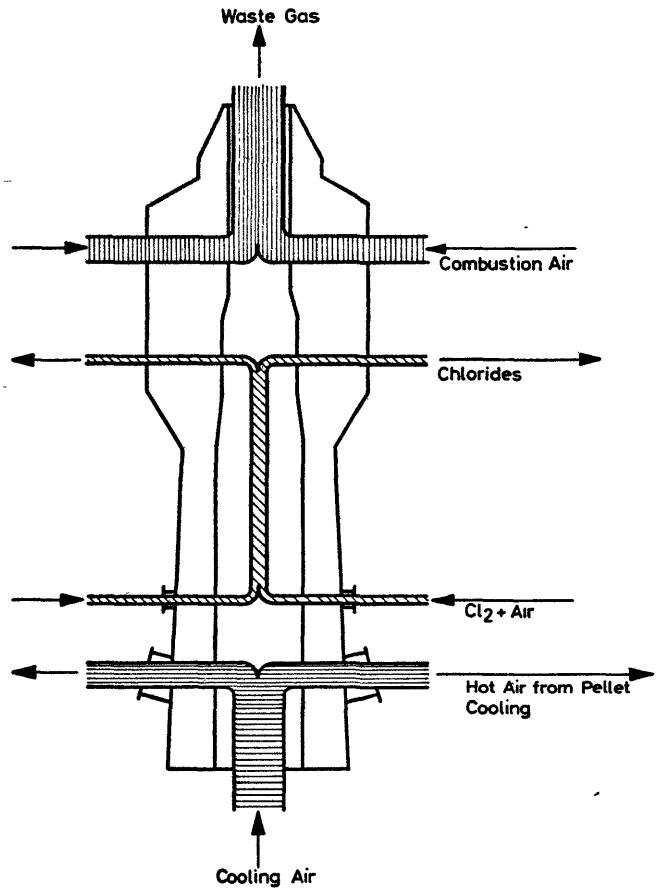

FIGURE 1A: GAS FLOW IN LDK SHAFT FURNACE

Separation of the gas flows is automatically maintained from pressure differential and chlorine analysis measurements.

novel features, has demonstrated its capabilities during extensive trials on pyrite cinders containing up to comparatively large amounts of the impurity metals Cu, Pb, Zn, Co, Ni, Au, Ag and As. The process has the following two aims:- a) the recovery of the valuable non-ferrous metals and b) the production of hardened hematite pellets suitable for use in the iron blast furnace. Green pyrite-cinder pellets are charged to the top of an ingenious three zone vertical shaft furnace; this furnace is illustrated in Figure 1A. In the uppermost zone the pellets are heated to about 1200°C by direct contact with combusting gases, this causes pellet hardening and residual-sulphur removal. In the central zone the pellets are reacted with chlorine. This enters (mixed with air) at the bottom of the zone, whilst at the top the gaseous chlorides are extracted into venturi scrubbers. In the lower zone the pellets are counter-current air cooled, this recovered heat helps reduce the overall thermal requirements of the process. The process has been operated at between 1100 and 1250°C with 5 - 17% Cl_2 in air and a chlorination zone residence time of about one hour. With the exception of cobalt, high recoveries of all non-ferrous values are reported; a typical set of results is given in Table 1A. Since high oxygen partial pressures were employed only minimal iron volatilisation occurred. Between about 1.2 and 1.8 times the theoretical chlorine requirements were needed to obtain high non-ferrous recoveries; the chlorine partial pressure was therefore quite high throughout the reaction zone. (Only by employing prohibitive chlorine excesses could

	Initial content wt %	Treated pellet content wt %	Percentage recovery
Fe	55.5	61.0	
Cu	1.78	0.016	99
Zn	2.58	0.15	94
Pb	0.44	0.06	86
Co	0.035	0.02	43
Au	1.7 gm/ton	0.1 gm/ton	94
Ag	18 gm/ton	2 gm/ton	89

TABLE 1A: NON-FERROUS REMOVALS AFTER LDK PROCESSING

high cobalt recoveries be obtained.) Decreased recoveries at above 1250°C were attributed to pellet densification and to the formation of spinels (eg $ZnFe_2O_4$). It is encouraging to note that no significant corrosion or handling problems were encountered during any stage of the process. Although technically sound, economic factors (described in the introduction to this thesis) have so far prevented its full scale commercial implementation.

An important part of chlorination-volatilisation processes is the recovery of the volatilised chlorides. In some cases the chlorides can be collected and handled as liquids (eg $TiCl_4$), however, when this is not possible, hydrometallurgical processing must be employed. Various treatments for chloride solutions from the LDK process are described by Walden[34].

1B1c Choridisation-volatilisation roasting:- The purification of pyrite cinders by chloridisation-roasting has been analysed and studied in some detail by Yazawa and Kameda[10]. Good non-ferrous recoveries were obtained by rapidly heating cinder pellets, containing comparatively small amounts of $CaCl_2$, to a holding temperature of between 1100 and 1200°C. The presence of H_2O in the roasting atmosphere caused lowered removals of a number of metals, whilst high residual sulphur contents caused premature $CaCl_2$ decomposition. For the same reasons as in the LDK process, temperatures in excess of about 1200°C resulted in decreased non-ferrous recoveries. A commercial process[11], largely the same as that studied by Yazawa and Kameda is at present in operation in Japan. Its major advantage over previous chloridisation processes is that the production of hardened heamatite-pellets and the recovery of the non-ferrous values both take place in one operation.

1B2 Chlorination-volatilisation of ilmenite

Due to the relative scarcity of rutile (TiO_2) deposits and the increasing world demand for titanium dioxide[131] (mainly for use as paint pigment) various different processes for upgrading ilmenite ($FeTiO_3$) have received attention in recent years. The standard free energy changes of the iron oxides and titanium dioxide chlorination reactions presented on graph 1A show that a chlorination-volatilisation separation process appears to be theoretically possible. An experimental investigation on ilmenite chlorination-volatilisation using HCl has been reported by Sankaran, Misra and Bhatnagar[12], whilst a similar investigation using CO - Cl_2 gas mixtures has been reported by Rabie, Saada and Ezz[13]. In both studies the aim was to extract the iron as a gaseous chloride and leave behind a residue of purified TiO_2. The experiments of Sankaran et al were performed at between 700 and 1100°C on briquettes of powdered ilmenite using HCl containing varied additions of H_2, Cl_2 and O_2; for the purposes of comparison some experiments

were also performed using pure Cl_2. At below 1075°C, contrary to basic thermodynamic predictions (see graph 1A), iron removal was more effective employing HCl as compared with when using Cl_2. Iron volatilised by reaction with HCl was in the form of $FeCl_2$ and $FeCl_3$, approximately in the ratio of 3:1 (the ilmenite sample investigated contained 26.6 wt % FeO and 17.8 wt % Fe_2O_3). Additions of greater than 8% Cl_2 to the HCl caused the iron to be volatilised only as $FeCl_3$. Increased iron volatilisation rates occurred with finer ilmenite powder. With their most successful experiments Sankaran et al were able to extract about 99% of the iron for the volatilisation of only about 1% of the titanium. Similarly efficient separations (including useful V, Mn and Cr extractions) were also obtained by Rabie and co-workers using CO-Cl_2 gas mixtures in a fluidised bed reactor. This process was most favourable at the highest temperature investigated (1000°C), using a CO/Cl_2 ratio of about 1.3:1. Carbon monoxide as a reducing agent, in comparison with carbon, has a low thermal yield. This is because the heat produced by the $C + \frac{1}{2}O_2 = CO$ reaction has already been liberated. Unfortunately, layering prevents carbon and ilmenite particles from being used together in a fluidised bed reactor. For either of these two proposed TiO_2 production routes to become a commercial success a chlorine recycle would be required (the rutile chlorination-volatilisation process for TiO_2 pigment production employs a highly efficient chlorine recycle).

1B3 Chromite beneficiation by selective chlorination-volatilisation

Steel production is the major user of chromium metal and for this purpose iron-chromium alloys are produced by a variety of routes from chromite ($FeO.Cr_2O_3$) ore. This ore is the only major source of chromium. The minimum Cr/Fe ratio suitable for the various smelting operations is about 2.8:1. Various attempts have therefore been made at beneficiating low grade chromite ores so that they may then be processed into ferro-chrome. Selective chlorination-volatilisation beneficiation processes have been studied by Athawale and Altekar[14] (using HCl) and Hussein and El-Barawi[15] (using Cl_2). Athawale et al employed a fluidised bed reactor, at between 600 and 1000°C, below which variable proportions of H_2 and Cl_2 were combusted to give the fluidising/reactant gas (the heat of combustion is -23 K cals/mole of HCl, this method of HCl production was claimed to improve the overall thermal economy of the system). The process was most effective at comparatively high reaction temperatures, however HCl utilisations were only between about 2-15%. Under the best reaction conditions about 50% of the iron and about 1% of the chromium were volatilised, thus leaving a residual powder with

a high Cr to Fe ratio. Some of the other findings made by Athawale and Altekar were: a) large excesses of H_2 caused lowered iron volatilisation, b) reduced particle size had no correlated effect on the volatilisation process, c) the iron volatilisation rate varied almost linearly with the HCl partial pressure and d) an apparent 'activation energy' of 6.1 K cals/mole was calculated from the iron extraction rate data. Hussein and El-Barawi performed their studies on an iron rich complex chormite ore - $(Mg.Fe)O(Cr.Al.Fe)_2O_3$ - using additions of carbon and reaction temperatures of between 600 and 1000°C. Unfortunately their paper presents few quantitative results, the exact degree of success of the process cannot thus be assessed.

1B4 Selective chlorination of laterite ores

Laterites, which account for about 20% of the known world iron reserves, contain concentrations of nickel and chromium which are too high to allow direct utilisation of the ore in iron production. Typical Ni and Cr concentrations are about 1 and 2 wt % respectively. Removal of these impurities by fluidised bed chlorination employing O_2-Cl_2 gas mixtures has been studied by Ohba et al[16], Furui et al[17] and Yagi et al[18]. There is good agreement between the results obtained by these three groups of workers, none of which found the process to be particularly satisfactory. Typical results showed that by using an 85% O_2 - 15% Cl_2 gas mixture at 1000°C 90% of the nickel and 10% of the iron contained in the ore were volatilised. Reduced iron volatilisation was obtained at lower chlorine concentrations (about 2%), however this necessitated long reaction times which in turn caused a considerable loss of charge due to elutriation.

1B5 Extraction of tin by fluidised bed chlorination-volatilisation

Application of the conventional tin ore smelting process to concentrates containing less than about 25% Sn results in the production of large amounts of slag into which a significant amount of tin is lost. A two-stage fluidised bed chlorination process suitable for low grade concentrates has been proposed by Nieuwenhuis[19]. By performing the process under reducing conditions ($CO/CO_2 > 0.3$) at about 800°C with HCl as the chlorinating gas stannous chloride (b.pt = 652°C) instead of stannic chloride (b.pt = 115°C) becomes the predominating tin chloride species ($SnCl_4$ is difficult to handle, also its formation requires twice the amount of HCl as does $SnCl_2$). The

thermochemical equilibria relevant to this process are given below:

a)* $SnO_{2(s)} + 2HCl_{(g)} = SnCl_{2(g)} + H_2O_{(g)} + \frac{1}{2}O_{2(g)}$ $\Delta G^\circ_{1000^\circ K} = 39.0$ K cals/mole

b)* $\frac{1}{2}SnO_{2(s)} + 2HCl_{(g)} = \frac{1}{2}SnCl_{4(g)} + H_2O_{(g)}$ $\Delta G^\circ_{1000^\circ K} = 3.3$ K cals/$\frac{1}{2}$mole

c)* $SnO_{2(s)} + 2HCl_{(g)} + H_{2(g)} = SnCl_{2(g)} + H_2O_{(g)} + CO_{2(g)}$

$\Delta G^\circ_{1000^\circ K} = -7.7$ K cals/mole

On the basis of a detailed analysis of the thermodynamics of the proposed process Niewenhuis predicts the following reactions:

1) Reaction reversal (to SnO_2 and $SnCl_4$) is theoretically possible during $SnCl_2$ condensation and collection; rapid exit gas quenching is therefore necessary.

2) Low grade concentrates contain significant amounts of sulphides and iron oxides. Under normal operating conditions volatilised sulphur would appear as H_2S rather than SO_2, whilst any heamatite would be reduced to magnetite.

3) Some loss of HCl would be caused by the formation of $FeCl_{2(g)}$.

4) Ag, Cu, As, Pb, Bi, Zn and Sb are often present in the concentrates at low concentrations. If in the form of oxides all would tend to be volatilised, their complete removal only being limited by their activities and their metal chloride partial pressures. If in the form of sulphides Ag, Cu and As would tend to be retained.

Preliminary experimental investigations using a 10 cm diameter fluidised bed reactor almost wholly confirmed these theoreticsl predictions. With an ore concentrate containing about 20% Sn Nieuwenhuis suggests using a two stage reactor** with successive tin contents of 9% and 0.5% together with a solids retention time of about 24 hours. He also suggests that by partially combusting a light fuel oil with air and chlorine, fluidisation, internal heating and production of the reactant gases can be achieved in parallel.

---

* Free energy data taken from reference 3

** If depleted solids are formed in a fluidised bed reactor their composition at removal will be the same as the mean composition of the solids throughout the bed. A single stage reactor containing solids at the tailings composition will have a low overall reaction rate. Use of two or more stages improves this situation and also gives the benefit of reducing the variation, about a mean, of the total solids retention time.

1B6 Extraction of iron from low grade ores by chlorination-volatilisation

A fluidised bed chlorination-volatilisation process for upgrading iron ores (the work was performed on chamositic type ores - $Al_2O_3.2SiO_2.3Fe(Mg)O.3H_2O$) containing as little as 20% Fe has been studied by Reeve[20]. The process, which is cyclic, depends upon the chemical reaction given below, the standard free energy of which can be obtained from graph 1A.

$$Fe_2O_{3(s)} + 6HCl_{(g)} = (FeCl_3)_{2(g)} + 3H_2O_{(g)}$$

By carefully controlling the P_{H_2O}/P_{HCl} ratio a forward chlorination reaction takes place in a first reactor (at about 300°C), whilst the reverse reaction occurs in a second reactor (at about 500°C) thus depositing high grade iron oxide. Unfortunately, since the equilibrium of the reaction given above is not particularly favourable it was necessary to circulate about 15X the stoichiometric HCl requirement in order to obtain a workable ferric chloride transport rate. In other respects the process was technically satisfactory, however, economic reasons prevented its commercial exploitation.

1B7 Chlorination-volatilisation of iron-manganese ores and slags

Cochran and Falke[21] have reviewed previous workers' attempts at separating manganese from iron-manganese slags and ores. They conclude that although the manganese oxide-chlorine reaction is thermodynamically more favourable than are the iron oxide-chlorine reactions, previous experimental studies have shown that volatilised managanese chloride is always accompanied by considerable iron transport thus necessitating further separation treatment. They therefore decided to investigate a chlorination-volatilisation process employing selective condensation separation. Their experiments consisted of passing pure chlorine over a reaction boat, held at between 800 and 1000°C, containing manganese and iron oxide. The volatilised $MnCl_2$ (b.pt 1231°C, m.pt 650°C)[3] was then collected in a condenser held at about 500°C whilst the $(FeCl_3)_2$ (b.pt 315°C, m.pt 307°C)[3] passed on into a separate air cooled condenser. Under the best operating conditions up to 99% of the manganese was recovered containing acceptably low concentrations of the transported impurities Mg, Ca, Fe, Cu, Ni, Co and Ag. It would be quite essential with this process to avoid the formation of ferrous chloride due to the comparative closeness of its boiling point (b.pt 1012°C, m.pt 677°C)[3] with that of manganese chloride. The formation of significant quantities of dichloride-trichloride gaseous complexes (see section 1C3b)

would also cause the process to become less effective. The chlorination-volatilisation of iron-manganese ores has also been studied by Okahara and Iwasaki[49]. Their experiments consisted of continuously monitoring the weights of oxide samples held in a furnace, programmed to heat up to 800°C at 10 degC/min, through which chlorine was passed. Their results on pure iron and manganese oxides led them to the conclusion that the oxygen released in the chlorination of lower oxides converted the remaining oxide to a higher oxidation state thereby making further reaction more difficult.

1B8 Chlorination-volatilisation of ores containing niobium and tantalum

In recent years many new applications have been found for niobium and tantalum metal. Their extraction and purification in the most economic and satisfactory manner is thus of considerable importance. In their naturally occurring states Nb and Ta are usually found together, each in the form of a pentavalent oxide. Since both form pentachlorides whose boiling points are very close to one another ($TaCl_5$ - 234°C, $NbCl_5$ - 250°C) chlorination-volatilisation extraction and separation processes have been investigated on a number of occasions. Multiple chlorination of graphite - ore concentrate mixtures has been studied by Hussain and Jena[22]. A concentrate containing 24% Ta was reacted with Cl_2 at between 540 and 600°C, the niobium and tantalum chloride condensates were then oxideised in a stream of oxygen and the chlorination was repeated. After five successive chlorination-oxidation stages the tantalum content in the transported niobium had been reduced to 0.14%. Investigations using CCl_4 as a combined chlorination-reduction agent caused the separation process to become even more lengthy. Three different chlorination routes for the extraction of niobium and tantalum from ores and slags have been explored by May and Engel[23]. These consisted of chlorinating (Cl_2) the following mixtures, alloys and compounds at between 500 and 800°C.

a) Oxide-slag/ore and carbon mixtures;
b) Iron-tantalum-niobium alloys produced by carbothermic reduction of slags and ores,
c) Niobium-tantalum-carbide produced by carbothermic reduction of slags and ores.

Tantalum and niobium recoveries of up to 99% were obtained, however significant amounts of iron were also chlorinated. This iron contamination

was reduced either by a pre-chlorination acid leaching or by use of sodium chloride. The sodium chloride was either added to the unreacted solid powder or packed into a column through which the product gases passed. The aim in both cases was to reduce the ferric chloride volatility by forming a mixed chloride complex (see section 1C3b). Chlorination routes have also been investigated by Harris and Jackson[24] in their attempts at developing a suitable process for extracting niobium from the rich ore deposit at Mrima Hill in Kenya.

1B9 Chloride-volatilisation in other systems

1B9a The TORCO* process:- This process (often known as the segregation process), which has been outlined in the introduction to this thesis, is dependent upon a local transport phenomenon by which gaseous cuprous chloride, formed by the chloridisation action of NaCl, is reduced at the surface of carbon particles to copper metal. A good account of the TORCO* process has been given by Pinkney and Plint[25]; Brittan and Liebenberg's[64] work on the kinetics of the copper segregation process is described in section 1D2c.

1B9b Chlorination-volatilisation of rutile:- Although the general aspects of rutile chlorination are well known, there appear to be few publications in the metallurgical literature on the fundamentals of the process. This may be due to reasons of strong commercial competition and also that the process engineering and handling problems warrant the most attention. Many patents exist, however by their very nature they are quite non-specific.

1B9c Chlorination-volatilisation of tungsten ores:- Using either carbon or sulphur dioxide as a reducing agent, Henderson Rhoads and Brown[26] have studied the chlorination of scheelite and wolframite ores. The separation of tungsten from molybdenum by the fractional distillation of mixtures of their chlorides, and oxychlorides was also investigated. The results of their various experiments indicate that a chlorination route for tungsten production is technically feasible.

---

* Treatment of refractory copper ores

1B9d Extraction of uranium:- The extraction of uranium from a low grade refractory ore (0.04 to 0.2% U) by chlorination-volatilisation (using Cl_2 of CCl_4) at a reaction temperature on between 600 and 800°C has been studied by Lapage and Marriage[50]. At 800°C 92-96% of the uranium was recovered (as UCl_4) together with relatively large amounts of the transported impurities Fe, Al, Ca and Mg.

1B9e Chlorination of rare earth metal ores:- Brugger and Greinacher[27] describe a production scale process, operated at 1200°C, for the chlorination of rare earth ores in an electric furnace. In the process fused high boiling point chlorides are tapped from the furnace bottom whilst volatilised chlorides are extracted from the top for condensation and further treatment.

1B9f Purification of nickel-cobalt sulphide matte:- Shimagaya[28] has studied the extraction of cobalt from molten (1100°C) sulphide matte by a chlorine jetting process. His results shown that cobalt is volatilised to a greater extent than is nickel, and that Co levels could be lowered from 10% to 1.5%.

1C THERMODYNAMIC STUDIES AND DETERMINATIONS

The fundamental importance of comprehensive and accurate quantitative thermodynamic data in the study and design of chloride-volatilisation processes is so apparent that it needs no explanation in this thesis further than that given in the introduction.

1C1 Available thermodynamic data

The heat capacities, heats of formation, heats of transformation, melting points and boiling points (and in many cases vapour pressures) of almost all metallurgically significant compounds and elements have over the years been experimentally determined with varying degrees of accuracy. These data alone have enabled estimates to be made of the free energy changes (and therefore equilibrium constants) of very large numbers of chemical reactions. In addition to these indirectly determined equilibrium constants, which may often be in error by important amounts, many equilibria have been quantified by direct experimental methods; in general these

are potentially the most accurate. At the present time equilibria for chloride-volatilisation reactions are not known to the same degree of accuracy as are those for oxide-reduction reactions. Very few oxide-chlorine (or hydrogen chloride) equilibria have been directly measured. With almost all oxide-chlorine reactions it is therefore necessary to establish their standard free energy changes by using various combinations of thermodynamic data. This method is not particularly satisfactory (especially when the free energy changes involved are relatively small) since the free energies of formation of many gaseous chlorides have themselves not been accurately established (see section 6C4) either by direct measurement or by calculations based upon other thermodynamic functions. No thermodynamic data reviews specifically on chlorine metallurgy appear to have been published in the English language for some considerable time[29,30]. However, many of the more recent papers presenting thermodynamic measurements relevant to chlorine metallurgy may be traced via some of the broader ranging data reviews[3,4,40,100,103]. In order to avoid repetition most of the published thermodynamic data relevant to this thesis, namely that for the compounds ZnO, CdO, CoO, Co_3O_4, $ZnCl_2$, $CdCl_2$ and $CoCl_2$, are not reviewed in this main section but are discussed in section 6C and Appendix L.

1C2 Direct determination of oxide-chlorine chemical equilibria

To measure experimentally the equilibrium constant of a chemical reaction of the type* shown below presents a number of difficulties.

$$MeO_{(s)} + Cl_{2(g)} = MeCl_{2(g)} + \tfrac{1}{2}O_{2(g)} \qquad (1)$$

The equilibrium constant for this reaction is:

$$K = \frac{P_{MeCl_2} \cdot P_{O_2}^{\frac{1}{2}}}{a_{MeO} \cdot P_{Cl_2}} \qquad (2)$$

By performing the reaction using pure metal oxide ($a_{MeO} = 1$) the three unknown variables to be determined are the oxygen, chlorine and metal chloride equilibrium partial pressures. High temperature solid electrolyte cells would be an ideal method by which to measure the P_{O_2} and P_{Cl_2} values.

---

* The reaction being used for the purpose of illustration involves a bivalent metal, however, the points being described are equally applicable to a metal of a different valency or one that exists in more than one valency state.

The metal chloride partial pressure could then be computed either from a mass balance on the chlorine or by considering the stoichiometry of the reaction together with the amount of oxygen produced by reaction. Unfortunately, although oxygen cells are available, chlorine cells have not yet been fully developed. It is therefore necessary to employ an experimental method in which the equilibrated gas mixture (oxygen-chlorine-metal chloride) is collected and analysed. Experiments of this general type (which can for example also be used for determinations of vapour pressures[40]) are normally performed under dynamic conditions; the method is variously called the flow, transpiration or entrainment method. In the case of the MeO + Cl_2 reaction, chlorine (often diluted in a carrier gas such as O_2, Ar, N_2 or He) is passed through an isothermal packed bed of the oxide under study, the gas flow and gas-solid contact area being chosen so that the various components achieve thermodynamic equilibrium before the bed exit. From the equilibrated gas mixture leaving the bed all the metal chloride is collected in a condenser whilst the unreacted chlorine is absorbed chemically. After running the experiment for a suitable period of time both collected components are determined by an accurate analytical method. The oxygen is then determined from the measured amount of transported metal and the reaction stoichiometry.

Although this technique appears to be comparatively simple, it can have two limitations, both of which make it difficult, if not often impossible, to measure accurately the equilibrium constants of the reactions that are normally of most interest, namely those with a large negative standard free energy change. The first limitation is caused by equilibrium shift during collection of the condensate. If $dK/dT > 0$ there is back reaction during cooling, conversely if $dK/dT < 0$ there is forward reaction during cooling. It is both the sign and magnitude of the heat of reaction which governs the direction and extent of any equilibrium shift.
The equation which relates the important parameters is Van't Hoff's isobar:

$$\frac{d(\log_e K)}{dT} = \frac{\Delta H^o}{RT^2}$$

This shows that endothermic reactions undergo a backward reaction shift

during cooling* whilst exothermic reactions undergo a forward reaction shift*. The tendency of a metal oxide and chlorine system to forward react during cooling is not a problem since, as there is no metal oxide in the condenser no reaction can take place; the amount of absorbed chlorine is therefore the same as the amount leaving the oxide bed. However, a system that back reacts during cooling causes the amount of chlorine absorbed after the condenser to be larger than the amount leaving the bed. (Back reaction does not prevent the bed exit metal chloride partial pressure from being calculated since it is the total metal content in the condenser that is determined, be it either in the form of chloride or oxide.) Under certain conditions a correction can be applied to account for the excess chlorine, this is carried out by analysing the condensate for both its oxygen (as oxide) content and its chlorine (as chloride) content. However, with an endothermic large negative free energy change reaction the correction may be very large, which therefore causes the corrected P_{Cl_2} to be in error by an unacceptable amount. With a positive free energy change reaction this correction need not be applied since the equilibrium constant can be calculated on the basis of the bed entry chlorine flow rate, the condensate analysis (transported metal) and the stoichiometry of the reaction. The need to apply a correction with endothermic negative free energy change reactions can be avoided by preventing the back reaction from taking place. This can be achieved by passing the uncooled equilibrated gas mixture through a bed of carbon so that most** of the oxygen reacts to form carbon monoxide and carbon dioxide.

The second limitation to the dynamic method of determining metal oxide + chlorine reaction equilibrium constants is that very small amounts of chlorine are difficult to collect and accurately analyse. Shown below are the relative amounts of metal chloride and chlorine to be collected and analysed from bivalent metal oxide chlorination-volatilisation reactions (as in equation (1)) performed at 1000°K having ΔG° values

---

* This is, of course, part of the classic principle of Le Chatelier.

** The gas would need to remain oxidising with respect to CCl_4 so as to prevent its formation, therefore $C\text{-}CO_2\text{-}CO\text{-}O_2$ equilibrium would have to be avoided.

of + and - 20000 cals/mole (it is assumed that back reaction does not take place during cooling and collection of the equilibrated components).

ΔG° cals/mole	chlorination gas	Amounts to be collected Cl_2	$MeCl_2$
+20000	Pure Cl_2	5 gms	0.355 gms
+20000	O_2 containing a trace of Cl_2	5 gms	0.045 gms
-20000	Pure Cl_2	58 μ gms	5 gms
-20000	O_2 containing a trace of Cl_2	101 μ gms	5 gms

Total pressure = 1 atmos $M.W._{MeCl_2} = 150$
T = 1000°K
$K = 4.23 \times 10^{-3}$ or 2.35×10^{4} atmos$^{\frac{1}{2}}$

The data given in the table show that positive standard energy change reactions are the easiest to study, especially when pure chlorine is used. As the magnitude of the equilibrium constant becomes larger it is progressively more difficult to measure experimentally its value. It would thus appear that K values in excess of about 10^4 cannot be determined directly using the flow method on a single oxide. However, a large but unknown equilibrium constant can be measured experimentally by simultaneously equilibrating the oxide under investigation and an oxide having a smaller but already known equilibrium constant. From the relative amounts of each metal chloride formed (and the oxygen partial pressure in the case of a metal whose oxide and chloride are of unequal valency) the unknown equilibrium constant can then be computed with reference to the known constant*. Full details on this method, which has been used in this study, are given in chapters five and six.

* Provided that the metal oxide activities are known.

1C2a Zinc oxide-chlorine equilibrium:- It appears that in recent years only one equilibrium study has been performed by the method described in the preceding section. These measurements were carried out by Orlov and Jeffes[31] on the

$$ZnO_{(s)} + Cl_{2(g)} = ZnCl_{2(g)} + \tfrac{1}{2}O_{2(g)}$$

system at between 800 and 1100°C. In their experiments an O_2-5% Cl_2 gas mixture, at a total pressure of 1 atmosphere, was passed through an 8-10 cm deep 12 mm diameter packed bed (typically weighing about 20 gms) of 0.7-1.7 mm diameter zinc oxide granules. By performing a number of experiments it was established that equilibrium was achieved before the bed exit when using a gas flow of 200 cc/min; each experiment was of 40 minutes' duration. The chlorine in the condenser exit gas was absorbed by two potassium iodide scrubbers and then determined by back titrating the liberated iodine against sodium thiosulphate. After the experiment the condensate was washed from the condenser with 10% nitric acid solution. The Zn^{++} was determined by EDTA complexiometric titration whilst the Cl^- was determined by titrating against silver nitrate; the back reaction correction being calculated from the difference between these two analyses. At 800°C it was found that 0.25% of the collected zinc was in the form of ZnO, this resulted in a 10% correction to the chlorine partial pressure. Since at higher temperatures the errors in the Zn^{++} and Cl^- analyses were comparable with the corrected chlorine partial pressure, only their $K_{800°C}$ value was reliable. Being unable to determine the entropy of reaction they assumed it to be equal to the mean of the values derived from four different thermodynamic data publications. Their final estimate of the standard free energy of reaction is

$$\Delta G^\circ_T = 21890 - 28.00\ T \text{ cals/mole}$$

estimated error $\pm$ 1000 cals/mole between 732 and 1000°C

The accuracy of this free energy data is discussed in section 6C1.

1C3 Gaseous metal chloride molecules

Many metals can form more than one type of gaseous metal chloride molecule. The three different types possible are: a) different valency chlorides of the same metal, b) metal chloride polymers, and c) complex molecules formed between different metal chlorides. Some of the metals which form more than one metal chloride are Al, Cr, Cu, Co, Fe, Ti, Ta, Sn, Nb, V

and U. Since the standard free energies of formation of most metal chlorides are known (to varying degrees of accuracy) it is usually possible to predict whether under a given set of conditions a metal chloride of a particular valency state may exist. For further consideration of the respective stabilities of different valency chlorides of the same metal, reference should be made to some of the various thermodynamic data publications[3,4,29,30,103]. The existence of gaseous chloride polymers and gaseous chloride complexes are not widely appreciated, the thermodynamics of the formation of these species therefore deserves some mention in this review.

1C3a Gaseous chloride polymers:- The discovery of low entropies of vapourisation and high apparent molecular weights in many metal chloride systems have led to the identification of various polymeric vapour species, principal amongst which have been dimers and trimers. The heats of formation of polymers from monomers are exothermic whilst their entropies of formation are negative. Therefore, all polymers tend to revert to a monomer (possibly via intervening states) as their temperature is increased. A polymer may thus be viewed as being an intermediate between a liquid, which has strong intermolecular bonds, and a monomeric gas, which has broken these bonds. Various experimentally determined heats of formation of polymers from monomers are given in table 1B, each value can be thought of as being a heat of partial condensation. Each metal chloride was studied at a temperature considerably below its boiling point, thus, although at these respective temperatures the vapours are predominantly polymeric, their absolute vapour pressures are very low. Some other polymers that have been studied are $(ZnCl_2)_2$[76,77], $(CdCl_2)_2$[78], $(AuCl_3)_2$[38], $(ReCl_3)_3$[40], $(AlCl_3)_2$[40] and $(CuCl)_3$[35,36]. At certain temperatures some chloride vapours are partitioned between a number of polymers eg $LiCl-(LiCl)_2-(LiCl)_3-(LiCl)_4$. Metal chloride vapour species are normally studied by using one of two different methods. These consist of: a) measuring the real vapour pressure and comparing it with the apparent vapour pressure as measured by the flow method[40], and b) coupling a Knudsen effusion cell to a mass spectrometer[37,38,39]. The second technique gives the best results since it positively identifies each different vapour species, however, at total pressures in excess of about 10^{-4} atmospheres complex differential vacuum pumping systems are required[38]. Research reports on Knudsen cell - mass spectrometer studies often describe the existence

Metal chloride	Polymer type	ΔH polymerisation K cals/mole of polymer at T°K		ΔH evap-monomer* K cals/mole of monomer at boiling point °K		Reference
LiCl	dimer	-50.1	800	36.0	1655	40
NaCl	dimer	-51.8	930	40.7	1738	40
KCl	dimer	-41.5	900	39.0	1680	40
$CrCl_2$	dimer	-47.9	985	47.0	1573	37
$MnCl_2$	dimer	-37.7	888	32.7	1691	37
$FeCl_2$	dimer	-36.3	665	30.0	1285	37
$CoCl_2$	dimer	-35.5	817	37.6	1298	37
$NiCl_2$	dimer	-39.6	754	53.8 sublimation	1243	37
AgCl	trimer	-97.3	900	42.5	1837	39

* Data from reference 3

TABLE 1B: HEATS OF POLYMERISATION AND EVAPORATION

of unusual valency ionised metal chloride species. These are largely of academic interest since they are only present in small amounts and are probably produced by interactions inherent to the mass spectrometer. Whether polymeric species are formed during a given process largely depends upon the temperature at which it is operated. At 1200°C, the normal operating temperature of the LDK process[9], volatilised $ZnCl_2$ exists only as its monomer whilst at 800°C, the normal operating temperature of the TORCO process[25], gaseous cuprous chloride exists mainly as its trimer. Metal chloride polymerisation causes metal oxide + chlorine reactions with small equilibrium constants to become more favourable in terms of the partition of chlorine between reacted and unreacted forms. The effect of polymerisation on mixed oxide chlorination reactions is examined in section 6B1. Since molecular diffusion coefficients and Kundsen flow coefficients decrease as the mass of the diffusing species increases, a metal chloride polymer diffuses more slowly than does its monomer.

1C3b Gaseous complexes:- Many different metal chlorides combine together to form large complex gaseous molecules. After having studied the formation of complexes between various different dichlorides and Al and Fe trichloride, Dewing[41] has postulated the existence of the species

MAl_2Cl_8, MAl_3Cl_{11} and MFe_2Cl_8. The most important effect resulting from the formation of these complexes is that they greatly increase dichloride volatilisation at temperatures where the intrinsic vapour pressures of the pure dichlorides are low. The heats of formation of complexes are exothermic and their entropies of formation are negative, their stabilities therefore decrease with increasing temperature. In a gaseous trichloride - solid dichloride system this causes the effective volatility of the dichloride to fall with increasing temperature, reach a minimum value and then increase as the intrinsic vapour pressure of the dichloride becomes significant; in some systems this phenomenon will occur over a wide temperature range. Some experimentally determined heats and entropies of formation (according to Dewing) are given in Table 1C.

It is interesting to note (from the data given in Table 1C) that the stabilities of different complexes of a given type are very similar and appear to be unrelated to their dichloride boiling points. Dewing interprets this to mean that the energy bonding a dichloride molecule into a gaseous complex is similar to the dichlorides' solid state bond energy. This therefore suggests that any divalent chloride would form complexes with iron and aluminium trichloride. Gaseous chloride complexes, formed at temperatures of up to 1400°K between various combinations of mono,di and trichlorides, have also been reported by Bloom[40]. Two adverse effects on chlorination processes might be caused by the formation of complexes: a) enhanced transport of undesirable elements, b) impaired selective condensation efficiency (both of these problems occur with $MgCl_2$ and $CaCl_2$ in the aluminium chloride process). However, the formation of complexes might be advantageous with some processes either for scrubbing one component from a mixture of chlorides, as studied by May and Engel[23] (see section 1B8) and Nieberlein[48], or as a method of increasing the volatility of high boiling point chlorides at low reaction temperatures.

1C4 The thermodynamic analysis of volatilisation processes and chemical transport reactions

The name 'chemical transport reaction' is used to describe a specific group of reaction processes which depend upon a cyclic mechanism of the

MCl_2	T^oK	Heat of formation at T^oK - K cals/ mole of complex	Entropy of formation at T^oK-cals/mole of complex ^oK	MCl_2* mpt ^oK	MCl_2* bpt ^oK
		$MCl_{2(s)} + 2AlCl_{3(g)} = MAl_2Cl_{8(g)}$			
$CaCl_2$	900	-17.8	-25.7	1045	2273
$CoCl_2$	750	-15.2	-19.4	1013	1298
$MgCl_2$	800	-13.8	-17.9	987	1691
$MnCl_2$	750	-15.8	-20.9	923	1504
$NiCl_2$	750	-16.3	-24.2		sub. 1243
		$MCl_{2(s)} + 3AlCl_{3(g)} = MAl_3Cl_{11(g)}$			
$CaCl_2$	900	-30.0	-40.5	1045	2273
$CoCl_2$	700	-36.6	-47.4	1013	1298
$MgCl_2$	750	-42.6	-55.4	987	1691
$MnCl_2$	750	-33.3	-42.0	923	1504
		$MCl_{2(s)} + 2FeCl_{3(g)} = MeFe_2Cl_{8(g)}$			
$CdCl_2$	700	-19.4	-20.9	841	1234
$CoCl_2$	800	-16.5	-17.2	1013	1298
$MnCl_2$	750	-19.1	-21.2	923	1504
$NiCl_2$	800	-19.7	-24.4		sub. 1243

*bpt $FeCl_3$ = 588^oK *bpt $AlCl_3$ = 433^oK

* Data from reference 3

TABLE 1C: HEATS AND ENTROPIES OF FORMATION OF COMPLEXES (According to Dewing[41])

general type illustrated below.

$A_{(s \text{ or } l)} + B_{(g)} = AB_{(g)}$ . . . . . at T_1

$AB_{(g)} = B_{(g)} + A_{(s \text{ or } l)}$ . . . . . at T_2

The essential feature of these reactions is the transport of an element or compound between two reaction zones by a gaseous intermediary (often a halide) whose stability varies with temperature. Two successful metallurgical chemical transport reaction processes are the Mond process for nickel and the Van Arkel process for zirconium. Two unsuccessful processes which have been studied are those due to Reeve[20] (see section 1B6) and Gross[46,47]. In addition to their use in metallurgical extraction and refining operations chemical transport reactions have found some unusual applications,eg the 'quartz-halogen' electric light bulb. Many of the investigations into chemical transport reactions have been reviewed by Schafer[44], whilst the basic thermodynamic requirements of such processes have been described by Alcock and Jeffes[42]. The chemical transport reaction process which has probably received the most attention over the last 25 years is the Gross process for refining aluminium. The process operates by controlling the reaction:

$$AlCl_{3(g)} + 2Al_{(l)} = 3AlCl_{(g)}$$

Despite numerous efforts (including an £8m-8000 tons per year Alcan plant at Arvida) the process has so far defied successful commercial exploitation. A process for titanium similar to that for aluminium has also been studied by Gross[45]. For any volatilisation process to be a success a detailed knowledge of all the possible chemical reactions and vapour species is essential. This point is emphasised by Kellogg[43] who shows how systems in which a number of reactions are possible can produce definite maximum metal-containing-species effective vapour pressures.

1D CHLORINATION KINETICS

1D1 Transport kinetics and chemical kinetics

The equilibrium positions of all chemical reactions are determined by their standard free energy changes. Any reacting system not at equilbrium has a free energy driving force tending to cause it to move into its equilibrium state. Although the free energy driving force indicates in which direction the reaction will take place it gives little if any information about the overall rate of the reaction. Heterogeneous reactions involve both chemical and transport processes. Since transport processes

(mass, momentum and heat) are governed by physical phenomena their rates can sometimes be estimated from empirical and theoretical data. However, the rates of chemical processes, which are governed by the energies involved in the interactions between groups of atoms, cannot be predicted. Experiments to elucidate the rate controlling mechanism of a given heterogeneous reaction are usually difficult to devise and complex to analyse. Many metallurgical processes (including the majority of those involving chloride-volatilisation) depend upon chemical reactions between gases and solids. Since the early sixties the study and analysis of the kinetics of this type of process has become well advanced. In this time there have been published many notable experimental studies on gas porous-solid reactions[54,55,56], theoretical studies on gaseous diffusion within porous solids[128,130], theoretical papers on fluid solid reaction models[58,59,60,120] and texts on transport processes[57,62,117,127]. However, although these works contain much valuable information, in order to understand and quantify the individual rate processes of a previously uninvestigated reaction, there are no substitutes for carefully designed and critically analysed experiments.

1D2 Oxide-chlorine and oxide-hydrogen chloride reaction kinetics

Only a few reports on the kinetics of metal oxide chlorination reactions can be found in the literature. No studies were found on any of the four oxides (ZnO, CdO, CoO, Co_3O_4) used in the experiments being reported in this thesis. The most notable and detailed series of experiments on the kinetics of chlorination-volatilisation reactions are by Fruehan and Martonik[51,52,53].

1D2a Chlorination-volatilisation of Fe_2O_3 and NiO with Cl_2 and HCl:-
By thermogravimetric analysis Fruehan et al[51] have studied the rates of the chemical reactions shown below:

$$NiO_{(s)} + Cl_{2(g)} = NiCl_{2(g)} + \tfrac{1}{2}O_{2(g)} \quad \ldots\ldots\ldots\ldots\ldots (1)$$

$$NiO_{(s)} + 2HCl_{(g)} = NiCl_{2(g)} + H_2O_{(g)} \quad \ldots\ldots\ldots\ldots\ldots (2)$$

$$Fe_2O_{3(s)} + 3Cl_{2(g)} = 2FeCl_{3(g)} + 1\tfrac{1}{2}O_{2(g)} \quad \ldots\ldots\ldots\ldots\ldots (3)$$

$$Fe_2O_{3(s)} + 6HCl_{(g)} = 2FeCl_{3(g)} + 3H_2O_{(g)} \quad \ldots\ldots\ldots\ldots\ldots (4)$$

These experiments, some of which were on laboratory prepared nickel ferrite, were performed using screened granules and round pellets (0.3 to 10 mm in diameter) of various porosities with Cl_2 (up to 3%) and HCl (up to 30%) diluted in He and Ar. Over the temperature range investigated, 800 - 1200°C. ferric chloride is predominantly monomeric whilst nickel chloride is entirely monomeric. The standard free energy changes of the reactions were computed from data taken from Kubachewski et al[3] (the same values are plotted on graph 1A). The accuracies of these data are difficult to assess*, but it would appear that only reaction (1) has a negative standard free energy change, the least favourable equilibrium being that of reaction (4). With all of the experiments steady-state reaction rates were obtained until at least 20% of the solid had been volatilised. Analysis of the various results was therefore confined to the initial period of reaction. This analysis consisted of plotting $\log_{10}\left(\frac{dw}{dt} \cdot \frac{1}{w}\right)$ against $\log_{10} d$ for a number of experiments performed under identical conditions except for a change in the pellet/granule size. With porous solids gradients of 0, -1 and -2 represent three different reaction regimes. These are: a) when the gradient is equal to zero reaction occurs uniformly throughout the pellet, the reaction rate is therefore chemically controlled; b) with a gradient of minus one the overall reaction rate is proportional to the external surface area of the pellet, the reaction rate is therefore limited by gaseous diffusion within the pellet; c) a slope of minus two indicates that the overall reaction rate is inversely proportional to the pellet diameter, the reaction is therefore controlled by gaseous diffusion through the boundary layer**. After reaction all of the pellets and granules were found to be surrounded by a thin fluffy layer of oxide, below which there appeared to have been no reaction. These layers decreased in thickness as the reaction temperature increased. Below about 1000°C the outer surfaces of the $NiFe_2O_3$ pellets which had been reacted in Cl_2 were composed of a very thin layer of Fe_2O_3. Fruehan et al concluded that since there was no build up of Fe_2O_3 the reaction

$$NiFe_2O_{4(s)} + Cl_{2(g)} = NiCl_{2(g)} + \tfrac{1}{2}O_{2(g)} + Fe_2O_{3(s)}$$

---

* Extrapolations were necessary with some of the data

** This is because the Sherwood number is approximately constant during most gas-solid thermogravimetric experimental investigations.

was controlling the rate. However, this deduction is inconsistent since whichever oxide appears on the surface must have the slower reaction rate. Over the whole temperature range investigated the oxide reaction rates were first order with respect to the chlorination gas partial pressure.

With the oxide + chlorine reactions two distinct regimes were found.
a) At below about 1000°C the overall reaction rates of the pellets were proportional to d^2 (slope = -1). Dense oxides* reacted between 15(Fe_2O_3) and 30(NiO) times more slowly than porous oxides*. Overall reaction rate constants (defined by Fruehan et al as $\dot{n}''_{\text{chloride}} = \bar{k} \cdot {}_bP_{Cl_2}$, which therfore makes $\bar{k}$ independent of the pellet size) varied between about 0.15 (800°C) and 12 (1000°C) cm/sec. The temperature dependences of the different reactions were similar, the mean apparent activation energy being about 40 K cals/mole. Under a given set of conditions the oxide reaction rates decreased in the order NiO-Fe_2O_3-$NiFe_2O_4$.

b) At above about 1000°C there was a progressive transition towards a slope of -2, and a gradual decrease in the temperature sensitivity of the reaction rates. By 1200°C the reaction rates of different oxide pellets of the same size were very similar (at 1200°C a typical $\bar{k}$ value** for a 0.5 cm diameter pellet was 32 cm/sec). Reaction rates in Cl_2-He mixtures were more rapid than in Cl_2-Ar mixtures.

With the first regime described avove the experimental evidence indicates that the reactions were taking place at and slightly below the pellet surfaces. The overall reaction rates were therefore limited by the combined effects of low diffusion rates in the porous oxides and comparatively low chemical reaction rates. The results obtained at above about 1000°C show that the reactions were becoming controlled by gaseous diffusion through the boundary layer. By assuming the surface chlorine partial pressure to be equal to zero and calculating the Cl_2 mass transfer

---

* BET surface area values for the dense and porous oxides were Fe_2O_3 - 0.008 vs 14 M^2/gm and NiO - 0.022 vs 3.92 M^2/gm

** The gas composition used to obtain this value was not stated, however, it is thought that it was He containing somewhere between 1 and 3% Cl_2.

coefficients from the equation

$$K_c^{Cl_2} = \frac{D_{Cl_2/He}}{d} \cdot (2 + 0.6\, Re^{\frac{1}{2}} Sc^{1/3}) \quad \ldots\ldots\ldots (5)$$

Fruehan et al compared the experimentally measured 1200°C - NiO reaction rates (various pellet sizes) with ones calculated using the equation

$$\dot{n}''_{NiCl_2} = \frac{K_c^{Cl_2}}{RT} \cdot b^{P_{Cl_2}} \quad \ldots\ldots\ldots\ldots\ldots\ldots\ldots (6)$$

Agreement between the measured and calculated rates was very good. The mass transfer coefficients predicted by the correlation above were between about 15 and 50 cm/sec. These values were large, despite comparatively low Sherwood numbers, since at 1200°C $D_{Cl_2/He}$ (as calculated from the Chapman-Enskog formula) is equal to 7.0 cm^2/sec.

Fruehan and Martonik found the oxide + hydrogen chloride experiments, which were performed at between 800 and 1000°C, more difficult to explain. Their results were briefly as follows. The fluffy surface layers were thinner than those produced by the oxide + chlorine reactions at the same temperatures. Porous pellets were found to react only about 2-3 times faster than dense ones. Both the dense and porous NiO pellets reacted more rapidly than the Fe_2O_3. Overall reaction rate constants *($\bar{k}$, defined as before) for 5 mm diameter pellets varied between a minimum value of 0.23 cm/sec (dense Fe_2O_3 - 800°C) and a maximum value of 3.5 cm/sec (porous NiO - 1000°C). With pellets of greater than 2 mm diameter the $\log_{10}\left(\frac{dw}{dt} \cdot \frac{1}{w}\right)$ vs $\log_{10} d$ plots had slopes of approximately -2(bounday layer diffusion control). However, with pellets of smaller sizes (the smallest used were about 0.3 mm in diameter) the slopes tended towards values of between 0 and -0.5. The apparent activation energies of the NiO and Fe_2O_3 reactions in the gradient = -2 regions were 15 and 8.1 K cals/mole respectively. The results which are summarised above seem to indicate that the rates of the oxide + hydrogen chloride reactions were mainly controlled by mass transfer through the boundary layer.

---

* Although not stated it is thought that these values were obtained using an He-HCl gas mixture.

Fruehan et al suggest that the transition in slope was caused by reacting groups of the smaller pellets together, thereby limiting the surface areas available for reaction as well as reducing the mass transfer coefficients. Rates calculated on the basis of ${}_sP_{HCl} = 0$ and equations (5) and (6) gave values an order of magnitude greater than were experimentally measured. This result is not surprising since although the rates seem to have been mainly controlled by boundary layer mass transport, the transport resistances were due to the product species ($FeCl_{3(g)}$ and $NiCl_{2(g)}$) and not the reactant species ($HCl_{(g)}$). If the heterogeneous equimolar chemical reaction shown below

$A_{(g)} = B_{(g)}$ at solid surface . . . . . (7)

is transport controlled its general rate equation becomes

$$-\dot{n}''_B = \dot{n}''_A = - \frac{K_c^A \cdot K_c^B}{K \cdot K_c^B + K_c^A} \cdot \frac{1}{RT} \cdot (K \cdot {}_bP_A - {}_bP_B) \quad . . . . . (8)$$

where K is the surface equilibrium constant ${}_sP_B / {}_sP_A$. Essentially this equation contains two terms, one gives the deviation of the bulk gas composition from the equilibrium composition (ie the driving force), the other is a mass 'conductivity' term. If K is large the reaction becomes reactant gas transport controlled and equation (8) approximates to

$$\dot{n}''_A = - \frac{K_c^A}{RT} \cdot {}_bP_A \quad . . . . . (9)$$

whilst if K is small the reaction becomes product gas transport controlled, eqation (8) then approximates to

$$\dot{n}''_A = - \frac{K_c^B}{RT} \cdot ({}_sP_B - {}_bP_B) \quad . . . . . (10)$$

Since the equilibrium constants of both the Fe_2O_3 and NiO + HCl reactions are small (+ve standard free energy changes) their rates were mainly influenced by product gas transport. This caused the reaction rates to be small for two reasons: a) $D_{FeCl_3/He}$ and $D_{NiCl_2/He}$ are both significantly smaller than $D_{HCl/He}$, and b) the driving force term is small.

1D2b Thermogravimetric analysis of the chlorination of Fe, Mn, Cu, Sn, Ni, Zn, Ca and Mg oxides:- The general reaction behaviours of each of these oxides with Cl_2 and HCl have been investigated by Titi-Manyaka and Iwasaki[63]. Since the experiments, which were performed on

pure powders using the method[49] described in section 1B7, were not theoretically analysed their results are only suitable for semi-quantitative predictions.

1D2c Kinetics of the chlorination of copper and tin minerals:- In connection with the TORCO process[25] Brittan[64] has studied the kinetics of copper volatilisation from fluidised beds of low grade copper ores (<4% Cu). The experiments, at temperatures of between 750 and 900°C using HCl-CO -N_2 gas mixtures, gave high reaction rates until about 80% of the copper had been removed. In comparison, the rates of volatilisation during the final stages of extraction were very low. The effect of increased temperature and carbon monoxide partial pressure (up to 0.1 atmos.) was to raise the point (eg from about 70 to 90%) at which the rapid-slow reaction rate transition occurred. Variations in particle size and fluidising/reactant gas velocity produced no measurable changes in the reaction rates. Brittan therefore concluded that gaseous diffusion was not limiting the overall reaction rates. Electron probe micro analysis indicated that reaction occurred uniformly throughout the ore particles. Brittan's results show many similarities with those obtained by workers studying the fluidised bed chlorination of pyrite cinder[5,6,7,8] (see section 1B1a). The reaction rates of both these processes appear to be chemically controlled. This is probably caused by the minor-component metal oxides being present at low activities in complex mineral matrices.

The chemical kinetics of the reaction

$$SnO_{2(s)} + 2HCl_{(g)} + H_{2(g)} = SnCl_{2(g)} + 2H_2O_{(g)} \quad \cdots\cdots\cdots (1)$$

at between 500 and 600°C have been investigated by Lythe and Prosser[65]. The reaction rates of groups of synthetic and natural, single and twin cassiterite crystals were studied (by a thermogravimetric technique) using various H_2-HCl gas mixtures of varying composition and total pressure. Some of their findings, listed below, illustrate the complexity of the chemical reaction process: a) chemical reaction rates were more influenced by the H_2 partial pressure than by the HCl partial pressure; b) small additions of either Fe_2O_3, NiO, Co_3O_4, Pt, MoO_3, V_2O_5 or TiO_2 catalysed the reaction, whilst Nb_2O_5 inhibited the reaction; c) under some reaction conditions there was an incubation period; d) reaction rates were enhanced by the presence of dislocations and inclusions; and

e) different crystallographic orientations reacted at different rates. From the results of their various experiments Lythe et al conclude that the first stage in the chemical reaction process is the reduction of SnO_2 to SnO by chemisorbed hydrogen.

1D3 Kinetics of the chlorination of metal sulphides

Thermogravimetric experiments on the chlorination of a number of sulphide minerals have been performed by Titi-Manyaka and Iwasaki[66] (their experimental technique has been outlined in section 1B7). Since no theoretical analysis was performed, their results are only semi-quantitative.

The rates of reaction of single pellets of ZnS, NiS, Cu_2S and PbS with chlorine, at between 550 and 800°C, have been measured by Gerlach and Pawlek[67]. At the lower reaction temperatures the chlorine partial pressures employed were high enough to cause formation of surface coatings of $NiCl_{2(s)}$, $ZnCl_{2(l)}$, $PbCl_{2(l)}$ and $CuCl_{(l)}$. The reaction rates therefore became controlled by two factors: a) the metal chloride vapour pressure, and b) the gaseous metal chloride mass transfer coefficient. Under this regime the apparent activation energies of the different reactions were very close to their respective metal chloride heats of vapourisation. At above about 720°C the ZnS and PbS reaction rates were very much less temperature sensitive. This was interpreted to mean that there were no surface coatings, and that the reactions were mass transport controlled.

1D4 Metal chlorination kinetics

Two interesting studies on the kinetics of the chlorination-volatilisation of metals, complementary to their work on oxides[51] (see section 1D2a), have been published by Fruehan[52] and Fruehan and Martonik[53]. The following systems were investigated, between the indicated temperature ranges, using Ar and He as dilutent

$2Fe_{(s)} + 3Cl_{2(g)} = (FeCl_3)_{2(g)}$ 255-648°C . . . . . (1)

$Ni_{(s)} + Cl_{2(g)} = NiCl_{2(g)}$ 617-976°C . . . . . (2)

$$Sn_{(s)} + 2Cl_{2(g)} = SnCl_{4(g)} \qquad 67\text{-}123^{\circ}C \quad \ldots\ldots\ldots (3)$$

$$Fe_{(s)} + 2HCl_{(g)} = FeCl_{2(g)} + H_{2(g)} \qquad 537\text{-}902^{\circ}C \quad \ldots\ldots (4)$$

$$Ni_{(s)} + 2HCl_{(g)} = NiCl_{2(g)} + H_{2(g)} \qquad 577\text{-}1067^{\circ}C \quad \ldots\ldots (5)$$

carrier gases. Reaction (3), even though it was studied at a low temperature was found to be reactant gas transport controlled. At comparatively low reaction temperatures the metals in reactions (1), (2), (4) and (5) became coated in very thin layers of solid chlorides ($NiCl_{2(s)}$ and $FeCl_{2(s)}$). The rates of reactions (2), (4) and (5) were then controlled by the vapourisation of the coatings, and were independent (above the critical values for the formation of the coatings) of the chlorination gas partial pressure*. Reaction (1) was found to be very slow, Fruehan therefore postulated that the rate was controlled by the chemical reaction.

$$2FeCl_{2(s)} + Cl_{2(g)} = (FeCl_3)_{2(g)} \quad \ldots\ldots\ldots\ldots\ldots (6)$$

This theory is supported by the result that the overall rate of reaction (1) was linearly dependent upon the chlorine partial pressure when the iron was coated in $FeCl_{2(s)}$. The apparent activation energies of the vapourisation controlled reactions were very close to their respective metal chloride heats of sublimation. The rates of these reactions (assuming a bulk gas metal chloride partial pressure of zero) can be written as:

$$\dot{n}''_{MeCl_2} = \frac{K_c^{MeCl_2}}{RT} \cdot {}^{s}P_{MeCl_2}$$

At the solid surfaces the metal chloride partial pressures would be equal to their equilibrium partial pressures, which to a first approximation are:

$${}^{s}P_{MeCl_2} = Ae^{-\frac{\Delta Hsub}{RT}}$$

Since the $\frac{K_c^{MeCl_2}}{RT}$ values are almost constant, the true activation energies** are therefore equal to their metal chloride heats of sublimation. (This analysis is also applicable to the findings of Gerlach et al[67] - see section 1D3). Under conditions where no solid chloride layers were

---

* The only effect produced by increasing the chlorination gas partial pressure was to increase the steady state thickness of the solid chloride layer.

** Since the individual rate controlling process has been identified it is justified to call these values 'true activation energies'.

formed reactions (1), (2), (4) and (5) were gas phase transport controlled. With reactions (1) and (2) chlorine transport controlled the rates, whilst due to small equilibrium constants reactions (4) and (5) were controlled by their product chlorides.

C H A P T E R T W O

AIMS OF THE INVESTIGATION: CHOICE OF OXIDE SYSTEMS: EXPERIMENTAL APPROACH AND STRATEGY

The three purposes of this chapter are: firstly to outline the general intentions and analytical approach in mind for carrying out this study; secondly, to give the reasons behind the choice of oxides used in the study; thirdly, to go through in sequence the necessary decisions and choices which had to be made before serious experimental work could begin. Having once discussed the above topics it will not be necessary to return to them at any length. After this chapter, reporting is only concerned with the actual work and analysis performed. In order to avoid repetition, none of the methods of theoretical analysis used in treating the results are given before the results have themselves been reported. At the end of this chapter is given a list of the chronological order in which the various experiments were carried out.

2A AIMS OF THE INVESTIGATION

Presented in this thesis are the results of a fundamental study on the chlorination-volatilisation of mixed metal oxides. The primary aim of the study has been to analyse and quantify various important parameters governing the extraction and separation of metals from oxide mixtures by high temperature reaction with elemental chlorine. In the literature there are many reports on oxide ore chlorination studies. However, due to the complexities involved, few have been particularly fundamental. Of those that have been fundamental, none can be directly compared with the present study. Consequently, with there being no available precedents to act as a guide, it was decided to investigate systems composed of two oxides, the metals involved being of some metallurgical significance.

From the outset it became immediately apparent that there would be two aspects to the work. It has already been explained that equilibria for reactions of the type 'OXIDE + CHLORINE' have often not been determined accurately enough to give good predictions of mixed-oxide equilibrium-

chlorination separations. Equilibrium separations would therefore have to be experimentally determined prior to kinetic studies of any type. Direct determinations of thermodata constitute a study in their own right. In this thesis equilibrium measurements are therefore reported separately from kinetic studies.

As a prelude to any mixed oxide kinetic studies, it was decided to perform some non-equilibrium experiments on a pure oxide whose oxide-chlorine equilibrium was already known from previous work[31]. This small amount of single oxide work demonstrated certain problems; theoretical ones concerning the analysis of results along with practical ones concerning the experimental methods. Once the relevant equilibrium data had successfully been determined, and once some non-equilibrium experience of both a theoretical and practical nature had been obtained, it was then possible to perform limited numbers of kinetics experiments on a two oxide mixture. The non-equilibrium work, in order that it should be of more than just empirical value, has been analysed in terms of a gas-solid reaction model. For this analysis a few additional experiments were carried out, along with extensive structural examinations of reacted and unreacted mixed oxide compacts. An overall mathematical model was as a result constructed to test theoretical predictions against experimental results.

2B CHOICE OF OXIDE SYSTEMS

In choosing oxides to work with, numerous considerations had to be made. The two most fundamental factors were: a) that with any metal oxides chosen, their respective chlorides needed to be thermodynamically more stable, and b) the chlorides were required to have appreciable vapour pressures in the proposed temperature range of investigation. It was desirable that each of the metals would form only a single valency chloride under the study conditions, and also, that complexing and polymerisation would not be present to a significant extent. Formation of compounds between the mixed oxides was undesirable since the activities of the component oxides would then become unknown. So that the work might show parallels with other systems, it was felt that it should be carried out at temperatures similar to those used in other studies involving chloride volatilisation. The proposed temperature range was therefore between the

approximate limits 700°C to 1100°C (exceeding this upper would have introduced significantly more experimental difficulties in furnace and reaction vessel design).

With these thoughts in mind an obvious first choice was zinc oxide. Orlov and Jeffes[31] have carried out fundamental studies on the zinc oxide-chlorine equilibrium (this work has been reported in section 1C2a). This system is therefore more precisely quantified than are many others. Employing one oxide of known thermodynamics is advantageous in that once its equilibrium chlorination separation from a binary mixture of oxides has been determined, the chlorination equilibrium for the other oxide becomes fixed. With zinc oxide having been chosen, the second most suitable oxide was determined to be cadmium oxide. Cadmium and zinc have similar chemistry, both form only one known oxide and one known chloride, these compounds are all bivalent. The boiling points (1 atmos) of the chlorides are similar, 961°C for $CdCl_2$[3] and 732°C for $ZnCl_2$[3]; the respective melting points are 568°C[3] and 318°C[3]. Existing thermodata indicated that, in other respects these oxides and chlorides adequately met the general thermochemical requirements of the study. With this system, the first experiments would determine the separation equilibrium, the second would study the parameters and configuration governing deviation from equilibrium.

In addition to the system ZnO/CdO, it was decided to study a chlorination equilibrium involving a mixture of oxides of unequal valency. The equilibrium separation in such a system is influenced by the applied oxygen partial pressure. Considering all the relevant criteria, cobalt oxide was found to be most suitable. At the temperatures of interest Co_3O_4 is stable to about 950°C, after which it decomposes to CoO. Two chlorides are formed: $CoCl_3$ and $CoCl_2$; however, the bivalent compound predominates at high temperature. The boiling point of $CoCl_2$ (1 atmos) is 1025°C[3], its melting point 740°C[3]. The other oxide chosen for this second equilibrium investigation was, for obvious reasons, ZnO.

The reactions that were selected for this study, together with their equilibrium constants and mixed-oxide equilibrium separation constants, are given below:

$$ZnO_{(s)} + Cl_{2(g)} = ZnCl_{2(g)} + \tfrac{1}{2}O_2 \quad \ldots\ldots\ldots\ldots\ldots\ldots (a)$$

$$K = \frac{P_{ZnCl_2} \cdot P_{O_2}^{\frac{1}{2}}}{P_{Cl_2} \cdot a_{ZnO}}$$

$$CdO_{(s)} + Cl_{2(g)} = CdCl_{2(g)} + \tfrac{1}{2}O_{2(g)} \quad \ldots\ldots\ldots\ldots\ldots\ldots (b)$$

$$K = \frac{P_{CdCl_2} \cdot P_{O_2}^{\frac{1}{2}}}{P_{Cl_2} \cdot a_{CdO}}$$

$$1/3Co_3O_{4(s)} + Cl_{2(g)} = CoCl_{2(g)} + 2/3O_{2(g)} \quad \ldots\ldots\ldots\ldots (c)$$

$$K = \frac{P_{CoCl_2} \cdot P_{O_2}^{2/3}}{P_{Cl_2} \cdot a_{Co_3O_4}^{1/3}}$$

$$CoO_{(s)} + Cl_{2(g)} = CoCl_{2(g)} + \tfrac{1}{2}O_{2(g)} \quad \ldots\ldots\ldots\ldots\ldots\ldots (d)$$

$$K = \frac{P_{CoCl_2} \cdot P_{O_2}^{\frac{1}{2}}}{P_{Cl_2} \cdot a_{CoO}}$$

When the component oxides in the mixtures are at unit activity.

From (a) and (b) $K_p = \dfrac{P_{CdCl_2}}{P_{ZnCl_2}}$

Equilibrium for exchange reaction

From (a) and (c) $K_p = \dfrac{P_{ZnCl_2}}{P_{CoCl_2} \cdot P_{O_2}^{1/6}}$

From (a) and (d) $K_p = \dfrac{P_{ZnCl_2}}{P_{CoCl_2}}$

2C EXPERIMENTAL APPROACH AND STRATEGY

2C1 Equilibrium determinations

In section 2B are shown the three equilibrium separation constants whose values were to be experimentally determined. Although the absolute vapour pressures of individual pure metal chlorides can be determined by a direct method[40], no satisfactory technique exists for the direct determination of equilibrium metal chloride pressures in mixed oxide-chlorine systems. One experimental method that could possibly have been developed to cater for the present study was the use of a Knudsen effusion cell coupled to a mass spectrometer. However, this technique would be both difficult and time consuming to develop. After what could be termed the static technique, there comes the dynamic method, variously known as the flow, transpiration, or entrainment method. All are essentially the same. The general method consists of contacting a flowing gas, which can be either inert, reactive, or a mixture of both with a solid or liquid using a physical configuration such that thermodynamic equilibrium is achieved between the phases. The gaseous products, after leaving the reaction zone, are then either condensed, absorbed or physically collected for subsequent analysis. This method is usually a one run technique since gaseous products are not often continuously analysed. Collection of all the products from a set time duration experiment is the normal procedure. With the above considerations in mind, together with reported information on the technique used by Orlov et al[31], it was decided to use a flow method for the equilibrium studies. The apparatus was therefore chosen to consist of a packed bed reaction vessel and a downstream condenser in which to collect the product chlorides.

2C2 Non-equilibrium determinations

Non-equilibrium determinations can sometimes be carried out by methods which produce steady state reaction; rate measurements are then relatively simple. If, however, a reaction is necessarily an unsteady state process then instantaneous rates must be either continuously monitored or measured at frequent intervals of time. Thermogravimetric methods are ideally suited for continuously following the overall extent of a reaction between a gas and a solid; that is provided the reacting

system is invariant and of known stoichiometry. Knowing the overall rate of weight change of a given solid undergoing reaction is, however, of little help in analysing the process if more than one reaction can occur at once. Thus, although thermogravimetric analysis is suitable for single oxide-chlorine reactions, it does not provide enough information for mixed oxides work. If in a mixed oxide system the metal chlorides formed are continuously or semi-continuously monitored, whilst the reaction stoichiometries are known, no worthwhile advantage is gained (except for mass balance purposes) in having overall weight change rates. The use of a thermobalance for kinetics studies was consequently rejected at an early stage. Any technique used for the mixed oxide kinetics work clearly needed to continuously or semi-continuously measure the individual chloride rates, the first of these two methods obviously being the most desirable.

In addition to deciding how to measure the individual chloride rates it was necessary to consider what physical form and reaction configuration the oxides should take. Reaction studies using powdered solids are often little related to gas-solid pyrometallurgical processes. This is because different forms of the same solid often exhibit great dissimilarities in reaction behaviour. It was therefore decided to use compacts of mixed oxide powders. From a theoretical standpoint spherical pellets are the easiest shape to analyse. This therefore made them a more desirable shape to work with as compared to irregular granules.

Thermogravimetric studies are usually performed upon small quantities of solid, often single pellet compacts, with gaseous reactant flows large enough to ensure that bulk gas compositions remain effectively unchanged by any reaction. This form of reaction configuration is also possible without a thermobalance. It would yield fundamental information on chemical and transport processes, however it would not give direct information on the overall behaviour of a reactor. Analysis of the information gained from a reactor is usually complex. This is so since many of the processes occurring are unsteady with respect to time and position. Reasonable approximations can however be made, thus allowing theoretical models to be developed and tested. Since a packed bed was to be used for the equilibrium studies, it was decided to concentrate on

using only a packed bed for all the studies. (In retrospect this appears to have been the best approach as various interesting behaviours specific to a packed bed reactor were observed and studied.)

Continuous analysis of the product metal chlorides was initially decided to be the best method by which to explore the reaction kinetics. A new analytical technique was therefore proposed with this as its aim. Briefly, the technique was planned to consist of passing part of the hot gases, emergent from the reactor, through an atmospheric-pressure microwave-induced argon plasma. In the plasma part of each chloride would become dissociated; metal atoms so formed give characteristic emissions of radiation due to various transitions in electron energies. The energies involved place the characteristic emissions in or near to the visible spectrum. By collimating some of the emitted radiation into a monochromator-detector system the intensities of the metal species resonant lines could then be measured. With suitable calibration of the instrumentation together with use of internal standards, it appeared to be possible to continuously measure the quantities of metal chlorides emerging from the reactor. Preliminary studies were initiated to gain experience with microwave-induced atmospheric-pressure argon plasmas, together with suitable monochromator-detector systems. Non-flowing spectral sources for Cd and Zn were made. A small high temperature flow system for Ar + Zn was constructed to give qualitative indications of detection limits and sensitivities. Although the technique showed considerable promise the development effort required to make it a working proposition was more than could be afforded. It was therefore decided to discontinue this line of research. A more complete description of the technique and the experimental results are given in appendix A.

With no other prospective methods available for continuously monitoring the chloride rates, a simple but not entirely satisfactory technique had to be used. It consisted of using easily replaceable condensers which could be removed and replaced in a reasonably short time. The non-equilibrium experiments were thus carried out in short stages with a holding time between each reaction period (while condensers were being changed). Rates obtained by this method (calculated on the basis of the condensate analysis and the reaction time) were the mean rates for the period of each reaction stage. These mean rates are approximately equal

to the true rates at the mid time of the particular stage involved. By suitable choice of reaction times for the successive reaction stages, the errors caused by this approximation were considerably reduced.

2C3 Oxide compacts, carrier gases, chemical analysis, materials of construction

2C3a Oxide compacts:- For the mixed-oxide equilibrium and non-equilibrium experiments, approximately spherical pelletised compacts were used. For the initial proving runs and single oxide non-equilibrium experiments, irregular shaped granular compacts were used. Description of compact manufacture is given in Chapter Four.

2C3b Gases:- The two essential gases needed for the study were chlorine and oxygen. So that both of their partial pressures could be varied independently, an inert third gas was required, and nitrogen was chosen. One advantage of using various different inert carrier gases is that influences due to mass transfer can often be highlighted. This is because molecular diffusivities of reactant and product species change with changing carrier gas molecular weight (this of course assumes that the carrier gas is present at a significant concentration). This method of testing for mass transfer effects has been used by Fruehan et al[51,52,53]. However, its use with the present study was not possible in the time available.

2C3c Chemical analysis:- Choosing a method for metal chloride analysis was relatively simple. Classical techniques have the potential of marginally greater accuracy over instrumental methods. However, they are time consuming and become more so if separations are involved (as would be necessary with Zn^{++}/Cd^{++} mixtures). Of the instrumental methods available it was obvious that by far the most suitable was atomic absorption spectrophotometry (AA). This was consequently the method used throughout this study, except for when EDTA complexiometric titrations were used for a few single oxide experiments. When compared with AA analysis the EDTA method showed only a minimal improved accuracy.

2C3d Materials selection:- The useful temperature range, thermal shock resistance and ease and versatility of fabrication of silica (fused vitreous quartz) gave it immediate preference as the material for reactor and

condenser construction. Its only characteristic in doubt was its chemical inertness to the reactants and products at elevated temperatures. A comparative inertness of chlorine towards silica is demonstrated by the free energy changes given for the two reactions below. From these ΔG^{o} [3] values, making reasonable extrapolations, it is evident that with relatively high oxygen potentials, silica reacts to no significant extent with chlorine.

$$SiO_{2(s)} + 2Cl_{2(g)} = SiCl_{4(g)} + O_{2(g)} \quad \ldots\ldots\ldots\ldots\ldots\ldots \text{(a)}$$

$$\Delta G^{o} = +60000 - 3.64T \log T + 2.4T \text{ cals/mole} \quad (700^{o}K - 1000^{o}K)$$

$$SiO_{2(s)} + Cl_{2(g)} = SiCl_{2(g)} + O_{2(g)} \quad \ldots\ldots\ldots\ldots\ldots\ldots \text{(b)}$$

$$\Delta G^{o} = +178300 + 4.18T \log T - 64.25T \text{ cals/mole} \quad (700^{o}K - 1000^{o}K)$$

The only other possible reactions that needed consideration were those between the oxides and silica. In the literature there appears to be no evidence suggesting the existence of cadmium silicate at atmospheric pressure. However, the zinc oxide-silica and cobalt oxide-silica phase diagrams[68] both show that silicates may form. The thermodata[3] for zinc silicate formation is given below.

$$2ZnO_{(s)} + SiO_{2(s)} = Zn_2SiO_{4(s)} \quad \ldots\ldots\ldots\ldots\ldots\ldots \text{(c)}$$

$$\Delta G^{o} = -7130 + 0.23T \text{ cals/mole} \quad (300^{o}K - 1300^{o}K)$$

To obtain some measure of the kinetics of silicate formation, a simple experiment was devised. For the purposes of this test a number of small silica (Vitreosil*) cups were attached, next to each other, to one end of a long hollow silica tube. For the tests, a sample of each powdered metal oxide (reagent grade) was placed in a different cup. The assembly of cups was then fairly rapidly pushed into an electric furnace and held there in air for a few hours at a steady temperature. The temperature at the bottom of each cup was measured by sliding a Pt/Pt13% Rh thermocouple up the support tube until its junction was in the required position. After a suitable time duration the assembly was quickly removed from the furnace and allowed to air cool. The condition of each cup and oxide was then carefully examined and noted down. Special attention was paid to discolouration, devitrification and spalling of the silica. Using the

---

* Vitreosil is the trade name of transparent fused quartz manufactured by Thermal Syndicate Ltd.

same assembly the furnace temperature was then raised and with new oxide in each cup the procedure was repeated. The temperature range investigated was from 700°C to 1140°C and the qualitative results are given in appendix B. From the experimental observations, as given in the appendix, it appeared that Vitreosil would be a suitable material for the condenser and reactor, provided that temperature ceilings were imposed at 930°C for cobalt oxide and 1000°C for zinc oxide. Since experiments were envisaged at higher temperatures, a reactor lining material was required. Thermal shock resistance could not be entirely sacrificed for chemical inertness. Thus mullite ($2Al_2O_3 . SiO_2$) was chosen for test since it has a minimal free silica content. Testing its compatibility with cobalt and zinc oxide was carried out by containing an approximately 50/50 mole % mixture of CoO/ZnO powder inside a short length of mullite* tube, which was then held at 1200°C for 24 hours. Although the ceramic tube was made blue in colour, since it did not noticeably react with the oxides it was proved to be a suitable lining material.

Materials selection was necessary for parts of the apparatus handling chlorine and chlorine containing gas mixtures. Actual experiments on the materials were not carried out as they were already well tried and tested. A special materials list for use with chlorine is given below along with the relevant sources of purchase.

1. Gas regulator made of monel (British Oxygen Co. Ltd.)
2. Needle valve and tubing made of monel (Hoke Ltd.)
3. Silicone rubber bungs and tubing (Jencons Scientific Ltd.)
4. Voltalef grease (BDH Chemicals Ltd.)
5. Polythene tubing
6. Pyrex glass
7. PTFE glands and sealing tape
8. Concentrated H_2SO_4 for U-tube manometers and chlorine drying

2C4 Chronological order of experiments

Since some experiments will be reported out of sequence, to remove any possibility of confusion it has been decided to list them in chronological order:

---

* Morgan Refractories Ltd.

1. ZnO proving runs
2. ZnO non-equilibrium runs
3. CdO/ZnO equilibrium runs
4. CdO/ZnO non-equilibrium runs
5. CdO/ZnO double bed non-equilibrium runs
6. Co_3O_4/ZnO equilibrium runs
7. CoO/ZnO equilibrium runs

CHAPTER THREE

EXPERIMENTAL APPARATUS

3A APPARATUS DESIGN

General design calculations were made for certain parts of the apparatus described below. However, with experimental apparatus of the type used in this study, numerous detailed calculations are usually inappropriate since unknown factors often play the major role in determining the overall performance. Under these conditions it is perhaps most realistic to design with large safety margins and use previous experience where possible. The main requirements of the experimental apparatus became fixed once the experimental configuration had been decided. The design of the apparatus was thus commenced by determining a suitable maximum reactor size. Once this decision had been made, the design of the remaining equipment then followed in logical progression.

3B FURNACE

A photograph of the multi-zone furnace used for all the chlorination experiments is shown on plate 1. Its main dimensions, together with its internal construction, are illustrated by a sectional drawing shown on figure 3A. The photograph shows the furnace in its vertical operating position, with a reactor and condenser in situ, together with all the gas lines and ancillary equipment connected up as for an experimental run. By disconnecting four gas lines, the furnace could then be rotated about its two central mountings into a horizontal position. Using a tilting furnace reduced overall height requirements for the rig, since condensers and reactors could then be introduced and removed horizontally. The experiments were conducted with the reactor vertically above the condenser. This gave two obvious advantages: firstly, the oxide charges supported by the reactor bottom were uniformly distributed in the reactor and therefore subject to minimal gas by-passing; secondly, since the reaction zone was necessarily hotter than the condensation zone, convective heat transfer in the annular space around the reactor-condenser (and gas shield tube) was minimised. When hot, but not in use, the furnace was left in the horizontal position.

PLATE 1:

CHLORINATION FURNACE

This photograph shows the multi-zone furnace in which the chlorination experiments were performed. A reactor and condenser are in position and the gas lines and electrical circuits are connected. In the background is the gas train, and in the top righthand corner the caustic scrubbers.

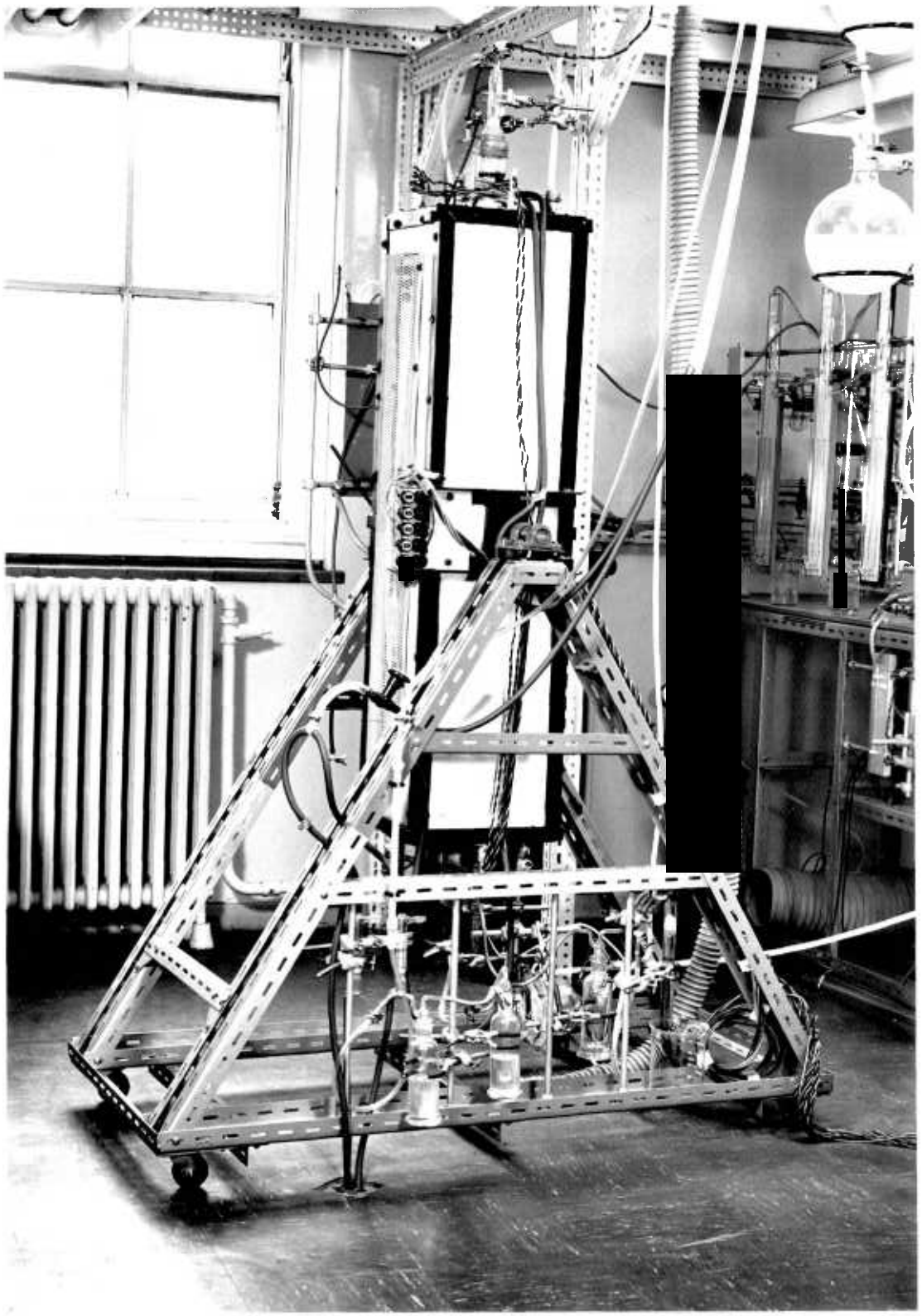

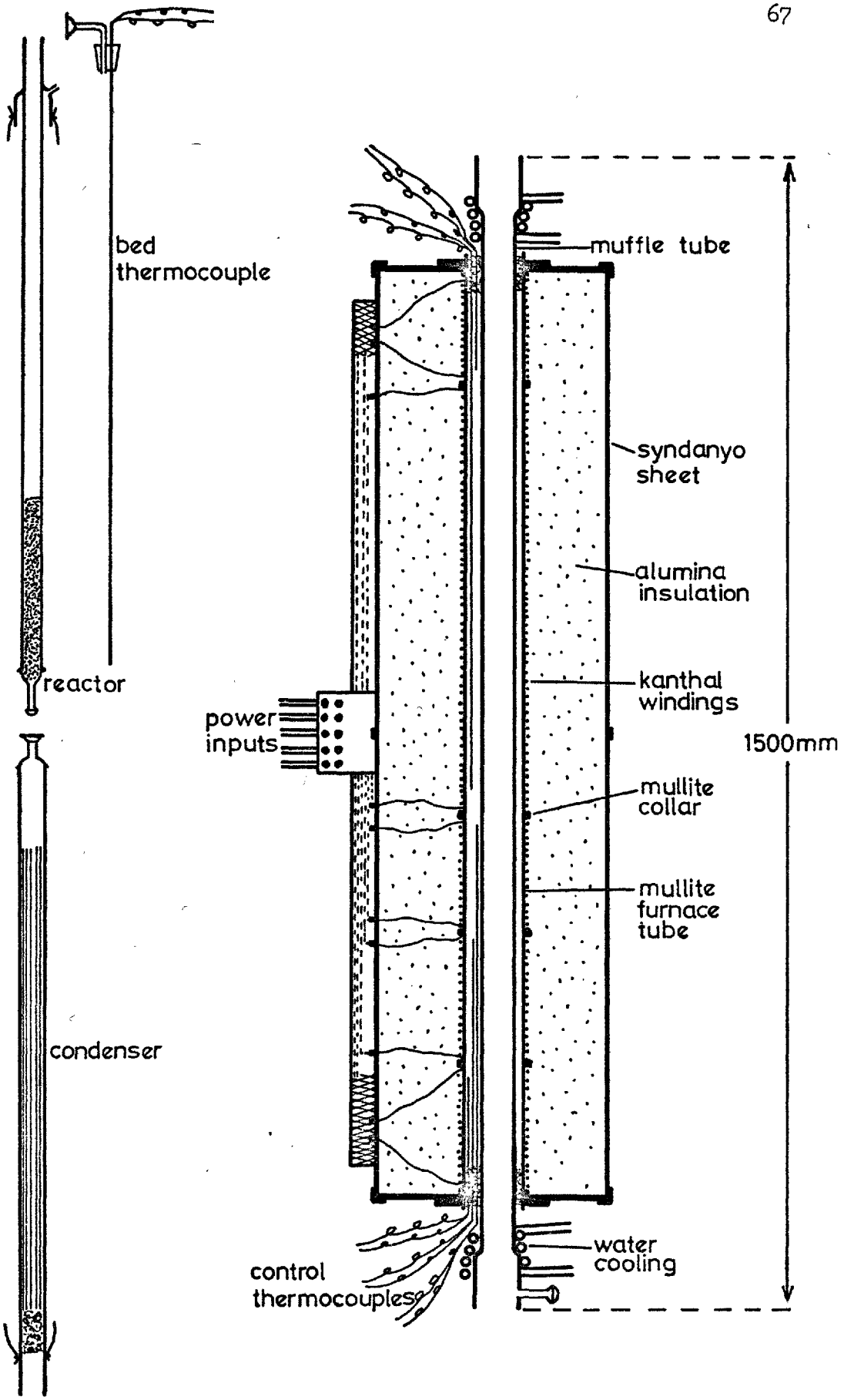

FIGURE 3A: DIAGRAM OF SECTIONED FURNACE, REACTOR AND CONDENSER.

3B1 Furnace tube and windings

The furnace was heated by means of Kanthal* A1 electric resistance heating wire; the maximum service temperature of this material is 1350°C. In view of the maximum proposed experimentation temperature, using this wire gave a reasonable safety margin against 'burn out'. Five separately controlled heat input zones were built into the furnace. This was necessary in order to produce both a long constant temperature region for the reactor, and a controlled temperature gradient for the condenser. Each of the zones was wound directly onto an 80 mm OD - 70 mm ID impervious mullite** tube of 1250 mm total length. Adjacent zones were separated from one another by 8 mm wide collars of mullite, which had been cut from a 95 mm OD - 80 mm ID tube. Both of the furnace ends-zones were differentially wound. Windings were cemented in place by a thin brushed-on layer of alumina slurry. This slurry was made from pure alumina powder and a 15% by volume aqueous solution of orthophosphoric acid. When the slurry had dried out the furnace tube and windings were fired at 1000°C. This firing, in conjunction with the acid, produced a very hard coating on and around the resistance wire.

All the detailed information concerning zone lengths and resistances, together with wire spacings and gauges, is shown on figure 3B. Heat loss calculations indicated that about $2\frac{1}{2}$ to 3KW would be required at maximum temperature. The winding scheme was thus devised on the basis of only two criteria. Firstly, the resistance of each zone should not be too low to allow use of a thyristor control unit; secondly, in the interests of long life, the surface loading of the wire in each zone should be as low as possible, (each zone should therefore contain as much wire as possible). To achieve both of these aims, the resistance, with each zone, was matched with the specific thyristor unit assigned to control that zone. This matching consisted of calculating the resistance required for the control unit to be able to employ near to its full power output (even though this would never be required). Lowering this optimised resistance would have caused the control unit to exceed its maximum power rating (thereby blowing its fuse); raising the resistance would have reduced the zones'

---

* Hall and Pickles Ltd.

** Andermans 10A material, maximum service temperature 1600°C

FURNACE TUBE

zone 1	zone 2	zone 3	zone 4	zone 5	
18 1·219	16 1·626	18 1·219	18 1·219	19 1·016	SWG & mm dia
11 - 9 - 7	6·5	10	10	9 - 11 - 13	turns per inch
15	26	17·3	19·9	29·5	ohms resistance
16	9·2	13·9	12·1	8·1	current at 240 volts
25	10	15	15	10	controller capacity amps

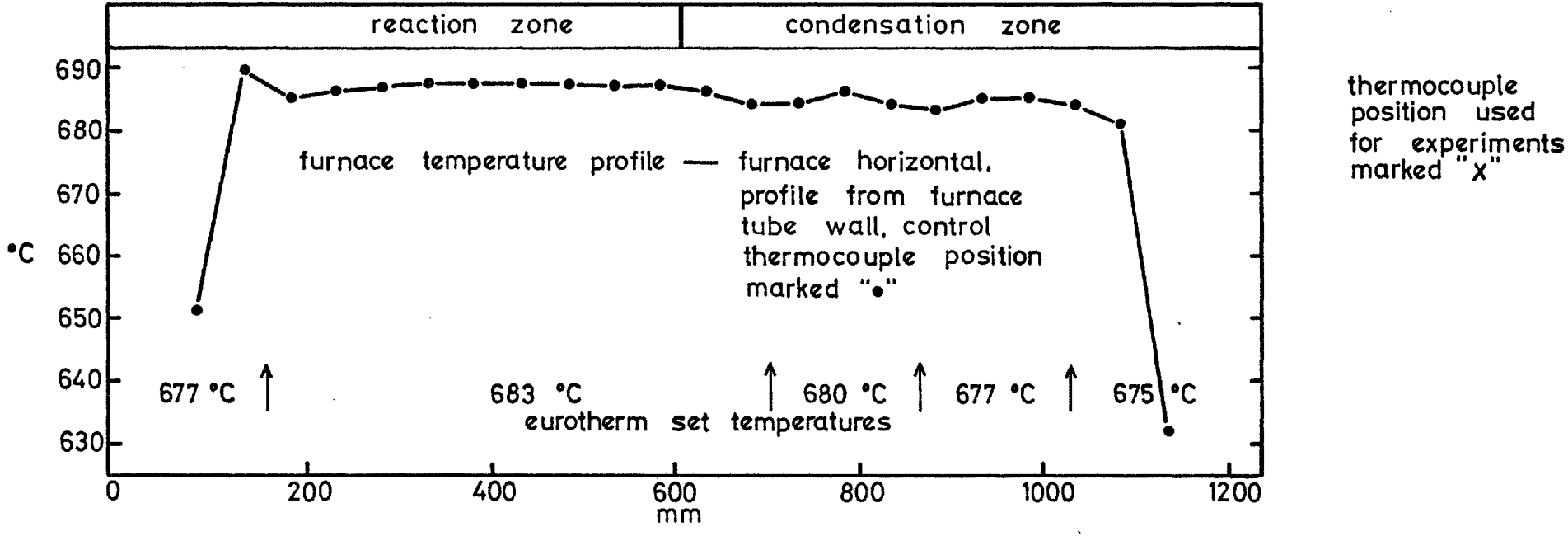

FIGURE 3B: FURNACE TEMPERATURE PROFILE AND DETAILS ON FURNACE WINDINGS

power capacity, but of more importance, reduced its safety margin, since smaller gauge wire would have been required, thereby raising its surface loading. Once the various resistances had been determined, wire was then selected for each zone which when wound as close together as was feasible, (wire spacing = wire diameter) gave the required resistance. If full mains voltage of 240 volts had been simultaneously applied across each zone, the total heat input would have been 14.2 KW. Under normal operating conditions, with the reaction zone at 1000°C, the furnace power consumption was about 1.5 KW. At this level of power input the wire surface loading in all the zones was two orders of magnitude less than the maximum recommended value.

3B2 Furnace assembly

The furnace tube was contained inside a rectangular box made of 1/4" thick Syndanyo sheet (compacted asbestos). This was held in place by a welded steel frame, onto which were attached the two pivot shafts. The ends of the furnace tube protruded about 20 mm out from each supporting end plate. These end plates incorporated an asbestos compression joint which allowed longitudinal expansion, but prevented insulation leakage. When being wound, an excess length of wire was left attached at the ends of each zone. On assembly these wires were cut as appropriate and were then clamped to 3/8" bolts which lead through to the outside of the furnace. It was through these bolts that electrical connection was made. The Kanthal leads inside the furnace box were threaded with porcelain insulating beads as a safety measure. Once the assembly had been completed, silica free calcined alumina, the furnace insulation, was introduced through a removable end plug. The insulation was topped up twice during the experimental campaign since it tended to gradually compact itself over a long period. The overall dimensions of the furnace were 305 mm x 305 mm x 1205 mm.

3C TEMPERATURE CONTROL

A photograph of the temperature control panel is shown on plate 2. Six individual control units were mounted on the panel; five were used for the chlorination furnace, the sixth (bottom right) was used to control a

small tube furnace in which the sintering experiments were carried out. This additional unit also acted as a spare for the main furnace. In the photograph the thermocouple inputs and power outputs are not connected up. These circuits were made to each unit through the plug sockets seen mounted under the ammeters.

3C1 Control units

All the controllers were Eurotherm* thyristor controlled models incorporating proportional, integral and derivative temperature control functions. The chlorination furnace units were 0-1600°C/Pt - Pt 13% Rh/fast cycling types** rated at (zones 1 to 5) 25, 10, 15, 15 and 10 amps respectively.

3C2 Thermocouples and temperature profiles

The furnace control thermocouples were situated inside the furnace tube, and were thus separated from the windings by the thickness of the tube. Not having the thermocouples in direct contact with the windings was slightly disadvantageous since speeds of response become lowered. However, this effect was outweighed by the ease with which the thermocouple positions could be varied to give the best possible temperature distribution along the furnace tube. The thermocouples themselves were made from 0.3 mm diameter Pt and Pt 13% Rh wire, threaded down 3 mm OD twin bore alumina thermocouple sheathing. Connections to the controllers were made via compensating cable. On figure 3B is plotted the furnace temperature profile which was obtained with the controllers set at the temperatures shown and with the thermocouples in the positions indicated "." During various temperature tests, it was found that each eurotherm unit controlled at a slightly different temperature to that which it indicated. The error with each unit was found to be effectively constant over the proposed range of use. Therefore, when the furnace was adjusted for an experiment, the predetermined correction was applied to each controller which thus resulted in the desired temperatures being obtained. The thermocouple positions marked "." on figure 3B were not quite the same as those used in the actual experiments. Best results, when a condensation zone

---

* Eurotherm Ltd.

** Phase angle controllers caused vibration of the windings due to inductive effects

temperature gradient was used, were obtained with the thermocouples in the positions marked "X". The reactor and condenser both sat inside a gas muffle tube. Slight local temperature differences at the furnace tube wall did not cause any problems since the presence of this muffle had a temperature smoothing effect.

The thyristor units had two adjustable controls, one was a current limit and this allowed the furnace to be heated or cooled slowly. At temperature each current limit was set at just above the zone's required current so as to prevent the occurrence of accidental overheating. The other control varied the control band width. These were kept at the minimum values which, with the given response times, did not produce temperature instability. The control units, furnace and frame were all earthed to prevent the incidence of electrical interference. When correctly set up, the temperature in the reaction zone of the furnace was maintained within $\pm \frac{1}{2}$ deg C of the desired value.

3D REACTORS AND CONDENSERS

Figure 3C shows a full-scale drawing of a reactor and a condenser sitting inside the gas muffle tube; both are in the position that they occupied during an experiment. The reactor shown had an ID of 27.5 mm; this was the largest reactor used. The condenser is a concentric tube type. Its main tube had an ID of 32 mm. During the study three different condensers were used, all were of the same basic design. With the reactors all were identical except for their diameters. One was of 17 mm ID, two were of 22 mm ID and one was of 27.5 mm ID. Two forms of condenser were employed; their socket joints and overall lengths were the same, but internal construction was different. With the initial chlorination experiments on ZnO, it was found that when high gas flow rates were used a single tube 22 mm bore condenser did not collect all the $ZnCl_2$ but allowed a fog to form. This problem was overcome by using condensers which contained three 600 m long concentrically mounted tubes, each supported from its outer neighbour by three thin spacing legs at both ends. The hot gases thus became split and flowed through the three annular passages and one central tube. By paying special attention to the temperature profile along the condenser, the increased gas-wall condensation area allowed the chlorides to be collected without any fog formation. Two of these modified

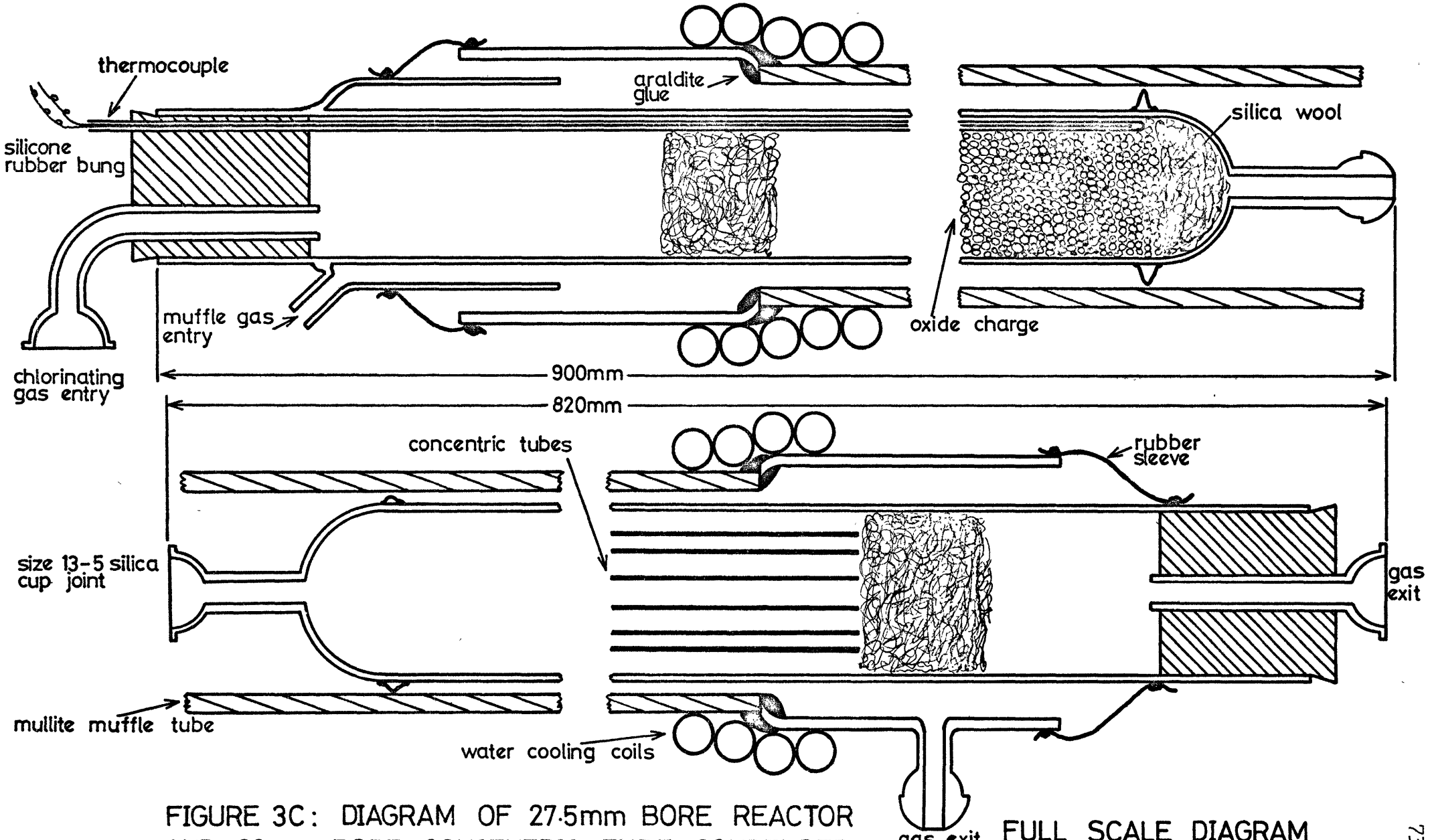

FIGURE 3C: DIAGRAM OF 27·5mm BORE REACTOR AND 32mm BORE CONCENTRIC TUBE CONDENSER FULL SCALE DIAGRAM

condensers were used; tube bores were 4, 14, 22 and 30 mm and 4, 13, 22 and 32 mm. All the condensers and reactors were assembled from standard sized silica* tubing and silica ball and cup joints.

3D1 Gas muffle and reactor-condenser joint

With the reactor and condenser, it was decided to make the necessary connection between them using a ball and cup joint. Since the performance of such joints at high temperature was rather an unknown quantity, a precaution against leakage was built into the overall experimental technique. By containing the ball and cup joint inside a chamber, full of an inert gas maintained at a slightly higher pressure than the gas passing through the joint, leakage would tend to be into the condenser rather than outward from the reactor. This positive pressure was maintained by operating the reactor and condenser inside an impervious mullite (10A material) muffle tube, the dimensions of which were 47 mm OD, 40 mm ID and 1380 mm long. On the ends of the muffle tube were glued (Araldite) 50 mm bore 60 mm long glass collars. Thin rubber seals secured by elastic bands then made the gas-tight connection between these collars and the reactor and condenser. The rubber connections were easily slipped on and off the glass collars when the reactor and condenser were being moved. Lead water cooling coils were wrapped around the glass-mullite glued joints to prevent overheating. The gas muffle was normally pressurised with argon taken from the gas train. When argon was required for the purposes of bed conditioning, the muffle was pressurised with nitrogen which was taken directly from a nitrogen cylinder pressure regulator. In both cases gas was introduced at the top of the apparatus and left after passage through the furnace to the bottom. Positive pressure was maintained by exiting the gas through a bubbler against a 10 cm head of concentrated sulphuric acid; this head was always greater than the chlorinating gas delivery head. The details of construction given in this sub-section can be seen on figure 3C.

Size 13-5 ball and cup joints were used; the spherical joint diameter with these standard connectors is 12.700 mm, the tube bore 5 mm. The cups were

---

* Vitreosil - supplied by Quartz Fused Products Ltd.

used with the condensers whilst the balls were used with the reactors. Once the silica apparatus had been assembled, the mating of the joints was very carefully checked. If there was any doubt about a joints gas tightness, the ball and cup were lapped against each other using a suspension of fine silicon carbide powder in water. Occasional relapping was carried out when the joint faces showed slight signs of deterioriation (due to devitrification and spalling). In this way, any reactor could safely be used with any condenser. Reactors and condensers were located approximately central to the muffle tube by short silica legs which were fused onto the outer surface of the tubes. The ball and cup joint connection was made by pushing the reactor and condenser together, and then rotating one against the other to check that there was no foreign matter between the faces. The joint was loaded by two effects; in the vertical operating position only the condenser was held, the reactor's entire weight was thus supported by the joint. Additional load was put on the joint by pushing the condenser up against the elastic restraining influence of the rubber gas seal. The total load on the joint is estimated to have been about 3 Kg_{force}. After the joint had been made (before chlorination was started) the muffle was pressurised (10 cms H_2SO_4) the gas was then turned off and the U tube manometer, giving the muffle tube excess pressure, was watched for any pressure drop indicating a leak. In not one experiment was even a slight gas leak detected. It would thus seem that at low pressures the ball and cup joints were completely gas tight. Fine silica wool was used to support oxide charges at the reactor bottom. After filling the reactor, a silica wool plug was pushed down from the entry until it was just above the start of the hot zone. This plug served to stop pulsing of the gas flow (a phenomena often encountered when a cold gas jet enters a hot chamber).

2D2 End connections

Connections to the ends of the reactors and condensers were made with suitable sized silicon rubber bungs. With the lower temperature runs, the chlorinating gas delivery tube (an FS13 glass cup) and a closed end silica thermocouple sheath both passed through the bung. The compression on the bung was sufficient to make the assembly gas tight. At the condenser exit, a bung and an FS13 socket were used only when the emerging gas was being filtered or scrubbed.

3D3 Bed thermocouple

For all experiments except those with the mullite liner, a 3.2 mm OD closed end silica thermocouple tube was used. This rested close to the inside wall of the reactor and reached to within 5 mm of the bed bottom. Inside the tube was the thermocouple. This was made from 0.3 mm Pt and Pt 13% Rh wire threaded through 1.6 mm OD twin bore alumina insulating sheathing. This thermocouple could be moved along the silica tube, and was thus able to measure the temperature at any place within the reactor. These silica thermocouple tubes were quite fragile and usually lasted only about 10 runs before being replaced.

3D4 Reactor liner and outside thermocouple

Due to the silica devitrification problem that has already been explained (see section 2C3d) a mullite liner was used for experiments carried out at above 930°C with CoO and 1000°C with ZnO. This liner was 870 mm long, had a bore of 20 mm and an outside diameter of 25.5 mm. It fitted inside the 27.5 mm bore reactor and was cushioned at the bottom by a silica wool plug. At the top it was sealed onto the reactor by a rubber sleeve in the same way that the gas muffle connections were made. Due to silicate formation, with experiments at the higher temperatures, it was not possible to use an internal silica thermocouple tube. Instead, the temperature outside the reactor had to be measured. For this purpose a long, closed end thin walled stainless steel tube, of 3 mm diameter, was attached by nichrome wire to the outside of the reactor; it also reached to within 5 mm of the bed bottom. A free moving thermocouple, as previously described, was mounted inside this tube. Stainless steel instead of silica was used for the external tube so that it could be earthed to prevent pick up of noise. This earthing was required since the noise picked up from the inductive effects of the furnace, when using unscreened thermocouples, increased dramatically above about 950°C.

3D5 Gas filter

In a few experiments, under which conditions there was a possibility of the formation of traces of chloride fog, an exit gas filter was used. This filter consisted of two FG100 flange joints, 103 mm in bore, each joined

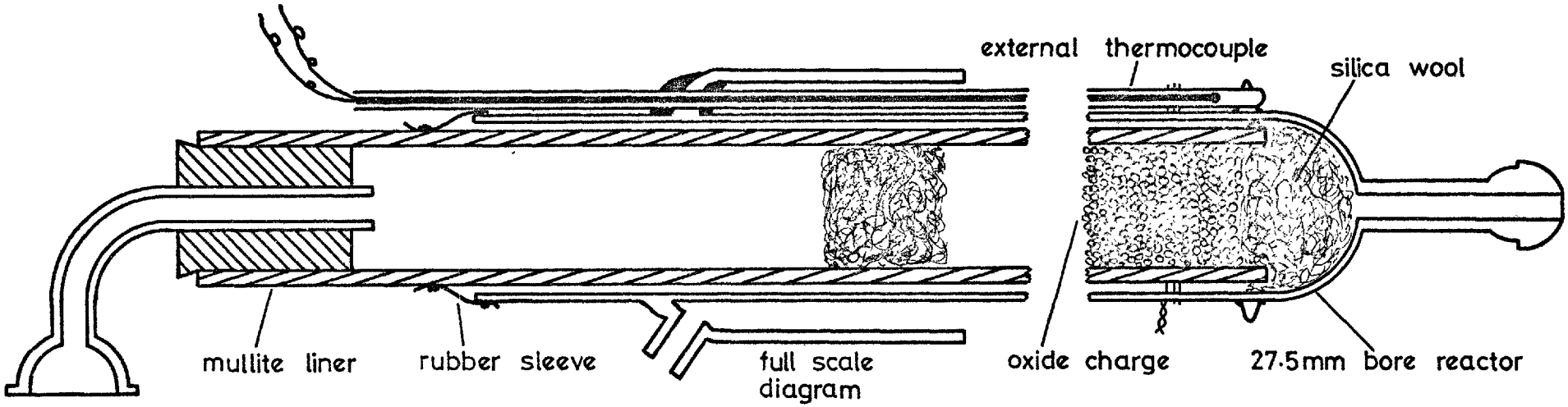

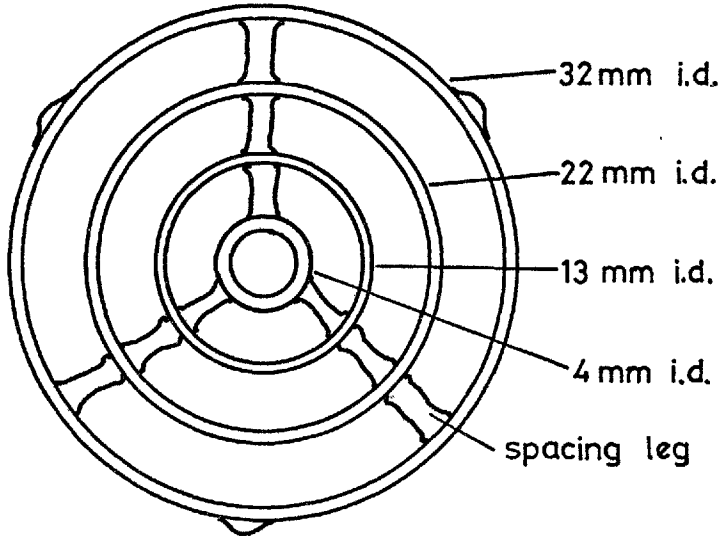

concentric tubes in condenser scale X2

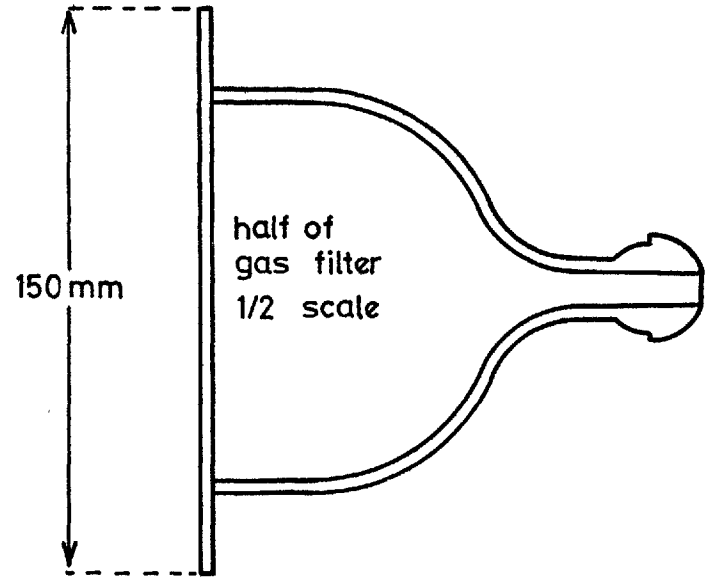

FIGURE 3D: DIAGRAM OF SECTIONED MULLITE LINED REACTOR; END VIEW OF CONCENTRIC TUBE CONDENSER; GAS FILTER.

to an MS19 ball joint. Between these flanges a 150 mm diameter filter paper could be clamped. This paper collected most of any chloride fog present in the exit gas. A few simple experiments passing nitrogen through various filter papers revealed that large pressure drops did not occur. A ΔP of 1 or 2 cms of H_2SO_4 was normal. Whatman no. 2 (2.9 to 1.4μ pores) and no. 32 (1.1 to 0.4μ pores) papers were used. The exit gas filtration was essentially a precautionary measure, since with the concentric tube condensers detectable quantities of metal chlorides were only occasionally found.

Figure 3D shows the modified reactor as used for the higher temperature runs; it also shows half the gas filter and an end view of the concentric tube condenser (32 mm bore).

3E GAS TRAIN

A photograph of the gas drying and metering train is shown on plate 2. From left to right this picture shows the gas bottles, the needle control valves, the argon, nitrogen, oxygen and chlorine orifice flow meters and the three way taps used for routing the gases; in the background are the drying columns and bubblers. A schematic diagram of the paths taken by the gases is given on figure 3E. From this diagram it can be seen that the N_2, O_2 and Ar control valves, drying columns, bubblers and liquid traps were the same. With all four gases the flow meters were identical.

3E1 Gases, supply and control

All the gases were drawn, via regulators, from pressurised storage cylinders. The nitrogen was BOC* oxygen free grade; the argon was BOC high purity grade; the oxygen was the normal BOC grade; the chlorine was Mathieson high purity grade (supplied by BOC). The chlorine cylinders contained 15 lbs of liquid, whose minimum purity was claimed to be 99.5%. Typical impurities and levels were quoted to be CO_2 - 500 ppm, O_2 - 200 ppm, N_2 - 100 ppm and H_2O - 10 ppm. The chlorine was reported to be free of HCl. A special monel regulator was necessary for the chlorine cylinder. The rates of chlorine use were always relatively low, thus evapouration of the liquid was never a problem. Flow rates of all the gases were controlled with needle valves. With the chlorine the valve was made of monel, with the other gases precision valves**were used.

---

* British Oxygen Company

** Field Tech Ltd.

PLATE 2:

GAS TRAIN AND TEMPERATURE CONTROLLERS

2a. Gas train. In the foreground from left to right are a) the gas cylinders and pressure regulators, b) the needle valves, c) the Ar, N_2,O_2 and Cl_2 orifice flow meters and d) the three-way stopcocks used for routing the gases. In the background are the drying columns, the excess pressure bubblers, the liquid traps, the variable head chlorine bubbler and the gas mixing chamber.

2b. Temperature controllers. On the left of the photograph is the furnace temperature control panel. This contains six separate units each consisting of a Eurotherm temperature controller, an ammeter, an on-off switch, and thermocouple input socket and a power output socket. On top of the panel are the potentiometer box and the Smiths two pen recorder. On the right of the photograph is the Perkin Elmer model 290B atomic absorption spectrophotometer.

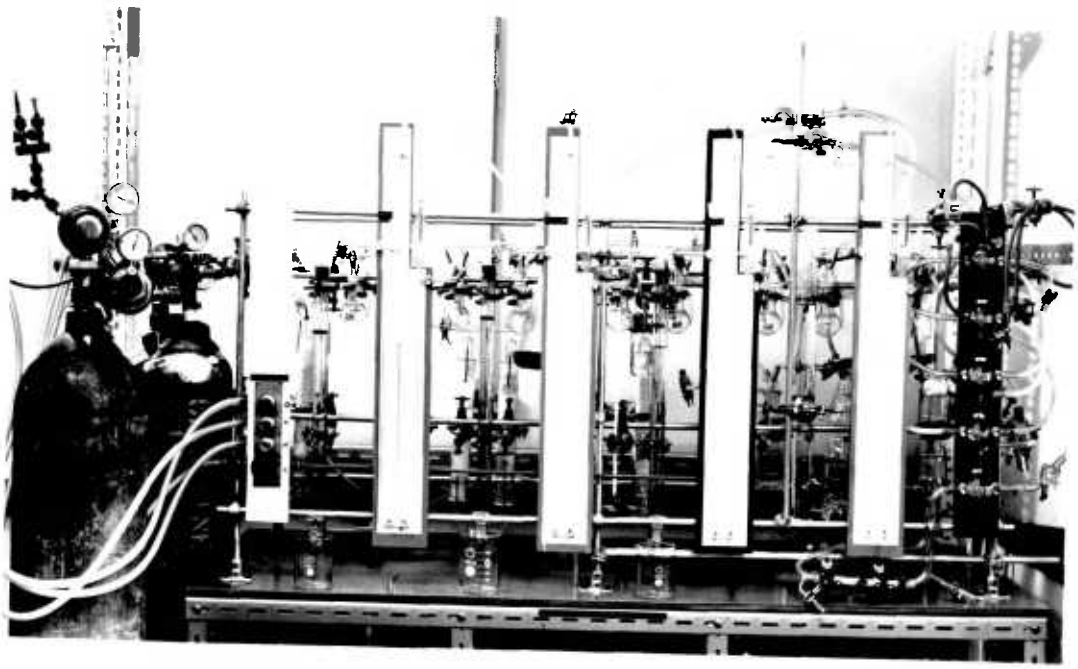

3E2 Gas Drying

All gases were dried prior to their flow meters. With the chlorine this was carried out by passing the gas up through a wash bottle containing about 400 mls of concentrated sulphuric acid; the gas was distributed in this vessel by a sintered glass disc. The Ar, N_2 and O_2 were dried with magnesium perchlorate and type 5A molecular sieve. Drying columns were made by joining two standard sized glass cone joints together to make a cylinder, the end connectors consisted of corresponding size socket joints joined to FS13 ball joints. Two slightly differing column sizes were used; the joints involved were B34/35 and B29/32; when assembled columns were about 18 cm long and 3 cm in bore. The loosely packed drying agents were held in the columns by glass wool plugs situated at each end. Three columns were used in each line. The gases first passed through two consecutive columns of magnesium perchlorate and then through one of molecular sieve.

3E3 Pressure and flow control

To guard against the possibility of excess pressure build up in either the Ar, N_2 or O_2 lines 'blow off's' were built into the system. These simply consisted of connections from the gas flow lines to long glass tubes held inside cylindrical containers full of concentrated sulphuric acid. If the pressure inside a gas line exceeded that exerted by the head of acid, gas was able to bubble up through the liquid and escape to atmosphere. The heads of acid (SG 1.84) were kept at between 35 and 40 cms. With a gauge pressure of about 10 PSI on the upstream side of the needle valves, and with a downstream pressure close to atmospheric, steady flow rates were easily reached with the O_2, N_2 and Ar. This was, however, not the case with chlorine. Steady flow rates could not be obtained using just the needle valve and regulator for control. This effect is thought to have been mainly due to the needle valve. It was not as sensitive as those used with the other gases, especially at very low flows; it also seemed to suffer from corrosion since, whenever it was examined or disassembled it was found to contain green debris around the seat and entry connector. To overcome this problem, a variable head bubbler was used to maintain the required chlorine pressure upstream of the flow meter. A diagram of this bubbler is shown on figure 3F. The central tube assembly was held rigid whilst the outer cylindrical container could be moved up

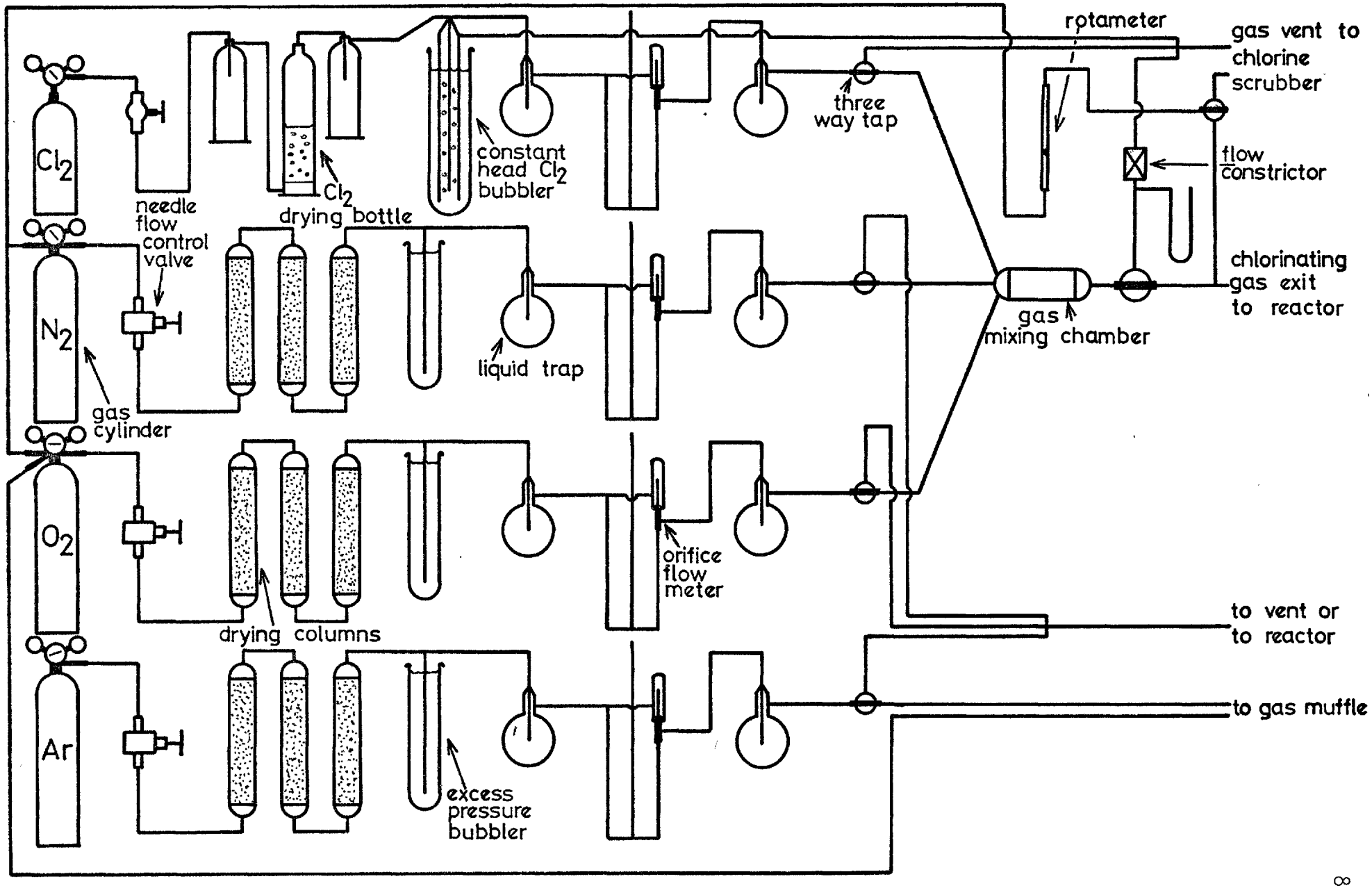

FIGURE 3E: SCHEMATIC DIAGRAM OF GAS TRAIN.

and down to vary the head. In operation an excess flow of chlorine was allowed to pass through the control valve, part of this flow escaped against the constant head of acid whilst the remainder passed through the orifice flow meter. The flow through the constant head device was kept fairly constant, at approximately 25 mls/min, by making sure that only 2 or 3 bubbles were rising through the acid at any one time. As long as the bubbles did not stop rising, a steady chlorine flow was maintained through the meter; the waste chlorine was piped away to a caustic scrubber.

3E4 Flow meters and calibration

A diagram showing the construction of a flow meter is given on figure 3F. The basic design is well known*, the only modification incorporated was the central tube which enabled the absolute pressure either side of the orifice to be measured instead of just the orifice pressure drop. Each assembly was made from standard 'Quickfit' glassware and 6 mm bore pyrex tubing. Meters were secured by means of 'Terry' clips onto wooden support boards; millimetre graph paper was mounted on these boards to facilitate the taking of pressure readings. The meters were mounted with their manometer tubes vertical; concentrated sulphuric acid was used as liquid. Two types of orifice were used, one kind was made by gluing, with Araldite an 0.25 mm thick nickel disc onto the end of a CNBIO socket. A suitable sized hole, giving the required flow range, was then drilled through the centre of the disc. The second type was made by melting over the end of a CNBIO socket until only a small hole was left. To get these orifices to give the right flow range was rather a case of trial and error; however, once this was achieved only periodic cleaning was necessary. Changing to different flow ranges was simply a case of taking off the spring loaded top cap and putting in the new orifice. When making these changes special care was taken to ensure that the two cone and socket joints involved were suitably greased.

Since the flow meter pressure drops of between 4 cms and 35 cms of H_2SO_4 were used, each orifice could span a flow variation of a factor of three. Once calibrated for a specific gas, orifices were not used with any other gas. Calibration of the orifices was carried out using various sized soap bubble meters and a three second sweep stop watch. The soap bubble meters

---

* The mechanics of operation are, however, generally misunderstood: see Appendix C

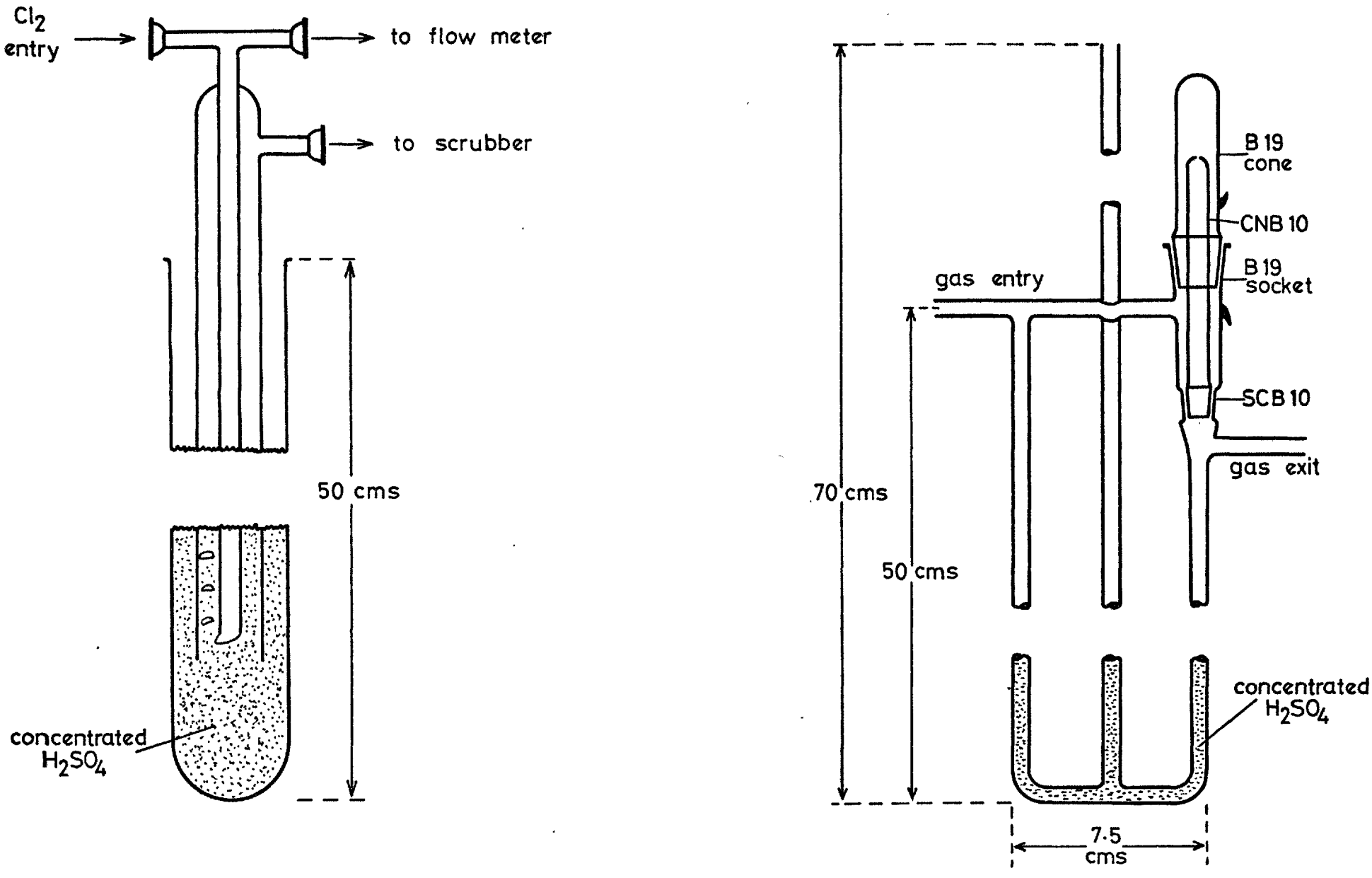

FIGURE 3F: ORIFICE FLOW METER DESIGN AND CONSTANT HEAD CHLORINE BUBBLER.

consisted of long pyrex tubes, or burettes, marked with suitable graduations. Gas entered at the bottom, and by using a rubber teat containing soapy water, a single bubble could be made to rise up the tube with the flowing gas. Flow rates were determined by timing the bubbles between set graduations. With each orifice the calibration readings taken spanned its effective flow range; all individual readings were repeated five times. Using a systematic routine for taking these readings, reproducibility with the O_2, N_2 and Ar was excellent. Each five values usually agreed to better than 0.3%. The only problem presented during calibration was that the chlorine fairly rapidly oxidised all the soaps and detergents used. Various organic bubble forming systems were found to be equally unstable. Since displacement methods were not favoured, calibrations with chlorine necessitated frequent changes of soap solution. Reproducibility of each set of five readings was within 0.5%.

As a check, one orifice for each of the gases Ar, N_2 and O_2 was recalibrated at the end of the experimental campaign some 18 months after the initial calibration. Comparison of the pairs of calibration plots showed no discernable differences. Under all experimental conditions the gas flows indicated by each meter were, on the basis of operative error, estimated to be accurate to within $\pm$ 1%. The concentrated sulphuric acid in the meters had a strong tendency to absorb water. A significant change in the density of the acid could have led to errors in calculating gas flows. Thus the acid level in each meter was regularly checked to see if and when the acid required changing. An outline of the fluid mechanics of these meters is given in appendix C, together with a typical calibration plot. As a safety precaution, liquid traps were placed either side of the parts of the gas train containing acid. So as to prevent any acid being ejected in the event of a sudden accidental pressure build up, PVC tubes leading to glass flasks were connected to the tops of the open ended manometers.

3E5 Gas routing and mixing: flow constrictors

Three-way ground glass stop cocks were employed for routing the gases; the various routes are shown on figure 3E. O_2-Cl_2, N_2-Cl_2 or N_2-O_2-Cl_2 gas mixtures could be obtained by directing the respective gases to a mixing chamber. This consisted of a shortened version of the drying

columns filled with glass wool. Gas mixtures leaving this chamber could then either be sent to a chlorine scrubber or to the reactor. In the line taking the gas mixture to the scrubber, there was a short section of silicon rubber tubing which could be constricted with a screw clip. The constriction was used to develop pressure drops somewhat greater than would occur across the reactor-condenser assembly during experiments. This enabled the flows of the constituent gases to be adjusted before starting the experiments. The ΔP across the venting route constrictor was made to be larger than that which would occur across the reactor-condenser, since the difference between the two was made up on starting an experiment by a similar constrictor placed in the reactor gas delivery line. This compensating constrictor could be finely adjusted to account for any changes in gas flow resistance which occurred during the course of the experiments. Thus, with this system of constrictors it was possible to set up each meter before an experiment, and then steadily maintain the same flow through the reactor for the duration of the experiment.

All the gases could, if necessary, be vented directly after their flow meters. This allowed for isolation of individual gas lines. With the O_2, Ar and N_2 by using various connectors from their venting lines, O_2-Ar and O_2-N_2 gas mixtures could be formed. These mixtures were used when conditioning the reactor and its contents of cobalt oxide(s)-zinc oxide at various oxygen partial pressures. Argon was used for the gas muffle except when it was needed for bed conditioning; then nitrogen, direct from a cylinder regulator, was used to maintain the excess pressure in the muffle.

When the chlorinating gas flow was stopped at the end of a run, residual gas in the delivery line and reactor was immediately pushed through the bed. This was carried out by using either pure nitrogen, pure oxygen, or an argon-oxygen mixure flowing at close to the same volume rate as used during the experiment. This flushing gas was taken either directly from the respective cylinder regulators via a rotameter, or from the gas train.

3E6 Manometers

U tube manometers filled with concentrated H_2SO_4 were used to indicate pressure differences at various places along the chlorinating gas flow routes. The pressures that were indicated are listed below.

1. Pressure before venting route constrictor
2. Pressure before delivery route constrictor
3. Chlorinating gas pressure at reactor entry
4. Pressure drop across reactor-condenser
5. Pressure in gas muffle

Of the pressures listed only 3. and 4. were recorded for each experiment, the others were used to help set up the chlorinating gas flow and to allow checks to be made during experiments.

3E7 Chlorine scrubber

Excess chlorine vented from the gas train, and unreacted chlorine from the condenser exit, were chemically absorbed by two bubblers each containing about one litre of 10N aqueous caustic soda solution. One of these bubblers can be seen in the top right hand corner of the photograph of the furnace assembly. The chlorine containing gas, together with some excess air, was drawn into the scrubber system by a vane pump situated downstream from the bubblers and liquid traps. If the reactor and gas train were together producing about 1.5 litres/min of gas for scrubbing, then the pump was throttled so as to draw about 3 litres/min (measured by an in-line rotameter) through the bubblers. The difference between these flow rates was made up with air which was drawn into the scrubber near to the condenser exit. This air bleed was arranged using a 'T' piece connector, one arm went to the scrubber, another to the condenser exit and gas vents, whilst the third arm was left open to the atmosphere. With this system all the chlorine could be collected for scrubbing without upsetting gas flows in any part of the reactor or gas train. With equilibrium runs, since the bed exit P_{Cl_2} was very low, scrubbing was not performed on the exit gas. Instead a fan extractor pumped the gases away to a fume chamber.

3E8 General assembly

The connections between different parts of the gas train were made with Quickfit ball and cup joints and flexible tubing. PVC of 1/4" bore was used with the Ar, O_2 and N_2 whilst 3/8" bore polythene was used with the chlorine; 1/4" bore monel and 6 mm bore glass was also used in certain places. The ground glass joints were spring loaded and sealed with Voltalef grease.

CHAPTER FOUR

OXIDE COMPACTS: EXPERIMENTAL PROCEDURES: PROVING RUNS

4A OXIDE COMPACTS

In this study two types of oxide compacts, both made from high purity oxide powders, were employed. Granular zinc oxide, used for the initial experiments and non-equilibrium work, was made by isostatic cold compaction. Since the resulting granules were in some ways unsatisfactory, all the mixed oxide compacts and single oxide compacts used for the subsequent experiments were made by pelletisation and hardening.

4A1 Granular zinc oxide

Analar grade ZnO* was isostatically cold compacted to 70 tons/sq.inch by a hydraulically operated press. The cylindrical compaction container, which fitted inside a large bolster, was 76.2 mm in diameter and 200 mm long. Removable end pads were 30 mm high, the bottom one was firmly supported by a base plate whilst the top one could slide downwards under the load applied by the ram. So that the load was applied isostatically to the oxide powder, 150 mm long, 'medium hard vinamould'** sleeves were cast, these had a wall thickness of 6 mm and just fitted inside the container. Under load this material behaves like a fluid and transmits pressure uniformly throughout its bulk. The procedure for compacting zinc oxide was as follows: Firstly the bottom pad was inserted into the cylinder, on top of this for sealing purposes was placed a close fitting thin neoprene disc, next the vinamould sleeve was pushed in. The sleeve was rammed full of zinc oxide powder, another neoprene sealing disc was then inserted followed by the top pad. The ram was then brought down onto this pad and the full press load of 500,000 Kg was rapidly applied; this load was not held but was quickly relieved. The whole loading-unloading step usually lasted no more than 15 seconds. Once completed, the oxide compact, both pads and the vinamould were pushed out of the cylinder by using the ram and a special support jig. Neither the neoprene discs nor the sleeve could be used more than once since they became severely damaged under load.

---

* Hopkins and Williams

** Alec Tiranti Ltd.

Compacts of zinc oxide consisted of rough surfaced cylinders weighing about 1 Kg; measured bulk densities were constant at 5.40 gms/cc, the voiding was therefore about 4%. No penetration of vinamould was detected, any thin coating found adhering to the oxide surface after compaction was easily peeled off. Once a number of compacts had been prepared they were broken into granules using a jaw crusher. These granules were then sieved into the following size fractions: -7* mesh + 14* mesh, - 3/16 inch + 7* mesh, -1/4 inch + 3/16 inch and - 3/8 inch + 1/4 inch. Each fraction was then stored in an air tight glass jar until needed for an experiment. A photograph of an equal mass of each size fraction is shown on plate 3. Although the granules produced by this method were very strong, for the purposes of the planned experiments they were not of a particularly satisfactory physical form. All had an irregular plate-like shape, consequently the specific surface area of a given size fraction (which consisted of a range of geometries) could not be estimated with any great accuracy. Furthermore, with their low voidage the granules were effectively impermeable; this feature would be undesirable with oxide mixtures. Finally, from the practical standpoint this technique was a lengthy procedure and was not suitable for production of relatively large quantities of compacts.

4A2 Pelletisation and hardening of single and mixed oxides

The specifications of the oxide powders used to make the various pellets are given in appendix D.

4A2a Pelletisation:- The pellets were made in a rotating pelletising drum 59 cms in diameter, 22 cms deep with an 8 cm lip at the open end to prevent spillage. The drum rotated about its central axis, which was inclined with its open end 15° above horizontal, at up to 40 revolutions per minute. The pellets were all directly made from the oxide powders. Oxide mixtures were homogenised by weighing exact quantities of constituent oxides into 35 cms tall - 14 cms diameter screw cap glass jars; these were never more than two thirds filled. For mixing, an expanded metal spoiler was fixed in each of the jars which were then placed on rollers (30 revs/min) for 24 hours. After rolling, the powder was very carefully examined to check on the homogeneity of the mixture. In all cases this was found to be satisfactory. No binders were added to the oxides, the

* 7 mesh = 2.5 mm, 14 mesh = 1.25 mm

only addition for this purpose was distilled water.

To start producing pellets about 1 Kg of powder was added to the rotating drum. This powder was then sprayed with fine droplets of water until a large number of small approximately spherical nuclei were formed. More dry powder together with suitable quantities of water were then added to the mass of nuclei, with the rolling action of the drum these stayed nearly spherical and gradually grew in size. Since CdO, ZnO and ZnO/CdO pellets of not greater than about 8.0 mm diameter, and 'CoO'/ZnO pellets of not greater than about 4.0 mm diameter were required, all the larger pellets were constantly broken up so as to allow a fairly narrow size range to develop. Once a suitable size distribution had been obtained, the pellets were left in the rotating drum for about 5 minutes to help produce as round pellets as was possible.

Since the pelletising process was very sensitive to the way it was operated, production of exactly similar pellets from different oxides and mixtures was not possible. During pelletisation it appeared that the CdO underwent a hydration reaction which caused the CdO and CdO/ZnO pellets to develop considerable green strengths. The rounding off procedure was thus fairly ineffective with these pellets, which consequently had to be made carefully and with some haste. For the purposes of the equilibrium experiments, some variation in the physical properties of the different pellets was of little consequence. For the ZnO/CdO non-equilibrium studies, where the properties of the pellets were of extreme importance, extensive structural examinations were carried out, these are reported in chapter eight. Although the CdO/ZnO and 'CoO'/ZnO pellets used for the equilibrium experiments were not examined structurally, by drawing parallels from the findings of the CdO/ZnO (non-equilibrium) structural examinations both sets of former pellets are thought to have had a voidage of about 15-25%, this essentially being made up of fairly uniform sized sub micron pores.

4A2b Pellet compositions:- The compositions of the various pellets produced are listed below:

1.	ZnO	Pure
2.	CdO	Pure
3.	CdO/ZnO	50.0 mole% CdO
4.	CdO/ZnO	26.6 mole% CdO
5.	CdO/ZnO	10.8 mole % CdO
6.	'CoO'/ZnO	nominally 50.0 mole % 'CoO'

Since the exact composition of the cobalt oxide (see appendix D) used for oxide mixture number 6 was unknown, it was for the purposes of weighing out, assumed to be CoO. If this assumption were correct, then the mixture on the basis of metal content contained 50 mole % Co. However, if the oxide were either entirely Co_3O_4 or entirely Co_2O_3, the mixture contained either 48.2 or 47.7 mole % Co respectively.

4A2c Pellet hardening:- Preliminary hardening tests on CdO/ZnO pellets showed that at temperatures above 1000°C three undesirable effects started to become pronounced; these were sintering, densification and cadmium volatilisation. Therefore, for hardening the CdO and CdO/ZnO pellets were placed in large alumina crucibles fairly rapidly (4 hours) heated (in air) to 1000°C, held at this temperature for 30 minutes, and then allowed to furnace cool. The resulting pellets were strong and appeared to be little changed in structure. Except for a few exposed CdO/ZnO pellets, which were always discarded, there were no signs of Cd loss. It was intended to heat treat the 'CoO'/ZnO pellets in the manner just described. However, the furnace being used for the heating cycle malfunctioned during the heat up. This caused the pellets to be heated up to 900°C and then immediately furnace cooled. On examination, since the pellets were found to be amply strong, no further heat treatment was carried out. The ZnO pellets were sintered at 1400°C for 24 hours; this produced very hard pellets having a voidage of about 2%. Since these pellets were only used for a small number of deep bed experiments (allowing the attainment of chemical equilibrium) their internal structure was unimportant.

4A2d Sieving:- The following sieves were employed for grading hardened pellets: 1.4, 1.6, 2.0, 4.0, 4.75, 5.6 , 6.7, 8.0 and 9.5 mm. The dimensions given are the lengths of one side of the square aperture of the sieve. Standard sieving procedures were followed, after which the pellet fractions were stored in air tight jars.

4B EXPERIMENTAL PROCEDURES

Although several types of experiments were carried out, the differences between the procedures were only slight. Thus, the detailed chronicle given below is appropriate to all the chlorination experiments. It is followed by additional information on each specific series of experiments.

4B1 Operational sequence of chlorination experiments

Once the aim of each experiment had been determined, it was necessary to decide upon values for the experimental variables which are listed below.

1. Reaction temperature
2. Chlorinating gas flow rate and composition
3. Bed mass, pellet composition and size fraction
4. Reaction time
5. Reactor and condenser size, condensation zone temperature gradient
6. Bed/reactor pre-conditioning and end flushing

After these variables had been determined, the experiment could commence. In the list below, readings were taken and recorded at operations marked with an asterisk.

4B1a Preparing for chlorination:-

1.* Insert correct orifices.
2. Set Eruotherm temperature controllers.
3. Wash reactor and condenser in water and then dry with acetone.
4.* Weigh empty reactor, silica wool plugs, thermocouple and attachments. Weigh empty condenser, silica wool plug and attachments. Record reactor and condenser size.
5. Fill reactor with oxide charge and insert thermocouple.
6.* Weigh full reactor. Measure initial bed depth.
7. Start to insert reactor and condenser into furnace (horizontal). This was carried out by moving both vessels inwards about 4 cms at a time. Slow insertion prevented thermal shock fracture of the mullite muffle tube. From start to finish the operation usually took about 20-25 minutes.
8.* Record reactor insertion starting time.
9. Start chlorine scrubbing system.
10. Start up gas train with gas mixture venting to scrubber. Adjust each gas flow. Set venting route constrictor.
11.* Record atmospheric pressure and gas train temperature.
12. When fully inserted into furnace, connect reactor to condenser. Attach rubber sealing sleeves to gas muffle. Load ball and cup joint.
13. Swing furnace vertical and secure.
14. Connect gas lines to gas muffle. Check gas tightness of ball and cup joint. Adjust gas supply to muffle. Connect thermocouple to potentiometer and pen recorder.

15.* If necessary, perform pre-chlorination bed conditioning. Record gases, flows and bed temperature.

16. Connect exit gas handling lines (and filter if required) to condenser. Flush out chlorinating gas delivery line and then connect to reactor.

17.* Check indicated Eurotherm temperatures. Record Eurotherm settings.

18.* Check for steady bed temperature. Record millivolt output from the thermocouple. Record potentiometer cold junction temperature.

19.* Check flow meter readings. Record all flow meter manometer readings. Mark acid level in one arm of chlorine flow meter.

4B1b Chlorination:-

20. Turn stopcock and route chlorinating gas to reactor. Start clock.

21. Adjust compensating constrictor until acid level in chlorine flow meter returns to marked position. (This ensures that the predetermined preadjusted gas flow is delivered to the reactor.)

22.* Record chlorinating gas entry pressure and reactor pressure drop. Record all flow meter readings. Record bed temperature (with certain experiments the thermocouple was moved upwards inside its sheath to measure any gradient down the bed). Check gas muffle pressure.

23. Readjust compensating constrictor if and when necessary.

24.* If unsteady re-measure, as necessary, bed temperature, reactor pressure drop and chlorinating gas entry pressure.

25. Stop chlorination by diverting gas to scrubber. Stop clock.

26.* Immediately chlorinating gas delivery is stopped, flush reactor through with inert gas; record flow, composition and time.

4B1c After chlorination:-

27.* Record reaction time.

28. Turn off all gas flows and scrubber systems.

29. Disconnect attachments to reactor and condenser. Swing furnace horizontal. Quickly remove reactor and condenser and allow to air cool.

30.* Record time of removal of reactor from furnace. When cool weigh reactor and condenser (about 15 to 30 minutes after removal from furnace).

31.* Record any relevant observations such as condition of reactor, oxide charge, condensate etc. File temperature trace if unsteady. Store reacted bed in air tight container.

32. Cool furnace if at greater than 900°C.

The sequence of events just described, for experiments in which the bed was chlorinated once, usually took up to about 2 hours to complete.

4B1d Collection of condensate:- The metal chloride(s) condensate was collected from within the condenser by the same method for all the experiments performed. 50 mls of concentrated analar hydrochloric acid (SG = 1.18) was added to approximately 250 mls of distilled water. This solution was heated to about 95°C and then poured into the condenser. For this operation the condenser was held vertical with its open end uppermost. The cup joint at the bottom was sealed with a ball shaped silicon rubber blank held in place by a spring clip. Since the amount of distilled water used to make up the acid solution was not accurately measured out, extra water was added to the condenser to bring the level over the silica wool end plug. When the solution within the condenser had cooled, it was poured together with the silica wool plug into a 1000ml (or 500 ml*) volumetric flask. Traces of solution adhering to the inside wall of the condenser were washed into the flask with distilled water. The contents of the flask were made up to the graduation mark when its temperature was between about 17 and 23°C. The silica wool plug was collected as part of the condensate in order to minimise the possible loss of metal chloride (its volume was always insignificantly small as compared with that of the flask).

4B1e Chemical and atomic absorption analysis:- For a number of the initial experiments on zinc oxide, the solution containing the condensate was analysed directly by EDTA complexiometric titration. This method was soon abandoned in favour of the more suitable and more rapid atomic absorption (AA) technique. The only potential disadvantage of this technique was that the 1000 ml 'master' solution invariably needed to be diluted (so as to produce a metal concentration in the solution being tested of between 1 and 10 ppm**). The dilutions used varied from one experiment (and component) to another; with major components the maximum dilution used was x 1000, in these cases 1 ml of 'master' solution was made up into a 1000 mls test solution. To investigate the absolute accuracies of the AA and EDTA techniques, and also to determine whether sample dilution was responsible for any significant errors, a number of $ZnCl_2$ solutions were subjected to various tests. The findings are listed below.

---

* 500 ml flasks were only used with ZnO - 22 mm condenser runs

** 1 ppm = 1 µgm/ml

1. On any one solution, repeated EDTA analysis gave results which varied by less than about ± 1% about a mean. Since analytical grade reagents were used throughout, it is assumed* that the absolute accuracy of this method was also better than about ± 1%.

2. On any one diluted solution, repeated AA analysis gave results which varied by less than about ± 2½% about a mean (this was also the level of internal reproducibility for Cd and Co AA analyses).

3. On any one undiluted master solution repeated AA analysis (each time involving a dilution) gave results which were also within about ± 2½% about a mean.

4. Agreement between the mean AA analysis and the mean EDTA analysis of any one solution was very good.

The two conclusions drawn from these results were a) careful sample dilution was not a significant error incurring operation, and b) the absolute accuracy of the AA-Zn method was within ± 3% (hopefully most analyses were even more accurate).

Since the same careful and systematic procedure was used for all the AA analyses (Cd, Co and Zn) it is claimed that the condensates were determined to within ± 3%. Details of the EDTA and AA methods are given in appendix E.

4B2 Details of procedures for individual series of experiments

Departures from, and additional details on, the procedure explained in section 4B1 will now be given. Information on each series of experiments is presented in the order in which they were performed.

---

* This assumption infers that there were no systematic errors

4B2a ZnO proving runs and non-equilibrium experiments

Temperature	700°C to 870°C. Internal thermocouple. Chart recorded
Oxide bed	-7m/+14m to -3/8"/+1/4" ZnO granules. New bed used with all experiments except for some proving runs. Beds 12 gms to 150 gms.
Chlorination gas mixtures	N_2-Cl_2 and N_2-O_2-Cl_2. Maximum Cl_2 content 25%. Maximum gas flow 5.5 litres/min.
Pre-chlorination bed conditioning	None
Post-chlorination gas flushing	O_2 for 4 to 7 minutes at same flow as total chlorination flow
Reactor size	22 mm bore
Condenser size	22 mm bore single tube condenser until D series experiments, then concentric tube condensers used.
Analysis	EDTA and one series by AA. For some experiments analysis was not performed.
Reaction time	7 to 20 minutes for non-equilibrium experiments.

4B2b ZnO/CdO equilibrium experiments

Temperature	702°C to 1072°C. Internal thermocouple for runs below 1050°C. Chart recorded.
Oxide bed	50.0 mole % CdO except for 4 runs with 10.8 mole % CdO. Beds 200 gms to 350 gms. Pellet size mostly -4 mm, a few runs at -4.75 mm and 2 at -5.6 mm. Some beds used once, others twice and one three times.
Chorination gas mixtures	N_2-Cl_2 except for 3 runs with O_2-Cl_2. Maximum total flow 400 mls_{NTP}/min. Maximum chlorine content 25%.
Pre-chlorination bed conditioning	None with N_2 carrier gas runs. O_2 purge before O_2-Cl_2 runs.
Post-chlorination gas flushing	O_2 for 8 minutes at same flow as total chlorination flow
Reactor size	22 mm bore reactor, 17 mm bore reactor and 27.5 mm reactor with 20 mm bore mullite liner.
Condenser size	22 mm bore single tube condenser, 30 mm and 32 mm bore concentric tube condensers.
Analysis	AA
Reaction time	10 to 50 minutes

4B2c ZnO/CdO non-equilibrium experiments

Temperature	750°C to 950°C. Internal thermocouple. Chart recorded.
Oxide bed	50.0, 26.6 and 10.8 mole % CdO. Bed weight 120 gms, size fraction -6.7mm/+5.6 mm. Each bed chlorinated in progressive stages.
Chlorination gas mixtures	N_2-Cl_2. Flows of 1200 mls_{NTP}/min N_2 and 55 mls_{NTP}/min Cl_2.
Pre-chlorination bed conditioning	None
Post-chlorination gas flushing	O_2 for 8 minutes at same flow as total chlorination flow.
Reactor size	27.5 mm bore
Condenser size	30 mm and 32 mm bore concentric tube condensers.
Analysis	AA
Reaction time	In stages of between 3 and 26 minutes. Maximum total chlorination time 90 minutes.

4B2d ZnO/CdO double bed non-equilibrium experiments

Temperature	750°C to 950°C. Internal thermocouple. Chart recorded.
Oxide bed	Twin layer bed: Upper 20 cm deep -4.0 mm/+2.0 mm ZnO; lower CdO/ZnO (50/50) - 8.0 mm/+6.7 mm or CdO -4.75 mm/+4.00 mm. Lower bed weight 70-80 gms.
Chlorination gas mixtures	N_2-Cl_2. Flows of 1200 mls_{NTP}/min N_2 and 55 mls_{NTP}/min Cl_2. Two runs with O_2 carrier gas at 1200 mls_{NTP}/min.
Pre-chlorination bed conditioning	None
Post-chlorination gas flushing	O_2 for 8 minutes at same flow as total chlorination flow.
Reactor size	27.5 mm bore
Condenser size	30 mm and 32 mm bore concentric tube condensers.
Analysis	AA
Reaction time	6 minutes.

4B2e Zinc oxide/Cobalt oxide(s) equilibrium experiments

Temperature	850°C to 1070°C. Chart recorded. External thermocouple used above 930°C
Oxide bed	-4.75 mm/+1.6 mm. Nominally 50 mole % CoO. 70 to 200 gms. Some beds used once most used twice.
Chlorination gas mixtures	N_2-Cl_2, N_2-O_2-Cl_2 and O_2-Cl_2. Maximum total flow 350 mls_{NTP}/min. Maximum chlorine content 9%.
Pre-chlorination bed conditioning	All beds were conditioned at various oxygen partial pressures prior to chlorination. Details are given in the relevant results section.
Post-chlorination gas flushing	Gas at the same oxygen partial pressure and total flow as during chlorination was passed for 10 minutes.
Reactor size	22 mm bore reactor below 930°C, 27.5 mm reactor with 20 mm bore mullite liner above this temperature.
Condenser size	30 mm and 32 mm bore concentric tube condensers.
Analysis	AA
Reaction time	10 to 25 minutes.

4C PROVING RUNS

With each series of experiments it was necessary to establish, by various means, that the conditions employed were actually producing the desired results. The equilibrium experiments required that thermodynamic equilibrium between the phases was achieved before the bed exit. The ZnO non-equilibrium experiments required that a quasi steady state approximation could be applied for theoretical analysis of the results. The CdO/ZnO non-equilibrium experiments could only be performed after the experimental procedures had been established. Therefore, prior to any specific experiments a number of proving runs were performed.

4C1 ZnO proving runs

The first test runs were carried out on the apparatus to check the reproducibility, accuracy and internal consistency of the overall

experimental procedure. Six identical chlorination runs were performed on ZnO granules at 800°C, with a reaction time of 21 minutes using the experimental procedure as given in section 4B2a. The gas mixture consisted of N_2(66%), O_2(19%) and Cl_2(15%) at a total flow of 420 mls_{NTP}/min. In each case a deep oxide bed, determined on the basis of Orlov and Jeffes[31] work (with an added safety factor included) was employed so that equilibrium would be obtained. With each of these experiments, the same gas flow, reaction temperature and reaction time was fairly easily achieved. Of most importance was the chlorine mass balance, figures for which are given below. (In brackets behind the mean values are given the maximum single deviations expressed as percentages of the mean.)

1. Mean gm-moles Cl_2 passed via flow meter = 0.0586 (-1.2%)
2. Mean gm-moles ZnO lost from reactor (by weight) = 0.0495 (-5.5%)
3. Mean gm-moles $ZnCl_2$ collected (by weight) = 0.0477 (+2.3%)
4. Mean gm-moles Zn^{++} by EDTA analysis = 0.0520 (+2.2%)

These first results were encouraging but not entirely satisfactory, thus eight more experiments were performed, this time at 850°C, using 'deep' ZnO beds and a total gas flow of 1000 mls_{NTP}/min [O_2(20%)-N_2(70%)-Cl_2(10%)]. Four runs were of 15 minutes, the other four were of 30 minutes. Since two reaction times were used, the results are presented as mean molar rates.

1. Mean gm-moles/min Cl_2 passed via flow meter = 0.00463 std. dev. = 0.8%
2. Mean gm-moles/min ZnO lost from reactor (by weight) = 0.00449 std. dev. = 4.3%
3. Mean gm-moles/min $ZnCl_2$ collected (by weight) = 0.00428 std. dev. = 1.7%
4. Mean gm-moles/min Zn^{++} by EDTA analysis = 0.00432 std. dev. = 1.0%
5. Mean gm-moles/min Zn by AA analysis (no sample dilution) = 0.00404 std. dev. = 5.7%

Next to each molar rate is given the standard deviation shown as a percentage of the mean.

The standard deviation for each series of values indicated that individually a given reading could be quite accurately reproduced. In comparison with the first runs, the better results were assumed to be due to an improvement in experimental operating technique. The chlorine rate indicated by the

flow meter varied least, the variation that did occur was due to operator error. The EDTA analyses were second smallest in degree of variance; in view of the discussion in section 4B1e, the calculated standard deviation value was very much as expected. The AA analyses were performed on concentrated $ZnCl_2$ solutions (up to 0.52N) using the low absorption 307.5 nm Zn line (see appendix E). The standard deviation of 5.7% for these results is larger than generally expected from the AA method: using concentrated solutions, for which the 290B AA instrument is not primarily designed, probably accounted for this result. The maximum weight changes of the reactor and the condenser used to calculate molar rates of ZnO reaction and $ZnCl_2$ condensation were 2.5% and 7.5% respectively. The magnitude of the percentage weight change greatly influences the error associated with rates determined by this method; the difference between the values of std. dev. = 1.7% ($ZnCl_2$) and std. dev. = 4.3% (ZnO) show this effect.

4C2 ZnO non-equilibrium proving runs

To test the general experimental procedure under non-equilibrium conditions, five experiments* were carried out on relatively shallow ZnO beds (-3/16" + 7m granules) at 700°C using total gas flows of 2000 mls_{NTP}/min (85% N_2 - 15% Cl_2). So that influences due to the reaction initiation and reaction termination periods could also be evaluated, reaction times were for 2, 4, 6, 10 and 15 minutes. The results of these runs are given below in table 4A. As expected, agreement between the ZnO weight loss, the $ZnCl_2$ weight collected and the Zn^{++} EDTA analysis improved as the amounts involved became larger. For the purposes of calculating the chlorine utilisation a constant chlorine flow entering the reactor of 0.0136 gm-moles/min was used for each experiment. To fully discuss the possible effects, on the chlorine reaction rate, of reaction initiation and termination periods would be inappropriate in this section. Essentially initiation is that time during which the chlorinating gas mixture displaces inert gas from the reactor; termination is the reverse of this process. With the experimental procedure employed, two other influences were also present, namely the time spent adjusting the compensating constrictor and the time between stopping the chlorinating gas flow and commencing to

* H series experiments: see appendix F

Mean bed weight - gms	Reaction time - mins	gm-moles ZnO lost (by weight) x 10^3	gm-moles $ZnCl_2$ collected (by weight) x 10^3	gm-moles Zn^{++} by EDTA x 10^3	gm-moles/min (from EDTA) x 10^3	% Cl_2 utilisation (from EDTA)
59.66	2.00	9.33	6.9	7.92	3.96	29.1
59.20	4.00	14.2	11.3	13.7	3.42	25.2
59.13	6.00	22.5	21.2	21.7	3.61	26.5
58.54	10.00	35.4	31.9	33.9	3.39	24.9
57.70	15.00	56.4	53.1	54.9	3.66	26.9

TABLE 4A: RESULTS OF ZnO NON-EQUILIBRIUM PROVING RUNS

flush the reactor. The key factors important to end effects were the total gas flow rate, the reaction time and the volume contained between gas train and reactor exit. The maximum possible dead volumes of the 4 reactors used are listed below.

17 mm bore reactor	200 cc
22 mm bore reactor	320 cc
27.5 mm bore reactor	500 cc
mullite lined reactor	270 cc

From the results given in table 4A it appears that (with the 22 mm reactor using a total flow of 2 litres/min) experiments of 4 minutes duration or over experienced end effects small in comparison with other sources of error. Considering that new beds were used with each experiment, none of which were equally depleted, the discrepancies in chlorine utilisations between the 4 longer runs were quite small.

4C3 Chlorine mass balance

With each experiment, a full mass balance on chlorine would have required determination of the combined-chlorine in the condensate, together with determination of the uncombined-chlorine in the exit gas. This mass balance was insufficiently important to justify the necessary effort involved in carrying out the analyses. Consequently the only reasonably reliable chlorine balance that could be obtained was with the equilibrium

experiments. With these runs the chlorine flow indicated by the meter was equated via stoichiometry to the analysis of the metal species in the condensate.

In chlorinating mixed oxides under equilibrium conditions, the oxide which has the larger - ve ΔG^{o} reaction value dominates the partition of chlorine between its combined and uncombined forms. During this study the lowest fractional chlorine utilisation, in an experiment operated under equilibrium conditions, would have occurred with the Zno proving runs at 800°C. According to Orlov and Jeffes[31]

$$K_{800^{o}C} = \frac{P_{ZnCl_2} \cdot P_{O_2}^{\frac{1}{2}}}{a_{ZnO} \cdot P_{Cl_2}} = 45.8$$

If it is assumed that $a_{ZnO} = 1$, and that chlorination is performed with oxygen containing only a trace of chlorine ($P_{O_2} = 1$), the partition of chlorine between combined and uncombined forms is 45.8:1. This situation of minimum chlorine reaction is equivalent to a utilisation of 97.9%. Thus for all practical purposes with the equilibrium experiments there was 100% chlorine utilisation. The percentage utilisation refers to the formation of metal chloride(s). It does not necessarily infer a low free chlorine concentration in the condenser exit gas since back reaction might possibly occur during cooling and condensation.

The mean chlorine utilisations for each series of experiments performed under equilibrium conditions are given below.

1. Cadmium oxide/zinc oxide 97.0%
2. Zinc oxide proving runs 93.3%
3. Zinc oxide/cobalt oxide 87.1%

These figures are lower than expected. The first and most obvious explanation is that the reactions did not proceed to equilibrium. However, the results that are presented in the next chapter clearly do not support this inference. The cause(s) for the low utilisation values must thus have been within the following possibilities:

a) The flow of Cl_2 indicated to have reached the reactor was incorrect.
b) The condensate analyses did not account for all the chlorides formed within the reactor.

Type b) effects can be sub-divided as below:

1. Systematic errors in the AA analyses.
2. Failure to wash all the condensate from the condenser.
3. Failure of the condenser to collect all the gaseous chlorides.
4. Leakage of reactor products at the reactor-condenser joint.

After careful consideration it was felt that the low appareant chlorine utilisations could not be explained by any of the above effects. Type a) effects come under 3 categories:

1. Leaks,
2. Flow meter error,
3. Impure chlorine.

After careful consideration it was felt that error sources 1. and 3. could be eliminated.

The mixed oxide equilibrium experiments all involved using the same chlorine orifice (numbered C5 in appendix C). After all the runs had been carried out the calibration of this orifice was checked. At a measured flow of 50.3 mls_{NTP}/min the calibration plot indicated, for the same pressure drop, a flow of 56.0 mls_{NTP}/min. This discrepancy in the calibration of orifice C5 accounts for the unsatisfactory chlorine mass balances but at the same time raises some other uncertainties. When originally tested orifice C5 gave a linear calibration plot which showed no obvious inconsistencies. A subsequent check on the raw data collected at the time of calibration revealed no errors in calculation. Ultimately with orifice C5, divergence between the true Cl_2 flow and the indicated Cl_2 flow must have been due to either a) a systematic but unknown error in the initial calibration procedure or b) a progressive obstruction or narrowing of the orifice. That these effects might have influenced other chlorine orifices will be discussed in the relevant sections.

CHAPTER FIVE

RESULTS OF EQUILIBRIUM EXPERIMENTS

In this chapter results of the equilibrium experiments are presented in their final form. Full sets of data for each experiment are given in appendix G for the system zinc oxide/cadmium oxide and appendix J for the system zinc oxide/cobalt oxide(s).

5A CONDITIONS FOR EQUILIBRIUM

The attainment of equilibrium in a dynamic gas-solid system is essentially dependent upon the contact time between the moving gas and the stationary solid. With the experimental configuration used in this study the key variables influencing gas-solid contact times were a) the mass, size distribution and structure of the pelletised-oxide beds and b) the flow rate of the chlorinating gas mixtures. (Assuming a bed voidage of 37%, ideal plug flow gas motion and no back mixing the residence times - the time of passage for an element of gas through the bed - ranged from 0.55 seconds (Run CZS5) up to 1.72 seconds (Run S27).) Orlov and Jeffes[31] in their experiments on ZnO achieved equilibrium at 800°C with 17 to 20 gm granular (up to 1.7 mm diameter) oxide beds and gas flows of 200 mls/min. Since with most systems chemical rates and mass transfer rates increase with increasing temperature, the conditions that are found to give equilibrium at the lowest operating temperature will almost certainly produce equilibrium at higher temperatures. The ZnO non-equilibrium chlorination experiments* demonstrated that the overall reaction rate of 96% dense granules was relatively high even at 700°C. Consequently, on the basis of the work of Orlov and Jeffes, the data collected during the non-equilibrium ZnO studies and the assumption that CdO would behave similarly to ZnO, it was decided to start experimentation on the ZnO/CdO system using oxide beds (-4.0 mm + 2.0 mm) of not less than about 200 gms mass and gas flows of not greater than about 400 mls_{NTP}/min. Once a state of equilibrium between reactant gases and solids is reached at some point through the reactor, any further gas-solid contact has no effect whatsoever on the emerging gas composition. This behaviour enables a check to be made on whether equilibrium is actually being achieved at any specific operating temperature. What is required is a variation in bed mass or

---

* reported in section 7A

gas flow, any resulting discrepancy in emerging gas composition outside of the expected experimental scatter then signifies deviation from equilibrium. With the ZnO/CdO experiments, beds were varied in mass from 195 gms to 348 gms whilst gas flows were varied from 203 mls_{NTP}/min to 412 mls_{NTP}/min; at no single temperature was there any evidence of divergence from equilibrium. That all the ZnO/CdO runs were true equilibrium determinations is further reinforced by the excellent consistenc that was obtained over the whole temperature range studied.

The lowest temperature at which cobalt oxide(s)/zinc oxide equilibrium experiments were performed was 850°C. For these runs, on the basis of experience gained from the ZnO/CdO work it was decided to use gas flows of about 350 mls_{NTP}/min whilst varying the bed mass between about 70 gms and 200 gms (-4.75 mm + 1.6 mm). The results obtained from this second system showed a somewhat lesser degree of reproducibility as compared with the ZnO/CdO work. However, the scatter in experimental results at 850°C did not correlate with variations in bed mass (12 different masses); the general level of reproducibility also stayed fairly constant over the whole temperature range studied. These two findings would thus appear to confirm that the cobalt oxide(s)/zinc oxide equilibrium runs were carried out under the necessary experimental conditions.

5B METAL CHLORIDE PARTIAL PRESSURES

Graph 5A shows vapour pressure curves for the monomeric species $ZnCl_2$, $CdCl_2$ and $CoCl_2$, each for the temperature range melting point - boiling point. The data for $ZnCl_2$ is due to Keneshea and Cubicciotti[76], their values are in good agreement with work by Bloom and Welch[77]. Neither pair of workers has measured vapour pressures at above 580°C, however, for present purposes extrapolation up to the boiling point[3] of 732°C is sufficiently accurate. As with $ZnCl_2$, the $CdCl_2$ data is due to Keneshea and Cubicciotti[78], once again it is in good agreement with measurements by Bloom and Welch[77]; the plot given has been extrapolated from 800°C to 961°C. The $CoCl_2$ vapour pressure curve is plotted according to data from Schafer and Krehl[79], it has been extrapolated for temperatures above 800°C. The purpose of giving these three vapour pressure curves is to show that with each equilibrium experiment the partial pressure of chlorine in the chlorinating gas mixture was always chosen to be appreciably below that which would produce liquid

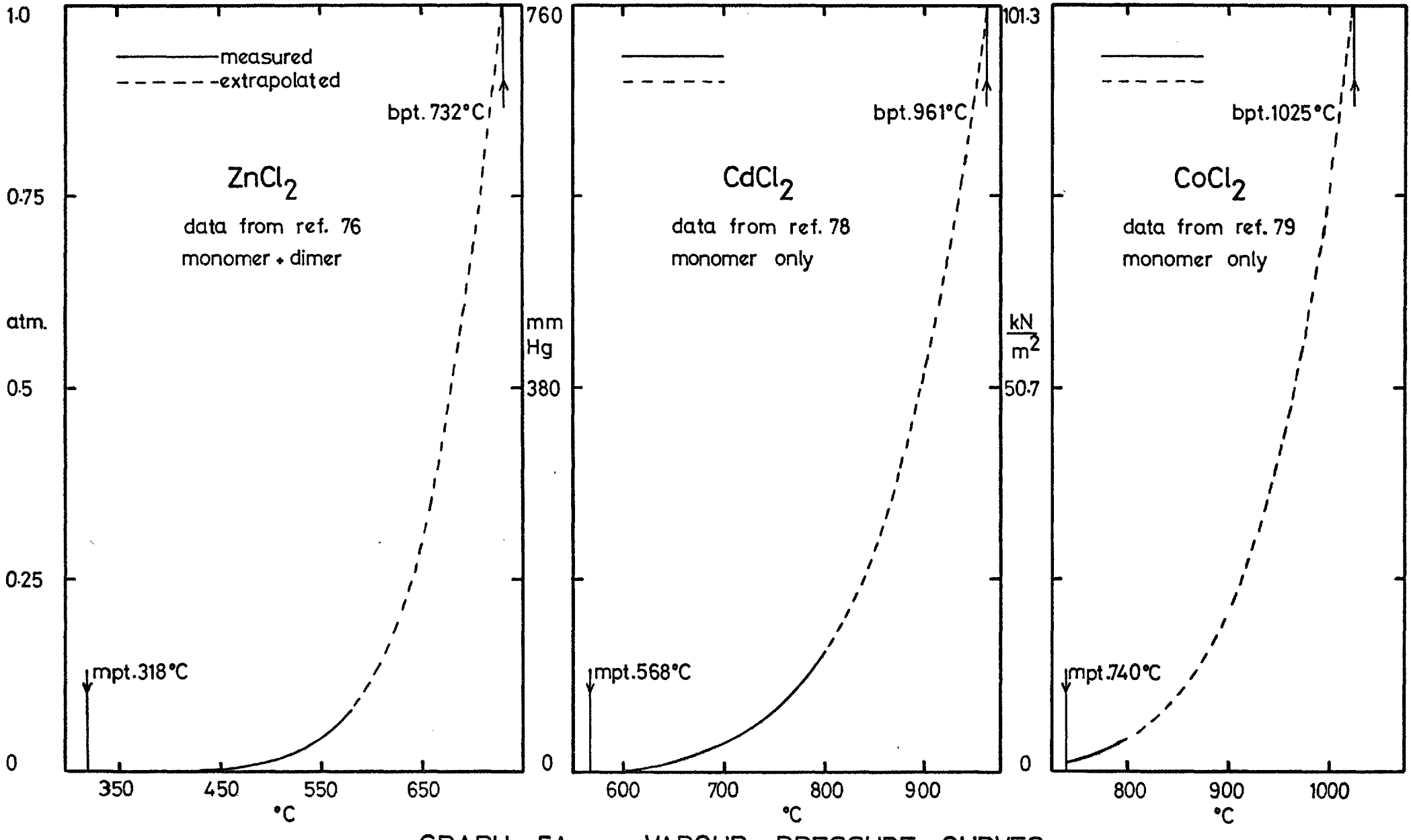

GRAPH 5A: VAPOUR PRESSURE CURVES

phase metal chloride.*

So as to highlight the formation of any complexes or polymeric species the chlorine partial pressure used with the CdO/ZnO experiments was constantly varied within the limit of the constraint just described. Taking these experiments as a whole, P_{Cl_2} values ranged in magnitude by a factor of x19. With the cobalt oxide(s) / zinc oxide system, experimental scatter was found to be a significant source of error. The P_{Cl_2} values used were thus not varied by large amounts since any relatively small effects caused by changes in metal chloride partial pressures would probably have gone undetected.

5C OXYGEN PARTIAL PRESSURE

By using nitrogen as an inert carrier gas in the chlorinating gas mixtures it was possible to vary both the oxygen and chlorine partial pressures independently of each other. The highest experimental P_{O_2} values employed were obtained by using O_2-Cl_2 gas mixtures in which there was a low chlorine partial pressure; under these conditions bed exit oxygen partial pressures of up to 0.95 atmos. were achieved. Since the chlorination experiments were not performed with reducing atmospheres (namely with gas containing CO/CO_2 mixtures) the lowest oxygen partial pressures that could be generated were with N_2-Cl_2 gas mixtures. When chlorine reacts with metal oxides oxygen is released into the gas phase; from knowledge of the stoichiometry of the particular oxide-chlorine reactions involved, the equivalence between chlorine reacted and oxygen released can be calculated. With the systems cobalt oxide(s)/zinc oxide and zinc oxide/cadmium oxide the equivalence $\frac{1}{2}Cl_2 = O_2$ was used for all calculations of bed exit oxygen partial pressures. There are two possible sources of error in using this value; firstly, ZnO, CdO and CoO might show some non-stoichimetry either in the form of a net oxygen excess or deficiency, and secondly, this equivalence is incorrect for the $Cl_2 + Co_3O_4$ reaction. These potential errors have however been neglected since if they were considered the required correction would be insignificant in comparison with other sources of error. With N_2-Cl_2 mixtures, by using lowest practicable chlorine concentrations, calculated minimum bed exit oxygen partial pressures of 0.035 atmos were obtained.

---

* See metal chloride partial pressure values given in tables 5A, 5B, 5C and 5D

For the system ZnO/CdO, where the ratio P_{ZnCl_2}/P_{CdCl_2} is predicted to be independent of oxygen pressure, all except three of the experiments were performed with N_2-Cl_2 mixtures. The three exceptions were O_2-Cl_2 runs which were carried out to confirm this prediction. The equilibrium ratio P_{ZnCl_2}/P_{CoCl_2} for the system Co_3O_4/ZnO is predicted to depend upon the oxygen partial pressure to the power of 1/6; for the CoO/ZnO system no oxygen partial pressure dependence is expected. Since the decomposition temperature* of Co_3O_4 is in the temperature range that was investigated, the cobalt oxide(s)/zinc oxide equilibrium experiments were performed over a range of oxygen pressures (0.95 atmos - 0.035 atmos). At 850°C, where Co_3O_4 is stable, a large number (21) of runs was carried out to investigate the $1/6^{th}$ power dependence. At higher temperatures P_{O_2} variation was still continued even into the region of CoO stability.

5D METAL OXIDE ACTIVITIES

All the cobalt oxide(s)/zinc oxide equilibrium experiments were carried out o pellets from one single batch which had a nominal cobalt content of 50.0 atom % (see section 4A2b). The possibility that any of the oxides were present at other than unit activity is examined in sections 6B3b and 6B3c. (For the purposes of calculating standard free energy changes, the activity relationships $a_{ZnO} = a_{Co_3O_4}$ and $a_{ZnO} = a_{CoO}$ have been adopted in this chapter.) 26 of the 30 CdO/ZnO equilibrium experiments employed 50.0 mole % CdO pellets; the remaining 4 runs used 10.8 mole % CdO pellets in order that any significant deviation from unit activities (or equal activities) would influence the measured P_{CdCl_2}/P_{ZnCl_2} ratios. The values of the activities of ZnO and CdO are discussed in section 6B3a. (For calculation of standard free energy changes, the relationship $a_{ZnO} = a_{CdO} = 1$ has been adopted in this chapter.)

5E CALCULATIONS BASED UPON EXPERIMENTAL DATA

Except in the case of precise measurements (weighings) final calculated values in the results tables are given to three significant figures: recalculation using these values may produce some disagreement between third figures, the most accurate computations may be performed by using data given in the appendices. The values** of $^xP_{CdCl_2} / {}^xP_{ZnCl_2}$ and

---

* The temperature at which the reaction $Co_3O_4(s) = 3CoO(s) + \frac{1}{2}O_2(g)$ produces an oxygen pressure of 1 atmosphere.

** x = Bed exit value

$^{x}P_{ZnCl_2}$ / $^{x}P_{CoCl_2}$ were taken to be the ratios of the gm-moles of the respective metal species, found by AA analysis in the condensates. All temperatures used in calculating ΔG^{o}_{T} values were those measured (to the nearest deg.C) at the exit end of the reactors. Calculation of bed-exit partial pressures $^{x}P_{CdCl_2}$, $^{x}P_{ZnCl_2}$, $^{x}P_{CoCl_2}$, and $^{x}P_{O_2}$ were based upon the following assumptions:

1. Each experiment was at steady state for the whole of the reaction period.
2. Chlorine utilisation was 100%.
3. The NTP molar volumes of each gaseous chloride were 22414 mls.
4. Each gas obeyed the equation of state of an ideal gas (PV = nRT).
5. The bed exit absolute pressure was equal to atmospheric pressure + 1 mm Hg.
6. The production of each mole of gaseous chloride was accompanied by the release of $\frac{1}{2}$ mole of oxygen.

Values used for R, the gas constant, and J, Joules equivalent, were 1.9872 cals$^{o}K^{-1}$mole^{-1} and 4.1868 Joules cals^{-1} respectively.

5F SYSTEM ZnO/CdO EQUILIBRIUM RESULTS

The two chemical reactions that proceeded to equilibrium during chlorination of the CdO/ZnO mixtures are given below.

$$CdO_{(s)} + Cl_{2(g)} = CdCl_{2(g)} + \tfrac{1}{2}O_{2(g)} \quad \ldots\ldots\ldots\ldots (1)$$

$$ZnO_{(s)} + Cl_{2(g)} = ZnCl_{2(g)} + \tfrac{1}{2}O_{2(g)} \quad \ldots\ldots\ldots\ldots (2)$$

5F1 Standard free energy change

From the experimental measurements recorded the standard free energy change (ΔG^{o}_{T}) for the reaction

$$CdO_{(s)} + ZnCl_{2(g)} = CdCl_{2(g)} + ZnO_{(s)} \quad \ldots\ldots\ldots\ldots (3)$$

can be calculated. In all reacting systems the equation

$$\Delta G = G(\text{Products}) - G(\text{Reactants}) \quad \ldots\ldots\ldots\ldots (4)$$

is valid. By considering either the concept of Van't Hoff's isothermal

reaction box[80] or chemical potentials[81] (due to J.W. Gibbs) the free energy change associated with reaction (3) for any arbitrary activities of reactants and products, is represented by the equation below (known as Van't Hoff's reaction isotherm.)

$$\Delta G_T = -RT \log_e K + RT \log_e \frac{F^a ZnO \cdot F^a CdCl_2}{I^a CdO \cdot I^a ZnCl_2} \text{ cals/mole} \quad . . (5)$$

Subscript I refers to the initial activities and F to the final activities of the various components. K, the equilibrium constant, is equal to:

$$\frac{eq^a CdCl_2 \cdot eq^a ZnO}{eq^a ZnCl_2 \cdot eq^a CdO} \quad . . . . . .(6)$$

where subscript eq refers to equilibrium activities. If reaction (3) takes place under conditions where the reactants are initially in standard states of unit activity and the products formed by reaction return to standard states of unit activity then equation (5) reduces to a special form which gives ΔG^o the standard free energy change of reaction.

$$\Delta G^o_T = -RT \log_e K \quad . . . . . .(7)$$

By convention, for gases the standard state of unit activity is taken to be that of unit fugacity[81] (symbol f, units atmospheres). By convention, for solids the standard state of unit activity is taken to be that of a pure solid under one atmosphere total pressure. Under the conditions employed for the ZnO/CdO experiments both metal oxides are assumed to have been present in their standard states of unit activity (see section 6B3a). The equilibrium constant for reaction (3) is thus simplified to:

$$K_f = \frac{f_{CdCl_2}}{f_{ZnCl_2}} \quad . . . . . .(8)$$

By making the assumption that gaseous $CdCl_2$ and $ZnCl_2$ behave as ideal gases (an acceptable assumption at low pressure) their fugacities then become equal to their partial pressures. Therefore,

$$K_p = \frac{P_{CdCl_2}}{P_{ZnCl_2}} \quad . . . . . (9)$$

The final equation used for calculating the standard free energy change of reaction (3) is:

$$\Delta G^{\circ}_{T} = -RT \log_e \frac{x_{P_{CdCl_2}}}{x_{P_{ZnCl_2}}} \quad \text{cals/mole} \quad \ldots\ldots\ldots (10)$$

5F2 Calculated standard free energy change

Calculated ΔG°_{T} values for reaction (3) together with other relevant experimental variables for the temperature range 702°C to 1072°C are presented in table 5A. The boiling point[3] of $ZnCl_2$ is 732°C, that of $CdCl_2$ is 961°C. That at below these respective temperatures neither species can exist in its defined standard states does not invalidate the calculated ΔG°_{T} values. Since the standard states for which the ΔG°_{T} values have been computed are clearly defined the tabulated data (and graphical data) may easily be referred to other standard states (eg liquid $CdCl_2$ and $ZnCl_2$) by applying simple corrections.

5F3 Analysis of calculated free energy data

The calculated standard free energy change values given in table 5A are plotted (ΔG°_{T} vs T) on graph 5B. Since there is some experimental scatter ΔC_p effects have been neglected, the data has thus been fitted to the linear equation.

$$\Delta G^{\circ}_{T} = \Delta H^{\circ} - T\Delta S^{\circ}$$

A best fit line of ΔG°_{T} from T has been computed by the method of least squares; a T from ΔG°_{T} line was not chosen since the main experimental errors are in the ΔG°_{T} values. The resulting line is drawn on graph 5B; its equation is given below.

$$\Delta G^{\circ}_{T} = -9670 + 1.23T \quad \text{cals/mole}$$

$$= -40500 + 5.15T \quad \text{joules/mole}$$

(T is in °K)

From this equation, which applies for the temperature range 975°K to 1345°K, the following ΔH° and ΔS° values are obtained:

Experiment number	Mole % CdO	Initial bed weight gms	Total gas flow mls_{NTP}/min [x]	$^{x}P_{O_2}$ Atmos $x10^{-2}$	$^{x}P_{CdCl_2}$ Atmos $x10^{-2}$	$^{x}P_{ZnCl_2}$ Atmos $x10^{-3}$	K_p	Temperature [x] ^{o}K	ΔG^{o} cals/mole
S21	50.0	238.94	203	0.571	1.13	0.149	75.5	975	-8378
S22	50.0		290	0.903	1.78	0.219	81.3	975	-8521
S17	50.0	276.83	301	1.26	2.48	0.398	62.3	1026	-8424
S18	50.0		412	1.59	3.14	0.494	63.2	1026	-8453
S27	50.0	348.40	359	94.1	5.22	0.961	54.3	1045	-8294
S23	10.8	283.42	318	2.23	4.36	0.889	49.1	1051	-8132
S15	50.0	240.41	235	4.45	8.72	1.73	50.4	1075	-8374
S16	50.0		316	3.27	6.41	1.27	50.3	1075	-8370
S1	50.0	223.37	391	5.08	9.91	2.49	41.8	1124	-8338
S4	50.0	212.95	273	5.71	11.1	2.69	41.4	1125	-8324
S6	50.0	280.64	330	10.5	20.5	4.74	43.2	1125	-8418
S28	50.0	348.40	363	93.5	5.90	1.51	39.0	1146	-8343
S24	10.8	282.53	329	3.05	5.93	1.64	36.2	1150	-8202
S7	50.0	201.74	317	11.1	21.6	5.96	36.2	1174	-8373
S8	50.0	200.54	285	7.04	13.7	3.92	34.9	1175	-8295

x = bed exit value

TABLE 5A (Part 1): CdO/ZnO EQUILIBRIUM RESULTS

Experiment number	Mole % CdO	Initial bed weight gms	Total gas flow mls_{NTP}/min [x]	$^{x}P_{O_2}$ Atmos $x10^{-2}$	$^{x}P_{CdCl_2}$ Atmos $x10^{-2}$	$^{x}P_{ZnCl_2}$ Atmos $x10^{-3}$	K_p	Temperature [x] ^{o}K	ΔG^{o} cals/mole
S19	50.0	204.80	312	3.73	7.25	2.14	33.9	1176	-8234
S20	50.0		390	6.14	11.9	3.35	35.6	1176	-8348
S25	10.8	236.86	299	3.61	6.98	2.39	29.2	1200	-8046
S9	50.0	200.50	281	7.19	13.9	4.64	30.0	1224	-8273
S10	50.0	214.97	272	5.55	10.7	3.74	28.7	1224	-8165
S29	50.0	348.40	362	93.8	5.59	2.06	27.1	1246	-8170
S26	10.8	235.64	310	3.48	6.69	2.62	25.6	1251	-8061
S11	50.0	280.21	318	10.7	20.6	7.89	26.0	1274	-8248
S12	50.0	270.75	345	5.00	9.62	3.88	24.8	1275	-8135
S31	50.0	195.24	343	7.00	13.4	5.96	22.5	1310	-8105
S30	50.0		356	3.90	7.45	3.55	21.0	1311	-7931
S13	50.0	300.03	353	5.07	9.67	4.78	20.2	1324	-7908
S14	50.0		329	10.4	19.7	10.4	19.0	1326	-7759
S32	50.0	198.30	344	6.57	12.6	5.83	21.5	1345	-8200
S33	50.0		337	3.12	5.95	2.97	20.1	1345	-8020

x = bed exit value

TABLE 5A (Part 2): CdO/ZnO EQUILIBRIUM RESULTS

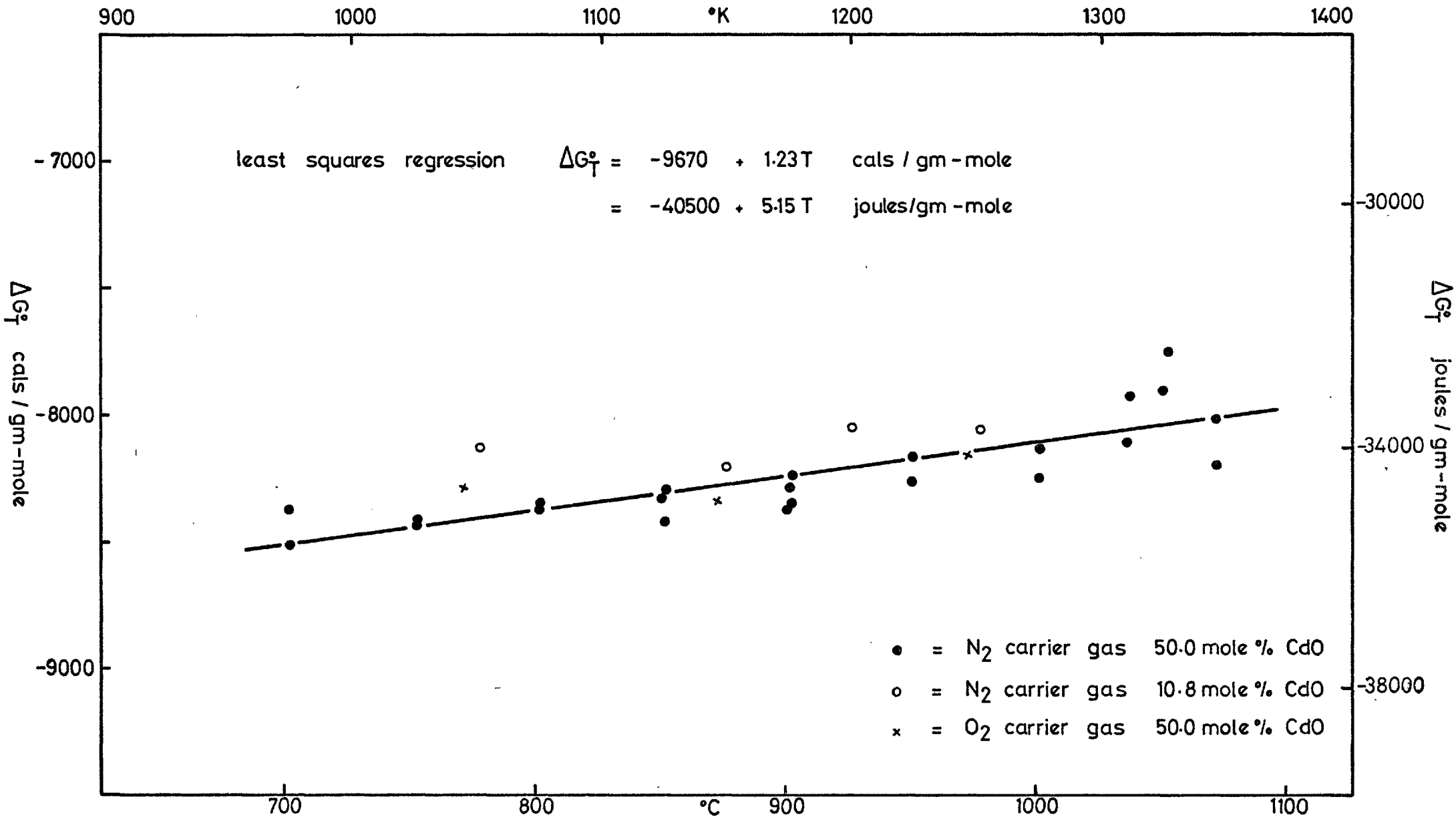

GRAPH 5B: STANDARD FREE ENERGY CHANGE OF REACTION

$ZnCl_{2(g)} + CdO_{(s)} = CdCl_{2(g)} + ZnO_{(s)}$

DATA FROM TABLE 5A

$\Delta H^{\circ}(975\text{-}1345^{\circ}K)$ = -9.67 K cals/mole
= -40.5 K joules/mole

$\Delta S^{\circ}(975\text{-}1345^{\circ}K)$ = -1.23 cals/mole $^{\circ}K$
= -5.15 joules/mole $^{\circ}K$

5G SYSTEM COBALT OXIDE(S)/ZINC OXIDE EQUILIBRIUM RESULTS

The experimental results that are reported in this section are for the systems Co_3O_4/ZnO and CoO/ZnO. The three chemical reactions involved are given below.

$$ZnO_{(s)} + Cl_{2(g)} = ZnCl_{2(g)} + \tfrac{1}{2}O_{2(g)} \quad \ldots\ldots\ldots\ldots (1)$$

$$CoO_{(s)} + Cl_{2(g)} = CoCl_{2(g)} + \tfrac{1}{2}O_{2(g)} \quad \ldots\ldots\ldots\ldots (2)$$

$$1/3Co_3O_{4(s)} + Cl_{2(g)} = CoCl_{2(g)} + 2/3\ O_{2(g)} \quad \ldots\ldots (3)$$

From the experimental measurements recorded, standard free energy changes for the reactions

$$CoCl_{2(g)} + ZnO_{(s)} = CoO_{(s)} + ZnCl_{2(g)} \quad \ldots\ldots\ldots\ldots (4)$$

$$CoCl_{2(g)} + ZnO_{(s)} + 1/6\ O_{2(g)} = 1/3\ Co_3O_{4(s)} + ZnCl_{2(g)} \quad \ldots (5)$$

can be calculated. Using the same arguments as applied in section 5F1 (but not necessarily assuming that the oxides were present within the pellets in their standard states, only that (1) $a_{ZnO} = a_{CoO}$ and (2) $a_{ZnO} = a_{Co_3O_4}$; for a full discussion see section 6B3b and 6B3c) the equilibrium constants* for reactions (4) and (5) are:

$$\text{reaction (4)} \quad K_p = \frac{x_{P_{ZnCl_2}}}{x_{P_{CoCl_2}}} \quad \ldots\ldots\ldots\ldots (6)$$

$$\text{reaction (5)} \quad K_p = \frac{x_{P_{ZnCl_2}}}{x_{P_{CoCl_2}} \cdot x_{P_{O_2}}^{1/6}} \quad \ldots\ldots\ldots\ldots (7)$$

---

* Bed exit values

From these equilibrium constants ΔG°_{T} can be calculated using the equation:

$$\Delta G^{\circ}_{T} = -RT \log_e K_p$$

5G1 Co_3O_4/ZnO results

5G1a Initial experiments - 904°C:- The first two cobalt oxide(s)/zinc oxide equilibrium experiments (CZS1 and CZS2) carried out at a nominal temperature of 904°C, were of an exploratory nature. With both runs the procedure was the same. The bed (the same one was used for each run) was first flushed with nitrogen for about 5 minutes, it was then chlorinated with a N_2-Cl_2 gas mixture for 10 minutes after which it was flushed with oxygen for 8 minutes. For both runs the temperature trace, obtained from an internal thermocouple situated close to the bed exit, was the same. The common features were:

a) During nitrogen flushing the recorded bed temperature fell by about 8 deg.C from its initial stable value.
b) Between ceasing the N_2 flush and commencing chlorination the bed temperature returned to its initial value.
c) During chlorination the bed temperature once again fell (but more slowly) to a steady value about 10 deg.C below that at the start of the run.
d) Between ceasing chlorination and starting oxygen flushing the bed temperature once again rose (at the same rate) to its initial value.
e) During oxygen flushing the bed temperature rapidly increased by about 45 deg.C and then slowly fell back to its initial value.

The behaviour just described was never experienced with any of the CdO/ZnO runs. It was thus due to neither the endothermic chlorination reactions nor the thermal demand of the chlorination gas mixture. The temperature fluctuations were caused by two processes, a) endothermic decomposition of Co_3O_4 to CoO and b) exothermic oxidation of CoO to Co_3O_4. Appendix K examines in detail the decomposition equilibrium

$$2Co_3O_4 = 6CoO + O_2$$

over the temperature range of interest to this study. From graph K1 shown in this appendix it is evident that at 904°C (the starting temperature for the two initial runs) under an oxygen pressure of 1 atmosphere, Co_3O_4 is the stable oxide of cobalt. The calculated bed exit oxygen partial

pressures operating during the chlorination stages of runs CZS1 and CZS2 were 0.031 and 0.040 atmos. respectively. The oxygen partial pressure in the nitrogen gas used during initial flushing would have had a minimum value of about 5×10^{-6} atmos. Graph K1 (appendix K) shows that under both these oxygen pressures CoO is the stable oxide of cobalt. It is thus clear that a) the initial N_2 purging gave rise to endothermic decomposition of Co_3O_4 to CoO, b) since this process did not go to completion it continued during chlorination and c) the use of oxygen for final flushing rapidly reoxidised (exothermically) the CoO to Co_3O_4. Although not all the Co_3O_4 decomposed during chlorination (with the result that CoO and Co_3O_4 were simultaneously present in the bed) it can be argued that these two experiments were true CoO/ZnO equilibrium runs; a full justification of this assertion is given in section 6A1.

5G1b Initial experiments - 850°C:- Since equilibrium relationships in the system $Co_3O_{4(s)}$-$O_{2(g)}$-$CoO_{(s)}$ are not precisely quantified it was decided against carrying out experiments in a region of some uncertainty. Thus for the next experiments the temperature was lowered to 850°C where under the proposed operating oxygen partial pressures Co_3O_4 appears to be stable. By using N_2-Cl_2 chlorinating gas mixtures, minimum bed exit P_{O_2} values of between 0.03 atmos. and 0.04 atmos. could be obtained. To check on whether Co_3O_4 at 850°C was stable under this minimum obtainable oxygen partial pressure a simple experiment was performed. 100.13 gms of cobalt oxide(s)/zinc oxide pellets* (-4.75 + 1.6 mm) were charged to the reactor which was then inserted into the furnace (set at 850°C). An Ar-O_2 gas mixture flowing at a total rate of 1002 mls_{NTP}/min, having a bed exit oxygen partial pressure of 0.043 atmospheres, was then passed through the reactor for 137 minutes. During this time the temperature recorded at the exit end of the bed remained constant at 852 $\pm \frac{1}{2}$°C. After the reactor had been removed from the furnace it was reweighed (cold); a weight loss of 0.39 gms was recorded. An approximate calculation shows that if before the experiment all the cobalt in the bed had been in the form of Co_3O_4 and this had subsequently decomposed to CoO a weight loss of about 2.5 gms would have occurred. The actual weight loss of 0.39 gms is therefore not entirely conclusive in proving that Co_3O_4 is stable at 852°C under an oxygen partial pressure of 0.043 atmos. There

---

* Considering the heat treatment that these pellets received during their manufacture the cobalt was expected to be present as Co_3O_4. X-ray diffraction analysis of unreacted pellets confirmed this belief. For full details see appendix M.

are two possible explanations for the small weight loss.

a) Combination of the effects of experimental error, desorption of water (observed after heating ZnO pellets which had been exposed to the atmosphere) and decomposition of Co_2O_3 to Co_3O_4.
b) Slow decomposition of Co_3O_4 to CoO.

A further experiment (involving bed CZS3 prior to its chlorination) was thus carried out in an attempt to clarify the situation. Firstly, pure oxygen was passed* through the mixed oxide bed (-4.75 + 1.6 mm pellets, 149.7 gms) for about 5 minutes; this was followed by an Ar-O_2 gas mixture (P_{O_2} = 0.041 atmos., flow = 1001 mls_{NTP}/min) flowing for 37 minutes; finally, pure oxygen was once again passed* for about 5 minutes. Throughout this procedure the recorded temperature near to the bed exit remained steady at 853 $\pm \frac{1}{2}^{o}C$. Consequently, it is felt that this result, especially as there was no detectable exothermic 're-oxidation' with the final oxygen flush, confirms that Co_3O_4 is stable at 853°C under a P_{O_2} of 0.041 atmos. This finding is in agreement with one of the sets of data given in appendix K (see graph K1).

5G1c Results of experiment series - Co_3O_4/ZnO - 850°C:- Details on the experimental procedure employed for this series of runs are given in section 4B2e. Three important points deserve special mention:

a) Prior to chlorination each bed was conditioned either with O_2-N_2, O_2-Ar or O_2 at an oxygen partial pressure close to that which would be in operation at the bed exit during chlorination. (This conditioning stage was also intended to oxidise any traces of CoO to Co_3O_4.)
b) After chlorination each bed was again flushed through with gas (as above) having an oxygen partial pressure close to that which operated at the bed exit during chlorination.
c) With each run the temperature near to the bed exit was chart recorded.

In this series of experiments 21 runs (CZS3 to CZS23 inclusive) were carried out, each within the temperature range 852°C - 854°C. At each oxygen partial pressure experiments were repeated at least four times. The bed mass was varied between about 70 gms and 200 gms whilst the chlorinating-gas flow was kept fairly constant at 350 mls_{NTP}/min, with

---

* The flow was not measured but is estimated to have been about 500 mls/min

a chlorine content of around 7% to 8%. Full sets of data for these runs are given in appendix J. The equilibrium constant* given for reaction - (5) section 5G is

$$K_p = \frac{{}^{x}P_{ZnCl_2}}{{}^{x}P_{CoCl_2} \cdot {}^{x}P_{O_2}^{1/6}} \quad \ldots\ldots\ldots\ldots\ldots (1)$$

The value of K_p is constant at a given temperature therefore

$$\log_{10}K_p + 1/6\log_{10}{}^{x}P_{O_2} = \log_{10}\left\{{}^{x}P_{ZnCl_2}/{}^{x}P_{CoCl_2}\right\} \quad \ldots\ldots (2)$$

(T - constant)

Presented in table 5B are the experimental results for runs CZS3-CZS23. The calculated values of $\log_{10}{}^{x}P_{O_2}$ and $\log_{10}\left\{{}^{x}P_{ZnCl_2}/{}^{x}P_{CoCl_2}\right\}$ have been plotted against each other on graph 5C. The predicted slope for this plot is 1/6, with an intercept of $\log_{10}K_p$. Three lines are drawn on graph 5C. The broken line has a gradient of 1/6, it is not related to the plotted data and has only been drawn for the purpose of comparison. Line A is a best fit [to equation (2)] line calculated for the least sum of the squares of $\log_{10}{}^{x}P_{ZnCl_2}/{}^{x}P_{CoCl_2}$ from $\log_{10}{}^{x}P_{O_2}$. The computed gradient and intercept of this line are 1/4.83 and 2.668 (K_p = 466 atmos$^{-1/6}$) respectively. Line B is also a best fit line calculated by the method of least squares, but in this case for $\log_{10}{}^{x}P_{O_2}$ from $\log_{10}{}^{x}P_{ZnCl_2}/{}^{x}P_{CoCl_2}$. The gradient and intercept of this line are 1/4.54 and 2.676 (K_p = 474 atmos.$^{-1/6}$) respectively.

In reporting these results (850°C - Co_3O_4/ZnO) mention should be made of an unusual phenomena detected on the chart records of the bed temperature. During both pre-chlorination bed conditioning and post-chlorination bed flushing the recorded temperature (near to the bed exit) remained steady to within $\pm \frac{1}{2}$ deg.C. However, the temperature recorded during the chlorination stage of each run was not steady for the whole of the reaction period. Although none of the temperature charts were identical they all showed the same general effect. Typically the temperature remained quite steady for about 4 to 10 minutes, it then fairly rapidly increased by between 2 to 7 deg.C. and then equally rapidly returned to the initial value. This effect on average took 4 minutes from start to finish. Of all the experimental variables, the only correlation appeared to be with bed mass. A relatively small bed (70 gms) produced the greatest temperature

---

* x = bed exit value

Experiment number	Initial bed weight - gms	Total gas[x] flow mls_{NTP}/min	$x_{P_{ZnCl_2}}$ Atmos. $\times 10^{-2}$	$x_{P_{CoCl_2}}$ Atmos. $\times 10^{-4}$	Temperature[x] °K	$\log_{10}\left(x_{P_{ZnCl_2}}/x_{P_{CoCl_2}}\right)$	$\log_{10} x_{P_{O_2}}$	$x_{P_{ZnCl_2}}/x_{P_{CoCl_2}}$	$x_{P_{O_2}}$ Atmos.	ΔG° cals/mole
CZS3	149.79	347	6.66	2.95	1126	2.354	-1.461	226	0.0346	-13380
CZS4	89.58	350	7.20	3.07	1126	2.369	-1.428	234	0.0373	-13430
CZS5	68.23	350	7.08	3.04	1126	2.368	-1.435	233	0.0367	-13430
CZS6	118.16	343	6.54	2.66	1126	2.390	-1.470	245	0.0339	-13570
CZS7	198.88	338	5.67	2.31	1125	2.391	-1.532	246	0.0294	-13620
CZS8	197.24	337	8.76	1.99	1125	2.644	-0.032	441	0.928	-13640
CZS9	99.59	350	7.44	1.51	1125	2.691	-0.026	491	0.941	-13870
CZS12	199.89	340	6.26	1.21	1126	2.712	-0.026	515	0.941	-13990
CZS13		349	7.87	1.50	1126	2.719	-0.034	524	0.925	-14040
CZS10	120.37	350	6.91	1.82	1125	2.580	-0.432	380	0.370	-13650
CZS11	100.60	346	6.96	1.75	1125	2.600	-0.430	398	0.371	-13750

x = bed exit value

TABLE 5B (Part 1): Co_3O_4/ZnO - 850°C EQUILIBRIUM RESULTS

Experiment number	Initial Bed weight - gms	Total gas flow mls_{NTP}/min	$x_{P_{ZnCl_2}}$ Atmos $x10^{-2}$	$x_{P_{CoCl_2}}$ Atmos $x10^{-4}$	Temperature ^{o}K	$\log_{10}\left(x_{P_{ZnCl_2}}/x_{P_{CoCl_2}}\right)$	$\log_{10} x_{P_{O_2}}$	$x_{P_{ZnCl_2}}/x_{P_{CoCl_2}}$	$x_{P_{O_2}}$ Atmos.	ΔG^{o} cals/mole
CZS14	153.16	347	6.36	1.65	1126	2.586	-0.436	385	0.366	-13700
CZS15		356	8.10	2.27	1126	2.552	-0.435	356	0.367	-13520
CZS16	140.41	347	7.15	2.29	1126	2.494	-0.717	312	0.192	-13470
CZS17		350	8.44	2.77	1126	2.484	-0.710	305	0.195	-13410
CZS18	145.16	343	7.09	2.19	1125	2.510	-0.714	324	0.193	-13540
CZS19		351	8.61	2.68	1125	2.507	-0.703	321	0.198	-13510
CZS20	165.95	345	6.71	1.64	1126	2.613	-0.182	410	0.658	-13620
CZS21		353	8.13	2.12	1126	2.584	-0.187	384	0.650	-13470
CZS22	158.12	343	6.57	1.50	1127	2.643	-0.180	440	0.660	-13790
CZS23		350	8.24	2.07	1126	2.600	-0.186	398	0.651	-13550

x = bed exit value

TABLE 5B (Part 2): Co_3O_4/ZnO - 850°C EQUILIBRIUM RESULTS

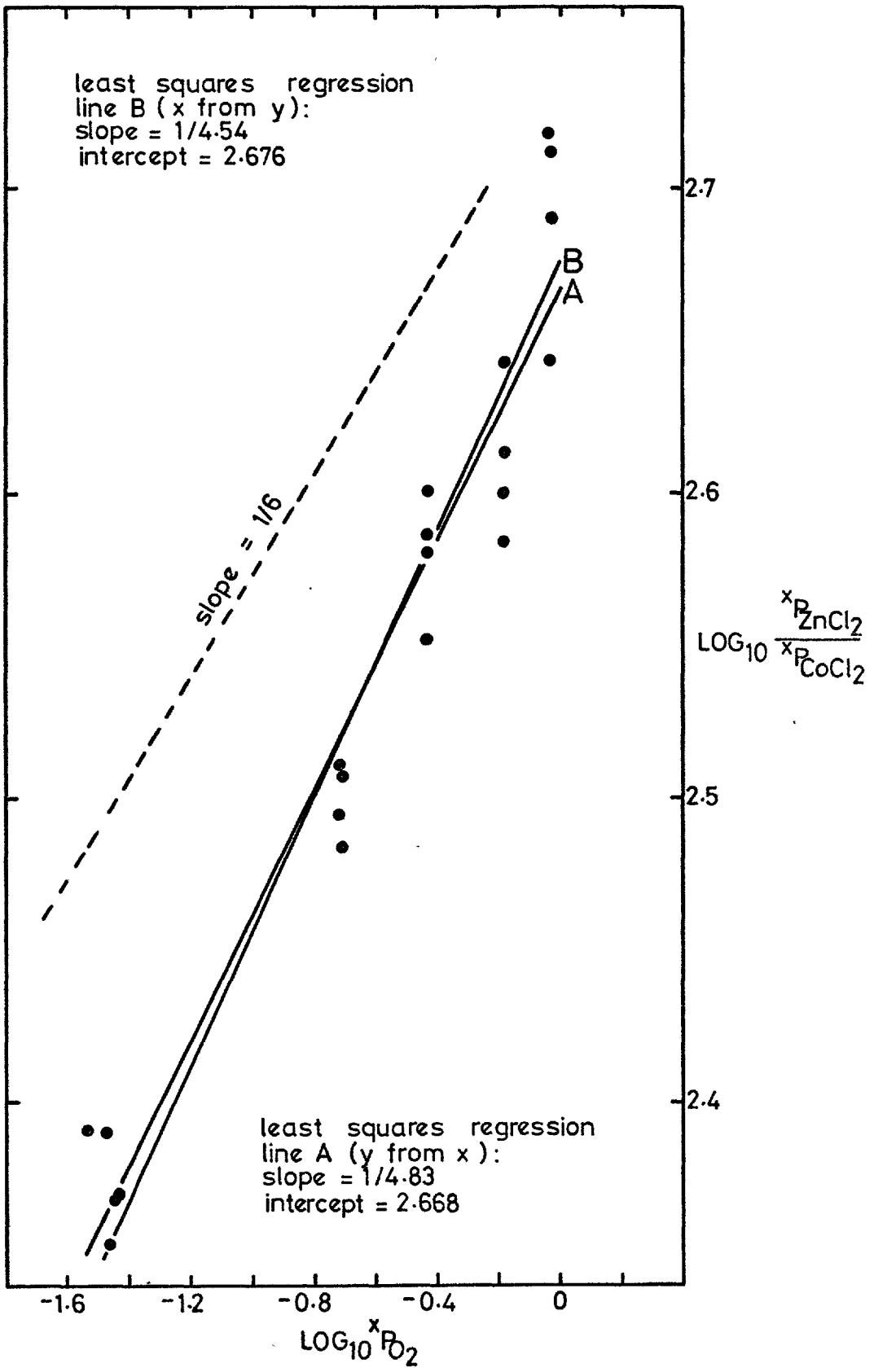

GRAPH 5C: MEASURED EFFECT OF OXYGEN PARTIAL PRESSURE ON THE Co_3O_4/ZnO CHLORINATION-VOLATILISATION EQUILIBRIUM. DATA FROM TABLE 5B.

rises, these being at an early stage of reaction; for relatively large beds (200 gms) the converse behaviour was observed. The overall appearance was that of a degrading temperature wave moving down the bed; a discussion of this effect appears in section 6A3.

5G1d Results of runs CZS26 and CZS27:- Six experiments (3 different sets of conditions - each performed twice) were carried out on the system cobalt oxide(s)/zinc oxide at 928-929°C. At the time they were performed it was assumed that CoO was the stable oxide of cobalt present under oxygen partial pressures used (P_{O_2} values of 0.039, 0.19 and 0.94 atmos.). Subsequent examination of the experimental results and the best available thermodynamic data on cobalt oxides shows that Co_3O_4 was stable at the highest P_{O_2} value employed. Four separate observations all confirm that runs CZS26 and CZS27 were on the system Co_3O_4/ZnO whilst the remaining four were on the system CoO/ZnO. These observations are:

a) Four of the five sets of data presented in appendix K (see graph K1) indicate that at 928°C under a P_{O_2} of 0.93 atmos. Co_3O_4 is the stable oxide of cobalt; they also show that under the other two oxygen partial pressures used CoO is stable.

b) Agreement between the measured weight decrease of the oxide bed and the calculated weight decrease (based on the condensate analysis) was good only with runs CZS26 and CZS27. The measured weight loss with the other runs was in each case over twice the calculated weight loss. The explanation of this apparent inconsistency is that at P_{O_2} = 0.93 atmos. measured weight changes were due only to ZnO and Co_3O_4 loss, however at the lower oxygen partial pressures weight change was caused not only by ZnO and CoO loss but also by Co_3O_4 decomposition.

c) With experiments at the two lower oxygen partial pressures values of $^xP_{ZnCl_2}/^xP_{CoCl_2}$ are in reasonably good agreement, however, they are not in agreement with the values for the high P_{O_2} runs. This behaviour is consistent with there having been a transition from the system Co_3O_4/ZnO to CoO/ZnO as the oxygen partial pressure was decreased.

d) During pre-chlorination bed conditioning at the lower oxygen partial pressures a temporary temperature drop of between 20 and 35 deg.C was recorded. This effect was not observed at the high oxygen partial pressure.

An explanation of this phenomena is given in section 5G1a. Full sets of data for these two experiments may be found in appendix J. Data relevant to this section is given in table 5C below.

Experiment number	Initial bed weight - gms	Total gas flow^{x} mls_{NTP}/min	$^{x}P_{ZnCl_2}$ atmos $x10^{-2}$	$^{x}P_{CoCl_2}$ atmos $x10^{-4}$
CZS26	136.52	344	6.98	4.36
CZS27		349	7.89	3.93

Experiment number	Temperature ^{o}K	$^{x}P_{O_2}$ atmos	$\frac{^{x}P_{ZnCl_2}}{^{x}P_{CoCl_2}}$	$\frac{^{x}P_{ZnCl_2}}{^{x}P_{CoCl_2} \cdot {}^{x}P_{O_2}^{1/6}}$
CZS26	1202	0.948	160	161
CZS27	1202	0.939	201	203

TABLE 5C: $928^{o}C$ - Co_3O_4/ZnO EQUILIBRIUM RESULTS
x = bed exit value

5G2 CoO/ZnO results

Experiments in this series were carried out according to the same procedure used for the Co_3O_4/ZnO runs; main details are given in section 4B2e. Two experiments were performed under each specific set of conditions. Complete sets of data for each run are given in appendix J. Calculated results for these experiments (CZS 1, 2, 24, 25, 28-41) are presented in table 5D. In this section no further explanation of the data is required, the only points to be made concern the temperature charts taken during each run.

At temperatures over $930^{o}C$, experiments on the system CoO/ZnO employed an external thermocouple for measuring the bed temperature (see section 3D4). Traces obtained from this thermocouple position indicated no detectable temperature variation with any of the experiments. However, since the thermocouple was directly viewed by the inside of the muffle tube whilst being separated from the oxides by a thickness of silica and mullite, steady temperature traces did not necessarily confirm the absence of small temperature variations within the reactor. Only the runs at

Experiment number	Initial bed weight - gms	Total gas flow^{x} mls_{NTP}/min	$^{x}P_{ZnCl_2}$ Atmos $x10^{-2}$	$^{x}P_{CoCl_2}$ Atmos $x10^{-4}$	$^{x}P_{O_2}$ Atmos	Temperature ^{o}K	$^{x}P_{ZnCl_2}/^{x}P_{CoCl_2}$ Dimensionless
CZS24	133.18	350	7.51	5.16	0.038	1201	146
CZS25		352	8.04	5.06	0.040	1201	159
CZS28	130.38	349	7.48	4.59	0.19	1201	163
CZS29		352	8.38	5.48	0.19	1201	153
CZS34	150.84	349	7.39	3.49	0.93	1237	212
CZS35		351	8.03	4.68	0.93	1237	172
CZS32	129.60	344	6.84	4.62	0.94	1277	148
CZS33		349	7.94	4.36	0.93	1277	182
CZS30	128.34	349	6.88	6.45	0.035	1276	107
CZS31		356	8.11	4.61	0.041	1276	176
CZS36	151.02	349	8.27	5.51	0.92	1306	150
CZS37		350	8.03	5.97	0.92	1306	135
CZS38	150.79	356	8.40	6.30	0.042	1305	133
CZS39		353	7.97	7.06	0.040	1305	113
CZS40	152.11	349	8.09	6.05	0.93	1339	134
CZS41		352	8.31	5.56	0.93	1339	150
CZS1	92.54	346	6.14	3.27	0.031	1177**	188
CZS2		355	7.98	3.25	0.040	1177**	245

x = bed exit value

** = Initial temperatures. Values of 1168 used for calculations

TABLE 5D: CoO/ZnO EQUILIBRIUM RESULTS

928-929°C employed an internal thermocouple (except also CoO/ZnO runs CZS1 and CZS2 at 904°C). The temperature traces from these four 928°C runs were exactly as expected, both in terms of previous experience and theoretical predictions. Once pre-chlorination bed conditioning had commenced a temperature drop of up to 35 deg.C was recorded. This persisted for nearly 20 minutes whilst the Co_3O_4 endothermically decomposed; over about 10 minutes the temperature then returned to the original steady value. During chlorination the same temporary temperature rise effect, as seen with all the previous cobalt oxide(s)/zinc oxide runs, was recorded. Post-chlorination reactor flushing produced no temperature fluctuations. Returning to the charts obtained using the external thermocouple, it seems reasonable to assume that the small temperature oscillation present in the below 930°C experiments did occur with the higher temperature runs but was not detected. With these higher temperature runs (964°C and upwards) a large temperature drop was not expected during bed conditioning since most of the Co_3O_4 would already have spontaneously decomposed due to its equilibrium oxygen dissociation pressure being appreciably greater than 1 atmosphere.

5G3 Calculated standard free energy changes for cobalt oxide(s)/zinc oxide experiments

In this section the calculated standard free energy changes for reactions (4) and (5) - section 5G are presented. Values of K_p, T and ΔG°_T for each experiment are given in table 5E. For the system Co_3O_4/ZnO three ΔG°_T values have been calculated, one each for runs CZS26 and CZS27 and one for 853°C (1126°K) runs CZS3-23. With this series of 21 experiments an arithmetic mean $\Delta G^\circ_{1126^\circ K}$ value is presented, the individual values from which this mean has been computed are given in table 5B. For the system CoO/ZnO 18 ΔG°_T values have been calculated; the only point of difference from data presented in table 5D is the use of T = 1168°K (895°C) for runs CZS1 and CZS2. This is 9 deg.K below the temperature at the start of the runs, but was the eventual steady reading at the bed exit. The computed standard free energy change values are plotted against T°K on graph 5D. The decomposition of Co_3O_4 has been examined in some detail in appendix K. From the presented data (appendix K) the most reliable dissociation temperature (at which Co_3O_4, CoO and O_2 may all coexist in their standard states) appears to be 1228°K (955°C). A vertical broken line has thus been drawn at 1228°K on graph 5D to indicate the regions of stability of the two oxides.

SYSTEM Co_3O_4/ZnO Decomposition temperature of Co_3O_4 = 1228°K (P_{O_2} = 1 atmos)

Experiment number	K_p Atmos$^{-1/6}$	Temperature °K	ΔG° cals/mole
CZS3-23	439	1126	-13620
CZS26	161	1202	-12140
CZS27	203	1202	-12700

SYSTEM CoO/ZnO

Experiment number	K_p Dimensionless	Temperature °K	ΔG° cals/mole
CZS1	188	1168	-12150
CZS2	245	1168	-12770
CZS24	146	1201	-11890
CZS25	159	1201	-12100
CZS28	163	1201	-12160
CZS29	153	1201	-12010
CZS34	212	1237	-13170
CZS35	172	1237	-12650
CZS32	148	1277	-12680
CZS33	182	1277	-13210
CZS30	107	1276	-11850
CZS31	176	1276	-13110
CZS36	150	1306	-13000
CZS37	135	1306	-12730
CZS38	133	1305	-12680
CZS39	113	1305	-12260
CZS40	134	1339	-13030
CZS41	150	1339	-13330

TABLE 5E: CALCULATED STANDARD FREE ENERGY CHANGES

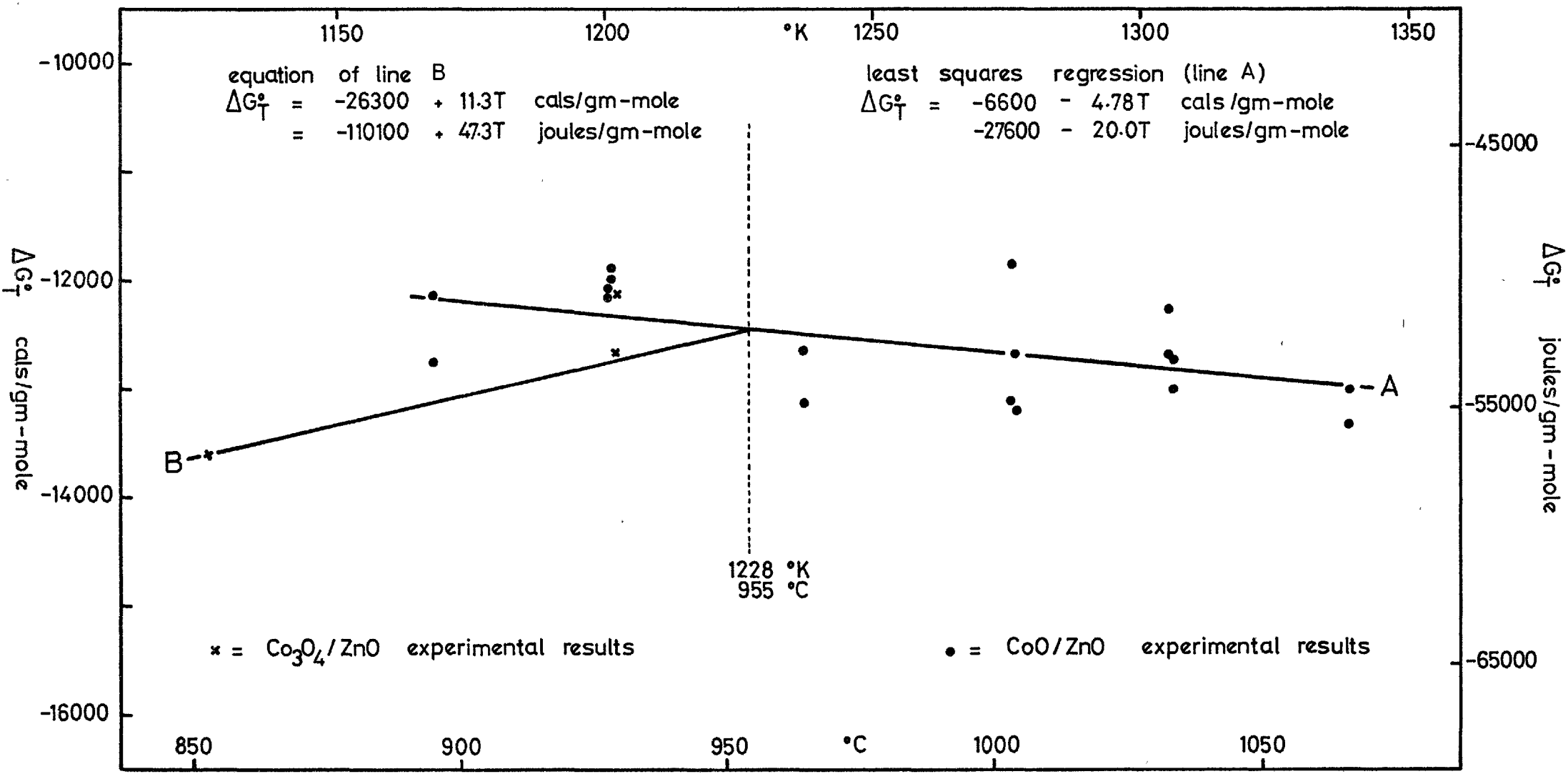

GRAPH 5D: STANDARD FREE ENERGY CHANGE OF REACTION

(B) $CoCl_{2(g)} + ZnO_{(s)} + 1/6O_{2(g)} = ZnCl_{2(g)} + 1/3Co_3O_{4(s)}$

(A) $CoCl_{2(g)} + ZnO_{(s)} = ZnCl_{2(g)} + CoO_{(s)}$

DATA FROM TABLE 5E

5G3a Analysis of calculated standard free energy changes:- Line A drawn on graph 5D is a best fit linear equation calculated by the method of least squares (ΔG°_{T} from T) for the CoO/ZnO data. The equation of this line is:

ΔG°_{T} = -6600 - 4.78T cals/mole
= -27600 - 20.0T joules/mole

it applies for the reaction

$CoCl_{2(g)} + ZnO_{(s)} = ZnCl_{2(g)} + CoO_{(s)}$

over the temperature range 1168°K to 1339°K. The standard enthalpy and entropy changes (within the specified temperature range) are:

ΔH° = -6600 cals/mole
-27600 joules/mole

ΔS° = +4.78 cals/mole°K
+20.0 joules/mole °K

Line B has been drawn between two points, a) the point given by the results of runs CZS3-23, b) the intersection of line A with the dissociation temperature of Co_3O_4. The equation of line B is:

ΔG°_{T} = -26300 + 11.3T cals/mole
-110100 + 47.3T joules/mole

it applies for the reaction

$CoCl_{2(g)} + ZnO_{(s)} + 1/6\ O_{2(g)} = ZnCl_{2(g)} + 1/3\ Co_3O_{4(s)}$

over the temperature range 1126°K to 1228°K. The standard enthalpy and entropy changes (within the specified temperature range) are:

ΔH° = -26300 cals/mole
-110100 joules/mole

ΔS° = -11.3 cals/mole °K
-47.3 joules/mole °K

The boiling point[3] of $CoCl_2$ is 1025°C. It thus cannot exist in its defined standard state at below this temperature. That at below 1025°C standard free energy changes have been calculated with reference to a hypothetical $CoCl_2$ standard state does not invalidate the presented equations and plots since correction to a new standard state (liquid $CoCl_2$) is a simple procedure.

CHAPTER SIX

DISCUSSION OF EQUILIBRIUM RESULTS

Discussion of the results of the equilibrium experiments can essentially be divided into three separate sections, the main contents of which are: a) the overall experimental method, b) treatment of the experimental results and c) comparison of the results with previous work. Since the same experimental technique and basic theoretical analysis was used for the CdO/ZnO, Co_3O_4/ZnO and CoO/ZnO studies it is possible, for the most part, to discuss in parallel matters common to each of these three systems. Only in the last section is it necessary to finally consider each system independently.

6A EXPERIMENTAL METHOD AND ERRORS

The experimental apparatus and experimental procedures used for the equilibrium runs are fully discribed, together with evaluations of some sources of errors, in chapters 3 and 4.

6A1 Gas-solid equilibrium

The foundation upon which the analysis of these experimental results is based, is that during each experiment chemical equilibrium (or an insignificant deviation from a state of equilibrium) was reached between flowing gases and stationary solids before the bed exit. It is thus of primary importance, before discussing other points, to briefly review the experimental evidence which confirms that the necessary equilibrium conditions were always employed.

6A1a CdO/ZnO runs:- With the CdO/ZnO experiments, over the whole temperature range studied (370 deg.C) variations in gas flow rate and bed size produced no evidence of divergence from equilibrium. Results obtained from this system also showed good individual run reproducibility and excellent overall consistency. In chapter 7 results of non-equilibrium experiments performed on this same system are reported. With these runs at between 750 and 950°C, using conditions at least an order of magnitude less favourable for the attainment of equilibrium in comparison to those used for the equilibrium runs, initial rates of production of $CdCl_{2(g)}$

and $ZnCl_{2(g)}$ (from a packed bed prior to significant depletion) were very close to those predicted by the equilibrium experiments. Results of the packed bed non-equilibrium ZnO chlorination experiments, reported in chapter 7, showed that overall reaction rates were high even at a temperature as low as 705°C. These two sets of results, even if only approximately applied to the CdO/ZnO equilibrium runs, predict a rapid and complete approach to equilibrium under the experimental conditions that were employed. As final confirmation of the true equilibrium nature of the experiments performed there are, for comparison, the results of previous workers[31].

6A1b Cobalt oxide(s)/Zinc oxide runs:- With the cobalt oxide(s)/zinc oxide experiments the gas flows were kept nearly constant however, variations in bed mass had no correlated effect on the results. Although this system showed the greater amount of experimental scatter it appeared that it was entirely random and could not be related to any single reaction parameter. Since closely similar conditions were employed for these experiments as were used for the CdO/ZnO runs, by analogy each set of results lends support to the other.

Before it can be finally accepted that all the cobalt oxide(s)/zinc oxide experiments were achieving true equilibrium, this section must examine what would have been the effect if Co_3O_4 and CoO (one being stable, the other unstable) had co-existed in the bed at the same time. Prior to their chlorination all the oxide charges were conditioned in order to ensure that only stable cobalt oxide (that corresponding to each particular operating temperature and oxygen pressure) would be present. X-ray diffraction analysis of chlorinated ZnO/CoO and ZnO/Co_3O_4 pellets showed that after reaction and cooling two oxides of cobalt were never simultaneously present in either of the oxide mixtures (see appendix M). However, since no simple means was available for testing if all the cobalt was oxidised before chlorination to one state only*, it was possible that Co_3O_4 and CoO may have been simultaneously present, although in disproportionate amounts, during part of some of the experiments.

---

* Following bed temperatures during bed conditioning clearly showed when oxidation or de-oxidation were occurring, however this effect gave no definite indication of the completeness of these reactions.

Intuitively it might be thought that if equilibrium in the system $Co_3O_{4(s)}$ - $O_{2(g)}$ - $CoO_{(s)}$ had not been fully arrived at, then this would have prevented the attainment of a true state of equilibrium between the gaseous chlorides ($ZnCl_2$ and $CoCl_2$) and the solid oxides (ZnO/Co_3O_4). With experiments CZS3-CZS23 (the 850°C - Co_3O_4/ZnO runs) since the oxygen partial pressure was always maintained above the equilibrium decomposition pressure there would have been no CoO formation. X-ray diffraction analysis of the unreacted pellets (see appendix M) showed that they consisted only of ZnO and Co_3O_4. For these runs the problem of the co-existence of CoO and Co_3O_4 therefore did not arise. As explained in section 5G1d, runs CZS26 and CZS27 (929°C) were carried out at an oxygen partial pressure under which Co_3O_4 is stable, whilst the other 929°C experiments were performed using conditions under which CoO is stable. Although with runs CZS26 and CZS27 a small amount of Co_3O_4 decomposition might have occurred during inserting the reactor (in air) into the furnace, a pre-chlorination bed conditioning of 21 minutes (547 mls_{NTP}/min, P_{O_2} = 0.93 atmos.) was carried out. The probability of there having been anything more than an insignificant trace of CoO present was thus extremely doubtful.

Experiments CZS1, 2, 24, 25, 28-41 employed temperatures and oxygen pressures at which the stable oxide system was CoO/ZnO. During the conditioning stage of these runs, prior to chlorination, the intention was to decompose any Co_3O_4 present to CoO. Although with runs CZS1 and CZS2 this aim was not realised (see section 5G1a) and with the other runs there was no certain check that full decomposition had been achieved, by considering the most probable overall decomposition behaviour (also valid for oxidation) of the bed of pellets it can be argued that the existence of small amounts of Co_3O_4 would not have interfered with the equilibrium being studied. The large recorded temperature falls (see section 5G2) and rises (see section 5G1a) due to Co_3O_4 decomposition and CoO oxidation indicated that with the packed bed configuration used, overall rates for these two reactions were quite high. In the literature[74,83,84] there are no reports indicating solid solubility between CoO and Co_3O_4, therefore (excluding the possible effects of solution with ZnO) both of these oxides would have been present at or near to unit activity. Even though the physical structure of the cobalt oxide(s)/zinc oxide pellets was not examined, since sub micron sized oxide powders were used for their

manufacture it is reasonable to assume that gaseous diffusion within the pellets (quite possibly under a Knudsen-molecular mixed regime) was the major rate controlling resistance to the oxidation and de-oxidation reactions, especially since the specific surface area of the cobalt oxide(s) was large, which would therefore have resulted in high overall interfacial rates. With pellets this relative condition of high chemical reactivity and low transport rates gives rise to a topochemical reaction (shrinking core) process. A partially decomposed (Co_3O_4 - CoO) pellet would thus have consisted of a shell of CoO/ZnO surrounding a core of Co_3O_4/ZnO. With an incompletely decomposed bed the upper pellet shell-thickness would be greater than that at the bed bottom; even so the exchange reaction

$$CoCl_{2(g)} + ZnO_{(s)} = ZnCl_{2(g)} + CoO_{(s)}$$

would be able to reach and maintain equilibrium before the bed exit. The dissociation oxygen pressure of Co_3O_4 exceeds 1 atmosphere at above about 950°C. Thus decomposition to CoO would have tended to occur spontaneously with experiments above this temperature, being accelerated to some degree by bed conditioning. The only experiments that could appear to be doubtful are CZS1 and CZS2 during which decomposition was still proceeding alongside chlorination. However, since a shell of CoO/ZnO almost certainly surrounded each pellet these two runs can be treated as true equilibrium determinations. In conclusion two points may be made:

a) If unstable cobalt oxide existed in any of the pellet charges during chlorination it was present in small to negligible amounts.
b) The physical distribution of any unstable cobalt oxide was such that it did not influence the equilibrium being measured.

Whilst considering qualitative reaction behaviour it is of interest to briefly outline the sequence of reactions occurring down the mixed oxide beds during chlorination. The following description has been quantitatively verified for the CdO/ZnO system (see chapters 7 and 8). Chemical reactivities at similar temperatures to those employed in this study, for reactions of the type OXIDE + CHLORINE = VOLATILE CHLORIDE + OXYGEN are comparatively high (provided ΔG° is -Ve). Consequently, with the systems studied in this work, on entering the packed beds, the chlorine would have tended to rapidly react with whichever oxide was first contacted: the rates of production of the respective chlorides being governed by chemical kinetic, mass transport and physical parameters. Even though it is probable that

in the uppermost section of each bed the oxide chlorine reaction having the largest -ve ΔG^{o} value would have initially predominated (before the top pellets were depleted of this their most reactive component thus setting up a diffusional resistance to reaction) it is very unlikely that the distribution of gaseous chlorides in this section of the bed would have been anything approaching that found at equilibrium*. The CdO/ZnO non-equilibrium results show that resistance to chemical reaction was much less than that to gaseous diffusion in the porous pellets. By considering a pelletised admixed-oxide system Ao/Bo (that forms chlorides Ac and Bc for which the equilibrium ratio Ac/Bc is large) having this same overall reaction behaviour the point being made can easily be explained. There are two possible reaction modes for a pellet in the chlorine reaction zone:

a) If Ao reacts with chlorine faster than does Bo, after passage of time a layer of Bo depleted of Ao will surround an Ao/Bo core. With this behaviour the rate of production of Ac quickly falls whilst that of Bc increases, this being in the opposite direction to that required for Ac-Bc equilibrium.

b) If Bo reacts faster than does Ao, then from the start of reaction production of Ac and Bc are in opposition to the equilibrium requirements. As the reaction proceeds, rates of Ac and Bc production do tend to move more towards equilibrium but not to a particularly signficant extent.

These two cases may be summed up as follows: in a mixed oxide-chlorine system where chemical reactivities are high in comparison to porous-solid gaseous diffusivities, there will always be significant deviation from equilibrium (that is if the Ac/Bc equilibrium constant is comparatively large and it is not at the very start of reaction) in the region where the chlorine is reacting. The oxide beds used for the equilibrium experiments can thus be seen in terms of two zones (in which there were different predominating reaction processes). There was a short initial zone where almost all the chlorine rapidly reacted, followed by a variable length 'scrubbing' zone where the exchange reaction Bc + Ao = Ac + Bo moved to equilibrium.

---

* Except when the bed entry was virtually unreacted.

6A2 Errors in experimental measurements

Sources of experimental error associated with the equilibrium results can be divided into four separate groups.

a) Temperature measurement
b) Collection and analysis of condensates
c) Gas flows (and purities)
d) Unidentified errors due to the experimental method, procedures and apparatus.

With the internal thermocouple the measured bed exit temperature is estimated to have been accurate to ± 1 deg.C. Using the external thermocouple the accuracy of the measured temperature was slightly less, being estimated at ± 2 deg.C. These two thermocouples are described in sections 3D3 and 3D4 respectively.

The method of condensate collection is described in section 4B1d (also see section 3D5 for information on condenser exit gas filtration). Analysis of the condensates, by atomic absorption spectrophotometry, is described in section 4B1e (and appendix E) where the maximum (random) error associated with Co, Zn and Cd analyses has been estimated to be ± 3%.

Details on the gas train, flow meters, their calibration and the purities of the different gases used are given in various subsections contained within section 3E. It has been estimated that the gas flows delivered via the flow meters were known to within about ±1%. One exception was, however, discovered; this concerned chlorine orifice "C5" (see section 4C3) where the error appeared to be as much as -12%. Since calculations for the equilibrium experiments did not rely upon knowing the chlorine flow rate this error, in relation to these experiments, is thus of no consequence.

The final grouping of errors includes all the unknown factors combined within the overall experimental procedure. Since no systematic or illegitimate errors could be identified under this category, they have been treated as random errors.

None of the errors reviewed in the preceding four paragraphs appear to be systematic, thus all errors in the calculated equilibrium results are taken as being random. Computed standard deviations are presented in section 6B5.

6A3 Temperature oscillation during cobalt oxide(s)/zinc oxide experiments

The small temperature fluctuation that was observed during the chlorination stage of the cobalt oxide(s)/zinc oxide experiments is described in section 5G1c (it is also referred to in section 5G2). This phenomena was not detected during the ZnO/CdO experiments. It is not thought to have been produced by variations in the furnace temperature. Therefore, it seems likely that it was due to an exothermic physical or chemical phenomenon that only occurred (or was detected) during chlorination of the cobalt oxide(s)/zinc oxide system. By considering the oxide bed in terms of two reaction zones, as described in section 6A1b, a possible qualitative explanation of this effect can be given. The work of Orlov and Jeffes[31], when corrected with respect to ΔS° (see section 6C1) indicates for the reaction $ZnO + Cl_2$* a ΔH° value of 17190 cals/mole. By combining this value with the standard free energy equations presented in chapter 5 the following standard heats of reaction have been computed:
$CdO + Cl_2$* — ΔH° = 8240 cals/mole, $CoO + Cl_2$* — ΔH° = 24510 cals/mole
$1/3Co_3O_4 + Cl_2$* — ΔH° = 44210 cals/mole. These enthalpy changes are quite strongly endothermic. During equilibrium chlorination the upper section of each bed, in which all the chlorine is considered to react is thus called upon to provide heat, which therefore results in a local temperature fall. In the remainder of the bed the METAL CHLORIDE - METAL OXIDE exchange reaction then proceeds to equilibrium. Experimental data shows that for exchange reaction $ZnCl_2$ - ZnO ΔH° is -9670 cals/mole; for exchange reaction $CoCl_2$ - CoO ΔH° is -6600 cals/mole and for exchange reaction $CoCl_2$ - $1/3Co_3O_4$ ΔH° is -26300 cals/mole. Therefore, as a result of these exothermic heats of reaction a temperature rise occurs in the 'scrubbing' zone of the oxide beds. From the start of a chlorination run an unsteady temperature profile would thus be set up down the bed. Although at the beginning of reaction the region affected might only be a small proportion of the total bed depth, the temperature peak would tend to be carried down towards the exit by the flowing gas whilst leaving behind it a gradually stabilising temperature distribution. This complex phenomenon could account for the temperature oscillation recorded with the cobalt oxide(s)/zinc oxide runs. Why it was not detected with the CdO/ZnO experiments may have been because of differences in bed sizes, in ΔH° values and in the degree of importance of the exchange reaction.

---

* Gaseous products

6B TREATMENT OF EXPERIMENTAL RESULTS

Basic assumptions made for the purposes of calculating final experimental results are given in section 5E. They need no further mention here since they are straightforward and introduce very small overall error. The assumptions that do however need some justification are those concerning the activities of the metal oxides and the identities of the transported gaseous species.

6B1 Polymeric species

Keneshea and Cubicciotti[76] have studied the composition of vapour in equilibrium with molten $ZnCl_2$ by measuring the absolute vapour pressure directly and the apparent vapour pressure by a transpiration method. Over the temperature range of their investigation (411 to 578°C) they identified $ZnCl_2$ and Zn_2Cl_4. At 412°C the dimer was responsible for 13% of the total measured vapour pressure, at 500°C it contributed 6% whilst at 575°C it was further reduced to 3.8%. Extrapolation of this data shows that even at the lowest experimental temperature employed (703°C) zinc chloride dimer is an insignificant species. Keneshea and Cubicciotti[78], using the same method as above, have also investigated vapour compositions and pressures over molten $CdCl_2$ at temperatures just above its melting point. A monomer and dimer have been identified, however, in comparison, this dimer is less prominent than is the $ZnCl_2$ dimer. The CdO/ZnO experiments were performed over a range of chlorine partial pressures so that the effects of any significant polymerisation would influence the measured $CdCl_2/ZnCl_2$ equilibrium ratios. Considering a two chloride system, A and B each of which form dimers, the effect of polymerisation can be simply illustrated. The chloride exchange reaction (oxides at unit activity) is described by:

$$P_A/P_B = K_1 \quad \ldots\ldots\ldots\ldots\ldots\ldots\ldots\ldots\ldots\ldots (1)$$

The two dimerisation reactions can be described by:

$$2A_{(g)} = A_{2(g)} \quad \ldots\ldots P_{A_2}/P_A^2 = K_2 \quad \ldots\ldots\ldots\ldots (2)$$

$$2B_{(g)} = B_{2(g)} \quad \ldots\ldots P_{B_2}/P_B^2 = K_3 \quad \ldots\ldots\ldots\ldots (3)$$

These equations refer to a state of equilibrium at a single temperature. From the condensate analyses the equivalent monomeric chloride partial pressures are calculated.

$$P_{Aequiv} = P_A + 2P_{A_2} \quad \ldots\ldots\ldots\ldots\ldots\ldots (4)$$

$$P_{Bequiv} = P_B + 2P_{B_2} \quad \ldots\ldots\ldots\ldots\ldots\ldots (5)$$

Re-arranging equations 2, 3, 4 and 5, the measured chloride distribution ratio becomes:

$$\frac{P_{Aequiv}}{P_{Bequiv}} = \frac{P_A + 2K_2P_A^2}{P_B + 2K_3P_B^2} \quad \ldots\ldots\ldots\ldots\ldots\ldots (6)$$

If polymerisation is insignificant K_2 and K_3 are very small and equation (6) is indistinguishable from equation (1). Alternatively, if polymerisation is important, the left hand term of equation (6) will not be independent of the absolute values P_A and P_B. Since not even the slight scatter in measured $CdCl_2/ZnCl_2$ ratios correlated with variations in the absolute values of $^xP_{CdCl_2}$ and $^xP_{ZnCl_2}$ this further confirms that at the temperatures employed chloride polymerisation was of no consequence.

Schafer and Krehl[79] have measured the absolute vapour pressure over $CoCl_2$ from its melting point upwards (see section 5B). However, they have not identified any gaseous species. Schoonmaker and co-workers[37], using Knudsen effusion cells coupled to a mass spectrometer, have studied vapour compositions over solid $CoCl_2$ at up to 700°C. They detected monomeric and dimeric cobalt chloride; their estimated ΔG° and ΔH° values for the reaction

$$2CoCl_{2(g)} = Co_2Cl_{4(g)}$$

at 817°K are +9K cals and -35.5K cals respectively. These figures are sufficient evidence to demonstrate that at the experimental temperatures, 852°C minimum, used in this study gaseous cobalt chloride is effectively monomeric.

6B2 Complexes and other gaseous species

6B2a Complexes:- $CoCl_2$, $CdCl_2$ and $ZnCl_2$ are known to form gaseous complexes with monochlorides and trichlorides[40,41] (see section 1C3b). However, in the literature there appear to be no reports on the formation of complexes between either $CdCl_2$ and $ZnCl_2$ or $ZnCl_2$ and $CoCl_2$. Two other considerations both seem to suggest that complex formation between these two pairs of gaseous chlorides is either unlikely or insignificant. Firstly, present literature[40,41] indicates that complexes are almost entirely confined to chlorides of unequal valency; secondly, heats of

formation of complexes are highly exothermic[41] therefore their stabilities decrease rapidly with increasing temperature.

6B2b Other valency chlorides:- Schafer and Krehl[79] have studied the equilibrium

$$CoCl_{2(g)} + \tfrac{1}{2}Cl_{2(g)} = CoCl_{3(g)}$$

at between 900 and 1100°K; from their results they calculate the standard free energy change to be

$$\Delta G^{o}_{T} = -16900 + 18.15T \text{ cals/mole}$$

If this data is extrapolated to 1125°K, the lowest temperature at which cobalt oxide(s)/zinc oxide equilibrium measurements were taken, the following equilibrium relationship is obtained:

$$0.12\ P_{Cl_2}^{\frac{1}{2}} = \frac{P_{CoCl_3}}{P_{CoCl_2}} \qquad \text{(at } 1125^{o}K\text{)}$$

The maximum calculated equilibrium chlorine partial pressure present at the bed exit during any of the 850°C Co_3O_4/ZnO runs was about 0.0012 atmospheres. Therefore, under these conditions only 0.4% of the cobalt chloride would have existed in the trivalent form. Although not exact, this calculation does show that $CoCl_3$ is an unimportant species. (Another data source[85] however goes further than saying that the species is insignificant by suggesting that even the existence of $CoCl_3$ is doubtful.) Corbett and Lynde[86] studying the system

$$Zn_{(g)} + ZnCl_{2(g)} = 2ZnCl_{(g)}$$

at between 320 and 950°C have determined the following thermodynamic values: $\Delta H^{o}_{1125^{o}K} = +43.9K$ cals/mole, $\Delta G^{o}_{1125^{o}K} = +33.4K$ cals/mole. $ZnCl_{(g)}$ formation is thus not of concern to this study. The reaction

$$CdCl_{2(g)} + Cd_{(g)} = 2CdCl_{(g)}$$

has been investigated by Buddy, Bruner and Corbett[87] who derive the following data:

$\Delta H^{o}_{1000^{o}K} = +34.1K$ cals/mole, $\Delta G^{o}_{1000^{o}K} = +23.6K$ cals/mole: these thermodynamic values show the monovalent species to be unimportant in the present context.

6B2c Metal oxide decomposition:- The boiling points[3] of Zn, Cd and Co metal are 907°C, 765°C and 2900°C respectively. Zinc and cadmium (gas phase) transport may thus occur at comparatively low temperatures. With regard to the experiments under discussion the important factors are, a) the stabilities of the oxides, and b) the operating oxygen partial pressures. The two reactions of interest are given below together with their standard free energies of reaction[3].

$$Zn_{(g)} + \tfrac{1}{2}O_{2(g)} = ZnO_{(s)}$$

$$\Delta G^{\circ}_{T} = -115420 - 10.35T \log_{10}T + 82.38T \text{ cals/mole} \quad (1170 \text{ to } 2000^{\circ}K)$$

$$Cd_{(g)} + \tfrac{1}{2}O_{2(g)} = CdO_{(s)}$$

$$\Delta G^{\circ}_{T} = -87520 + 49.95T \text{ cals/mole} \quad (1242 \text{ to } 1379^{\circ}K)$$

The highest temperature employed during the equilibrium studies, 1345°K, was with the ZnO/CdO system. Using the free energy data given above to calculate the relevant equilibrium constants gives:

$$\frac{P_{O_2}^{\frac{1}{2}} \cdot P_{Zn}}{a_{ZnO}} = 1.5 \times 10^{-8} \quad (\text{at } 1345^{\circ}K) \qquad \frac{P_{O_2}^{\frac{1}{2}} \cdot P_{Cd}}{a_{CdO}} = 5.5 \times 10^{-4} \quad (1345^{\circ}K)$$

At the maximum chlorination temperature the lowest oxygen partial pressure used was 0.0312 atmospheres; assuming that the oxides were present at unit activity the predicted equilibrium Zn and Cd partial pressures are

$P_{Cd} = 3.1 \times 10^{-3}$ atmos

$P_{Zn} = 8.5 \times 10^{-8}$ atmos

These values indicate two important facts:

a) Although Zn atoms existed in the gas phase during chlorination, their contribution to the total quantity of zinc volatilised was insignificant.

b) For cadmium transport the effective "Cd" partial pressure may be written:

$$P_{"Cd"} = P_{Cd} + P_{CdCl_2}$$

The calculated bed exit $CdCl_2$ partial pressure (in reality $P_{"Cd"}$) for the 1345°K - P_{O_2} = 0.0312 atmos* experiment was 0.0595 atmospheres. Therefore if the equilibrium P_{Cd} value had been reached by the bed exit cadmium atoms would have accounted for about 5% of the total amount of

---

* Run S33

transported cadmium. This calculation is for the experiment in which the contribution due to gaseous Cd was potentially greatest.

If this same calculation is performed for some of the lower temperature runs the following results are obtained:

Run S32	1345°K	$Cd_{(g)}$ contribution = 1.7%
Run S30	1310°K	$Cd_{(g)}$ contribution = 1.6%
Run S11	1274°K	$Cd_{(g)}$ contribution = 0.13%
Run S10	1224°K	$Cd_{(g)}$ contribution = 0.09%

The calculated values given above are not claimed to be exact; they do however demonstrate that only at near to the maximum experimental temperature was $Cd_{(g)}$ transport in any way significant. It is felt that any attempt to apply corrections for this effect would not be worthwhile since there would be no noticeable change in the computed ΔG° values.

6B2d Vapour transport of oxides:- Kellogg[43] gives examples of metal oxide vapour species (eg $(PbO)_x$, $(SnO)_x$ and In_2O) and of complex metal oxide vapour species (eg $CaMoO_4$, $MgWO_3$, Sb_3AsO_6 and HBO_2). However, he points out that when zinc oxide and cadmium oxide are thermally decomposed the species $CdO_{(g)}$ and $ZnO_{(g)}$ are insignificant in comparison to $Cd_{(g)}$ and $Zn_{(g)}$. With regard to cobalt, there appears to be no evidence to suggest that there are any volatile oxide species.

6B3 Metal oxide activities

The crystal structures of the four oxides involved in this study are given below.

a) ZnO - Wurtzite hexagonal structure
b) CdO - NaCl cubic structure
c) Co_3O_4 - 2.3 type normal spinel
d) CoO - NaCl cubic structure

Radii of the various ions are[107]

Zn^{++}	= 0.074 nm	Cd^{++}	= 0.097 nm
Co^{++}	= 0.074 nm	Co^{+++}	= 0.063 nm
O^{--}	= 0.14 nm		

The different structures and cation radii of CdO and ZnO suggests that there may not be extensive solid solubility between them. Since the radii of Zn^{++} and Co^{++} are effectively the same, despite differences in crystal structure some solid solubility in the two systems ZnO-CoO and ZnO-Co_3O_4 would seem possible.

6B3a System CdO-ZnO:- Brown and Hummel[89] have studied solid solubility and compound formation between CdO and ZnO. Although no compounds were identified small regions of solid solubility of Cd^{++} in ZnO and Zn^{++} in CdO were detected. Solid solutions were examined in detail at 800°C and 1000°C using high angle X-ray diffraction methods with silicon powder as an internal standard. By performing suitable lattice parameter calculations the experimental results indicated solid solubility of less than 1 mole % CdO in ZnO at 800°C and 3 mole % at 1000°C. At the other boundary it was found that about 1 mole % ZnO is soluble in CdO at 800°C, increasing to about 2 mole % at 1000°C. In this system the equilibrium activities of ZnO and CdO may therefore be safely approximated to unity over the whole temperature range of the chlorination experiments. Whether solid state equilibrium was actually attained during the course of the chlorination experiments is difficult to assess; best possible approximations concerning solid state diffusion rates are given in section 6B3d. Four of the CdO/ZnO equilibrium runs were performed on 10.8 mole% CdO pellets (as opposed to 50.0 mole % CdO pellets). The work of Brown and Hummel shows that this composition is in the two phase region, thus 50.0 mole % measurements should be the same as those obtained using 10.8 mole % pellets. This prediction is supported by the experimental results.

6B3b System Co_3O_4 - ZnO:- Although aspects of this oxide system have been studied on various occasions a phase diagram suitable for making accurate predictions cannot be constructed from the available published data. In 1929 Holgersson and Karlsson (see reference 108 or 109) identified the compound $ZnCo_2O_4$. This has a spinel structure: with the ionic radii of Zn^{++} and Co^{++} being almost identical the unit cell dimension is, not surprisingly, very close to that of Co_3O_4. As an ionic crystal $ZnCo_2O_4$ might be viewed in terms of a compound between Co_2O_3 and ZnO, however, since Co_2O_3 has a limited range of stability[85] it is thought unlikely that zinc cobaltite would be stable at above about 400°C.

Robin[108] has studied solid solubility and compound formation between zinc oxide and cobalt oxides*. He presents a phase diagram which, unfortunately, is extrapolated in the region of the temperatures at which the present Co_3O_4/ZnO equilibrium measurements were performed. His samples were

---

* He also studied the nickel oxide-cobalt oxides and magnesium oxide-cobalt oxides systems.

prepared from mixtures of hydrated nitrates which were firstly fused and secondly decomposed to the respective oxides, these were then held at the required temperatures for between 10 and 72 hours. (This method of sample preparation has the advantage that components are initially brought together on an atomic scale thus reducing solid state diffusion effects during equilibration.) Phase boundary measurements were based upon various X-ray powder diffraction techniques, however, Robin points out that quantitative measurements were very difficult since the lattice parameters of the solid solutions involved varied very little with compositional changes. Below 400°C at the cobalt end of the system $ZnCo_2O_4$ was identified as a compound, above this temperature progressive decomposition was noted; no data at above 600°C are given for Co_3O_4-ZnO. Since with the NiO-Co_3O_4 system (radius Ni^{++} = 0.072 nm[107]) only a metastable compound spinel was found, whilst with the MgO-Co_3O_4 system (radius Mg^{++} = 0.065 nm[107]) none was detected, Robin found it 'remarkable' that at between 66.6 atom % Co and 100 atom % Co there exists the spinel $Zn_{(1-x)}Co_{(2+x)}O_4$. Robin attributed this behaviour to ionic-covalent mixed bonding by the cobalt. Robin chose to extrapolate the single phase compound spinel region to a point showing about 20 atom % Zn^{++} solubility at 850°C. Cobalt solubility at the ZnO end of the phase diagram is given as 4 atom % Co^{++} at 850°C, this figure having been determined by extrapolation of higher temperature measurements. Since heat treatments were performed in air the presented equilibrium diagram is for an oxygen partial pressure of 0.21 atmospheres.

Although he did not study the ZnO-Co_3O_4 system with the intention of elucidating phase distributions, the work of Lotgering[109] is valuable since it examines the stability and magnetic behaviour of $ZnCo_2O_4$. The compound was prepared from both nitrate and oxalate mixtures which were heat treated for the relatively short period of only 2 hours. At up to 350°C $ZnCo_2O_4$ was found to be stable, above this temperature it decomposed into two phases, one with a spinel structure (Co_3O_4) the other with a hexagonal structure (ZnO); however, no estimates were made concerning solubility limits. Magnetic susceptibility tests on $ZnCo_2O_4$ gave results that could only be explained in terms of predominantly covalent bonding. The importance of knowing what were the activities of the Co_3O_4 and ZnO during the equilibrium chlorination experiments is readily apparent. As explained in the preceding paragraphs the phase diagram for these two compounds is

not known with any certainty. An experimental approach was therefore adopted so as to try and reach some conclusion concerning the oxide activities. The investigation, which is fully described in appendix M, consisted of making up various Co_3O_4/ZnO mixtures (from the same powders used to make the pellets) a part of each of which was then heat treated. By X-ray powder diffraction analysis using a Guinier camera the heat treated and un-heat treated mixtures were then compared. The results are summarised below; the cobalt was in the form of Co_3O_4 (as used in appendix K), the zinc as ZnO; heat treatment was carried out in air.

a) 5 atom % Co + 95 atom % Zn - 6 hours 851°C. With the un-heat treated mixture ZnO lines and Co_3O_4 lines were clearly visible, the latter being at fairly low intensity. No significant changes could be detected after heat treatment.

b) 5 atom % Zn + 95 atom % Co - 6 hours 851°C. With the unfired mixture Co_3O_4 lines were very prominent but the ZnO lines were quite faint. After firing the ZnO lines could not be detected.

c) 10 atom % Zn + 90 atom % Co - 3 hours 850°C. The spinel lines were once again very pronounced both before and after firing. The ZnO lines although relatively faint were seen to be little changed by the heat treatment.

d) 5 atom % Zn + 95 atom % Co - 3 hours 850°C. Once again the ZnO lines were faint in the unfired mixture, however, after firing they were still just discernible.

There are two possible explanations which either individually or in conjunction could account for these findings. These are: a) mutual solid solubilities between ZnO and Co_3O_4 at 850°C are only of the order of a few percent, and b) the solid state diffusion processes involved were relatively slow. Before making any conclusions concerning the activities of the ZnO and Co_3O_4 during the chlorination experiments, approximate solid state diffusion rates are considered in section 6B3d.

6B3c System CoO-ZnO:- At 900°C the equilibrium diagram presented by Robin[108] indicates solid solubilities of about 9 atom % Co^{++} in ZnO and 30 atom % Zn^{++} in CoO, both solubilities are shown to rise with increasing temperature.

Bates and co-workers[110] have directly measured ZnO-CoO mutual solid solubilities at between 600°C and 800°C using an electron probe microanalyser. This technique is more accurate than calculating solubilities from small changes in lattice constants (measured by X-ray methods). Their determined solubility limits at 800°C are 6.5 atom % Co^{++} in ZnO and 22 atom % Zn^{++} in CoO.

Navrotsky and Muan[111] have studied activity-composition relations in the system CoO-ZnO at 1050°C. Solid solubility limits of 17 atom % Co^{++} in ZnO and 22 atom % Zn^{++} in CoO were measured. Two independent methods were used to determine the oxide activities; one (used only for a_{CoO} in the cobalt rich single phase, and the two phase regions) consisted of equilibrating the solid solution(s) with CO/CO_2 gas mixtures and determining the ratio at which pure cobalt metal first appeared. The second technique (used for both a_{ZnO} and a_{CoO}) was to study the ternary system $ZnO-Al_2O_3-CoO$ in two and threee phase regions (spinel + zincite, spinel + rocksalt*, spinel + zincite + rocksalt*). There is good reason to believe that the spinel $(Co,Zn)Al_2O_4$ behaves as an ideal solution, in addition it is possible by X-ray analysis to identify its composition. Therefore, by firstly equilibrating suitable $ZnO-Al_2O_3-CoO$ mixtures, then determining what phases were present together with the spinel composition, it was possible using phase diagram conjugation lines to estimate values for a_{ZnO} and a_{CoO}. Integration of the Gibbs-Duhem equation using the CO/CO_2 reduction results was performed to check the consistency of the data. Results obtained by the two different methods were in excellent agreement. Within the limits of experimental error solid solubilities and activities were found to be the same in air (P_{O_2} = 0.21 atmos) as at oxygen pressures just above that at which cobalt metal is precipitated (P_{O_2} of about 10^{-10} atmos). As expected, from a terminal solid solubility system which does not form compounds, there was no negative deviation from ideality. The ZnO activity in zincite from N_{ZnO} = 1 to saturation at N_{ZnO} = 0.83 was effectively ideal whilst the cobalt oxide activity showed strong positive deviation. At the other end of the composition range there was small positive deviation (mean

---

* CoO based solid solutions

activity coefficient = 1.13) in the activity of CoO up to saturation where $N_{CoO} = 0.78$, $a_{CoO} = 0.88$; once again the solute exhibited strong positive deviation.

In relation to the present chlorination study these findings can be portrayed in the following way. At equilibrium in the system CoO-ZnO, at 1050°C, between the composition limits $N_{ZnO} = 0.83$ and $N_{ZnO} = 0.22$ two solid solutions exist, in each of which $a_{ZnO} = 0.83$ and $a_{CoO} = 0.88$. The pellets used for the chlorination experiments contained a nominal CoO mole fraction of 0.50, thus if solid state equilibrium had been achieved at 1050°C the activities of ZnO and CoO would have been equal to the values just quoted. In order to gain some understanding of the rates of solution of CoO in ZnO and ZnO in CoO simple tests, as with the Co_3O_4-ZnO system, were carried out; these are fully reported in appendix M. The results are summarised below; the CoO/ZnO mixtures were made from the same powders used for pellet manufacture (CoO was prepared by heating Co_3O_4 at 950°C and then cooling the product all under a continuously maintained vacuum); so as to prevent oxidation samples were sealed in silica tubes under an argon atmosphere prior to their heat treatment.

a) 90 atom % Zn + 10 atom % Co - 3 hours 1000°C. The X-ray analysis of the unfired mixture produced strong ZnO reflections together with readily visible CoO lines. After heating the CoO reflections were slightly less intense as well as being a little displaced from their previous 2θ positions. An estimate of the decrease in CoO line intensity suggested that less than half had dissolved. The lattice spacing changes indicated that a significant quantity of Zn^{++} had diffused into the remaining CoO.

b) 90 atom % Co + 10 atom % Zn - 3 hours 1000°C. The ZnO reflections were faint in the unheat treated mixture, whilst after firing they could not be detected. This result cannot be taken as confirmation that all the ZnO had dissolved, but only that a major proportion had dissolved.

Since the solid solubility boundaries of this system are quite accurately known, solid state diffusion rates were clearly the limiting factors in the two tests reported above. Before any conclusions are made concerning the activities of the CoO and ZnO during the equilibrium chlorination experiments, approximate solid state diffusion rates are considered in the

next section. However, from published data it is evident that activity - composition relations in the CoO-ZnO system (at equilibrium) may be predicted with good accuracy.

6B3d Approximate solid state diffusion rates:- It is beyond the scope of this section to give a full thoeretical treatment of solid state diffusion, if required this can be obtained from a suitable text on the subject[112]. Due to the complexities of the interdiffusing systems under consideration and the uncertainties surrounding the diffusion coefficients involved, the calculations in this section are necessarily only approximate and may therefore be incorrect by an order of magnitude or more. Interdiffusion between contacting particles of two different metal oxides is an unsteady state process. To be able to calculate 'time-concentration-distance' relationships Ficks' second law equation has to be solved. The general form of this equation is:

$$\frac{dc_i}{dt} = D_i \cdot \left(\frac{d^2 c_i}{dx^2}\right) \quad \ldots\ldots\ldots\ldots\ldots\ldots\ldots\ldots (1)$$

where c_i is the concentration of species "i" and D_i its diffusion coefficient; strictly speaking this equation only applies for thermodynamically ideal systems. A solution of this equation has been obtained[113] for unidirectional diffusion into a semi-infinite medium with the surface (or interface) concentration remaining constant. Under these conditions the concentration at any point reaches a value halfway between the initial and final concentration when

$$\frac{X}{\sqrt{D_i t}} = 0.954 \quad \ldots\ldots\ldots\ldots\ldots\ldots\ldots\ldots (2)$$

This relationship when approximated to

$$X^2 = D_i t \quad \ldots\ldots\ldots\ldots\ldots\ldots\ldots\ldots\ldots (3)$$

is very useful for quickly calculating what diffusion time will produce a significant approach to the final concentration attainable by a diffusing species. To apply this equation to the three oxide systems under discussion requires knowledge of solid state diffusion coefficients and oxide powder particle sizes.

The mean crystallite size of the ZnO powder, as quoted by the manufacturers (see appendix D) was 2.1×10^{-5} cms. An examination of this powder using a scanning electron microscope (see section 8A3a) confirmed that individual grains were all submicron in size. The CdO powder which was similarly

examined consisted of comparable sized grains. No examination of the cobalt oxide(s) powder was performed; since it appeared to be equally as fine as the cadmium and zinc oxide it is assumed also to have been submicron sized.

Evaluating diffusion coefficients presents several problems. These are: a) being difficult to measure they are often subject to large errors; b) many systems, especially two component ones, have not been studied; c) since solid state diffusion is an activated process it is very temperature sensitive, and d) crystal defects, which are dependent on many parameters, greatly influence diffusion rates. The work of various authors on tracer self diffusion coefficients in spinels has been reviewed by Schmalzried[114]. No studies appear to have been performed on cobalt spinel (Co_3O_4) or any cobaltites (MCo_2O_4) however data are available for many aluminates, chromites and ferrites. Measured self diffusion coefficients in these systems vary, at a given temperature, by as much as four orders of magnitude. It would be easy to enter into a long discourse on the probable values of tracer diffusion coefficients in cobaltites (if indeed any exist at high temperatures) and cobalt spinel, but this would serve little useful purpose. Therefore, because of its similarity* with the Co_3O_4-ZnO system, data for zinc ferrite ($ZnFe_2O_4$) will be used. At 850°C the self diffusion coefficient of Zn^{++} in zinc ferrite is about 5×10^{-14} cms^2/sec, this is a mean value from two determinations showing reasonably good agreement. A very comprehensive review of solid state diffusion in metal oxides has been published by Kofstad[115], information for CoO and ZnO are taken from this book. In the case of CdO only its oxygen self diffusion coefficient is reported, that for Cd^{++} has probably not been studied, thus as a rough approximation it will be assumed that it behaves in the same way as does Zn^{++} in ZnO. Values of tracer diffusion coefficients are given below, since they vary with oxygen pressure the figures are for 10^{-1} atmospheres of oxygen.

Co^{++} in CoO		Zn^{++} in ZnO	
1050°C	9×10^{-8} cms^2/sec	1050°C	8×10^{-13} cms^2/sec
950°C	5×10^{-9} cms^2/sec	950°C	1×10^{-13} cms^2/sec
		850°C	1×10^{-14} cms^2/sec
		750°C	1×10^{-15} cms^2/sec

---

* At.No. Fe = 26 At.No. Co = 27 Ionic radii in nanometres[107]
Co^{++} = 0.074 , Fe^{++} = 0.076, Co^{+++} = 0.063, Fe^{+++} = 0.064

Only in the case of complete solid solubility in a system of known thermodynamics with diffusion coefficients (tracer) of similar magnitude can an interdiffusivity coefficient be calculated with any accuracy. So that some approximate calculations may be made it has been assumed that solute cations have a diffusivity equal to that of the solvent cations in their own lattices.

Temp °C / Solvent	750	850	950	1050
ZnO lattice	4×10^{5}	4×10^{4}	4×10^{3}	5×10^{2}
CoO lattice	-	-	8×10^{-2}	4×10^{-3}
Co_3O_4 lattice	-	8×10^{3}	-	-

TABLE 6A: Approximate mid-concentration diffusion times for interdiffusion of solute cations into 2×10^{-5} cms diameter oxide grains - seconds (1 hour = 3.6×10^{3} seconds)

The calculated times given in table 6A must be treated with some caution since equation (3) applies for simple boundary conditions different from those in a mixed oxide pellet, also the diffusion coefficients have been derived by means of an 'educated guess'. Bearing in mind these two points the estimated diffusion times suggest that the possibility of significant interdiffusion between the different oxides (within solid solubility limits) cannot be discounted.

6B3e Metal oxide activities - final estimates:- Estimated diffusion times for the CdO-ZnO system indicate that at 850°C and below solid state diffusion is a relatively slow process. Only at temperature of 950°C and above do rates appear to become signficant in relation to the time scale of the experiments. An approach to solid state equilibrium may therefore have occurred with the higher temperature runs. Structural examinations (see section 8A3b) which were carried out upon ZnO/CdO pellets used in non-equilibrium experiments showed that sintering and bulk densification were relatively gradual at 750°C but very pronounced at 950°C. Since sintering is greatly influenced by solid state diffusion, these findings are in good general agreement with the predictions of table 6A. However, as outlined in section 6B3a, solid solubility limits in the CdO-ZnO system are only about 2 to 3%; activity-composition

relationships for ZnO and CdO would probably show positive 'solvent' deviations and therefore the assumption that both oxides were present at unit activity is very well justified, regardless of whether the chlorinated pellets consisted of an admixture of oxides or two equilibrium solid solutions.

The diffusion times for system $ZnO\text{-}Co_3O_4$ given in table 6A are inconclusive due to the large potential errors associated with the calculations involved. The works of Robin[108] and Lotgering[109], discussed in section 6B3b, do not give accurate 850°C mutual solid solubility limits for this oxide pair. According to Robin, solubility of Co^{++} in ZnO at 850°C is about 4 atom %, Bates et al[110] report a value of 6.5 atom % at 800°C. The cause of this disagreement may have been that, in the Co_3O_4-ZnO system solubility of Co^{++} can be controlled by the equilibrium

$$[CoO]_{ZnO}(s) + 1/6\ O_{2(g)} = 1/3\ Co_3O_4(s)$$

As regards Zn^{++} solubility in Co_3O_4 it is questionable whether Robin's extrapolation to 20 atom % at 850°C is justified. Under test conditions at 850°C 5 atom % Zn^{++} did not dissolve in 3 hours but appeared to in 6 hours; this rate of solution is relatively low, thus suggesting that only a small amount of Zn^{++} was taken in by the Co_3O_4 during chlorination runs on this system. To calculate ΔG°_T values from the Co_3O_4/ZnO equilibrium chlorination results the ratio $a_{ZnO}/a_{Co_3O_4}^{1/3}$ was assumed to be equal to unity; from the preceding discussion it is evident that there could be some error in this assumption. If the two solid solutions involved behave ideally, solubility limits being 20 atom % Zn^{++} and 6 atom % Co^{++} then the activity ratio above becomes 1.013. With almost any realistic combination of equilibrium activities, or effective activities under non-equilibrium (but equilibrating) conditions, it is very doubtful whether the activity ratio above could have varied outside the range 1.0 ± 0.1. The maximum error due to this possible uncertainty factor is less than ± 250 cals/mole and therefore within the claimed accuracy of the present work.

Although the interdiffusion times for CoO and ZnO given in table 6A differ by several orders of magnitude both sets of values suggest that mutual solution could have been pronounced during the CoO/ZnO equilibrium chlorination experiments. The 3 hour heat treatment tests were in

agreement with the trend of these calculations in that solution of Zn^{++} in CoO was more rapid than solution of Co^{++} in ZnO. Once again, as with the previous system discussed, it is not possible to make any categorical statements concerning the effective activities of the oxides involved. Best indications are that the CoO-ZnO mutual solution rates were relatively high over the whole temperature range studied, however, it would appear that only with the higher temperature runs (>1033°C) was there a close approach to equilibrium. As reported in section 6B3c Navrotsky and Muan[111] have determined equilibrium acitivities in this system at 1050°C, for the two phase region (saturated solid solutions) they found $a_{ZnO} = 0.83$ and $a_{CoO} = 0.88$. In order to calculate ΔG°_{T} values from the CoO/ZnO equilibrium results the ratio a_{ZnO}/a_{CoO} was taken to be equal to unity. Under all experimental conditions it is estimated that this activity ratio (or effective activity ratio) was within the range 1.0 ± 0.15. The potential error that this generous assessment could incur is less than the accuracy claimed for these results.

6B4 Oxygen partial pressure dependence

With both the CdO/ZnO and the CoO/ZnO equilibrium chlorination experiments there was no correlation between oxygen partial pressure and bed-exit metal chlorides partial pressure ratios: this is as predicted by theoretical considerations.

With Co_3O_4/ZnO equilibrium chlorination the ratio P_{ZnCl_2}/P_{CoCl_2} depends upon the one sixth power of the oxygen partial pressure.[2] When investigated at a temperature of 852°C the experimentally measured dependency was between 1/4.83 and 1/4.54 (best fit values from two least squares analyses). In view of this relative insensitivity to oxygen pressure the disagreement between the measured and the theoretical exponents is thought to be small especially when it is remembered that, taken as a whole, the cobalt oxide(s)/zinc oxide results contained an appreciable element of random scatter. The large number of experiments performed at 852°C to obtain the oxygen pressure exponent allowed K_p, the equilibrium constant at this temperature, to be measured with considerable accuracy. It is therefore felt that the $\Delta G^{\circ}_{1126^{\circ}K}$ value on graph 5D is the most accurate single point given on the plot.

6B5 Standard deviations

Sources of error in the equilibrium measurements are discussed in section 6A2. Since no systematic of illegitimate errors were identified all experimental scatter is assumed to have been random. The standard deviation* of the 30 CdO/ZnO ΔG°_{T} values from the calculated least squares best fit ΔG°_{T} vs T line (plotted on graph 5B) is $\pm$ 112 cals/mole ($\pm$ 470 joules/mole). The standard deviation* of the 18 CoO/ZnO ΔG°_{T} values from the calculated least squares best fit ΔG°_{T} vs T line (plotted on graph 5D) is $\pm$410 cals/mole ($\pm$ 1720 joules/mole). The standard deviation of the 21 852-854°C Co_3O_4/ZnO ΔG°_{T} values is $\pm$185 cals/mole ($\pm$776 joules/mole).

6C COMPARISON OF EXPERIMENTAL RESULTS WITH PREVIOUS WORK

Only one oxide-chlorine high temperature equilibrium study involving either CdO, CoO, Co_3O_4 or ZnO has been discovered in the literature: that determination, as reported in section 1C2a, was performed on ZnO by Orlov and Jeffes[31]. As a result of this lack of specific information, ΔG° values given in chapter five can only be compared with compilations of previous measurements. In order not to overburden this section with comparative analyses of a multitude of previous works, reported standard free energies of formation of CoO, Co_3O_4, CdO, ZnO, $ZnCl_2$, $CdCl_2$ and $CoCl_2$ are reviewed in appendix L.

6C1 Zinc oxide-chlorine equilibrium

The work of Orlov and Jeffes[31] is described in section 1C2a. It is particularly relevant to the present study since if their data is accurate, using the ΔG° values of the present work, it enables cobalt oxide(s)-chlorine and cadmium oxide-chlorine equilibria to be determined more precisely than was previously possible. Back reaction in the condenser prevented Orlov and Jeffes from performing measurements over a range of temperatures; $\Delta G^{\circ}_{1073^{\circ}K}$ was thus the only reliable free energy change value obtained. Since they were unable to calculate ΔS° from their results they assumed a value which was the mean of four literature

---

* These standard deviations are necessarily minimum possible values since the best fit lines were calculated to give the least sum of the squares of the deviations. It can be shown mathematically that σ, 2σ and 3σ are the respective deviations (about either the arithmetic mean or the least-squares-plot) within which 68.3%, 95.4% and 99.7% of the experimental readings fall. These are known as the percentage confidence limits of a series of results.

compilations. This somewhat unsatisfactory method of estimating the entropy change was subsequently criticised by Lumsden[101] who suggested a new value, the basis of which was more scientific than that of the initial estimate. For the reaction

$$ZnO_{(s)} + Cl_{2(g)} = ZnCl_{2(g)} + \tfrac{1}{2}O_{2(g)}$$

at 800°C Orlov and Jeffes determined

$$\Delta G^{\circ}_{1073^{\circ}K} = -8160 \text{ cals/mole} \quad \ldots\ldots\ldots\ldots\ldots\ldots (1)$$

with their assumption that $\Delta S^{\circ} = 28.0$ cals/mole°K they obtained the equation

$$\Delta G^{\circ}_{T} = 21890 - 28.0T \text{ cals/mole} \quad \ldots\ldots\ldots\ldots\ldots\ldots (2)$$

Using Lumsden's estimated entropy change figure ($\Delta S^{\circ} = 24.3$ cals/mole°K) the free energy equation for the reaction given above becomes

$$\Delta G^{\circ}_{T} = 17910 - 24.3T \text{ cals/mole} \quad \ldots\ldots\ldots\ldots\ldots\ldots (3)$$

Since this 'corrected' equation appears to be the more accurate of the two it has been adopted for all the remaining calculations. The temperature range over which it is valid and its absolute accuracy are difficult to assess. The main error is due to ΔS°, $\Delta G^{\circ}_{1073^{\circ}K}$ is probably accurate to within $\pm$ 100 cals/mole as claimed by the authors. It would seem quite safe therefore to assume an accuracy of $\pm$1000 cals/mole over the temperature range 700-1100°C. A comparison between equation (3), the corrected free energy change, and a compilation based upon what in the present author's opinion are the best currently available alternative data is shown on graph 6B; the full line is the corrected data, the broken line is based upon values from references 98 and 95 (see appendix L). It is immediately evident that agreement between the two lines is good. Both the sets of data used to derive the line of comparison have been available for some time. Orlov and Jeffes, whose work was published after these studies, obtained their literature data exclusively from texts on thermochemistry, which it would appear do not give the most accurate values. There are thus two interesting points which can be made. These are: a) a thorough search of the literature is always essential if critical thermodata is required; and b) the long published (1930) work of Wachter and Hildebrand[98] has in general been neglected, it was however an accurate and notable study.

6C2 CdO/ZnO equilibrium results

On graph 6A is plotted the experimentally determined standard free energy change line for the reaction

$ZnCl_{2(g)} + CdO_{(s)} = CdCl_{2(g)} + ZnO_{(s)}$ . . . . . (1)

as reported in chapter five. Also plotted on this graph is a complied line of comparison based upon values derived from references 94, 97, and 31 – corrected. $CdCl_2$ literature data were taken from Lorenz and Velde[97] in preference to Lantratov (see Lumsden[100]) since ΔS° as given by the former workers is, when corrected for phase changes, in better agreement with the most recently published[103] $\Delta S^\circ_{298^\circ K}$ value (see appendix L for more details). One comment made about the $ZnCl_2$ data in the previous section is also applicable to the $CdCl_2$ data: Lorenz and Velde[97] published their work in 1929; it appears to be of commendable accuracy but has been passed by on many occasions. The full line of graph 6A is from chapter five, the compiled free energy change values are plotted as a broken line. Agreement between the two sets of data are good; the small discrepancy is probably due, in the main, to the $CdCl_2$ data and to neglect of ΔC_p during compilation.

Lumsden[100] reports the work of Jellinek who studied the reaction given below:

$ZnCl_{2(l)} + Cd_{(l)} = CdCl_{2(l)} + Zn_{(l)}$ . . . . . (2)

Recalculating the original data using accurate Cd-Zn activities whilst assuming that the chlorides form an ideal solution Lumsden finds

$\Delta G^\circ_{873^\circ K}$ = 7400 cals/mole . . . . . (3)

At 873°K the standard free energies of formation of ZnO[95] and CdO[94] are -62640 cals/mole and -39840 cals/mole respectively. (ΔH_{evap}Cd = 23.9 ± 0.3 K cals/mole — 1038°K[3]). Thus for the reaction

$ZnCl_{2(l)} + CdO_{(s)} = CdCl_{2(l)} + ZnO_{(s)}$ . . . . . (4)

using the preceding sets of values

$\Delta G^\circ_{873^\circ K}$ = -15400 cals/mole . . . . . (5)

This value may be compared with one derived from the free energy data given in chapter five, a change in standard states is however necessary. Quoted[3] heats of evaporation and boiling points for $CdCl_2$ and $ZnCl_2$ are 29.6 ± 0.8 K cals/mole — 1224°K and 28.5 ± 3.0 K cals/mole —1005°K respectively. Applying the required corrections, using these figures, the ΔG° value given below is obtained for reaction (2):

$\Delta G^{\circ}_{873^{\circ}K}$ = -13350 cals/mole . . . . . .(6)

Agreement between (6) and (5) is quite good. It is thought that the discrepancy is mainly the result of combinations of errors in value (5) and therefore that value (6) is more accurate.

6C3 Co_3O_4/ZnO and CoO/ZnO equilibrium results

The experimentally determined standard free energy equations given in chapter five for the systems Co_3O_4/ZnO and CoO/ZnO are plotted, as full lines, on graph 6A. For comparison compiled data for these two systems are drawn, as broken lines, on the same graph. Three literature sources were used to evaluate the lines of comparison. These were 3, 90, and 31-corrected. Agreement between the experimental and compiled lines is seen to be rather poor; essentially this is caused by the $CoCl_2$ data[3] being demonstrably inaccurate (details are given in the next section). The errors in the cobalt oxides data[90] are relatively small. Full details on Co_3O_4, CoO and $CoCl_2$ are given in appendix L.

Consistency between the Co_3O_4/ZnO and CoO/ZnO experimental results may be checked by computing the standard free energy change for the reaction below:

$CoO_{(s)} + 1/6\ O_{2(g)} = 1/3\ Co_3O_{4(s)}$ . . . . . (1)

From the two exchange-reaction free energy equations given in section 5G3a

ΔG°_{T} = -19700 + 16.1T cals/mole (CoO) . . . . . .(2)

According to Bugden and Pratt[90]

ΔG°_{T} = -15780 + 13.03T cals/mole (CoO) . . . . . (3)

(estimated error $\pm$ 100 cals)

Over a wide temperature range disagreement between these equations would be very significant. The Co_3O_4/ZnO system was, however, only studied at 1126°K and above. From equation (2) $\Delta G^{\circ}_{1126^{\circ}K}$ = -1570 cals/mole. From equation (3) $\Delta G^{\circ}_{1126^{\circ}K}$ = -1110 cals/mole. The discrepancy between the two values above is within the combined accuracy limits of the Co_3O_4/ZnO and CoO/ZnO results. Therefore, on the basis of reaction (1) the cobalt oxide(s)/zinc oxide equilibrium results are consistent.

6C4 Metal oxide - chlorine equilibria

Having recalculated the zinc oxide-chlorine equilibrium in section 6C1 it is now possible to derive standard free energy changes for the reactions

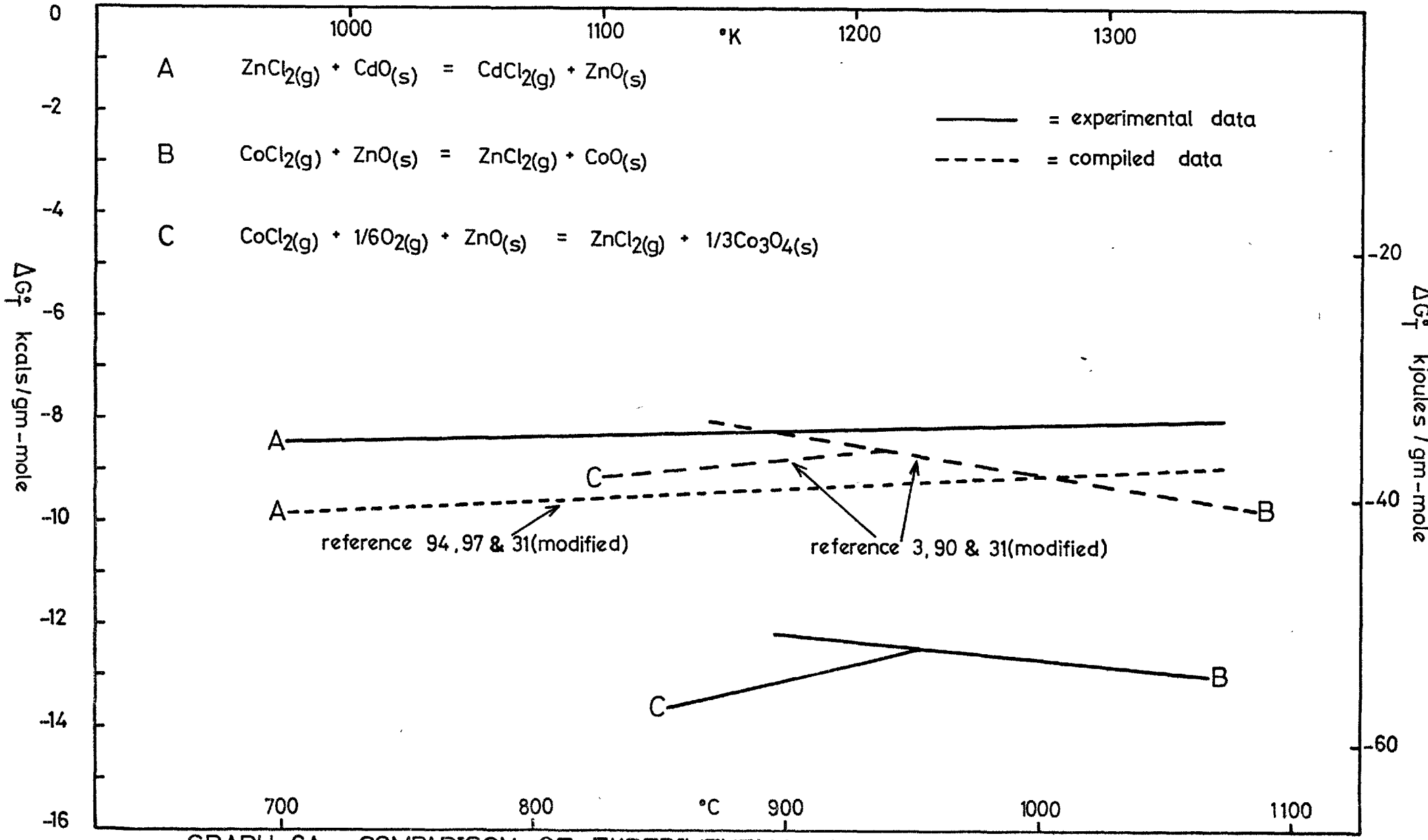

GRAPH 6A: COMPARISON OF EXPERIMENTALLY MEASURED AND COMPILED EXCHANGE REACTION STANDARD FREE ENERGY CHANGE DATA.

$CdO + Cl_2$, $1/3\ Co_3O_4 + Cl_2$ and $CoO + Cl_2$ with an accuracy greater than has been hitherto possible. On the bases of the results given in chapter five and the corrected work of Orlov and Jeffes the following free energy data has been computed:

$$CdO_{(s)} + Cl_{2(g)} = CdCl_{2(g)} + \tfrac{1}{2}O_{2(g)} \quad \ldots\ldots\ldots\ldots (1)$$

$$\Delta G^\circ_T = 8240 - 23.1T \text{ cals/mole} \quad \ldots\ldots\ldots\ldots\ldots (2)$$
$$(975 - 1345^\circ K)$$

$$1/3\ Co_3O_{4(s)} + Cl_{2(g)} = CoCl_{2(g)} + 2/3\ O_{2(g)} \quad \ldots\ldots (3)$$

$$\Delta G^\circ_T = 44210 - 35.6T \text{ cals/mole} \quad \ldots\ldots\ldots\ldots\ldots (4)$$
$$(1126 - 1228^\circ K)$$

$$CoO_{(s)} + Cl_{2(g)} = CoCl_{2(g)} + \tfrac{1}{2}O_{2(g)} \quad \ldots\ldots\ldots\ldots (5)$$

$$\Delta G^\circ_T = 24510 - 19.5T \text{ cals/mole} \quad \ldots\ldots\ldots\ldots\ldots (6)$$
$$(1168 - 1339^\circ K)$$

Equations (2), (4) and (6) are plotted on graph 6B as full lines, the broken lines of comparison, also on this graph have been compiled from the best currently available sets of data (references 90 and 3 for the cobalt oxides and 94 and 97 for cadmium oxide). The discrepancy between the new CdO line and the compiled line is comparable with that between the corrected and compiled ZnO lines which are also drawn on graph 6B. In absolute terms agreement between both new lines and their compiled lines is good, always being within 1500 cals/mole over a wide temperature range. With the CoO and $1/3\ Co_3O_4$ lines there is significant variance between the new and compiled data. It is the author's belief that this discrepancy is almost entirely due to errors in the $CoCl_{2(g)}$ literature data. The standard free energies of formation of CoO and Co_3O_4 are well documented[3,4,75,82,88,90,92] (see appendices K and L for details). This is not the case for $CoCl_2$, especially in the gas phase. Only two recent studies on the free energy of formation of $CoCl_{2(s)}$ could be found in the literature; none were discovered for $CoCl_{2(1)}$ or $CoCl_{2(g)}$. As shown in appendix L, $CoCl_2$ phase transformation thermodata is in a state of considerable uncertainty, this therefore precludes the possibility of making reasonable solid - liquid - gas extrapolations. However, the two recent $CoCl_{2(s)}$ studies may be compared with solid-phase data obtained from thermodynamic data reviews. Egan[105] reports standard free energies of formation of:

$$\Delta G^\circ_{673^\circ K} = -52730 \text{ cals/mole} \quad \ldots\ldots\ldots\ldots\ldots (7)$$

$$\Delta G^\circ_{723^\circ K} = -51280 \text{ cals/mole} \quad \ldots\ldots\ldots\ldots\ldots (8)$$

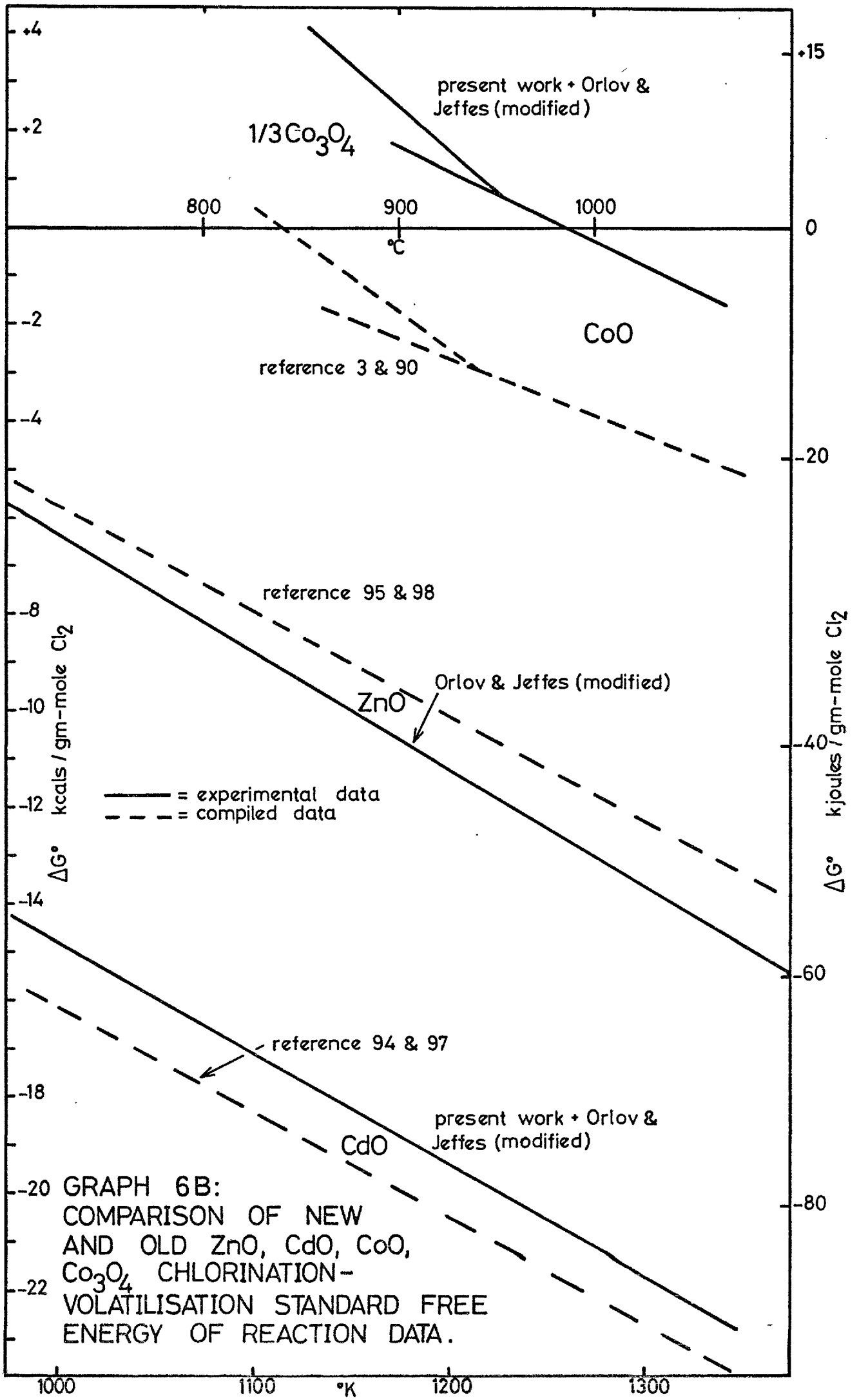

GRAPH 6B: COMPARISON OF NEW AND OLD ZnO, CdO, CoO, Co_3O_4 CHLORINATION-VOLATILISATION STANDARD FREE ENERGY OF REACTION DATA.

In good agreement is the work of Gee[106].

$\Delta G^{\circ}_{673^{\circ}K}$ = -52160 cals/mole* . . . . . (9)
-51670 cals/mole**

$\Delta G^{\circ}_{723^{\circ}K}$ = -50500 cals/mole* . . . . . (10)
-50090 cals/mole**

Values from the reviews[3,4,29,30] are all very similar since each appears to incorporate, with minor modifications, the same original data. Figures from Kubaschewski[3] et al are given below.

$\Delta G^{\circ}_{673^{\circ}K}$ = -55410 cals/mole . . . . . (11)

and

$\Delta G^{\circ}_{723^{\circ}K}$ = -53840 cals/mole . . . . . (12)

These values are about 3000 cals/mole larger (negative sense) than those of either Egan or Gee (error limits quoted by the authors of the review[3] are $\pm$ 3000 cals/mole). The free energy equations which are given by the reviews[3,4,29,30] for $CoCl_{2(l)}$ and $CoCl_{2(g)}$ are based upon exptrapolations of solid phase data. The 3 K cals/mole error would therefore be carried through, with the possibility of it's being added to by errors in the heats of transformation and estimated ΔC_p's (the estimated error limits given by Kubaschewski[3] et al for ΔG°_T - $CoCl_{2(g)}$ are $\pm$ 4000 cals/mole). The 3-4 K cals/mole discrepancy between the compiled and new cobalt oxides lines drawn on graph 6B can thus be primarily attributed to a 3-4 K cals/mole error in the literature values of the standard free energy of formation of $CoCl_{2(g)}$. The new 1/3 Co_3O_4 + Cl_2 and CoO + Cl_2 lines drawn on graph 6B show that the free energy driving forces for chlorination volatilisation of cobalt oxides are lower than were previously predicted. This helps explain why in the LDK process[9] (see section 1B1b) cobalt extraction was always found to be relatively low. It also helps explain why Orlov and Piskunov[6,7] and Orlov[8] (see section 1B1a) observed significant decreases in cobalt volatilisation rates when either O_2 or H_2O were added to their chlorination gas mixtures.

---

* $Fe/FeCl_2$ reference
** $Ni/NiCl_2$ reference

See appendix L for details

6C5 Final listing of reactions, free energy equations, estimated errors and temperature ranges

1. $ZnCl_{2(g)} + CdO_{(s)} = CdCl_{2(g)} + ZnO_{(s)}$

$\Delta G^{\circ}_{T} = -9670 + 1.23T$ cals/mole

$= -40500 + 5.15T$ joules/mole

$T = 975\text{-}1345^{\circ}K$

standard deviation $= \pm$ 112 cals/mole

$= \pm$ 470 joules/mole

2. $CoCl_{2(g)} + ZnO_{(s)} = ZnCl_{2(g)} + CoO_{(s)}$

$\Delta G^{\circ}_{T} = -6600 - 4.78T$ cals/mole

$= -27600 - 20.0T$ joules/mole

$T = 1168\text{-}1339^{\circ}K$

standard deviation $= \pm$410 cals/mole

$= \pm$1720 joules/mole

3. $CoCl_{2(g)} + ZnO_{(s)} + 1/6\ O_{2(g)} = ZnCl_{2(g)} + 1/3\ Co_3O_{4(s)}$

$\Delta G^{\circ}_{T} = -26300 + 11.3T$ cals/mole

$= -110100 + 47.3T$ joules/mole

$T = 1126\text{-}1228^{\circ}K$

$\Delta G^{\circ}_{1126^{\circ}K} = -13620$ cals/mole

$= -57020$ joules/mole

standard deviation $= \pm$ 185 cals/mole

$= \pm$ 780 joules/mole

4. $ZnO_{(s)} + Cl_{2(g)} = ZnCl_{2(g)} + \frac{1}{2}O_{2(g)}$

$\Delta G^{\circ}_{T} = 17910 - 24.3T$ cals/mole

$= 74990 - 102T$ joules/mole

$T = 973\text{-}1373^{\circ}K$

estimated error $= \pm$ 1000 cals/mole

$= \pm$ 4190 joules/mole

5. $CdO_{(s)} + Cl_{2(g)} = CdCl_{2(g)} + \frac{1}{2}O_{2(g)}$

ΔG°_{T} = 8240 - 23.1T cals/mole

= 34500 - 96.7T joules/mole

T = 975-1345°K

estimated error = $\pm$ 1000 cals/mole

= $\pm$ 4190 joules/mole

6. $1/3\ Co_3O_{4(s)} + Cl_{2(g)} = CoCl_{2(g)} + 2/3\ O_{2(g)}$

ΔG°_{T} = 44210 - 35.6T cals/mole

= 185100 - 149T joules/mole

T = 1126-1228°K

estimated error = $\pm$ 1000 cals/mole

= $\pm$ 4190 joules/mole

7. $CoO_{(s)} + Cl_{2(g)} = CoCl_{2(g)} + \frac{1}{2}O_{2(g)}$

ΔG°_{T} = 24510 - 19.5T cals/mole

= 102600 - 81.6T joules/mole

T = 1168-1339°K

estimated error = $\pm$ 1000 cals/mole

= $\pm$ 4190 joules/mole

CHAPTER SEVEN

RESULTS OF NON-EQUILIBRIUM EXPERIMENTS

In this chapter the results of three series of packed bed non-equilibrium chlorination experiments are reported, the order being the same as that in which they were performed. The first non-equilibrium experiments were carried out on packed beds of dense zinc oxide granules (these were the same type of granules used for the proving runs described in section 4C); complete sets of experimental data on all of these runs are given in appendix F. Although it was not the prime intention of this study to examine single oxide chlorination kinetics, the work on ZnO served several useful purposes. Some of the areas in which valuable information was obtained are listed below:

a) Experience was gained with all aspects of experimental procedure.
b) A simple mathematical analysis of a packed bed reactor was performed.
c) The unsuitability of granular oxide charges became apparent.
d) Wall effects and physical changes in reacted granules were observed.
e) Relatively high overall reaction rates were shown to be difficult to study using packed beds.
f) Temperature decreases during chlorination were recorded.
g) Some semi-quantitative rate data was obtained.

The theoretical analysis used for the ZnO results is relatively simple; it is therefore given as part of this chapter. Since the results in general do not warrant a more detailed treatment they receive no further analysis (except during discussion) in any other part of this thesis.

The second series of non-equilibrium experiments was performed on packed beds of porous CdO/ZnO pellets (the same type of pellets as those used for the CdO/ZnO equilibrium runs); complete sets of data for these experiments are given in appendix H. Based upon gas-solid reaction theory a mathematical model which attempts to describe the kinetics of chlorination of a packed bed of CdO/ZnO pellets has been developed. Extensive structural examinations of reacted and unreacted CdO/ZnO pellets were carried out in order to a) measure the effect of sintering and densification, b) suppl fundamental data for the mathematical model and c) determine reaction modes and elucidate various other phenomena. So that the CdO/ZnO

experimental results may initially be viewed on their own, the results of the structural examinations together with the theoretical development and predictions of the mathematical model are not presented in this chapter but are fully described in chapter eight.

The third and shortest series of non-equilibrium experiments (double bed experiments) each employed a deep bed of ZnO pellets above a bed of either CdO pellets or CdO/ZnO pellets, complete sets of data on these runs are given in appendix I. The experiments were carried out in order to test various theoretical predictions and to qualitatively investigate one possible exchange reaction mechanism. The results of the runs are given in this chapter, their significance is however discussed in chapter nine.

7A ZnO NON-EQUILIBRIUM EXPERIMENTS

Since it was not possible to continuously, or even semi-continously, monitor reactor exit gas compositions during ZnO chlorination runs, an experimental procedure was used such that with each experiment reaction was occurring as an approximately steady state process. By carrying out relatively short experiments, using low chlorine content gas mixtures, bed depletions* were kept as small as was practically possible. Therefore, during any such run the reaction could be approximated to a steady state process. The maximum bed depletion that occurred during this series of experiments, as calculated from the reactor weight loss, was about 18% (run D8). The arithmetic mean value for the runs (as plotted on graph 7A) reported in this section has been calculated to be 8.1%. Performing runs of too short a duration would have resulted in significant reaction initiation and termination effects. The ZnO non-equilibrium proving runs showed that if a total swept volume of chlorinating gas of 8 litres or more was employed these effects, with a 22 mm bore reactor, became insignificant in comparison to the overall level of experimental reproducibility. All chlorination runs reported in this section employed more than this minimum safe swept volume of gas, the lowest swept volume was about 14 litres (B series runs), the average near 20 litres and the maximum 110 litres (run G1). With each experiment only the bed entry and bed exit gas compositions could be determined. More important than the bed exit gas composition was how the chlorine and therefore zinc chloride concentration varied with position down each bed. This could only be

---

* The fraction of the total bed mass that was volatilised

studied by performing a number of runs using the same gas composition and flow, oxide size fraction, temperature and reaction time whilst varying the depth of the packed bed. A series of runs thus consisted of repeating a given experiment a number of times with all conditions identical except for carefully chosen variations in bed mass. It is evident that due to the necessary experimental constraints and approximations, the overall complexity of the reaction process and the time consuming nature of the experiments, the reactor-condenser configuration employed in this study is not particularly well suited to investigating single oxide chlorination kinetics. However, as discussed in section 2C, this technique was devised in order to carry out several different types of experiments, the least important of which were those on zinc oxide.

7A1 Details of experimental procedure

A general list of the sequence of operations which were carried out when performing a chlorination experiment is given in section 4B1. Specific details concerning the ZnO runs are reported in section 4B2a. Two different methods were used for determining the amount of zinc chloride formed (equivalent to the amount of zinc oxide lost) in the reactor during the course of each experiment. With some runs the condensate was chemically analysed by EDTA complexiometric titration, this technique has been described in section 4B1e. With the remaining runs the amount of chlorine to have reacted, which is what the EDTA analyses quantified, was taken to be equal to half the sum of the gm-moles of ZnO lost and the gm-moles of $ZnCl_2$ collected $[\frac{1}{2}(n_{ZnO} + n_{ZnCl_2})]$ these molar quantities having been calculated from the recorded reactor weight loss and condenser weight gain. Determining the extent of reaction by this last method is potentially more inaccurate than the analytical technique, however, the error is not as large as might be first imagined. With each non-equilibrium proving run (described in section 4C2) agreement between the EDTA - Zn^{++} analysis, the ZnO weight loss and the weight of $ZnCl_2$ collected was good; in addition, the values determined by analysis always lay between the two weight change values. For the five proving runs reported in table 4A the average disagreement between the EDTA - Zn^{++} analyses and the mean weight change values is 2.2%, with the 16 non-equilibrium ZnO experiments whose condensates were analysed chemically this figure is 1.4%. With each ZnO experiment an internal thermocouple situated near to the bed exit (about 5 mm before the exit) was

used to measure, and continously display on a chart recorder, the bed temperature. The granular zinc oxide charges used for the experiments were manufactured by first isostatically compacting zinc oxide powder, then crushing the resulting compacts and finally separating the granules into different size fractions by sieving. The full manufacturing procedure is described in section 4A1. Experiments were performed on the following four size fractions: -3/8 inch + 1/4 inch, -1/4 inch + 3/16 inch, -3/16 inch +7*mesh -7*mesh + 14* mesh. Plate number 3 is a photograph of an equal mass (4.98 gms) of the four different size fractions, each of which has been spread out over an area 3 inches square. The range of solid geometries within each size fraction was observed to be very similar, the photgraph shows that a typical granule had an irregular plate-like shape. The measured density of the granules was 5.40 gms/cc as compared with a theoretica density of 5.68 (calculated from X-ray measurements) and a density of 5.61 quoted by the Handbook of Chemistry and Physics. On the basis of these two figures the granules were either 95.1% or 96.3% dense, and therefore in either case effectively impermeable.

7A2 Theoretical analysis of results.

Excluding the effects of heat transfer, namely assuming the reacting system to be isothermal, either or both of two different rate processes control the overall rate of the reaction given below:

$$Cl_{2(g)} + ZnO_{(s)} = ZnCl_{2(g)} + \tfrac{1}{2}O_{2(g)} \quad \ldots\ldots\ldots\ldots (1)$$

The two processes referred to are gas phase mass transport and chemical reaction at the gas-solid interface. All chemical reactions are dynamic processes; the net rate of any chemical process is therefore given by the general equation below:

NET RATE = TOTAL FORWARD RATE − TOTAL BACKWARD RATE . . .(2)

If, with a heterogeneous system, chemical rates are high in comparison to transport rates**, the overall reaction rate becomes transport controlled and conditions at the reaction surface approach chemical equilibrium. With the converse situation the reaction rate becomes chemically controlled and the net rate is then described by equation (2). When reactants and products are present at the reaction surface in such proportions that there is a large deviation from equilibrium, the net reaction rate becomes dominated by the concentrations of the reactants. It is then safe to assume a zero

---

* 7 mesh = 2.5 mm 14 mesh = 1.25 mm

** Clearly in any heterogeneous reacting system transport and chemical rates are equal. The word 'rate' is therefore being used as a general expression describing the magnitude of the chemical and transport rate coefficients.

reverse reaction rate. From the data given in section 6C1 it is clear that the equilibrium constant for reaction (1) is relatively large over the whole temperature range studied. Since with all the ZnO non-equilibrium runs the bed exit gas compositions deviated very significantly from equilibrium, if the reaction were chemically controlled the backward reaction rate could be neglected. Alternatively, if the reaction rate were gas phase mass transport controlled, since the equilibrium constant is large, control would lie with the reactant species and not the product species (this behaviour is mathematically described in section 1D2a). Therefore under either chemical, transport or mixed control the overall rate of reaction (1) was determined by chlorine rate processes.

Chlorine transport is a first order process with respect to chlorine partial pressure. In the literature there appear to be no reports on the chemical kinetics of zinc oxide chlorination. An assumption is thus necessary regarding the order of chemical reaction (1) with respect to chlorine partial pressure. Fruehan and Martonik[51] established that the chemical rates of reaction of NiO and Fe_2O_3 with HCl and Cl_2 at 800°C and above are first order with respect to the partial pressure of the chlorinating species. (During chlorination of Fe and Ni metal zero order rates, due to surface coatings of product chlorides, were observed by these workers[52,53]. Since the ZnO experiments were carried out at temperatures and chlorine partial pressures such that $ZnCl_2$ liquid would not appear a product layer effect may be disregarded.) Chemisorbed chlorine (or hydrogen chloride) very probably plays an important part in metal oxide chlorination reaction - mechanisms. However, that the reaction rates of NiO and Fe_2O_3 with chlorine were found to be first order indicates that only a small fraction of the available active sites were ever occupied by chemisorbed molecules. On the basis of these considerations it would therefore seem reasonable to assume that the zinc oxide-chlorine reaction is, under the experimental conditions that were employed, first order with respect to P_{Cl_2}. The rate of chlorine reaction per unit area of ZnO surface can now be calculated for a mixed control reaction; uniform conditions are assumed to hold over the surface being considered.

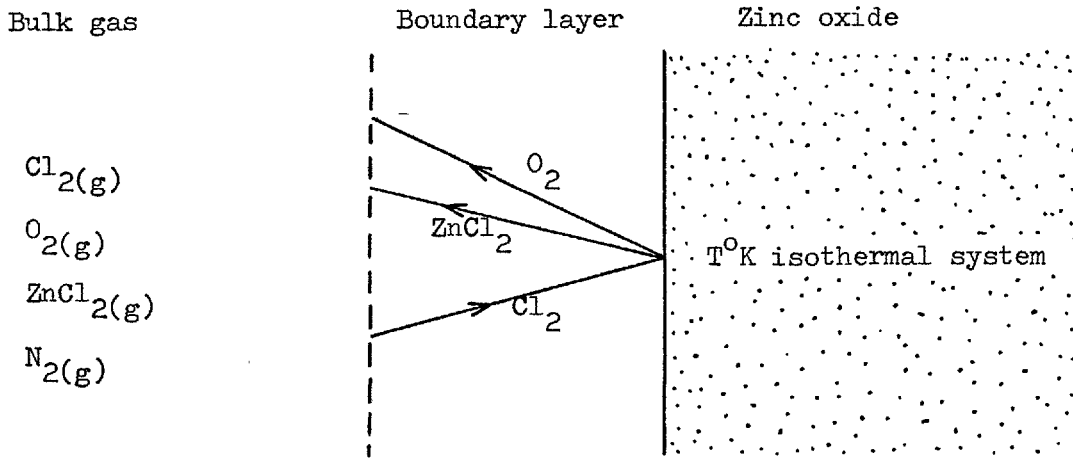

k_{Cl_2} = chemical rate constant

$K_c^{Cl_2}$ = effective boundary layer Cl_2 mass transfer coefficient

${}_bP_{Cl_2}$ = bulk gas phase chlorine partial pressure

${}_sP_{Cl_2}$ = surface chlorine partial pressure

From stoichiometry $\dot{n}''_{Cl_2} = -\dot{n}''_{ZnCl_2}$ . . . . . (a)

Chlorine transport* $\dot{n}''_{Cl_2} = -\frac{K_c^{Cl_2}}{RT} \cdot ({}_bP_{Cl_2} - {}_sP_{Cl_2})$ . . (b)

Chemical reaction $\dot{n}''_{ZnCl_2} = \frac{{}_sP_{Cl_2}}{RT} \cdot k_{Cl_2}$ . . . . . (c)

By combining equations (a), (b) and (c) the following mathematical expression is obtained for the overall zinc chloride rate:

$$\dot{n}''_{ZnCl_2} = \frac{{}_bP_{Cl_2}}{RT} \cdot \frac{K_c^{Cl_2} \cdot k_{Cl_2}}{K_c^{Cl_2} + k_{Cl_2}} \quad \text{. . . . . (d)}$$

If $K_c^{Cl_2}$ is comparatively large, then the reaction is chemically controlled; if it is comparatively small, the reaction is transport controlled. Defining an overall rate constant:

---

* The effective chlorine mass transfer coefficient includes the effect of bulk flow.

$$\dot{n}''_{ZnCl_2} = \frac{b P_{Cl_2}}{RT} \cdot \bar{k}_{Cl_2} \text{ gm-moles/sec cm}^2 \quad \ldots\ldots(3)$$

Using equation (3) it is now possible to derive an expression for the reaction of chlorine in a packed bed of zinc oxide. This is carried out by performing a differential mass balance, the assumptions that have been made are listed below.

a) The reaction is a steady state process, there is thus no accumulation term $\left(\frac{\partial_x c_{Cl_2}}{\partial t}\right) = 0$

b) There is no back mixing.

c) Gas flow distribution is uniform over the bed cross section; there are thus no wall or channeling effects.

d) The effective rate constant does not change with bed position.

e) The bed is isothermal and at constant total pressure, the gases behave ideally.

f) The oxide charge is uniformly distributed in the bed.

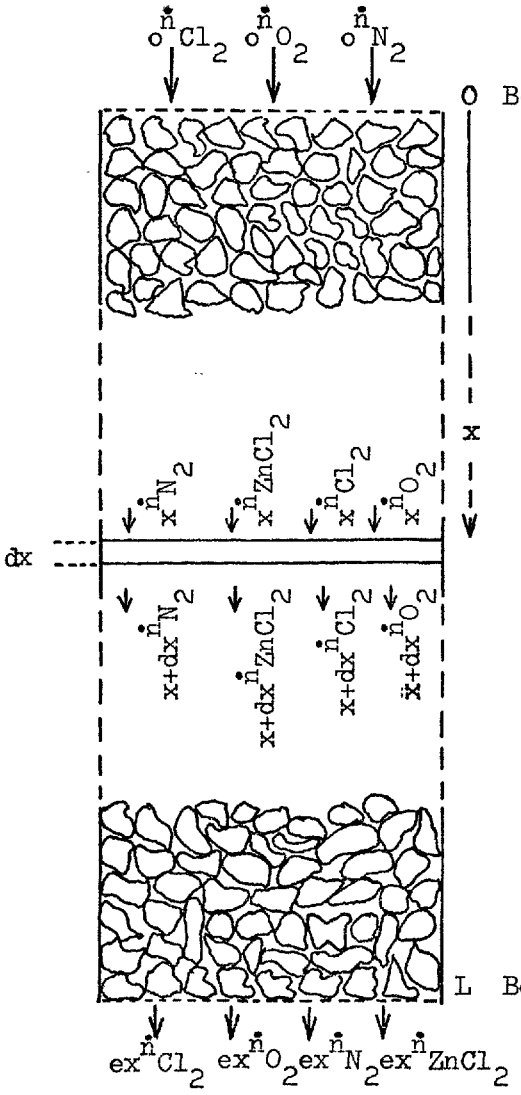

M_L = bed mass per unit length - gms/cm

S_M = surface area per unit mass of oxide charge - cms^2/gm

P = total pressure - atmos

T = temperature - ^oK

sign convention

reaction of reactants -ve

production of products +ve

M = total bed mass - gms

A mass balance on the differential element dx gives the four equations below.

$$d_x\dot{n}_{Cl_2} = x+dx\dot{n}_{Cl_2} - x\dot{n}_{Cl_2} \quad \ldots\ldots\ldots\ldots\ldots (e)$$

$$d_x\dot{n}_{ZnCl_2} = x+dx\dot{n}_{ZnCl_2} - x\dot{n}_{ZnCl_2} \quad \ldots\ldots\ldots\ldots\ldots (f)$$

$$d_x\dot{n}_{O_2} = x+dx\dot{n}_{O_2} - x\dot{n}_{O_2} \quad \ldots\ldots\ldots\ldots\ldots (g)$$

$$d_x\dot{n}_{N_2} = 0 \quad \ldots\ldots\ldots\ldots\ldots (h)$$

From reaction stoichiometry the following relationships are obtained:

$$-d_x\dot{n}_{Cl_2} = d_x\dot{n}_{ZnCl_2} = 2d_x\dot{n}_{O_2} \qquad (i)$$

Applying equation (3) to describe the total reaction rate in the differential element dx, where $_xP_{Cl_2}$ is the bulk chlorine-partial pressure

$$d_x\dot{n}_{ZnCl_2} = dx.M_L S_M.\frac{{}_xP_{Cl_2}}{RT}.\bar{k}_{Cl2} \quad \ldots\ldots\ldots\ldots (j)$$

It is now necessary to derive an expression for $_xP_{Cl_2}$ in terms of $x\dot{n}_{Cl_2}$

$${}_xP_{Cl_2} = P.\frac{x\dot{n}_{Cl_2}}{x\dot{n}_{Cl_2} + x\dot{n}_{ZnCl_2} + x\dot{n}_{O_2} + x\dot{n}_{N_2}} \quad \ldots (k)$$

At position x the total molar gas flow rate (the denominator in the equation above) is:

$$o\dot{n}_{N_2} + o\dot{n}_{Cl_2} + o\dot{n}_{O_2} + \tfrac{1}{2}(o\dot{n}_{Cl_2} - x\dot{n}_{Cl_2}) \quad \ldots\ldots\ldots (l)$$

where subscript 'o' refers to bed entry molar flow rates.

Defining $C = o\dot{n}_{N_2} + o\dot{n}_{O_2} + 1\tfrac{1}{2}o\dot{n}_{Cl_2} \quad \ldots\ldots\ldots\ldots (m)$

therefore

$${}_xP_{Cl_2} = P.\frac{x\dot{n}_{Cl_2}}{C - \tfrac{1}{2}x\dot{n}_{Cl_2}} \quad \ldots\ldots\ldots\ldots\ldots (n)$$

combining equations (i), (j) and (n)

$$-d_x\dot{n}_{Cl_2}\ \frac{(C - \tfrac{1}{2}x\dot{n}_{Cl_2})}{x\dot{n}_{Cl_2}} = dx\, M_L S_M \cdot \frac{P}{RT} \cdot \bar{k}_{Cl_2} \quad \ldots\ldots (o)$$

Integrating between the limits $x = 0$, $x\dot{n}_{Cl_2} = o\dot{n}_{Cl_2}$, and $x = L$, $x\dot{n}_{Cl_2} = ex\dot{n}_{Cl_2}$

$$\int_{o\dot{n}_{Cl_2}}^{ex\dot{n}_{Cl_2}} \left[\tfrac{1}{2}x\dot{n}_{Cl_2} - C\log_e x\dot{n}_{Cl_2}\right] = \int_0^L \left[M_L S_M.\frac{P}{RT}\cdot\bar{k}_{Cl_2}\right] \quad \ldots (p)$$

Rearranging equation (p) with M equal to the total bed mass (LM_L) gives:

$$C\log_e\left(\frac{{}_o\dot{n}_{Cl_2}}{{}_{ex}\dot{n}_{Cl_2}}\right) + \tfrac{1}{2}{}_{ex}\dot{n}_{Cl_2} = MS_M\,\frac{P}{RT}\cdot\bar{k}_{Cl_2} + \tfrac{1}{2}{}_o\dot{n}_{Cl_2} \quad \ldots\ldots (4)$$

where subscript 'ex' refers to the bed exit molar flow rate.

Equation (4) is of the form $y = mx + c$. A plot of the terms on the left of the equation versus bed mass for a number of experiments, all carried out under the same conditions except for variations in bed mass, should therefore yield a straight line with a slope of $S_M \cdot \frac{P}{RT} \cdot \bar{k}_{Cl_2}$ and an intercept of $\frac{1}{2}{}_o\dot{n}_{Cl_2}$.

7A3 Presentation of results

The results presented in this section are derived from the experimental data given in appendix F. The constant

$$C = {}_o\dot{n}_{N_2} + {}_o\dot{n}_{O_2} + 1\tfrac{1}{2}{}_o\dot{n}_{Cl_2}$$

has been calculated, for each run, from the flow rates recorded by the respective flow meters (the NTP molar volumes used for the N_2, O_2 and Cl_2 are given on page 303). The ${}_{ex}\dot{n}_{Cl_2}$ values have been calculated by subtracting ${}_{ex}\dot{n}_{ZnCl_2}$ from ${}_o\dot{n}_{Cl_2}$. The values of

$$C\log_e\left(\frac{{}_o\dot{n}_{Cl_2}}{{}_{ex}\dot{n}_{Cl_2}}\right) + \tfrac{1}{2}{}_{ex}\dot{n}_{Cl_2} \quad \text{gm-moles/sec}$$

are referred to as 'Y' in results table 7A. Since the oxide beds were depleted during chlorination, mean bed masses are used for the data plots. The final calculated data for each run are listed in table 7A; the parameter and values given are a) the predicted Y axis intercepts, b) the oxide size fractions, c) the initial and final recorded bed temperatures, d) the bed entry total pressures, e) the mean bed masses and d) the computed 'Y' values. Plots of 'Y' versus 'mean bed mass' for each series of experiments are shown on graph 7A. No attempt has been made at mathematical curve-fitting since the sets of data do not warrant exact treatment, the 7 lines have thus been drawn by inspection. One B series data point has been disregarded (B1) since it is considered to be a wild result, possibly having been caused by channeling in the bed. Most of the plots exhibit curvature

Run number	oxide size fraction and $\frac{1}{2}\dot{n}_{O}\dot{n}_{Cl_2}$	Initial bed temp °C	Final bed temp °C	Bed entry total pressure Atmos.	Mean bed mass gms	$Y.10^3$ gm-moles /sec
B1		851	848	1.01	114.97	2.44
B2		851	847	1.01	62.62	2.09
B3	-1/4" + 3/16"	851	842	1.01	45.24	1.69
B4		851	836	1.02	30.92	1.13
B5	0.0000604 gm-moles/sec	850	835	1.01	24.10	1.26
B6		849	837	1.01	13.73	0.71
C1		868	863	1.02	58.29	4.50
C2	-3/8" + 1/4"	871	863	1.02	37.57	3.37
C3		875	869	1.01	19.46	1.66
C4	0.0000749 gm-moles/sec	878	876	1.02	81.75	6.56
D1		719	703	1.01	56.99	0.954
D2	-3/16" + 7 mesh	721	698	1.01	28.18	0.699
D3		714	706	1.02	86.81	1.17
D4		727	700	1.02	18.89	0.585
D5	0.000262 gm-moles/sec	720	698	1.01	42.89	0.787
D6		721	716	1.02	140.08	1.57
D7		719	713	1.04	105.75	1.35
D8		721	710	1.03	11.07	0.497
J1		706	698	1.02	46.12	0.426
J2	-1/4" + 3/16"	705	700	1.02	83.62	0.563
J3		706	702	1.02	149.65	0.759
J4	0.000114 gm-moles/sec	705	696	1.02	25.00	0.335
I1		706	702	1.02	98.05	0.750
I2	-3/16" + 7 mesh	706	703	1.02	147.69	0.910
I3		705	693	1.02	29.97	0.436
I4	0.000113 gm-moles/sec	706	700	1.01	55.66	0.549
K1		705	696	1.03	58.49	0.761
K2	-7 mesh + 14 mesh	704	699	1.03	150.55	1.09
K3	0.000115 gm-moles/sec	705	699	1.03	87.88	0.876
E1	-1/4" + 3/16"	859	863	1.02	68.27	4.37
E2	0.0000229 gm-moles/sec	859	863	1.01	28.45	2.37

TABLE 7A: ZnO NON-EQUILIBRIUM CHLORINATION RESULTS

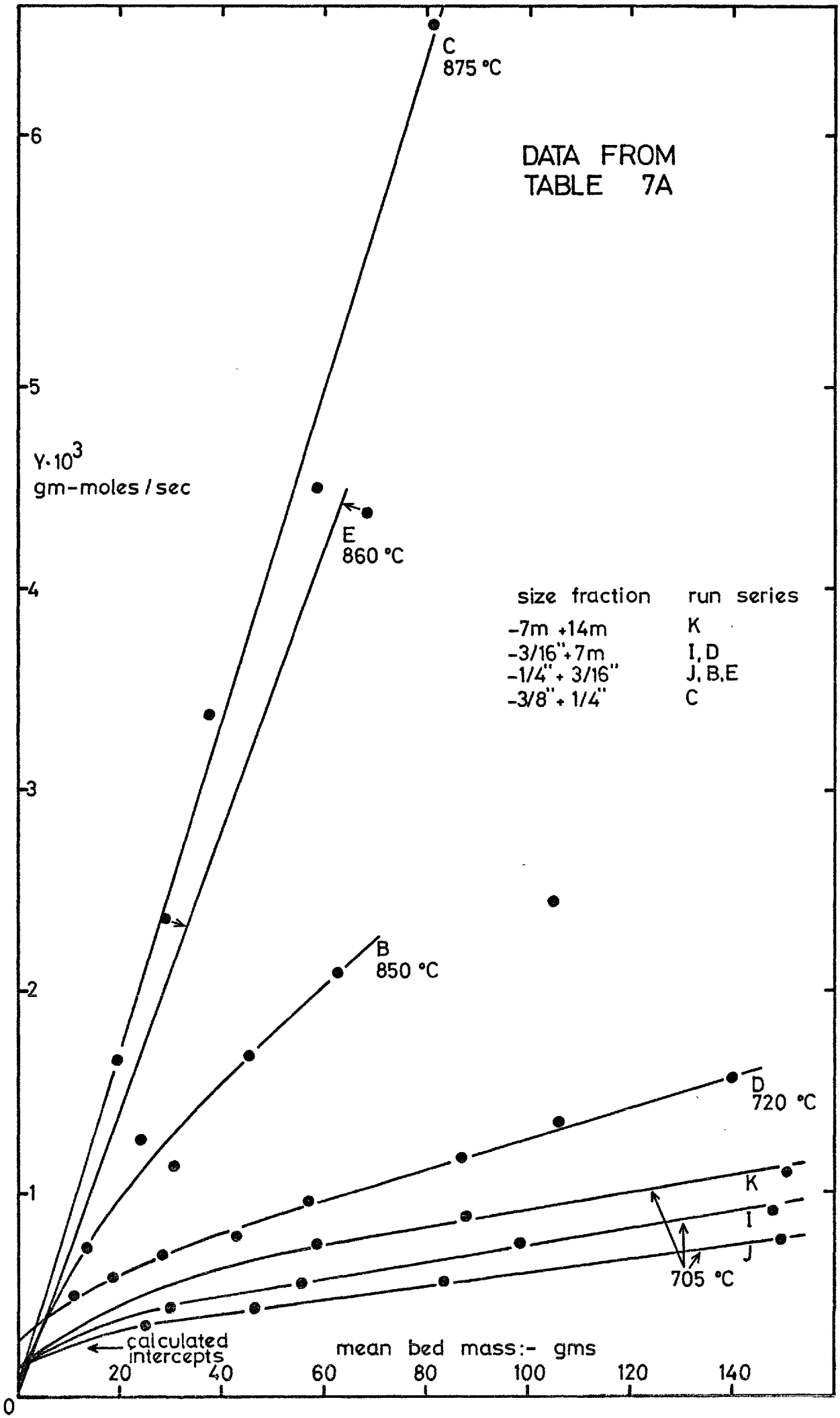

GRAPH 7A: ZnO CHLORINATION RATE ANALYSIS PLOTS

in the region of comparatively small bed size, this phenomenon is discussed in section 9A3. The computed gradient of the linear portion of each line (as drawn) is given in table 7B.

Experiment series	Nominal temperature ^{o}C	Gradient gm-moles sec^{-1} gms^{-1}
C	873	7.8×10^{-5}
E	860	7.0×10^{-5}
B	850	2.6×10^{-5}
D	720	7.9×10^{-6}
K	705	4.4×10^{-6}
I	705	4.1×10^{-6}
J	705	3.4×10^{-6}

TABLE 7B: $S_{\bar{M}} \cdot \frac{P}{RT} \cdot \bar{k}_{Cl_2}$ VALUES

In order to determine overall rate constants from the gradients given in table 7B values of S_M (surface area/unit mass) are required for each of the four different zinc oxide size fractions.

7A3a Granular ZnO - surface area estimates:- Accurate measurement of the true surface area* of irregular shaped solids is a difficult, if not often impossible, task. The only quantitative method that exists for experimentally determining a solid surface area genuinely representative of the true surface area is due to Brunauer, Emmett and Teller (BET). Their method[116], published in 1938, depends upon the adsorption of a monolayer (or multi-layers) of gaseous molecules onto the surface of the solid under test. For large surface areas it is a sensitive technique but loses in accuracy as the surface area per unit mass decreases; there are no reports of determinations at less than about 50 cm^2/gm; at these levels results are difficult to obtain and are susceptible to large errors. BET analysis was therefore not considered to be a suitable means for determining the specific surface areas** of the zinc oxide granules used in this study; it has thus been necessary to estimate the values. Careful visual examination of

* At an atomistic level the concept of surface area is difficult to define. However, what is of significance is the value of the number of constituent atoms or molecules that are exposed to the surroundings; the true surface area is therefore taken to be an area value that is directly related to this quantity.

** surface area/ unit mass = S_M

a large number of different sized ZnO granules showed that the range of solid geometries within any narrow size gradation appeared to remain constant, confirmation of this observation may be obtained from plate 3. It is therefore safe to assume that the 'average geometry' of a large population of each of the four different size fractions is the same. The specific surface area of any given geometric shape is inversely proportional to its linear dimension (the constant of proportionality will of course vary with the actual shape and also with which dimension is taken eg length, breadth, height, diameter, circumference etc). Therefore, by halving the linear size of a given shape its specific surface area is doubled. The effective specific surface area of each of the four ZnO size fractions are thus approximately in the ratio of the inverse of their mean sieve sizes. Another method of calculating the ratios of the specific surface areas of different size fractions is to compare equal masses of the different fractions. Any given solid object may in theory be transformed into a number of smaller replicas. If the replicas are all made to be half the linear size of the original, 8 will be obtained. From the preceding discussion it is evident that the specific surface of the smaller objects will be twice that of the original. In general, by dividing a given solid object into N equal sized smaller replicas an increase in specific surface of $N^{1/3}$ is obtained. The ratios of the specific surfaces of the four ZnO size fractions are thus approximately equal to the ratios of the cube roots of the number of granules from each fraction that comprise the same mass of solid (that is, provided reasonably large numbers of granules are involved).

It is now necessary to find a method by which to estimate the actual specific surface of one of the size fractions. Since it is impossible to estimate the 'roughness' of the surface of the zinc oxide granules, only a 'geometric' specific surface ($S_{\overline{M}}$) can be gauged. This geometric specific surface (equally important as the specific surface in cases of gas phase mass transport control) assumes each ZnO granule to be macroscopically smooth. The ratios of the geometric surface area to the projected surface area for flat lying thin plates and cubes and for spheres are 2, 6 and 4 respectively. Since they were essentially plate like the zinc oxide granules all tended to lie flat when spread out to be photographed. It is thus estimated that the ratio of the geometric to projected surface area for the granules shown on plate 3 is about 3. In addition, it is estimated

that the smallest size fraction granules shown on this plate cover about 35% of the 3 inch square within which they lie. Their projected surface area is therefore about 20.3 cms^2, their geometric surface area about 60.9 cms^2 and their geometric specific surface about 12.2 cms^2/gm. By using this last value it is now possible to determine the approximate geometric specific surfaces of the other size fractions.

Size fraction	Arithmetic mean size mm	Number of granules on plate 3	Ratios of inverse of mean size	Ratios of (number of granules)$^{1/3}$	Estimated geometric specific surface cms^2/gms
+14M-7M	1.87	285	4.24	3.85	12.2
+7M-3/16"	3.63	30	2.18	1.82	6.0
+3/16"-1/4"	5.56	10	1.43	1.26	4.1
+1/4"-3/8"	7.94	5	1	1	3.0

TABLE 7C: ZnO GRANULES - ESTIMATED GEOMETRIC SPECIFIC SURFACE VALUES

In the table 7C are given the $S_{\bar{M}}$ estimates and the data upon which they are based. The geometric specific surface ratios used were the mean of the 1/diameter and $N^{1/3}$ ratios; the $S_{\bar{M}}$ values were then calculated from these mean ratios and the estimated $S_{\bar{M}}$ value of the smallest size fraction. It is not necessary to further explain that the $S_{\bar{M}}$ estimates are only approximate, however, it is the author's opinion that the errors in the values are probably within a factor of about x2.

7A3b Overall rate constants:- Using the gradients given in table 7B and the geometric specific surfaces in table 7C the following overall rate constants have been calculated:

Run series	Temperature ^oC	$\bar{k}_{Cl_2}$ cms/sec
C	873	2.4
E	860	1.6
B	850	0.58
D	720	0.13
K	705	0.030
I	705	0.055
J	705	0.066

7A3c Additional observations on the ZnO experiments:- In table 7A are given the initial* and final* bed temperatures that were recorded during each experiment. The two facts apparent from these values are a) significan temperature gradients could exist down the beds, and b) they were caused by the endothermic nature (ΔH° = 17910 cals/mole, see section 6C1) of the chlorination reaction. The three largest ΔT's occurred during D series runs, relatively small beds were being reacted whilst the chlorine flow rate was the highest used for any of the ZnO experiments. The values of the temperature drops were 27, 23 and 22 deg. C respectively, the largest bed of the D series runs produced a ΔT of 6 deg. C. With the lowest chlorine flow rate runs, series E, during which the flow was x11.4 less than for series D, the maximum temperature drop was 4 deg. C. The ΔT's given above are maximum values since they are the differences between the initial and final bed temperatures. Bed temperature chart recordings were taken for all the experiments. These showed that once the chlorinating gas mixture reached the bed the temperature started to fall relatively rapidly, a quasi steady state value was however reached after about only 4 to 5 minutes. After chlorination the granules that had reacted to a significant extent were somewhat reduced in size, more rounded and covered with a very thin pure white soft powdery coating of zinc oxide, estimated to have been at maximum** less than about 1/20 mm thick. The extent of this alteration in physical appearance was most pronounced with granules from the top of each bed, those from the bottom of deep beds were virtually unchanged. Post-chlorination examination of in situ oxide beds showed that the areas of zinc oxide in close proximity with the reactor wall were relatively little reacted. Whilst removing the reacted beds, further low reacted areas were observed at points of granule-granule contact.

7B CdO/ZnO NON-EQUILIBRIUM EXPERIMENTS

The factors which governed the choice of the experimental technique and reaction configuration used to study the non-equilibrium chlorination of CdO/ZnO mixtures have been discussed in section 2C2. Having made the decision to use a packed bed reactor-condenser system it then became clear that in order to gain a reasonable understanding of mixed oxide chlorination kinetics reaction would need to be performed under non-steady state

---

* The initial temperature was taken before chlorination commenced, the final temperature just before it was completed.

** The powdery surface coatings were noted to be very much thinner with the higher temperature (>850°C) experiments.

conditions (rather than those approximating to a steady state as had been used for the ZnO work). Unsteady state processes are best analysed using continuously measured experimental rate data. However, instantaneous rate data measured at frequent intervals of time during the process may often be used equally effectively. Neither continuous nor instantaneous rate data could be obtained from the CdO/ZnO non-equilibrium experiments; it was therefore necessary to perform step wise chlorination experiments* from which mean rates for the duration of each step could be calculated. The number of possible experimental variables involved in the chlorination process were many (viz - temperature, gas flow and composition, pellet size and composition, bed mass and reaction time); in addition, since the experiments were performed in a step wise manner each was a relatively lengthy procedure. Under these circumstances it was therefore decided to limit the experiments to a study of the effects of variations in temperature and pellet composition. So that changes in the $ZnCl_{2(g)}$ and $CdCl_{2(g)}$ rates would be small enough to be conveniently measured by runs of not less than a few minutes duration, whilst at the same time maintaining a moderate total gas flow, a low chlorine partial pressure (0.045 atmos) was used for all the experiments. In order that the chlorination experiments would provide critical data** a number of preliminary runs, under different reaction conditions were carried out to obtain approximate $ZnCl_{2(g)}$ and $CdCl_{2(g)}$ rates (these runs are not reported in this thesis). From these results it was possible to estimate with reasonable accuracy what combination of operating conditions were required to produce the maximum quantity of critical experimental data.

7B1 Details of experimental procedure

A list of the sequence of operations carried out whilst performing a chlorination experiment together with details on condensate collection

---

* With regard to the results presented in this section the word 'experiment' describes the total number of chlorination stages performed on one bed; the word 'run' describes one such stage.

** For any scientific experiment to be of maximum efficiency it is essential that the results obtained are of a critical nature, namely that they highlight the interrelation(s) between the parameters being investigated. For example, it would be worthless investigating mixed oxide non-equilibrium chlorination separation under conditions that were either very close to chemical equilibrium or gave no separation.

and analysis are given in section 4B1. Additional details specific to the CdO/ZnO non-equilibrium experiments are given in section 4B2c. All condensates were anlysed, by atomic absorption spectrophotometry, for zinc and cadmium. The reactor I.D. was 27.5 mm. The temperature before and during runs was measured and recorded from an internal thermocouple located close to the bed exit. As has been previously described, each bed was chlorinated in stages. The time interval between the end of one chlorination step and the start of the next (during which time the reactor was kept in the furnace) was controlled by the following two factors: a) the slow speed (about 20 to 25 minutes) at which a cold condenser could be introduced into the hot furnace, and b) only two concentric tube condensers were employed, the condensates within them therefore had to be collected (see section 4B1d) before either could be re-used. Typically, an experiment for which the total reaction time was 90 minutes resulted in the bed being at temperature for about 6 hours; full details are given in Appendix H.

7B2 Presentation of results

Full sets of experimental data for all the CdO/ZnO non-equilibrium runs (SK3-SK61) are given in Appendix H. All the experiments employed N_2-Cl_2 chlorinating gas mixtures, the nominal flows were 1200 mls_{NTP}/min and 55 mls_{NTP}/min respectively. Experiments were performed at 750°C, 850°C and 950°C; each employed an initial bed mass of close to 120 gms; this quantity of pellets produced beds which were on average about 8 cms deep. Pellets of three different compositions were studied, these contained 50.0, 26.6 and 10.8 mole % CdO; their manufacture is described in section 4A2. The pellets used for all the experiments were within the size range -6.7 mm + 5.6 mm. A photograph of 6 randomly selected unreacted pellets of this size range, for each composition, is shown on plate 3. Cadmium oxide powder is dark brown in colour whilst zinc oxide powder is white, the 10.8 mole % CdO pellets were therefore considerably lighter in colour than were the 50.0 mole % pellets; this difference is partly visible from the photograph of the pellets. It is also evident from the photograph that the degree of success at making the pellets spherical was somewhat variable, the reasons for deviations from roundness are discussed in sections 4A2a and 8A1a. Reactor-condenser pressure drops were never more than about 4 mm of Hg, the total pressure in each bed during chlorination was thus only slightly greater that the then current atmospheric pressure.

The experimental results have been treated in the following manner. From the amounts of Zn and Cd found (by AA analysis) in the condensate from each run mean bed exit $ZnCl_{2(g)}$ and $CdCl_{2(g)}$ rates have been calculated. As a best approximation, rates determined in this way have been assumed to be equal to the actual rates at the mid-time of each of the chlorination stages comprising each experiment. Calculated bed-exit $ZnCl_{2(g)}$ and $CdCl_{2(g)}$ rates for each chlorination stage of each experiment together with the total reaction time to the middle of these stages are given in table 7D. Also given in this table are the bed-entry chlorine rates as determined from the flow meter readings, the reaction temperatures, the pellet compositions and the total chlorination time for each experiment. The data given in table 7D are plotted on graphs 7B, 7C and 7D, the plots are of zinc chloride and cadmium chloride rate against time. Graph 7B shows the experimental results (750°C, 850°C and 950°C) for the 50.0 mole % CdO pellets, 7C for the 26.6 mole % CdO pellets, 7D for the 10.8 mole % CdO pellets. The average total chloride ($ZnCl_2$ + $CdCl_2$) volatilisation rate for the runs on each of the three different composition pellets are:

50.0 mole % CdO - 38.8×10^{-6} gm-moles/sec
26.6 mole % CdO - 38.5×10^{-6} gm-moles/sec
10.8 mole % CdO - *40.4×10^{-6} gm-moles/sec

From the values given above bed exit zinc and cadmium chloride rates corresponding to 'zero separation' have been calculated, these are shown as broken lines on graphs 7B, 7C and 7D. Zero separation is taken to be the point at which the ratio of the rate of zinc to cadmium chloride is equal to the ratio of the ZnO to CdO initially in the pellets. Thus, for the 50.0 mole % CdO pellets zero separation is when the zinc and cadmium chloride rates are equal, for the 26.6 mole % CdO pellets when the cadmium chloride rate is 26.6% of the total-chloride rate and for the 10.8 mole % CdO pellets when the cadmium chloride rate is 10.8% of the total-chloride rate. The average chloride-volatilisation rates given above would not be of any significance if there were more than only very slight variations in chlorine utilisations over the range of different reaction temperatures and conditions employed. Given in table 7E are the average chlorine utilisations at each reaction temperature.

---

* This is the average of the 850°C and 950°C runs only. The 750°C experiment has been omitted from the calculation since the chloride rates for its last three stages were about 10% low. See appendix H.

Run number	Temperature, pellet composition and total chlorination time	Total reaction time to middle of runs - mins.	$ZnCl_{2(g)}$ rate $\times 10^6$ gm-moles/sec	$CdCl_{2(g)}$ rate $\times 10^6$ gm-moles/sec	Metered bed entry chlorine rate $\times 10^6$ gm-moles/sec
SK15	753°C	2.50	0.66	38.0	41.7
SK16		7.50	0.68	39.0	41.7
SK17	50.0 mole % CdO	14.0	0.82	37.7	41.5
SK18		23.5	1.16	37.7	41.5
SK19		36.5	1.53	37.0	41.5
SK20	90.1 minutes	54.0	2.38	34.7	41.5
SK21		77.0	3.68	34.3	41.5
SK3	852°C	2.50	0.96	37.3	41.7
SK4		7.50	1.13	38.3	41.7
SK5	50.0 mole % CdO	15.0	2.66	35.5	41.5
SK6		27.5	4.33	35.0	41.5
SK7	53.0 minutes	43.0	7.66	32.0	41.5
SK8	951°C	2.50	1.34	37.0	41.7
SK9		7.50	4.63	34.7	41.7
SK10	50.0 mole % CdO	14.0	12.2	26.7	41.5
SK11		23.5	15.4	23.7	41.5
SK12	90.0 minutes	36.5	16.7	22.8	41.5
SK13		54.0	17.3	21.8	41.5
SK14		77.0	18.0	20.5	41.5
SK22	752°C	2.50	0.71	38.3	41.7
SK23		7.50	1.03	38.5	41.5
SK24	26.6 mole % CdO	14.0	1.60	37.0	41.5
SK25		23.5	2.97	35.5	41.7
SK26	90.0 minutes	36.5	4.77	33.3	41.7
SK27		54.0	7.38	29.8	41.7
SK28		77.0	11.4	25.9	41.5
SK36	851°C	2.50	1.88	36.2	40.7
SK37		7.58	5.38	32.7	40.5
SK38	26.6 mole % CdO	14.2	7.76	30.6	40.5
SK39		23.7	12.0	26.5	40.5
SK40		36.7	14.9	23.0	40.5
SK41	90.2 minutes	54.2	18.1	19.3	40.5
SK42		77.2	22.0	16.4	40.5

TABLE 7D (part 1): CdO/ZnO NON-EQUILIBRIUM CHLORINATION RESULTS

Run number	Temperature, pellet composition and total chlorination time	Total reaction time to middle of runs - mins.	$ZnCl_{2(g)}$ rate $\times 10^6$ gm-moles/sec	$CdCl_{2(g)}$ rate $\times 10^6$ gm-moles/sec	Metered bed entry chlorine rate $\times 10^6$ gm-moles/sec
SK43	951°C	2.50	2.68	36.5	41.2
SK44		7.50	14.5	25.3	41.2
SK45	26.6 mole % CdO	14.0	25.7	14.3	41.2
SK46		23.6	27.0	12.4	41.2
SK47	90.1 minutes	36.6	28.2	11.7	41.2
SK48		54.1	27.0	11.0	41.2
SK49		77.1	28.1	10.2	41.2
SK29	752°C	2.50	0.91	38.0	41.5
SK30		7.50	2.46	35.2	41.7
SK31	10.8 mole % CdO	14.0	4.87	34.0	41.5
SK32		23.5	8.11	29.4	41.5
SK33	90.0 minutes	36.5	13.3	21.2	42.0
SK34		54.0	20.0	14.9	41.8
SK35		77.0	25.4	7.05	41.5
SK50	851°C	1.50	1.09	38.5	41.2
SK51		5.00	2.75	37.8	41.2
SK52	10.8 mole % CdO	9.50	5.99	34.0	41.2
SK53		16.0	10.2	30.6	41.2
SK54	53.0 minutes	26.5	16.2	24.5	41.3
SK55		43.0	22.8	17.5	41.3
SK56	952°C	1.50	3.94	35.7	41.8
SK57		5.00	21.7	19.8	41.8
SK58	10.8 mole % CdO	9.50	28.3	11.6	41.7
SK59		16.0	31.0	9.17	41.8
SK60	52.0 minutes	27.5	33.1	8.26	41.7
SK61		42.5	33.0	7.43	41.7

TABLE 7D (part 2): CdO/ZnO NON-EQUILIBRIUM CHLORINATION RESULTS

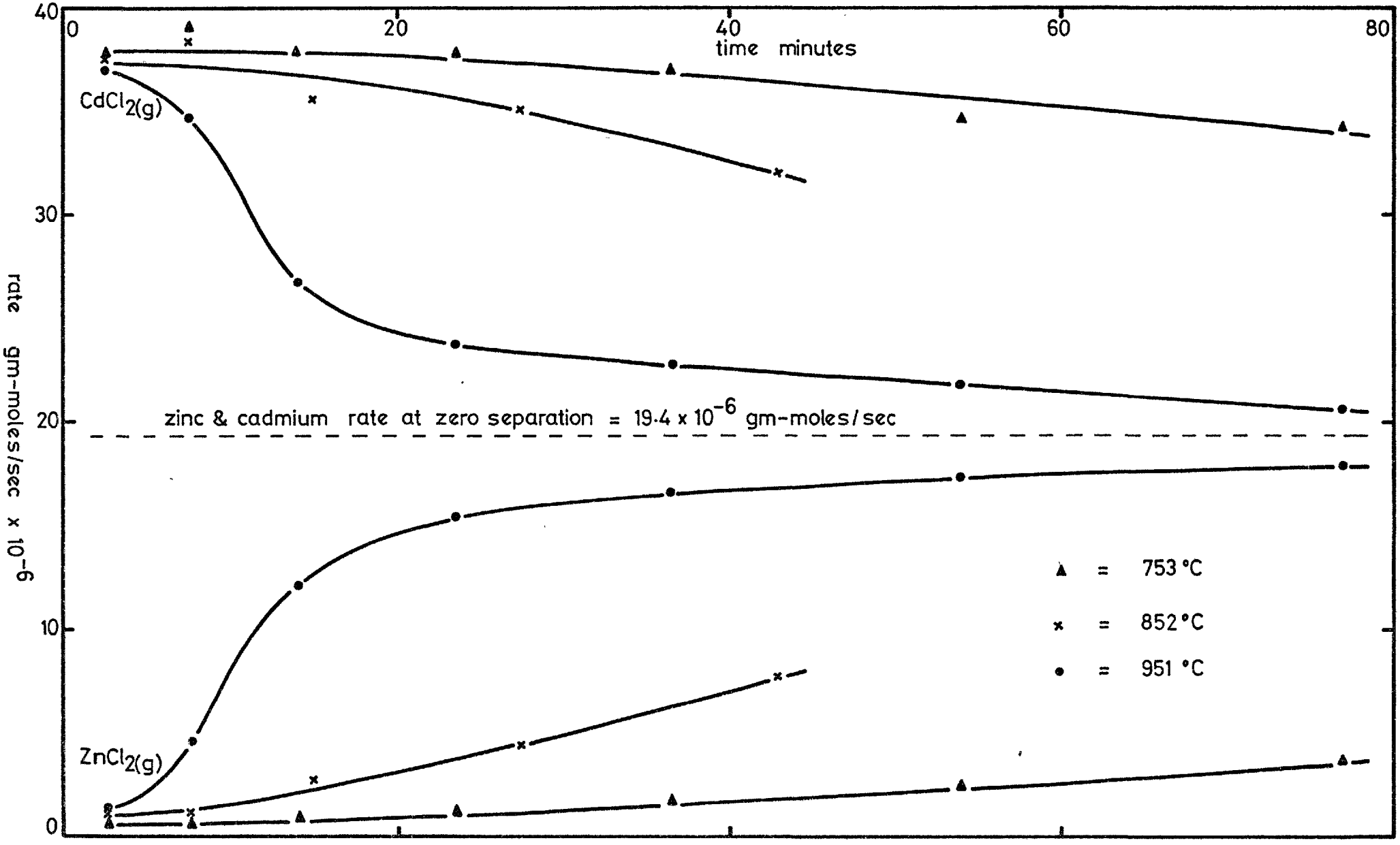

GRAPH 7B: 50·0 MOLE % CdO NON-EQUILIBRIUM RESULTS; $CdCl_{2(g)}$ AND $ZnCl_{2(g)}$ RATE vs TIME CURVES. DATA FROM TABLE 7D

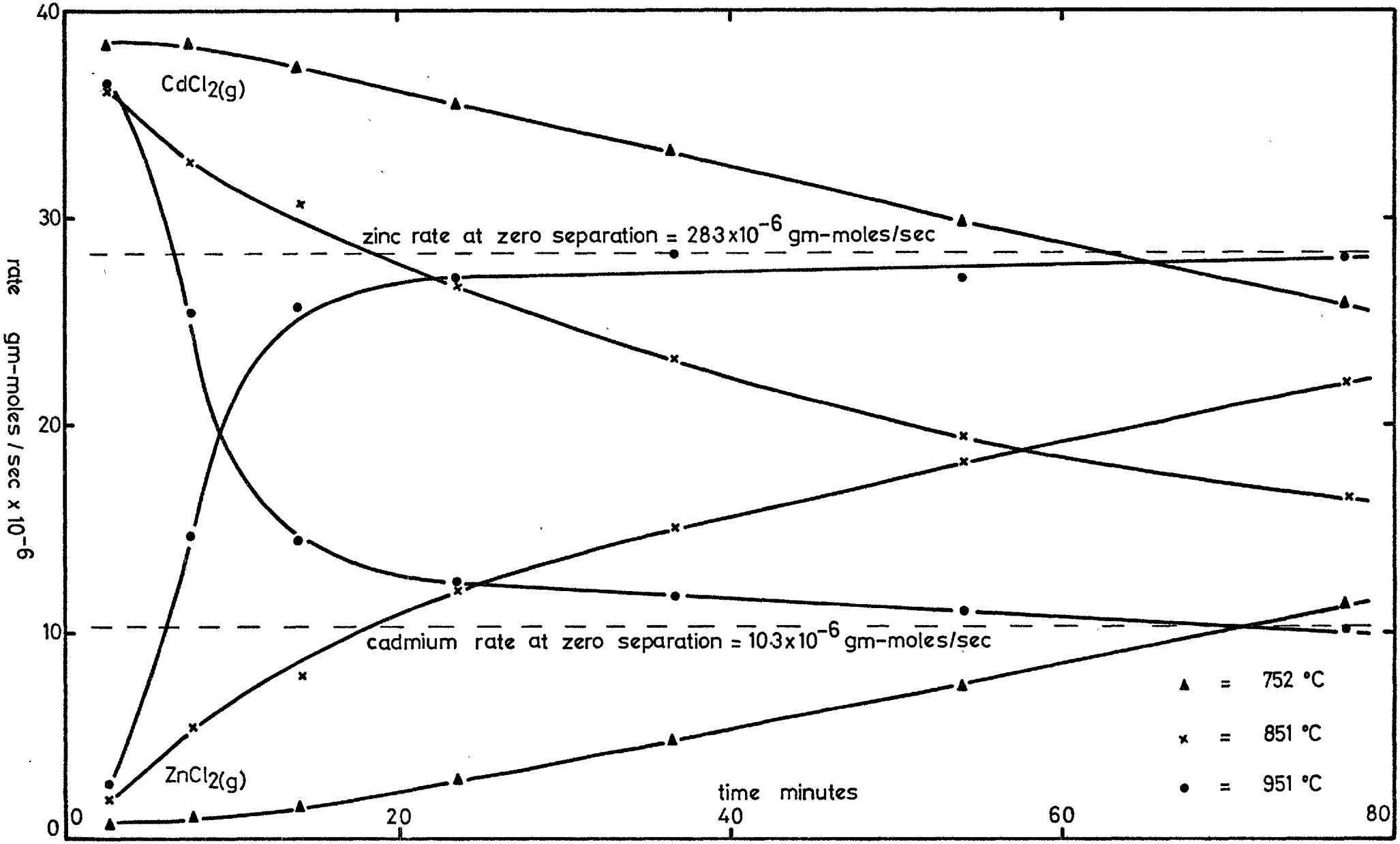

GRAPH 7C : 26·6 MOLE % CdO NON-EQUILIBRIUM RESULTS; $CdCl_{2(g)}$ AND $ZnCl_{2(g)}$ RATE vs TIME CURVES. DATA FROM TABLE 7D

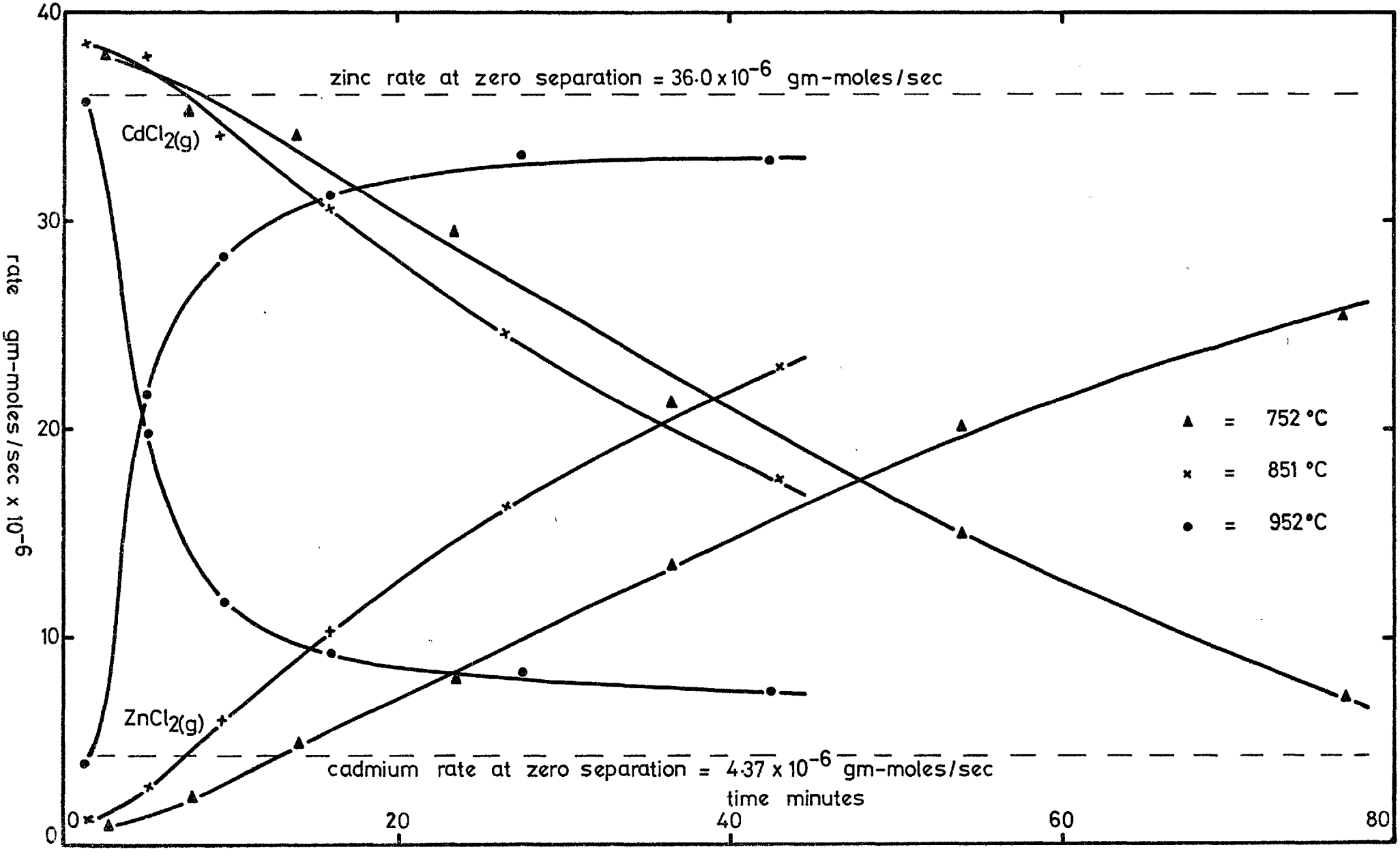

GRAPH 7D: 10·8 MOLE % CdO NON-EQUILIBRIUM RESULTS; $CdCl_{2(g)}$ AND $ZnCl_{2(g)}$ RATE vs TIME CURVES.

DATA FROM TABLE 7D

Nominal temperature °C	Average Cl_2 rate gm-moles/sec	Average chloride rate gm-moles/sec	Average Cl_2 utilisation %
750	*41.6×10^{-6}	*38.4×10^{-6}	*92.3
850	41.1×10^{-6}	39.1×10^{-6}	95.2
950	41.5×10^{-6}	39.5×10^{-6}	95.2

TABLE 7E: Indicated chlorine utilisations for CdO/ZnO non-equilibrium experiments

The chlorine flow rates for all the CdO/ZnO non-equilibrium experiments were measured by use of orifice "C5". In section 4C3, whilst discussing chlorine mass balances, it has been pointed out that orifice "C5" for a given pressure drop passed less chlorine than was indicated from its calibration plot. Overall utilisations (using "C5") for the CdO/ZnO equilibrium experiments and the ZnO proving runs were 97.0% and 93.3% respectively, however both were expected to be close to 100%. The utilisations given in table 7E are thus very probably a few per cent low. It would therefore seem safe to assume effective chlorine utilisations of 100% for all the CdO/ZnO non-equilibrium runs.

The lines plotted on graphs 7B, 7C and 7D have been drawn as smooth curves through the experimental data points. There are several interesting features common to all the curves. For every experiment the cadmium rate curve and the zinc rate curve are, within experimental error, mirror images of each other. This has been caused by the total chloride rate ($ZnCl_2$ + $CdCl_2$) remaining constant, at very close to the bed entry Cl_2 rate over the duration of each experiment. Under all experimental conditions the cadmium rate decreased and the zinc rate increased as chlorination proceeded. Without comparing the experiments this general behaviour is in no way surprising. However, when they are compared, what is most striking is that for each pellet composition the respective decrease and increase in rates became progressively greater with increasing temperature. With increasing temperature the degree of separation of cadmium from zinc therefore decreases far in excess of the decrease that occurs in the equilibrium ratio P_{CdCl_2}/P_{ZnCl_2}. For example, at 750°C

* Excluding the 10.8% CdO experiment

850°C and 950°C for the 26.6 mole % CdO experiments, the percentages of cadmium and zinc volatilised (based upon initial amounts present) over the 90 minute period of chlorination were 50.0% and 3.63%, 34.9% and 8.90% and 21.4% and 14.6% respectively. In table 7F are given the ratios of the cadmium rate to the zinc rate for the first chlorination stage of each experiment, also shown are the equilibrium ratios P_{CdCl_2}/P_{ZnCl_2} (oxides at unit activity, equilibrium data taken from section 5F3)[2] corresponding to the three reaction temperatures.

Nominal temperature °C	Equilibrium ratio P_{CdCl_2}/P_{ZnCl_2}	Ratio of Cd rate to Zn rate for first stage of experiment		
		50.0 mole % CdO	26.6 mole % CdO	10.8 mole % CdO
750	62.7	57.6	53.9	41.8
850	41.0	38.8	19.3	35.3
950	28.8	27.6	13.6	9.06

TABLE 7F: Ratios of $CdCl_2$ to $ZnCl_2$ rates for first stage of chlorination experiments

It is extremely doubtful whether, at any stage during chlorination of the mixed oxide pellets, the equilibrium P_{CdCl_2}/P_{ZnCl_2} ratios could be exceeded anywhere in the reactor except at the surface of the CdO micro particles contained in the pellets. The equilibrium separation ratios may therefore be seen as being equal to the maximum possible cadmium chloride rate to zinc chloride rate ratios that could be obtained from the beds. The figures in table 7F show that during the first stage of chlorination of each bed equilibrium ratios were never exceeded but were often closely approached. This would seem to indicate that the bed exit gas composition tended to equilibrium at the start of each experiment. Deviation away from the equilibrium ratio at a given temperature occurred more rapidly and also to a greater extent with pellets containing lesser amounts of CdO. With the extreme cases of decreasing cadmium rate - increasing zinc rate, namely those experiments at 950°C, conditions of zero separation were closely approached at an early stage of chlorination.

7B3 Additional observations on the CdO/ZnO non-equilibrium experiments

Due to a error in flow meter adjustment the N_2 carrier gas flow rate was about 14% high with runs SK51 to SK55 (850°C - 10.8 mole % CdO). The total-chloride rates during the last three stages of the 750°C - 10.8 mole % CdO experiment were between about 8.4 and 15% low. The chlorine flow meter reading was however constant throughout the experiment. The low rates, real or apparent, must have thus been due either to a chlorinating gas leak, a loss of chlorides, an error in analysis or channeling in the bed. The effect produced by this experimental error is visible on graph 7D. The temperature close to the bed exit was measured and continuously recorded for every run; there were never any detectable variations in temperature at this position. During some experiments the thermocouple was slowly moved, inside its sheath, up to the bed; only slight temperature fluctuations of up to about $\pm$ 3 deg. C were ever detected. Agreement between the measured weight of condensate and the calculated* weight of condensate was good in the case of every run. Since the reactor was not weighed between runs only measured weight losses over the several chlorination stages of each experiment could be obtained. Agreement between these values and calculated* reactor weight losses was excellent, disagreement at worst was 4.1% at best 0.5%. Comprehensive descriptions (together with photographs) of the different physical properties of the various reacted and unreacted CdO/ZnO pellets are given in section 8A.

7C CdO/ZnO DOUBLE BED NON-EQUILIBRIUM EXPERIMENTS

The double bed runs reported in this section were performed after a detailed analysis of the CdO/ZnO non-equilibrium experiments had produced clear evidence indicating that, with these experiments, the exchange reaction

$$ZnCl_{2(g)} + CdO_{(s)} = CdCl_{2(g)} + ZnO_{(s)} \quad \ldots\ldots\ldots\ldots (1)$$

was a very important process. Details of the experimental and theoretical evidence supporting this assertion are given in chapter eight. In brief; it was found that volatilisation of cadmium from the beds of CdO/ZnO

---

* Based on condensate analysis

pellets was a topochemical process (shrinking core); due to the physical structure of the pellets, and the high reaction rate of chlorine with both zinc oxide and cadmium oxide, penetration of $Cl_{2(g)}$ into the pellets was minimal; cadmium oxide chlorination, except at the start of reaction, was therefore by $ZnCl_{2(g)}$. To obtain some measure of the exchange reaction rate it was therefore decided to perform chlorination experiments on CdO/ZnO and CdO beds using $ZnCl_{2(g)}$ as the chlorinating species. These experiments were carried out by placing two oxide beds in the reactor at once, the lower bed consisted of either CdO/ZnO pellets or CdO pellets, whilst sitting on top of this, separated by a silica wool plug, was a deep bed of small ZnO pellets; the mass of the upper bed was never less than 340 gms. During each run almost all the chlorine* entering the upper bed thus reacted to form zinc chloride, this then passed into the second bed where exchange reaction (1) took place.

7C1 Details of experimental procedure

A list of the operations performed whilst carrying out a chlorination experiment along with details on condensate collection and analysis are given in section 4B1. Details specific to the double bed runs are given in section 4B2d. The same 27.5 mm I.D. reactor as used for the CdO/ZnO non-equilibrium experiments was employed together with an internal thermocouple. Each experiment consisted of only one relatively short period of chlorination.

7C2 Presentation of results

Full sets of experimental data for all the double bed runs (SMK1, SMK4-14) are given in appendix I; also given are data for two CdO chlorination runs (SMK2-3). Since no CdO experiments had yet been carried out these last two runs were performed simply to investigate whether there were any unusual phenomena associated with CdO chlorination. Experiments, each of which lasted for 6 minutes (except for run SMK12 which was 6.7 minutes in duration) were performed at 750°C, 850°C and 950°C. As with the CdO/ZnO non-equilibrium experiments the gas flow entering the reactor for each

---

* Under the experimental conditions employed it is thought that a very close approach to equilibrium would have been achieved in the ZnO beds. Under such circumstances at least 98% of the chlorine entering the reactor would have emerged from the upper bed in the form of $ZnCl_{2(g)}$.

run consisted of Cl_2 diluted in a carrier gas, the nominal flows being 55 mls_{NTP}/min and 1200 mls_{NTP}/min respectively. For 12 of the runs nitrogen was used as carrier gas, the remaining two employed oxygen. The manufacture of the ZnO, CdO and CdO/ZnO pellets is described in section 4A2. The size fractions used were: ZnO -4.0 + 2.0 mm, CdO -4.75 + 4.0 mm and CdO/ZnO - 8.0 + 6.7 mm. Zinc oxide beds, their size not being critical, were between 340 and 430 gms in mass; the cadmium oxide beds were of 70 gms mass and the mixed oxide beds were of 80 gms mass. The mixed oxide pellets* contained 50.0 mole % CdO. As with the single bed mixed oxide non-equilibrium runs, chlorine utilisations (calculated from condensate analyses and indicated Cl_2 flow rates) were lower than expected; the mean utilisation of the 12 double bed runs was 94.8%. This discrepancy is attributed to the previously described error associated with orifice "C5". Agreement between the measured and calculated reactor weight loss, and between the measured and calculated condenser weight gain, was good for each run performed. Measured pressure drops across the reactor-condenser assembly were between 3.2 and 8.9 mm of Hg. The results of the double bed experiments are summarised in table 7G. Those runs employing a CdO/ZnO lower bed were repeated once in order to determine their degree of reproducibility. Since the runs on CdO/ZnO pellets were found to be insufficiently reproducible to allow quantitative analysis, whilst those on CdO were inconclusive, double bed experiments were discontinued. To clarify the CdO/ZnO experimental data presented in table 7G the results are displayed on graph 7E. On this plot the amounts of zinc and cadmium found in the condensate from each run are shown for each of the three different reaction temperatures (to bring run SMK12 data into line its zinc and cadmium analyses have been multiplied by 0.90 to account for the slightly longer reaction time). The broken line near the top of the graph represents the average gm-moles of condensate ($ZnCl_2$ + $CdCl_2$) for the runs plotted.

Qualitatively the results, in general agreement with the CdO/ZnO single bed non-equilibrium runs, show that under the given reaction conditions an increase in temperature produced an increased deviation from equilibrium. Specifically, the double bed runs show that the overall rate of the exchange reaction decreased with increasing temperature. The results

---

* These were not from the same batch of pellets as used for the single bed non-equilibrium experiments but from a second batch made under identical conditions.

Run number	Bed Top-Bottom	Temperature °C	gm-moles Cd in condensate $x10^3$	gm-moles Zn in condensate $x10^3$	Total gm-moles of condensate $x10^3$	Equilibrium separation constant
SMK1	ZnO-CdO	752	5.87	8.17	14.0	62.7
SMK6	ZnO-CdO	854	2.14	12.3	14.4	41.0
SMK7	ZnO-CdO	952	3.04	11.6	14.6	28.8
SMK4	ZnO-CdO/ZnO	753	13.2	0.78	14.0	62.7
SMK14	ZnO-CdO/ZnO	754	13.8	0.48	14.3	62.7
SMK5	ZnO-CdO/ZnO	854	10.2	3.90	14.1	41.0
SMK13	ZnO-CdO/ZnO	853	12.5	1.41	13.9	41.0
SMK8	ZnO-CdO/ZnO	953	7.52	6.88	14.4	28.8
SMK10	ZnO-CdO/ZnO	954	10.1	4.21	14.3	28.8
SMK11	ZnO-CdO/ZnO	953	7.43	6.50	13.9	28.8
SMK9*	ZnO-CdO/ZnO	952	6.98	7.34	14.3	28.8
SMK12*	ZnO-CdO/ZnO	952	9.74	4.89	14.6	28.8

* Oxygen carrier gas

TABLE 7G: DOUBLE BED NON-EQUILIBRIUM RESULTS

are, however, quite scattered and cannot be treated quantitatively. The two oxygen carrier gas experiments were performed to investigate whether oxygen would have an effect on the overall exchange reaction rate. Regardless of mechanism(s) no net quantity of oxygen is consumed during the exchange reaction process, however it is possible for oxygen to influence the chemical reaction rate. The two most obvious mechanisms by which the exchange reaction might take place are shown below:

a) Direct exchange

$$ZnCl_{2(g)} + CdO_{(s)} \rightarrow CdCl_{2(g)} + ZnO_{(s)}$$

b) Indirect exchange

$$ZnCl_{2(g)} + \tfrac{1}{2}O_{2(g)} \rightarrow Cl_{2(g)} + ZnO_{(s)}$$

$$CdO_{(s)} + Cl_{2(g)} \rightarrow \tfrac{1}{2}O_{2(g)} + CdCl_{2(g)}$$

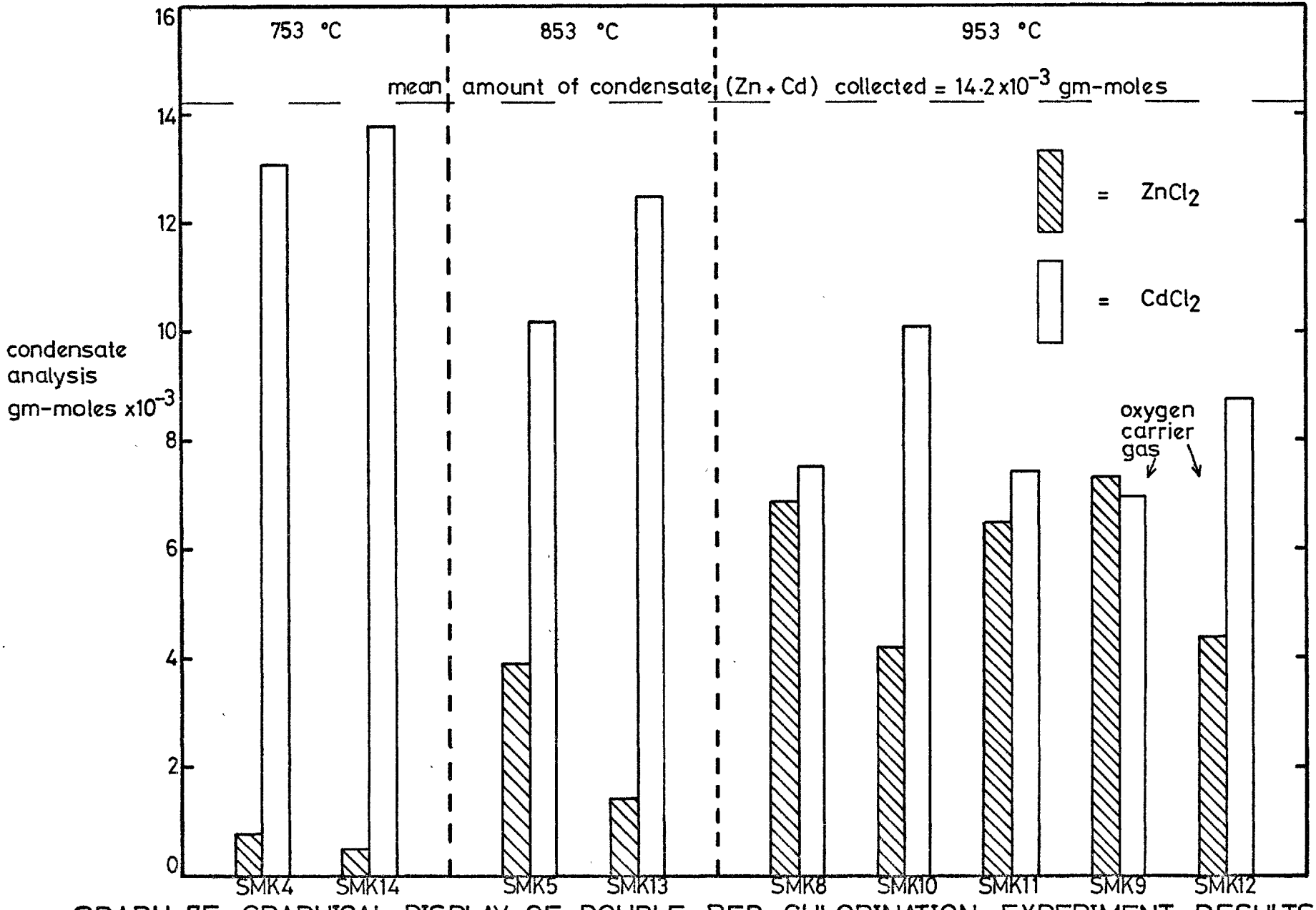

GRAPH 7E: GRAPHICAL DISPLAY OF DOUBLE BED CHLORINATION EXPERIMENT RESULTS. DATA FROM TABLE 7G.

With direct exchange, the surface reaction mechanism could be quite complex but the general effect would be to coat each cadmium oxide micro particle with a layer of zinc oxide. With the indirect mechanism, chlorine generated at the zinc oxide surface would be transported to the cadmium oxide surface where it would then react to form cadmium chloride, this is illustrated on the diagram below:

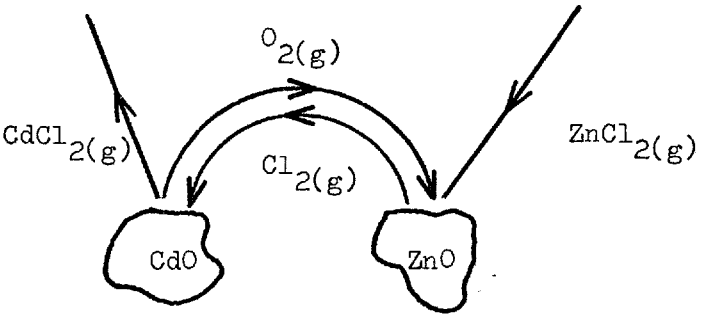

Since gas phase mass transport resistance between neighbouring micro particles is probably low, whilst the $Cl_{2(g)} + CdO_{(s)}$ rate constant is high, the exchange reaction rate might be expected to be controlled by the rate of chlorine production*. If on the other hand chlorine production were comparatively rapid (an unlikely situation), the higher the chlorine partial pressure at the surface of the zinc oxide particles the higher would be the exchange reaction rate*. With either of these limiting cases a high oxygen partial pressure increases the exchange reaction rate since it raises the chlorine partial pressure at the zinc oxide surface. Graph 7E shows that it is not possible to distinguish between the high P_{O_2} runs(SMK9 and 12) and the low P_{O_2} runs (SMK8, 10 and 11). This however, is an inconclusive result since it neither proves nor disproves either exchange reaction mechanism theory.

The three CdO double bed runs have not been plotted on graph 7E since they do not show any clear trend with increasing temperature; nevertheless, departure from equilibrium in each case was very considerable.

7C3 Additional observations on the double bed non-equilibrium experiments

After each CdO/ZnO experiment the reacted pellets (those from the lower bed) were visually examined whilst still in place in the reactor, surfaces of individual pellets were then examined with the naked eye and also with a relatively low powered (x50) deep-field binocular microscope. After

---

* Provided $ZnCl_{2(g)}$ transport was not the rate controlling step.

even a cursory examination it became immediately apparent, from the varied surface appearance of the different pellets, that there had been a progressive decrease in the extent of the exchange reaction with increasing temperature.

Pellets reacted at 750°C (experiments SMK4 and 14) ranged in colour from almost pure white at the top of each bed to a mottled light brown at the bottom. About six to eight small dark brown approximately round areas could be seen on each pellet, these were due to $ZnCl_{2(g)}$ starvation at and near the points of pellet-pellet and pellet-wall contact. Although the surfaces of pellets taken from the top of each bed were not closely similar to those from the 750°C - single bed CdO/ZnO experiments, under the microscope the white surfaces appeared relatively smooth, soft and easily scratched. Moving down each bed, since the pellets became less reacted, these effects became less pronounced. That the zinc oxide layer on the surface of each pellet was soft suggests a) that there was no appreciable sintering, and b) that the exchange reaction did not cause coalescence of the oxide micro-particles. Examination of a number of sectioned pellets taken from near to the top of each bed showed the ZnO-CdO/ZnO interface to be sharp.

General surface appearances and properties of the "850°C" pellets (experiments SMK5 and 13) were between those of the "750°C" and "950°C" pellets. None of the pellets became white in colour, those from near to the top of each bed were sand coloured, those from near to the bottom were medium brown overlayed with light brown speckles; points of contact could once again be identified; the surfaces of the pellets were quite hard. The pellets from each of the five 950°C experiments (SMK8, 9, 10 11 and 12) exhibited the same characteristics. Pellets from near to the top of each bed were covered, over most of their surface, by a thin hard layer of sand coloured oxide. At the tips of the numerous small protrusions (formed during pellet manufacture; see plate 3) which were the 'high' regions of the roughness comprising the surface of each pellet, the oxide layer was exceptionally thin; it was therefore possible to see through to the underlying CdO/ZnO mixture. In the 'low' regions between the protrusions the extent of reaction, as gauged by the amount of zinc oxide deposited, was greatest. Pellets taken from the bottom of

each bed were only slightly different from those just described. Taking into consideration the differences between the reaction times, pellets from the single bed 950°C experiments (except those from near to the top of each bed) were remarkably similar in outward appearance to those from the 950°C double bed experiments. A full description (together with photographs) of the external features of the 950°C-reacted CdO/ZnO single bed pellets is given in section 8A1b.

The recorded bed exit temperatures varied by no more than about +2 deg.C during the course of double bed experiments. These slight temperature rises were a result of the exchange reaction being exothermic.

As a final comment it is worth recording that the CdO pellets from runs SMK2 and 3, which were reacted with chlorine at 750°C developed only brown, hard, matt surfaces and not fluffy surfaces (as were developed by the zinc oxide granules; see section 7A3c).

CHAPTER EIGHT

PHYSICAL STRUCTURES AND PROPERTIES OF REACTED AND UNREACTED CdO/ZnO PELLETS: A MATHEMATICAL ANALYSIS OF THE NON-EQUILIBRIUM CHLORINATION OF PACKED BEDS OF CdO/ZnO PELLETS

The results of the CdO/ZnO non-equilibrium chlorination experiments are reported in section 7B. Before these results could be analysed in any detail it was necessary to examine the physical structures and properties of the various reacted and unreacted CdO/ZnO pellets. The techniques which were employed to study the pellets are listed below:

a) Optical microscopy
b) "Stereoscan" scanning electron microscopy
c) "Geoscan" electron probe microanalysis
d) Mercury porosimetry.

The results obtained from each of these investigations are presented in the first part of this chapter. On the basis of the results of the chlorination experiments and the results of the pellet studies it has been possible to qualitatively characterise the reaction behaviour of individual CdO/ZnO pellets. Through application of the concepts of gas-solid reaction theory this characterisation has led to the construction of a mathematical description of single pellet chlorination kinetics. By introducing this single pellet model into an ideal packed bed* a mathematical model of the chlorination of packed beds of CdO/ZnO pellets has been developed. Using various combinations of estimated, calculated and measured parameters this overall reaction model has been solved (using a computer) for the same sets of conditions as were used for the CdO/ZnO experiments. Full details on the mathematical model, its various predictions, and comparisons between these and the experimental results are given in the second part of this chapter.

---

* What is meant by an ideal packed bed is explained in section 8B7; in brief, it is an isothermal, uniform property packed bed in which the gas flow is evenly distributed over the bed cross-section.

8A PHYSICAL STRUCTURES AND PROPERTIES OF REACTED AND UNREACTED CdO/ZnO PELLETS

Since the contents of this section are of very great importance to the second part of the chapter the individual results and the inferences drawn from them are presented together.

8A1 Exterior features of the pellets

8A1a Unreacted pellets:- A photograph of six randomly selected unreacted pellets (-6.7 + 5.6 mm) of each of the three different compositions is shown on plate 3; their manufacture is described in section 4A2. Of the different pellets, those containing 26.6 mole % CdO were the most approximately spherical. Variations in the geometries of the other two compositions were similar, the 10.8 mole % CdO pellets, however, had the most nodular surfaces. Variations in shape and surface roughness between the pellets of the three different compositions were caused by an inability to precisely control the manufacturing procedure (the mechanism of pelletisation is essentially the same as that employed when making a large snowball from a small snowball nucleus and a snow covered field). The following three main problems were encountered during pelletisation, a) it was difficult to form a large number of similar sized small nuclei, b) many pellets tended to be formed by the coalescence of smaller pellets rather than from grown nuclei, c) hydration of the CdO caused premature hardening of the pellets and thus prevented them from rounding off. Photographs from which both the coalesced structures and the concentric layered structures can be see are given on plates 5, 7, 8, and 9. The nodular surfaces of the 10.8 mole % CdO pellets were caused by small pellets becoming only partially incorporated into larger pellets. Since during manufacture the protruding parts of irregular shaped and nodular surfaced pellets were able to make contact with the pelletising drum and other pellets, the high regions on pellets became comparatively smooth and compacted whilst the low interlying areas, being inaccessible, remained loosely packed.

8A1b Reacted pellets:- After chlorination, each bed of reacted pellets was examined whilst still in place in the reactor. In all cases pellets near to the top of the bed were considerably reduced in size; however, pellets in over half of each bed were apparently little changed in size,

PLATE 3:

UNREACTED CdO/ZnO PELLETS AND
UNREACTED ZnO GRANULES

3a. Unreacted -6.7 + 5.6 mm CdO/ZnO pellets. The 10.8 mole % CdO pellets (top) have the most nodular surfaces, the 26.6 mole % CdO pellets (middle) are the most nearly spherical and the 50.0 mole % pellets (bottom) are the hardest.

3b. Unreacted ZnO granules. This photograph shows a random selection of 4.98 gms of each of the different size fractions (-7 mesh + 14 mesh, -3/16" + 7 mesh, -1/4" + 3/16" and -3/8" + 1/4") spread out in a 3 inch square. The range of geometries and surface appearances within each size fraction are very similar. A typical granule has a comparatively smooth surface and an irregular plate-like shape.


CENTIMETRES

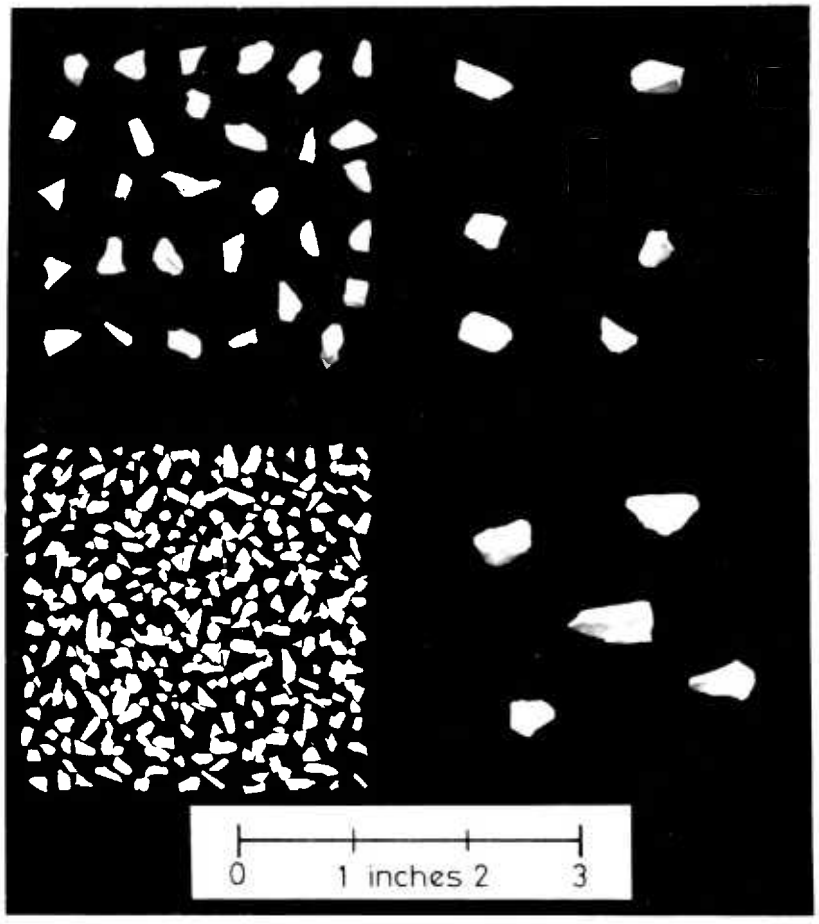
0
1 inches 2
3

especially those from the 850 and 950°C experiments. Photographs of the top 40 pellets taken from the beds of the 750, 850 and 950°C - 26.6 mole % CdO experiments* are shown on plate 4; each of these experiments was of 90 minutes total reaction time. Several significant features are illustrated by these photographs. The progressive decrease in pellet size with increasing temperature can only be consistent with an increasing overall chlorine reaction rate constant. Surfaces of the 750°C - 26.6 mole % CdO reacted pelletswere soft and fluffy**; surfaces of the 850°C and 950°C pellets were quite smooth and (especially with the 950°C pellets) hard. These surface textures can in part be observed on plate 4. The variations in surface properties between the three sets of pellets are consistent with there having been a small amount of chlorine penetration at 750°C, but very little at 850 and 950°C. The predominantly or totally white colour of all the pellets clearly indicates that CdO is somehow removed from the pellets in preference to ZnO (as is already known from the experimental results given in section 7B). Small areas of exposed CdO can be seen in numerous places on the surfaces of the 950°C pellets; this would appear to support the theory that there was insignificant chlorine penetration at this temperature. Reference to graph 7C shows that during the final stage of reaction the 950°C bed was giving no effective separation, the final-stage separations given by the other two beds may also be seen on this same graph. The final piece of information that can be obtained from plate 4 is that as the pellets became quite small they also became misshapen. This would appear to have been due to the effects of pellet-pellet and pellet-wall contact. The various features of the reacted pellets taken from the 26.6 mole % CdO experiments, which have been described and illustrated above,were in all respects qualitatively the same for the other two series of experiments.

Colour photographs showing 4 reacted pellets from the 750, the 850 and the 950°C - 10.8 mole % CdO experiments are shown on plate 8. Each set of pellets was selected from that part of the bed in which the pellets were little changed in size, even so the photographs accurately display the range of appearances (except sizes) found throughout each 10.8 mole % CdO bed. At 750°C the pellets in the upper regions of the 10.8 mole % CdO

---

* Although of equal initial mass, the largest number of pellets comprising a bed was 202, the lowest number 193.

** It is estimated that the fluffy surface layers were up to about 1/10 mm thick.

PLATE 4:

REACTED CdO/ZnO PELLET SIZE DISTRIBUTIONS

4a. Size distribution of the top 40 pellets* from the 750°C - 26.6 mole % CdO experiment, (reaction time = 90.0 minutes). After reaction at this temperature the surfaces of the pellets were soft and fluffy.

4b. Size distribution of the top 40 pellets* from the 850°C - 26.6 mole % CdO experiment (reaction time 90.2 minutes). Pellets reacted at 850°C had smooth surfaces.

4c. Size distribution of the top 40 pellets* from the 950°C - 26.6 mole % CdO experiment (reaction time 90.1 minutes). Areas of exposed CdO are visible on many of the pellets. The smaller pellets have become misshapen due to variations in reaction rates over their surfaces.

---

* Shown on the left of each photograph, for the purpose of comparison, are four unreacted 26.6 mole % CdO pellets; each photograph is to the same scale.

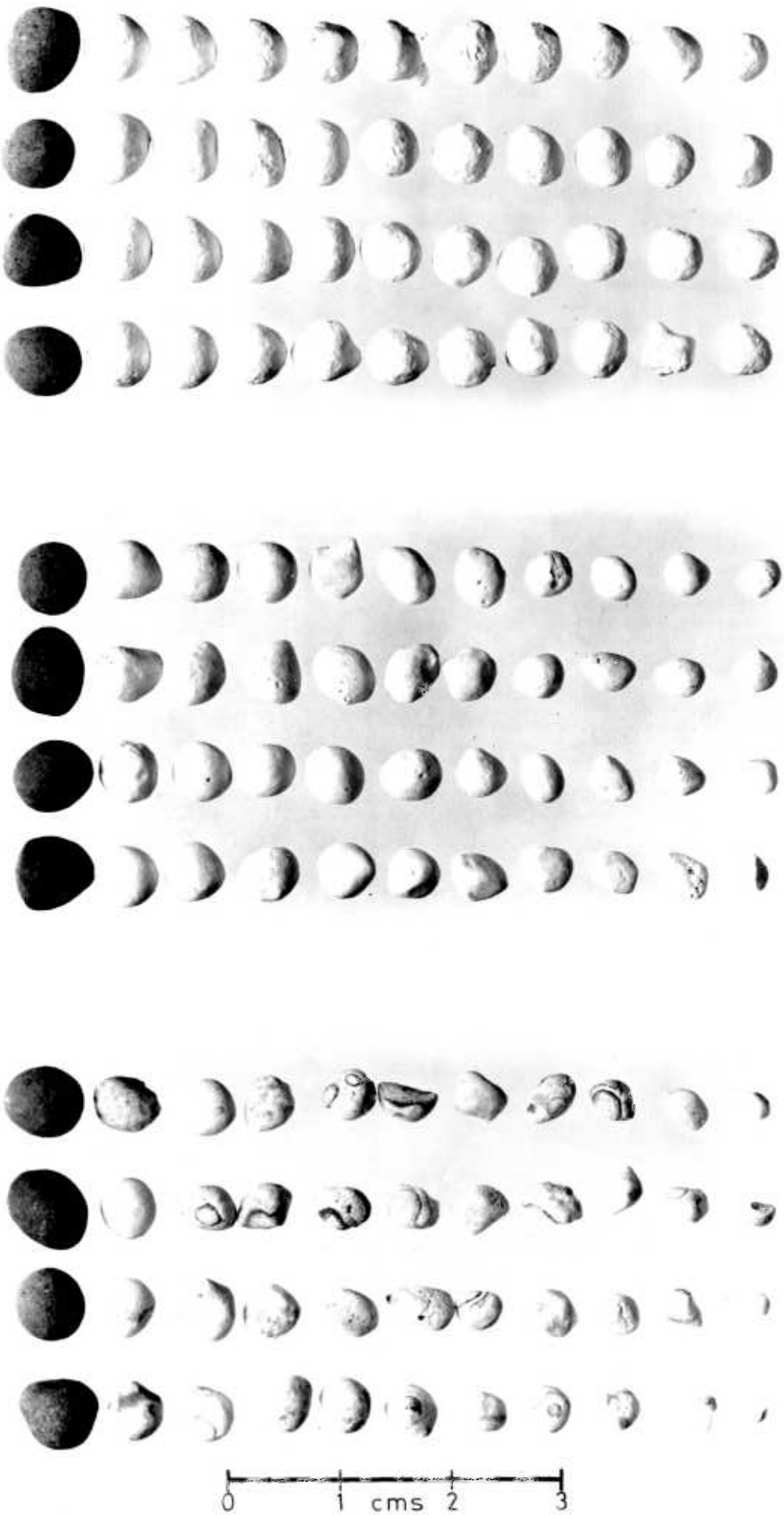
0
1 cms 2
3

bed had pure white soft fluffy surfaces, in the lower regions the surfaces were relatively hard and smooth and light brown in colour. At 850°C there were no soft surfaced pellets, only the top 15 to 20% were white whilst the remainder were various shades of yellow-brown (increasingly so towards the bed exit). The appearance of the 950°C pellets was most striking. Nowhere in the bed were there any all white pellets, those from near to the top were mottled white-dirty brown in colour whilst those from the lower regions were covered in distinct areas of yellow and of brown. The lower pellets are of special interest since the different coloured areas are directly associated with specific physical features on their surfaces. As described in section 8A1a the 10.8 mole % CdO pellets developed nodular surfaces due to problems of manufacture. A brief examination of photograph C on plate 8 shows that the brown areas cover the protruding nodules whilst the yellow areas are in the interlying depressions (accounting for the differences in reaction time and CdO content, the reacted 10.8 mole % CdO pellets just described were qualitatively the same in external appearance as pellets from the 50.0 mole % CdO - 950°C double bed experiments; see section 7C3). The yellow and the brown areas are consistent with there having been differences in structure between the nodules and the low interlying regions. For present purposes it is asserted that these type of pellets came from a part of the bed where only insignificant amounts of chlorine were available. Also that nodules, because of their greater degree of compaction, in conjunction with the effects of sintering, presented a virtual barrier to gaseous diffusion whereas the low lying areas were in comparison relatively permeable. The reacted 26.6 mole % CdO and 50.0 mole % CdO pellets both exhibited essentially the same features as have just been described for the 10.8 mole % CdO pellets. The only two notable differences were a) as the CdO content of the pellets increased their various colours all became progressively darker; and b) having more approximately spherical geometries and smoother surfaces, larger areas of the 26.6 mole % CdO and 50.0 mole % CdO - 950°C pellets had the appearance of being nearly impermeable. However, the 'densely packed - loosely packed' effect could still be detected in many places.

8A2 Examination of sectioned pellets

As part of the investigations into the internal structures of the reacted and unreacted CdO/ZnO pellets, polished pellet sections were examined both visually and with the aid of an optical mocroscope. The first stage of specimen preparation consisted of grinding away (on silicon carbide paper) almost half of each pellet initially selected for examination*; in so doing it was possible to obtain an approximate idea of the condition of the inside of each pellet and thus decide whether or not to carry out a detailed examination. Having chosen a suitable number of interesting pellets these were then mounted, flat sides facing outwards, in cold curing polyester resin. After setting, the mounted pellets and surrounding resin were carefully ground flat on 600 grade silicon carbide paper. Two different methods were employed for the polishing that followed. The first specimens to be examined were polished in the conventional manner on a diamond impregnated cloth polishing wheel. However, this technique was found to be unsatisfactory since it produced damage on the surfaces being polished. This damage, consisting of surface unevennesses and voids, seemed to be mainly caused by the weakness of the pellets in conjunction with the shear forces which were imposed by the polishing. To overcome these problems a slow acting vibro-polishing technique was employed. The polisher consisted of a horizontal spring-mounted shallow pan connected to a 50Hz vibrator unit; on the bottom of the pan was a flat glass plate which could be covered with a suitable polishing cloth. For polishing, ultra fine alumina powder and 10 mm depth of water were added to the pan, a number of weighted specimens were then placed face downwards on the cloth. The polisher was constructed so that the vibrator would impart both vertical and rotary motion to the pan, the amplitude** of which could be adjusted. When in operation the specimens very slowly moved around the pan; optimum surface polish was obtained after about 24 hours. Even with this refined technique the polish produced, when examined at a microscopic level, was rather poor. This result is attributed to the unsuitability of the mixed oxide specimens to polishing. However, at a macroscopic level the polish was very good, there were also no signs of spurious macro-porosity.

---

* When a reacted bed was the subject of investigation a large number of pellets (20 to 30) chosen from a range of different bed positions, were sectioned in order to obtain a good representation of the various structures present.

** No details of the amplitude of vibration were given by the manufacturers - McLean Research Eng. Co. Ltd. - the maximum dispacement used is estimated to have been of the order of $\pm$ 0.1 mm (vertical).

8A2a Macrostructure:- Sectioned and polished unreacted pellets of each of the three different compositions were examined and compared with reacted pellets. Small cracks and macro-pores were present in all the unreacted* 50.0 mole % CdO pellets, most were concentrated towards the centre of each pellet, few extended to the surface. After reaction these features had grown both in size and in number, especially with increasing temperature. Cracks and macro-pores within reacted 50.0 mole % CdO pellets may be seenin photographs (a) and (b) on plate 7 and in photograph (a) on plate 9. Fewer cracks, but a similar number of macropores were present in the unreacted 26.6 mole % CdO pellets. After reaction approximately circular internal cracks (possibly spherical within a whole pellet) were found (see plate 5). These appeared to be associated with the boundaries (or where these boundaries had been prior to reaction) between the successive CdO/ZnO layers which formed most of these pellets. The unreacted 10.8 mole % CdO pellets contained very few cracks but a significant number of macropores; after reaction no real changes in structure could be detected. The various findings described above suggest that a) the CdO was responsible for causing the cracking, the magnitude of which increased with increasing temperature, and b) the cracking was not related to the chlorination reactions, but was due to sintering and densification.

The technique used for mixing together the ZnO and CdO powders (see section 4A2a) proved itself to be completely successful since, even at high magnification, no regions of unmixed CdO and only very occasional white specks of unmixed ZnO were seen within the unreacted pellets. Various features observed within the pellets (both unreacted and reacted) could be traced to the events and mechanisms of manufacture. As has already been explained, pellet growth occurred by two mechanisms: a) coalescence of smaller pellets, and b) agglomeration of powder onto a single pellet. No pellets were formed by one of these mechanisms only, however the 10.8 mole % CdO pellets were formed mainly by mechanism (a) whilst the 26.6 mole % CdO pellets were mainly formed by mechanism (b). Photograph (c) on plate 7 and photograph (e) on plate 9 each show a single pellet mainly comprised of an aggregate of smaller pellets. Pellets which were 'grown'

---

* All the unreacted pellets examined were from the same batch and size fraction as used for the chlorination experiments.

by the mechanism of powder agglomeration developed an annular banded structure; this effect was caused by the pelletisation procedure. Ideally it would have been best to continuously add powder and water to the pelletising drum so as to obtain uniformly developed pellets. Unfortunately it was difficult to control the pelletisation process, therefore, in most cases the pellets were grown in stages. If pellets were left to round off between each addition of powder and water, their exposed surfaces tended to become more compacted than their interiors. A pellet which was grown in several stages, each separated by a period of rounding off, thus consisted of a number of overlying shells connected by thin zones of more densely packed oxide. These concentric layers and their thin boundaries can be seen within the unreacted portions of the pellets shown on plate 5. In the reacted parts of the pellets some of the thin boundaries appear to have retained small amounts of CdO; this effect is particularly noticeable with the sectioned pellet shown in photograph (b) on plate 9. This retention was probably caused by a small fraction of the CdO particles becoming entirely surrounded by ZnO and thus effectively separated from the reactant gas. It is probable that these thin boundaries were of reduced permeability, and possible that they were partly responsible for the circular cracks which developed. No photographs of unreacted pellets are presented since all their various features can be seen within the unreacted cores of the different reacted pellets.

The photographs presented on plates 5, 7, 8 and 9 illustrate the various macrostructures developed by the reacted pellets. The sectioned pellets in the three photographs on plate 5 are from the three experiments (750, 850 and 950°C) performed on the 26.6 mole % CdO beds; those in the three colour photographs on plate 8 are from the three experiments performed on the 10.8 mole % CdO beds. In each photograph the 9 pellets shown are a fair representation of the range of macrostructures found in the lower 70 to 80% of the bed. Colour photographs of individual sectioned-pellets are presented on plate 9; low magnification photographs of specific features are presented on plate 7. In all these photographs the ZnO-CdO/ZnO interfaces, except for minor variations, appear to be sharply defined. This effect is a classic feature of a reaction whose rate is controlled by the gaseous diffusion of either reactant or product or reactant and product species through a layer of porous solid. When this

PLATE 5:

SECTIONED REACTED 26·6MOLE% CdO PELLETS

5a. Typical range of macrostructures from the 750°C - 26.6 mole % CdO experiment. After chlorination 50.0% of the CdO and 3.63% of the ZnO had been removed from the bed. The arrow indicates the ZnO-CdO/ZnO boundary which was examined using the electron probe microanalyser.

5b. Typical range of macrostructures from the 850°C - 26.6 mole % CdO experiment. After chlorination 34.9% of the CdO and 8.90% of the ZnO had been removed from the bed.

5c. Typical range of macrostructures from the 950°C - 26.6 mole % CdO experiment. After chlorination 21.6% of the CdO and 14.6% of the ZnO had been removed from the bed.

The sectioned pellets were taken from the lower 70-80% of the beds; each photograph is to the same scale; the dark central areas are CdO/ZnO, the light areas are CdO depleted, the specimens are mounted in transparent resin.

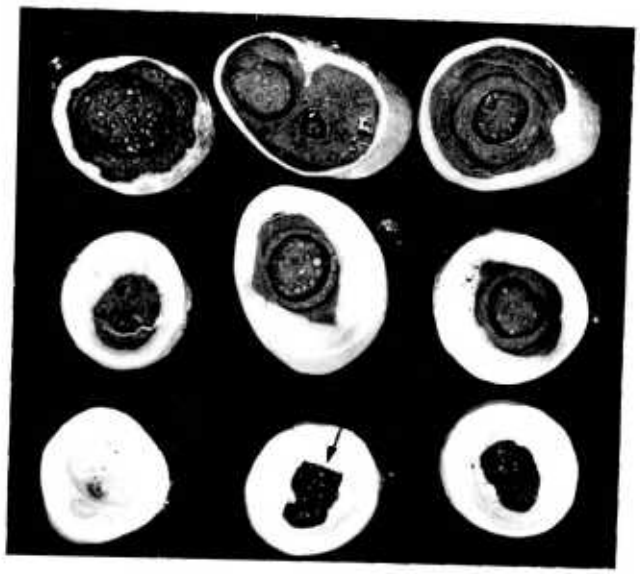

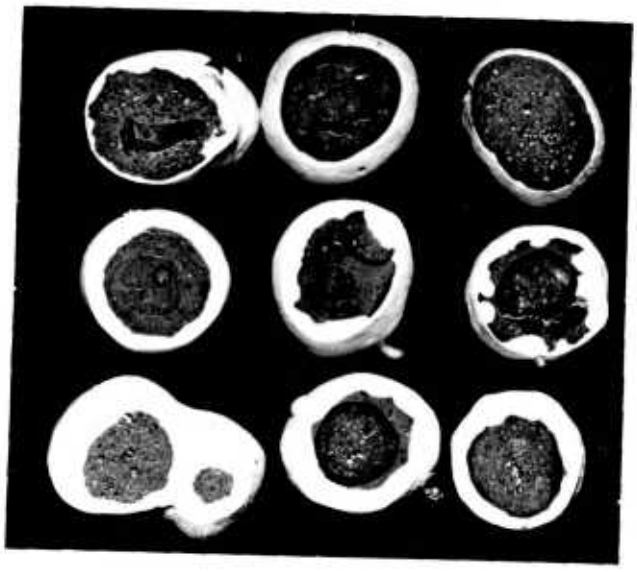

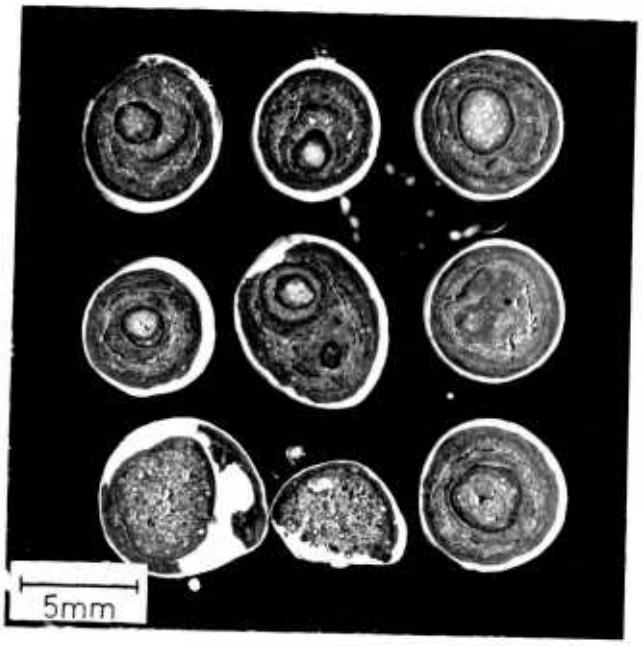
5mm

type of reaction occurs within a uniform property spherical pellet the solid reactant behaves as a shrinking spherical core. The photographs on plates 5, 8 and 9 show that this was the mode of reaction of many of the pellets. When a CdO/ZnO core was found within a pellet taken from the top of a bed, the ZnO-CdO/ZnO interface also appeared to be sharply defined.

Pellets significantly reduced in size (namely those taken from near to the top of each bed) had, according to their initial composition and to the temperature at which they were reacted, the following macrostructures.

a) None of the reacted pellets which had initially contained 50.0 mole % CdO were found to be without a CdO/ZnO core. At 750°C the smallest pellets (for comparison see plate 4) had CdO/ZnO cores which were a little below half their external diameter. At 850°C* the cores made up over half the diameter of the pellets (which were reduced in overall size). At 950°C the cores comprised most of the pellets (which were further reduced in overall size).

b) Some of the reacted pellets which had initially contained 26.6 mole % CdO were found to be without a CdO/ZnO core. However, in many cases inhomogeneities within 'CdO free' pellets had caused traces of CdO to remain unreacted, the general distribution of these traces were similar to those in photograph (b) on plate 9. At 750°C CdO/ZnO cores were absent from pellets that were less than about half the initial pellet size. At 850°C only those pellets reduced to about 1/4 their initial size were without cores. At 950°C even the smallest pellets each contained a core reaching nearly to their external surface.

c) Many of the reacted pellets which had initially contained 10.8 mole % CdO were without a CdO/ZnO core. Since 70.2% of the CdO that was within the pellets at the start of the 750°C experiment had been removed by the end of chlorination, the majority of the pellets from this bed (all those from its upper regions) were without CdO/ZnO cores. At 850°C* pellets of less than about half their initial diameter were without cores. At 950°C*

---

* Shorter total reaction time employed

no pellets were without irregular shaped regions of CdO/ZnO. In some places the unreacted oxide mixture reached to within a very small distance of the surface, in other places it went both deep into and through the pellets. No true symetric cores were found; typical structures were very similar to those of the more reacted pellets shown in photograph (f) on plate 8.

The most significant feature exhibited by the reacted pellets as illustrated by the various macrographs was the apparent sharpness of the ZnO-CdO/ZnO boundaries. This behaviour, as has already been briefly explained, is characteristic of a reaction whose overall rate is effectively controlled by the rate of transport of one or more gaseous species through a porous solid. Under such conditions resistance to transport is governed by the structure of the porous solid and the properties of the gas or mixture of gases. It would seem safe to assume that (except in areas influenced by either pellet-pellet or pellet-wall contact) the driving force, or forces, which caused the $CdO_{(s)} \rightarrow CdCl_{2(g)}$ reaction to take place were, at a given instant of time, constant over the surface of any given pellet undergoing reaction. Therefore, significant divergences away from the symetric shrinking-core reaction mode can, with each pellet, be attributed to local variations in transport resistance. Since the intrinsic transport properties of the various gaseous reactant and product species were nearly independent of the reactor gas composition (see section 8B3c), the unusual ZnO-CdO/ZnO boundary shapes present in many of the reacted pellets must therefore have been caused by structural inhomogeneities that originated during pellet manufacture and were subsequently intensified by the action of sintering and densification.

Most of the different features exhibited by the reacted pellets* are readily apparent from the various photographs shown on plates 5, 8 and 9. Since the important features are also outlined in each accompanying caption no useful purpose is served by discussing them here. However, the micrographs shown on plate 7 deserve special mention. The irregular shaped surfaces that were developed by some of the pellets are described in

---

* Although a sequence of reacted 50.0 mole % CdO pellets is not shown, their structures may be inferred from a combination of their experimental results given in chapter 7, the earlier descriptions and the following photographs: (a) and (b) plate 7; (a) plate 9.

PLATE 6:

MICROGRAPHS AND SURFACE STRUCTURE OF POLISHED SECTIONS OF REACTED CdO/ZnO PELLETS

6a (top left). Micrograph* of a ZnO-CdO/ZnO boundary within a 26.6 mole % CdO pellet reacted at 750°C.

6b. Micrograph* of a ZnO-CdO/ZnO boundary within a 26.6 mole % CdO pellet reacted at 850°C.

6c. Micrograph* of a ZnO-CdO/ZnO boundary within a 50.0 mole % CdO pellet reacted at 850°C.

6d. Micrograph* of an irregular shaped ZnO-CdO/ZnO boundary within a 50.0 mole % CdO pellet reacted at 950°C.

6e. Stereoscan photograph of the surface of a 'polished' pellet section.

6f (bottom right). As 6e. These two photographs show that surface unevennesses produced deceptive features in the micrographs.

*The micrographs are all at the same magnification; the dark areas are CdO/ZnO, the light areas are CdO depleted, the black areas are the mounting resin.

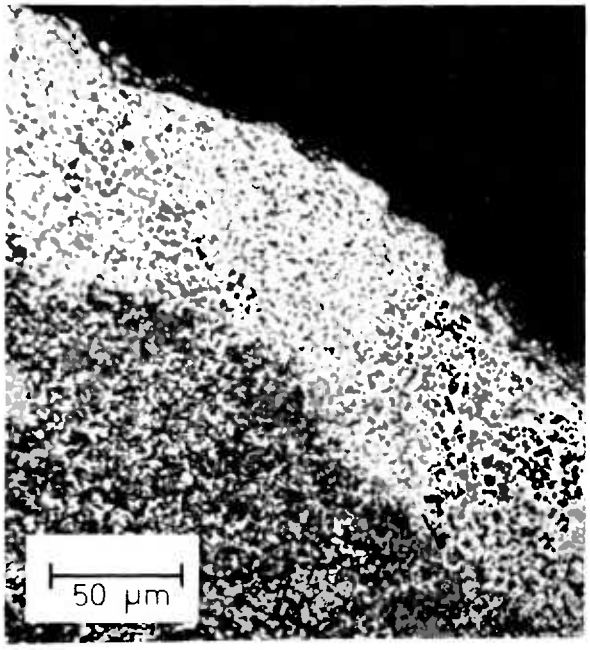
50 µm

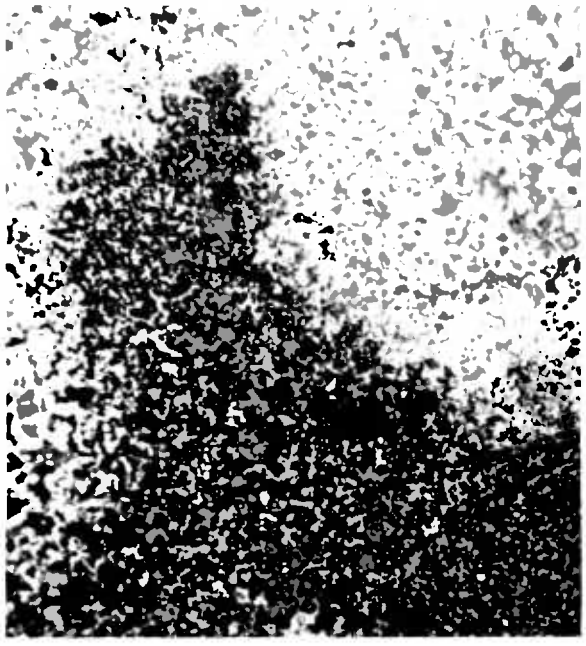

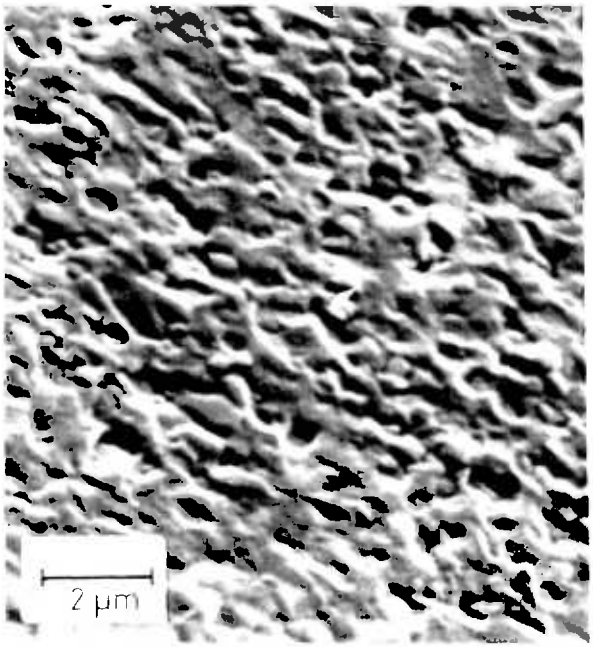
2 µm

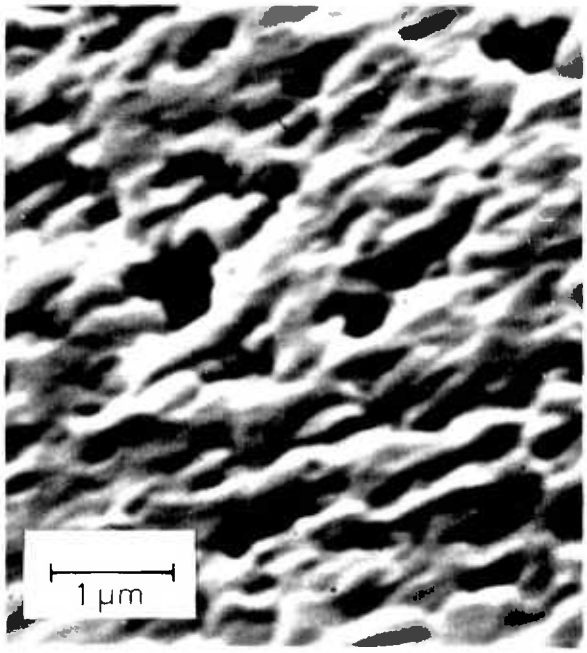
1 µm

PLATE 7:

MACROGRAPHS OF SECTIONED ASYMMETRICALLY REACTED CdO/ZnO PELLETS

7a (top left). 50.0 mole % CdO pellet reacted at 750°C. The surface depression has resulted in an increased CdO reaction rate; note also the retained CdO at the boundaries between the successive layers of oxide picked up during pelletisation.

7b. 50.0 mole % CdO pellet reacted at 850°C. Surface depression as at 7a. Note the macropores and cracks. The pure white area is ZnO that remained unmixed during powder preparation.

7c. 10.8 mole % CdO pellet reacted at 850°C. The surface protrusion has become almost totally impermeable to the reactant gas. Note that the pellet is mainly made up of an aggregate of small pellets.

7d. 10.8 mole % CdO pellet reacted at 850°C. Surface depression as 7a; the CdO reaction rate may also have been increased by the presence of the crack.

7e. 10.8 mole % CdO pellet reacted at 950°C. Surface protrusion similar to 7c.

7f (bottom right). 10.8 mole % CdO pellet reacted at 950°C. Surface protrusion as 7c; the CdO depleted area appears to have been formed, in part, by the diffusion of reactant gas down a crack.

All of the photographs are at the same magnification; the dark areas are CdO/ZnO, the light areas are CdO depleted, the black areas are the transparent mounting resin.

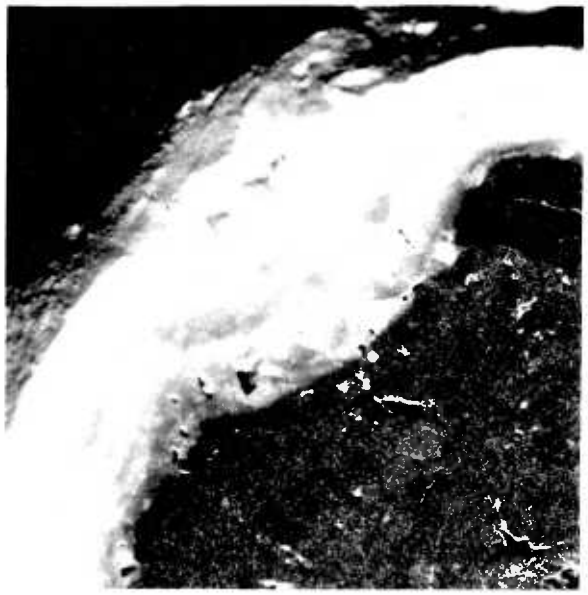

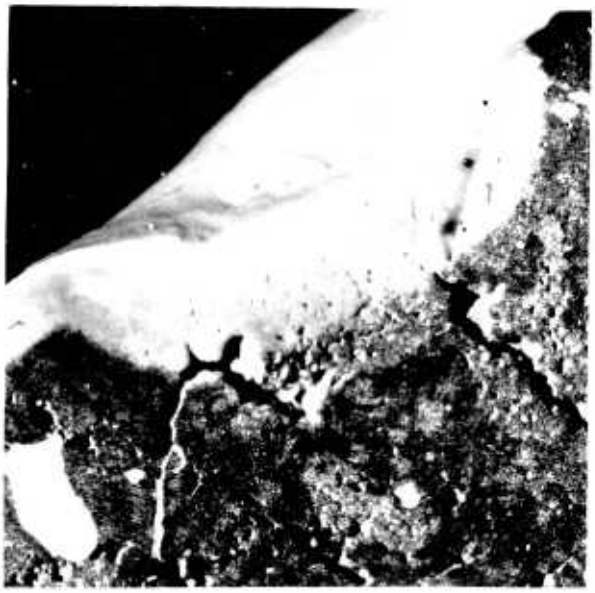

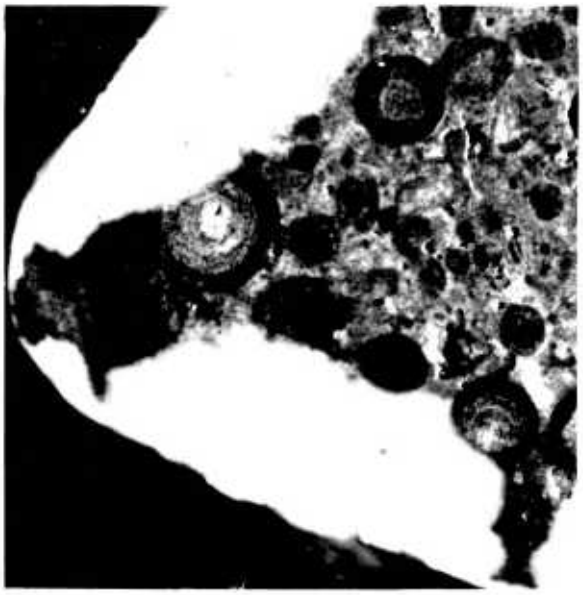

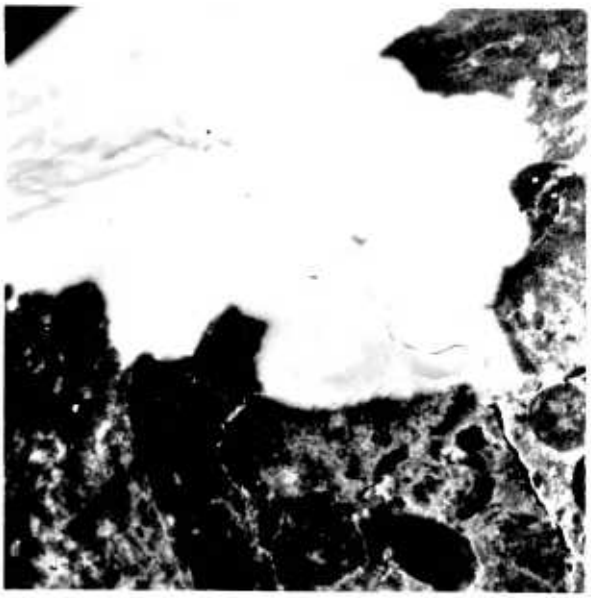

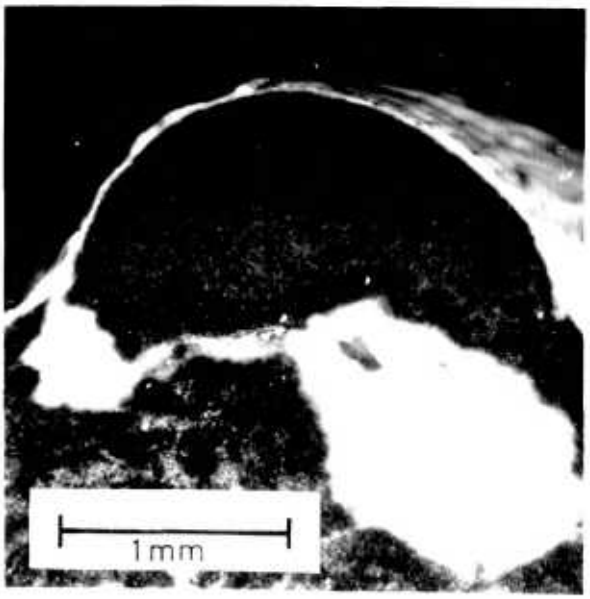
1mm

PLATE 8:

SECTIONED REACTED 10·8MOLE%CdO PELLETS AND
EXTERNAL FEATURES OF REACTED 10·8MOLE%CdO PELLETS

8a (top left). External appearances of pellets from the 750°C - 10.8 mole % CdO experiment. The two lighter coloured pellets were taken from near to the top of the bed, the two darker ones from near to the bottom.

8b. External appearances of pellets from the 850°C - 10.8 mole % CdO experiment. As with 8a, the darker pellets came from the lower regions of the bed. The brown colouration is due to retained CdO.

8c. External appearances of pellets from the 950°C - 10.8 mole % CdO experiment. As with 8a, the lighter pellets came from the upper regions of the bed. The dark nodules are covered by a very thin transparent layer of impermeable ZnO.

8d. Typical range of macrostructures from the 750°C - 10.8 mole % CdO experiment. After chlorination 70.2% of the CdO and 6.81% of the ZnO had been removed from the bed. The pellets appear to contain fairly uniform amounts of retained CdO.

8e. Typical range of macrostructures from the 850°C - 10.8 mole % CdO experiment. After chlorination 53.9% of the CdO and 3.84% of the ZnO had been removed from the bed. Some of the CdO cores have reacted in an asymmetric manner.

8f. (bottom right). Typical range of macrostructures from the 950°C - 10.8 mole % CdO experiment. After chlorination 22.6% of the CdO and 7.48% of the ZnO had been removed from the bed. The CdO within each of the pellets has reacted in an asymetric manner.

The pellets shown on this plate all came from the lower 70-80% of the beds; 8a, 8b, and 8c are to the same scale; 8d, 8e, and 8f are to the same scale.

X4

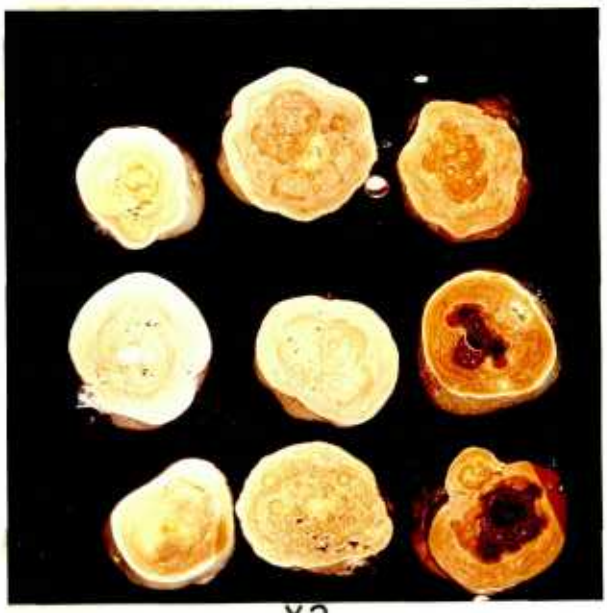

X3

PLATE 9:

VARIOUS SECTIONED REACTED CdO/ZnO PELLETS AND ELECTRON PROBE PHOTOGRAPH OF A ZnO-CdO/ZnO BOUNDARY

9a (top left). 50 mole % CdO pellet reacted at 750°C. Note the extensive cracking towards the centre of the pellet, (which appears to have produced an increased CdO reaction rate) and also the retained CdO.

9b. 26.6 mole % CdO pellet reacted at 750°C. CdO is retained at the boundaries between the successive layers of oxide which were added to the pellet during its manufacture.

9c. 26.6 mole % CdO pellet reacted at 850°C. This malformed pellet shows no distinct areas of retained CdO; two CdO/ZnO cores have developed.

9d. 10.8 mole % CdO pellet reacted at 850°C. The CdO within this pellet has reacted as a symmetric shrinking core. There is no retained CdO similar to that in either 9a or 9b.

9e. 10.8 mole % CdO pellet reacted at 950°C. Reactant gas has diffused to the pellet interior through the surface concavities. There has been virtually no reaction of the CdO situated below the protruding parts of the pellet's surface.

9f (bottom right). Electron probe area scan of the ZnO-CdO/ZnO boundary (750°C - 26.6 mole % CdO) shown on plate 5. Each spot corresponds to one photon of Cd-L_{α} radiation.

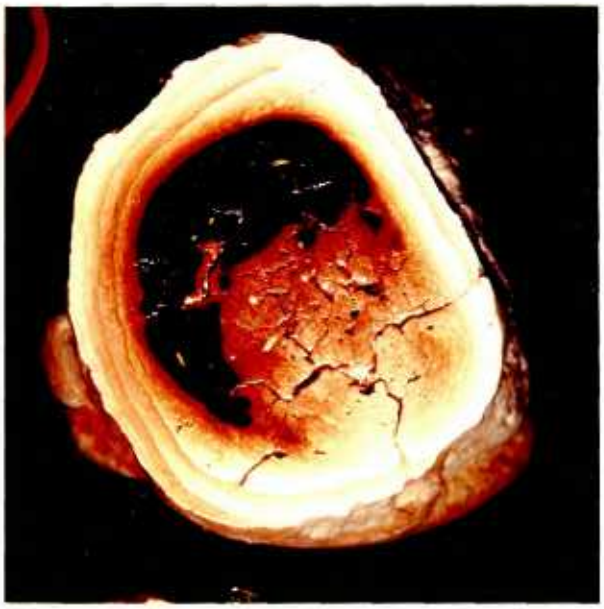

X11

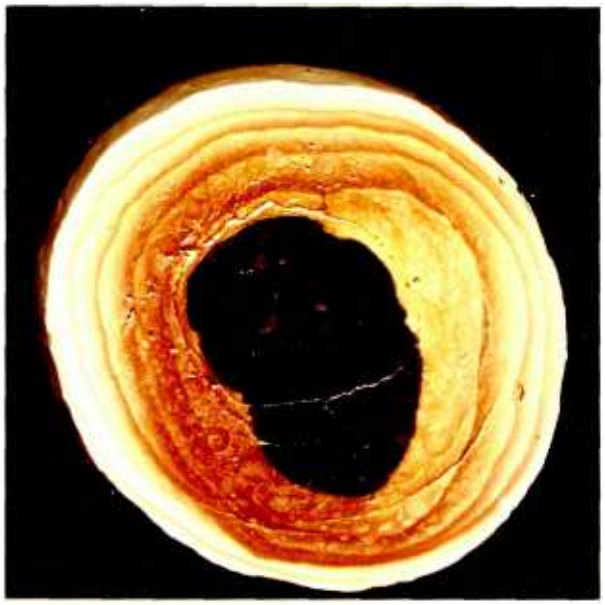

X12

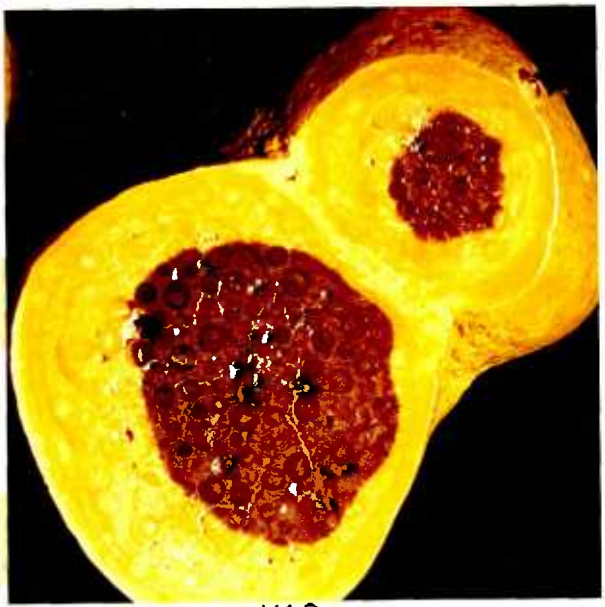

X10

X12

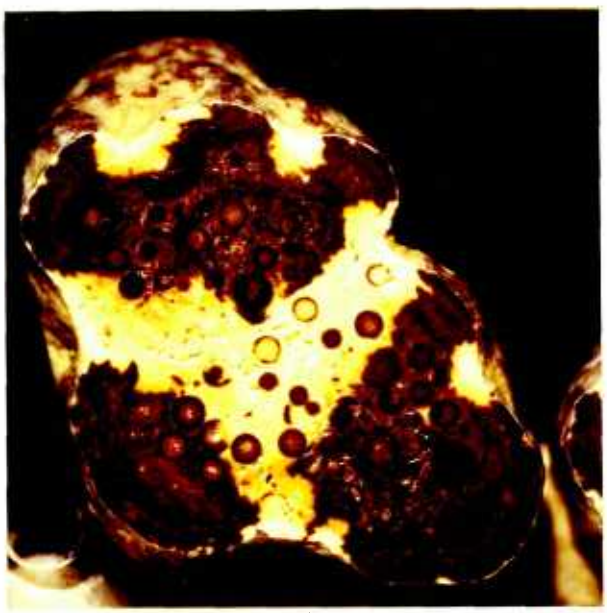

X9

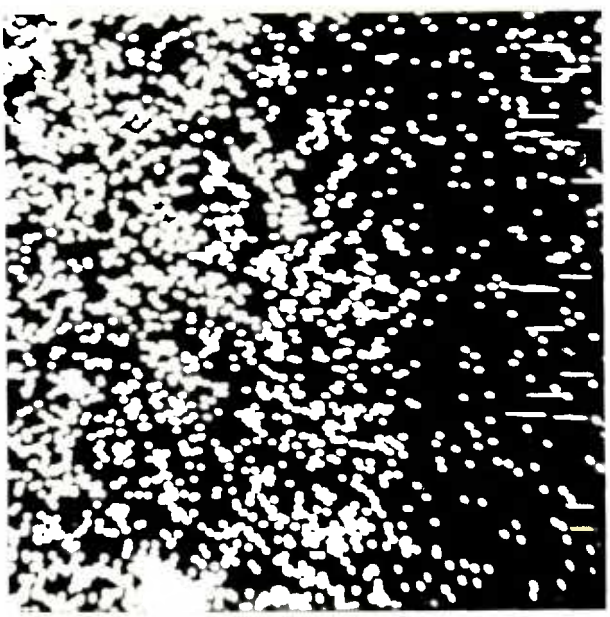

20µm

section 8A1b, surface layer compaction due to rounding off is described in the present section. Together these two effects helped cause concave surface regions of some pellets to remain relatively permeable but convex regions to become relatively impermeable. The photographs on plate 7 show concave surface areas that have allowed preferential gaseous diffusion and convex surface areas that have remained effectively impenetrable.

8A2b Microstructure:- The microstructures of the various unreacted and reacted pellets were examined with an optical microscope. Using magnifications of greater than about x50 the vibro-polished sectioned-pellet surfaces exhibited features which at first could not be interpreted. To solve this problem the polished surfaces were examined by using a scanning electron microscope. Photographs (a), (b), (c) and (d) on plate 6 each show a ZnO-CdO/ZnO boundary at high magnification under normal incident lighting. Photographs (e) and (f) on the same plate show the structure of the 'polished' surfaces as seen at very high magnification on the Stereoscan. With the light microscope investigations two effects caused the surface features to be obscure. Under normal incident lighting (as opposed to oblique lighting which was employed for the macroscopic examinations and photographs) the reflectivities of the ZnO and the CdO/ZnO regions were almost the same. Reacted-unreacted boundaries were therefore difficult to observe and equally difficult to photograph. The second obscuring effect was due to the complete unevenness of all the apparently polished pellet surfaces. At high magnification the optical microscope can only accommodate very small depths of field, the pellet surfaces thus falsely appeared to consist of many large pores. The ZnO-CdO/ZnO boundary shown on each micrograph on plate 6 is very sharp. No diffuse boundaries, excepting the occasional incidences of areas appearing to contain retained CdO, were found within any of the reacted pellets examined. No other features on the micrographs are of any particular significance; the porous* structures of all the unreacted and reacted pellets were too fine to resolve.

---

* micropores

8A3 Stereoscan results

The surface and internal structures of the unreacted and reacted pellets were examined and photographed using a 'Cambridge model S600' scanning electron microscope. The CdO and ZnO powders used for pellet manufacture were similarly investigated. Each pellet chosen was first broken into two or more segments; a suitable portion was then lightly glued onto a flat-headed aluminium rivet; the mounted specimen was then covered in a very thin layer of gold (less than 50 Å) using a vacuum evaporator unit. Powder samples were mounted and prepared in the same manner.

8A3a Structures of oxide powders and unreacted pellets:- The ZnO powder was composed of irregular shaped sub-micron particles, a range of sizes were observed, these appeared to be in agreement with the mean crystallite size (0.21μ; see appendix D) that was quoted by the manufacturer. A SEM photograph showing a typical group of ZnO particles is shown on plate 10. They are not accurately resolved since the instrument was at its magnification limit of x50,000. On the same plate is shown a SEM photograph of a typical group of CdO particles. No details on the CdO powder were given by the manufacturer but their mean particle size is estimated to have been a little larger than that of the ZnO powder. Although not fully resolved the CdO particles appeared to be similar in shape to the ZnO particles.

Three SEM photographs (c, d and e) of the typical internal structures of unreacted CdO/ZnO pellets are shown on plate 10. Only slight differences could be detected between the 50.0, 26.6 and 10.8 mole % CdO pellets. All the unreacted pellets consisted of an interconnecting matrix of irregular shaped particles*. Individually these particles were larger than the crystallites which comprised the raw oxide powders. Each particle must therefore have been formed from a number of crystallites which had coalesced through the action of sintering whilst the pellets were being hardened (30 minutes at 1000°C). All the micropores between the particles were within a fairly narrow size range, most being below a micron in neck 'diameter'. It was difficult to estimate the porosity of the pellets since the surfaces being examined probably appeared to be more porous than were their interiors, however, a bulk voidage of about 35% seemed most

* It was not possible to distinguish between ZnO and CdO particles.

reasonable. There were no real differences in observed structure between the external and interior surfaces of the pellets. Traverses across pellets did not reveal any variations in internal microstructure; this was a little surprising in view of the proven existence of macroscopic inhomogeneities (formed during pelletising). Various sized and shaped macropores were found within all the pellets examined, however they only constituted a very small fraction of the total voidage (an approximately round section macropore is shown in photograph (e) on plate 10). The only two observed differences between the various composition pellets were, a) the particles making up the 10.8 mole % CdO pellets appeared to be relatively amorphous as compared with those in the 50.0 mole % CdO pellets, and b) the particles in the 50.0 mole % CdO pellets seemed to be more fully joined together than those in the 10.8 mole % CdO pellets. A difference in sintering rate between the ZnO and CdO was probably the cause of both these effects.

8A3b Structures of reacted pellets:- Several very important features were discovered during the SEM investigations on the reacted pellets. Before these are listed the structures found at each different reaction temperature will be briefly described. The pellets selected for examination were in each case smaller (by more than about 20% in diameter) than their unreacted counterparts; also they all contained CdO depleted regions.

a) - 750°C. After reaction at this temperature the particles making up the bulk of each pellet were like curved faced faceted spheroids, these varied little in size, typically being about 1μ in diameter. The bulk porosity of the pellets was high, it was also uniform (except for occasional macropores). In comparison with the unreacted pellets the reacted pellets had a slightly coarser structure. As far as could be judged, the structures of the three different composition reacted pellets were indistinguishable from one another. There were no detectable differences between CdO/ZnO and ZnO* regions, therefore no ZnO-CdO/ZnO boundaries could be identified. The external surfaces of the pellets were composed of a wide size range of interconnecting particles (the largest were about 1μ in diameter); the pellet surfaces were also much more porous than their interiors. This increased porosity, gradually decreasing with distance,

---

* Except for ZnO regions close to the external surfaces.

PLATE 10:

STEREOSCAN PHOTOGRAPHS

10a (top left). ZnO powder used for pellet manufacture. Magnification x 50,000

10b. CdO powder used for pellet manufacture.

10c. Internal structure of an unreacted 50.0 mole % CdO pellet. The individual grains are slightly larger than the crystallites comprising the oxide powders. Magnification x 20,000

10d. Internal structure of an unreacted 10.8 mole % CdO pellet. The individual grains are amorphous in comparison with those in 10c.

10e. Macro pore within unreacted 10.8 mole % CdO pellet. Magnification x 5,000

10f. Centre of a 50.0 mole % CdO pellet reacted at 750°C. It was not possible to distinguish between the CdO/ZnO and the CdO depleted regions of the pellet. Magnification x 10,000.

10g. About 20μm below the surface of a 50.0 mole % CdO pellet reacted at 750°C. Note the increased porosity.

10h (bottom right). External surface of a 50.0 mole % CdO pellet reacted at 750°C. Note the range of particle sizes and the increased porosity.

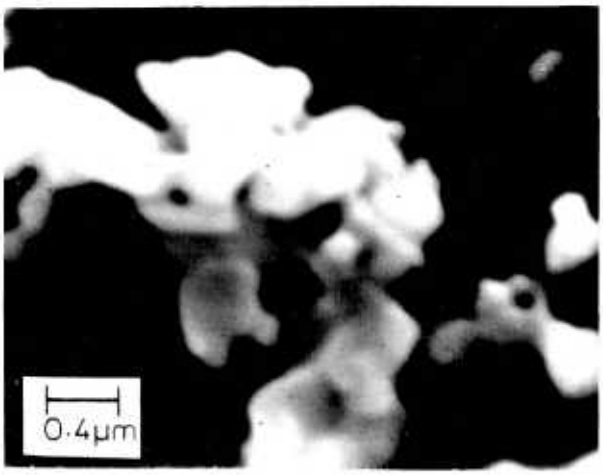
0·4μm

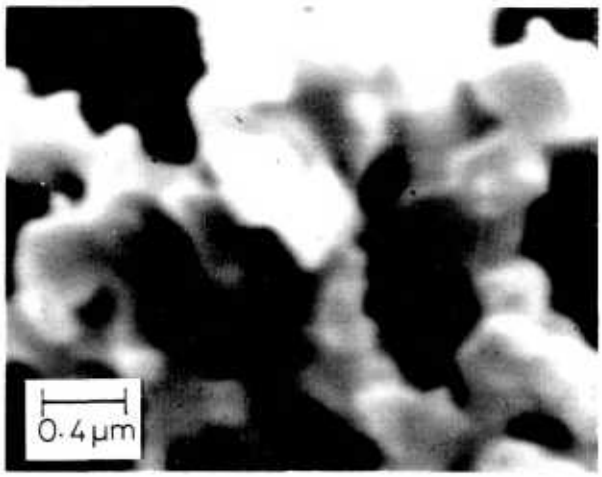
0·4μm

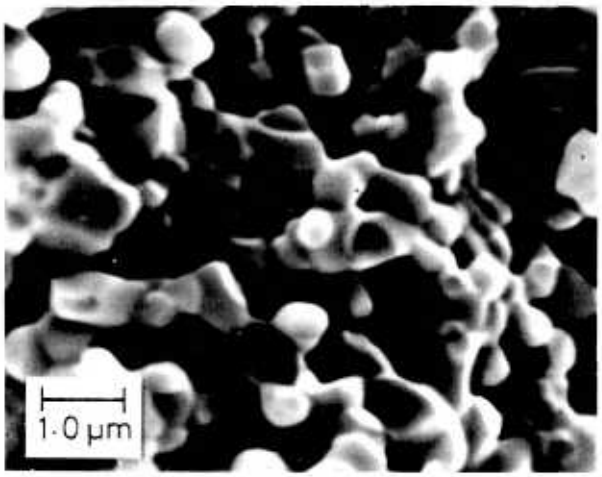
1·0μm

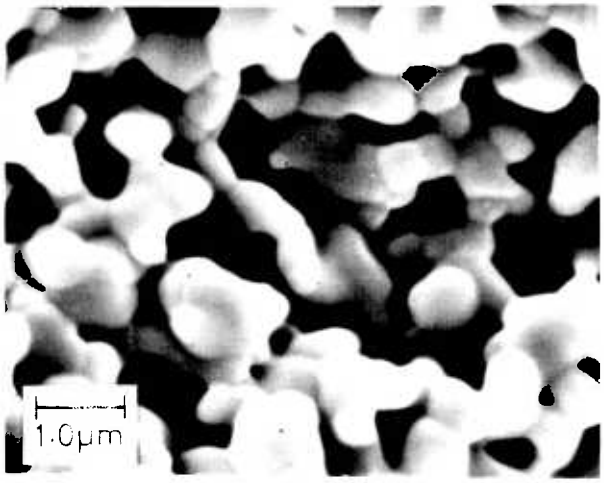
1·0μm

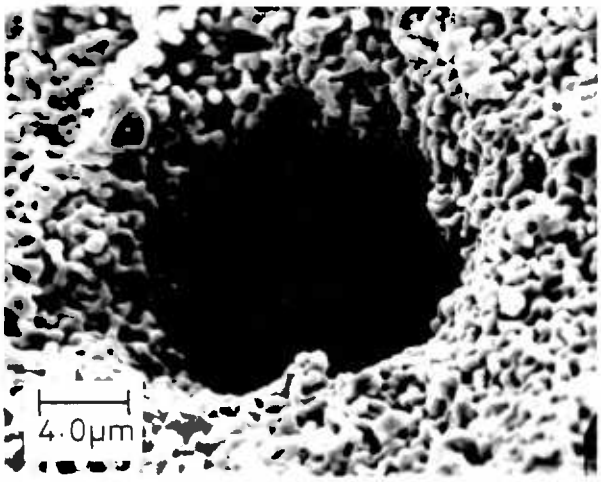
4·0μm

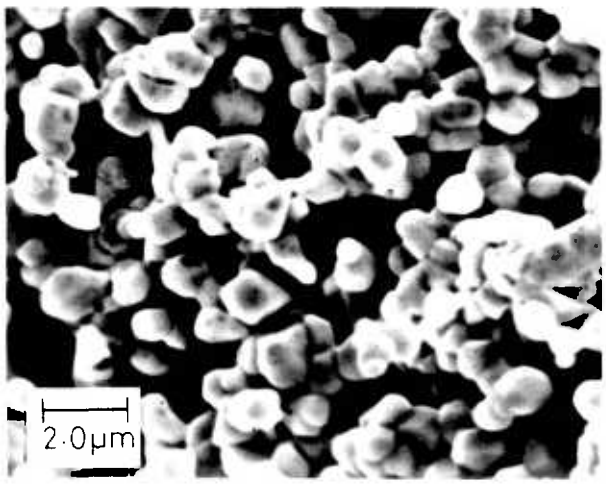
2·0μm

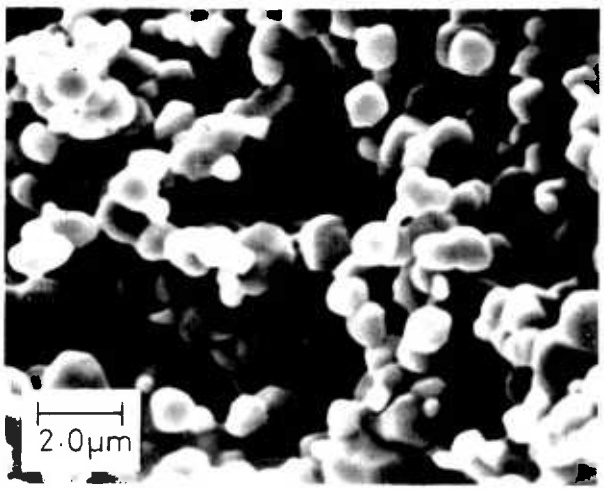
2·0μm

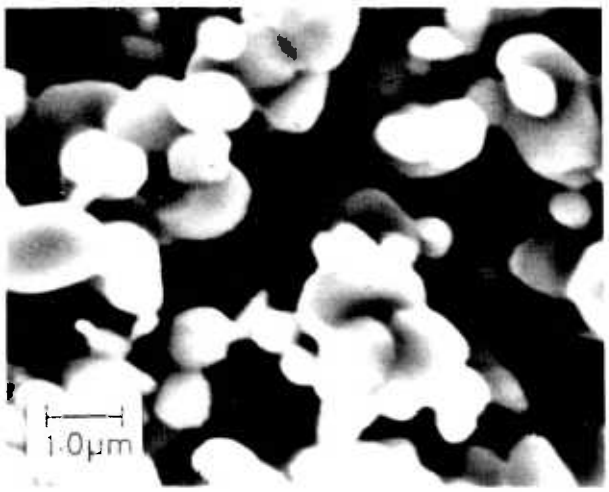
1·0μm

extended to about 100μ below the surfaces. Photographs (f), (g) and (h) on plate 10 and (a) and (b) on plate 11 illustrate the various features described above.

b) - 850°C. After reaction at 850°C the internal structure of all the pellets consisted of closely merged faceted particles about 2μ in diameter (approximately twice as large as those found after the 750°C experiments). The bulk porosities of all the reacted pellets were lower (but still significant) than their initial values. Passageways between interconnecting pores appeared to be more tortuous at 850°C than at 750°C. Any real differences in structure between the different composition pellets were indiscernable. There were no variations in structure* across the pellet sections except for occasional macropores. No ZnO-CdO/ZnO boundaries could be identified. Particles at the surfaces of the pellets covered a wide size range, the largest being just below 2μ in diameter. With each pellet the increased surface porosity appeared only to extend to a depth of about 30μ. Photographs (c), (d), (e) and (f) on plate 11 illustrate the various features described above.

c) - 950°C. Pellets reacted at 950°C had a highly sintered, low porosity, coarse structure. This structure bore very little resemblance to that of the unreacted pellets. Individual particles, in effect, no longer existed. Once again the internal structures of the different composition pellets were indistinguishable from one another. No ZnO-CdO/ZnO boundaries could be identified. The external surfaces of the pellets were similar to those developed at 750 and 850°C, however the increased porosity only reached about 10μ below the surface. Typical internal structures of the 950°C pellets are shown in photographs (g) and (h) on plate 11 and in photographs (a),(b) and (c) on plate 12.

Three very significant characteristics that were common to all of the reacted pellets are listed below.

a) The surfaces of the pellets were very porous. This high porosity only extended a short distance into each pellet. The oxide particles at the surfaces covered wide size ranges.

---

* Except for ZnO regions very close to the external surfaces.

PLATE 11:

STEREOSCAN PHOTOGRAPHS

11a (top left). CdO depleted region midway to the centre of a 10.8 mole % CdO - 750°C reacted pellet. The pellet is still quite porous (compare with 10d).

11b. External surface of a 10.8 mole % CdO pellet reacted at 750°C. The structure is very similar to that shown in 10h.

11c. Internal structure of a CdO depleted region of a 50.0 mole % CdO pellet reacted at 850°C; the same structure was found in the CdO/ZnO core. Compare with 11a.

11d. About 10-20 μm below the surface of a 50.0 mole % CdO pellet reacted at 850°C.

11e. Internal structure of a CdO depleted region of a 10.8 mole % CdO pellet reacted at 850°C. Although the grains are sintered together the structure has remained comparatively porous.

11f. External surface of 10.8 mole % CdO pellet reacted at 850°C.

11g. CdO/ZnO region of a 10.8 mole % CdO pellet reacted at 950°C.

11h (bottom right). As 11g. Compare with 11a and 11e.

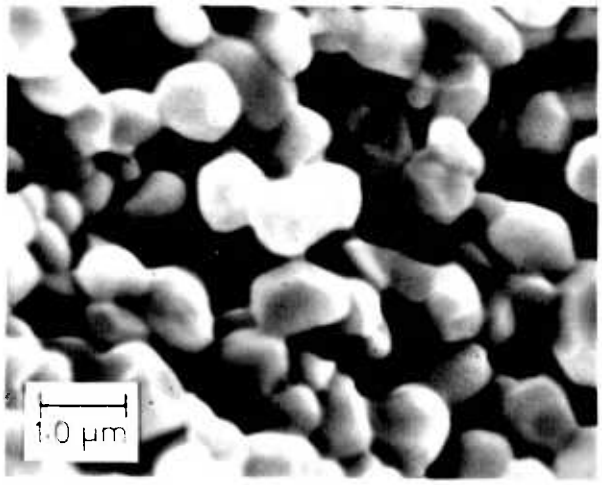
1·0 μm

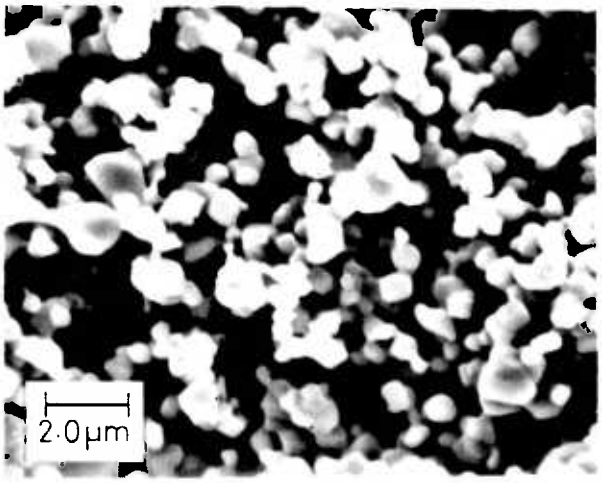
2·0μm

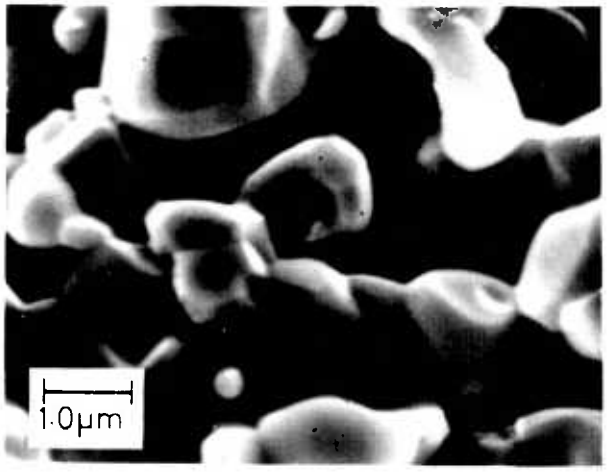
1·0μm

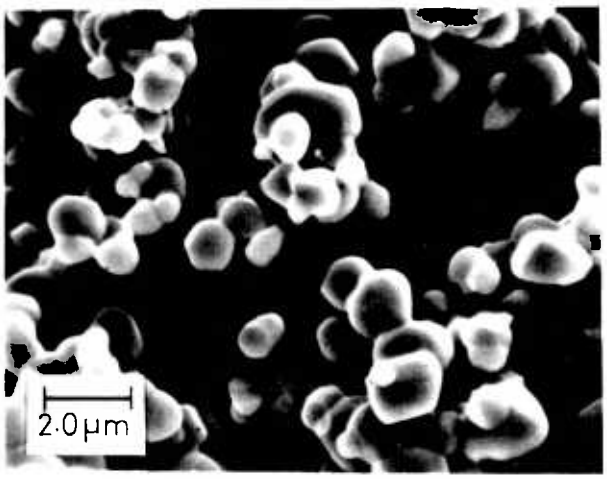
2·0μm

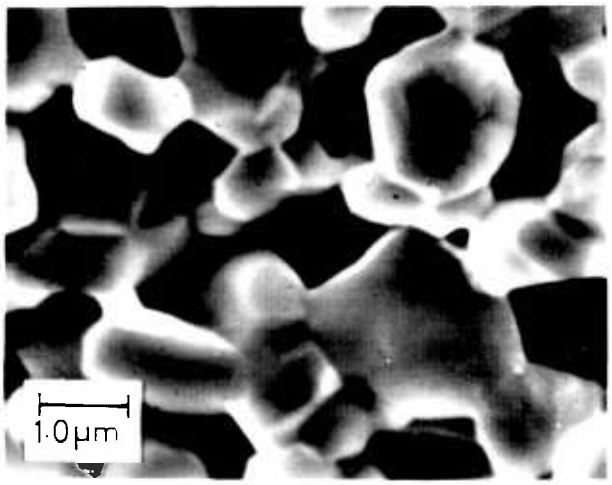
1·0μm

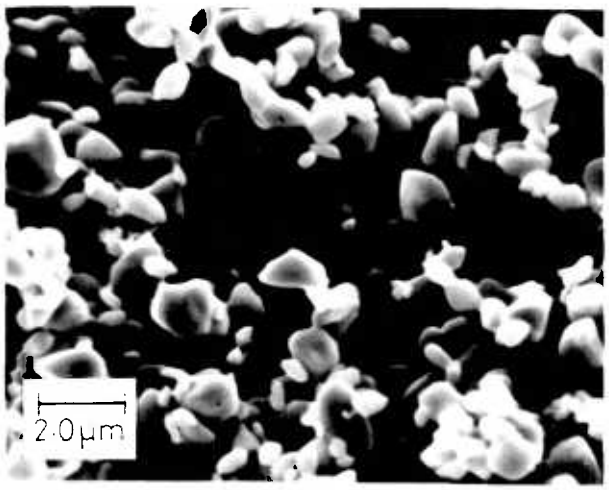
2·0μm

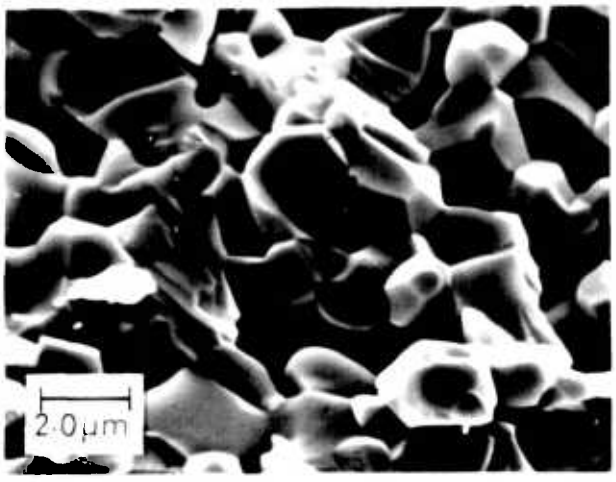
2·0μm

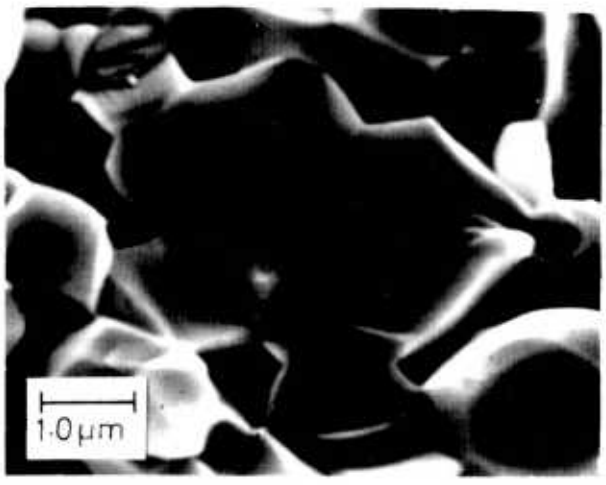
1·0μm

b) The structure of any given reacted pellet, other than at very close to its external surface, was (except for macropores) uniform throughout its bulk. The ZnO-CdO/ZnO boundaries could not therefore be detected.

c) The kinetics of sintering and densification, which could not be related to the composition of the pellets, became very much more rapid as the reaction temperature was increased.

If chlorine had reacted with the CdO contained within the pellets, the ZnO-CdO/ZnO boundaries would have appeared as discontinuities in bulk porosity*, especially those in the 50.0 mole % CdO pellets. Reduced porosity caused by the removal of oxide through reaction with chlorine was only detected near to the surfaces of the pellets. No variation in porosity was observed in the vicinity of any ZnO-CdO/ZnO boundary. The qualitative reaction behaviour of a partially depleted single pellet exposed to a chlorine containing atmosphere was therefore as follows. The chlorine, after diffusing through the gaseous boundary layer, reacted with ZnO at and slightly below the pellet surface. Zinc chloride, from either the pellet surface regions or the pellet surface regions and the bulk gas phase diffused through the porous ZnO shell and exchange reacted with the CdO. This second reaction was mass transport controlled. With increasing reaction temperature the permeability of the porous ZnO shell decreased due to the action of sintering and densification.

8A3c Structures of sintered pellets:- Sintering experiments were performed on unreacted pellets of the three different compositions. These were carried out as part of the investigations into the porosities of the various unreacted and reacted pellets, the results of the tests are reported in section 8A5b. For sintering some of the pellets were held at 950°C for 5 hours; this was about the length of time it took to perform one of the CdO/ZnO non-equilibrium experiments. It was therefore decided to examine these pellets under the Stereoscan and compare their structures with those of the 950°C - reacted pellets. Photographs (d), (e), (f), (g) and (h) on plate 12 illustrate the typical structures of the five hours -

* Provided that there was no collapse of structure.

PLATE 12:

STEREOSCAN PHOTOGRAPHS

12a (top left). Internal structure of a 10.8 mole % CdO pellet reacted at 950°C.

12b. Internal structure of 26.6 mole % CdO pellet reacted at 950°C

12c. As 12b. All of the pellets which had been reacted at 950°C had highly sintered low porosity structures.

12d. Internal structure of a 10.8 mole % CdO pellet sintered for 5 hours at 950°C

12e. Internal crack within a 10.8 mole % CdO pellet sintered for 5 hours at 950°C.

12f. As 12d. This structure, as in 12g, appears to be impermeable.

12g. Internal structure of a 26.6 mole % CdO pellet sintered for 5 hours at 950°C

12h (bottom right). As 12g.

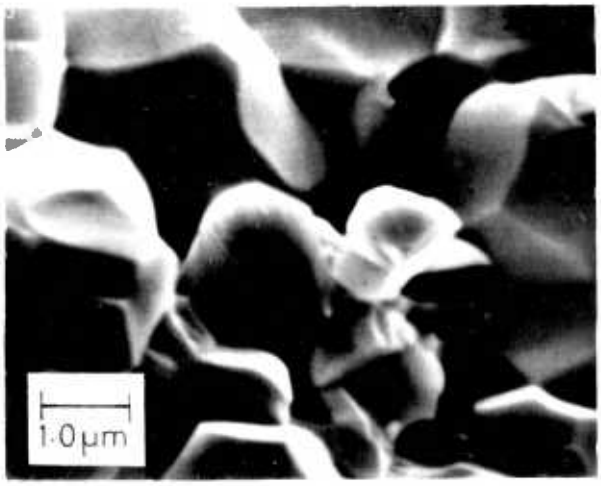
1·0μm

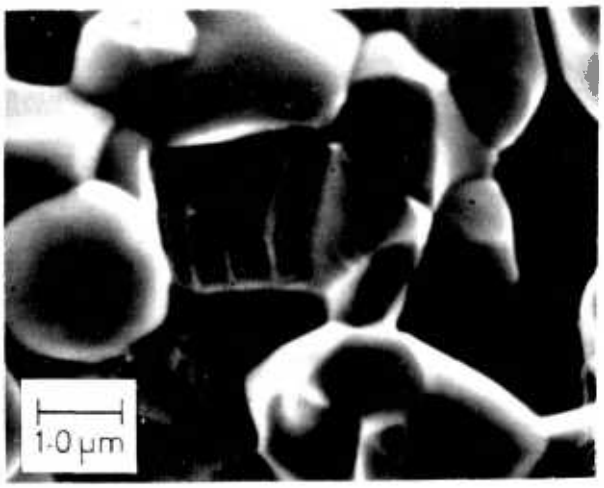
1·0μm

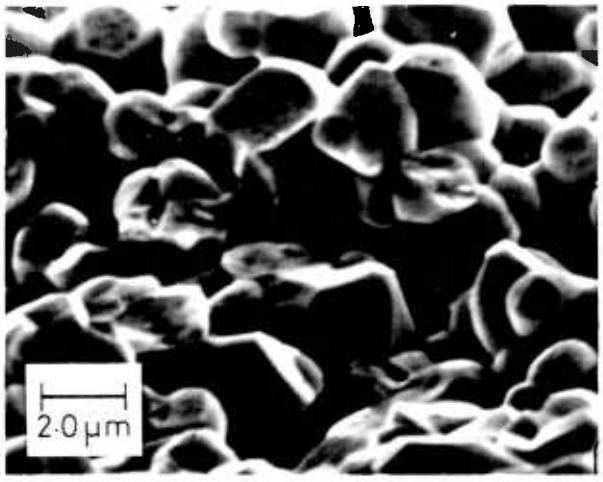
2·0μm

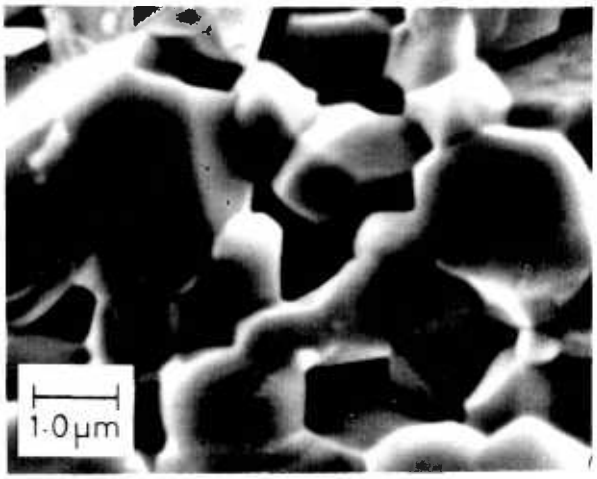
1·0μm

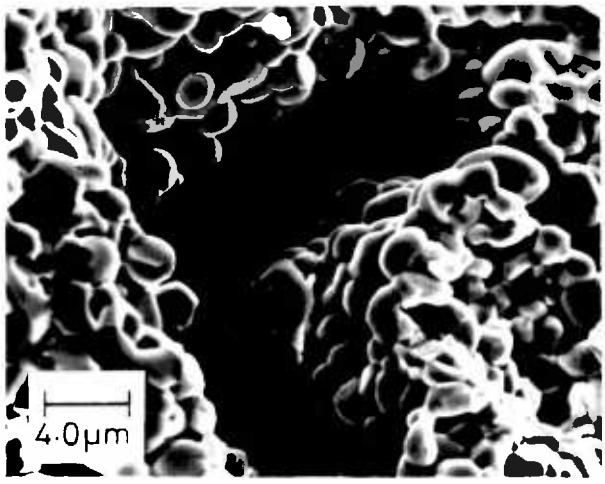
4·0μm

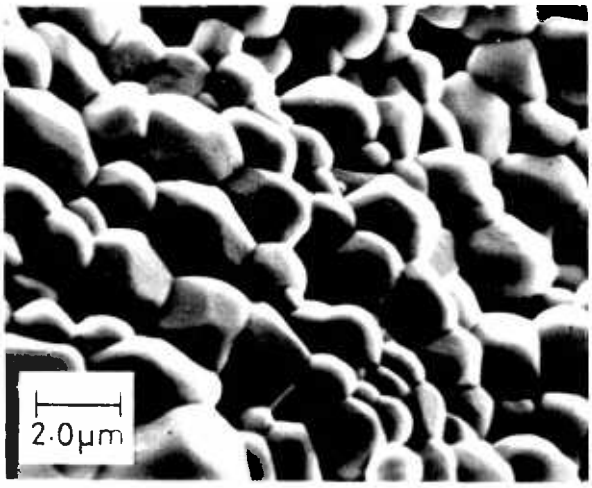
2·0μm

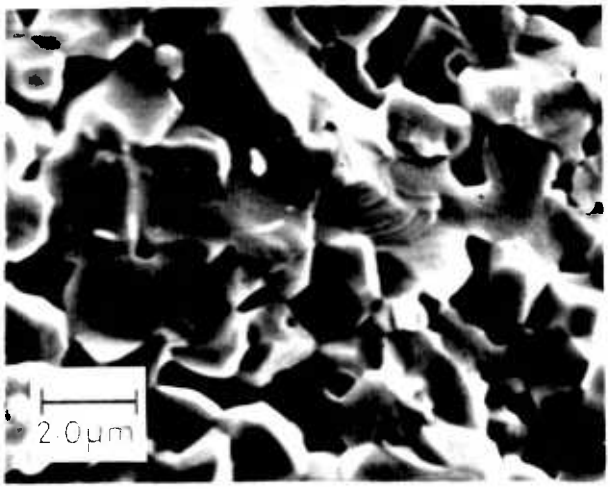
2·0μm

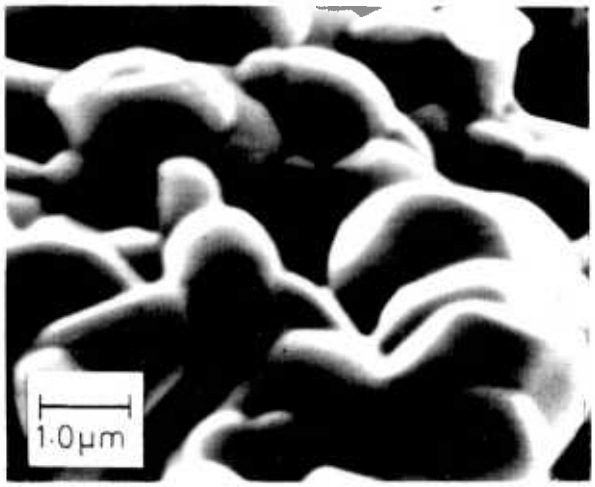
1·0μm

950°C sintered pellets. After this treatment it was not possible to distinguish between the three different composition unreacted pellets since all had dense highly sintered structures. Although there were differences between the bulk structures of the 950°C - reacted and the 950°C - sintered pellets, none were apparent from the SEM examinations.

8A4 Geoscan results

This investigation was performed with a Cambridge Geoscan electron probe microanalyser. Several operational modes were possible, those used were:

a) characteristic X-ray emission (area scanning)
b) characteristic X-ray emission (line scanning)
c) back scattered electron intensity (area scanning).

The electron beam, about 1-2μ in diameter, was accelerated with a potential of 20KV. Some of the electrons hitting the specimen surface caused X-ray emissions to occur, these included emissions characteristic of the metals present (Cd and/or Zn). Other electrons were back scattered. To measure the intensity of a particular characteristic emission a colimated beam of the radiation was sent to a crystal monochromator. By suitable positioning of the crystal, the desired radiation then passed to a photon counter. In this manner the Zn-K_α (Lithium flouride - 200 reflection) and Cd-L_α (pentaerythritol - 001 reflection) emission intensities were measured. Under the operating conditions employed, the characteristic X-rays were generated within a pear drop shaped volume which extended about 3-4μ into the specimen surface.

8A4a 750°C - 26.6 mole % CdO ZnO-CdO/ZnO boundary:- The 750°C - 26.6 mole % CdO specimen from which the results in this section were obtained is shown in photograph (a) on plate 5. The specimen surface, except for the addition of a thin carbon coating, was studied whilst in the same condition as that shown in the photograph. Photograph (f) on plate 9 maps the Cd distribution at the ZnO-CdO/ZnO boundary (area scanning); each white spot was produced by one quantum of Cd-L_α radiation. The boundary was clearly very sharp, however it is interesting to note that a small amount of Cd still remained in the ZnO. This retained Cd was probably in two forms: a) CdO encased in ZnO and b) Cd^{++} in solid solution with the ZnO (see section 6B3a). The Cd-scanned area shown on plate 9 was also examined using the back scattered electron operating mode, and

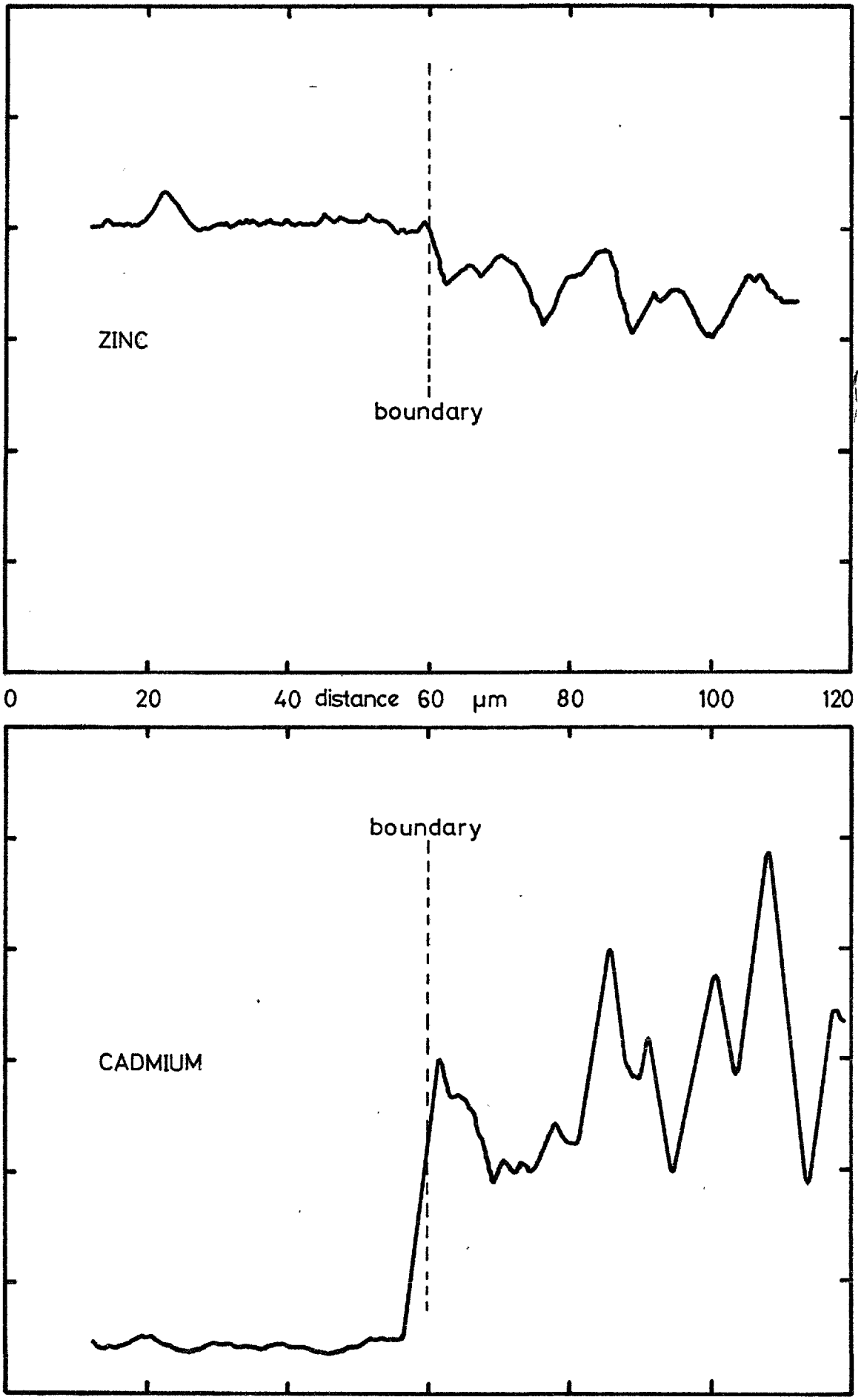

GRAPH 8A: ELECTRON PROBE Zn & Cd LINE SCANS ACROSS A ZnO-CdO/ZnO BOUNDARY.

also with an optical microscope. All three images* corresponded perfectly; each showed that the boundary had a small concavity towards its left hand side (see plate 9). On graph 8A are shown facsimiles of Zn and Cd line (about 2μ wide) scans** that were taken from the top to the bottom of the area that is shown in photograph (f) on plate 9. The two traces cannot be treated as accurate quantitative measurements since due to statistical variations no scan would ever be twice the same. However, the following three important points are demonstrated:

a) The ZnO-CdO/ZnO boundary was very sharp.
b) The ZnO contained a fairly uniform distribution of retained Cd.
c) The ZnO region appeared to contain a greater concentration of Zn than did the CdO/ZnO region.

Points (a) and (b), as expected, are in agreement with the Cd area-scan shown on plate 9. The most significant finding is point (c). The discontinuity in the Zn trace, provided that it was a genuine+ effect, supports the reaction behaviour described at the end of section 8A3b; namely, that the $CdO_{(s)}$ reacted with $ZnCl_{2(g)}$ (other than at the start of reaction).

8A5 Mercury porosimetry

The results presented in the first four main sections of this chapter show that the CdO reaction rate was mass transport controlled++. It was therefore important to quantify the effective diffusion coefficients of the reactant and product species in the various porous pellets. Effective diffusion coefficients within porous solids can be measured by direct experimental techniques[117,118]. These types of measurement, which can be of good accuracy, are normally obtained at room temperature, and are then modified for use at higher temperatures. When direct measurements are

---

* The intensity of the back scattered electrons was greatest from the high Cd regions since cadmium atoms are relatively more massive than zinc atoms.

** The line scans were recorded by photographing an oscilloscope display screen.

\+ It would not be a genuine effect if it had been caused either by a characteristic of the Geoscan technique, or by the collapse of the ZnO shell.

++ Other than, perhaps, at the start of reaction.

not possible, effective diffusion coefficients have to be estimated. An estimate can be accurate if the structure of the porous solid is analysed in detail. The important structural features to know are the sizes of the pores, the orientation of the pores and the total porosity. During reaction the CdO/ZnO pellets were subject to sintering and densification. Effective diffusion coefficients thus varied over the period of each experiment (more so with increasing temperature). A comprehensive and detailed analysis, by a direct method, of the varying transport properties of the different pellets would therefore have been very difficult, it would also have been somewhat inappropriate. It was thus decided to study the structures of the unreacted, reacted and sintered pellets and then estimate the values of the effective diffusion coefficients.

The pore structures of the different pellets are described and illustrated in section 8A3. These results, although of considerable significance, are essentially only semi-quantitative in nature. Any estimates, based on the Stereoscan results, of the total porosities, or various pore sizes of the different pellets would thus only be approximate. One established method for measuring pore sizes (and total porosities) is mercury porosimetry. Most solid surfaces are not wetted by mercury. To force mercury into a small capillary an external pressure is required. The simple force balance equation for a cylindrical capillary is given below:

$$\pi . r^2 . P = 2 . \sigma . r . \pi . \text{Cos}(180-\theta) \quad \ldots\ldots (1)$$

P = external applied pressure

r = capillary radius

σ = surface tension of mercury

θ = wetting angle

It has been established[117] that the wetting angle (angle of contact) between mercury and a great number of different solids, such as metal oxides and charcoals, varies only within the range 135° to 142°. The surface tension of uncontaminated mercury is 484 dynes/cm at $25^\circ C$, falling slightly to 472 dynes/cm at $50^\circ C$. Using an average contact angle value of 141° equation (1) reduces to

$$r = \frac{75000}{P} \quad \ldots\ldots (2)$$

r = pore radius - Å

P = applied pressure - atmos.

Different r.P ratios have been used by other workers[117] (eg 62000) but a figure of 75000 seems to be generally accepted. An exact r.P value is not essential since, pores rarely being cylindrical, only effective pore radii are measured. Mercury being forced into a long irregular shaped pore will not uniformly occupy its cross section. The first mercury that enters does so as a cylindrical column*. Only when the pressure is increased (all the more easily entered regions then being full) does the mercury start to flow into the 'tight corners' of the pore. A further complication brought about by irregular shaped pores concerns 'necks'. If large pores are connected to each other by small passages, then the pressure required to force mercury from one pore to the next (provided that there are no other flow routes) is governed by the size of the neck and not the size of the pore. Fortunately these factors are not always dominant. Their general effect is however to make the pores appear to be smaller than they really are.

From the Stereoscan results it can be seen that the pore structures of the various pellets were relatively simple. The porosimetry results obtained during this study were thus fairly easy to interpret. The effective pore radii given below have been determined by using equation (2).

8A5a Experimental procedure:- The standard instrument used for the pore size studies was a Carlo Erba model 70 mercury porosimeter. Its maximum operating pressure is 2000 atmospheres, it is thus capable of measuring extremely small pores (based on equation (2) – 37Å). The operating principal of the instrument is as follows: The specimen under test is placed in a test tube shaped glass vessel, which is then connected by a greased cone joint, to a precision bore glass tube. Using a special holding jig, the vertically held container and tube are then pumped down to about 0.1 torr. The assembly is then filled nearly to the top with pure mercury. The container and tube are then transferred to the instrument's pressure vessel. Through the top of this vessel is a long threaded contact rod. This is screwed down until it just touches the top of the mercury in the tube. An electrical circuit is employed for the purposes of establishing contact; the current passes down the rod, through the mercury and out of the bottom of the glass vessel via a

---

* A complex pore may be filled by several columns of mercury before they finally join together.

sealed in tungsten wire. The entire pressure vessel and pressure supply line are then filled with methyl alcohol, and sealed shut. Pressure, generated by a hydraulically operated pressure intensifier unit, is then applied to the system. The circuitry of the instrument is arranged so that when continuity between the mercury in the tube and the contact rod is lost, the intensifier unit ceases to increase the pressure. A servo motor then screws down the contact rod to complete the circuit, pressurisation then continues until more mercury is taken in by the specimen and the process is repeated. The graphical output of the instrument is a plot of applied pressure (gauge) vs. contact rod displacement. Various sizes of precision bore tubes are available, the one used in this study was 3.00 mm in bore and 100 mm long, this allowed total pore volumes of up to about 0.7 cc to be studied. One system correction is required, this accounts for the compressibility of the mercury and the elasticity of the pressure vessel. Since no specimens studied were less than 95% filled by 100 atmospheres pressure this correction was always small. However, at high pressures (1000 atmos.) this correction is critical since small pores (having very small volumes) can easily be 'lost' by an inaccurate correction.

Other than when premature depressurisation occurred (seal failure) all the pellets were taken up to the maximum working pressure. To obtain maximum sensitivity from the porosimeter, each sample tested was chosen to have as large a total pore volume as permissible. In all instances several pellets from the same specimen batch were therefore tested at once. One potential problem with the technique is that after the specimen vessel has been filled, on re-admitting air to the system, pores of greater than 7.5μ immediately become filled with mercury. To check that this effect did not occur during this study, each filling routine was carefully watched. Fortunately the uptake at 1 atmosphere was invariably small or negligible with all the specimens tested.*

To calculate the bulk porosities of the specimens tested it was necessary to measure their external bulk volumes. These measurements were carried out by using a simple mercury displacement rig; its construction has been described by Campbell[118]. Briefly, the technique consisted of submerging partially evacuated pellets (about 500-600 mm Hg) in a given volume of mercury. The displacement of the mercury from its original position (measured to ±0.005 cc) then gave the external volume of the pellets.

---

* Macropores did exist; this result therefore indicates that either few emerged at the surface of the pellets, or that they were of very small sum total volume.

8A5b Porosimetry results:- Porosimeter tests were performed on unreacted, reacted and sintered pellets of each of the three different compositions. The sintering treatments were carried out by pushing the pellets straight into a furnace held at the predetermined temperature, and then equally quickly removing them after the sintering time (between 1 and 5 hours) had elapsed. This comparatively rapid thermal cycling did not cause the pellets to crack. The results from each test were calculated as follows*: a) the bulk density was calculated from the mass of the pellets and their bulk volume, b) the bulk porosity was calculated from the bulk volume of the pellets and the volume of mercury which was forced into them by the porosimeter, and c) the solid's density was calculated from the mass of the pellets and the difference between their bulk volume and the volume of mercury forced into them. Given in table 8A (parts 1, 2 and 3) are the results of 30 porosimeter tests. The four plots given on graph 8B cover the range of different pore size distributions encountered during these tests. Various different sizes of pellets were studied since insufficient numbers of unreacted pellets, of the same size used for the chlorination experiments (-6.7 + 5.6 mm) were available. With reacted pellets a range of sizes from the same bed were tested together, these pellets were then dissolved in hydrochloric acid and analysed (AA) to discover their mean composition, results of these analyses are given in table 8A. Since only 4 pore size distribution plots are presented, with each of the sets of results three data-points from their pore size graphs are given in table 8A. These data points are the pore sizes above which 10%, 50% and 90% of the total pore volume is composed. Solids' densities have been calculated for the unreacted and sintered pellets for the purpose of comparing the consistency of the results. The measured solids density of unreacted and sintered pellets of the same composition should be very nearly constant**. The theoretical densities[119] of CdO and ZnO calculated from X-ray measurements are 8.238 and 5.675 gms/cc respectively (at 26°C); the measured densities[119] are given to be 8.15 and 5.61 gms/cc. Calculated

---

* The methods of calculating the density and porosity results are given since the results tables show some slight inconsistencies: eg run numbers 35 and 26.

** Provided that all the pores became full of mercury.

Run number	Pellet size fraction - mm	Bulk density gms/cc	Solids density gms/cc	Mole % CdO in pellets	Condition of pellets	Porosity %	X% of total pore volume made up of pores greater than Y microns in radius		
							X = 10%	X = 50%	X = 90%
16	-9.5 + 8.0	4.83	6.47	50.0	unreacted	25.3	0.40(Y)	0.26(Y)	0.18(Y)
14	-6.7 + 5.6	5.02	6.61	50.0	unreacted	24.1	0.40	0.25	0.17
4	-6.7 + 5.6*	4.67	-	45.5	reacted 750°C	25.1	0.80	0.52	0.23
5	-6.7 + 5.6*	4.92	-	46.2	reacted 850°C	23.5	1.10	0.65	0.34
6	-6.7 + 5.6*	5.38	-	48.5	reacted 950°C	16.4	1.20	0.60	0.01
25	-9.5 + 8.0	5.39	6.25	50.0	5 hrs-950°C	13.6	0.85	0.60	0.31
26	-9.5 + 8.0	4.87	6.54	50.0	1 hr-950°C	17.6	0.65	0.37	0.22
35	-9.5 + 8.0	4.93	6.31	50.0	5 hrs-850°C	21.9	0.58	0.39	0.22
31	-9.5 + 8.0	4.81	6.34	50.0	5 hrs-750°C	24.1	0.55	0.33	0.20

* Initial size

Calculated solids density = 6.93 gms/cc

TABLE 8A (part 1): POROSIMETRY RESULTS - 50.0 mole % CdO PELLETS

Run number	Pellet size fraction - mm	Bulk density gms/cc	Solids density gms/cc	Mole % CdO in pellets	Condition of pellets	Porosity %	X% of total pore volume made up of pores greater than Y microns in radius		
							X = 10%	X = 50%	X = 90%
1	-8.0 + 6.7	4.62	5.92	26.6	unreacted	22.0	0.21(Y)	0.15(Y)	0.11(Y)
18	-9.5 + 8.0	4.92	6.13	26.6	unreacted	19.8	0.21	0.17	0.12
7	-6.7 + 5.6*	4.07	-	15.3	reacted 750°C	27.9	0.63	0.38	0.20
9	-6.7 + 5.6*	4.86	-	22.2	reacted 850°C	16.4	0.63	0.33	0.15
8	-6.7 + 5.6*	5.29	-	24.7	reacted 950°C	12.3	0.55	0.28	0.05
43	-8.0 + 6.7	5.75	5.81	26.6	2 hrs-1000°C	1.14	-	0.18	0.07
20	-8.0 + 6.7	5.59	5.83	26.6	5 hrs-950°C	4.12	0.45	0.24	0.09
42	-8.0 + 6.7	5.61	6.09	26.6	2 hrs-950°C	7.90	0.33	0.10	0.02
22	-8.0 + 6.7	5.34	6.14	26.6	1 hr-950°C	13.0	0.36	0.15	0.05
34	-8.0 + 6.7	5.22	6.06	26.6	5 hrs-850°C	13.7	0.22	0.12	0.07
38	-8.0 + 6.7	4.96	5.93	26.6	2 hrs-850°C	16.4	0.28	0.19	0.11
32	-8.0 + 6.7	5.10	6.07	26.6	5 hrs-750°C	16.1	0.25	0.14	0.07
23	-8.0 + 6.7	5.03	6.14	26.6	1 hr-750°C	18.1	0.23	0.17	0.11

* Initial size

Calculated solids density = 6.32 gms/cc

TABLE 8A(part 2): POROSIMETRY RESULTS - 26.6 mole % CdO PELLETS

Run number	Pellet size fraction - mm	Bulk density gms/cc	Solids density gms/cc	Mole % CdO in pellets	Condition of pellets	Porosity %	X% of total pore volume made up of pores greater than Y microns in radius		
							X = 10%	X = 50%	X = 90%
13	-6.7 + 5.6	4.14	5.65	10.8	unreacted	26.7	0.20(Y)	0.16(Y)	0.12(Y)
10	-6.7 + 5.6*	3.74	-	5.28	reacted 750°C	31.9	0.75	0.40	0.24
11	-6.7 + 5.6*	4.15	-	5.27	reacted 850°C	24.4	0.56	0.37	0.22
12	-6.7 + 5.6*	4.88	-	10.2	reacted 950°C	11.7	0.70	0.41	0.23
24	-6.7 + 5.6	5.18	5.49	10.8	5 hrs-950°C	5.54	0.60	0.23	0.10
27	-6.7 + 5.6	5.01	5.63	10.8	1 hr-950°C	11.0	0.32	0.19	0.10
36	-6.7 + 5.6	4.86	5.67	10.8	5 hrs-850°C	14.4	0.25	0.17	0.10
37	-6.7 + 5.6	4.32	5.56	10.8	5 hrs-750°C	22.4	0.23	0.17	0.12

* Initial size

Calculated solids density = 5.90 gms/cc

TABLE 8A (part 3): POROSIMETRY RESULTS - 10.8 mole % CdO PELLETS

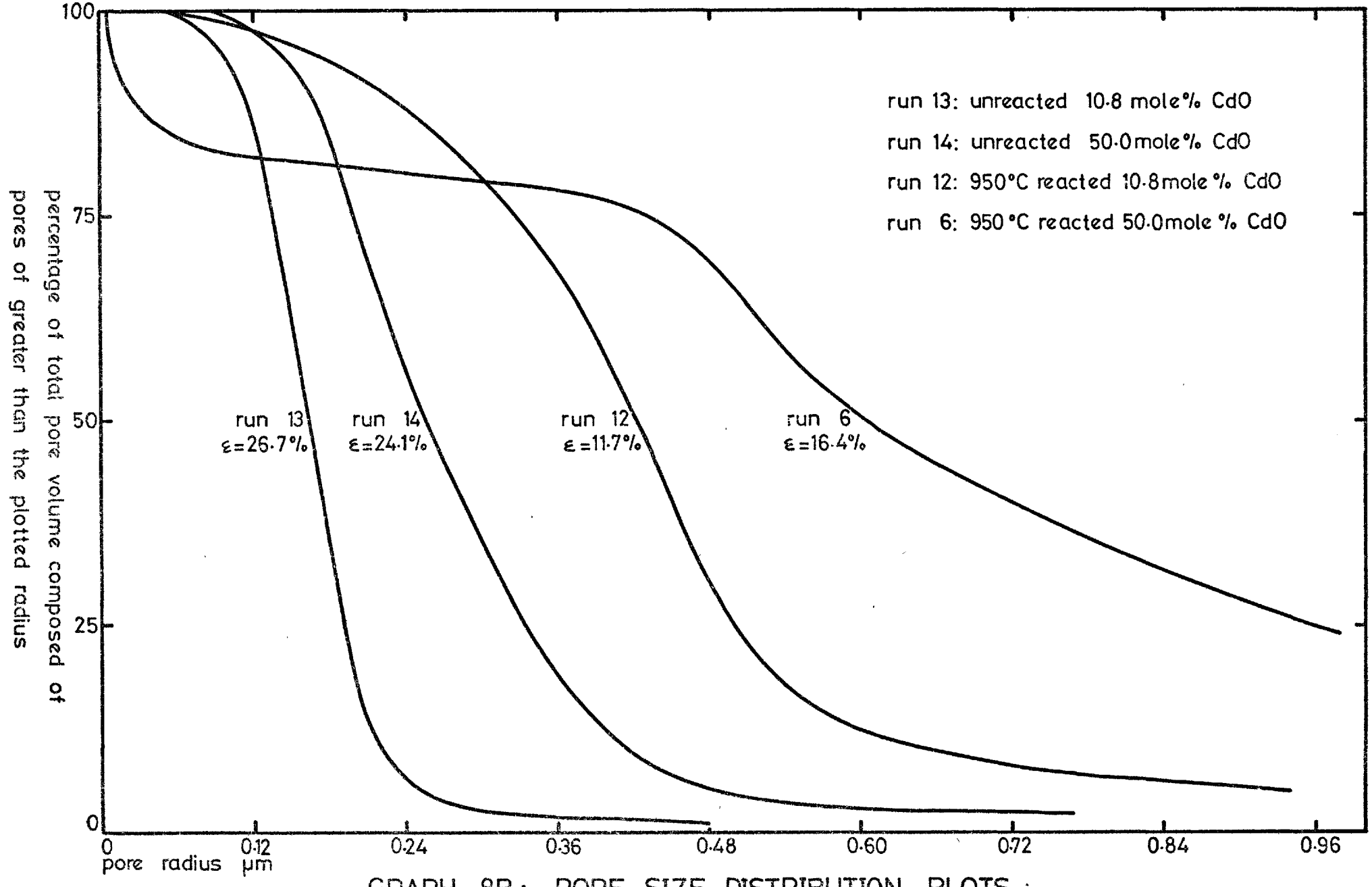

GRAPH 8B: PORE SIZE DISTRIBUTION PLOTS.

solids densities (as admixtures) of the pellets of the three different compositions, based upon these measured densities, are given at the bottom of table 8A.

The porosimetry results indicate that the pore structures within all the various pellets tested were unimodal. The only pellets that had an apparent tendency towards a bimodal structure were from the 950°C - 50.0 mole % CdO chlorination experiment. It is thought, however, that distinct small pores were not present in these pellets, the effect was probably due to the larger pores having many 'tight corners'. The narrowest size ranges of pores were found in the unreacted pellets. 80% of the total pore volume contained within both the unreacted 10.8 and 26.6 mole % CdO pellets was made up of pores between about 0.21 and 0.12μ radius. The unreacted 50.0 mole % CdO pellets contained pores that were between about 30 and 40% larger. The largest pores were present in the reacted pellets. Those in the sintered pellets, although somewhat smaller, were appreciably larger (depending upon the sintering treatment) than those in the unreacted pellets. A detailed description of the pore sizes and distributions found in all of the various pellets would be lengthy, however the data given in table 8A and on graph 8B convey all the relevant information.

The bulk porosities of all the reacted and sintered pellets fell by very significant amounts with increasing temperature. This bulk densification was more pronounced with the lower CdO content pellets. However, it is thought that macro cracks and pores were mainly responsible for the maintenance of relatively high bulk porosities within the 50.0 mole % CdO pellets (see section 8A2a). The 26.6 and 10.8 mole % CdO - 750°C pellets both showed slight increased porosities as compared with their unreacted counterparts. This could have been caused by the combined effects of a) some Cl_2 penetration, b) no effective densification and c) the molar volume* of CdO is greater than that of ZnO. The measured

---

* Molar volume ZnO = 14.52 cc
Molar volume CdO = 15.76 cc
Data from reference 119

solids densities of the unreacted pellets of each composition showed some variation, also, the values were on average about 5% (10.8 and 26.6 mole % CdO pellets) to 9% (50.0 mole % CdO pellets) below the calculated values. These disagreements were probably caused by experimental inaccuracies and closed pores. Considering the dissimilarities between their sintering conditions, the differences between the reacted and sintered pellets were not unexpected.

The one major disadvantage with the porosimeter tests was that bulk pellet properties were under investigation as opposed to those of the ZnO shells. The results given in this section are in good general agreement with the Stereoscan observations.

8A A MATHEMATICAL ANALYSIS OF THE NON-EQUILIBRIUM CHLORINATION OF PACKED BEDS OF CdO/ZnO PELLETS

8B1 Reaction characterisation

Before a mathematical model describing the non-equilibrium experiments could be constructed it was necessary to critically evaluate all the available experimental data so as to obtain a qualitative understanding of the various reaction processes. The most significant results obtained from the chlorination experiments and the subsequent structural analyses are listed below:

1. With the experiments at 750, 850 and 950°C chlorine utilisations were effectively 100% (see section 7B2 and table 7E).

2. The overall chlorine reaction rate constant increased with increasing temperature (see section 8A1b. This same constant rapidly increased with increasing temperature during the ZnO chlorination experiments; see section 7A3b).

3. The CdO reaction rate within each pellet was controlled by the diffusion of gaseous species through the surrounding porous ZnO shell (see sections 8A2a, 8A2b and 8A4).

4. Due to sintering and densification the CdO reaction rate decreased with increasing temperature (see section 8A3b, 8A3c and 8A5b).

5. Penetration of Cl_2 into the porous pellets appeared to be slight even at 750°C (see section 8A3b).

6. Although not entirely conclusive there was strong evidence to suggest that within the CdO/ZnO pellets the CdO reacted with gaseous $ZnCl_2$ (see section 8A3b and 8A4).

7. At 750°C the overall rate of the $ZnCl_{2(g)}$ + CdO exchange reaction could be comparatively high. When taking place in a packed bed of CdO/ZnO pellets the overall rate of this reaction decreased with increasing temperature (see section 7C2 and table 7G).

8. Temperature variations during chlorination were very small (see section 7B3).

Six of the features described above require no further discussion since they are well proven by the experimental results. However, the two most important points listed (numbers 5 and 6), although well evidenced by the experimental results, require some theoretical support.

The extent of penetration by diffusion of a gaseous reactant into a porous solid is governed by two factors. These are a) the effective diffusivity of the reactant species through the porous solid, and b) the intrinsic chemical reactivity of the solid. Under all real conditions there will be some penetration. However, slow diffusion through a high reactivity solid will result in very little penetration, and conversely, rapid diffusion through a low reactivity solid will result in signficant or almost total penetration. The phenomena of simultaneous reaction and diffusion can be mathematically analysed once a number of simple assumptions have been made. The analysis that now follows is, within the limitations imposed by the assumptions, applicable to the diffusion of chlorine into a porous zinc oxide spherical pellet. The reaction taking place is

$$ZnO_{(s)} + Cl_{2(g)} = ZnCl_{2(g)} + \tfrac{1}{2}O_{2(g)} \quad \cdots\cdots\cdots\cdots \quad (1)$$

The simplifying assumptions are a) reaction 1 is irreversible* (therefore the reaction proceeds only in a forward direction); b) reaction (1) is first order with respect to chlorine partial pressure; c) the chemical reaction rate constant is constant throughout the pellet; d) the internal surface area of the pellet is uniformly distributed throughout its bulk; e) the effective diffusion coefficient of Cl_2 is constant throughout the pellet; f) gaseous diffusion can be described by Fick's first law; and g) the pellet is isothermal. The schematic diagram below represents a ZnO pellet (since only chlorine is involved in the equations no "Cl_2" subscripts are used with c_{Cl_2}, $D^{eff}_{Cl_2}$ and k_{Cl_2}).

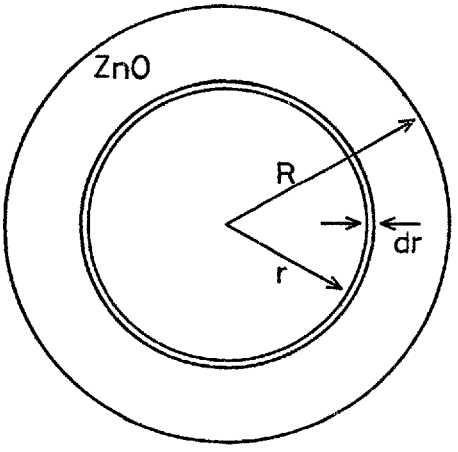

Using the pseudo-steady-state approximation the shell mass balance on Cl_2 for the differential element dr is:

(Rate of inward diffusion at r = r + dr) - (Rate of inward diffusion at r = r) = Rate of reaction in differential element dr . . . (2)

Transforming equation (2) into mathematical form the following differential equation is obtained:

$$-4\pi(r + dr)^2.D^{eff}.\left(\frac{dc}{dr} + \frac{d^2c}{dr^2}dr\right) + 4\pi r^2.D^{eff}.\frac{dc}{dr}$$

$$= -4\pi r^2 dr.S_v.k.c \quad \ldots\ldots\ldots\ldots\ldots\ldots\ldots\ldots\ldots\ldots (3)$$

sign convention: reaction of reactant -ve

inward diffusion -ve

S_v = internal surface area per unit vol - cm^2/cm^3

k = Cl_2 chemical rate constant - cm/sec

c = Cl_2 concentration - gm-moles/cm^3

$\frac{dc}{dr}$ = Cl_2 concentration gradient at radius r - gm-moles/cm^4

D^{eff} = effective chlorine diffusion coefficient - cm^2/sec

---

* This is a valid assumption for reactions that are signficantly away from equilibrium.

Expanding equation (3) and rearranging gives:

$$\frac{d^2c}{dr^2} + \frac{2}{r} \cdot \frac{dc}{dr} = \frac{S_v.k.c}{D^{eff}} \quad \ldots\ldots\ldots\ldots\ldots\ldots\ldots\ldots\ldots\ldots (4)$$

Equation number (4) is well known in the study of catalysis, from it is defined the Thiele modulus (shown here for a first order reaction and spherical geometry).

$$Th = R \cdot \left(\frac{k.S_v}{D^{eff}} \right)^{\frac{1}{2}} \quad \ldots\ldots\ldots\ldots\ldots\ldots\ldots\ldots\ldots\ldots (5)$$

This is a dimensionless number which is a measure of the ratio of the resistance to diffusion to the resistance to chemical reaction. In terms of the Thiele modulus (Th) equation (4) becomes:

$$\frac{d^2c}{dr^2} + \frac{2}{r} \cdot \frac{dc}{dr} = \left(\frac{Th}{R}\right)^2 \cdot c \quad \ldots\ldots\ldots\ldots\ldots\ldots\ldots (6)$$

In the context of catalysis (for the purposes of calculating effectiveness factors) this equation has been solved by Satterfield[117]. An analogous equation has been solved by Wen[120] in his comprehensive paper on noncatalytic heterogeneous solid-fluid reaction models. From this paper is taken graph 8C; this shows plots of dimensionless concentration (concentration at r/concentration at R) versus dimensionless radius (r/R) for varying Thiele moduli.

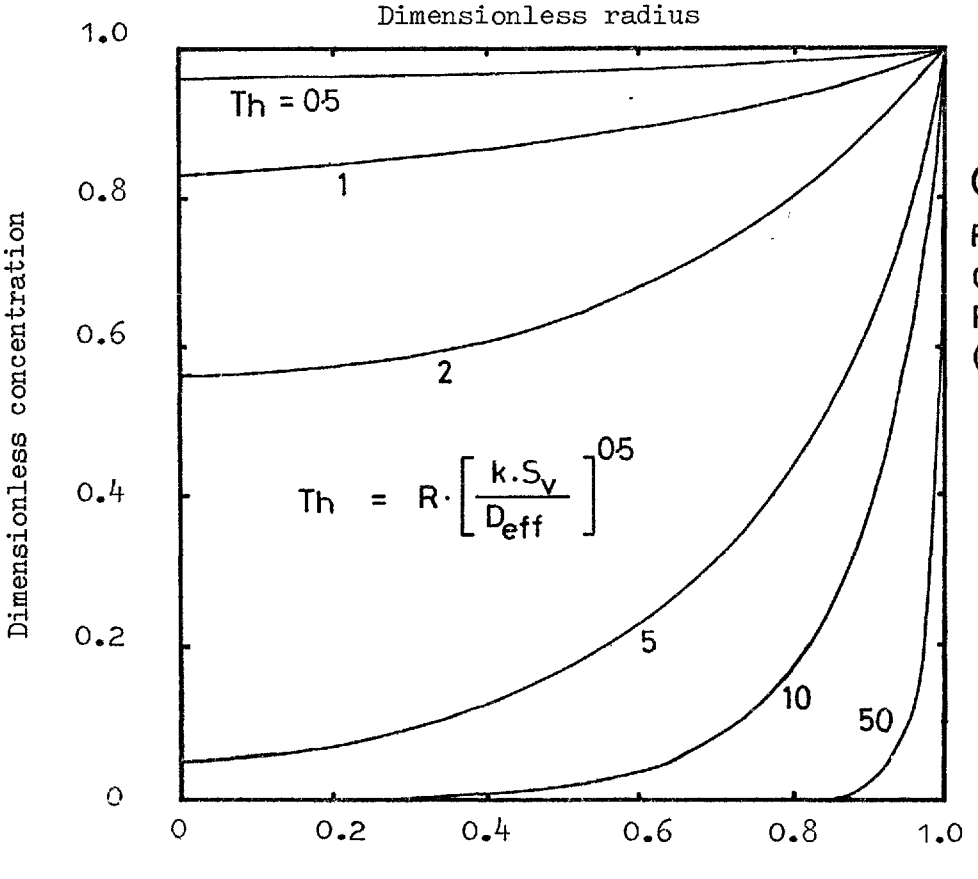

GRAPH 8C: REACTANT GAS PENETRATION (from Wen[120]).

Graph 8C shows that when the Thiele modulus starts to approach a value of about 50 reactant gas penetration becomes very limited. The problem that now arises is to estimate a Thiele modulus value for the porous ZnO shells which surrounded the CdO/ZnO cores. Values are required for the parameters k_{Cl_2}, $_{ZnO}S_v$ and $D^{eff}_{Cl_2}$; these will be estimated for a temperature of $750^{\circ}C$.

a) Even though the gas composition varied throughout the reactor during each chlorination experiment at a given temperature the molecular diffusion coefficient of Cl_2 in these changing gas mixtures remained fairly constant. At $750^{\circ}C$ a good estimate of $D_{Cl_2/m}$ is 1.0 cm^2/sec. If the pellets are assumed to have had a porosity of 25% and a tortuosity factor of 4, an effective diffusion coefficient, including a Knudsen flow contribution, of about $0.1 cm^2/sec$ would thus appear to be a generous estimate.

b) $_{ZnO}S_v$, the ZnO surface area per unit volume, may be estimated from the Stereoscan results. Typical internal structures of the $750^{\circ}C$ - reacted pellets are illustrated by photographs (f) and (g) on plate 10 and (a) on plate 11. For the purposes of calculating a surface area value it would seem quite safe to treat the pellets as being made up of 1μ diameter spherical micro particles. Thus, using a porosity of 25% and a particle radius of 0.5μ the calculated surface area per unit volume becomes $4.5 \times 10^4 cm^{-1}$.

c) To make a reasonable estimate of the chemical rate constant would be impossible without at least some general overall rate data, fortunately the ZnO non-equilibrium results supply this information. Presented in section 7A3b are the overall rate constants that have been calculated from the ZnO non-equilibrium results. By interpolating these results an overall rate constant of 0.15 cm/sec at $750^{\circ}C$ is obtained.

Using the values given above together with a pellet radius of 0.61 cms (mean diameter of the -6.7 + 5.6 mm pellets) the calculated Thiele modulus is 158. A critical assessment of this calculation suggests that the surface area and diffusion parameters have been reasonably accurately estimated but that the rate constant is potentially in error by a large amount. The assumption that the ZnO + Cl_2 chemical rate constant is equal to the overall rate constant infers that boundary layer gas phase transport resistance is negligible. Although

this might be incorrect, for the purposes of this calculation the assumption is safe since it underestimates rather than overestimates the value of the chemical rate constant. The source of the large potential error is that the ZnO + Cl_2 overall rate constants (given in section 7A3b) incorporate estimated geometric surface area values (see section 7A3a). The true surface areas of the various ZnO size fractions, under experimental conditions, were almost certainly significantly greater than these estimates*. The chemical rate constant value of 0.15 cm/sec used for the Thiele modulus calculation would therefore appear to be too large. However, if this rate constant is reduced by a factor of 10 the modulus becomes 50, and if it is reduced by a factor of 100 the modulus becomes 16. Since it is thought extremely unlikely that the true chemical rate constant was more than x10 less than the value first used, the calculated Thiele moduli (in conjunction with graph 8C) indicates that at 750°C chlorine penetration** was very slight. Chemical reactions are activated processes, their rates are thus extremely temperature sensitive. Therefore, if chlorine penetration was only very slight at 750°C it would have been even less at 850°C and negligible at 950°C.

8B2 Rate controlling mechanisms

The results and calculations presented in the preceding section clearly demonstrate that (except near the start of reaction) during the various chlorination experiments $CdCl_{2(g)}$ was formed by the overall exchange reaction

$$ZnCl_{2(g)} + CdO_{(s)} = CdCl_{2(g)} + ZnO_{(s)} \quad \ldots\ldots\ldots\ldots (1)$$

It has also been shown that this reaction was mass transport controlled. However, what has not been established is the Cl_2 reaction rate controlling mechanism(s). The overall rate constants calculated from the ZnO non-equilibrium results (see section 7A3b) suggest that at between 705 and 720°C resistance to reaction was mainly due to chemical processes at the

---

* This statement is based upon the observation that the ZnO granules had developed thin powdery coatings by the end of chlorination.

** The calculations apply for a porous solid which is not 'volatilised', they therefore best describe the initial stages of chlorination of a ZnO pellet. After a significant period of chlorination, although there would be a ZnO concentration gradient near to the pellet surface, Cl_2 penetration would not be much greater than that indicated by graph 8C.

ZnO surface (estimated packed bed mass transfer coefficients supply the evidence upon which this belief is based: see section 8B4). At between 850 and 870°C the calculated overall rate constants are of the same order of magnitude as the estimated packed bed mass transfer coefficients. No ZnO non-equilibrium data is available for 950°C, however, by extrapolating the lower temperature results it appears that the controlling mechanism would probably be boundary-layer gas-phase mass transfer. These tentative deductions have been made upon the basis of results that are not entirely conclusive. A mixed-control (chemical and mass transfer) packed bed mathematical model would be difficult to develop, any reasonable simplifications would thus be very desirable. Hills[54] suggests that the best method of analysing a high temperature gas-solid reaction is to first assume that it is transport controlled*; only if the reaction proceeds significantly more slowly than is predicted on the basis of this assumption should a chemical mechanism be considered.

With these various considerations in mind it was decided to construct a mass transport controlled reaction model. As regards the chlorine reaction rate, this type of model is not as inflexible as might at first be imagined. The boundary layer chlorine mass transfer coefficient acts as an overall reaction rate constant, therefore by using low mass transfer coefficients this simulates, in part, the effects of a low chemical rate constant (see equation (3), section 7A2).

8B3 Gas phase ordinary molecular diffusion

There are several distinct types of molecular diffusion, the type described in this section, known as ordinary molecular diffusion, is caused by a concentration gradient of a molecular species. A mixture of gases tends towards a uniform composition as a result of all the component species diffusing down their concentration gradients. This phenomenon can be analysed and understood by using the kinetic theory of gases (eg Stefan-Maxwell equations). For a full analysis of this subject reference should be made to Hirschfelder, Curtiss and Bird[121]. Practical applications of the theory of ordinary diffusion are given by Satterfield[117] and by Bird, Stewart and Lightfoot[62].

---

* Either heat or mass or heat and mass transport controlled.

8B3a Diffusion in binary systems:- With reference to the plane of no net molar transport the rate of diffusion of component "i" in a binary gas mixture ("i"-"j") is given by Fick's first law equation

$$J_i = -D_{ij} \cdot \frac{dc_i}{dx} \quad \ldots\ldots\ldots\ldots\ldots\ldots\ldots\ldots\ldots\ldots (1)$$

(diffusion is in the x-direction)
J_i is the flux (gm-moles/sec cm^2) of gas "i"
dc_i/dx the concentration gradient (gm-moles/cm^4) of gas "i" and
D_{ij} the diffusion coefficient (cm^2/sec) of gas "i" in the mixture (diffusion of "i" into "j" is the same as diffusion of "j" into "i", therefore $D_{ij} = D_{ji}$ and $J_i = -J_j$). Equation (1) is of limited use since most cases of diffusion require solution with respect to fixed axes. In these circumstances an additional term is required to describe bulk flow, the resulting equation is given below:

$$\dot{n}''_i = N_i \cdot (\dot{n}''_i + \dot{n}''_j) - D_{ij} \cdot \frac{dc_i}{dx} \quad \ldots (2)$$

Total flux of "i" in x-direction w.r.t. fixed axes	Flux resulting from net molar bulk flow, determined by stoichiometry of system	Flux due to diffusion

$\dot{n}''_i$ and $\dot{n}''_j$ are the fluxes of species "i" and "j" with respect to fixed axes, N_i is the mole fraction of "i". In the case of equimolar counter diffusion $\dot{n}''_i = -\dot{n}''_j$, therefore there is no bulk flow term; alternatively, if "i" is diffusing through stagnant "j" $\dot{n}''_j = 0$.

In low pressure binary gas mixtures for a given gas pair D_{ij} is inversely proportional to pressure, increases with increasing temperature and is almost independent of composition. Diffusivities of many gas pairs have been experimentally measured at room temperature, whilst some of the more common systems have been measured at higher temperatures. However, it is frequently necessary to estimate D_{ij} values by using various theoretical equations. For the most accurate results the Chapman-Enskog[62] formula should be used. This equation, developed from the kinetic theory of gases, is capable of predicting D_{ij} values to within an accuracy of better than 10%. The equation is shown below:

$$D_{ij} = \frac{0.001858T^{3/2}[(M_i+M_j)/M_i.M_j]^{\frac{1}{2}}}{P.\sigma_{ij}^2 \cdot \Omega_D} \quad \ldots\ldots\ldots\ldots (3)$$

D_{ij} = diffusivity - cm^2/sec

T = temperature - ^oK

M_i = molecular weight of "i"

M_j = molecular weight of "j"

Ω_D = Collision integral (dimensionless function of temperature and intermolecular potential field for one molecule of "i" and one of "j")

σ_{ij} = "collision diameter" ("i"-"j") - Å

P = pressure - atmospheres

The Lennard-Jones empirical potential energy function is normally used to calculate Ω_D and σ_{ij}. The characteristic collision diameters (Lennard-Jones) of many molecules are known and can be used in the approximation $\sigma_{ij} = \frac{1}{2}(\sigma_i + \sigma_j)$. When they are not known the following empirical relationships may be used:

$$\sigma = 1.166V_{b,liq}^{1/3} \quad \text{or} \quad \sigma = 1.222V_{m,sol}^{1/3} \quad \ldots\ldots\ldots (4)$$

$V_{b,liq}$ = molar volume of liquid at boiling point (1 atmos)

$V_{m,sol}$ = molar volume of solid at melting point (1 atmos)

The dimensionless parameter Ω_D can be obtained from tables[62,117,121] in which it is listed against kT/e_{ij} (k = Boltzmann's constant, T = temp^oK and e_{ij} = maximum energy of attraction between molecule "i" and molecule "j"). Values of e are known for many molecules, for dissimilar molecules the approximation $e_{ij} = \sqrt{e_i.e_j}$ is used. When e is not known it is calculated from one of the following empirical relationships:

$$e/k = 1.15T_b \quad \text{or} \quad e/k = 1.92T_m \quad \ldots\ldots\ldots\ldots (5)$$

T_m = melting point ^oK

T_b = boiling point ^oK (both at 1 atmos)

8B3b Diffusion in multicomponent systems:- A rigorous mathematical description of ordinary diffusion in multicomponent systems is very complex. The exact Stefan-Maxwell equations, as rearranged by Curtiss

and Hirschfelder, are[62,121]:

$$\frac{dc_i}{dx} = \sum_{j=1}^{n} \frac{1}{D_{ij}} (N_i \cdot \dot{n}''_j - N_j \cdot \dot{n}''_i) \quad \ldots\ldots\ldots\ldots\ldots\ldots (1)$$

Similarly for all other species (these equations apply for an n component ideal gas mixture).

With diffusion calculations applied to multi-component systems it is often convenient to define an equation (with respect to fixed axes) that is analogous to the binary diffusion equation (equation 2 in section 8B3a).

$$\dot{n}''_i = N_i \sum_{j=1}^{n} \dot{n}''_j - D_{im} \cdot \frac{dc_i}{dx} \quad \ldots\ldots\ldots\ldots\ldots\ldots (2)$$

D_{im} = effective "binary" diffusivity of species "i" in mixture m

Combining equations (1) and (2) the effective diffusivity of species "i" in mixture "m" becomes

$$D_{im} = \frac{\dot{n}''_i - N_i \sum_{j=1}^{n} \dot{n}''_j}{\sum_{j=1}^{n} (1/D_{ij})(N_j \cdot \dot{n}''_i - N_i \cdot \dot{n}''_j)} \quad \ldots\ldots\ldots\ldots (3)$$

It can be seen from equation (3) that except when all the D_{ij} are equal, D_{im} is dependent upon composition (and therefore upon position). Two simple solutions for this equation are a) when gases 2,3, 4, ...n are present at very low concentrations in gas 1, equation (3) can be approximated to $D_{im} = D_{i1}$, and b) when gases 2,3,4,....n are stationary (no flux)

$$D_{1m} = \frac{1 - N_1}{\sum_{j=2}^{n} \frac{N_j}{D_{ij}}} \quad \ldots\ldots\ldots\ldots\ldots\ldots\ldots\ldots (4)$$

This equation, together with its application to mass transfer, has been examined in some detail by Wilke[122].

8B3c Diffusion in Cl_2-O_2-N_2-$ZnCl_2$-$CdCl_2$ mixtures:- The complex nature of diffusion in multicomponent gases makes it almost immpossible to obtain exact solutions for concentration gradients and mass fluxes even when only one species is diffusing. During the CdO/ZnO chlorination experiments four species (O_2, Cl_2 $ZnCl_2$ and $CdCl_2$) were simultaneously diffusing through stagnant nitrogen. Since the D_{ij} values of the 10 gas-pair combinations in the reactor gas mixtures are not equal it became apparent that some approximations

would be necessary. The first stage in evaluating a suitable approximation was to calculate the binary diffusivities of the 10 component gas-pairs by using the Chapman-Enskog equation. For Cl_2, O_2 and N_2 the Lennard-Jones parameters, and e/k, have been experimentally determined; in the case of $CdCl_2$ and $ZnCl_2$ it is necessary to estimate them. For these two metal chlorides using various data sources[40, 123, 124] the following molar volume values were arrived at:

$ZnCl_2$ - molar volume of liquid at boiling point = 60.6 cc
- molar volume of solid at melting point = 51.7 cc

$CdCl_2$ - molar volume of liquid at boiling point = 59.8 cc
- molar volume of solid at melting point = 47.1 cc

Using these data in the empirical equations given in section 8B3a, collision diameter parameters were calculated for $CdCl_2$ and $ZnCl_2$ (each being based upon the mean of two values). Mean e/k parameters for the two gaseous metal chlorides were also estimated by using the empirical equations given in section 8B3a (the melting point and boiling point data were taken from reference 3). Using the Lennard-Jones function tables given by Bird Stewart and Lightfoot[62] the following binary diffusivities for 1 atmosphere total pressure, were calculated.

D_{ij} \ Temperature °C	750	800	850	950
$D_{CdCl_2/ZnCl_2}$	0.21	0.23	0.25	0.30
D_{CdCl_2/O_2}	0.75	0.81	0.88	1.03
D_{CdCl_2/N_2}	0.76	0.83	0.90	1.04
D_{CdCl_2/Cl_2}	0.37	0.41	0.44	0.52
D_{ZnCl_2/O_2}	0.78	0.84	0.92	1.06
D_{ZnCl_2/N_2}	0.79	0.86	0.93	1.08
D_{ZnCl_2/Cl_2}	0.41	0.44	0.48	0.57
D_{O_2/N_2}	1.67	1.81	1.95	2.24
D_{O_2/Cl_2}	0.90	0.98	1.06	1.24
D_{N_2/Cl_2}	1.08	1.18	1.27	1.47

TABLE 8B: CALCULATED BINARY DIFFUSIVITIES - cm^2/sec

The chlorinating gas mixtures used for the CdO/ZnO non-equilibrium experiments contained about 4.4% Cl_2 (in N_2). It therefore appeared reasonable to use the approximation $D_{i/m} = D_{i/N_2}$. However, to check upon the possible error in this assumption, equation (4) - section 8B3b was used to calculate $D_{i/m}$ values for diffusion of a single species through Cl_2-O_2-N_2-$ZnCl_2$-$CdCl_2$ mixtures. A mixture of 7% Cl_2 in nitrogen (at 800°C - 1 atmos P.) was chosen for this calculation; reaction of chlorine was assumed to produce $CdCl_2$ and $ZnCl_2$ in the ratio of 9 to 1. The following results summarise the calculations (D_{ij} values were taken from table 8B; units of cm^2/sec).

a) At the start of chlorination - gas composition 93% N_2, 7% Cl_2 - $D_{Cl_2/m}$ (= D_{Cl_2/N_2}) = 1.18

b) Four sevenths of chlorine reacted - gas composition 2.94% Cl_2, 3.53% $CdCl_2$, 0.39% $ZnCl_2$, 1.96% O_2 and 91.2% N_2 - $D_{Cl_2/m}$ = 1.09, $D_{CdCl_2/m}$ = 0.79 $D_{ZnCl_2/m}$ = 0.76 and $D_{O_2/m}$ = 1.68

c) All chlorine reacted - gas composition 6.08% $CdCl_2$, 0.68% $ZnCl_2$, 3.38% O_2 and 89.9% N_2 - $D_{CdCl_2/m}$ = 0.81, $D_{ZnCl_2/m}$ = 0.73 and $D_{O_2/m}$ = 1.67

Comparison of the 800°C - D_{i/N_2} values in table 8B with the $D_{i/m}$ values above shows that when only one species is diffusing $D_{i/m} = D_{i/N_2}$ is a reasonable approximation. Since the chlorinating gas mixtures used with the CdO/ZnO experiments only contained about 4.4% chlorine it is felt that this approximation would still be justified for simultaneous diffusion of 4 minor components. According to Bird et al[62] and Satterfield[117] this approximation gives good results when calculating mass transfer rates but less accurate predictions of concentration gradients.

8B4 Boundary layer mass transfer coefficients in packed beds

Many dimensionless correlations which describe mass transfer in packed beds are available in the literature. Unfortunately, these correlations are somewhat inaccurate at low Reynolds numbers; this is because most studies have been made at high Reynolds numbers and are then extrapolated. For a single isolated sphere the Ranz-Marshall[125] correlation

$$Sh = 2.0 + 0.6(Re)^{\frac{1}{2}}(Sc)^{1/3} \quad \ldots\ldots\ldots\ldots\ldots\ldots\ldots (1)$$

appears to be most frequently used*. A comprehensive review paper by Rowe and Claxton[61] gives the correlation

$$Sh = A + B(Sc)^{1/3}(Re)^{n} \quad \ldots\ldots\ldots\ldots\ldots\ldots\ldots\ldots\ldots\ldots (2)$$

$$A = 2/(1-(1-\varepsilon)^{1/3})$$

$$B = 2/3\varepsilon$$

ε = bed voidage

$$(2 - 3n)/(3n - 1) = 4.65\ Re^{-0.28}$$

for mass transfer in a packed bed of spheres. Hougen et al[126] give, in terms of the well known Chitton-Colburn j_m factor for mass transfer in packed beds, the correlation

$$j_m = 0.57(Re)^{-0.41} \text{ for } Re > 50 \quad \ldots\ldots\ldots\ldots\ldots\ldots\ldots (3)$$

$$j_m = 0.84(Re)^{-0.51} \text{ for } Re < 50 \quad \ldots\ldots\ldots\ldots\ldots\ldots\ldots (4)$$

where $j_m = \dfrac{Sh}{Re(Sc)^{1/3}}$

Although the Ranz-Marshall correlation is not strictly applicable to a packed bed it is worth comparing the mass transfer coefficients that are predicted by the three different correlations. For the purpose of this calculation the same gas composition as used in example (b) section 8B3c has been chosen (namely when 4/7 of the chlorine had reacted to form $CdCl_2$ and $ZnCl_2$ in the ratio of 9 to 1). The imaginary experimental conditions that have been chosen are as follows: a) chlorinating gas = 7% Cl_2 in N_2, b) total gas flow rate = 1300 mls_{NTP}/min, c) bed void fraction = 0.41, d) temperature = 800°C, e) reactor diameter = 2.8 cms, f) pellet diameter = 0.62 cms, and g) total pressure = 1 atmosphere. The mass transfer coefficients given in the table below have been calculated using D_{im} values. The highest mass transfer coefficients are predicted by Rowe and Claxton, however, if this calculation is examined it is found that in each case the factor "A" (see equation (2)) accounts for over 75% of the value of K_c. No constant is present in the Hougen et al correlation, consequently their predicted packed bed mass transfer coefficients are lower than those predicted for a single pellet by Ranz and Marshall. Whilst briefly discussing the question of packed bed mass transfer coefficients two general points can be made:

---

* Sh = Sherwood number = $\dfrac{K_c^i \cdot d_p}{D_{im}}$

Sc = Schmidt number = $\dfrac{\mu_m}{\rho_m \cdot D_{im}}$

Re = Reynolds number = $\dfrac{\rho_m \cdot U_o \cdot d_p}{\mu_m}$

Correlation \ Mass transfer coefficient cms/sec	$K_c^{Cl_2}$	$K_c^{O_2}$	$K_c^{CdCl_2}$	$K_c^{ZnCl_2}$
Ranz-Marshall[125] single pellet	6.6	9.5	5.0	5.0
Rowe and Claxton[61] packed bed	27	40	20	19
Hougen et al[126] packed bed	4.1	5.5	3.3	3.3

Gas composition 2.94% Cl_2, 1.96% O_2, 3.53% $CdCl_2$ 0.39% $ZnCl_2$ and 91.2% N_2. Diffusivities $D_{Cl_2/m}$ = 1.09, $D_{O_2/m}$ = 1.68, $D_{CdCl_2/m}$ = 0.79 and $D_{ZnCl_2/m}$ = 0.76 - cm^2/sec

Re = 8.5, Pellet diameter = 6.2 mm

TABLE 8C: ESTIMATED MASS TRANSFER COEFFICIENTS AT 800°C - cm/sec

a) During the CdO/ZnO non-equilibrium experiments pellet Reynolds numbers (based upon the superficial gas velocity) were low, typically being (depending mainly upon the size of the pellet) between about 2 and 9.

b) Schmidt numbers* for gases vary little, usually being in the range 0.6-1.5. When using mass transfer correlations for the gas phase the factor $(Sc)^{1/3}$ is therefore approximately equal to 1.

The packed bed mass transfer coefficients given in table 8C are insufficiently reliable to be directly applied in the ZnO/CdO - chlorination model. However, the values did act as a very useful guide in choosing a range of coefficients to use when testing the model.

* Schmidt numbers were calculated for table 8C by using the Chapman-Enskog viscosity equation in conjunction with a formula for the viscosity of a multicomponent gas developed by Wilke (see appendix N).

8B5 Diffusion in porous solids

The three main types of gaseous diffusion that can occur in porous solids* are surface diffusion[127], ordinary molecular diffusion and Knudsen flow[117,118,127]. Surface diffusion becomes important only when surface areas are very large (1000 m^2/gm) and there is significant adsorbtion of gaseous species; this phenomenon therefore need not be considered in the present study. Ordinary molecular diffusion in porous solids obeys the normal laws of diffusion as described in section 8B3. However, the structure of a porous solid modifies diffusion coefficients for three obvious reasons: a) if the pores are randomly dispersed, the mean free cross section available for diffusion is equal to the void fraction of the porous solid, b) if pores are randomly orientated then the distance over which diffusion must take place is greater than the linear distance in the direction of diffusion, and c) pores through which diffusion takes place are rarely uniform in cross section, these shape irregularities lead to reduced diffusion rates. Therefore, to obtain an effective ordinary molecular binary diffusion coefficient in a porous solid the ordinary molecular binary diffusion coefficient (D_{ij}) is modified by three terms

$$D_{ij}^{eff} = D_{ij} \cdot \frac{\epsilon}{L.S} \quad \ldots\ldots\ldots\ldots\ldots\ldots\ldots\ldots\ldots (1)$$

ϵ = void fraction

L = length factor

S = shape factor

With most real porous solids it is impossible to measure separately, or even estimate, S and L; they are thus combined into one term "τ" known as the tortuosity factor. Various theoretical models[117] have been developed for predicting tortuosity factors, however, due to the complex structures encountered in real porous solids none of these models are suitable for general application. Typical tortuosities mainly range between about 2 and 10; in the absence of reliable data the approximation $\tau = 1/\epsilon$ would appear to be a reasonable method of making a rough estimate.

The description given above refers to conditions under which molecule-molecule collisions are very much greater in frequency than are molecule-pore wall collisions; this is known as the molecular diffusion regime.

---

* There are other types of diffusion - forced, thermal, and pressure, however, they are of no significance in the present context.

When molecule-wall collisions predominate, diffusion* enters the Knudsen controlled regime. With porous solids this occurs if the gas density is low (the mean free path therefore being high) or if the pores are small (or if both are true). In the Knudsen regime molecules colliding with the pore walls are momentarily adsorbed and then diffusively reflected (random direction), this phenomenon causes a resistance to flow. In 1909 M. Knudsen, using the kinetic theory of gases, developed equations to describe this type of flow in narrow capillaries; these are:

$$\dot{n}_i'' = D_{k,i} \cdot \frac{dc_i}{dx} \quad \ldots\ldots\ldots\ldots\ldots\ldots\ldots\ldots\ldots\ldots (1)$$

where

$$D_{k,i} = \frac{4r}{3} \cdot \left(\frac{2RT}{\pi M_i}\right)^{\frac{1}{2}} \cdot (2-f)/f \quad \ldots\ldots\ldots\ldots\ldots\ldots\ldots (2)$$

$D_{k,i}$ = Knudsen diffusion coefficient for species "i"
M_i = molecular weight of "i"
r = capillary radius
f = proportion of molecules striking surface which are diffusively reflected (usually taken to be equal to 1)

From these equations it can be seen that Knudsen flow is governed by a Ficks law type flux equation, and that the Knudsen diffusion (flow) coefficient of a given species is independent of any other species that might be present and also independent of pressure (unlike molecular diffusion). With f=1 equation (2) reduces to

$$D_{k,i} = 9700.r.(T/M_i)^{\frac{1}{2}} \quad \ldots\ldots\ldots\ldots\ldots\ldots\ldots\ldots\ldots (3)$$

This equation applies for flow in a circular capillary, its application to porous media therefore necessitates some modifications. Using the same arguments as applied to molecular diffusion:

$$D_{k,i}^{eff} = D_{k,i} \cdot \frac{\varepsilon}{\tau} \quad \ldots\ldots\ldots\ldots\ldots\ldots\ldots\ldots\ldots (4)$$

To calculate a Knudsen flow coefficient for a porous solid a representative pore radius is required. For a round capillary the volume to surface area ratio is $\frac{1}{2}r$, by analogy the effective pore radius of a porous solid is $2\varepsilon/S_v$. A better method of determining pore radii is mercury porosimetry, however results from this technique can be difficult to utilise since a porous solid with a range of pore sizes will have a Knudsen flow coefficient that varies with position.

*Strictly speaking the word flow instead of diffusion should be used to describe transport in the Kundsen regime.

When molecule-molecule and molecule-wall collisions are of a comparable frequency, transport becomes controlled by both Knudsen flow and molecular diffusion; this is known as the transition region*. Expressions for mixed-control diffusion have been developed by Scott and Dullien[128] and Evans et al[130]. Their equation for transport of species "i" in a binary gas mixture (i-j) at constant total pressure is

$$\dot{n}_i'' = - \frac{\frac{dc_i}{dx}}{\frac{1 - (1 + \dot{n}_j''/\dot{n}_i'')N_i}{D_{ij}^{eff}} + \frac{1}{D_{k,i}^{eff}}} \quad \ldots\ldots\ldots (5)$$

If there is no bulk flow (namely, there is equimolar counter diffusion)

$$\dot{n}_i'' = - \frac{\frac{dc_i}{dx}}{1/D_{ij}^{eff} + 1/D_{k,i}^{eff}} \quad \ldots\ldots\ldots (6)$$

In this case the mixed-control effective diffusion coefficient is therefore related to the effective molecular diffusion coefficient and the effective Knudsen flow coefficient by the equation**

$$\frac{1}{D_{mixed,i}^{eff}} = \frac{1}{D_{ij}^{eff}} + \frac{1}{D_{k,i}^{eff}} \quad \ldots\ldots\ldots\ldots\ldots (7)$$

Transition region diffusion in three component gas mixtures has recieved attention from Cunningham and Geankoplis[129].

8B5a Diffusion in CdO/ZnO pellets:- An exact analysis of the processes of diffusion of $ZnCl_{2(g)}$ and $CdCl_{2(g)}$ in the porous CdO/ZnO pellets would be very difficult, it would also be somewhat inappropriate. However, by making reasonable approximations, estimates of effective diffusivities have been made for use in the mathematical model.

It is safe to assume that within the mixed oxide pellets thermodynamic equilibrium was achieved at the Zno-CdO/ZnO interfaces. Since the equilibrium ratio P_{CdCl_2}/P_{ZnCl_2} is comparatively large (over ZnO and CdO at comparable activities) the CdO reaction rate was reactant gas ($ZnCl_2$)

---

* A given system can be brought into the transition region by reducing the overall pressure

** This equation is analogous to the summing of series resistances.

transport controlled rather than product gas transport controlled (see section 8B6b). Thus, under these conditions it is most important to estimate the effective transport coefficients of the $ZnCl_{2(g)}$, those of the $CdCl_{2(g)}$ being very much less critical. For simplicity it has therefore been assumed that within the same pellet the $CdCl_{2(g)}$ and $ZnCl_{2(g)}$ effective transport coefficients were equal*. Presented in table 8D are estimated effective diffusion coefficients for $ZnCl_{2(g)}$ for the various different CdO/ZnO pellets at each reaction temperature. These estimates have been calculated in the following manner:

a) For molecular diffusion it has been assumed that $D_{ZnCl_2/m} = D_{ZnCl_2/N_2}$. The D_{ZnCl_2/N_2} values have been taken from table 8B.

b) $ZnCl_{2(g)}$ Knudsen flow coefficients have been claculated on the basis of the porosimetry results. The effective pore radius for the pellets from each chlorination experiment has been taken to be equal to the experimentally determined pore radius above which size 50% of the total pore volume was composed (these values have been taken from the reacted pellets porosimetry results given in table 8A).

c) In each case the tortuosity factor of the reacted pellets has been taken to be equal to the reciprocal of their void fraction (as given in table 8A).

d) Since $ZnCl_{2(g)}$ and $CdCl_{2(g)}$ were counter-diffusing through a stagnant gas mixture (predominantly N_2) transition region diffusion coefficients have been calculated by using equation (7), section 8B5.

---

* This would be a reasonable approximation even if $CdCl_{2(g)}$ transport had been the rate controlling step since, $ZnCl_{2(g)}$ and $CdCl_{2(g)}$ behave in a similar manner to each other under both molecular and Knudsen regimes.

Chorination experiment $T^{o}C$ - mole % CdO	Molecular diffusion coeff. D_{ZnCl_2/N_2} - cm^2/sec	Knudsen flow coeff. $D_{k_2ZnCl_2}$ - cm^2/sec	Transition region $ZnCl_2$ diffusion coeff - cm^2/sec	Effective diffusion coeff. - cm^2/sec
750-50.0	0.79	1.33	0.50	0.032
750-26.6	0.79	1.01	0.44	0.034
750-10.8	0.79	1.06	0.45	0.046
850-50.0	0.93	1.81	0.61	0.034
850-26.6	0.93	0.92	0.46	0.012
850-10.8	0.93	1.03	0.49	0.029
950-50.0	1.08	1.74	0.67	0.018
950-26.6	1.08	0.81	0.63	0.010
950-10.8	1.08	1.19	0.57	0.0079

TABLE 8D ESTIMATED $ZnCl_{2(g)}$ EFFECTIVE DIFFUSION COEFFICIENTS

The values of the calculated molecular diffusion coefficients given in table 8D show that under all experimental conditions diffusion was within the Knudsen-molecular transition region. It can also be seen from the results in this table that the effective diffusion coefficients underwent significant decreases as the reaction temperature increased. However, it must be emphasised that these estimated effective diffusion coefficients are possibly in error by a sizeable amount, due to the numerous approximations made during their evaluation.

8B6 Mathematical model

8B6a General description of the packed bed:- During the CdO/ZnO non-equilibrium experiments, the various rate processes taking place in the reactor were unsteady with respect to both time and position. To analyse the reactor performance it was therefore necessary to set up partial differential conservation equations describing the time and position dependences of the concentrations of the different reactant and product species. At a given instant of time the conservation equation for a gaseous species "i" over a differential bed element dx is:

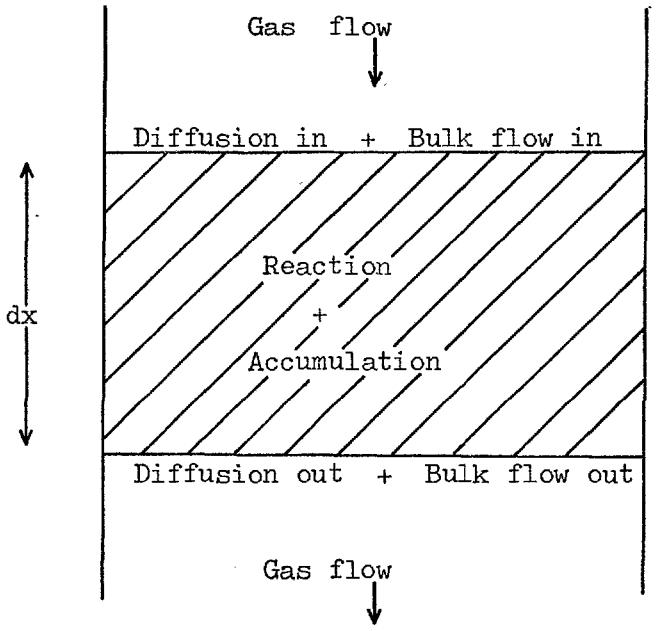

Conservation of species "i" over a differential control volume

$$ {}_f\dot{n}_i - \bar{A} \cdot D_{im} \cdot \left(\frac{dc_i}{dx}\right) + R\dot{n}_i'' \cdot dx \cdot Sx = $$

(bulk flow in) + (diffusion in) + (reaction) =

$$ {}_f\dot{n}_i + \left(\frac{d\,{}_f\dot{n}_i}{dx} \cdot dx\right) - \bar{A} \cdot D_{im} \cdot \left(\frac{dc_i}{dx} + \frac{d^2c_i}{dx^2} \cdot dx\right) + \bar{A}\,\frac{dc_i}{dt} \cdot dx \quad \ldots (1) $$

(bulk flow out) + (diffusion out) + (accumulation)

where

${}_f\dot{n}_i$ = total bulk flow of species "i" into differential element

$R\dot{n}_i''$ = rate of reaction (or production) of species "i" per unit of solid surface area (reaction of reactant -ve, production of product +ve)

$\bar{A}$ = solid-free bed cross sectional area

Sx = surface area of pellets/unit bed length

This equation assumes that there is no back mixing of gas in the reactor. Under the conditions of the non-equilibrium experiments, in comparison with the bulk flow and reaction terms the diffusion and accumulation terms were very small and could therefore be neglected. Thus equation (1) reduces to:

$$ \left(\frac{d\,{}_f\dot{n}_i}{dx}\right)_t - (R\dot{n}_i'' \cdot Sx)_{x,t} = 0 \quad \ldots (2) $$

Equation (2) can be used to describe the time and position dependences of the concentrations of the Cl_2, O_2, $ZnCl_2$ and $CdCl_2$ in the packed bed

reactor. Since an analytical solution for this set of equations is not possible they have been solved by a numerical method. The model used for the reaction terms $(_R\dot{n}''_i)_{x,t}$ assumes that all the reaction processes were mass transport controlled.

8B6b Reaction of single pellet:- The various stoichiometry, equilibrium and rate equations will now be derived by considering a reacting single pellet containing a ZnO-CdO/ZnO interface. The subscripts "i", "s" and "b" (in most cases prefixed) denote ZnO-CdO/ZnO interface, pellet surface and bulk gas phase values repectively. A shematic diagram of a partially reacted pellet on which the gas partial pressures and transport coefficients are marked is shown on figure 8A. The rate equations are derived for the pseudo-steady-state condition.

a) Transport of chlorine from pellet surface to bulk gas:- using equation (2) - section 8B3b the $Cl_{2(g)}$ flux from the pellet surface to the bulk gas is (per unit of pellet surface area)

$$\dot{n}''_{Cl_2} = N_{Cl_2}(\dot{n}''_{ZnCl_2} + \dot{n}''_{CdCl_2} + \dot{n}''_{Cl_2} + \dot{n}''_{O_2}) - D_{Cl_2/m} \cdot \frac{dc_{Cl_2}}{dx} \quad \ldots(a)$$

rearranging the bulk flow term and substituting $c_{Cl_2} = N_{Cl_2} \cdot \frac{P}{RT}$ gives:

$$\dot{n}''_{Cl_2} = - \frac{D_{Cl_2/m} \cdot P}{RT(1+\frac{1}{2}N_{Cl_2})} \cdot \frac{dN_{Cl_2}}{dx} \quad \ldots\ldots\ldots\ldots(b)$$

Integrating this equation over the boundary layer where at $x = 0$, $N_{Cl_2} = {}_sN_{Cl_2}$ and $x = L$, $N_{Cl_2} = {}_bN_{Cl_2}$ gives:

$$\dot{n}''_{Cl_2} \cdot \Big[x \Big]_0^L = - \frac{2P.D_{Cl_2/m}}{RT} \Big[\log_e(1+\tfrac{1}{2}N_{Cl_2}) \Big]_{{}_sN_{Cl_2}}^{{}_bN_{Cl_2}} \quad \ldots(c)$$

Defining the boundary layer mass transfer coefficient as

$$K_c^{Cl_2} = \frac{D_{Cl_2/m}}{L}$$ equation (c) reduces to:

$$\dot{n}''_{Cl_2} = - 2K_c^{Cl_2} \frac{P}{RT} \cdot \log_e \left(\frac{1 + \frac{1}{2} \cdot \frac{{}_bP_{Cl_2}}{P}}{1 + \frac{1}{2} \cdot \frac{{}_sP_{Cl_2}}{P}} \right) \quad \ldots\ldots\ldots\ldots (M1)$$

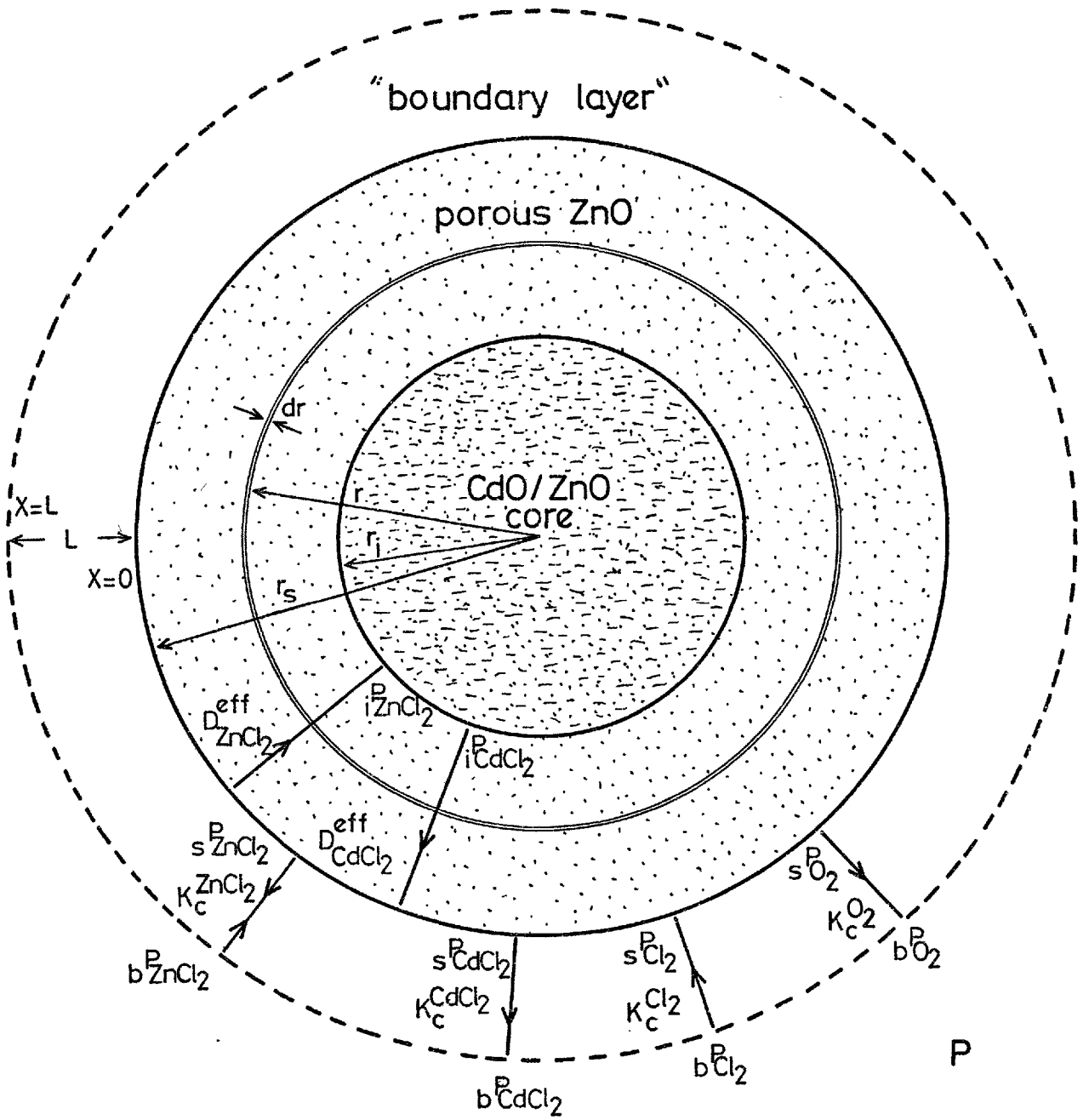

surface equilibrium $\dfrac{s^P_{ZnCl_2} \cdot s^P_{O_2}{}^{0.5}}{s^P_{Cl_2}} = s^K$

interface equilibrium $\dfrac{i^P_{CdCl_2}}{i^P_{ZnCl_2}} = i^K$

$PV = nRT$

K_c = boundary layer mass transfer coefficient.

D^{eff} = effective diffusivity.

subscripts: b=bulk, s=surface, i=interface.

P = total pressure. P = partial pressure.

+ve fluxes outwards, -ve fluxes inwards.

the "boundary layer" may not be of equal "thickness" for the different species

FIGURE 8A: SYMBOLS FOR REACTION MODEL.

Since ${}_bP_{Cl_2}$ is never less than ${}_sP_{Cl_2}$ the negative sign signifies that chlorine is always transported down to the pellet surface.

b) Transport of oxygen from pellet surface to bulk gas:- using equation (2) - section 8B3b the $O_{2(g)}$ flux from the pellet surface to the bulk gas is (per unit of pellet surface area)

$$\dot{n}''_{O_2} = N_{O_2}(\dot{n}''_{ZnCl_2} + \dot{n}''_{CdCl_2} + \dot{n}''_{Cl_2} + \dot{n}''_{O_2}) - D_{O_2/m} \cdot \frac{dc_{O_2}}{dx} \quad \ldots\ldots (d)$$

rearranging the bulk flow term and substituting $c_{O_2} = N_{O_2} \cdot \frac{P}{RT}$ gives:

$$\dot{n}''_{O_2} = - \frac{D_{O_2/m} \cdot P}{RT(1-N_{O_2})} \cdot \frac{dN_{O_2}}{dx} \quad \ldots\ldots\ldots\ldots (e)$$

Integrating this equation over the boundary layer where at x=0, $N_{O_2} = {}_sN_{O_2}$ and x=L, $N_{O_2} = {}_bN_{O_2}$ gives:

$$\dot{n}''_{O_2} \cdot \Big[\, x \,\Big]_0^L = \frac{P \cdot D_{O_2/m}}{RT} \cdot \Big[\, \log_e(1-N_{O_2}) \,\Big]_{{}_sN_{O_2}}^{{}_bN_{O_2}} \quad \ldots (f)$$

Defining the boundary layer mass transfer coefficient as $K_c^{O_2} = \frac{D_{O_2/m}}{L}$

equation (f) reduces to:

$$\dot{n}''_{O_2} = K_c^{O_2} \cdot \frac{P}{RT} \cdot \log_e \left(\frac{1 - \frac{{}_bP_{O_2}}{P}}{1 - \frac{{}_sP_{O_2}}{P}} \right) \ldots\ldots\ldots\ldots\ldots (M2)$$

Since ${}_sP_{O_2}$ is never less than ${}_bP_{O_2}$ the logarithmic term is never negative therefore the oxygen is always transported from the pellet surface to the bulk gas.

c) Transport of zinc chloride from pellet surface to bulk gas:- using equation (2)-section 8B3b, the $ZnCl_{2(g)}$ flux from the pellet surface to the bulk gas is (per unit of pellet surface area):

$$\dot{n}''_{ZnCl_2} = N_{ZnCl_2}(\dot{n}''_{ZnCl_2} + \dot{n}''_{CdCl_2} + \dot{n}''_{Cl_2} + \dot{n}''_{O_2}) - D_{ZnCl_2/m} \frac{dc_{ZnCl_2}}{dx} \quad \ldots (g)$$

rearranging the bulk flow term and substituting $c_{ZnCl_2} = N_{ZnCl_2} \cdot \frac{P}{RT}$ gives:

$$\dot{n}''_{ZnCl_2} = - \frac{D_{ZnCl_2/m} \cdot P}{RT\left(1 - N_{ZnCl_2} \cdot \frac{\dot{n}''_{O_2}}{\dot{n}''_{ZnCl_2}}\right)} \cdot \frac{dN_{ZnCl_2}}{dx} \quad \ldots\ldots\ldots \text{(h)}$$

Integrating this equation over the boundary layer where at x=0, $N_{ZnCl_2} = {}^{s}N_{ZnCl_2}$ and x=L, $N_{ZnCl_2} = {}^{b}N_{ZnCl_2}$ gives:

$$\dot{n}''_{ZnCl_2} \cdot \left[x \right]_0^L = \frac{\dot{n}''_{ZnCl_2}}{\dot{n}''_{O_2}} \cdot \frac{P \cdot D_{ZnCl_2/m}}{RT} \cdot \left[\log_e\left(1 - N_{ZnCl_2} \cdot \frac{\dot{n}''_{O_2}}{\dot{n}''_{ZnCl_2}}\right) \right]_{{}^{s}N_{ZnCl_2}}^{{}^{b}N_{ZnCl_2}} \quad \ldots \text{(i)}$$

Defining the boundary layer mass transfer coefficient as $K_c^{ZnCl_2} = \frac{D_{ZnCl_2/m}}{L}$ equation (i) reduces to:

$$\dot{n}''_{O_2} = K_c^{ZnCl_2} \cdot \frac{P}{RT} \cdot \log_e \left(\frac{1 - \frac{{}^{b}P_{ZnCl_2}}{P} \cdot \frac{\dot{n}''_{O_2}}{\dot{n}''_{ZnCl_2}}}{1 - \frac{{}^{s}P_{ZnCl_2}}{P} \cdot \frac{\dot{n}''_{O_2}}{\dot{n}''_{ZnCl_2}}} \right) \quad \ldots \text{(j)}$$

Defining $H = e^{\left(\frac{\dot{n}''_{O_2} \cdot RT}{P \cdot K_c^{ZnCl_2}}\right)}$ equation (j) when rearranged gives:

$$\dot{n}''_{ZnCl_2} = \frac{\dot{n}''_{O_2}}{P(1-H)} \cdot ({}^{b}P_{ZnCl_2} - {}^{s}P_{ZnCl_2} \cdot H) \quad \ldots\ldots\ldots\ldots \text{(M3)}$$

Since H is never less than 1, when ${}^{b}P_{ZnCl_2}$ is greater than ${}^{s}P_{ZnCl_2}$ the zinc chloride flux is negative (namely $_2$ from the bulk gas to the pellet surface).

d) Transport of cadmium chloride from pellet surface to bulk gas:- Using equation (2)-section 8B3b the $CdCl_{2(g)}$ flux from the pellet surface to the bulk gas is (per unit of pellet surface area).

$$\dot{n}''_{CdCl_2} = N_{CdCl_2}(\dot{n}''_{ZnCl_2} + \dot{n}''_{CdCl_2} + \dot{n}''_{Cl_2} + \dot{n}''_{O_2}) - D_{CdCl_2/m} \cdot \frac{dc_{CdCl_2}}{dx} \quad \ldots(k)$$

rearranging the bulk flow term and substituting $c_{CdCl_2} = N_{CdCl_2} \cdot \frac{P}{RT}$ gives:

$$\dot{n}''_{CdCl_2} = \frac{-D_{CdCl_2/m} \cdot P}{RT\left(1 - N_{CdCl_2} \cdot \frac{\dot{n}''_{O_2}}{\dot{n}''_{CdCl_2}}\right)} \cdot \frac{dN_{CdCl_2}}{dx} \quad \ldots\ldots\ldots(l)$$

Integrating this equation over the boundary layer where at x=0, $N_{CdCl_2} = {}_sN_{CdCl_2}$ and x=L, $N_{CdCl_2} = {}_bN_{CdCl_2}$ gives:

$$\dot{n}''_{CdCl_2} \cdot \Big[\, x \,\Big]_0^L = \frac{\dot{n}''_{CdCl_2}}{\dot{n}''_{O_2}} \cdot \frac{P \cdot D_{CdCl_2/m}}{RT} \Big[\log_e\left(1 - N_{CdCl_2} \cdot \frac{\dot{n}''_{O_2}}{\dot{n}''_{ZnCl_2}}\right)\Big]_{{}_sN_{CdCl_2}}^{{}_bN_{CdCl_2}} \quad \ldots(m)$$

Defining the boundary layer mass transfer coefficient as $K_c^{CdCl_2} = \frac{D_{CdCl_2/m}}{L}$ equation (m) reduces to:

$$\dot{n}''_{O_2} = K_c^{CdCl_2} \cdot \frac{P}{RT} \cdot \log_e\left(\frac{1 - \frac{{}_bP_{CdCl_2}}{P} \cdot \frac{\dot{n}''_{O_2}}{\dot{n}''_{CdCl_2}}}{1 - \frac{{}_sP_{CdCl_2}}{P} \cdot \frac{\dot{n}''_{O_2}}{\dot{n}''_{CdCl_2}}}\right) \quad \ldots\ldots\ldots(n)$$

Defining $HA = e^{\left(\frac{\dot{n}''_{O_2} \cdot RT}{P \cdot K_c^{CdCl_2}}\right)}$ equation (n) when rearranged gives:

$$\dot{n}''_{CdCl_2} = \frac{\dot{n}''_{O_2}}{P(1 - HA)} \cdot ({}_bP_{CdCl_2} - {}_sP_{CdCl_2} \cdot HA) \quad \ldots\ldots\ldots(M4)$$

Since HA is never less than 1 and ${}_sP_{CdCl_2}$ is never less than ${}_bP_{CdCl_2}$ the cadmium chloride flux is always positive (namely from the pellet surface to the bulk gas).

e) Transport of zinc chloride from ZnO-CdO/ZnO interface to pellet surface:- the total flux of $ZnCl_{2(g)}$ passing between the pellet interface and surface is given by the equation*

$$\dot{n}_{ZnCl_2} = -4\pi r^2 \cdot D^{eff}_{ZnCl_2} \cdot \frac{dc_{ZnCl_2}}{dr} \quad \ldots\ldots\ldots\ldots\ldots\ldots (o)$$

rearranging this equation, substituting $c_{ZnCl_2} = N_{ZnCl_2} \cdot \frac{P}{RT}$

and integrating between the limits $r = r_i$, $N_{ZnCl_2} = {}_iN_{ZnCl_2}$ and $r = r_s$ $N_{ZnCl_2} = {}_sN_{ZnCl_2}$ gives:

$$\dot{n}_{ZnCl_2} \cdot \Big[-\frac{1}{r}\Big]_{r_i}^{r_s} = -4\pi \cdot D^{eff}_{ZnCl_2} \cdot \frac{P}{RT} \cdot \Big[N_{ZnCl_2}\Big]_{{}_iN_{ZnCl_2}}^{{}_sN_{ZnCl_2}} \quad \ldots (p)$$

By inserting the limits and dividing by the external surface area of the pellet the $ZnCl_{2(g)}$ flux per unit of pellet surface area becomes:

$$\dot{n}''_{ZnCl_2} = -\frac{r_i \cdot D^{eff}_{ZnCl_2}}{r_s(r_s - r_i)RT} \cdot ({}_sP_{ZnCl_2} - {}_iP_{ZnCl_2}) \quad \ldots\ldots\ldots (M5)$$

Since ${}_sP_{ZnCl_2}$ is never less than ${}_iP_{ZnCl_2}$ the negative sign signifies that zinc chloride is always transported from pellet surface to interface.

---

* Since $\dot{n}''_{ZnCl_2} = -\dot{n}''_{CdCl_2}$ there is no bulk flow term. The effective diffusivity accounts for Knudsen, molecular and structural effects. It is assumed that there is no variation in total pressure through the pellet.

f) Transport of cadmium chloride from ZnO-CdO/ZnO interface to pellet surface:- by using an exactly analogous treatment as above the $CdCl_{2(g)}$ flux per unit of pellet surface area becomes:

$$\dot{n}''_{CdCl_2} = \frac{r_i \cdot D^{eff}_{CdCl_2}}{r_s(r_s - r_i)RT} \cdot ({}_iP_{CdCl_2} - {}_sP_{CdCl_2}) \quad \ldots\ldots\ldots \text{(M6)}$$

since ${}_iP_{CdCl_2}$ is never less than ${}_sP_{CdCl_2}$ the positive sign signifies that the cadmium chloride is always transported from pellet interface to surface.

g) Reaction stoichiometry:- the following relationships between the fluxes of the various components (expressed as fluxes per unit of pellet surface area) are dictated by reaction stoichiometry.

Transport through the boundary layer (s→b)

$$\dot{n}''_{CdCl_2} + \dot{n}''_{ZnCl_2} + \dot{n}''_{Cl_2} = 0 \quad \ldots\ldots\ldots\ldots\ldots\ldots \text{(M7)}$$

$$\dot{n}''_{O_2} = -\tfrac{1}{2}\dot{n}''_{Cl_2} \quad \ldots\ldots\ldots\ldots\ldots\ldots\ldots\ldots\ldots \text{(M8)}$$

Transport through the ZnO (i → s)

$$-\dot{n}''_{ZnCl_2} = \dot{n}''_{CdCl_2} \quad \ldots\ldots\ldots\ldots\ldots\ldots\ldots\ldots\ldots \text{(M9)}$$

Transport through the ZnO (i → s) and transport through the boundary layer (s → b)

$$\dot{n}''_{CdCl_2}\ (i \rightarrow s) = \dot{n}''_{CdCl_2}\ (s \rightarrow b) \quad \ldots\ldots\ldots\ldots\ldots \text{(M10)}$$

h) Equilibrium relationships:- since the mathematical model assumes that the reaction processes are mass transport controlled, thermodynamic equilibrium is achieved at the pellet surface and interface. Therefore, with the ZnO and CdO both present at unit activity, the following two relationships are obeyed:

Pellet surface:-
$$\frac{{}_sP_{ZnCl_2} \cdot {}_sP_{O_2}^{\frac{1}{2}}}{{}_sP_{Cl_2}} = {}_sK \quad \ldots\ldots\ldots\ldots \text{(M11)}$$

ZnO-CdO/ZnO interface:-
$$\frac{{}_iP_{CdCl_2}}{{}_iP_{ZnCl_2}} = {}_iK \quad \ldots\ldots\ldots\ldots \text{(M12)}$$

Using equations (M5),(M6),(M9) and (M12) the following expression is obtained for the cadmium oxide reaction rate in terms of the rate of transport of $ZnCl_{2(g)}$ through unit area of pellet surface:

$$\dot{n}''_{ZnCl_2} = -\left(\frac{D^{eff}_{ZnCl_2}}{{}_iK + \frac{D^{eff}_{ZnCl_2}}{D^{eff}_{CdCl_2}}}\right) \cdot \left(\frac{r_i}{r_s(r_s-r_i)}\right) \cdot \left(\frac{1}{RT}\right) \cdot \left({}_iK_s P_{ZnCl_2} - {}_sP_{CdCl_2}\right)$$

Since ${}_iK$ is large whilst $D^{eff}_{ZnCl_2}$ and $D^{eff}_{CdCl_2}$ are almost equal, the CdO reaction rate is reactant-gas ($ZnCl_2$)-transport-controlled (conversely, if ${}_iK$ were very small, the CdO reaction rate would be product-gas ($CdCl_2$)-transport-controlled).

8B6c Application of the single pellet model to a packed bed:- Under given reaction conditions the bulk gas composition, the various transport coefficients and the equilibrium constants are 'known' variables. The twelve simultaneous equations (M1)-(M12) therefore contain the following twelve unknowns: a) surface partial pressures ${}_sP_{ZnCl_2}$, ${}_sP_{CdCl_2}$, ${}_sP_{Cl_2}$ and ${}_sP_{O_2}$ b) interface partial pressures ${}_iP_{ZnCl_2}$ and ${}_iP_{CdCl_2}$ c) boundary layer fluxes $\dot{n}''_{ZnCl_2}$, $\dot{n}''_{CdCl_2}$, $\dot{n}''_{Cl_2}$ and $\dot{n}''_{O_2}$ and d) surface-interface fluxes $\dot{n}''_{CdCl_2}$ and $\dot{n}''_{ZnCl_2}$. Equations (M1),(M2),(M3),(M4) and (M11) are non linear, the remainder are linear. An analytical solution of these simultaneous equations, if possible, would be very complex; it has thus been necessary to solve them by an iterative method (for details of this method of numerical solution see appendix O). From the solution of these pseudo-steady-state equations the four ${}_R\dot{n}''_i$ reaction* rate terms (in differential equation (2)-section 8B6a) are obtained for a given differential element of the bed at a given moment of time. To determine the performance of the reactor at any given instant of time, equations (M1)-(M12) have to be simultaneously employed at numerous positions throughout the bed, so as to obtain an approximate continuous** reactor-

---

* Here the subscript "i" refers to species "i"

** The word continuous refers to the analytical solution of the reactor, since with this solution (possibly imaginary) a continuum of values could in theory be calculated.

solution. Furthermore, to determine the reactor performance over the period of a chlorination experiment new solutions at each of the numerous bed positions have to be determined after frequent short periods of reaction, so as to obtain an approximately continuous reactor-time-solution. For these computations the packed bed was initially divided into 50 equal sized sections (that is, containing an equal number of pellets); later it was divided into sections of three different sizes, 100 sections in total. By computing the same 'chlorination experiment' using different short reaction periods (15 seconds - 2 minutes) it was established that 30 seconds was a suitable time interval with which to obtain approximately continuous reactor-time solutions.

There are many finite-difference approximations for solution of partial differential equations. Application of one of these techniques in the present context would require simultaneous solution of 50 (or 100) sets of equilibrium and rate equations [(M1)-(M12)]. Since some of these equations are non linear the computer time required to perform this kind of solution would have been extremely large; especially since great difficulty was encountered in obtaining convergence for a single solution. Therefore, a slightly more approximate but equally satisfactory method was employed to calculate the reactor performance at given instances in time. As described above the bed was divided into a large number of sections each of which contained a given fraction of the total number of pellets making up the CdO/ZnO charge, one of these sections is represented below.

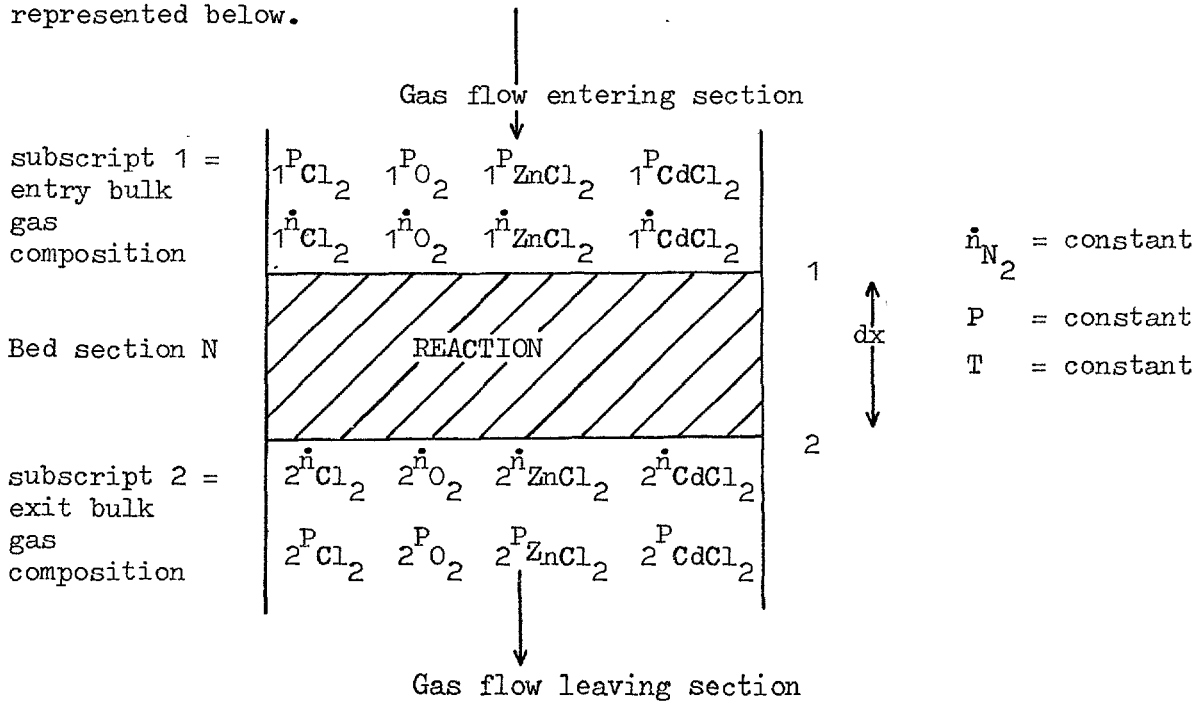

The reaction rate in a given section was calculated by solving equations (M1)-(M12) for the bulk gas composition that entered the section (namely using bulk gas partial pressures $_1P_{Cl_2}$, $_1P_{O_2}$, $_1P_{ZnCl_2}$ and $_1P_{CdCl_2}$ together with the relevant r_i and r_s values; the transport coefficients and equilibrium constants being constant throughout the whole of a given bed). Applying these computed reaction/production rates to the total pellet surface area contained in the section, the section exit bulk gas composition and flow ($_2P_{Cl_2}$, $_2\dot{n}_{Cl_2}$ .... etc.) was then calculated, this being the bulk gas composition entering the next section. The main assumption contained in this method of determining the reactor performance is that each section behaves as a "well stirred tank" containing gas at the inlet composition. When the size of each section tends towards the limit dx = 0 (namely the number of sections tends towards infinity) this assumption is perfectly correct*. Even when only a relatively small number of sections (50 or 100) are used the assumption is very satisfactory since divergences from the analytical (imaginary) bed-solution are self correcting. (before this point is explained a simple description of the calculation routine will be given).

Before the calculations could be started the 'experimental conditions' were read into the computer storage. These were the bed entry gas flow rate, and composition, the equilibrium constants, the transport coefficients, the mean pellet diameter, the pellet composition, the total number of pellets in the bed and the steady-state-reaction time interval. All reactor-solution calculations started at the bed entry, the gas in the first section therefore always consisted of nitrogen and chlorine. With the bed in an unreacted state (time = 0) the pseudo-steady-state reaction rate equations were solved for the first section so as to give the gas flow rate and composition entering the second section, which in turn was solved to give the gas flow rate and composition entering the third section and so forth down the bed until the last section. In a similar manner to the sectioning of the bed, the total reaction time was divided into short steady state time intervals. By using the computed reaction rates together with this predetermined time interval the pellet(s) contained in each section were then 'reacted' by the required amount, after which the new r_i and r_s values were stored in place of the previous values. Before

* Within the approximation that back mixing, diffusion and accumulation can be neglected.

recommencing the calculation on the reacted bed, various values were written out from storage. Frequent repetition (150 to 200x) of this procedure thus gave a good step-wise approximation to the analytical* solution of the 'chlorination experiment'. The self correcting behaviour that occurs from section to section and from time interval to time interval is simply explained. In comparison to the analytical (imaginary) reactor-solution the section by section solution will show small disagreement. In the first section the computed chlorine reaction rate is higher than would be predicted by the analytical solution; this is because the effective chlorine partial pressure** in the section is clearly less than the inlet partial pressure. The computed chlorine partial pressure entering the second section is therefore <u>less</u> than the analytical solution value (the oxygen, zinc chloride and cadmium chloride partial pressures are greater). This computed chlorine partial pressure will quite possibly+ be <u>less</u> than the second section effective chlorine partial pressure**. If this is so it will cause the computed chlorine reaction rate to be <u>less</u> than would be predicted by the analytical solution, thereby causing the computed chlorine partial pressure entering the third section to be <u>greater</u> than the analytical solution value. The computed values of the chlorine partial pressure (and the $ZnCl_2$, $CdCl_2$ and O_2 partial pressures) entering the different sections down the bed therefore oscillate about the analytical solution values. This self correcting effect is illustrated in the diagram below.

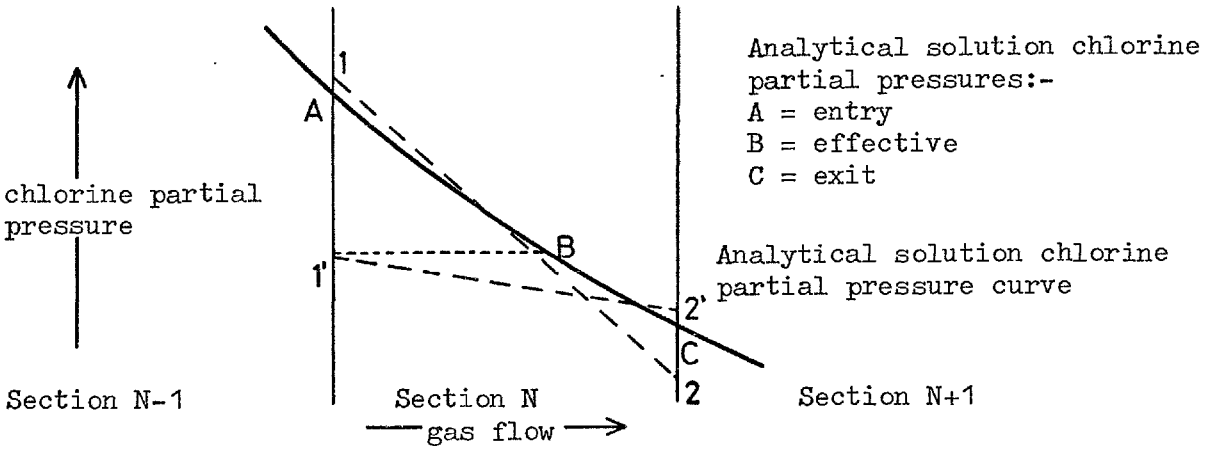

* An analytical solution is probably not possible, therefore this refers to the imanginary analytical solution.

** The effective chlorine partial pressure is that value which if applied throughout the section would produce the same total amount of reaction as predicted by the analytical solution.

\+ It is possible that the computed chlorine partial pressure (the entry value) used for the second section might be above the effective chlorine partial pressure, however, the effect described above would occur with the first section in which this was not the case.

If the computed section (N) entry P_{Cl_2} (1) is greater than the analytical solution effective value (B), the computed P_{Cl_2} (2) entering the next section (N +1) will be less than the analytical solution value (C). Alternatively, if the computed section (N) entry P_{Cl_2} (1') is less than the analytical solution effective value (B) then the computed P_{Cl_2} (2') entering the next section (N + 1) will be greater than the analytical solution value (C). Provided that the bed is divided into a sufficiently large number of sections, for a given bed condition the computed P_{Cl_2}, $\dot{n}_{Cl_2}$ .... etc values only oscillate about the analytical solution values by an insignificantly small amount. Pellets in a section which has become over 'reacted' during the first time interval will, if they are of smaller size than their analytical solution second time interval effective diameter*, become under 'reacted' during the second time interval. This therefore causes a time interval to time interval self-correcting effect (provided the time intervals are suitably short) analogous to the section to section self correcting effect. A flow chart of the computer program is given on figure 8B. A full listing of the computer program, together with the namelist and a description of the method of solution of equations (M1)-(M12) are given in appendix O.

8B7 Results of computer runs

After program HALBED had been carefully tested (to be certain that it was performing the desired calculations correctly) it was run about 40 times so as a) to obtain a range of general predictions, and b) to compare predicted 'experimental' results with actual experimental results. However, before these results are presented a few important points will be explained. The calculations were based upon the following assumptions (excluding those made in section 8B6).

a) The bed was isothermal, therefore ${}_iK$ and ${}_sK$ were constant for a given run.

b) For a given run the various transport coefficients were independent of time and bed position.

---

* This is the pellet diameter which, if combined with the analytical solution effective reaction rate would give the same total extent of reaction as indicated by the analytical solution over the duration of the time interval.

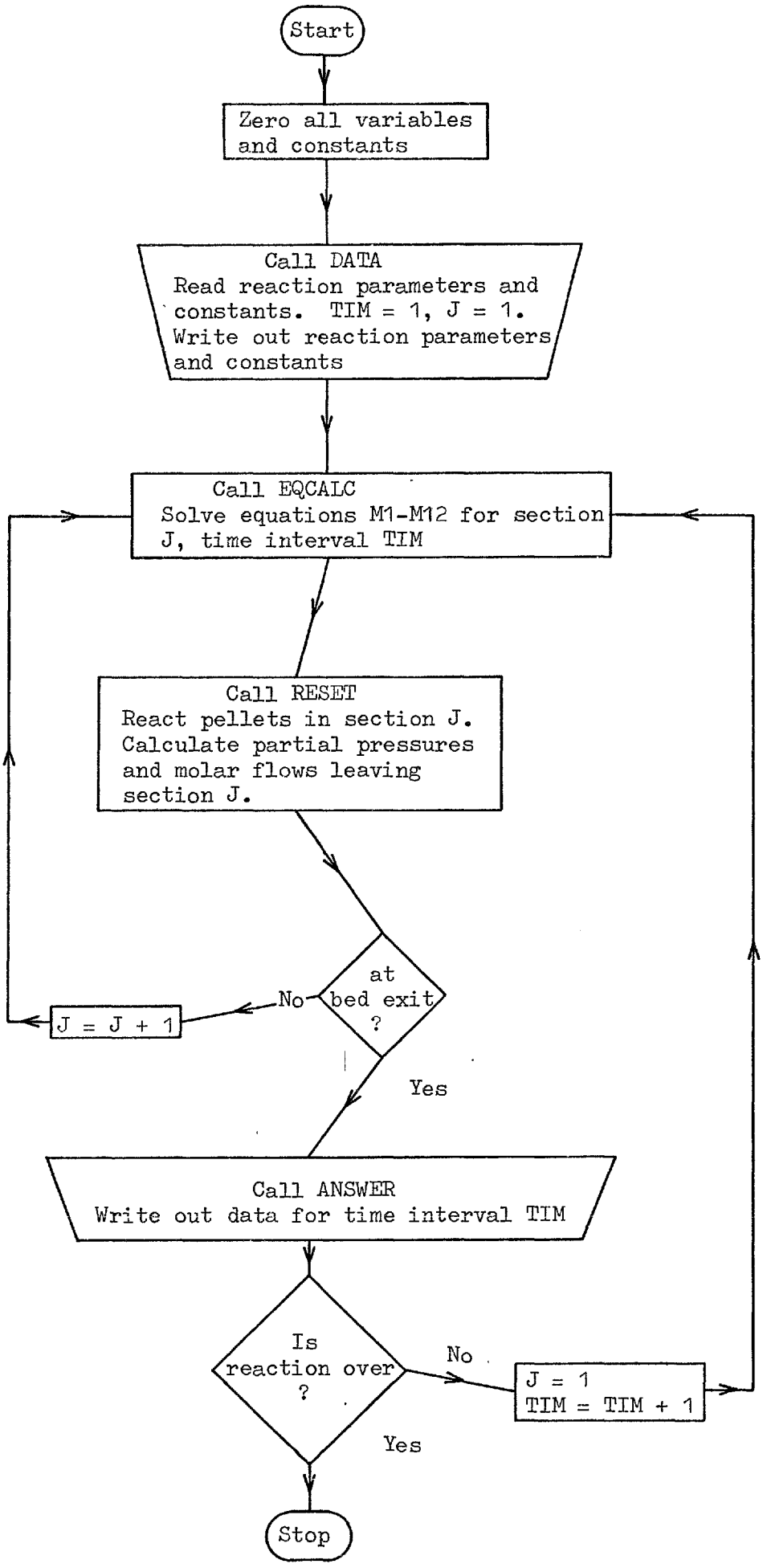

FIGURE 8B: COMPUTER PROGRAM FLOW CHART

c) The gas flow was uniformly distributed over the bed cross-section.

d) There were no pellet-pellet or pellet-wall effects.

e) $D^{eff}_{ZnCl_2}$ and $D^{eff}_{CdCl_2}$ were taken to be equal (except for two runs when reactant-gas mass transport control was being investigated).

f) The values of the boundary layer mass transfer coefficients $K^{O_2}_c$ $K^{Cl_2}_c$, $K^{ZnCl_2}_c$, and $K^{CdCl_2}_c$ were taken to be in the ratios 2:1½:1:1 (this assumption was made firstly because $_sK$ is large and secondly because of the calculated K_c values given in table 8C).

The first four runs* were carried out to determine a suitable steady state time interval. Given below are the bed exit $ZnCl_2$ and $CdCl_2$ partial pressures that were calculated after reaction times of 10.0, 20.0 and 50.0 minutes by using time intervals of 15.0, 30.0 and 60.0 seconds.

Time interval - secs	Reaction time - mins 10.0	20.0	50.0
60.0	0.0463	0.0462	0.0372
30.0	0.0463	0.0462	0.0369
15.0	0.0463	0.0462	0.0368
Bed exit P_{CdCl_2} - atmospheres			
60.0	0.000917	0.000985	0.00992
30.0	0.000918	0.00100	0.0102
15.0	0.000918	0.00101	0.0103
Bed exit P_{ZnCl_2} - atmospheres			

Since there was little difference between the results given by using a time interval of either 30.0 or 15.0 seconds it was decided, in the interests of economy of computer time, to employ a value of 30.0 seconds for all further runs. Values of $_iK$ were calculated from the standard

---

* The reaction conditions employed were: 200 6.32 mm diameter 24% porous 26.6 mole % CdO pellets, $K^{Cl_2}_c$ = 7.5 cm/sec, $D^{eff}_{ZnCl_2}$ = 0.02 cm^2/sec, 800°C, 60 mls_{NTP}/min chlorine and 1200 mls_{NTP}/min nitrogen.

free energy change data presented in section 5F3, $_sK$ values were calculated from the data presented by Orlov and Jeffes[31] (see section 1C2a). At 750°C $_iK$ = 62.3, $_sK$ = 27.7 at 850°C $_iK$ = 42.4, $_sK$ = 72.3 at 950°C $_iK$ = 29.4, $_sK$ = 161.

8B7a Variation of boundary layer mass transfer coefficients:- Plotted on graph 8D are a series of bed exit zinc chloride and cadmium chloride rate vs. time curves obtained by using $K_c^{Cl_2}$ values of 18.0, 12.0, 6.0, 3.75, 1.5, 0.75 and 0.525 cm/sec. Only the K_c values were varied between the runs, the other reaction parameters were kept constant at: 200 6.32 mm diameter 24% porous 26.6 mole % CdO pellets, $D_{ZnCl_2}^{eff}$ = 0.01 cm^2/sec, 700°C, 60 mls_{NTP}/min Cl_2 and 1200 mls_{NTP}/min N_2. With the computer run which employed a $K_c^{Cl_2}$ value of 18.0 cm/sec the bed was divided into 100 sections, whilst with the other runs 50 sections were used. Varying the bed temperature between 700 and 900°C (and therefore $_iK$ and $_sK$) for a given bed size, gas flow and composition and set of transport coefficients produced only slight changes in bed performance. Thus the curves on graph 8D illustrate the effects of variations in K_c values for a fairly wide temperature range. Given below are the percentage chlorine utilisations computed at reaction times of 1, 20 and 80 minutes using the different $K_c^{Cl_2}$ values.

Reaction time - mins	$K_c^{Cl_2}$ - cm/sec 0.525	0.75	1.5	3.75	6.0
1.0	82.75	92.00	99.42	99.99	99.99
20.0	82.38	91.71	99.35	99.98	99.99
80.0	81.18	90.70	99.01	99.77	99.79

Percentage chlorine utilisations

In the chlorination model $K_c^{Cl_2}$ acts as the overall reaction (Cl_2) rate constant. From the values given in the table above it is evident that if the overall rate constant exceeds about 1.5 cm/sec the chlorine utilisation is predicted to be greater than 99.0% over the whole period (90 minutes maximum) of the chlorination experiment. If $K_c^{Cl_2}$ is below this value, progressively increasing amounts of unreacted chlorine leave the bed. Using very large $K_c^{Cl_2}$ values (12.0 - 18.0 cm/sec) the model predicts that thermodynamic equilibrium (between $ZnO_{(s)}$-$CdO_{(s)}$-$Cl_{2(g)}$ -$O_{2(g)}$-$ZnCl_{2(g)}$-$CdCl_{2(g)}$) is attained before the bed exit during the

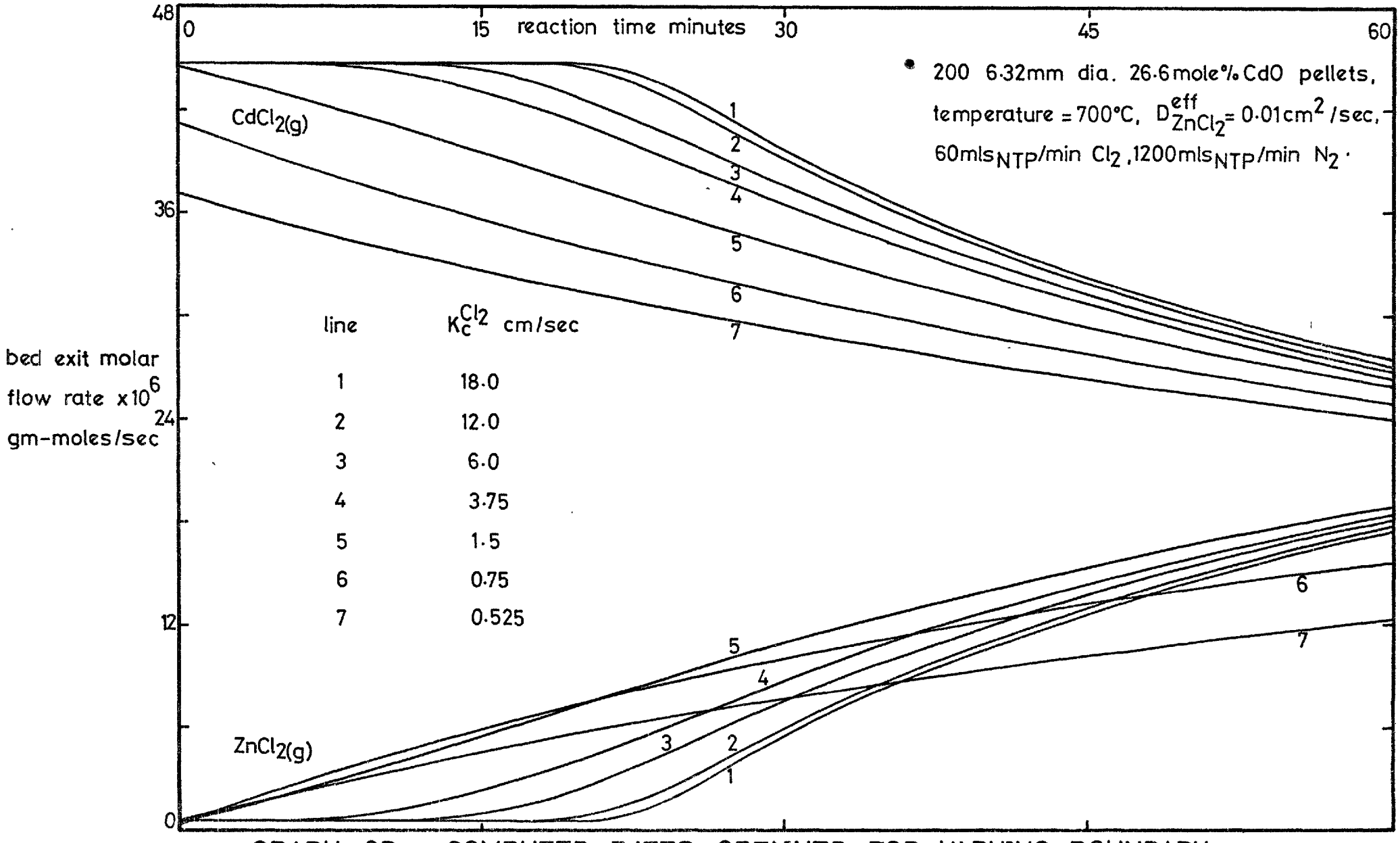

GRAPH 8D: COMPUTED RATES OBTAINED FOR VARYING BOUNDARY LAYER MASS TRANSFER COEFFICIENT VALUES.

first few minutes of reaction (provided that $D^{eff}_{ZnCl_2}$ is not very small).

Plotted on graph 8E are the size distributions (r_s) of the top 50 pellets after 40.5 minutes of reaction for the 'experiments' shown on graph 8D. It is immediately apparent from the plot that as $K^{Cl_2}_c$ increases, chlorine reaction becomes concentrated in the initial part of the bed. Using a $K^{Cl_2}_c$ value of 18.0 cm/sec the model calculates that by this stage of reaction (40.5 minutes) the first 6 pellets have been completely volatilised, whilst with lower values it shows that chlorine reaction extends progressively further into the bed. Although they are for different reaction times, it is interesting to compare the predicted pellet size distributuions given on graph 8E with those shown on plate 4.

8B7b Variation of $D^{eff}_{ZnCl_2}$:- Plotted on graph 8F are a series of cadmium chloride and zinc chloride rate vs. time curves obtained by using various different $D^{eff}_{CdCl_2}$ and $D^{eff}_{ZnCl_2}$ values (whilst holding all the other reaction variables constant at:- 200 6.32 mm diameter 24% porous 26.6 mole % CdO pellets, $K^{Cl_2}_c$ = 3.75 cm/sec, 700°C, 60 mls_{NTP}/min chlorine and 1200 mls_{NTP}/min nitrogen). With four of the computer runs $D^{eff}_{ZnCl_2}$ and $D^{eff}_{CdCl_2}$ were equal; these values being 0.002, 0.01, 0.02 and 0.03 cm^2/sec. Two other runs each employed a $D^{eff}_{ZnCl_2}$ value of 0.02 cm^2/sec but $D^{eff}_{CdCl_2}$ values of 0.2 and 0.002 cm^2/sec. Only 5 pairs of curves are plotted on graph 8F since the runs with $D^{eff}_{ZnCl_2}$ = 0.02, $D^{eff}_{CdCl_2}$ = 0.2 and $D^{eff}_{ZnCl_2}$ = 0.02, $D^{eff}_{CdCl_2}$ = 0.02 were for practical purposes identical, therefore, one pair of curves represents both of these runs. None of the runs predicted that a state of thermodynamic would be reached before the bed exit, even at the very start of reaction*. However, the initial rates of $CdCl_2$ and $ZnCl_2$ production were the same for each run; these rates being effectively in the ratio of the 700°C - equilibrium P_{CdCl_2}/P_{ZnCl_2} ratio. Deviation from this state of pseudo-equilibrium occurred more rapidly and to a greater extent with decreasing $D^{eff}_{ZnCl_2}$ values. The plots on graph 8F were found to be relatively insensitive to temperature (some of the runs were repeated at 900°C and compared with those obtained at 700°C). Thus (similarly to graph 8D) the plots demonstrate the effects of variations in the D^{eff} values for a fairly wide temperature span. At no stage during any of the different

---

* Had a larger $K^{Cl_2}_c$ value been used thermodynamic equilibrium would have been predicted.

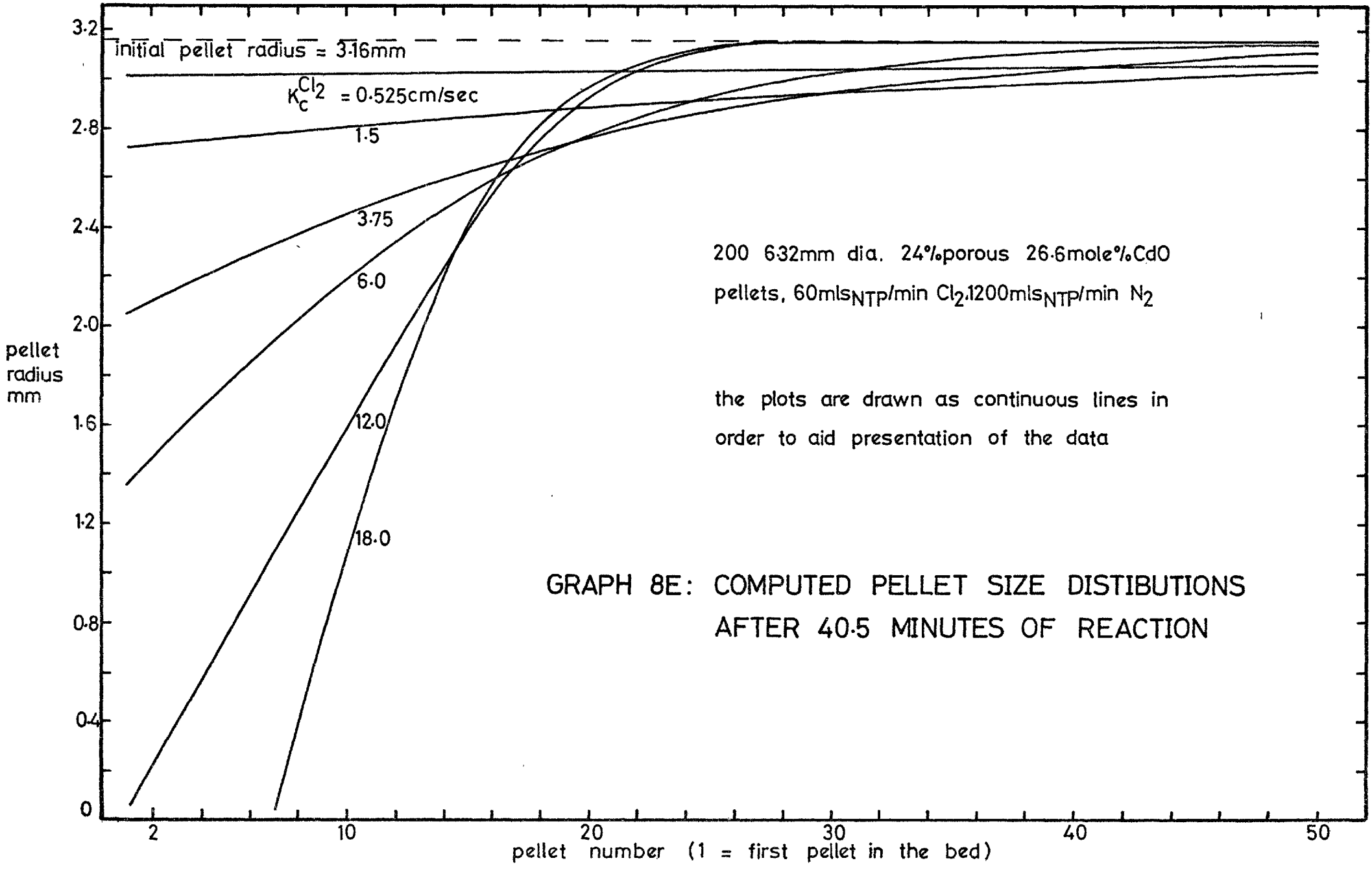

GRAPH 8E: COMPUTED PELLET SIZE DISTIBUTIONS AFTER 40·5 MINUTES OF REACTION

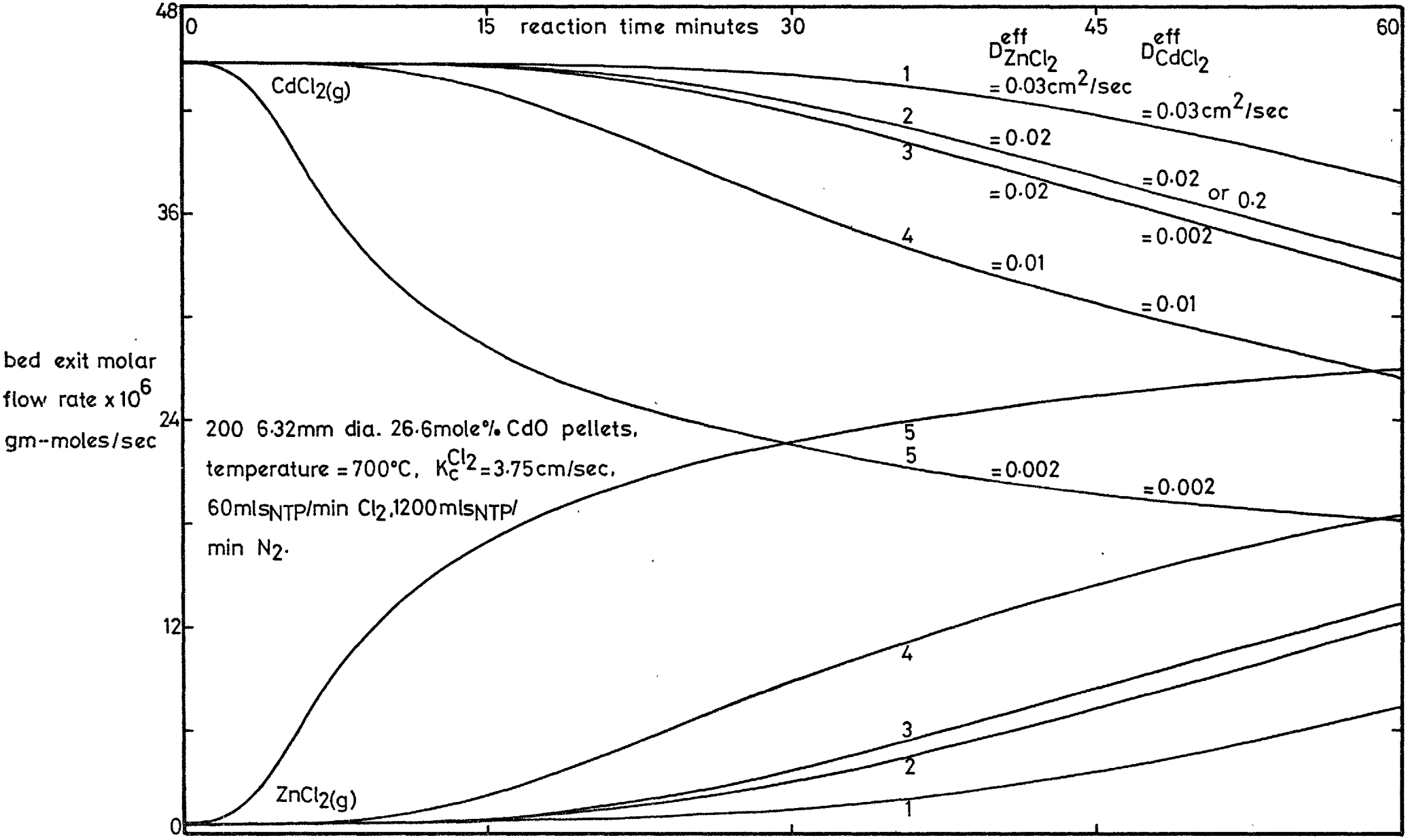

GRAPH 8F: COMPUTED RATES OBTAINED FOR VARYING $D^{eff}_{ZnCl_2}$ AND $D^{eff}_{CdCl_2}$ VALUES.

runs plotted on graph 8F did the chlorine utilisation fall below 99.5%. Given in the table below are the computed amounts of ZnO and CdO volatilised (presented as a percentage of the amount initially present in the bed) after 10.0, 30.0 and 60.0 minutes of reaction for the four runs (shown on graph 8F) in which $D^{eff}_{ZnCl_2}$ and $D^{eff}_{CdCl_2}$ were equal. It is interesting to note that a change in the value of $D^{eff}_{ZnCl_2}$ by a factor of x15 did not cause as much variation in the amount of CdO volatilised as might at first be expected. Two of the runs plotted on graph 8F display that the CdO reaction rate was controlled by the diffusion of $ZnCl_{2(g)}$ through the porous ZnO. As explained earlier in this paragraph increasing $D^{eff}_{CdCl_2}$ from 0.02 to 0.2 cm^2/sec whilst maintaining $D^{eff}_{ZnCl_2}$ equal to 0.02 cm^2/sec had virtually no effect on the bed exit zinc chloride and cadmium chloride rates. Conversely, when $D^{eff}_{CdCl_2}$ was reduced to 1/10 th of the value of $D^{eff}_{ZnCl_2}$ only a small decrease in the bed exit cadmium chloride rate occurred.

$D^{eff}_{ZnCl_2}$	Reaction time 10 mins		30 mins		60 mins	
cm^2/sec	CdO	ZnO	CdO	ZnO	CdO	ZnO
0.002	6.65	0.33	14.8	2.69	24.4	7.37
0.01	7.18	0.044	20.3	0.59	35.3	3.22
0.02	7.19	0.038	21.3	0.21	39.7	1.56
0.03	7.20	0.037	21.5	0.14	41.5	0.86

CdO and ZnO percentage depletions

8B7c Comparison of predicted experimental results with actual experimental results:- Employing the same conditions as used for the experiments reported in section 7B, predicted experimental results were obtained from program HALBED for various different D^{eff} and K_c values (with each of these runs $D^{eff}_{ZnCl_2}$ and $D^{eff}_{CdCl_2}$ were equal, whilst the O_2, Cl_2, $ZnCl_2$ and $CdCl_2$ K_c values were in the ratios $2:1\frac{1}{2}:1:1$). Each bed was divided into 100 separate sections, the first 40 of which each contained $1/240^{th}$ of the total number of pellets, the next 20 $1/120^{th}$ and the final 40 $1/60^{th}$. The reaction conditions used for the computations were determined in the following way:

a) Because the accuracy of orifice "C5" was in doubt (see section 4C3) the chlorine flow rates were not taken to be equal to the rates indicated

by the flow meter. Instead it was assumed that with all the non-equilibrium experiments chlorine utilisations had been 100% (see section 7B2); the steady chlorine flow rate for a given experiment was therefore taken to be equal to the mean of the $ZnCl_2$ + $CdCl_2$ rates of the different stages of the experiment.

b) With each experiment the nitrogen flow was taken to be equal to the mean rate indicated by the nitrogen flow meter.

c) The total gas pressure for a given computer run was taken to be equal to the mean measured bed-entry gas pressure.

d) For computer runs on beds of the same composition the same number of pellets were used; this number was taken to be the mean of the number used in the 3 experiments on the same composition bed.

e) The same pellet diameter was used for different computer runs on beds of the same composition. These values (for the beds of each composition) were calculated on the basis of the mean mass of the three beds of each composition, the mean number of pellets in these beds (as in (d)) and the unreacted pellet densities* given in table 8A (part 1-3).

On graphs 8G, 8H, 8I and 8J are plotted the predicted bed-exit $ZnCl_2$ and $CdCl_2$ rate vs. time curves together with the experimentally determined curves (as plotted in section 7B2). The parameters used for the various computed curves are as follows:

a) Graph 8G:- 951°C-50.0 mole % CdO. (1) $K_c^{Cl_2}$ = 3.0 cm/sec, $D^{eff}_{ZnCl_2}$ = 0.001 cm^2/sec, pellet diameter = 6.358 mm, total number of pellets = 178, Cl_2 flow = 48.6 mls_{NTP}/min and N_2 flow = 1168 mls_{NTP}/min.

b) Graph 8H:- 852°C-26.6 mole % CdO. (1) $K_c^{Cl_2}$ = 3.0 cm/sec, $D^{eff}_{ZnCl_2}$ = 0.008 cm^2/sec, pellet diameter = 6.19 mm, total number of pellets = 197, Cl_2 flow = 50.5 mls_{NTP}/min and N_2 flow = 1155 mls_{NTP}/min. (2) as

---

* The molar concentrations of ZnO and CdO in the unreacted pellets were calculated to be : 50.0 mole % CdO pellets - 0.0239 moles CdO and ZnO per cc, 26.6 mole % CdO pellets - 0.0384 moles ZnO and 0.0139 moles CdO per cc, 10.8 mole % CdO pellets - 0.0451 moles ZnO and 0.00547 moles CdO per cc.

above except $D^{eff}_{ZnCl_2}$ = 0.005 cm^2/sec.

c) Graph 8I:- 952°C - 10.8 % mole CdO. (1) $K^{Cl_2}_c$ = 3.75 cm/sec, $D^{eff}_{ZnCl_2}$ = 0.0015 cm^2/sec, pellet diameter = 6.292 mm, total number of pellets = 211, Cl_2 flow = 53.6 mls_{NTP}/min and N_2 flow = 1182 mls_{NTP}/min. (2) as above except $K^{Cl_2}_c$ = 9.0 cm/sec and $D^{eff}_{ZnCl_2}$ = 0.0009 cm^2/sec.

d) Graph 8J:- 851°C-10.8 mole % CdO. (1) $K^{Cl_2}_c$ = 3.75 cm/sec, $D^{eff}_{ZnCl_2}$ = 0.017 cm^2/sec, pellet diameter = 6.292 mm, total number of pellets = 211, Cl_2 flow = 53.4 mls_{NTP}/min and N_2 flow = 1304 mls_{NTP}/min. (2) as above except $K^{Cl_2}_c$ = 7.5 cm/sec and $D^{eff}_{ZnCl_2}$ = 0.015 cm^2/sec.

At no stage during any of the computer runs plotted on graph 8G, 8H, 8I and 8J did the calculated chlorine utilisation fall below 99.8%. In addition, none of these runs predicted the complete volatilisation of the pellets contained in any of the bed sections. Compared in the table below, for the experiments plotted on graphs 8G, 8H, 8I and 8J, are the experimentally measured and computed CdO and ZnO bed-depletions at the end of reaction.

Temperature pellet composition (and graph number)	Data source	Reaction time - mins	$D^{eff}_{ZnCl_2}$ cm^2/sec	ZnO depletion %	CdO depletion %
951°C-50.0 mole % CdO 8G	experiment	90.0	-	14.3	22.5
	computed	90.0	0.001	13.6	23.2
852°C - 26.6 mole % CdO 8H	experiment	90.2	-	8.90	34.9
	computed	90.2	0.008	7.43	39.0
	computed	90.2	0.005	8.93	34.9
952°C - 10.8 mole % CdO 8I	experiment	52.0	-	7.48	22.6
	computed	52.0	0.0015	6.99	26.1
	computed	52.0	0.0009	7.34	23.4
851°C - 10.8 mole % CdO 8J	experiment	53.0	-	3.84	53.9
	computed	53.0	0.017	3.48	56.3

Experimentally measured and computed CdO and ZnO depletions at the end of reaction.

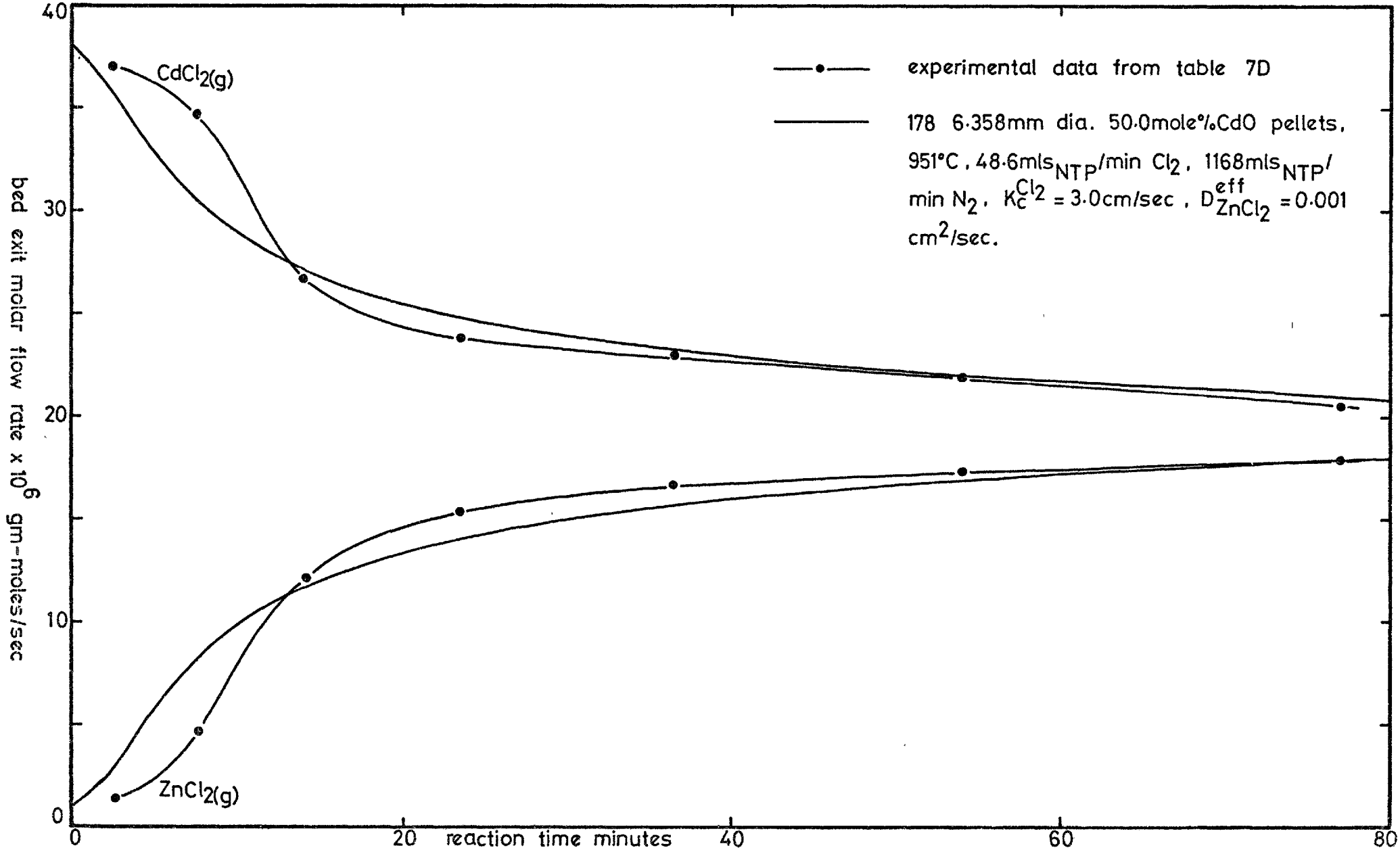

GRAPH 8G: COMPARISON OF 951°C-50.0MOLE% CdO EXPERIMENT AND COMPUTED RESULTS.

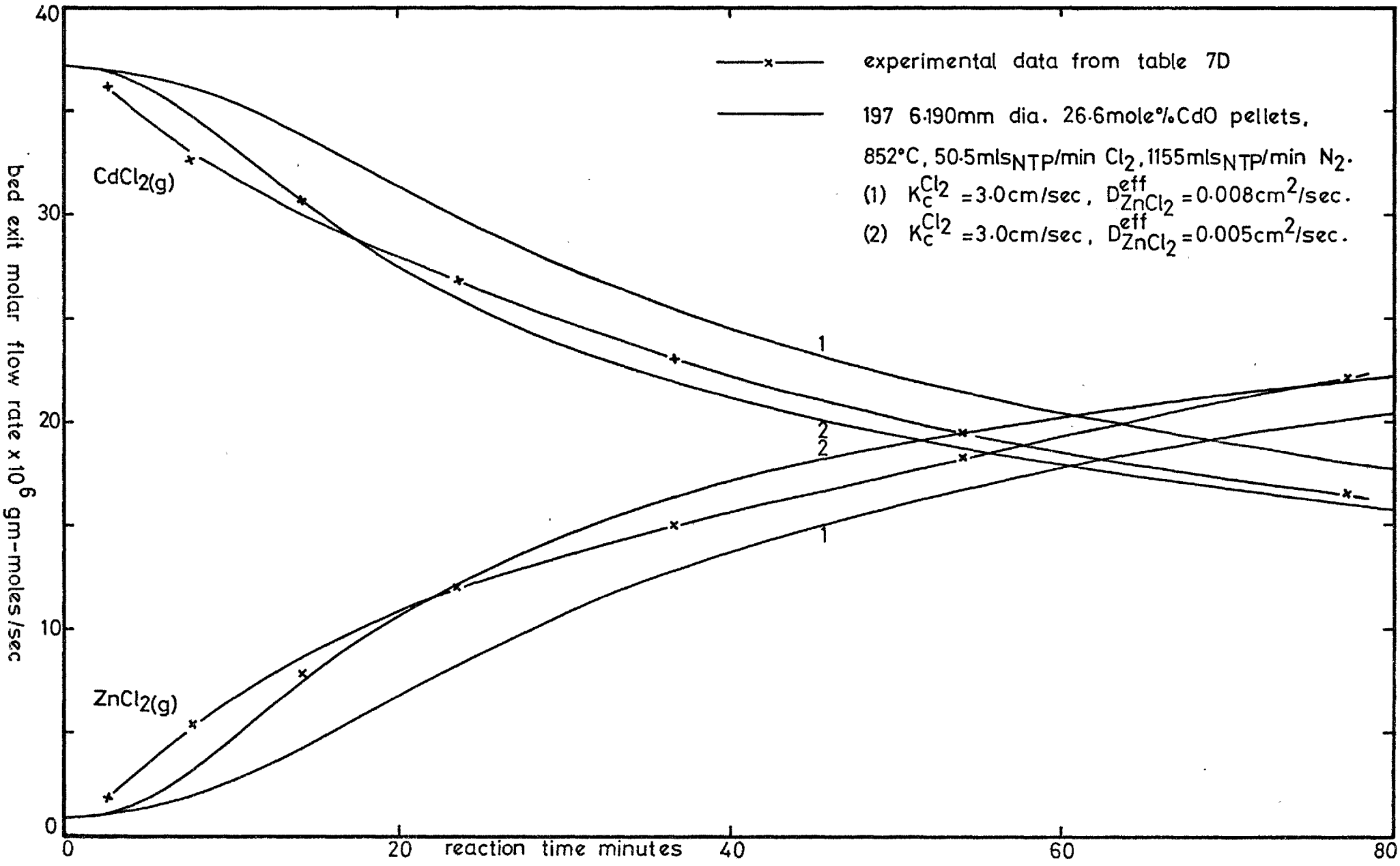

GRAPH 8H: COMPARISON OF 852°C -26·6MOLE%CdO EXPERIMENT AND COMPUTED RESULTS.

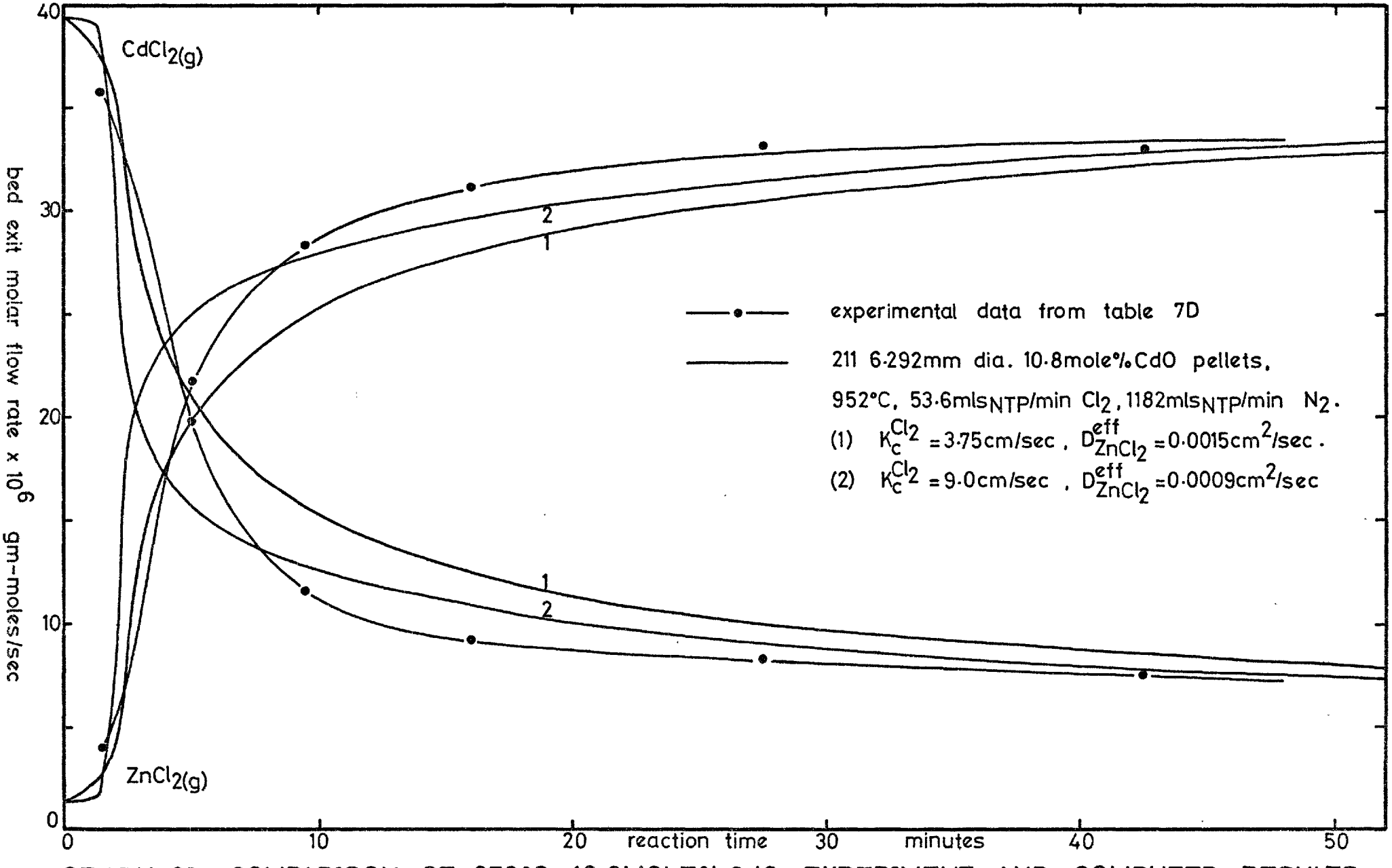

GRAPH 8I: COMPARISON OF 952°C -10·8MOLE% CdO EXPERIMENT AND COMPUTED RESULTS.

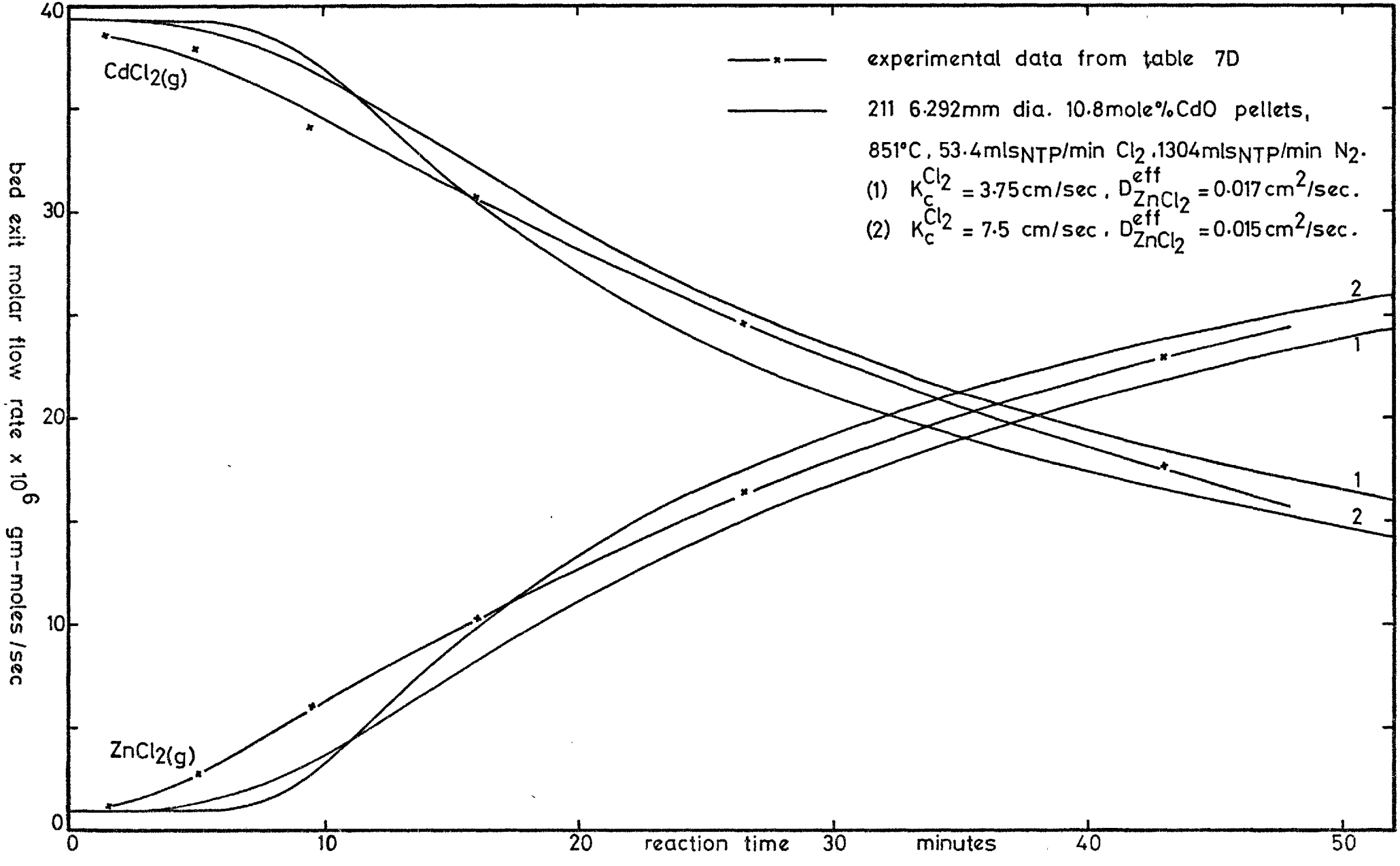

GRAPH 8J: COMPARISON OF 851°C-10·8MOLE% CdO EXPERIMENT AND COMPUTED RESULTS.

Shown on graph 8K are two typical pellet and core size distribution plots as predicted by program HALBED. One plot is the size distribution predicted by the 851°C-10.8 mole % CdO-$D^{eff}_{ZnCl_2}$ = 0.017 cm^2/sec computer run after 40.5 minutes of reaction (see graph J). The other plot is the size distribution predicted by the 852°C-26.6 mole % CdO - $D^{eff}_{ZnCl_2}$ = 0.008 cm^2/sec computer run after 80.5 minutes of reaction (see graph 8H). It is interesting to compare these plots with the photographs and descriptions given in section 8A2a.

Shown on graph 8L are the $ZnCl_2$, $CdCl_2$, O_2 and Cl_2 bulk gas partial pressure distributions predicted by the 851°C-10.8 mole % CdO-$K_c^{Cl_2}$ = 7.5 cm/sec-$D^{eff}_{ZnCl_2}$ = 0.015 cm^2/sec computer run after 20.5 minutes of reaction (see graph 8J). By this stage of reaction the bed depth was computed to be 96.3% of its initial depth, the bed to be 30.6% depleted of CdO, 0.57% depleted of ZnO and the first section pellet size to be 4.76 mm in diameter (as compared to an initial diameter of 6.292 mm). In addition, the computed $ZnCl_2$ partial pressures midway down the bed in the bulk gas, at the pellet surface and at the ZnO-CdO/ZnO interface were 0.0256, 0.0237, and 0.000898 atmospheres respectively. These values show that, with the transport coefficients given above, almost all of the resistance to the $ZnCl_{2(g)} + CdO_{(s)}$ exchange reaction was due to diffusion in the ZnO shell.

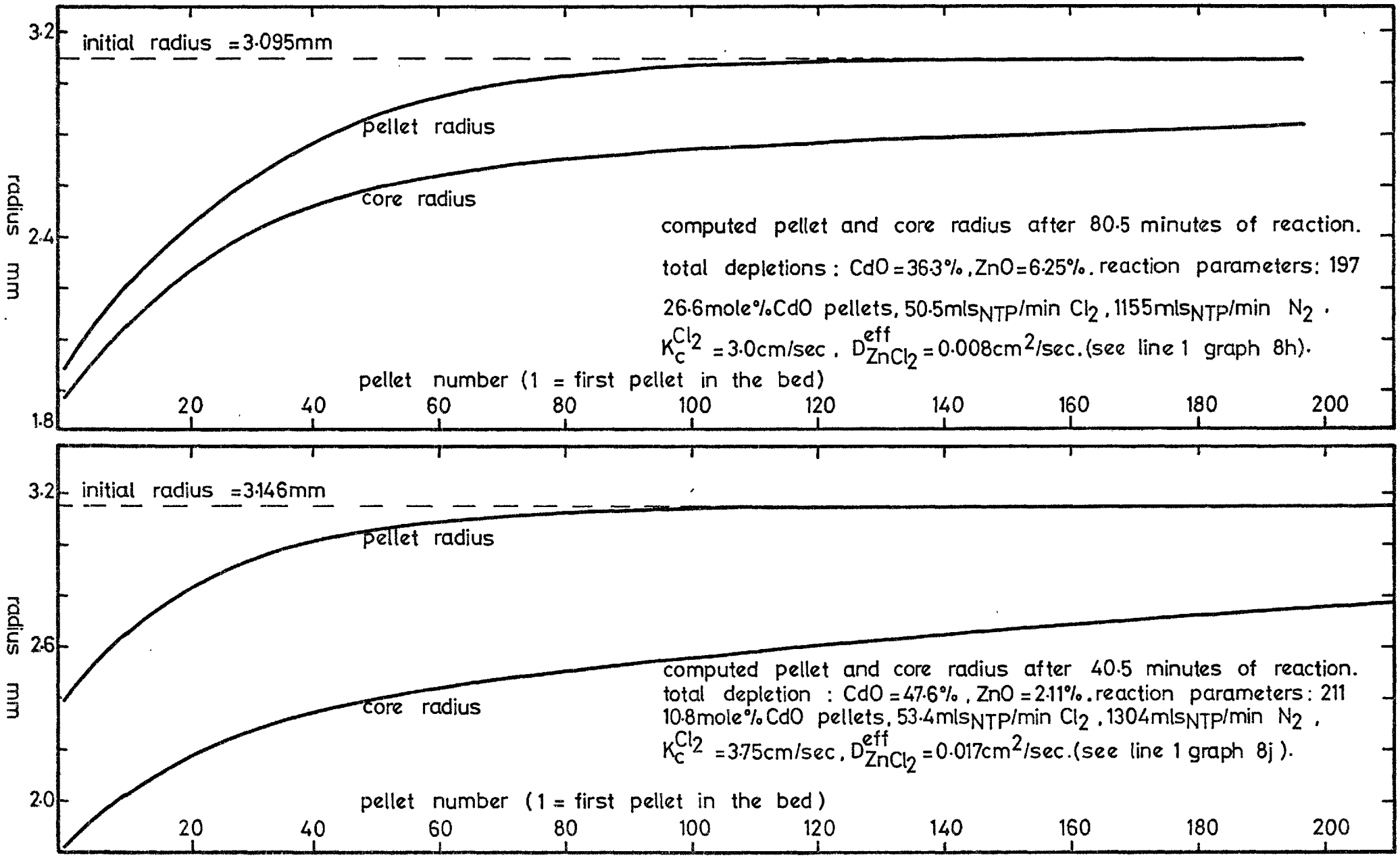

GRAPH 8K: COMPUTED PELLET AND INTERFACE RADIUS vs BED POSITION PLOTS.

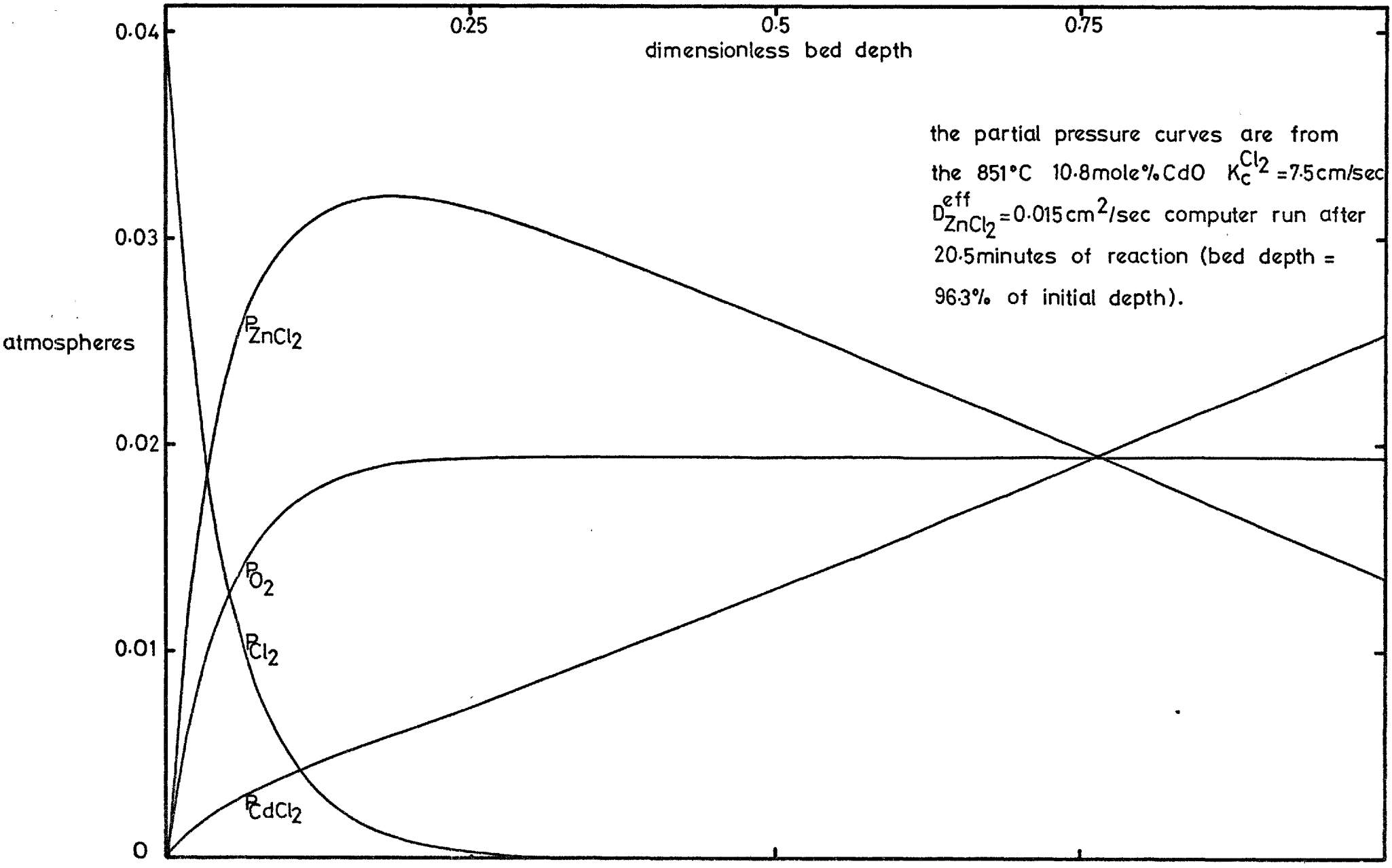

GRAPH 8L: COMPUTED PARTIAL PRESSURE vs BED POSITION CURVES.

CHAPTER NINE

DISCUSSION OF THE NON-EQUILIBRIUM EXPERIMENTS

There are few reports on the kinetics of oxide chlorination-volatilisation reactions in the literature. The most fundamental study has been by Fruehan and Martonik[51], this is reviewed in section 1D2a. No detailed studies have been performed on either ZnO or CdO. The only paper on the separation of metals from an admixture of metal oxides (NiO/ZnO) by a chlorination (HCl)-volatilisation process[32] which was found in the literature unfortunately contains little quantitative data. It is therefore not possible to make any direct comparisons with the results presented in Chapters 7 and 8.

9A ZnO NON-EQUILIBRIUM EXPERIMENTS

9A1 Experimental method

The ZnO + Cl_2 experiments described in Chapter 7 were the first of the experiments reported in this thesis to be performed. They were carried out in order to help develop various experimental procedures whilst at the same time obtain some data on the rate of the ZnO chlorination-volatilisation reaction. The greatest experimental difficulty with packed bed studies is the continuous measurement of either the reaction rates through the bed or the reaction rate of the bed as a whole. If it is not possible to obtain continuous or semi-continous measurments, then the reaction must be performed as an approximately steady state process. Before performing either any ZnO or CdO/ZnO non-equilibrium experiments attention was first directed at trying to develop a method for continuously measuring the overall rate of the reactor. For this purpose two different analytical techniques were considered:

a) continuous analysis of metal chlorides by emission spectrophotometry,

b) continuous analysis of chlorine by visible spectrum absorption spectrophotometry. A feasibility study was performed on the first of these methods (see Appendix A). The results of this investigation showed that a large amount of work would be required to develop it into an accurate analytical technique. The second method is already used in

a number of processes*. Its application with the non-equilibrium experiments was not,however, investigated in detail because of reasons of cost, time and the limited use to which it would be put. Since no comparatively simple method could be devised for either continuously or semi-continuously monitoring the reaction rates of the zinc oxide beds, these experiments were performed under approximately steady state conditions.

The overall reaction rate of a packed bed reactor is always unsteady unless either a) it is a pseudo-steady-state process eg ironmaking, or b) it is a steady state catalytic process. Although the ZnO experiments were in neither of these categories, by only reacting a small fraction of each bed** each experiment could be approximated to a steady state process and analysed accordingly. This approximation, which assumes that the overall reaction rates of the beds remained constant for the duration of the experiments, was not experimentally investigated. However, results obtained by other workers support the approximation (Fruehan et al[51] found that steady reaction rates were obtained from single pellets and granules of Fe_2O_3, NiO and $NiFe_2O_4$ until they were at least 20% reacted; see section 1D2a). With some packed bed reactions a further approximation is possible. If a reactant flows through a uniform property packed bed very rapidly in comparison to the rate at which it reacts, its reaction rate becomes nearly independent of position. Overall rate data are then comparatively easy to analyse (an analogous situation exists with thermogravimetric studies where the reactant flow is chosen to be sufficiently large to insure that its concentration in the bulk gas remains effectively unchanged by the reaction). Since the ZnO + Cl_2 reaction was found to be relatively rapid, the gas flows that would have been needed to make the ZnO react at an approximately constant rate through the beds were prohibitively large. During each ZnO experiment the chlorine reaction rate therefore varied with changing bed position. The conditions employed for the ZnO experiments are described in section 7A. To recapitulate briefly; bed depletions were minimised by using a combination of low chlorine partial pressures and short reaction times, but not at the expense of allowing significant interferences

---

* An on line chlorine analyser is marketed by ETHER CONTROLS. Named an 'okometer' it is used by various industries for monitoring chlorine concentrations (between 0.2 and 100%) in process streams and exhaust gases; one such instrument was employed in the LDK pilot plant (see section 1B1b).

** The average bed depletion of the ZnO experiments presented in Chapter seven was 8.1%.

from reaction initiation and termination effects. Some of the complications and limitations imposed by the overall experimental method are listed below:

a) With each experiment the proportion of the total surface area of the ZnO granules freely exposed to the reactor gas flow was significantly reduced due to granule-granule and granule-wall contact. These two effects were particularly pronounced since the granules were plate shaped and the reactor was comparatively small (22 mm bore). (The generally accepted reactor diameter/pellet diameter ratio above which pellet-wall interferences can be neglected[33] is 10:1.) At low Reynolds numbers* in small reactors containing large granules gas velocity gradients across the bed section may be significant.

b) High reaction rates could not be successfully studied since for this purpose short beds, large granules, low chlorine partial pressures and high gas flows were required. Fog formation caused difficulty when condensing $ZnCl_{2(g)}$ from rapidly flowing gas streams.

c) The beds became progressively less reacted in the direction of gas flow, this therefore set up temperature gradients.

d) Packed bed mass transfer coefficient correlations are somewhat unreliable at low Reynolds numbers (see section 8B4).

e) Large amounts of ZnO granules were required.

f) Detailed theoretical analysis of packed bed processes is difficult.

More information on the kinetics of the ZnO + Cl_2 reaction would have been obtained, for the expenditure of less effort, by studying single pellets or granules with a thermobalance. Packed bed reactors should only be employed for gas-solid reaction kinetics studies when one of the following two criteria applies: a) single pellet/granule rate data is already

---

* The granule Reynolds numbers, calculated using the mean sieve size and the superficial gas velocity through the reactor, with the ZnO experiments varied between about 7 (K series runs) and 40 (C series runs).

available, the study is therefore specifically concerned with the performance of a packed bed reactor; b) despite the complexities of a packed bed reactor no alternative reaction configuration is suitable.

9A2 Theoretical analysis

The theoretical analysis used for the ZnO experiments is fully described in section 7A2. The most fundamental assumption made in this analysis is that the chemical reaction rate, over the temperature investigated, is first order with respect to chlorine partial pressure. Two considerations support this assumption: a) at similar temperatures and chlorine partial pressures to those used with the ZnO experiments Fruehan and Martonik[51,52] found the rates of reaction of Fe_2O_3, NiO, $NiFe_2O_4$, Fe and Ni to be first order with respect to P_{Cl_2}, except when surface coatings were formed; b) the chlorine partial pressures used for the ZnO experiments were insufficiently high to form liquid zinc chloride. Several approximations had to be made before equation (3) - section 7A2 could be used in developing an expression to describe the overall reaction rate of the ZnO beds. The most important of these, that the reactions were steady state processes, is partly discussed in the previous section. This approximation clearly becomes more valid as the reaction time is decreased (within the limitations imposed by reaction initiation and termination effects). If the reaction was boundary layer mass transport controlled then the overall reaction rate would decrease only as the size of the granules decreased. However, if the process was chemically controlled it might be possible, due to the granules developing porous surfaces thereby exposing increased areas of ZnO to the chlorine, for the overall reaction rate to reach a maximum value shortly after the start of reaction. The approximation that the rate constant $\bar{k}_{Cl_2}$ was constant throughout the bed was most valid when the overall reaction rates were low. With comparatively high reaction rates the beds developed temperature differences of up to 25 deg.C down their lengths. If under these conditions the reaction was chemically controlled $\bar{k}_{Cl_2}$ would vary by a significant amount with changing bed position. The uniformity of gas flow over the bed cross section, one of the approximations in the analysis, was subject to disturbances from three sources: a) the thermocouple sheath would have promoted uneven gas flow, b) the gas flow velocity would have been reduced at near to the reactor wall, and c) the packing distribution in packed beds is adversely affected by low reactor diameter/pellet

diameter ratios[33]. Since the flow of gas through packed beds is a very complex phenomenon it is difficult to quantify these three effects. However, elementary considerations indicate that the gas flows were most uniform in the beds composed of the smallest granules. At each set of reaction conditions studied, experiments were performed using a range of bed sizes. Each of these beds was assumed to be a random sample of granules from the particular sieve fraction being used. However, since the granules spanned a range of geometries (see plate 3) the specific surfaces of small beds of large granules were subject to sampling errors.

9A3 Results

The results of the ZnO non-equilibrium experiments are plotted on graph 7A according to the theoretical analysis given in section 7A2. The plots, all of which are predicted to be linear, of the J, I, K, D and B series experiments are non-linear at small bed sizes. Curvature in these plots could possibly have been due to one or more of the following causes: a) a greater than first order reaction, b) a decrease in the value of $\bar{k}_{Cl_2}$ down the beds, c) an error in the measured chlorine flow rates. It is thought unlikely that the ZnO reaction is other than first order with respect to chlorine. If the indicated chlorine flow rates (that is those used for calculating the plotted results) had been incorrect, then re-calculating the plotted data using either a positive or a negative $_o\dot{n}_{Cl_2}$ correction would not make the plots become linear*. The most plausible explanation for the curvatures exhibited by the plots therefore seems to be that the granules in the upper regions of the beds, since their surfaces became fluffy and porous, exposed larger areas of ZnO for reaction, thereby causing $\bar{k}_{Cl_2}$ to be highest at the bed entry (this of course assumes that the reactions were chemically controlled).

In order to calculate $\bar{k}_{Cl_2}$ values from the gradients of the plots on graph 7A, it was necessary to know the geometric specific surfaces ($S_{\bar{M}}$) of the different ZnO size fractions. Since the granules were irregularly shaped, a complicating factor which is best to avoid with gas-solid studies, the values had to be

---

* Orifice C5 was found to give slightly erroneous readings (see section 4C3), however it was only used with ZnO experiments E1 and E2.

estimated. These estimates and the method by which they were calculated are discussed in section 7A3a. The $\bar{k}_{Cl_2}$ values given in section 7A3b are insufficiently reliable to be used for an apparent activation energy plot. However, a $\bar{k}_{Cl_2}$ value of between 0.030 and 0.066 cm/sec at 705°C clearly indicates chemical control, whilst a $\bar{k}_{Cl_2}$ value of 2.4 cm/sec at 873°C suggests that the reaction is under mixed control (see table 8C for calculated $K_c^{Cl_2}$ values). Surface textures developed by oxide compacts during chlorination-volatilisation reactions are strongly influenced by the rate controlling mechanism. The results of the ZnO experiments, as well as the results obtained by Fruehan and Martonik[51] (see section 1D2a) indicate that fluffy surface layers are characteristic of low chemical rate constant reactions, whilst smooth surfaces are characteristics of mass transport controlled reactions.

9B CdO/ZnO NON-EQUILIBRIUM EXPERIMENTS

9B1 Experimental method*

The factors which were considered when choosing a suitable experimental technique for investigating the kinetics of the chlorination-volatilisation of ZnO/CdO pellets are described and discussed in section 2C2. The two most serious disadvantages with the step-wise chlorination technique which was adopted were: a) only the average reaction rates during each reaction stage could be calculated, and b) the sintering which occurred between each reaction stage was unrelated to the reaction process. Although it did not affect the results, another disadvantage of the overall experimental method was that since each experiment was quite a lengthy operation only a limited number of parameters could be investigated. However, in most other respects the experiments were satisfactory. The use of approximately spherical pellets (which were comparatively easy to manufacture) avoided surface area values from having to be estimated, promoted uniformity of gas flow and helped simplify the theoretical analysis. The concentric tube condensers collected all the $ZnCl_{2(g)}$ and $CdCl_{2(g)}$ formed in the reactor, both of which were then analysed by an accurate and convenient method. The Zn + Cd mass balances were very good. By using low chlorine partial pressures the reacting beds were kept effectively isothermal. A larger diameter reactor

---

1 Single CdO/ZnO bed experiments

would have been desirable in order to reduce the fraction of the total number of pellets in each bed which were in contact with the reactor wall. The reactor diameter/pellet diameter ratio at the start of the CdO/ZnO experiments was about 4.5:1. In a simple experiment about 500 -6.7 + 5.6 mm unreacted CdO/ZnO pellets were randomly packed into the 27.5 mm diameter reactor, 61% made contact with the wall, repeating the experiment gave a value of 63%. This shows that the obstructed surface areas, disturbances in gas flow patterns and local variations in mass transfer coefficients produced by pellet-wall contact would have had some effect on the majority of pellets comprising each bed.

9B2 Structural investigations

The results of the optical microscopy, porosimetry, scanning electron microscope and electron probe investigations are reported and interpreted in section 8A. In this section the important aspects of these findings are summarised and discussed.

The results of the structural investigations show that over the temperature range studied the general reaction behaviour of the CdO/ZnO pellets was governed by the following three factors:

a) The CdO reaction rate was controlled by transition region diffusion of $ZnCl_{2(g)}$ through the porous zinc oxide shell.

b) At the lowest reaction temperature chlorine only penetrated a small distance into the pellets; penetration decreased with increasing temperature.

c) Pellet sintering and bulk densification became very rapid as the reaction temperature was increased. This caused the effective diffusivity of the $ZnCl_{2(g)}$ and therefore the CdO reaction rate to decrease with increasing temperature. Structural inhomogeneities formed during pelletisation and intensified by sintering caused asymetric reaction of the CdO at the higher reaction temperatures.

During the chlorination experiments the ZnO/CdO pellets were exposed to $ZnCl_2$-$CdCl_2$-Cl_2-O_2-N_2 and O_2 atmospheres, there was also deposition of ZnO at the ZnO-CdO/ZnO boundaries. Under these conditions many factors could have been influencing the processes of sintering and densification.

No work on the high temperature kinetics of CdO sintering could be found in the literature. However, since CdO has been reported[134] to sinter at as low as 300°C its sintering rate at between 750-950°C is likely to be very rapid. The sintering of ZnO has been studied on a number of occasions. Gupta and Coble[132] found that ZnO compacts, initially 25% porous, held in air at 900°C were 15% porous after 10 minutes, 8% porous after 20 minutes, and 6% porous after 3 hours. Rates of densification were higher in oxygen than in air. Increased ZnO densification rates due to the presence of oxygen in the sintering atmosphere have also been reported by Roberts and Hutchings[133]. No deductions on the comparative rates of sintering of the different composition pellets can be made from the stereoscan results. However, the results of the macroscopic examinations (see section 8A2) show that the 50.0 mole % CdO pellets contained many more internal cracks than did the 10.8 mole % CdO pellets. This suggests that the CdO sintered and densified more rapidly than the ZnO, thereby producing internal stresses which in turn resulted in cracking. Internal cracking, by this mechanism, would appear to be the reason why the bulk voidage of the 50 mole % CdO 5 hours - 950°C sintered pellets remained fairly high (see table 8A) despite their having a highly sintered structure.

Photograph C on plate 8 shows surface areas covered by very thin layers of ZnO through which the underlying CdO can be seen (this feature was also exhibited by some of the 950°C-reacted pellets of the other compositions and also by the pellets from the 950°C double bed experiments). Pellets with these very thin, virtually transparent ZnO coatings were only found after reaction at 950°C. All had been exposed to gas containing a comparatively high concentration of $ZnCl_2$, yet there had been very little reaction. The only explanation for this behaviour is that the ZnO coatings, partly deposited by the exchange reaction, were effectively impermeable. Since neither individual CdO or ZnO grains, nor regions of deposited ZnO could be identified, little can be said about the exchange reaction mechanism. However, the sharpness of the ZnO-CdO/ZnO boundaries at each reaction temperature clearly indicates that the chemical mechanism(s) of the exchange reaction was always very rapid. Two possible exchange reaction mechanisms are described in section 7C2. Reaction by indirect exchange would not cause the CdO grains to become coated in ZnO, whereas direct exchange would. It appears that at 950°C, regardless of reaction mechanism(s), the

deposited ZnO together with the ZnO initially present tended to sinter and densify (aided by the holding time between each reaction stage) into a $ZnCl_{2(g)}$ diffusion barrier. At 750°C if the reaction had taken place by direct exchange, then the ZnO coatings must have been permeable since the Geoscan showed the ZnO-CdO/ZnO boundary to be extremely sharp (not what would be expected if a solid state diffusion process through dense ZnO was occurring).

The ZnO side of the ZnO-CdO/ZnO boundary examined with the Geoscan was found to contain retained CdO, this result is illustrated on graph 8A and plate 9. Areas of ZnO containing retained CdO can also be seen in some of the macrographs on plates 7, 8 and 9. CdO could be retained in one of two forms: a) discrete CdO particles encased in ZnO and b) Cd^{++} in solid solution with ZnO. Since the solid solubility of Cd^{++} in ZnO is fairly low (about 2½% at 950°C - see section 6B3a) it is doubtful whether pure ZnO and ZnO saturated with Cd^{++} would appear much different in colour. The retained CdO visible in the macro-sections was thus in the form of discrete particles. The formation of these concentric layers is explained in section 8A2a. Retained encased CdO particles were probably also responsible for the external surfaces of some of the pellets being coloured various shades of brown. Under all reaction conditions most of any cadmium oxide retained in solid solution in the ZnO in the essentially CdO-depleted regions would have tended to be slowly removed by the $ZnCl_2$ which was diffusing through to the ZnO-CdO/ZnO boundary.

Slight penetration of chlorine into the pellets reacted at 750°C, in conjunction with a low rate of sintering, caused their surfaces to become soft and relatively porous. Hard surfaces were found at the higher reaction temperatures since sintering was more rapid and chlorine penetration considerably reduced.

9B3 Double bed experiments

The results of the double bed experiments are fully described in section 7C2. They show that the overall rate of the exchange reaction decreased with increasing temperature. However, since the results were not accurately reproducible they could not be analysed in detail. The features exhibited by the reacted pellets (see section 7C3) indicate that: a) the exchange

reaction rates were controlled by the diffusion of $ZnCl_{2(g)}$ through the ZnO shells and b) as the reaction temperature increased the ZnO shells became very much less porous. Information on the mechanism of the exchange reaction, which it was hoped might be provided by some of the double bed experiments, was not obtained since the chemical reaction process did not directly influence the overall reaction rates.

9B4 Reaction regimes

A number of different reaction regimes could explain the CdO/ZnO experimental results which are plotted on graphs 7B, 7C and 7D. Clearly established features of these experiments are a) the CdO reaction rate was reactant gas transport controlled; and b) pellet sintering and densification caused the CdO reaction rate to decrease with increasing reaction temperature. However, what was controlling the chlorine reaction rate cannot be conclusively deduced from the available experimental results. Illustrated in this section are the three different reaction regimes which could have been controlling the chlorine reaction rate, together with the experimentally established $ZnCl_{2(g)} + CdO_{(s)}$ exchange reaction regime. The common feature between these regimes is that chemical reaction of the CdO at the ZnO-CdO/ZnO boundary is very rapid. To simplify the discussion figures 9A, 9B, 9C and 9D are drawn for planar geometry.

Figure 9A is a representation of the mass transport reaction regime in a part of the bed where the chlorine bulk partial pressure is comparatively high. (This is the regime that is mathematically analysed and modelled in section 8B.) At the pellet surface there is thermodynamic equilibrium between $ZnO_{(s)}$, $Cl_{2(g)}$, $ZnCl_{2(g)}$ and $O_{2(g)}$; whilst at the ZnO-CdO/ZnO boundary there is thermodynamic equilibrium between $ZnCl_{2(g)}$, $CdO_{(s)}$, $CdCl_{2(g)}$ and $ZnO_{(s)}$. The chlorine surface partial pressure is effectively zero, the ZnO reaction rate (equal to the net reaction rate) is therefore exclusively controlled by the boundary layer chlorine mass transfer coefficient and the chlorine bulk partial pressure. Of the $ZnCl_{2(g)}$ generated at the pellet surface part diffuses through to the ZnO-CdO/ZnO boundary, the remainder is transported to the bulk gas. The rate of transport of $ZnCl_{2(g)}$ through to the ZnoO-CdO/ZnO boundary, which is the rate controlling step for the exchange reaction, is governed by three factors: a) the effective diffusivity of the $ZnCl_{2(g)}$ through the ZnO

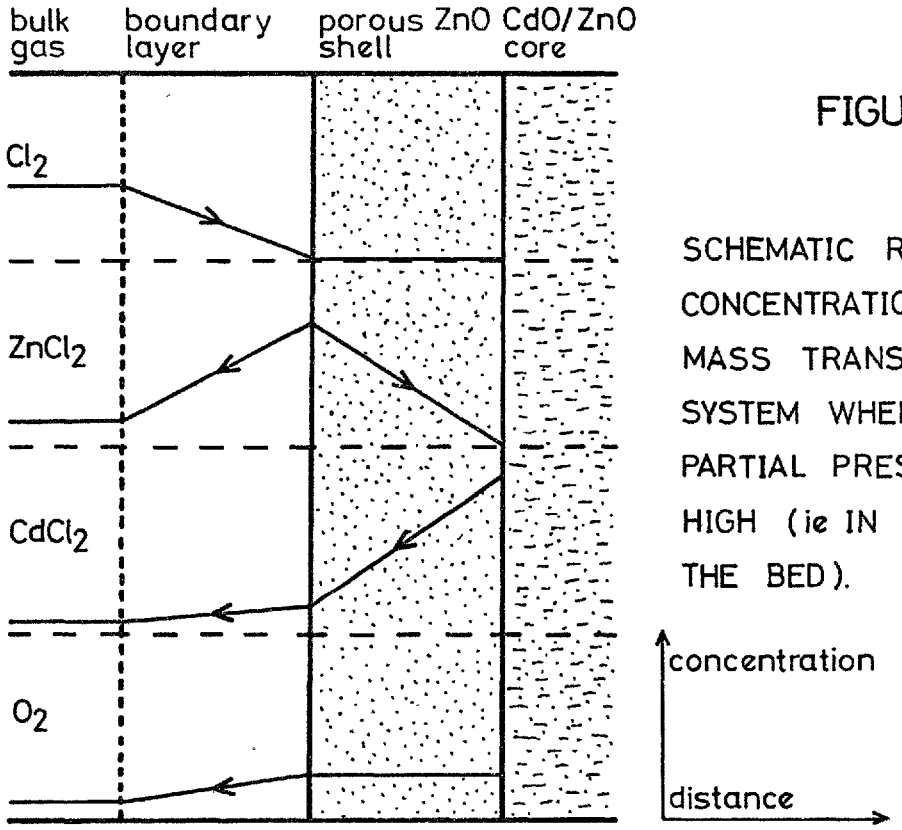

FIGURE 9A:

SCHEMATIC REPRESENTATION OF THE CONCENTRATION GRADIENTS IN A MASS TRANSPORT CONTROLLED SYSTEM WHEN THE CHLORINE BULK PARTIAL PRESSURE IS COMPARATIVELY HIGH (ie IN THE UPPER PART OF THE BED).

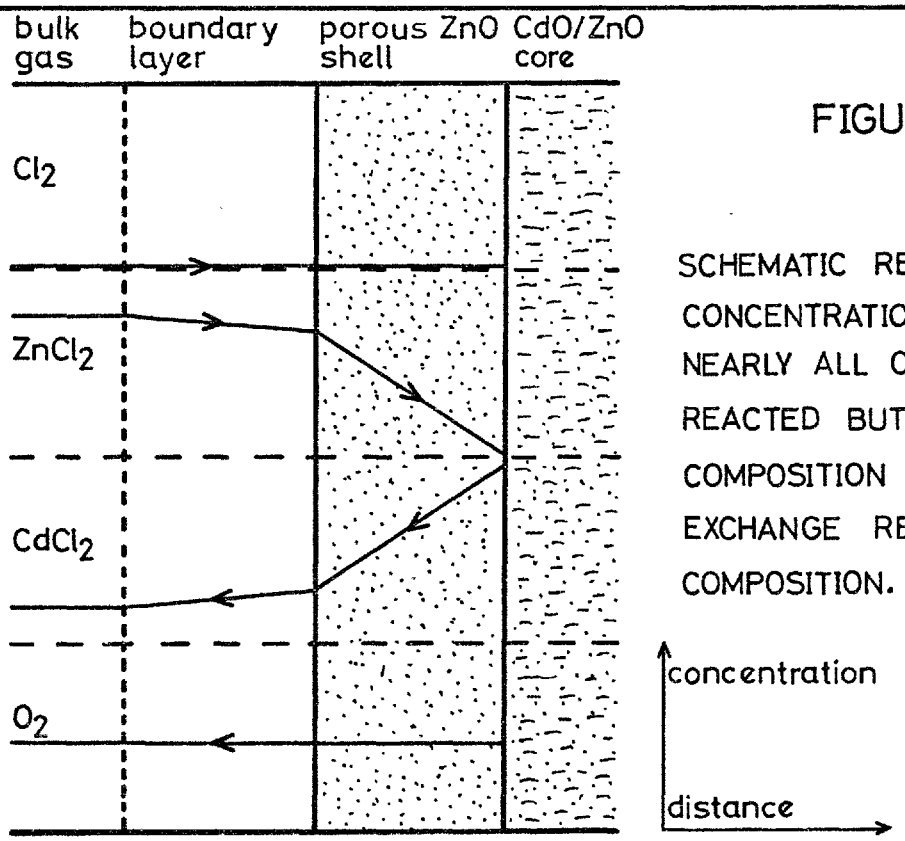

FIGURE 9B:

SCHEMATIC REPRESENTATION OF THE CONCENTRATION GRADIENTS WHEN NEARLY ALL OF THE CHLORINE IS REACTED BUT THE BULK GAS COMPOSITION IS NOT AT THE EXCHANGE REACTION EQUILIBRIUM COMPOSITION.

shell; b) the ZnO shell thickness, and c) the zinc chloride surface partial pressure (the zinc chloride partial pressure at the ZnO-CdO/ZnO boundary being effectively equal to zero). The first of these three factors is dependent only upon the physical structure of the porous ZnO and the molecular and Knudsen diffusion coefficients of the $ZnCl_{2(g)}$. The second factor is dependent upon the amount of CdO that has reacted. The third factor, for a given chlorine reaction rate ($\dot{n}''_{Cl_2}$), is very much dependent* upon the boundary layer zinc chloride mass transfer coefficient, (but effectively independent of the boundary layer oxygen mass transfer coefficient); a low coefficient causes the zinc chloride surface partial pressure to be high, conversely for a high coefficient. For the mass transfer control model to give reliable predictions for the region of the bed where the chlorine is reacting it is thus necessary to accurately know both $K_c^{Cl_2}$, $D^{eff}_{ZnCl_2}$ and $K_c^{ZnCl_2}$. Shown on graph 8L is a typical set of computer-predicted bulk partial pressure vs bed position curves for a bed in which all the chlorine is effectively reacted by about 1/4 distance (also see the last paragraph in chapter eight for full details on graph 8L). Graph 8L corresponds to 20.5 minutes of reaction, at this same time the following data was computed for a position $1/20^{th}$ the distance into the bed (bed entry P_{Cl_2} = 0.040 atmos, $K_c^{Cl_2}$ = 7.5 cm/sec, $K_c^{ZnCl_2}$ = 5.0 cm/sec and $D^{eff}_{ZnCl_2}$ = 0.015 cm^2/sec):- pellet diameter = 5.90 mm; ZnO shell thickness = 0.41 mm; $CdCl_2$, $ZnCl_2$ and Cl_2 bulk partial pressures 0.0026, 0.024 and 0.013 atmospheres respectively; $CdCl_2$, $ZnCl_2$ and Cl_2 surface partial pressures 0.0050, 0.040 and 0.00074 atmospheres respectively; $CdCl_2$ and $ZnCl_2$ interface partial pressures 0.044, and 0.0010 atmospheres respectively; $CdCl_2$, $ZnCl_2$ and Cl_2 surface to bulk fluxes 0.13 x 10^{-6}, 0.88 x 10^{-6} and 1.0 x 10^{-6} gm-moles/cm^2sec respectively. These data show that: a) the surface chlorine partial pressure is effectively zero; b) the interface** zinc chloride partial pressure is also effectively zero, and c) 88% of the $ZnCl_2$ produced at the pellet surface is transported to the bulk gas even though the ZnO shell is only 0.41 mm thick.

Figure 9B is a representation of the general reaction regime for the condition where nearly all the chlorine has reacted+ but the bulk gas is not at the exchange reaction equilibrium composition. (This is the reaction behaviour that occurs in what is termed the 'scrubbing zone' of the mixed

---

* It is also of course dependent upon factors a) and b) above.

** ZnO-CdO/ZnO interface

\+ Under either boundary layer mass transport or internal reaction-diffusion control.

oxide beds; this behaviour is also briefly described, with reference to the equilibrium experiments, in section 6A1b.) If the ZnO shell is very thin then the exchange reaction rate is controlled by the transport of $ZnCl_{2(g)}$ through the boundary layer (the $CdO_{(s)} + ZnCl_{2(g)}$ chemical reaction being very rapid, as is assumed in the first paragraph of this sub-section). This would be the case with mass transport controlled double bed experiments at the start of reaction. Once a CdO depleted layer of any thickness develops almost the entire resistance to reaction is due to diffusion of $ZnCl_{2(g)}$ through the porous ZnO (the lower 80% of the bed illustrated on graph 8L is reacting in this manner).

Figure 9C is a representation of the internal reaction-diffusion regime when the chlorine only penetrates a small distance into the ZnO. (The transition between the regime shown on figure 9A and that shown on figure 9C is caused by a reduced $ZnO_{(s)} + Cl_{2(g)}$ chemical reaction rate constant.) The overall reaction rate of the chlorine is mainly controlled by the combined effects of its low chemical reaction rate and its comparatively low effective diffusivity through the porous ZnO. The extent of chlorine penetration under this type of reaction control is discussed (in terms of $D^{eff}_{Cl_2}$, k_{Cl_2} and S_v) in section 8B1. $CdCl_{2(g)}$ is produced only by the reaction of $ZnCl_{2(g)}$ with CdO at the ZnO-CdO/ZnO boundary. This reaction is essentially transport controlled, its overall rate being equal to the overall rate of $ZnCl_{2(g)}$ production in the porous ZnO which is on the inner side of the maximum point in the zinc chloride partial pressure curve. A detailed mathematical analysis of this reaction regime would be very complex since in the region of the pellet where the chlorine reacts there is: a) simultaneous reaction and diffusion, b) bulk flow, c) a ZnO concentration gradient, and d) varying D^{eff} values. Fruehan and Martonik[51] (see section 1D2a) have observed internal reaction-diffusion control during the chlorination-volatilisation of single pellets/granules of NiO, Fe_2O_3 and $NiFe_2O_4$, they have not however mathematically analysed the reaction process. The reduction of iron oxides under this general type of reaction regime has been studied and analysed by Tien and Turkdogan[135]. Theoretical models for various internal reaction-diffusion controlled processes are given by Wen[120], Szekely[60] and Szekely and Evans[136]. The development of an internal reaction-diffusion control oxide chlorination-volatilisation reaction model would best be undertaken in parallel with single pellet thermogravimetric experiments. An approximate expression for the rate of chlorine reaction under the partial penetration regime can be developed from the analysis presented in section 8B1. The total chlorine reaction rate is equal to the total amount of chlorine which diffuses into the pellet at $r = R_p$. Under the conditions of reaction defined in

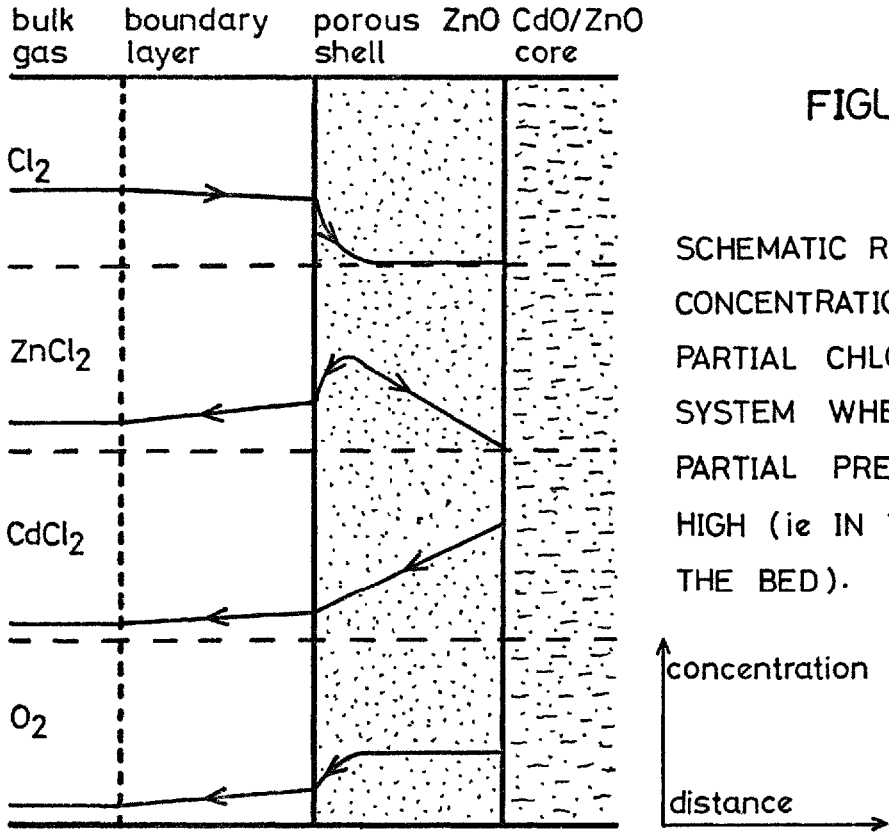

FIGURE 9C:

SCHEMATIC REPRESENTATION OF THE CONCENTRATION GRADIENTS IN A PARTIAL CHLORINE-PENETRATION SYSTEM WHEN THE CHLORINE BULK PARTIAL PRESSURE IS COMPARATIVELY HIGH (ie IN THE UPPER PART OF THE BED).

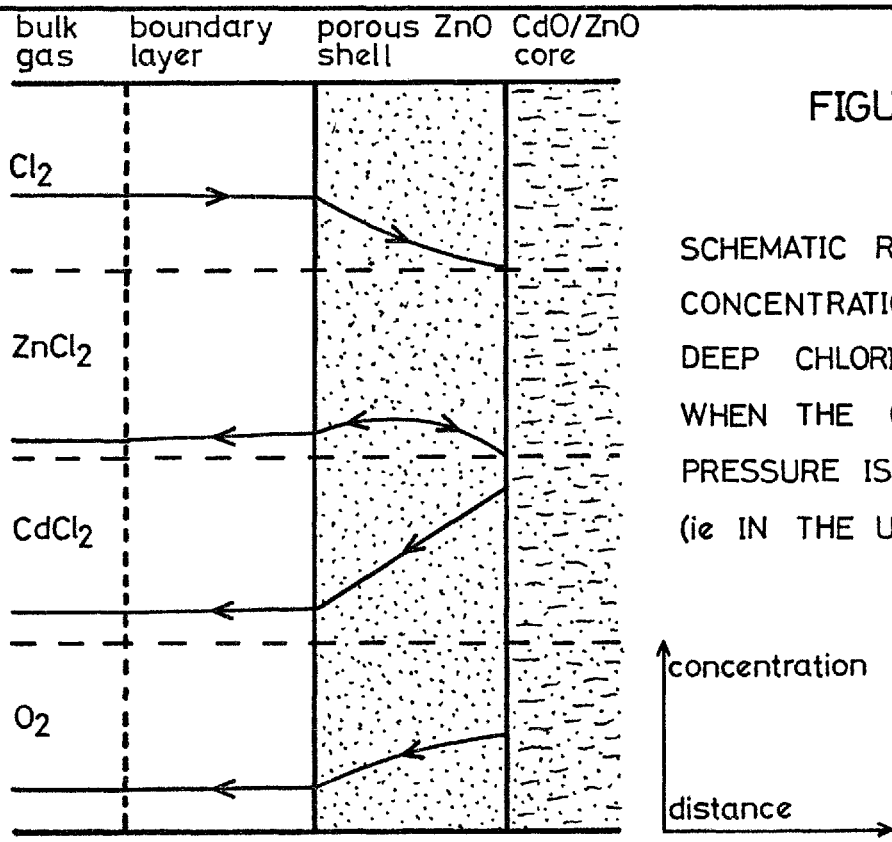

FIGURE 9D:

SCHEMATIC REPRESENTATION OF THE CONCENTRATION GRADIENTS IN A DEEP CHLORINE-PENETRATION SYSTEM WHEN THE CHLORINE BULK PARTIAL PRESSURE IS COMPARATIVELY HIGH (ie IN THE UPPER PART OF THE BED)

section 8B1 an analytical solution[117] for the Cl_2 concentration gradient at $r = R_p^*$ can be substituted into Fick's first law equation to give:

$$\dot{n}''_{Cl_2} = -\frac{s^P Cl_2}{RT} \cdot Th \cdot \frac{D^{eff}_{Cl_2}}{R_p} \cdot \left(\frac{1}{\tanh(Th)} - \frac{1}{Th} \right) \quad \ldots\ldots\ldots (1)$$

When Th = 2.65 tanh(Th) = 0.99, therefore with partial penetration (the Thiele moduli being large) the term in brackets is effectively equal to unity. Equation (1) thus reduces to:

$$\dot{n}''_{Cl_2} = \frac{s^P Cl_2}{RT} \cdot \left(k_{Cl_2} \cdot ZnO^{S_v} \cdot D^{eff}_{Cl_2} \right)^{\frac{1}{2}} \quad \ldots\ldots\ldots\ldots\ldots (2)$$

For a porous solid in which S_v and D^{eff} are constant (eg an unpoisoned catalyst) equation (2) is a very good approximation for Thiele modulus values of >5. However, in the case of partial penetration chlorination-volatilisation reactions, it is more approximate since S_v and D^{eff} are a function of position.

Figure 9D is a representation of the deep chlorine-penetration reaction regime. At the ZnO-CdO/ZnO boundary $CdCl_{2(g)}$ is formed from both $Cl_{2(g)}$ and $ZnCl_{2(g)}$. $ZnCl_{2(g)}$ and $O_{2(g)}$ are produced throughout the ZnO shell. The overall chlorine reaction rate, except at the start of reaction, is lower than with either of the other reaction regimes. The CdO reaction rate, however, is comparable with the other regimes since a) $Cl_{2(g)}$ has higher molecular and Knudsen diffusivities than does $ZnCl_{2(g)}$, and b) the chlorine partial pressure at the pellet surface is relatively high. As with the partial penetration regime, a mathematical analysis of the deep penetration regime would be very complex.

9B5 Mass transfer controlled reaction model

The reasons a mass transfer control model was developed in preference to a mixed control model are given in section 8B2. A critical assessment of the available experimental results shows that this model is not, however, applicable to the 750°C - CdO/ZnO chlorination experiments**. The following key results indicate that at 750°C although the CdO reaction rate was reactant gas transport controlled, the chlorine was reacting under a partial penetration internal reaction-diffusion regime (its reaction rate therefore being only partly controlled by diffusion through the boundary

---

* R = gas constant, R_p = pellet radius

** No computer runs were therefore performed for comparison with the results of the 750°C experiments.

layer): a) the overall rate constant computed from the 720°C granular - ZnO results (see section 7A3b) is considerably smaller than the packed bed mass transfer coefficients given in section 8B4; b) CdO/ZnO pellets reacted at 750°C developed thin, comparatively porous surface coatings; c) the figures given in table 7E suggest that the average chlorine utilisation with the 750°C - CdO/ZnO experiments was about 3% lower than with the 850 and 950°C experiments (utilisations with these higher temperature experiments, when the error in orifice C5 is accounted for, appear to have been 100%); d) the pellet size distributions found after the 750°C - CdO/ZnO experiments are not consistent with a boundary layer mass transfer controlled chlorine reaction rate.

All of the various assumptions and approximations made whilst developing the mass transport controlled reaction model are given at the relevant places in section 8B. An explanation of the boundary layer mass transport equations derived in section 8B6b is however relevant. The assumption that a solid whilst reacting with a flowing gas is surrounded by a stable gas film through which the reactant and product species diffuse is a mathematical simplification, employed since the complexities of the different transport mechanisms do not permit the formulation of rigorous equations. Mass transfer in gas-solid systems takes place by one or more of the following mechanisms: (1) molecular diffusion through a stable gas film, (2) diffusion into/out of naturally convected gas, and (3) diffusion into/out of forced convected gas. Various different theories[137] on the relative importance of these mechanisms exist. In a stationary gas only mechanism (1) operates, if the gas is not flowing but density differences exist mechanisms (1) and (2) operate, whilst if the gas is flowing all three may operate. Most mass transfer correlations for both single spheres and beds of spheres are of the form:

$$Sh = A + B.Re^{n} . Sc^{m}$$

In these correlations the Sherwood number is made up of a constant which accounts for mechanism (1) and a variable term which accounts for mechanism (3). A separate term to account for mechanism (2) is not normally incorporated since its contribution is comparatively small. For a single sphere the theoretical value of A is 2, this figure has been verified experimentally on a number of occasions. Values of B, n and m for single spheres and packed beds are given in section 8B4. Mass transfer coefficients over the surfaces of spherical objects in stationary gases are constant. However, since the extent and degree of turbulence around a spherical object

situated in a flowing gas varies with position, mass transfer coefficients incorporating forced convection contributions are average surface values. The transition between laminar and turbulent flow around a sphere starts to gradually occur at above about Re = 1. For gas flowing through a bed of spheres there is thus no sharp transition between laminar and turbulent flow. Since the pellet Reynolds numbers were always below about 10 the gas flows in the CdO/ZnO beds were probably part laminar and part turbulent. With the computer runs the boundary layer mass transfer coefficients were assumed to be independent of pellet size. This is thought to be a reasonable assumption, especially since the smallest pellets became misshapen and fell into the interstices between the larger pellets, thereby reducing their freely exposed surface areas. With a constant $K_c^{Cl_2}$ value for pellets exposed to a steady bulk chlorine partial pressure dr/dt = const.

9B6 Computer predictions vs experimental results

The $CdCl_2$ and $ZnCl_2$ rate vs reaction time plots given on graphs 8D and 8F illustrate that it is possible, by employing a suitable choice of transport coefficients, for the mass transport controlled packed bed reaction model to predict results consistent with the experimentally measured results given on graphs 7B, 7C and 7D. However, since some of the $K_c^{Cl_2}$ values employed in obtaining the curves on graph 8D are as much as perhaps an order of magnitude smaller than the values to be expected in the ZnO/CdO* beds, it is clear that obtaining reasonably good agreement between experimentally measured and computer-predicted $ZnCl_2$ and $CdCl_2$ rate vs. time curves is <u>not</u> confirmation that the chlorine reaction rate is mass transport controlled. This point is further illustrated by the fact that it would have been possible to obtain reasonably good agreement between 750°C - computer curves and the 750°C - experiment curves even though in the preceding section it is deduced that at this temperature the chlorine reaction rate was not primarily controlled by boundary layer mass transport. On the bases of comparisons between a) the computer - predicted chlorine utilisations given in section 8B7a and the 750°C chlorine utilisation given in

---

* As is shown in section 8B4, mass transfer coefficients in packed beds cannot be predicted accurately at low Reynolds numbers. However, it is thought that the $K_c^{Cl_2}$ values in the ZnO/CdO beds were around 4-8 cm/sec.

table 7E (after having accounted for an error of about 5% caused by orifice C5) and b) the 750°C pellet size distributions shown on plate 4 and the computer-predicted pellet size distributions plotted on graphs 8E and 8K, it is estimated that at 750°C the overall chlorine reaction rate constant ($\bar{k}_{Cl_2}$) was about 1 to 1.5 cm/sec. Using these same arguments for the 850°C and 950°C results it is estimated that their overall chlorine reaction rate constants were between about 4-8 cm/sec, and that at both these temperatures the chlorine reaction rate was therefore mass transport controlled.

The agreements shown between the various computer-predicted and experimentally measured $ZnCl_2$ and $CdCl_2$ rate vs. time curves shown on graphs 8G, 8H, 8I and 8J are good considering that a) each computer curve was calculated using a constant $D^{eff}_{ZnCl_2}$ value even though the pellets became progressively more densified during the course of the experiments, and b) in the computer model the CdO within each pellet reacted as a shrinking spherical core, whereas the structural examinations showed that the CdO frequently reacted in an asymetric manner. The $D^{eff}_{ZnCl_2}$ values used in computing the comparison curves are in each case less than the corresponding $D^{eff}_{ZnCl_2}$ values given in table 8D (these are the values that were estimated from the porosimetry results). However, the $D^{eff}_{ZnCl_2}$ values used in the 850°C computer runs and the estimated 850°C $D^{eff}_{ZnCl_2}$ values are in much closer agreement than are their 950°C counterparts; these values are compared below:

Experiment and graph number	Origin of data	$D^{eff}_{ZnCl_2}$ cm^2/sec
850°C-10.8 mole % CdO (8J)	Table 8D	0.029
	computer model	0.017
	computer model	0.015
850°C-26.6 mole % CdO (8H)	Table 8D	0.012
	computer model	0.008
	computer model	0.005
950°C-10.8 mole % CdO (8I)	Table 8D	0.0079
	computer model	0.0015
	computer model	0.0009
950°C-50.0 mole % CdO (8G)	Table 8D	0.018
	computer model	0.001

The larger disagreements between the $D^{eff}_{ZnCl_2}$ values at 950°C as compared with 850°C can be attributed to a) the 950°C pellets maintaining comparatively high bulk voidages despite having highly densified microstructures and b) the 950°C pellets developing virtually impermeable areas over their external surfaces.

On graph 8K are shown two typical pairs of computer-predicted pellet radius and interface radius vs. bed position curves (one pair of curves is from the $D^{eff}_{ZnCl_2} = 0.008$ cm^2/sec run on graph 8H, the other is from the $D^{eff}_{ZnCl_2} = 0.017$ cm^2/sec run on graph 8J). In general the computer-predicted core size distributions and the observed core size distribution (as illustrated on plates 5 and 8, and described in section 8A2a) were not in particularly good agreement. Within the range of transport coefficients investigated the computer model predicted that only very small pellets at the top of the beds would be completely depleted of CdO; whilst at the bed exit the ZnO shells surrounding the CdO/ZnO cores were predicted to be thicker than were observed. It is thought that these disagreements were mainly due to the computer model not accounting for changing $D^{eff}_{ZnCl_2}$ values as the reactions progressed.

As is apparent from the preceding discussion the results of the CdO/ZnO experiments did not provide sufficient information from which to determine accurately the overall chlorine reaction rate constant at each of the different reaction temperatures. Should an investigation on the chlorination-volatilisation of packed beds of mixed oxides be undertaken again, considerable advantage in understanding and quantifying the various reaction processes would be gained if, in conjunction with the packed bed studies, thermogravimetric studies were performed on the pure component oxides.

CHAPTER TEN

CONCLUSIONS

An experimental method for studying the chlorination-volatilisation of packed beds of compacts of mixed oxides has been successfully developed. Preliminary investigation of a proposal to analyse continuously gaseous metal chlorides by argon-plasma emission-spectrophotometry showed that a considerable amount of development work would be required before the potential of the technique could be assessed. The first part of the experimental program, the study of the chemical equilibria

$$ZnCl_{2(g)} + CdO_{(s)} = CdCl_{2(g)} + ZnO_{(s)}$$

$$CoCl_{2(g)} + ZnO_{(s)} + 1/6\ O_{2(g)} = ZnCl_{2(g)} + 1/3Co_3O_4(s)$$

$$CoCl_{2(g)} + ZnO_{(s)} = ZnCl_{2(g)} + CoO_{(s)}$$

by chlorinating CdO/ZnO, Co_3O_4/ZnO and CoO/ZnO mixtures, was very successful. Over the whole temperature range investigated (975-1345°K) the CdO/ZnO results were consistent and reproducible. The Co_3O_4/ZnO (1126-1228°K) and CoO/ZnO (1168-1339°K) results were also consistent but, in comparison with the CdO/ZnO results, somewhat less reproducible. Two possible causes for the lower degree of reproducibility are thought to be: a) the P_{ZnCl_2}/P_{CoCl_2} equilibrium ratios were comparatively large, and b) solid solubilities in the CoO-ZnO and Co_3O_4-ZnO systems are more extensive than in the CdO-ZnO system. Experimental investigations on the CdO/CoO and CdO/Co_3O_4 systems, as a means of establishing consistency between the CoO/ZnO, Co_3O_4/ZnO and CdO/ZnO results, were not possible since the P_{CdCl_2}/P_{CoCl_2} equilibrium ratios would have been too large (typically between about 9000 and 3000) to measure accurately. Results were obtained which are in good agreement with the 1/6th power oxygen partial pressure dependence of tne chlorination of Co_3O_4/ZnO mixtures. There is no evidence to suggest that significant quantitites of either gaseous chloride polymers or gaseous chloride complexes were present in any of the three systems studied. By combining the experimentally determined free energy data with thermodynamic data from the literature it has been possible to calculate the standard free energy changes of the CdO + Cl_2, 1/3 Co_3O_4 + Cl_2 and CoO + Cl_2 reactions. The standard free energy of formation of $CoCl_2$ (solid, liquid and gas) as quoted in a number of thermodynamic data reviews, is shown to be about 3 Kcals/mole to large (-ve sense). From a review of the literature it is evident that the values of the standard free energies of formation of the oxides of Cd, Zn and Co are more accurately known than are the values for their chlorides.

Experiments on the kinetics of the chlorination of packed beds of ZnO and CdO/ZnO compacts were more difficult to perform, and analyse, than were the equilibrium experiments. In terms of the amount of quantitative rate data obtained for the amount of effort expended the granular-ZnO chlorination experiments were not particularly productive. Thermogravimetric analysis would appear to be the best technique for fundamental investigations into the kinetics of the chlorination of single oxides. At 705°C the ZnO + Cl_2 reaction was found to be chemically controlled. The results obtained at the highest temperature studied, 873°C, are inconclusive. However, boundary layer mass transport appears to have been at least partly influencing the overall reaction rate. The results of the CdO/ZnO chlorination experiments were governed by the following factors:

a) At 750°C chlorine penetrated only a small distance into the pellets, penetration decreased with increasing temperature.

b) Except when CdO was present either at or close to the external surface of the pellets in gas containing unreacted chlorine, $CdCl_2$ was produced by the exchange reaction

$$ZnCl_{2(g)} + CdO_{(s)} = CdCl_{2(g)} + ZnO_{(s)}$$

c) The rate of this reaction was controlled by transition region diffusion of $ZnCl_{2(g)}$ through porous ZnO.

d) Pellet sintering and densification caused the effective diffusivity of the $ZnCl_{2(g)}$ and therefore the efficiency of separating the cadmium from the zinc, to decrease with increasing reaction temperature.

e) Structural inhomogeneities formed during pelletisation and intensified by sintering caused asymetric reaction of the CdO.

A mass transfer control reaction model was developed in order to help analyse the CdO/ZnO results. Predictions made by this model, in conjunction with various experimental observations, show that a) at 750°C the chlorine reacted under a partial penetration internal reaction-diffusion control regime, and b) the chlorine reaction rates at 850 and 950°C are consistent with boundary layer mass transfer control. Effective diffusivity values based on the results of the porosimetry tests performed on the 950°C reacted pellets were inaccurate since although the pellets were porous, the pellets developed barriers to diffusion.

FUTURE WORK

The standard free energy changes of the $CoO + Cl_2$ and $1/3\ Co_3O_4 + Cl_2$ reactions could be studied by using the direct experimental metnod described in section 1C2. This would be a comparatively simple way of checking the cobalt oxides data presented on graph 6B. This direct method could also be used for the oxides Fe_2O_3 and NiO, and under reducing conditions (CO/CO_2 mixture) for Fe_3O_4. Some of the oxide pairs whose exchange reaction equilibria it might be possible to measure by using the same technique as used in this study are: a) without reducing conditions PbO/CdO, PbO/ZnO, ZnO/MnO, MnO/CoO, NiO/MnO, CoO/NiO, Fe_2O_3/CoO, Fe_2O_3/Co_3O_4 and NiO/Fe_2O_3; and b) with reducing conditions (CO/CO_2 mixture) MnO/FeO, NiO/Fe_3O_4 and CoO/Fe_3O_4. The technique could however encounter some difficulty with systems in which there is extensive solid solubility.

Thermogravimetric studies on the kinetics of ZnO and CdO chlorination would be of very considerable relevance to the results presented in this thesis. Such studies could lead to the development of a mathematical model of the internal reaction-diffusion control regime. With this type of model, together with a mass transfer model similar to that used in the present work, it should be possible to make reasonable predictions of the rates of chlorination of admixtures of oxides using data obtained from studying each component oxide.

L I S T O F S Y M B O L S

$\mathring{A}$	angstrom = 10^{-8} cm
a_i	activity of species "i"
b(subscript)	bulk
bpt	boiling point
^oC	temperature - degrees centigrade
c_i	concentration of species "i"; gm-mole/cm^3
C_p	specific heat at constant pressure; cals/gm-mole^oK
D_{ij}	binary diffusivity; cm^2/sec
D_{im}	effective "binary" diffusivity of species "i" in mixture "m"; cm^2/sec
D_{ij}^{eff}	effective binary diffusivity; cm^2/sec
$D_{k,i}$	knudsen flow coefficient of species "i"; cm^2/sec
$D_{k,i}^{eff}$	effective knudsen flow coefficient of species "i"; cm^2/sec
D_i^{eff}	effective diffusivity of species "i"; cm^2/sec
d	diameter; cm
d_p	pellet diameter; cm
dx	length of differential element; cm
$(\frac{\partial x}{\partial y})$	partial differential
ΔG^o	standard free energy change; cals/gm-mole
ΔH^o	standard enthalpy change; cals/gm-mole
ΔH_{evap}	latent heat of evaporation; cals/gm-mole
ΔH_{fusion}	latent heat of fusion; cals/gm-mole
ΔH_{sub}	latent heat of sublimation; cals/gm-mole
ΔP	pressure drop (units defined locally)
ΔS^o	standard entropy change; cals/gm-mole^oK
ΔT	temperature change; degrees centigrade
ϵ	void fraction; dimensionless
f_i	fugacity of species "i"; atmospheres
(g)	gas
i (subscript)	interface
J	joules equivalent; joules/cal
J_i	Diffusion flux of species "i" relative to the plane of no net molar transport; gm-mole/cm^2 sec

k_i first order chemical reaction rate constant for species "i"; cm/sec

$\bar{k}_i$ overall reaction rate constant for species "i"; cm/sec

^oK absolute temperature; degrees Kelvin

K_c^i mass transfer coefficient for species "i" (excludes the effect of bulk flow); cm/sec

$\bar{K}_c^i$ mass transfer coefficient for species "i" (includes the effect of bulk flow); cm/sec

K equilibrium constant

K_f equilibrium constant expressed in terms of fugacity

K_p equilibrium constant expressed in terms of partial pressure

L distance; cm

(l) liquid

M_L mass per unit bed length; gm/cm

M_i molecular weight of species "i"

M mass; gm

m (subscript) mixture

mls_{NTP} millilitre volume at 0^oC - 760.0 mm Hg

mpt melting point

N_i mole fraction of species "i"

n_i moles of species "i"; gm-moles

$\dot{n}_i$ molar rate of species "i"; gm-moles/sec

$\dot{n}_i''$ molar rate per unit area of species "i"; gm-moles/cm^2sec

nm nanometre = 10^{-9} metres

P total pressure; atmospheres

P_i partial pressure of species "i"; atmospheres

^xP_i bed exit partial pressure of species "i"; atmospheres

ρ density; gm/cm^3

R gas constant

R_p pellet radius; cm

r radius; cm

Re Reynolds number = $\rho_m \cdot U_o \cdot d_p/\mu_m$; dimensionless

Sc Schmidt number = $\mu_m/\rho_m \cdot D_{im}$; dimensionless

Sh Sherwood number = $K_c^i \cdot d_p/D_{im}$; dimensionless

Th Thiele modulus for first order reaction and spherical geometry = $R_p(k_i \cdot S_v/D_i^{eff})^{\frac{1}{2}}$; dimensionless

s (subscript) surface

(s) solid

S_M specific surface; cm^2/gm

S_x	surface area per unit bed depth; cm^2/cm
S_v	specific surface; cm^2/cm^3
T	temperature; ^oK (unless otherwise stated)
t	time; seconds
τ	tortuosity; dimensionless
U_o	superficial gas velocity; cm/sec
μ_i	viscosity of species "i"; gm/cm sec
μ_m	viscosity of mixture "m"; gm/cm sec
μ	10^{-6} metres
μm	10^{-6} metres
V	volume; cm^3
w	mass; gm
x	distance; cm

LIST OF CONSTANTS AND CONVERSION FACTORS

NTP molar volume of ideal gas	22414 mls
NTP molar volume of $Cl_{2(g)}$	22063 mls
NTP molar volume of $O_{2(g)}$	22392 mls
NTP molar volume of $N_{2(g)}$	22403 mls
NTP molar volume of $Ar_{(g)}$	22390 mls
Gas constant R (for thermodynamic calculations)	1.9872 cals/^{o}K gm-mole
Gas constant R (for mass transfer calculations	82.057 atmos. cc/gm-moles ^{o}K
Joules equivalent J	4.1868 joules/cal
Faradays constant F	23066 cal/volt
Molecular weight of Zn	65.38
Molecular weight of Cd	112.41
Molecular weight of Co	58.94
Molecular weight of Cl_2	70.91
Molecular weight of O_2	32.00
Molecular weight of N_2	28.02
Density of $CdO_{(s)}$	8.15 gms/cc
Density of $ZnO_{(s)}$	5.61 gms/cc

prefix n 10^{-9}

prefix μ 10^{-6}

prefix m 10^{-3}

prefix c 10^{-2}

prefix K or k 10^{3}

1 inch = 25.4 mm

1 standard atmosphere = 101.325 kN/m^2 = 760.0 mm Hg

A P P E N D I X A

ON LINE ANALYSIS OF GASEOUS METAL CHLORIDES BY ATMOSPHERIC-PRESSURE MICROWAVE-INDUCED ARGON PLASMA EMISSION SPECTROPHOTOMETRY

A1 Introduction

In the literature there are reports on the use of argon plasmas at both atmospheric[69,71] and reduced pressure[70] for trace analysis of metal species. The systems used have employed flowing argon gas to which is added, prior to the plasma, a small liquid sample containing the metal to be determined. In passing through the plasma the metal moves into an atomic state with an electronic excitation temperature as high as 10,000°K; under these conditions it emits its characteristic emission spectra. This radiation is collected, and by using a monochromator-photomultiplier system the emission intensity of specific lines can be measured and recorded. By suitable calibration the system can then be used for sample analysis; reported[69] detection limits are extremely good with Cd at 2.0×10^{-13} gms and Zn at 8.0×10^{-11} gms.

A2 System used for feasibility study

A schematic diagram of the complete apparatus as used for the investigations on flowing argon plasmas containing traces of zinc vapour is shown on figure A1. The same apparatus, without the small furnace, was also used for studying the characteristics of flowing argon plasmas and Ar/Zn and Ar/Cd discharge tubes.

A3 Plasma production apparatus

Plasma support was by a magnetron value operated Microtron 200* microwave power generator. Its fixed operating frequency is 2450 MHz (12.25 cms) with a maximum output of 200 watts incident power. In order not to damage

---

* Microtron 200 Mk II EMS200L Electro-Medical Supplies Ltd.

SCHEMATIC DIAGRAM OF PLASMA EMISSION APPARATUS

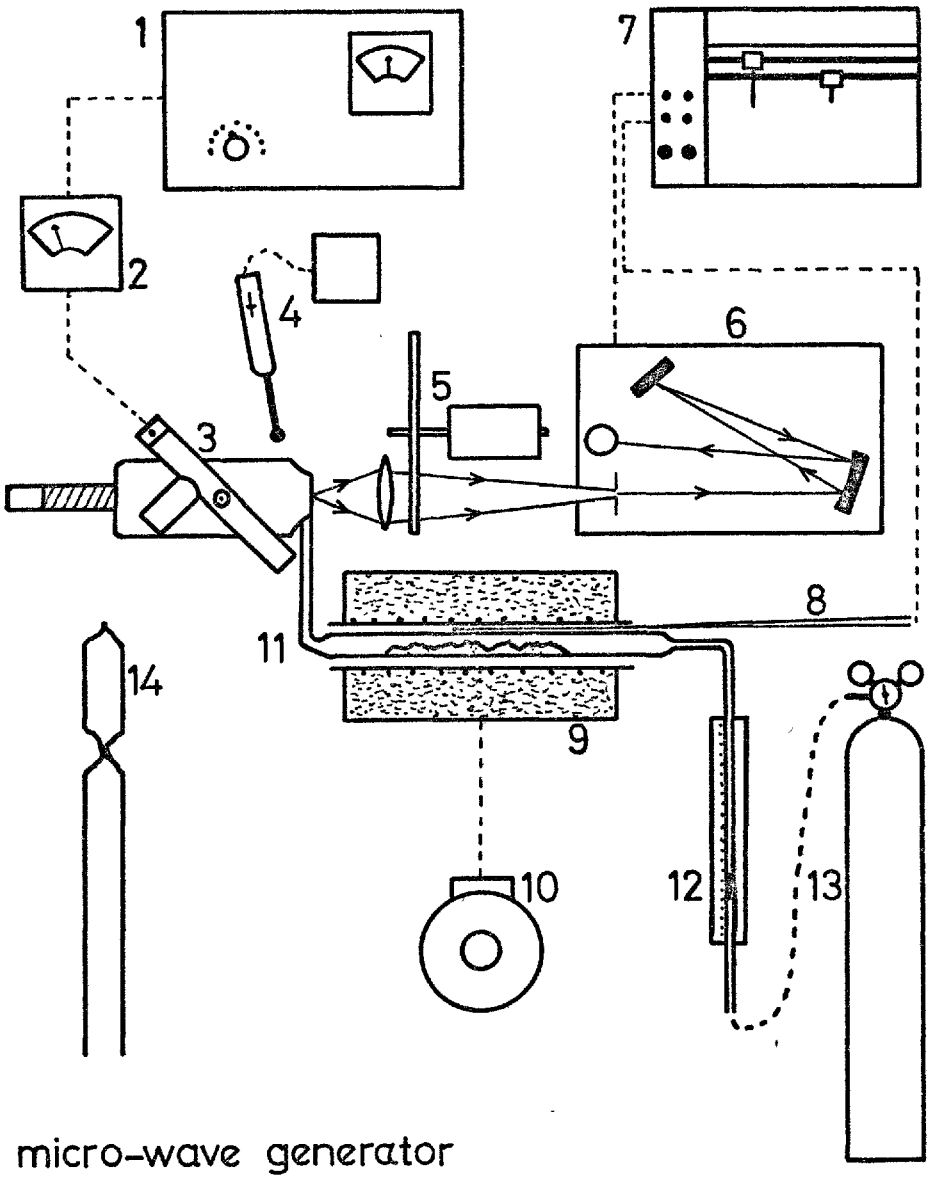

1 micro-wave generator
2 reflected power meter
3 1/4 wave resonant cavity
4 tesla coil
5 chopper
6 monochromator-detector system
7 pen recorder
8 thermocouple
9 furnace
10 variac
11 silica tube containing ZnO powder
12 rotameter
13 argon
14 discharge tube

FIGURE A1

the magnetron valve a reflected power meter* is placed between generator and resonant cavity, the reflected power limit is 50 watts. Power was coupled with the plasmas using a variable tuning resonant cavity. Two types were used in the study, a 3/4 wave** and 1/4*** wave cavity, the second type gives greatest coupling, this cavity is shown in figure A1. Power transmission between generator, reflected power meter and cavity involved using a special coaxial cable. Two types of configuration were used for the flowing gas plasmas. In one kind the plasma was entirely contained inside a vitreosil (silica) tube placed inside the cavity, the gas flow being vented to the atmosphere through the open end of the tube about 5 cms above the cavity. Vitreosil is transparent to visible spectrum radiation, its presence between the spectral source and detector system therefore produced no interfrerence. With argon flows containing Zn vapour, plating out inside the silica tube was a problem, to overcome this effect the silica tube was cut off just below the middle of the cavity. The argon plasma then extended a few millimetres out of the top of the tube into free space. The size of plasmas so formed were smaller than ones contained in a tube; this size reduction was caused by air entrainment. Small sealed discharge tubes did not suffer from plating out as after a short running period they became sufficiently hot to prevent deposition. Plasmas were initiated by running a tesla coil next to the cavity whilst about 100 watts incident power was applied from the generator.

A4 Optical system

Spectral emissions from the plasmas were studied using the flame emission operating mode of a Perkin Elmer 290B atomic absorption spectrophotometer; the output from this instrument was chart recorded using a Smiths Servoscribe 2 pen recorder. In the instrument's optical system, light is collected by an objective lens which focusses an image on to a narrow slit

---

* EMS2002L

** 210L

*** 214L Electro-medical Supplies Ltd.

leading into the monochromator, the lens aperture is approximately f/6. Light passing to the slit is modulated into the form of an approximate square wave by a motor driven chopper; this allows the instrument's AC amplification circuit to be used. The slit, acting as an intense line source to the monochromator system, permits light to fall onto a concave mirror which reflects a parallel beam onto a Littrow grating. At the grating, a reflection type, spectral dispersion occurs. All incident light of the same wavelength is diffracted through the same angle consequently all light of a specific wavelength leaves the grating as a parallel beam. This diffracted light returns to the concave mirror and is thus focussed as a series of images of the entry slit, each being of a different wavelength light, the limit of resolution is governed by a combination of the grating ruling (1800 lines/mm) and the incident slit width. In the plane of the monochromated images is a second slit of equal width to the first, behind it is a photomultiplier tube which measures the total intensity of any incident radiation. The spectral dispersion of the monochromated slit images is approximately 16 Å/mm (1600 nm/m), with the smallest slits in position the spectral resolution of the instrument could be reduced to 2Å (0.2 nm). Although this is insufficient resolution for line spectra from complex emissions, it is adequate for the characteristic emission spectra of many metals since their prominent lines are often comparatively few in number. Different 2Å wide sections of any suitable spectrum could be brought to the fixed photomultiplier tube by rotating the grating. The system could thus be used either to continuously monitor a 2Å wide section of any light source, or to scan over a range of wavelengths with a resolution of 2Å. Automatic scanning could be carried out using a reversible electric motor with variable gearing, connnected to the grating rotation mechanism. Scan speeds of between 4Å/min and 40Å/min were possible with standard Perkin Elmer equipment. Had the technique been fully developed, an automatic unit would have been designed to give any desired scanning programme; this would be necessary for metals with widely spaced determination lines.

A5 Gases

The argon gas used to make the plasmas was British Oxygen Company (BOC) high purity grade; for most of the flow system experiments it was taken directly from the cylinder regulator and delivered via a rotameter. The exception to this procedure was when Ar/O_2 mixtures were under test. Here the Ar and O_2 (BOC N_2 free grade) were delivered from the chlorinating gas train described in section 3E.

A6 Silica tubes

For unseeded flowing argon plasmas Vitreosil tubes of 10, 5, 3 and 1.8 mm bore were used at the resonant cavity. For the Zn seeded flow system a 5 mm ID tube was used in the furnace; this led into a 1.8 mm tube which ended just below the centre of the cavity. Discharge tubes were made from 10 mm ID tubing.

A7 Discharge tubes

The Zn and Cd discharge tubes contained argon gas at approximately 3 torr pressure inside a sealed 15 mm longbulb of vitreosil tubing. Prior to pump down about 20µgm of either $ZnCl_2$ or $CdCl_2$ was added to the tubes.

A8 Zn/Ar flow system and furnace

Zinc chloride was not used for these tests since control of its vapourisation rate into the flowing argon could not be easily achieved. As only a trace quantity of metal atoms was required, these were obtained by thermally decomposing ZnO into the argon stream. The silica tube inside the furnace was half filled along its length with analytical grade zinc oxide powder. This was held in place by silica wool end plugs. Argon gas was thus able to flow over the top of the powder and pick up gaseous Zn and O_2. The decomposition reaction is given below together with the relevant thermochemical data[3].

$ZnO(s) = Zn(g) + \frac{1}{2}O_2(g)$ . . . . . (a)

$\Delta G^\circ_T = 483240 + 43.3\ T \log T - 344.9T$ joules/mole

$T_{\text{evaporation Zn (1 atmos)}} = 907^\circ C$

To calculate the zinc content in the flowing argon gas entails several assumptions:

1. that the pure argon was oxygen free
2. that the zinc was only volatilised as Zn atoms
3. that no ZnO powder was picked up
4. that equilibrium was achieved for reaction (a).

By using the ΔG°_T data given above, the reaction stoichiometry and a ZnO activity of unity, P_{Zn} and corresponding Zn concentration values have been calculated for various temperatures, this data is given below in table A1.

$T^\circ C$	P_{Zn} Atmos.	Zn concentration moles/cc	gms/cc
900	1.36×10^{-7}	1.41×10^{-12}	9.22×10^{-11}
1000	1.61×10^{-6}	1.54×10^{-11}	1.00×10^{-9}
1100	1.32×10^{-5}	1.17×10^{-10}	7.65×10^{-9}

TABLE A1: Equilibrium Zn concentrations

Of the assumptions, 2. and 3. are probably most valid, 1. is probably a good approximation and 4. is likely to be incorrect. The net effect is that lower zinc contents than those calculated were actually being studied; the detection limit of the system, bearing in mind these considerations, was thus extremely good.

The furnace tube was 11 mm in bore and 100 mm long, heating was by 'Nichrome' electric resistance wire, the current being supplied and controlled via a 'Variac'. 'Triton Kaowool' and asbestos string were used for insulation. The temperature in the furnace could be recorded from a Pt - Pt 13% Rh thermocouple.

A9 Emission spectra

The argon spectrum produced in the plasma consisted of a continuous low-intensity stable background emission upon which were superimposed a number of prominent lines known as the argon blue series. Zinc and cadmium gave only their characteristic line spectra; under the prevailing conditions of excitation these are relatively simple for both metals. Various unresolved bands were recorded in certain spectral regions, these were probably molecular spectra caused by the presence of O_2, N_2 and H_2O. They produced no interference in the areas of interest.

In table A2 given below are shown the wavelengths and relative intensities of prominent lines from the emission spectra of Cd, Zn and Ar; this data is taken from references 72 and 73.

Argon	Cadmium		Zinc	
Wavelength nm	Wavelength nm	Relative Intensity	Wavelength nm	Relative Intensity
415.8	214.438*	60	213.856*	1000**
418.1	226.502*	110	307.590*	26
419.1	228.802*	1500**	328.233	20
420.0	326.106*	32	330.259	90
427.2	340.365	80	330.294	28
430.0	346.620	250	334.502	140
462.8	346.766	80	334.557	30
470.2	361.051	360	468.014	40
	361.288	70	472.216	100
	467.816	80	481.053	140
	479.992	140		
	508.582	280		
	643.847	26		

* Resonant lines
** Raies Ultimaes

TABLE A2: Ar, Cd and Zn line spectra

Resonant lines emanate from electron transitions involving the ground state. In flames and low power plasmas most atoms tend to be in the ground state and consequently resonant lines are the most intense. In agreement with the data in table A2, the 213.856 nm Zn line and the 228.802 nm Cd line were found to be most intense under all experimental conditions.

A10 Experimental observations

The experiments carried out were largely qualitative in nature, important findings will now be briefly outlined.

A11 Characteristics of argon plasmas

The work described under this heading was performed using the 3/4 λ cavity with 10, 5, 3 and 1.8 mm bore, long vitreosil tubes. Measured argon flow rates were from 2.5 litres/min down to approximately zero, the gas being taken via a rotameter direct from the cylinder.

A11a Initiation

Plasma initiation using the tesla coil was always possible at about 100 watts incident power except when argon flows were lower than about 80 mls/min. At the lowest flows 200 watts, the maximum available power, did not support a plasma; these low flow effects were probably due to the entry of diatomic gaseous impurities by diffusion or entrainment.

A11b Tube size

Plasmas produced in the larger tubes (10 and 5 mm) consisted of a number of unconnected vibrating low intensity blue filaments in line with the tube axis; these filaments were not symmetrically spaced either with respect to each other or the tube axis. With high power inputs up to five could be obtained whilst at just above the extinction power only one was present. With smaller bore sizes progressively more stable, higher intensity, single filament blue plasmas were produced; at 1.8 mm bore the plasma was axi-symmetric and nearly filled the tube.

A11c Power input

In general it was found that high power inputs gave the least stable plasmas, this effect being most pronounced with larger tubes. Plasma intensities always increased with raised power input; this effect was most pronounced with small tubes. As the power input was increased the plasmas would extend out of either end of the cavity, in this way excitations of up to 100 mm long could be obtained. Plasma extinction was fairly insensitive to most variables, always occurring at between 20 and 30 watts.

A11d Gas flows

The most surprising aspect of gas flow variation was that once initiated the plasma could not be 'blown out' even by as much as about 5 litres/min (nominal velocity - 32.5 m/sec) flow through the smallest tube with only low incident power input. Relatively low gas flows (500-100 mls/min) produced wide, stable, intense plasmas; the converse was so for high flows (>500 mls/min). Flows lower than about 100 mls/min produced very intense plasmas; as extinction was approached, their colours changed from blue to green and finally to orange.

A11e $1/4\lambda$ cavity, tuning and temperature

With the $1/4\lambda$ cavity, general effects were found to be the same as described above. There were two main specific differences between the cavities. The better coupling $1/4\lambda$ type not surprisingly gave higher intensity emissions, also it was more sensitive to tuning and to the positioning of the silica tube. The increase in heat content of the argon after passage through the cavities can only be estimated since actual temperature rises were not recorded. A simple calculation indicates that very high gas enthalpies were possible. For a gas flow of 1 litre/min, assuming a coupled power of 50 watts and using a Cp argon value of $5R/2$ the calculated temperature rise is approximately $3500^{\circ}K$. The great uncertainty inherent in this calculation is due to the estimate of coupled power. It is very probable that only a small fraction of the incident power actually couples with the argon; most lost power is dissipated in

the metal cavity. The remainder is reflected back to the generator. Under all operating conditions the cavities gradually heated up; it is estimated that at steady state the 1/4λ type may on occasions have reached about 300°C. At high power/flow ratios the smallest silica tube could be made to glow red hot at the cavity centre (1/4λ). On the basis of actual observations it would thus seem that the plasmas, under certain operating conditions, obtained high thermal temperatures; however, the power coupling efficiency of both cavities appears to have been relatively low. An excessively high enthalpy content produces doppler broadening of emission lines; with simple spectra this is not a real problem unless the temperature is unsteady.

A11f Ar/O_2 plasmas

The effects of oxygen additions to the Ar gas were studied under several conditions, using the 1/4λ cavity. The experiments were carried out by firstly setting up a free venting pure argon plasma using a 2 mm bore tube. The 427.2 nm argon line intensity was then continuously recorded as gradually increasing oxygen additions were made to the argon. The influence of oxygen was much the same under all conditions. The 427.2 nm line intensity was very much reduced by small oxygen additions. Under no conditions could a plasma be maintained with more than a 5% O_2 content. Increasing the power input did not raise the lowered intensity emission by any significant amount.

A11g Observed spectra

The spectra obtained from the Cd and Zn lamps and the flowing argon were as expected. Resonant lines were the most prominent; some close lines were not separately resolved.

A11h Observations from Zn/Ar flow system

Graph A1 shows two curves obtained from a Zn/Ar experiment. One curve gives the temperature measured at the furnace centre whilst the other

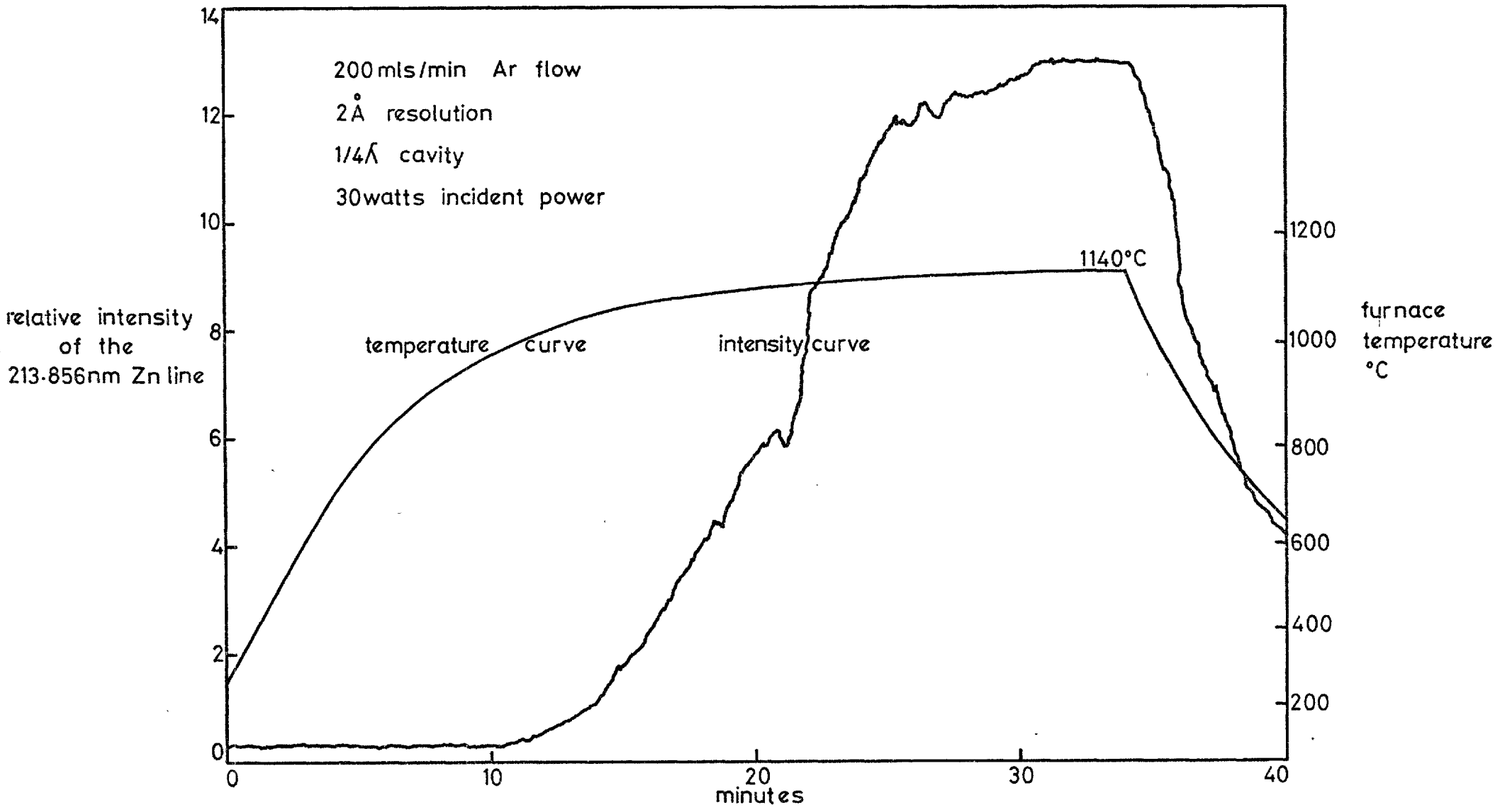

GRAPH A1: Zn/Ar FLOW SYSTEM FURNACE TEMPERATURE AND EMISSION INTENSITY CURVES.

gives the relative intensity of the 213.856 nm Zn line; both curves correspond to each other with respect to time. The final temperature that the furnace reached was 1140°C. At this steady state a constant emission intensity was recorded. From the behaviour of the curves it is evident that no Zn was carried into the plasma as ZnO powder; only after the furnace temperature reached 1000°C did significant quantities of Zn become vapourised. On switching off the furnace the emission intensity was not related to temperature in exactly the same way as during heat up; this was probably due to a memory effect.

A12 Application to gaseous chloride systems

Whether the technique just outlined can be applied to continuous analysis of gaseous metal chloride mixtures depends upon two major factors. The development effort required to overcome these two potential problems was at the time of the study judged to be too great to warrant continuation of the work.

The first of these two problems is essentially one of designing and engineering an integrated apparatus which connects a chlorination section to an analytical section. Since analysis of full reactor flows would not be possible, controlled flow splitting would be needed so as to let only trace quantities of volatile chlorides reach the plasma. To prevent condensation the whole gas flow route would need to be at high temperature; with very low chloride partial pressures the temperatures involved would be near to the respective chloride melting points; even so this might require 600°C to 800°C. With consideration to the instrumentation, continuously monitoring more than one species would require either rapid scanning or two detector systems. It is felt that these engineering problems can be solved. The success of the technique, therefore, mainly rests upon devising a suitable method for calibration. Calibration is necessary since even using a photon counter the method is not absolute. No suitable answer to this problem was found during the time that the technique was under consideration; however, using a tracer technique would seem to be one possible solution.

APPENDIX B

OXIDE-SILICA COMPATIBILITY TESTS

Nominal temp °C	Holding time hrs	Observations on oxide-silica interaction	
700	4.0	CdO	no effect
		ZnO	no effect
		Co_3O_4	no effect
780	3.25	CdO	no effect
		ZnO	no effect
		Co_3O_4	slight whitening of silica
830	7.0	CdO	no effect
		ZnO	no effect
		Co_3O_4	slight blue coloured devitrification
880	3.5	CdO	no effect
		ZnO	no effect
		Co_3O_4	crazed surface; deeper blue
930	6.0	CdO	no effect
		ZnO	no effect
		CoO	surface spalling
980	7.0	CdO	slight smoking of surface
		ZnO	some devitrification
		CoO	serious spalling
1030	6.0	CdO	more smoking of surface
		ZnO	serious devitrification
		CoO	incompatible
1080	5.0	CdO	smoked surface - no devitrification
		ZnO	incompatible
		CoO	incompatible
1140	3.0	CdO	smoked surface - no devitrification
		ZnO	incompatible
		CoO	incompatible

APPENDIX C

C1 FLOW METER MECHANICS

Contrary to popular belief, the orifice meter design used in this study is not the type that is normally referred to in texts on fluid flow measurement. A true orifice meter, flow nozzle or venturi meter causes moving fluid to be accelerated through a constriction placed in the flow line. With conventional meters the volume flow rate of the fluid is related to the pressure differential between the slow and fast moving fluid regions by a mechanical energy balance; potential energy changes due to gravitational acceleration are usually negligible. With proper pressure tappings these meters work for virtually any fluid. The ideal fluid is of course inviscid and incompressible. With this fluid, the sum of the pressure energy and kinetic energy of any volume element is constant and independent of position. Therefore, if the constriction is situated in a constant bore tube no permanent pressure loss occurs between undisturbed upstream and downstream regions. With real fluids, some energy is lost through the existence of local velocity gradients within the fluid. In the region of converging flow where fluid is being accelerated, losses are usually small. The flow rate - pressure drop relationships are thus adjusted by various coefficients which account for the small amounts of energy lost (as heat) between the points of maximum pressure differential. With an orifice it is in the region of diverging flow after the constriction that most of the overall energy loss occurs, here fast moving fluid entrains stagnant fluid thus forming eddies. These eddies cause a mechanical energy loss which is manifested as a permanent pressure drop between the pre-orifice and developed downstream flows.

The 'orifice' meters used in this study depend upon viscous gases to generate the pressure differences that are recorded. If an inviscid fluid could be used with these meters no pressure drop would occur between the pressure taps incorporated in the design. Figure C1 clearly shows that the meter pressure taps measure the permanent pressure loss caused by the flow disturbance after the orifice. If ΔP_{12} instead of ΔP_{13} were measured, the meter would be a true orifice meter. With the sizes of orifices used in this study only very little pressure recovery occurs. An estimated pressure plot is shown of figure C1.

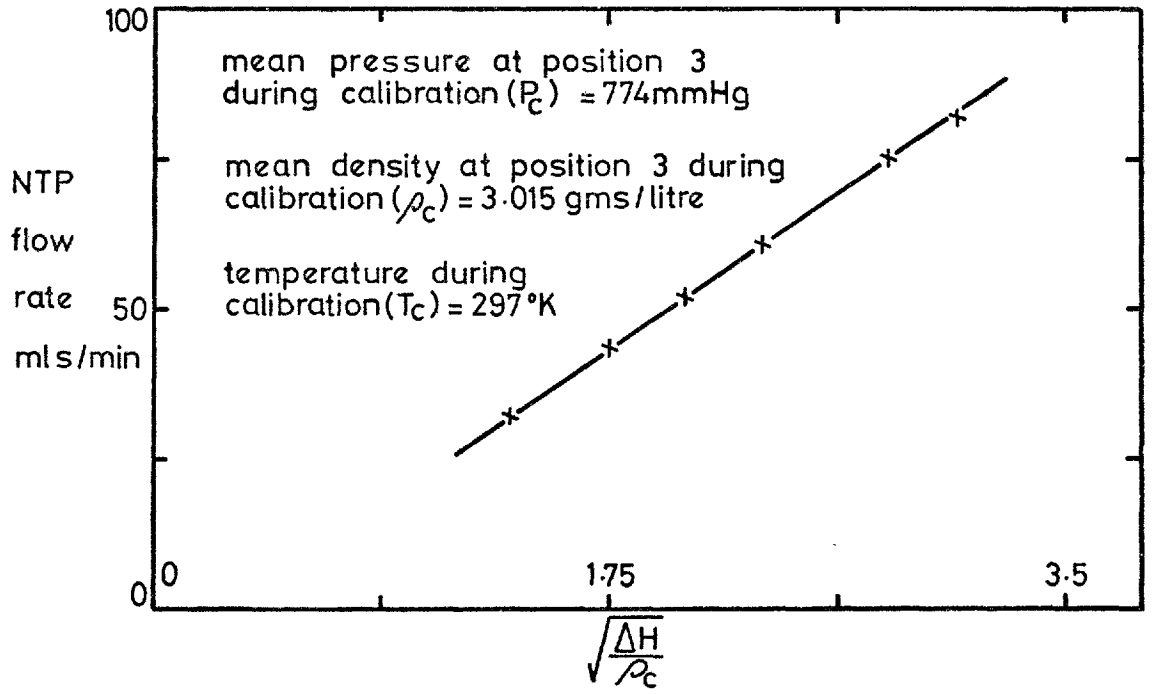

CHLORINE ORIFICE C5 CALIBRATION PLOT

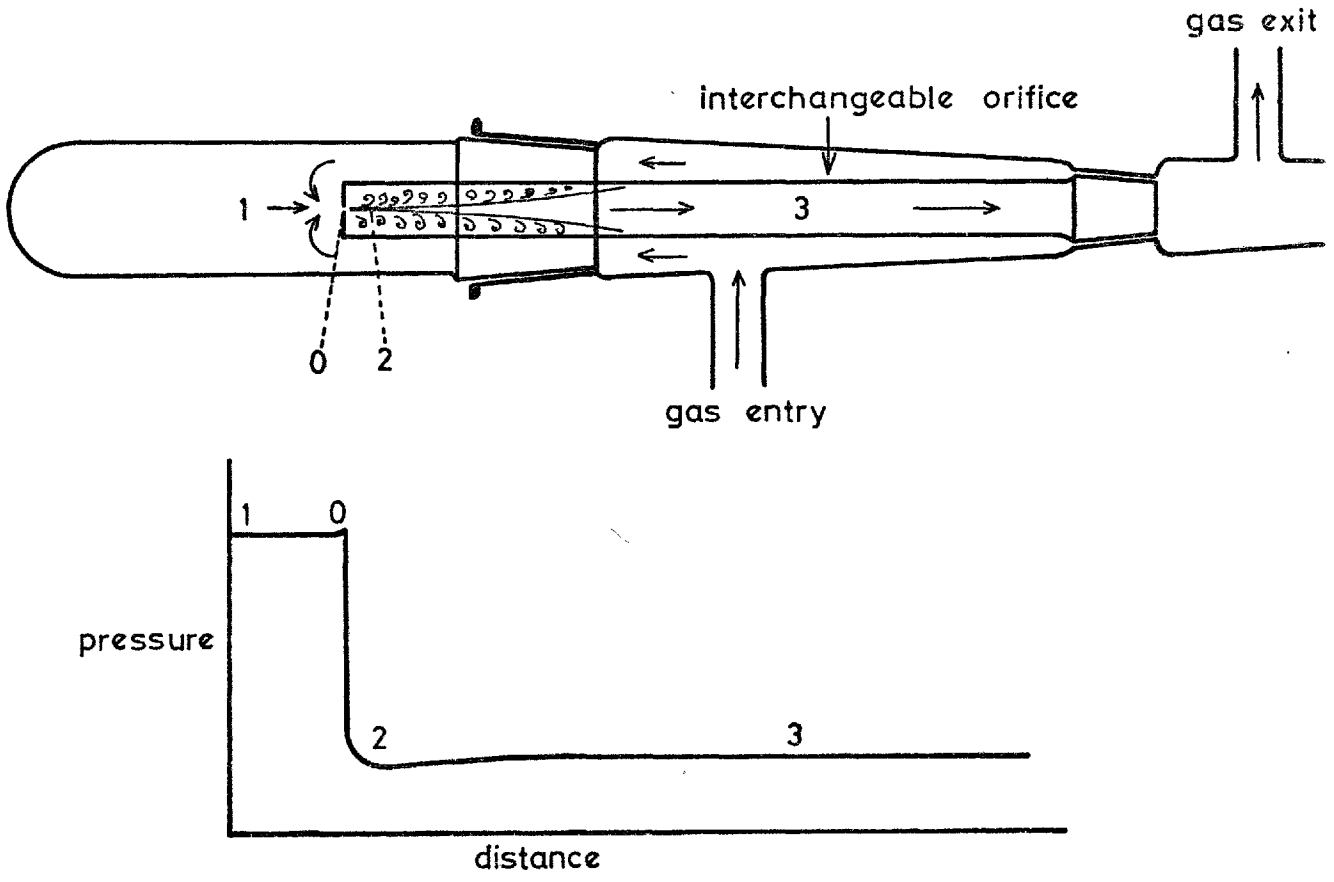

FIGURE C1: PRESSURE DISTRIBUTION IN FLOW METER

A full analysis of the orifice meter is given by Bennett and Myers*. The following general equation, for the relationship between the fluid flow rate and the permanent pressure drop, can be derived from their text.

$$\dot{Q} = C \cdot \sqrt{\frac{\Delta P_{13}}{\rho}}$$

C is constant for a given orifice (and gas) over a moderate range of Reynolds numbers. $\dot{Q}$ is the volume flow rate of gas.

C2 Flow meter calibration and corrections

With each orifice, readings obtained during calibration were treated in the following way: the measured flow rate was corrected to NTP (760 mm Hg 0°C) and then plotted against $\sqrt{\frac{\Delta H}{\rho}}$.

ΔH was the centimetre head of pure concentrated sulphuric acid (SG 1.84) recorded by the flow meter manometer tubes. ρ was the density of the gas at ambient temperature and position 3 pressure.

With the calibration data, plotting gas flows as NTP volume rates would be undesirable if, when using the meter under different conditions, the volume flow rate specific to the different conditions was required. To obtain a volume flow rate for pressure and temperature conditions different to those at calibration would require conversion of the indicated NTP flow rate back to the measured flow rate at the calibration temperature and pressure. However, by a suitable correction, NTP flow rates corresponding to pressures and temperatures different to those at calibration can be directly read from an NTP-flow vs $\sqrt{\frac{\Delta H}{\rho}}$ plot. The basic flow meter equation is

$$\dot{Q}_{P,T} = C \cdot \sqrt{\frac{\Delta H}{\rho_{P,T}}} \quad \ldots\ldots\ldots\ldots\ldots\ldots\ldots\ldots\ldots\ldots\ldots\ldots (1)$$

C is constant for a given orifice and flow configuration. Correcting the calibration flow to NTP (subscript C refers to calibration).

$$\dot{Q}_{NTP} = C \cdot \frac{P_c}{760} \cdot \frac{273}{T_c} \cdot \sqrt{\frac{\Delta H}{\rho_c}} \quad \ldots\ldots\ldots\ldots\ldots\ldots\ldots\ldots\ldots\ldots (2)$$

---

* Momentum Heat and Mass Transfer - McGraw Hill 1962

The calibration plots thus consist of $\dot{Q}_{NTP}$ vs $\sqrt{\frac{\Delta H}{\rho_c}}$. With a ΔH reading taken during an experiment (subscript e) at a new temperature and pressure, calculating the value $\sqrt{\frac{\Delta H}{\rho_e}}$ and reading an NTP flow rate off the calibration plot gives a flow which needs two corrections. One to refer it back to the calibration flow at T_c and P_c and one from this flow back to NTP from P_e and T_e. Thus the true flow rate is:

$$\dot{Q}_{NTP} \text{ indicated} \cdot \frac{T_c}{T_e} \cdot \frac{P_e}{P_c} \quad \ldots\ldots\ldots\ldots\ldots\ldots\ldots\ldots\ldots\ldots (3)$$

As the calibration plot is linear this true NTP flow rate could be obtained by looking up the corrected $\sqrt{\frac{\Delta H}{\rho_e}}$ given below.

$$\frac{T_c \cdot P_e}{T_e \cdot P_c} \sqrt{\frac{\Delta H}{\rho_e}} \quad \ldots\ldots\ldots\ldots\ldots\ldots\ldots\ldots\ldots\ldots (4)$$

but $\rho_e = \rho_c \cdot \frac{P_e}{P_c} \frac{T_c}{T_e}$

Re-arranging equation (4) gives

$$\sqrt{\frac{\Delta H}{\rho_c \frac{P_e}{P_c} \cdot \frac{T_c}{T_e}}} \quad \ldots\ldots\ldots\ldots\ldots\ldots\ldots\ldots\ldots\ldots (5)$$

Thus, by using equation (5) NTP flow rates corresponding to any temperature and pressure could be read directly from the calibration plots.

Seventeen different orifices were used during this study; all gave prefectly linear calibration plots. No useful purpose would be served by reproducing each of these plots in this appendix. One typical calibration plot is however shown since it illustrates the excellent linearity that was obtained.

A P P E N D I X D

SPECIFICATIONS OF OXIDE POWDERS

D1 Imperial Smelting Corporation: Special Grade Zinc Oxide

Arsenic	nil
Cadmium oxide	0.005%
Ferric oxide	0.001%
Lead oxide	0.009%
Sulphur trioxide	nil
Chlorine	nil
Insoluble matter	0.007%
Loss on ignition	0.035%
Water soluble salts	0.040
Mean particle size	0.21μ
Particle shape	Irregular crystallites
Specific surface area	5.1 sq m/gm
Coarse particles retained by 240 B.S. Sieve	0.010%
Zinc oxide	99.94%

D2 Blythe Colours: Cadmium Oxide

Lead	50-100 ppm
Zinc	15 ppm
Iron	10 ppm
Copper	4 ppm
Aluminium	3 ppm
Nickel	3 ppm
Calcium	1 ppm
Chromium	less than 1 ppm
Magnesium	less than 1 ppm
Silica	less than 1 ppm
Sodium	less than 1 ppm
Silver	less than 1 ppm

D3 Cobalt Oxides

Some uncertainties surround commercially available oxides of cobalt since there are various opinions concerning the valence states of the oxides involved. Oxides under the names cobalt, cobaltous and cobaltic are available. The cobalt oxide is claimed to consist of variable proportions of Co_2O_3 and Co_3O_4. The cobaltic oxide can only be assumed to be Co_2O_3, whilst the cobaltous oxide suggests CoO.

It is undisputed that CoO and Co_3O_4 do exist as specific oxides (see Appendix K), however Co_2O_3 appears to be stable only as a hydrate[74.85].

The two oxides relevant to this study are CoO and Co_3O_4; each has a definite range of stability under which conditions the cobalt is uniformly oxidised to one form only. It was thus unimportant as to which was the claimed state of oxidation of the oxide purchased provided that under any given experimental conditions the oxide present was stable with respect to the prevailing oxygen partial pressure. With the equilibrium experiments this was brought about by conditioning each oxide bed prior to its chlorination. The cobalt oxide(s) used to make pellets for the zinc oxide/cobalt oxide(s) equilibrium experiments was a mixture of oxide(s) obtained from two sources*; in each case it was the highest purity offered. The only specifications given were maximum Fe and Ni levels (0.01% and 0.04% respectively). In view of the oxide production route, other impurities are thought to have been insignificant.

D4 ZnO/CdO Mixtures

In calculating the amounts of zinc oxide and cadmium oxide to use for the pellets of three different compositions, each oxide was assumed to be 100% pure. The only small error in this assumption could be due to the fact that both oxides absorb water (or hydrate) to a significant extent. However, as the oxides were carefully stored, this source of error is discounted.

---

* (a) BDH Chemicals; (b) Hopkins and Williams

A P P E N D I X E

ANALYSIS OF CONDENSATES

E1 EDTA complexiometric titration

The standard solutions used for this volumetric method are listed below, analar reagents and deionised water were used throughout.

a) 0.2N and 0.4N EDTA solution ($C_{10}H_{14}O_8N_2Na_2.2H_2O$ MW = 372.24 disodium dihydrogen ethylenediamine tetra-acetate dihydrate)

b) Buffer solution - 444 mls NH_4OH (SG = 0.88) and 56 gms of NH_4Cl made up to 2 litres

c) Eriochrome black T indicator - 0.2 gms of dye dissolved in 15 mls of triethanolamine and 5 mls of ethanol.

The titration of the Zn^{++} solutions was carried out in the following manner: 25 mls of sample was transferred by pipette into a conical flask, to this was added about 6 drops of indicator. This solution, which was quite acidic, was then neutralised with the buffer, a slight excess of which was used to keep the solution at a PH of 9 to 10. The point at which the solution became neutral was detected by the appearance of a gelatinous precipitate of zinc hydroxide, this dissolved once the solution became alkaline. (Provided that enough buffer was added to dissolve the precipitate, the PH of the solution was suitable for titration; an excess of buffer was not detrimental.) Once it had been prepared, the solution was then titrated against the standard EDTA, the end point was indicated by a sharp change in colour from wine red to blue-black.

E2 Atomic absorption analysis

All the $ZnCl_2$ + $CdCl_2$ and $ZnCl_2$ + $CoCl_2$ condensates, and some of the $ZnCl_2$ condensates were analysed on a Perkin Elmer model 290B atomic absorption spectrophotometer, this is a single beam model which was fitted with an air-acetylene burner-nebuliser system. The instrument was at all times used under the standard operating conditions recommended by the manufacturer. Co, Cd and Zn single element hollow cathode lamps were used, and the linear output signal was recorded on a Smiths Servoscribe 2 pen recorder.

E2a Absorption lines and working ranges

Only resonant lines were used for analysis, these together with slit widths are listed below.

1. Cobalt 240.7 nm line 0.2 nm slit
2. Cadmium 228.8 nm line 0.7 nm slit
3. Zinc 213.8 nm line 2.0 nm slit
   307.5 nm line 0.2 nm slit

With the longer wavelength zinc line the absorption coefficient was very low, a plot of absorbance vs concentration thus showed good linearity even with solutions of up to 1N strength. A few undiluted $ZnCl_2$ condenser solutions were analysed with this line; however, since the burner system was adversely affected by concentrated solutions the Zn in mixed chloride solutions was not analysed in this way.

The details given in the remainder of this appendix refer only to determinations of mixed chloride solutions using sensitive absorption lines and sample dilution. Figure E1 shows typical calibration curves for Co, Cd and Zn. The Zn and Cd curves both show serious non-linearity at high concentrations; listed below are the maximum concentrations and typical working ranges used:

Zn max 8 ppm - usual range 1 to 4 ppm
Cd max 9 ppm - usual range 1 to 6 ppm
Co max 11 ppm - usual range 1 to 11 ppm

E2b Preparation of standards

The Cd, Co and Zn standards were all manufactured from metal of the

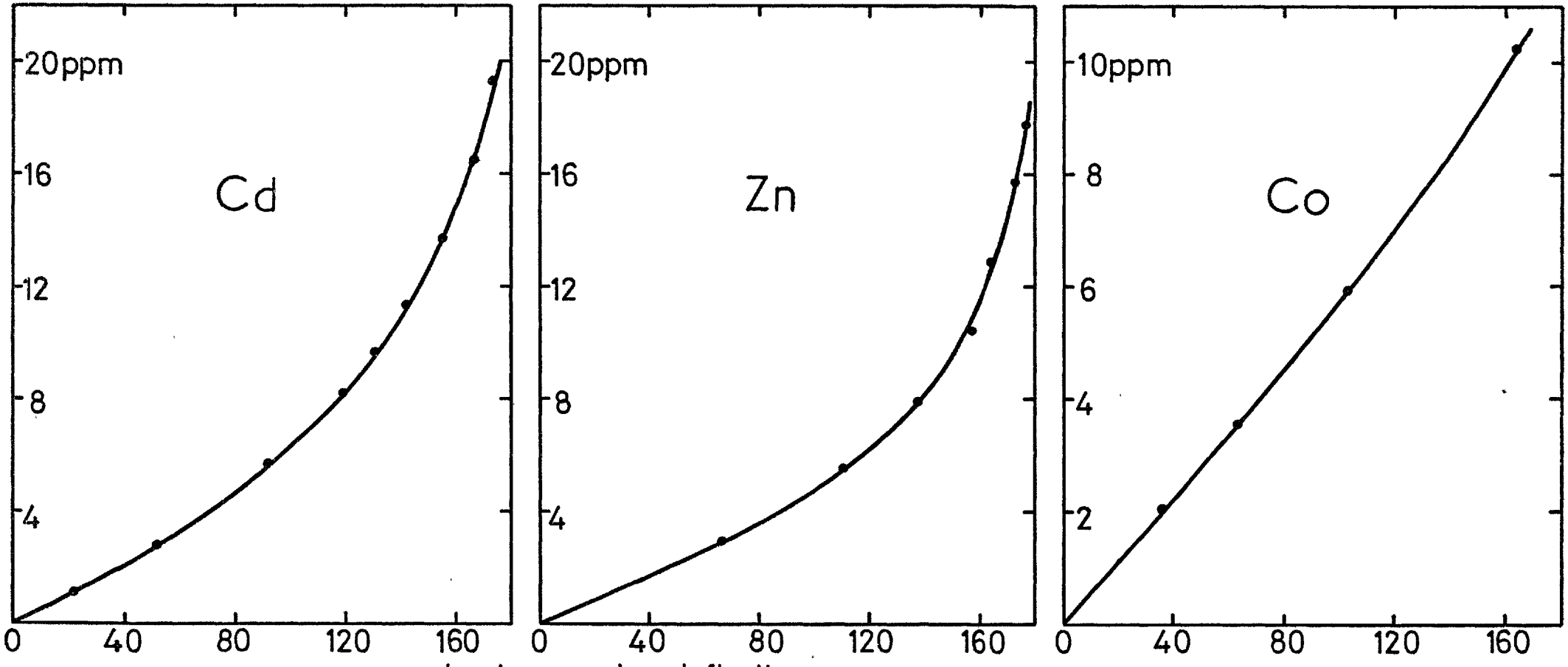

1ppm = 1micro-gm / ml

FIGURE E1: AA CALIBRATION CURVES

purities listed below:

Cd -	>99.999%
Co - high purity cathode cobalt	>99.0%
Zn -	>99.95%

The standards required could not be made up directly since the quantities of metal involved were too small to be accurately weighed, standards were thus made up in two stages. Firstly 1 and 2 litre solutions containing between 50 and 5000 ppm were made up for each metal. This was done by dissolving, inside the volumetric flasks, precisely weighed quantities of metal in an excess of concentrated acid (HCl for Cd and Zn - HNO_3 for Co). Once the metal had dissolved the solutions were made up to the mark with distilled water at the correct graduation temperature of 20°C. These concentrated solutions were then used to make up AA standards containing between 1 and 11 ppm; dilutions ranged between x10 and x500. Zn and Co standards were made up in 5% V/V HCl, the Cd being in 2% V/V HCl. At least two independent batches of standards were made for each metal species, these were checked against each other for internal consistency by running them on the AA instrument. Comparative and internal disagreements between the standards were never more than the percentage reproducibility of the method as a whole; it is thus fair to assume that the standards were of a high degree of absolute accuracy.

E2c Interferences

A slight matrix effect was detected with hydrochloric acid when compared with distilled water. To neutralise this interference all samples under text were made up in hydrochloric acid solution of corresponding strength to that in the standards, also the base line in any determination was taken to be that given by aspirating aqueous HCl solution of the same strength. With Cd/Zn solutions when one of the two species was being determined, the presence of the second, even at high concentration (up to 500 ppm) did not produce any interference. With Co/Zn solutions the cobalt did not interfere during zinc determinations; however, very slight interference occurred during cobalt analysis since a solution containing 5 ppm Co typically contained 1500 ppm Zn. On investigation of this interference it was found that the maximum artificial increase in indicated cobalt concentration was about 1%. This effect was not corrected since it was so small.

E2d Production of diluted samples

Dilutions of up to x1000 were made by using various pipettes together with 500 and 1000 ml volumetric flasks. Co and Zn were made up in 5% V/V HCl; Cd was made up in 2% V/V HCl.

E2e Method of running samples

The lamp, flame and instrumentation were adjusted and then stabilised for about 40 minutes before analysis started. About 6 standards, which spanned the concentration range of the samples, were run twice (against blank acid solution); if the instrument was stable and there was agreement between the standards the analysis proceeded. For analysis, about 4 samples were run, followed by 2 standards. This was repeated until the last sample had been completed, then all the standards were re-run. If all the standards were consistent, then a calibration curve was drawn from the peak heights on the chart recorder output and the known strengths of the standards. The concentrations of the solutions under test were measured off from this calibration plot.

Experiment number		B1	B2	B3	B4	B5	B6	C1	C2	C3	C4
Common Data		ZnO size fraction = 1/4" + 3/16" nominal temperature = 850°C $\frac{1}{2}\dot{o}\dot{n}Cl_2$ = 0.0000604 gm-moles/sec						ZnO size fraction = -3.8" + 1/4" nominal temp. = 875°C $\frac{1}{2}\dot{o}\dot{n}$ Cl_2 = 0.0000749 gm-moles/sec			
Reaction time - mins		10.02	10.00	10.00	10.00	10.00	10.00	7.00	7.00	7.50	7.00
Gas	N_2	1210	1205	1210	1205	1210	1210	3010	3005	3000	3000
Flow	O_2	72	71	71.5	71.5	74	74	71	71.5	71	71
$MLS_{ntp/min}$	Cl_2	161	162	161	161	161.5	152.5	199	198	198	198.5
Chlorinating gas entry P. mm Hg		767.3	766.4	769.9	772.2	770.8	770.1	777.3	771.3	769.2	777.3
Initial bed weight - gms		117.64	65.17	47.51	32.75	25.98	14.93	60.49	39.50	20.82	84.17
Initial bed depth - cms		14.3	7.7	5.6	3.6	3.2	1.7	7.5	5.2	2.7	9.8
Final bed depth - cms		12.0	7.0	5.5	3.5	3.0	1.7	7.0	5.0	-	-
Initial bed temp. - °C		851	851	851	851	850	849	868	871	875	878
Final bed temp. - °C		848	847	842	836	835	837	863	863	869	876
gm-moles ZnO lost (by wt)		0.0656	0.0625	0.0558	0.0451	0.0462	0.0295	0.0542	0.0474	0.0334	0.0596
gm-moles $ZnCl_2$ collected (by wt)		0.0636	0.0606	0.0549	0.0453	0.0485	0.0284	0.0508	0.0451	0.0306	0.0571
gm-moles $ZnCl_2$ by analysis		0.0645 (EDTA)	0.0617 (EDTA)	0.0562 (EDTA)	0.0455 (EDTA)	0.0485 (EDTA)	0.0288 (EDTA)	No analysis performed			
% chlorine utilisation		88.2	84.1	77.0	62.4	66.3	41.7	83.2	73.7	47.5	92.7
Y x 10^3 gm-moles/sec		2.44	2.09	1.69	1.13	1.26	0.71	4.50	3.37	1.66	6.56
Mean bed weight - gms		114.97	62.62	45.24	30.92	24.10	13.73	58.29	37.57	19.46	81.75

Chronological order of experiments - B,C,D,E,F,G,H,I,J, and K

Experiment number	D1	D2	D3	D4	D5	D6	D7	D8
Common Data	ZnO size fraction = -3/16" + 7m $\frac{1}{2}o\dot{n}Cl_2$ = 0.000262 gm-moles/sec					nominal temperature = 720°C		
Reaction time - mins	8.00	8.00	8.00	8.00	8.00	8.00	8.00	8.00
Gas N_2	2080	2075	2098	2095	2085	2085	2040	2100
Flows O_2	none	none	none	none	none	none	none	none
$MLS_{ntp/min}$ Cl_2	696	697	696	700	698	700	658	705
Chlorinating gas entry P. - mm Hg	768.3	767.3	777.5	773.6	770.8	778.3	793.9	783.0
Initial bed weight - gms	59.96	30.18	90.43	20.37	45.23	144.81	109.80	12.19
Initial bed depth - cms	6.8	3.5	10.9	2.5	5.3	15.7	-	-
Final bed depth - cms	6.6	-	-	2.2	5.2	15.3	-	-
Initial bed temp - °C	719	721	714	727	720	721	719	721
Final bed temp - °C	703	698	706	700	698	716	713	710
gm-moles ZnO lost (by wt)	0.0729	0.0493	0.0890	0.0362	0.0570	0.116	0.0994	0.0276
gm-moles $ZnCl_2$ collected (by wt)	0.0694	0.0464	0.0853	0.0336	0.0451	0.115	0.0970	0.0255
gm-moles $ZnCl_2$ by analysis	0.0704 (EDTA)	0.0475 (EDTA)	0.0876 (EDTA)	0.0358 (EDTA)	0.0557 (EDTA)	0.116 (EDTA)	no analysis performed	
% Cl_2 utilisation	27.9	18.8	34.7	14.1	22.0	45.7	41.2	10.4
Y x 10^3 gm moles/sec	0.954	0.699	1.17	0.585	0.787	1.57	1.35	0.497
Mean bed weight - gms	56.99	28.18	86.81	18.89	42.89	140.08	105.75	11.07

Experiment number	J1	J2	J3	J4	I1	I2	I3	I4	K1	K2	K3
Common data	ZnO size fraction = -1/4" + 3/16" $\frac{1}{2}o\dot{n}Cl_2$ = 0.000114 gm-moles/sec nominal temperature = 705°C				Zno size fraction = -3/16" + 7m $\frac{1}{2}o\dot{n}Cl_2$ = 0.000113 gm-moles/sec nominal temperature = 705°C				ZnO size fraction = -7m + 14m $\frac{1}{2}o\dot{n}Cl_2$ =0.000115 gm-moles/sec nominal temperature = 705°C		
Reaction time - mins	10.00	10.00	10.00	10.00	10.50	10.00	10.00	10.00	10.00	10.50	10.00
Gas flow N_2	1710	1710	1710	1695	1720	1710	1725	1710	1720	1710	1720
$Mls_{NTP/min}$ O_2	none	none	none	none	none	none	none	none	none	none	none
Cl_2	304	302	304	301	301	301	302	298	304	302	305
Chlorinating gas entry P. - mm Hg	772.4	775.3	778.5	775.1	773.2	773.1	776.7	765.5	781.4	783.1	780.7
Initial bed weight - gms	47.19	85.14	151.65	25.80	100.03	150.02	31.01	57.10	60.49	153.38	90.15
Initial bed depth - cms	5.8	10.0	18.0	2.9	11.1	17.5	3.5	6.8	7.0	17.0	10.1
Final bed depth - cms	-	-	-	-	-	-	-	-	-	-	-
Initial bed temp. - °C	706	705	706	705	706	706	705	706	705	704	705
Final bed temp. - °C	698	700	702	696	702	703	693	700	696	699	699
gm-moles Zno lost (by wt.)	0.0262	0.0375	0.0490	0.0197	0.0487	0.0571	0.0256	0.0354	0.0491	0.0695	0.0557
gm-moles $ZnCl_2$ collected (by wt)	0.0249	0.0324	0.0458	0.0178	0.0464	0.0541	0.0266	0.0319	0.0458	0.0667	0.0525
gm-moles $ZnCl_2$ by analysis	no analysis performed				0.0488 (EDTA)	0.0555 (EDTA)	0.0261 (EDTA)	0.0339 (EDTA)	no analysis performed		
% Cl_2 utilisation	18.5	25.5	34.4	13.7	34.1	40.7	19.1	25.1	34.4	47.4	39.1
Y x 10^3 gm-moles/sec	0.426	0.563	0.759	0.335	0.750	0.910	0.436	0.549	0.761	1.09	0.876
Mean bed weight - gms	46.12	83.62	149.65	25.00	98.05	147.69	29.97	55.66	58.49	150.55	87.88

Experiment number		E1*	E2*	F1*	G1*	H1	H2	H3	H4	H5
Common data		ZnO size fraction = -1/4" + 3/16" $\frac{1}{2}o^{\dot{n}}Cl_2 = 2.29 \times 10^{-5}$ moles/s nominal temp = 860°C		-1/4"+3/16" 860°C	-3/8"+1/4" 860°C	ZnO size fraction = 3/16" + 7m nominal temperature = 700°C				
Reaction time - mins		20.00	20.00	20.00	20.00	2.00	4.00	6.00	10.00	15.00
Gas flow	N_2	2040	2030	4490	5560	Nitrogen flow = 1700				
$Mls_{NTP/min}$	O_2	none	none	none	none	No oxygen flow				
	Cl_2	60.6	60.5	60.5	103	Chlorine flow = 300				
Chlorinating gas entry P. - mm Hg		772.9	769.3	771.7	795.0	-	-	-	-	-
Initial bed weight - gms		70.40	30.16	50.42	60.16	59.66	59.20	59.13	58.54	57.70
Initial bed depth - cms		8.5	-	-	-	7.3	7.1	7.1	6.8	6.9
Final bed depth - cms		-	-	-	-	-	-	-	-	-
Initial bed temp - °C		859	863	862	861	708	707	705	706	705
Final bed temp - °C		860	863	851	-	-	702	698	700	698
gm-moles ZnO lost (by wt)		0.0524	0.0419	0.0510	0.0695	0.00933	0.0142	0.0225	0.0354	0.0564
gm-moles $ZnCl_2$ collected (by wt)		0.0505	0.0430	0.0481	0.0741	0.00690	0.0113	0.0212	0.0319	0.0531
gm-moles $ZnCl_2$ by analysis		No analysis performed		N.A.P.	N.A.P.	0.00792	0.0137	0.0217	0.0339	0.0549
% Cl_2 utilisation		93.5	77.4	90.3	76.9	29.1	25.2	26.5	24.9	26.9
Y x 10^3 gm-moles/sec		4.37	2.37	-	-	-	-	-	-	-
Mean bed weight - gms		68.27	28.45	-	-	-	-	-	-	-

* Filter analysis negligible

Experiment number	*S1	*S4	*S6	*S7	*S8	*S9	*S10	*S11	*S12	*S13
Temperature - ^{o}C	851	852	852	901	902	951	951	1001	1002	1051
Bed composition - mole % CdO	50.0	50.0	50.0	50.0	50.0	50.0	50.0	50.0	50.0	50.0
Bed size fraction - mm	+2/-4	+2/-4	+2/-4	+2/-4	+2/-4	+4/ -4.75	+4/ -4.75	+4/ -4.75	+4/ -4.75	+4.75 -5.6
Initial bed weight - gms	223.37	212.95	280.64	201.74	200.54	200.50	214.97	280.21	270.75	300.03
Bed depth - cms	19.0	19.0	25.5	18.0	18.0	20.0	20.5	27.5	27.0	29.0
N_2 flow - $MLS_{ntp/min}$	329	226	227	212	225	221	227	218	294	300
Cl_2 flow - $MLS_{ntp/min}$	42.5	31.6	69.1	68.8	40.0	40.5	29.4	66.9	34.9	35.2
Zn analysis (AA) x 10^3 gm-moles	1.07	1.33	1.80	2.09	1.49	1.74	0.895	2.75	1.82	1.85
Cd analysis (AA) x 10^3 gm-moles	44.8	55.1	77.8	75.7	52.0	52.2	25.7	71.6	45.1	37.4
Measured condensate weight - gms	8.33	10.13	14.19	13.56	9.50	9.60	4.73	13.05	8.68	6.94
Calculated condensate weight - gms	8.36	10.29	14.51	13.62	9.74	9.81	4.83	13.50	8.52	7.10
Weight of oxide lost - gms	5.90	7.24	10.02	9.69	6.81	6.85	3.45	9.52	6.08	-
Calculated weight of oxide lost - gms	5.84	7.18	10.14	9.89	6.80	6.84	3.37	9.42	5.94	-
Chlorinating gas entry P. - mm Hg	772.0	749.9	766.0	765.2	763.2	763.2	769.4	773.8	773.6	773.2
ΔP reactor/condenser - mm Hg	1.2	1.5	1.3	1.6	1.1	0.9	1.1	1.2	1.6	1.6
Reaction time - mins	25.00	40.00	26.00	25.00	30.00	30.00	20.00	25.00	31.00	25.00

For runs S11 and S12 the same CdO/ZnO bed was used

* 22mm-bore reactor

Experiment number	*S14	**S15	- S16	**S17	- S18	**S19	- S20	**S21	- S22
Temperature - ^{o}C	1053	802	802	753	753	903	903	702	702
Bed composition - mole % CdO	50.0		50.0		50.0		50.0		50.0
Bed size fraction - mm	+4.75 -5.6		+2/-4		+2/-4		+2/-4		+2/-4
Initial bed weight - gms	-		240.41		276.83		204.8		238.94
Bed depth - cms	-		34.5		44.0		34.0		37.5
N_2 flow $MLS_{ntp/min}$	228	204	285	285	392	277	318	200	282
Cl_2 flow $MLS_{ntp/min}$	66.6	-	-	-	-	-	48.3	-	-
Zn analysis (AA) x 10^3 gm-moles	3.00	0.359	0.425	0.257	0.364	0.688	1.17	0.0681	0.114
Cd analysis (AA) x 10^3 gm-moles	56.9	18.1	21.4	16.0	23.0	23.3	41.7	5.14	9.27
Measured condensate weight - gms	10.52	3.33	3.93	2.90	4.20	4.36	-	0.94	1.59
Calculated condensate weight - gms	10.85	3.36	3.98	2.97	4.27	4.36	-	0.95	1.71
Weight of oxide lost - gms	12.62		5.14		5.09		8.50		1.91
Calculated weight of oxide lost - gms	12.50		5.14		5.06		8.40		1.87
Chlorinating gas entry P. - mm Hg	773.0	768.1	768.7	756.2	757.6	757.2	758.4	755.9	756.9
Δ P reactor/condenser - mm Hg	1.3	1.1	1.8	2.8	4.3	4.3	5.0	1.5	2.5
Reaction time - mins	20.00	20.00	24.00	35.00	40.00	23.00	20.00	50.00	40.00

S13 and S14 were a double-chlorination experiment

Cl_2 flow rates when not given were too low to measure

* 22mm-bore reactor

** 17mm-bore reactor

Experiment number	*S23	*S24	*S25	*S26	*S27	- S28	- S29	**S30	- S31	**S32	- S33
Temperature - ^{o}C	778	877	927	978	772	873	973	1038	1037	1072	1072
Bed composition - mole % CdO	10.8	10.8	10.8	10.8		50.0			50.0		50.0
Bed size fraction - mm	+1.6/-4	+1.6/-4	+1.6/-4	+1.6/-4		+1.0/-4.0			+1.4/-4.75		+1.4/-4.75
Initial bed weight - gms	283.42	282.53	236.86	235.64		348.40			195.24		198.30
Bed depth - cms	28.0	28.0	24.0	23.0		28.0			-		-
N_2 flow $Mls_{ntp/min}$	297	299	267	278	$0_{2_{330}}$	$0_{2_{330}}$	$0_{2_{330}}$	315	272	277	306
Cl_2 flow $Mls_{ntp/min}$	-	-	-	-	-	-	-	28.4	49.5	47.0	-
Zn analysis (AA) gm-moles x 10^3	0.127	0.242	0.320	0.399	0.232	0.369	0.502	1.39	1.35	1.50	1.32
Cd analysis (AA) gm-moles x 10^3	6.23	8.76	9.34	10.2	12.6	14.4	13.6	29.2	30.4	32.3	26.5
Measured condensate weight - gms	1.09	1.59	1.69	1.82	2.35	2.54	2.46	5.65	5.74	6.16	5.08
Calculated condensate weight - gms	1.16	1.64	1.76	1.92	2.34	2.69	2.56	5.54	5.76	6.13	5.04
Weight of oxide lost - gms	0.89	1.21	1.34	1.46		5.55			-		-
Calculated weight of oxide lost - gms	0.81	1.14	1.22	1.34		5.30			-		-
Chlorinating gas entry P. - mm Hg	756.1	756.5	759.0	759.4	755.8	756.6	756.6	770.5	770.1	771.0	770.7
ΔP reactor/condenser - mm Hg	1.2	0.8	0.9	1.1	2.7	3.5	3.6	3.8	3.2	3.4	3.0
Reaction time - mins	10.00	10.00	10.00	11.00	15.00	15.00	15.00	25.00	15.00	17.00	30.00

For runs S23-S24 and S25-S26 the same bed was used

Cl_2 flow rates when not given were too low to measure

* 22mm-bore reactor

** 27.5mm-bore reactor with 20mm bore mullite liner

Experiment 750°C 50.0 mole % CdO

Nominal reaction temperature - °C	750
Composition of pellets - mole % CdO	50.0
Initial bed weight - gms	120.07
Initial bed depth - cms	7.7
Size fraction of pellets - mm	-6.7 + 5.6
Number of pellets	176
Equilibrium separation constant	62.7
Total weight of oxide volatilised - gms	26.83
Calculated total weight of oxide volatilised - gms	25.97
Total moles Cd volatilised - gm-moles	0.195
Total moles Zn volatilised - gm-moles	0.0116
Initial moles ZnO in bed - gm-moles	0.572
Initial moles CdO in bed - gm-moles	0.572
% bed depletion Zn	2.02
% bed depletion Cd	34.1
Total time of bed at temperature - hours	6.42
Sum total time of chlorination - mins	90.08

Run number	SK15	SK16	SK17	SK18	SK19	SK20	SK21
Temperature - °C	753	753	753	753	753	752	751
Reaction time - mins	5.00	5.00	8.00	11.00	15.00	20.00	26.08
Cl_2 flow - Mls_{NTP}/min	54.6	54.5	54.0	54.6	54.6	54.6	54.7
N_2 flow - Mls_{NTP}/min	1163	1172	1166	1167	1170	1175	1175
Gas delivery P - mm Hg	756.7	757.0	756.8	757.0	756.8	757.0	756.7
ΔP reactor/condenser - mm Hg	1.3	1.6	1.4	1.6	1.4	1.6	1.3
Cd analysis (AA)x10^3 - gm-moles	11.4	11.7	18.1	24.9	33.4	41.6	53.8
Zn analysis (AA)x10^3 - gm-moles	0.20	0.206	0.395	0.771	1.38	2.87	5.77
Measured condensate weight -gms	2.02	2.13	3.24	4.63	6.30	8.39	10.47
Calculated condensate wt - gms	2.12	2.18	3.37	4.67	6.32	8.02	10.65
Cd rate x 10^6 gm-moles/sec	38.0	39.0	37.7	37.7	37.0	34.7	34.3
Zn rate x 10^6 gm-moles/sec	0.66	0.68	0.82	1.16	1.53	2.38	3.68
Sum total chlorination time to middle of run - mins	2.50	7.50	14.00	23.50	36.50	54.00	77.04
Cl_2 supplied x 10^3 gm-moles/min	2.50	2.50	2.49	2.49	2.49	2.49	2.49
gm-moles condensate/min x 10^3	2.32	2.38	2.31	2.33	2.31	2.22	2.28

CdO/ZnO NON-EQUILIBRIUM CHLORINATION EXPERIMENTAL DATA

Experiment 850°C 50.0 mole % CdO

Nominal reaction temperature - °C	850
Composition of pellets - mole % CdO	50.0
Initial bed weight - gms	120.17
Initial bed depth - cms	7.8
Size fraction of pellets - mm	-6.7 + 5.6
Number of pellets	182
Equilibrium separation constant	41.0
Total weight of oxide volatilised - gms	15.54
Calculated total weight of oxide volatilised - gms	15.31
Total moles Cd volatilised - gm-moles	0.110
Total moles Zn volatilised - gm-moles	0.0148
Initial moles ZnO in bed - gm-moles	0.573
Initial moles CdO in bed - gm-moles	0.573
% bed depletion Zn	2.59
% bed depletion Cd	19.2
Total time of bed at temperature - hours	5.17
Sum total time of chlorination - mins	53.00

Run number	SK3	SK4	SK5	SK6	SK7
Temperature - °C	851	851	852	852	852
Reaction time - mins	5.00	5.00	10.00	13.00	20.00
Cl_2 flow - Mls_{NTP}/min	53.9	53.9	53.9	53.9	53.9
N_2 flow - Mls_{NTP}/min	1155	1152	1161	1161	1155
Gas delivery P. - mm Hg	741.2	-	741.3	741.0	741.0
ΔP. reactor/condenser - mm Hg	2.7	-	3.0	2.7	2.1
Cd analysis (AA) $x10^3$ - gm-moles	11.2	11.5	21.3	27.4	38.4
Zn analysis (AA) $x10^3$ - gm-moles	0.29	0.34	1.60	3.40	9.20
Measured condensate weight - gms	2.02	2.01	4.08	5.27	8.13
Calculated condensate weight - gms	2.09	2.15	4.13	5.49	8.30
Cd rate x 10^6 - gm-moles/sec	37.3	38.3	35.5	35.0	32.0
Zn rate x 10^6 - gm-moles/sec	0.96	1.13	2.66	4.33	7.66
Sum total chlorination time to middle of run - mins	2.50	7.50	15.00	27.50	43.00
Cl_2 supplied x 10^3 - gm-moles/min	2.50	2.50	2.49	2.49	2.49
gm-moles condensate/min x 10^3	2.30	2.37	2.29	2.36	2.38

Experiment 950°C 50.0 mole % CdO

Nominal reaction temperature - °C	950
Composition of pellets - mole % CdO	50.0
Initial bed weight - gms	120.18
Initial bed depth - cms	8.0
Size fraction of pellets - mm	-6.7 + 5.6
Number of pellets	176
Equilibrium separation constant	28.8
Total weight of oxide volatilised - gms	23.76
Calculated total weight of oxide volatilised - gms	23.23
Total moles Cd volatilised - gm-moles	0.129
Total moles Zn volatilised - gm-moles	0.0820
Initial moles ZnO in bed - gm-moles	0.573
Initial moles CdO in bed - gm-moles	0.573
% bed depletion Zn	14.3
% bed depletion Cd	22.5
Total time of bed at temperature - hours	7.17
Sum total time of chlorination - mins	90.00

Run number	SK8	SK9	SK10	SK11	SK12	SK13	SK14
Temperature - °C	951	951	952	951	951	951	952
Reaction time - mins	5.00	5.00	8.00	11.00	15.00	20.00	26.00
Cl_2 flow - Mls_{NTP}/min	54.4	54.4	54.5	54.5	54.7	54.5	54.5
N_2 flow - Mls_{NTP}/min	1170	1168	1170	1167	1169	1168	1162
Gas delivery P. - mm Hg	759.0	760.0	759.9	760.1	759.8	760.1	759.9
ΔP. reactor/condenser - mm Hg	-	3.8	3.7	3.9	3.6	3.9	3.7
Cd analysis (AA) $x10^3$ gm-moles	11.1	10.4	12.8	15.6	20.6	26.3	32.1
Zn analysis (AA) $x10^3$ - gm-moles	0.404	1.39	5.85	10.2	15.0	20.9	28.3
Measured condensate wt - gms	1.96	2.04	2.97	4.23	5.58	7.58	9.86
Calculated condensate wt - gms	2.09	2.11	3.15	4.24	5.83	7.67	9.75
Cd rate x 10^6 - gm-moles/sec	37.0	34.7	26.7	23.7	22.8	21.8	20.5
Zn rate x 10^6 - gm-moles/sec	1.34	4.63	12.2	15.4	16.7	17.3	18.0
Sum total chlorination time to middle of run - mins	2.50	7.50	14.00	23.50	36.50	54.00	77.00
Cl_2 supplied x 10^3 gm-moles/min	2.50	2.50	2.49	2.49	2.49	2.49	2.49
gm-moles condensate/min x 10^3	2.30	2.36	2.33	2.35	2.37	2.35	2.31

Experiment 750°C 26.6 mole % CdO

Nominal reaction temperature - °C	750
Composition of pellets - mole % CdO	26.6
Initial bed weight - gms	120.28
Initial bed depth - cms	7.5
Size fraction of pellets - mm	-6.7 + 5.6
Number of pellets	202
Equilibrium separation constant	62.7
Total weight of oxide volatilised - gms	25.27
Calculated total weight of oxide volatilised - gms	24.68
Total moles Cd volatilised - gm-moles	0.171
Total moles Zn volatilised - gm-moles	0.0341
Initial moles ZnO in bed - gm-moles	0.940
Initial moles CdO in bed - gm-moles	0.341
% bed depletion Zn	3.63
% bed depletion Cd	50.0
Total time of bed at temperature - hours	6.25
Sum total time of chlorination - mins	90.00

Run number	SK22	SK23	SK24	SK25	SK26	SK27	SK28
Temperature - °C	752	752	752	752	752	751	751
Reaction time - mins	5.00	5.00	8.00	11.00	15.00	20.00	26.00
Cl_2 flow - Mls_{NTP}/min	55.1	54.9	54.9	55.1	55.1	55.1	55.0
N_2 flow - Mls_{NTP}/min	1186	1181	1176	1179	1180	1179	1178
Gas delivery P. - mm Hg	773.0	-	773.1	773.3	773.1	773.4	773.0
ΔP. reactor/condenser - mm Hg	2.7	-	2.8	3.0	2.8	3.1	2.7
Cd analysis (AA)x10^3 - gm-moles	11.5	11.6	17.8	23.4	30.0	35.8	40.5
Zn analysis (AA)x10^3 - gm-moles	0.214	0.309	0.771	1.96	4.30	8.87	17.7
Measured condensate wt - gms	1.96	2.15	3.33	4.53	6.08	7.80	9.63
Calculated condensate wt - gms	2.13	2.16	3.37	4.56	6.08	7.77	9.84
Cd rate x10^6 - gm-moles/sec	38.3	38.5	37.0	35.5	33.3	29.8	25.9
Zn rate x10^6 - gm-moles/sec	0.710	1.03	1.60	2.97	4.77	7.38	11.4
Sum total chlorination time to middle of run - mins	2.50	7.50	14.00	23.50	36.50	54.00	77.00
Cl_2 supplied x10^3 gm-moles/min	2.50	2.49	2.49	2.50	2.50	2.50	2.49
gm-moles condensate/min x10^3	2.34	2.37	2.32	2.30	2.28	2.23	2.24

Experiment 850°C 26.6 mole % CdO

Nominal reaction temperature - °C	850
Composition of pellets - mole % CdO	26.6
Initial bed weight - gms	120.08
Initial bed depth - cms	7.8
Size fraction of pellets - mm	-6.7 + 5.6
Number of pellets	196
Equilibrium separation constant	41.0
Total weight of oxide volatilised - gms	23.13
Calculated total weight of oxide volatilised - gms	22.52
Total moles Cd volatilised - gm-moles	0.122
Total moles Zn volatilised - gm-moles	0.0835
Initial moles ZnO in bed - gm-moles	0.938
Initial moles CdO in bed - gm-moles	0.341
% bed depletion Zn	8.90
% bed depletion Cd	34.9
Total time of bed at temperature - hours	5.32
Sum total time of chlorination - mins	90.17

Run number	SK36	SK37	SK38	SK39	SK40	SK41	SK42
Temperature - °C	852	852	852	851	851	852	850
Reaction time - mins	5.00	5.17	8.00	11.00	15.00	20.00	26.00
Cl_2 flow - Mls_{NTP}/min	53.8	53.7	53.7	53.7	53.7	53.7	53.7
N_2 flow - Mls_{NTP}/min	1155	1156	1155	1155	1155	1155	1155
Gas delivery P. - mm Hg	736.5	736.7	736.7	736.8	736.7	736.9	736.5
ΔP. reactor/condenser - mm Hg	3.2	3.4	3.4	3.5	3.4	3.6	3.2
Cd analysis (AA)x10^3 - gm-moles	10.8	10.1*	14.7	17.5	20.7	23.2	25.5
Zn analysis (AA)x10^3 - gm-moles	0.566	1.67	3.73	7.92	13.4	21.8	34.4
Measured condensate wt - gms	1.92	2.04	3.09	4.27	5.47	7.34	9.27
Calculated condensate wt - gms	2.06	2.08	3.20	4.29	5.63	7.23	9.37
Cd rate x 10^6 gm-moles/sec	36.2	32.7	30.6	26.5	23.0	19.3	16.4
Zn rate x 10^6 gm-moles/sec	1.88	5.38	7.76	12.0	14.9	18.1	22.0
Sum total chlorination time to middle of run - mins	2.50	7.58	14.16	23.66	36.66	54.16	77.16
Cl_2 supplied x 10^3 gm-moles/min	2.44	2.43	2.43	2.43	2.43	2.43	2.43
gm-moles condensate/min x 10^3	2.28	2.29*	2.30	2.31	2.28	2.25	2.30

* Cd not analysed. Value calculated from Zn analysis and mean condensate rate

Experiment 950°C 26.6 mole % CdO

Nominal reaction temperature - °C	950
Composition of pellets - mole % CdO	26.6
Initial bed weight - gms	120.46
Initial bed depth - cms	7.9
Size fraction of pellets - mm	-6.7 + 5.6
Number of pellets	193
Equilibrium separation constant	28.8
Total weight of oxide volatilised - gms	21.17
Calculated total weight of oxide volatilised - gms	20.57
Total moles Cd volatilised - gm-moles	0.0733
Total moles Zn volatilised - gm-moles	0.137
Initial moles ZnO in bed - gm-moles	0.941
Initial moles CdO in bed - gm-moles	0.342
% bed depletion Zn	14.6
% bed depletion Cd	21.4
Total time of bed at temperature - hours	4.72
Sum total time of chlorination - mins	90.13

Run number	SK43	SK44	SK45	SK46	SK47	SK48	SK49
Temperature - °C	952	951	951	951	951	952	951
Reaction time - mins	5.00	5.00	8.00	11.13	15.00	20.00	26.00
Cl_2 flow Mls_{NTP}/min	54.6	54.6	54.6	54.6	54.6	54.6	54.6
N_2 flow - Mls_{NTP}/min	1174	1180	1178	1165	1158	1172	1172
Gas delivery P. - mm Hg	745.4	745.9	745.5	745.8	745.6	745.9	745.6
ΔP. reactor/condenser - mm Hg	2.2	2.7	2.3	2.6	2.4	2.7	2.4
Cd analysis (AA)x10^3 - gm-moles	10.9	7.61	6.85	8.32	10.5	13.2	15.9
Zn analysis (AA)x10^3 - gm-moles	0.803	4.36	12.3	18.0	25.4	32.4	43.9
Measured condensate wt - gms	2.02	1.96	2.65	3.82	5.00	7.11	9.21
Calculated condensate wt - gms	2.11	1.98	2.92	3.98	5.39	6.83	8.90
Cd rate x10^6 - gm-moles/sec	36.5	25.3	14.3	12.4	11.7	11.0	10.2
Zn rate x10^6 - gm-moles/sec	2.68	14.5	25.7	27.0	28.2	27.0	28.1
Sum total chlorination time to middle of run - mins	2.50	7.50	14.00	23.57	36.63	54.13	77.13
Cl_2 supplied x 10^3 gm-moles/min	2.47	2.47	2.47	2.47	2.47	2.47	2.47
gm-moles condensate/min x 10^3	2.35	2.39	2.39	2.37	2.39	2.28	2.30

Experiment 750°C 10.8 mole % CdO

Nominal reaction temperature - °C	750
Composition of pellets - mole % CdO	10.8
Initial bed weight - gms	120.19
Initial bed depth - cms	8.9
Size fraction of pellets - mm	-6.7 + 5.6
Number of pellets	218
Equilibrium separation constant	62.7
Total weight of oxide volatilised - gms	21.27
Calculated total weight of oxide volatilised - gms	20.43
Total moles Cd volatilised - gm-moles	0.106
Total moles Zn volatilised - gm-moles	0.0844
Initial moles ZnO in bed - gm-moles	1.24
Initial moles CdO in bed - gm-moles	0.150
% bed depletion Zn	6.81
% bed depletion Cd	70.2
Total time of bed at temperature - hours	5.92
Sum total time of chlorination - mins	90.00

Run number	SK29	SK30	SK31	SK32	SK33	SK34	SK35
Temperature - °C	752	752	753	752	752	752	752
Reaction time - mins	5.00	5.00	8.00	11.00	15.00	20.00	26.00
Cl_2 flow - Mls_{NTP}/min	55.0	55.1	55.0	55.0	55.6	55.3	55.0
N_2 flow - Mls_{NTP}/min	1200	1200	1182	1183	1202	1189	1180
Gas delivery P. - mm Hg	773.7	773.4	773.7	773.4	773.5	773.5	773.7
ΔP. reactor/condenser - mm Hg	1.9	1.6	1.9	1.6	1.7	1.7	1.9
Cd analysis(AA)x10^3 - gm-moles	11.4	10.5	16.3	19.4	19.1	17.9	11.0
Zn analysis(AA)x10^3 - gm-moles	0.275	0.740	2.34	5.35	12.0	24.1	39.6
Measured condensate wt - gms	2.04	2.03	3.17	4.22	5.50	6.43	7.62
Calculated condensate wt - gms	2.12	2.03	3.31	4.29	5.14	6.62	7.41
Cd rate x 10^6 - gm-moles/sec	38.0	35.2	34.0	29.4	21.2	14.9	7.05
Zn rate x 10^6 - gm-moles/sec	0.910	2.46	4.87	8.11	13.3	20.0	25.4
Sum total chlorination time to middle of run - mins	2.50	7.50	14.00	23.50	36.50	54.00	77.00
Cl_2 supplied x 10^3 gm-moles/min	2.49	2.50	2.49	2.49	2.52	2.51	2.49
gm-moles condensate/min x 10^3	2.33	2.26	2.33	2.25	2.07	2.10	1.95

Experiment 850°C 10.8 mole % CdO

Nominal reaction temperature - °C	850
Composition of pellets - mole % CdO	10.8
Initial bed weight - gms	120.02
Initial bed depth - cms	9.3
Size fraction of pellets - mm	-6.7 + 5.6
Number of pellets	210
Equilibrium separation constant	41.0
Total weight of oxide volatilised - gms	14.11
Calculated total weight of oxide volatilised - gms	14.27
Total moles Cd volatilised - gm-moles	0.0810
Total moles Zn volatilised - gm-moles	0.0475
Initial moles ZnO in bed - gm-moles	1.24
Initial moles CdO in bed - gm-moles	0.150
% bed depletion Zn	3.84
% bed depletion Cd	53.9
Total time of bed at temperature - hours	4.12
Sum total time of chlorination - mins	53.00

Run number	SK50	SK51	SK52	SK53	SK54	SK55
Temperature - °C	851	851	851	851	851	851
Reaction time - mins	3.00	4.00	5.00	8.00	13.00	20.00
Cl_2 flow - Mls_{NTP}/min	54.6	54.6	54.6	54.6	54.7	54.7
N_2 flow - Mls_{NTP}/min	1169	1335*	1330*	1330*	1331*	1330*
Gas delivery P. - mm Hg	757.9	758.2	758.2	757.9	758.5	758.1
ΔP. reactor/condenser - mm Hg	3.5	3.8	3.8	3.5	4.1	3.7
Cd analysis (AA)x10^3- gm-moles	6.94	9.07	10.2	14.7	19.1	21.0
Zn analysis (AA)x10^3- gm-moles	0.196	0.661	1.80	4.89	12.6	27.4
Measured condensate wt- gms	1.23	1.64	2.01	3.12	4.98	7.25
Calculated condensate wt - gms	1.29	1.75	2.12	3.36	5.22	7.58
Cd rate x 10^6 - gm-moles/sec	38.5	37.8	34.0	30.6	24.5	17.5
Zn rate x 10^6- gm-moles/sec	1.09	2.75	5.99	10.2	16.2	22.8
Sum total chlorination time to middle of run - mins	1.50	5.00	9.50	16.00	26.50	43.00
Cl_2 supplied x 10^3 gm-moles/min	2.47	2.47	2.47	2.47	2.48	2.48
gm-moles condensate/min x 10^3	2.38	2.43	2.40	2.45	2.44	2.42

* N_2 Carrier gas flow rate about 14% high

Experiment 950°C 10.8 mole % CdO

Nominal reaction temperature - °C	950
Composition of pellets - mole % CdO	10.8
Initial bed weight - gms	120.42
Initial bed depth - cms	9.1
Size fraction of pellets - mm	-6.7 + 5.6
Number of pellets	205
Equilibrium separation constant	28.8
Total weight of oxide volatilised - gms	11.99
Calculated total weight of oxide volatilised - gms	11.93
Total moles Cd volatilised - gm-moles	0.0340
Total moles Zn volatilised - gm-moles	0.0929
Initial moles ZnO in bed - gm-moles	1.24
Initial moles CdO in bed - gm-moles	0.151
% bed depletion Zn	7.48
% bed depletion Cd	22.6
Total time of bed at temperature - hours	4.22
Sum total time of chlorination - mins	52.03

Run number	SK56	SK57	SK58	SK59	SK60	SK61
Temperature - °C	953	952	952	952	952	951
Reaction time - mins	3.00	4.00	5.00	8.00	13.00	19.03*
Cl_2 flow - Mls_{NTP}/min	55.3	55.3	55.2	55.3	55.2	55.2
N_2 flow - Mls_{NTP}/min	1180	1181	1184	1184	1181	1181
Gas delivery P. - mm Hg	765.4	765.7	765.3	765.6	765.3	765.6
ΔP. reactor/condenser - mm Hg	3.9	4.2	3.8	4.1	3.8	4.1
Cd analysis (AA) x 10^3 - gm-moles	6.43	4.76	3.47	4.40	6.45	8.50
Zn analysis (AA) x 10^3 - gm-moles	0.709	5.20	8.49	14.9	25.8	37.8
Measured condensate wt - gms	1.08	1.43	1.49	2.56	4.47	6.86
Calculated condensate wt - gms	1.27	1.58	1.79	2.84	4.70	6.71
Cd rate x 10^6 - gm-moles/sec	35.7	19.8	11.6	9.17	8.26	7.43
Zn rate x 10^6 - gm-moles/sec	3.94	21.7	28.3	31.0	33.1	33.0
Sum total chlorination time to middle of run - mins	1.50	5.00	9.50	16.00	27.50	42.50
Cl_2 supplied x 10^3 - gm-moles/min	2.51	2.51	2.50	2.51	2.50	2.50
gm-moles condensate/min x 10^3	2.38	2.49	2.39	2.41	2.48	2.43

* Run time not recorded accurately - value calculated on basis of amount of condensate

A P P E N D I X I

Experiment number		SMK2***	SMK3***	SMK1	SMK6	SMK7	SMK9	SMK12
Temperature - °C		749	749	752	854	952	952	952
Upper ZnO Bed	weight - gms	-	-	349.76	346.01	344.52	342.10	388.84
	size fraction - mm	-	-	+2.0 -4.0	+2.0 -4.0	+2.0 -4.0	+2.0 -4.0	+2.0 -4.0
	depth - cms	-	-	20.5	20.5	20.0	22.0	20.0
Reaction time - mins		6.00	6.00	6.00	6.00	6.00	6.00	6.67
Lower Bed	mole% CdO	100.0	100.0	100.0	100.0	100.0	50.0**	50.0**
	size fraction - mm	-4.75 +4.0	-4.75 +4.0	-4.75 +4.0	-4.75 +4.0	-4.75 +4.0	-8.0 +6.7	-8.0 +6.7
	weight - gms	70.08	70.09	70.10	70.19	70.19	80.38	80.07
	number of pellets	221	212	224	232	232	69	72
	depth - cms	3.3	3.1	3.5	3.2	3.0	-	5.0
N_2 flow - Mls_{NTP}/min		1175	1180	1190	1192	1200	O_2* 1210	O_2* 1213
Cl_2 flow - Mls_{NTP}/min		54.5	54.7	55.5	55.5	55.7	54.8	50.2
Cd analysis x 10^3 - gm-moles		13.9	14.2	5.87	2.14	3.04	6.98	9.74
Zn analysis x 10^3 - gm-moles		-	-	8.17	12.3	11.6	7.34	4.89
Ratio molesCd/moles Zn		-	-	0.718	0.714	0.262	0.951	1.99
Equilibrium separation constant		-	-	62.7	41.0	28.8	28.8	28.8
Measured oxide weight loss - gms		1.80	1.86	1.48	1.38	1.36	-	1.89
Calculated oxide weight loss - gms		1.78	1.82	1.42	1.28	1.33	-	1.65
Measured weight of condensate - gms		2.63	2.42	2.06	1.90	2.00	2.29	2.39
Calculated weight of condensate - gms		2.55	2.60	2.19	2.07	2.14	2.28	2.45
gm-moles Cl_2 passed x 10^3		14.8	14.9	15.1	15.1	15.1	14.9	15.2
gm-moles of condensate x 10^3		13.9	14.2	14.0	14.4	14.6	14.3	14.6
ΔP. reactor/condenser - mm Hg		2.0	1.9	3.2	5.4	4.7	4.7	8.9
Chlorinating gas delivery P. - mm Hg		770.2	768.4	768.9	772.9	781.5	762.7	770.8

* Oxygen carrier gas
** Batch 2 50/50 pellets
*** Single bed CdO chlorination runs

CdO/ZnO DOUBLE BED NON-EQUILIBRIUM CHLORINATION EXPERIMENTAL DATA

Experiment number		SMK4	SMK14	SMK13	SMK5	SMK8	SMK10	SMK11
Temperature - °C		753	754	853	854	953	954	953
Upper ZnO Bed	weight - gms	343.23	430.82	387.09	347.44	343.29	366.33	364.90
	size fraction - mm	+2.0 -4.0	+2.0 -4.0	+2.0 -4.0	+2.0 -4.0	+2.0 -4.0	+2.0 -4.0	+2.0 -4.0
	depth - cms	20.0	25.0	21.5	20.0	20.5	21.5	19.0
Reaction time - mins		6.00	6.00	6.00	6.00	6.00	6.00	6.00
Lower Bed	mole % CdO	50.0**	50.0**	50.0**	50.0**	50.0**	50.0**	50.0**
	size fraction - mm	-8.0 +6.7	-8.0 +6.7	-8.0 +6.7	-8.0 +6.7	-8.0 +6.7	-8.0 +6.7	-8.0 +6.7
	weight - gms	80.09	80.66	79.77	80.05	80.04	80.17	80.33
	number of pellets	70	72	72	70	70	72	73
	depth - cms	4.9	5.1	5.1	5.2	5.3	-	5.0
N_2 flow - Mls_{NTP}/min		1200	1166	1170	1200	1196	1193	1185
Cl_2 flow - Mls_{NTP}/min		54.9	54.6	54.8	55.5	55.5	55.3	54.0
Cd analysis x 10^3 gm-moles		13.2	13.8	12.5	10.2	7.52	10.1	7.43
Zn analysis x 10^3 - gm-moles		0.780	0.483	1.41	3.90	6.88	4.21	6.50
Ratio molesCd/moles Zn		16.9	28.6	8.9	2.62	1.09	2.4	1.14
Equilibrium separation constant		62.7	62.7	41.0	41.0	28.8	28.8	28.8
Measured oxide weight loss - gms		-	1.85	1.93	1.73	1.58	1.96	1.74
Calculated oxide weight loss - gms		-	1.81	1.72	1.63	1.53	1.64	1.48
Measured weight of condensate -gms		2.55	2.58	2.52	2.35	2.25	2.30	2.20
Calculated weight of condensate - gms		2.53	2.60	2.48	2.40	2.32	2.43	2.25
gm-moles Cl_2 passed x 10^3		14.9	14.8	14.9	15.1	15.1	15.0	14.7
gm-moles condensate x 10^3		14.0	14.3	13.9	14.1	14.4	14.3	13.9
ΔP. reactor/condenser - mm Hg		5.3	4.4	5.6	6.5	6.5	6.3	5.4
Chlorinating gas delivery P. - mm Hg		784.7	760.1	762.6	785.6	782.0	775.9	767.8

** Batch 2 50/50 pellets

A P P E N D I X J

Experiment number		CZS3	CZS4	CZS5	CZS6	CZS7*	CZS8*	CZS9
Temperature - °C		853	853	853	853	852	852	852
Atmospheric P. - mm Hg		772.0	771.6	758.9	759.0	767.5	769.4	771.9
Oxide Bed	size fraction - mm	-4.75 +1.6	-4.75 +1.6	-4.75 +1.6	-4.75 +1.6	-4.75 +1.6	-4.75 +1.6	-4.75 +1.6
	weight - gms	149.79	89.58	68.23	118.16	198.88	197.24	99.59
	depth - cms	20.5	13.0	9.5	16.0	26.0	26.0	13.8
Pre-chlorination Bed/reactor Conditioning	O_2 flow Mls_{NTP}/min	41	43	42.5	42.5	41	approx 1000	approx 1000
	N_2 flow Mls_{NTP}/min	none	none	none	none	none	none	none
	Ar flow Mls_{NTP}/min	960	955	960	953	952	none	none
	purge time - mins	37.00	5.00	7.00	7.00	7.00	13.00	6.00
	Po_2 - atmos**	0.042	0.044	0.042	0.043	0.042	1.01	1.02
Chlorination gas flow	O_2 flow - Mls_{NTP}/min	none	none	none	none	none	308	311
	N_2 flow - Mls_{NTP}/min	313	313	313	309	309	none	none
	Cl_2 flow Mls_{NTP}/min	29.5	31.0	29.5	29.3	29.5	29.0	29.8
	Po_2 - atmos**	0.0346	0.0373	0.0367	0.0339	0.0294	0.928	0.941
Reaction time - mins		20.00	15.00	15.00	15.00	20.00	20.00	15.00
Zn analysis x 10^3 - gm-moles		20.3	16.6	16.6	15.0	16.9	26.0	17.1
Co analysis x 10^4 - gm-moles		0.899	0.709	0.712	0.611	0.687	0.590	0.348
Ratio Zn/Co		225.8	234.1	233.1	245.5	246.0	440.7	491.4
Weight of condensate - gms		2.91	2.34	2.29	2.10	2.41	-	2.26
Calculated weight of condensate - gms		2.77	2.26	2.26	2.04	2.30	-	2.33
Weight loss of oxide - gms		1.95	1.52	1.48	1.42	1.64	-	1.42
Calculated weight loss of oxide - gms		1.65	1.35	1.35	1.22	1.37	-	1.39
gm-moles condensate x 10^3		20.4	16.7	16.7	15.1	17.0	26.1	17.1
gm-moles Cl_2 passed x 10^3		26.7	21.1	20.0	19.9	26.7	26.3	20.3
ΔP. reactor/condenser - mm Hg		2.6	1.7	1.7	1.9	2.6	3.0	1.7

* Same bed used for each run
** Based on a total pressure of Atmospheric + 1 mm Hg

COBALT OXIDE(S)/ZINC OXIDE EQUILIBRIUM CHLORINATION EXPERIMENTAL DATA

Experiment number		CZS12 *	CZS13	CZS10	CZS11	CZS14 *	CZS15	CZS16*
Temperature - °C		853	853	853	852	853	853	853
Atmospheric P. - mm		762.7	762.7	764.8	765.0	762.0	762.1	764.0
Oxide Bed	size fraction - mm	-4.75 / +1.6		-4.75 +1.6	-4.75 +1.6	-4.75 / +1.6		-4.75 +1.6
	weight - gms	199.89		120.37	100.60	153.16		140.41
	depth - cms	28.7		16.5	-	21.0		21.0
Pre-chlorinating Bed/reactor Conditioning	O_2 flow - Mls_{NTP}/min	approx 500	approx 500	116	119	116	118.5	56
	N_2 flow - Mls_{NTP}/min	none	none	none	none	none	none	none
	Ar flow - Mls_{NTP}/min	none	none	196	196	198	196.5	226
	purge time - mins	5.00	5.00	9.00	11.50	8.00	12.00	14.00
	Po_2 - Atmos.**	1.00	1.00	0.37	0.38	0.37	0.38	0.20
Chlorination gas flow	O_2 flow - Mls_{NTP}/min	308	308	116.5	115.5	115.5	115.5	53.5
	N_2 flow - Mls_{NTP}/min	none	none	197	195	198	197	256
	Cl_2 flow - Mls_{NTP}/min	29.9	29.9	29.7	29.7	29.5	30.0	29.7
	Po_2 - Atmos.**	0.941	0.925	0.370	0.371	0.366	0.367	0.192
Reaction time - mins		25.00	20.00	20.00	15.00	20.00	20.00	25.00
Zn analysis x 10^3 - gm-moles		23.6	24.4	21.4	16.0	19.6	25.6	27.5
Co analysis x 10^4 - gm-moles		0.458	0.466	0.563	0.402	0.509	0.718	0.882
Ratio Zn/Co		515.3	523.6	380.1	398.0	385.1	356.5	311.8
Weight of condensate - gms		3.12	3.42	2.89	2.31	2.75	3.42	3.75
Calculated weight of condensate - gms		3.22	3.32	2.92	2.18	2.67	3.49	3.75
Weight loss of oxide - gms		3.64		1.68	1.30	3.74		-
Calculated weight loss of oxide - gms		3.90		1.74	1.30	3.68		-
gm-moles condensate x 10^3		23.6	24.4	21.5	16.0	19.7	25.7	27.6
gm-moles Cl_2 passed x 10^3		32.8	27.1	26.9	20.2	26.7	27.2	33.6
ΔP. reactor/condenser - mm Hg		1.3	1.7	3.3	1.5	1.3	1.3	1.0

* Double chlorination experiment

** Based on a total pressure of Atmospheric + 1mm Hg

Experiment number		CZS17*	CZS18*	CZS19	CZS20*	CZS21	CZS22*	CZS23
Temperature - °C		853	852	852	853	853	854	853
Atmospheric P. - mm Hg		764.0	765.4		771.5		772.2	
Oxide Bed	size fraction - mm	-4.75 +1.6	-4.75/+1.6		-4.75/+1.6		-4.75/+1.6	
	weight - gms	140.41	145.16		165.95		158.12	
	depth - cms	21.0	19.0		21.5		22.0	
Pre-chlorination Bed/reactor Conditioning	O_2 flow - Mls_{NTP}/min	53	56	53.5	215	212	212	211
	N_2 flow - Mls_{NTP}/min	none	none	none	none	none	none	none
	Ar flow - Mls_{NTP}/min	225	226	228	118	118	118	119
	purge time - mins	8.00	12.00	8.00	15.00	6.00	15.00	5.00
	Po_2 - Atmos.**	0.19	0.20	0.19	0.66	0.65	0.65	0.65
Chlorination gas flow	O_2 flow - Mls_{NTP}/min	53	53.5	53.5	212	212	212	210
	N_2 flow - Mls_{NTP}/min	253	253	252	98.5	98.5	98	97.5
	Cl_2 flow - Mls_{NTP}/min	30.0	30.2	29.7	29.7	29.4	29.5	29.8
	Po_2 - Atmos.**	0.195	0.193	0.198	0.658	0.650	0.660	0.651
Reaction time - mins		20.00	25.00	20.00	25.00	20.00	20.00	20.00
Zn analysis x 10^3 - gm-moles		26.2	26.9	26.7	25.4	25.2	19.8	25.3
Co analysis x 10^4 - gm-moles		0.860	0.831	0.831	0.619	0.657	0.450	0.636
Ratio Zn/Co		304.6	323.7	321.3	410.3	383.6	440.0	397.8
Weight of condensate - gms		3.49	3.80	3.47	3.55	3.51	2.59	3.44
Calculated weight of condensate - gms		3.57	3.67	3.64	3.46	3.43	2.69	3.45
Weight loss of oxide - gms		4.36***	4.50		4.10		3.61	
Calculated weight loss of oxide - gms		4.37***	4.36		4.12		3.67	
gm-moles condensate x 10^3		26.3	27.0	26.8	25.5	25.3	19.8	25.4
gm-moles Cl_2 passed x 10^3		27.2	34.2	26.9	33.6	26.6	26.7	27.0
ΔP. reactor/condenser - mm Hg		0.8	1.9	1.9	1.7	1.5	1.2	1.5

* Double chlorination experiment
** Based on a total pressure of Atmospheric + 1mm Hg
*** Sum of CZS17 and CZS16

Experiment number		CZS24 *	CZS25	CZS26 *	CZS27	CZS28 *	CZS29
Temperature - °C		928	928	929	929	928	928
Atmospheric P. - mm Hg		773.2	773.2	773.5	773.5	769.9	769.9
Oxide Bed	size fraction - mm	-4.75/+1.6		-4.75/+1.6		-4.75/+1.6	
	weight - gms	133.18		136.52		130.38	
	depth - cms	18.5		19.0		19.5	
Pre-chlorination Bed/reactor Conditioning	O_2 flow - Mls_{NTP}/min	42	42	500	492	102.5	53
	N_2 flow - Mls_{NTP}/min	none	none	47	46.5	none	none
	Ar flow - Mls_{NTP}/min	965	970	none	none	526	275
	purge time - mins	42	5.00	21.00	8.00	55.00	5.00
	Po_2 - Atmos.**	0.042	0.042	0.93	0.93	0.16	0.16
Chlorination gas flow	O_2 flow - Mls_{NTP}/min	none	none	308	308	52.5	52.5
	N_2 flow - Mls_{NTP}/min	311	310	none	none	258	256
	Cl_2 flow - Mls_{NTP}/min	29.8	29.8	29.8	29.7	29.7	29.7
	Po_2 - Atmos.**	0.0378	0.0405	0.948	0.939	0.190	0.193
Reaction time - mins		20.50	20.00	20.00	20.00	20.00	20.00
Zn analysis x 10^3 - gm-moles		23.6	24.8	21.0	24.1	23.0	26.0
Co analysis x 10^4 - gm-moles		1.62	1.56	1.31	1.20	1.41	1.70
Ratio Zn/Co		145.7	159.0	160.3	200.8	163.1	152.9
Weight of condensate - gms		3.34	3.71	2.90	3.48	3.22	3.64
Calculated weight of condensate - gms		3.24	3.41	2.87	3.30	3.15	3.57
Weight loss of oxide - gms		8.32		4.46		8.32	
Calculated weight loss of oxide - gms		3.97		3.69		4.01	
gm-moles condensate x 10^3		23.8	25.0	21.1	24.2	23.1	26.2
gm-moles Cl_2 passed x 10^3		27.3	26.6	26.6	26.5	26.5	26.5
ΔP. reactor/condenser - mm Hg		2.0	2.0	1.7	2.0	1.5	1.9

* Double chlorination experiment
** Based on a total pressure of Atmospheric + 1mm Hg

Experiment number		CZS30 - * CZS31		CZS32 - * CZS33		CZS34 - * CZS35		CZS1*
Temperature - °C		1003	1003	1004	1004	964	964	904
Atmospheric P. - mm Hg		771.8	771.8	766.0	766.0	765.2	765.2	779.0
Oxide Bed	size fraction - mm	-4.75/+1.6		-4.75/+1.6		-4.75/+1.6		-4.75 +1.6
	weight - gms	128.34		129.60		150.84		92.54
	depth - cms	-	-	-	-	-	-	12.5
Pre-chlorination Bed/reactor Conditioning	O_2 flow - Mls_{NTP}/min	none	none	none	none	none	400	none
	N_2 flow - Mls_{NTP}/min	none	none	none	none	none	none	unknow
	Ar flow - Mls_{NTP}/min	960	750	950	950	930	none	none
	purge time - mins	16.00	10.00	15.00	5.00	16.00	5.00	5.00
	Po_2 - Atmos.**	0	0	0	0	0	1.00	0
Chlorination gas flow	O_2 flow - Mls_{NTP}/min	none	none	300	308	310	309	none
	N_2 flow - Mls_{NTP}/min	313	313	none	none	none	none	315
	Cl_2 flow - Mls_{NTP}/min	30.0	30.1	29.7	29.7	29.5	29.5	30.2
	Po_2 - Atmos.**	0.035	0.041	0.94	0.93	0.93	0.93	0.031
Reaction time - mins		15.00	15.00	15.08	15.00	15.00	15.00	10.00
Zn analysis x 10^3 - gm-moles		15.8	19.0	15.7	18.4	17.1	18.7	9.25
Co analysis x 10^4 - gm-moles		1.48	1.08	1.06	1.01	0.808	1.09	0.493
Ratio Zn/Co		106.7	175.9	148.1	182.1	211.6	171.6	187.6
Weight of condensate - gms		2.43	2.93	2.41	2.63	2.57	2.62	1.39
Calculated weight of condensate - gms		2.17	2.60	2.15	2.52	2.34	2.56	1.26
Weight loss of oxide - gms		-	-	-	-	-	-	2.33
Calculated weight loss of oxide - gms		-	-	-	-	-	-	1.75
gm-moles condensate x 10^3		15.9	19.1	15.8	18.5	17.2	18.8	9.30
gm-moles Cl_2 passed x 10^3		20.0	20.1	19.9	19.9	19.7	19.7	13.5
ΔP. reactor/condenser - mm Hg		3.6	3.4	4.3	3.4	3.7	3.6	1.3

* Double chlorination experiment
** Based on a total pressure of Atmospheric + 1mm Hg

Experiment number		CZS36 - * CZS37		CZS38 - * CZS39		CZS40 - * CZS41		CZS2*
Temperature - °C		1033	1033	1032	1032	1066	1066	904
Atmospheric P. - mm Hg		764.0	764.0	775.4	775.4	772.2	772.2	779.0
Oxide Bed	size fraction - mm	-4.75/+1.6		-4.75/+1.6		-4.75/+1.6		-4.75 +1.6
	weight - gms	151.02		150.79		152.11		92.54
	depth - cms	-	-	-	-	-	-	12.5
Pre-chlorination Bed/reactor Conditioning	O_2 flow - Mls_{NTP}/min	none	400	none	none	none	400	none
	N_2 flow - Mls_{NTP}/min	none	none	none	none	none	none	unknown
	Ar flow - Mls_{NTP}/min	945	none	895	350	930	none	none
	purge time - mins	15.00	5.00	24.00	7.00	15.00	7.00	5.00
	Po_2 - Atmos.**	0	1.00	0	0	0	1.02	0
Chlorination gas flow	O_2 flow - Mls_{NTP}/min	306	308	none	none	306	308	none
	N_2 flow - Mls_{NTP}/min	none	none	312	311	none	none	313
	Cl_2 flow - Mls_{NTP}/min	29.5	29.3	29.5	30.6	29.4	30.0	29.8
	Po_2 - Atmos.**	0.92	0.92	0.042	0.040	0.93	0.93	0.040
Reaction time - mins		15.00	15.00	15.00	15.00	17.00	15.00	10.00
Zn analysis x 10^3 - gm-moles		19.2	18.7	19.6	18.4	21.4	19.6	12.3
Co analysis x 10^4 - gm-moles		1.28	1.39	1.47	1.63	1.60	1.31	0.501
Ratio Zn/Co		150.0	134.5	133.3	112.9	133.7	149.6	245.5
Weight of condensate - gms		3.10	2.62	3.13	2.76	3.44	3.16	1.84
Calculated weight of condensate - gms		2.63	2.56	2.68	2.52	2.93	2.68	1.68
Weight loss of oxide - gms		-	-	-	-	-	-	2.33
Calculated weight loss of oxide - gms		-	-	-	-	-	-	1.75
gm-moles condensate x 10^3		19.3	18.8	19.7	18.5	21.5	19.7	12.30
gm-moles Cl_2 passed x 10^3		19.7	19.6	19.7	20.5	22.3	20.0	13.3
ΔP. reactor/condenser - mm Hg		4.5	4.2	4.6	4.0	5.0	-	1.6

* Double chlorination experiment
** Based on a total pressure of Atmospheric + 1mm Hg

APPENDIX K

DECOMPOSITION OF Co_3O_4

According to different literature sources, the decomposition* of Co_3O_4 to CoO and O_2 occurs at between about 890°C and 970°C. For the reaction

$6CoO + O_2 = 2Co_3O_4$ . . . . . .(1)

three literature values of ΔG°_T are given below (each for 2 gm-moles of Co_3O_4).

(a)[82] - 79200 + 64.9T cals (T = 298 - 1200°K)

(b)[3] - 87600 + 70.8T cals (T = 298 - 1300°K)

(c)[4] - 70900 + 14.72T $\log_e$T - 0.01046T^2 + 6.72 x 10^5 x T^{-1} - 31.34T cals (T = 718 - 1000°K)

Other workers[75,88] have studied the stability boundary between CoO and Co_3O_4 (T and P_{O_2} varied). Their results, which are in very good agreement, were not originally presented in terms of the standard free energy change; however, re-calculating their data gives:

ΔG°_T = - 71500 + 57.7T cals (T = 1068 - 1238°K)

These data sources are not in good enough agreement to precisely predict the decomposition behaviour of Co_3O_4. Since an experimental apparatus for directly determining dissociation pressures was available, it was decided to try to clarify the available data by measuring equilibrium oxygen pressures over decomposing Co_3O_4.

K1 Measurement of decomposition oxygen pressures

Since the object of these few experiments was to aid interpretation of existing data rather than to be a new and exact determination only essential details will be reported. The apparatus used for the measurements consisted of a closed end silica reaction tube connected by a cone and socket joint to a mercury manometer and a three way vacuum stop cock. Built into the system was a small bore sealed end silica tube which reached to the end of the reaction vessel. Along this a thermocouple could be inserted to measure the temperature directly above a silica boat containing the decomposing oxide. With a vacuum pump the apparatus could be thoroughly evacuated; then, by turning the tap, the system could be sealed. Heating of the oxide was by a small kanthal wound furnace. This

---

* The temperature at which P_{O_2} = 1 atmos.

was mounted on rails so that it could slide to a position in which the oxide then sat at the furnace centre. Co_3O_4 was prepared by heating cobaltous oxide* powder at 850°C for 24 hours in an atmosphere of pure oxygen. After this treatment the black powder was rapidly cooled, and then stored in an airtight jar.

For the experiment, about 5 gms of oxide was placed in a short silica boat, this was then pushed to the end of the reaction tube. During assembly of the apparatus all the ground glass joints incorporated in the system were carefully sealed with silicone high vacuum grease. The apparatus was then pumped down and checked for leaks. Once the cold apparatus was found to be leak free, the furnace was moved into position and heated to about 700°C. At this temperature the system was further evacuated in order to remove any desorbed gases; it was then sealed from the atmosphere and checked for leaks over a period of two days. Once it was found that there were no leaks, the temperature of the oxide was raised to 830°C (the lowest temperature at which the decomposition oxygen pressure could be measured with reasonable accuracy). As the oxide decomposed, the pressure in the apparatus gradually increased until it attained its equilibrium value; equilibrium was assumed once there had been no change in the oxygen pressure for a period of one hour. By recording both the atmospheric pressure and the manometer pressure, the equilibrium oxygen pressure could be calculated by subtraction. The temperature about 10 mm above the oxide charge was measured to the nearest °C using a Pt/Pt 13% Rh termocouple and a potentiometer box. Readings were taken from 830°C up to just below the P_{O_2} = 1 atmos. decomposition temperature. An attempt was made to check the reversibility of the reacting system by comparing readings taken during 'heat up' with those taken during 'cool down'. Unfortunately the re-combination reaction proceeded so slowly that it was impractical to continue taking readings. Consequently, all data presented here was obtained at progressively increasing temperatures.

---

* British Drug Houses

K2 Presentation of literature and experimental data

If it is assumed that CoO and Co_3O_4 are both present at unit activity, then the equilibrium oxygen partial pressure is related to ΔG°_T by the following equation:

$$\Delta G^\circ_T = RT \log_e P_{O_2} \text{ - cals/1 gm-mole } O_2 \quad \ldots\ldots\ldots\ldots \quad (2)$$

where P_{O_2} is measured in atmospheres. There are several possible ways of plotting oxygen pressure against temperature. Since ΔG°_T for most reactions can be satisfactorily expressed in the form of the linear equation:

$$\Delta G^\circ_T = \Delta H^\circ - T\Delta S^\circ \quad \ldots\ldots\ldots\ldots\ldots\ldots\ldots\ldots \quad (3)$$

by re-arranging equation (2) the following relationship is obtained:

$$\frac{\Delta H^\circ}{4.576T} - \frac{\Delta S^\circ}{4.576} = \log_{10} P_{O_2}$$

Therefore, a plot of $\log_{10} P_{O_2}$ vs $\frac{1}{T}$ should give either a straight line or a close approximation to a straight line; the gradient and intercept of which are governed by ΔH° and ΔS° respectively. Plotting experimental data in this way would be invalid if the assumption of unit activities for the two oxides was incorrect. The only way that variations from unit activity could occur would be by CoO - Co_3O_4 solid solution formation. Searches through the literature[74,83,84] have not, however, revealed any evidence of solid solubility in this system. Experimentally determined data, for the temperature range 830°C to 940°C is given in table K1 below.

Temp °C	P_{O_2} Atmos.	$\text{Log}_{10} P_{O_2}$	$\frac{1}{T^\circ K} \times 10^4$
830	0.051	-1.295	9.066
836	0.062	-1.207	9.017
859	0.122	-0.913	8.834
888	0.251	-0.602	8.613
918	0.505	-0.296	8.396
933	0.748	-0.126	8.292
940	0.862	-0.063	8.244

TABLE K1 Co_3O_4 DECOMPOSITION RESULTS

On Graph K1 are given plots of $\log_{10} P_{O_2}$ vs $\frac{1}{T^\circ K}$ for the experimental

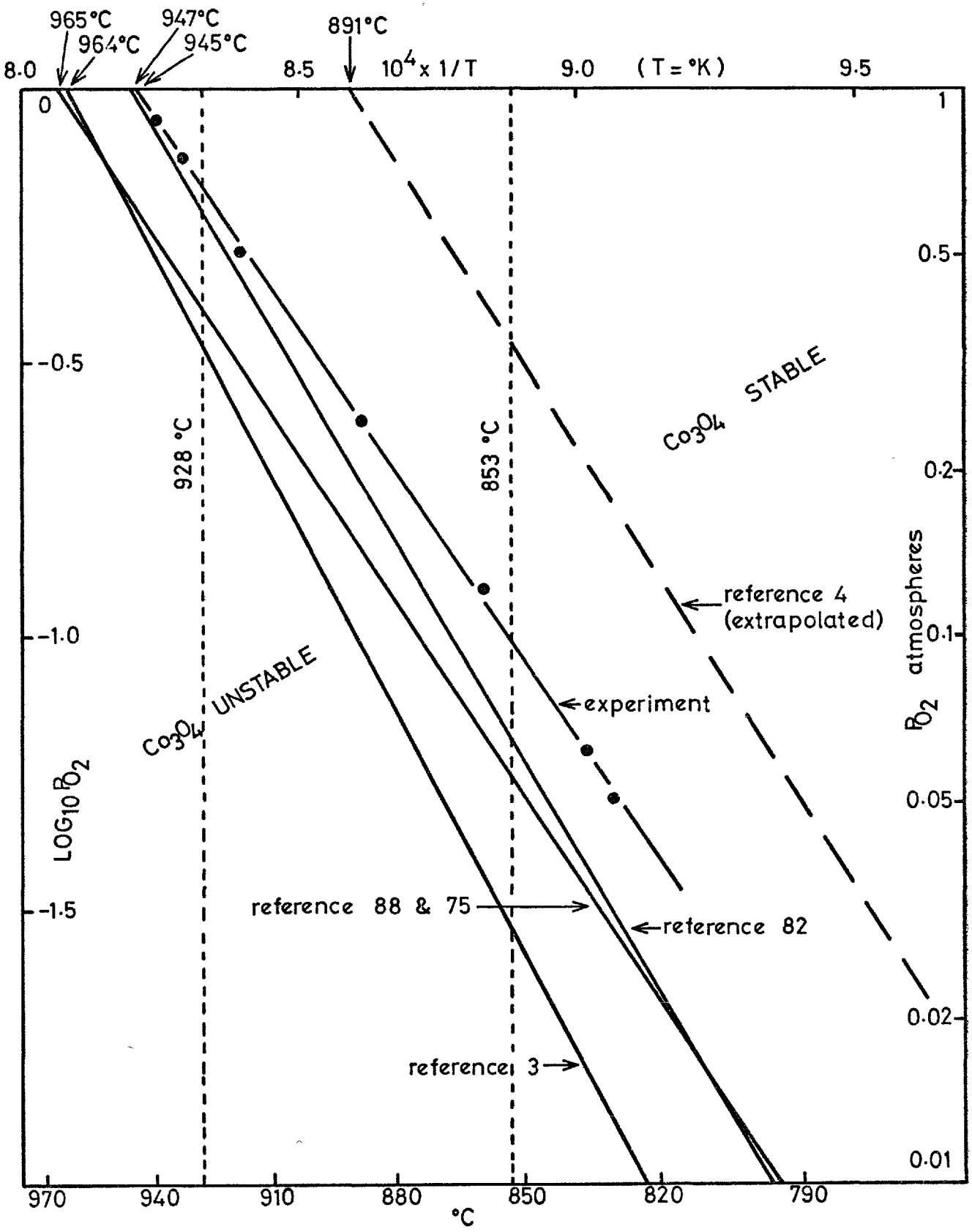

GRAPH K1:

$LOG_{10}P_{O_2}$ vs 1/T FOR THE DECOMPOSITION REACTION

$2Co_3O_{4(s)} = 6CoO_{(s)} + O_{2(g)}$

(OXIDES AT UNIT ACTIVITY)

measurements and the four sets of literature data. The plot for reference 4 data is shown as a broken line since it has been extrapolated from lower temperatures (1000°K).

K3 Discussion - Decomposition of Co_3O_4

The information given in reference 4 is mostly based upon a compilation of specific heat data (species CoO, Co_3O_4, Co and O_2). Its suggested accuracy appears a little ambitious, also the plotted data has been extrapolated from 1000°K. The other lines given on graph K1 have been mainly derived from data obtained by more direct means (measurement of chemical equilibria). Reference 4 data is thus thought to be unreliable and will not be considered again.

Agreement between the four remaining sets of data is reasonable. The predicted decomposition temperatures are 965°C (references 75 and 88), 964°C (reference 3), 947°C (reference 82) and 945°C (experiment). Since there appears to be no evidence for the existence of solid-solubility in the system CoO - Co_3O_4, the experimentally measured oxygen decomposition pressures are probably in error only as a result of experimental inaccuracies. A critical assessment of all the errors associated with the experimental procedure and apparatus does not deserve consideration here since only a few readings, of a confirmatory nature, were taken. However, two points can be made:

1. Assuming that the system did not leak, and that chemical equilibrium was achieved, the oxygen pressures could be quite accurately recorded.
2. The largest errors were almost certainly in the values of the measured temperatures. The thermocouple, from whose thermoelectric output the temperature was recorded, sat about 10 mm above the centre of a 30 mm long silica boat containing the decomposing oxide. Since at the temperatures investigated, radiative heat transfer predominates, the actual temperatures recorded would have been strongly influenced by the temperature distribution in the surrounding silica tube. Another potential error was that the furnace used could not be claimed to have had anything more than an 'approximately-constant' temperature zone. It is estimated that the temperature differential along the silica boat <u>might</u> have been as great as 10°C.

Data from reference 82 is due to Kubaschewski and Catterall who, it is presumed, compiled the most reliable information available at the time of their publication in 1956. Reference 3 data is due to Kubaschewski, Evans and Alcock who once again, it is presumed, compiled the best available pre-publication (1967)thermodata. Unfortunately their sources of information are not documented; thus the discrepancy between reference 3 and reference 82 data cannot be attributed to any particular more accurate or more recent determinations. There is a tendency, often for good reason, to assume that the most recent thermochemical data is the most reliable. However, of the four seemingly reliable plots on graph K1, considering the information available on their derivation, no one line can be favoured.

With the system cobalt oxide(s)/zinc oxide, no equilibrium experiments were performed between the temperatures 853°C and 928°C. Results of the experiments carried out at each of these two temperatures, under various oxygen partial pressures, are in fairly good agreement with predictions from the four sets of data under consideration. These results are reported and discussed in chapters 5 and 6 respectively.

The computed standard free energy change for reaction 1, based upon the experimental results presented in this appendix is given below.

$\Delta G^{\circ}_{T} = -68300 + 56.1T$ cals $\quad (T = 1103 - 1213^{\circ}K)$

APPENDIX L

STANDARD FREE ENERGIES OF FORMATION OF CoO, Co_3O_4, CdO, ZnO, $ZnCl_2$, $CdCl_2$ AND $CoCl_2$

In this appendix, whenever possible, directly determined (by experiment) standard free energy changes are reported in preference to compiled values. In many cases data extrapolations have been necessary; for this purpose only reliable phase transformation data have been used. ΔCp effects have, however, been neglected since the Cp data required is either not available or is of limited accuracy. It is felt that this omission does not reduce the general accuracy of the computed ΔG° values by a significant amount. Hypothetical standard states (a standard state in which the species concerned cannot exist) are used in a number of places in this appendix. At below certain temperatures the ΔG° results presented in chapter 5 refer to hypothetical standard states, namely $ZnCl_{2(g)}$, $CdCl_{2(g)}$ and $CoCl_{2(g)}$. Thus for the purposes of direct comparison the free energy changes tabulated in this appendix, for reactions involving metal chlorides, refer to a gaseous-chloride standard state. In addition, gaseous standard states have been adopted for Zn and Cd to aid comparison of different sets of data and to simplify various calculations. The marking "*" indicates the use of a hypothetical standard state, "**" indicates extrapolated data.

L1 CoO

For the reaction

$$Co_{(s)} + \tfrac{1}{2}O_{2(g)} = CoO_{(s)}$$

there are several sources of data which give the standard free energy of formation of CoO. Kubaschewski and Catterall[82] whose data are based upon a compilation of the results obtained by various workers, report

$\Delta G^\circ_T = -56950 + 18.55T$ cals/mole $\quad (T = 298 - 1400^\circ K)$

A direct determination by Tretjakow and Schmalzried[91] using solid electrolyte cells, gave

$\Delta G^\circ_T = -57600 + 18.61T$ cals/mole $\quad (T = 1000 - 1500^\circ K$, estimated error $\pm$ 100 cals)

Kuabschewski, Evans and Alcock[3], who do not cite their data source(s), give

ΔG°_{T} = -55900 + 16.9T cals/mole

(T = 298 - 1400°K, estimated error ± 1000 cals)

From solid electrolyte EMF measurements Moriyama[92] and co-workers report

ΔG°_{T} = -56000 + 16.91T cals/mole (T = 1120 - 1400°K)

The most recent study appears to be that by Bugden and Pratt[90], who, using calcia and magnesia stabilised zirconia solid electrolyte cells with either the sytem Cu/Cu_2O or Ni/NiO for reference, obtained the following free energy data

ΔG°_{T} = -55697 + 16.96T cals/mole

(T = 880 - 1250°K, estimated error ± 300 cals)(Cu/Cu_2O reference)

ΔG°_{T} = -55693 + 16.99T cals/mole

(T = 890 - 1200°K estimated error ± 300 cals)(Ni/NiO reference)

The data given above are best summarised by comparing the calculated ΔG°_{T} values given in the table below.

$\Delta G^{\circ}T$ cals/mole

Ref \ T°K	1150	1200	1250	1300	1350
(82)	-35620	-34690	-33760	-32830	-31910
(91)	-36200	-35270	-34340	-33410	-32480
(3)	-36460	-35620	-34770	-33930	-33080
(92)	-36550	-35710	-34860	-34020	-33170
(90)	-36170	-35320	-34480	-33630**	-32780**

TABLE L1 $CoO_{(s)}$

Agreement between all five different sets of data is good. It is particularly good for sources 3, 92 and 90.

L2 Co_3O_4

Some of the available thermodynamic data for the reaction

$6CoO_{(s)} + O_{2(g)} = 2Co_3O_{4(s)}$

have been examined in appendix K. Bugden and Pratt[90], in their recent work on cobalt oxides, have determined the standard free change for the reaction given above; their reported values are:

G°_{T} = -94104 + 77.62T cals/ 2 moles

(T = <1200°K, estimated error ± 600 cals, Ni/NiO reference)

and:

ΔG°_{T} = -95246 + 78.76T cals/2 moles

(T = <1200°K, estimated error ± 500 cals)(Ni/NiO reference)

The data for Co_3O_4 are summarised in the table below.

ΔG°_{T} cals/2 moles

Ref \ T°K	1100	1150	1200
(82)	-7810	-4560	-1320
(3)	-9720	-6180	-2640
(75)(88)	-8030	-5140	-2260
Present study	-6590	-3780	-980
(90)	-8660	-4760	-847

TABLE L2 $Co_3O_{4(s)}$

From these calculated ΔG°_{T} values it is evident that there is considerable disagreement between the different data sources. The ΔH° and ΔS° values vary by up to 25K cals/2 moles and 22 cals/2 moles°K respectively. Since the solid oxide electrolyte EMF method is potentially very accurate, as well as being direct, the work of Bugden and Pratt[90] would appear to be the most reliable.

L3 CdO

Only two direct determinations of the equilibrium

$Cd_{(g)} + \frac{1}{2}O_{2(g)} = CdO_{(s)}$

could be found in the literature. Both studies employed the entrainment method. Gilbert and Kitchener[93] report a standard free energy change of

ΔG°_{T} = -86120(±2900) + 48.84(±2.5)T cals/mole (T = 1150 - 1374°K)

In good agreement with this data is the work of Glemser and Stoecher[94]. Their reported values are

ΔG°_{T} = -87240 + 49.95T cals/mole (T = 1242 - 1379°K)

Calculated ΔG°_{T} values for both of these determinations are given in the table below.

$\Delta G^{\circ}T$ cals/mole

Ref \ T°K	1000*	1050	1100	1150	1200	1250	1300
(93)	-37280**	-34840**	-32400**	-29950	-27510	-25070	-22630
(94)	-37290**	-34800**	-32290**	-29800**	-27300**	-24800	-22300

Table L3 $CdO_{(s)}$

Agreement between these two data sources is seen to be very good.

L4 ZnO

For the reaction

$Zn_{(g)} + \frac{1}{2}O_{2(g)} = ZnO_{(s)}$

Kubaschewski[3] et al, who do not give their data sources, report a standard free energy change of

$\Delta G^{\circ}_{T} = -115420 - 10.35T \log_{10}T + 82.38T \pm 2000$ cals/mole

$(T = 1170 - 2000^{\circ}K)$

Wicks and Block[4] whose data appear to be derived from compiled Cp values (excluding ΔH°, the heat of reaction) give for the formation of $ZnO_{(s)}$ from liquid zinc

$\Delta G^{\circ}T = -85600 - 0.63T \log_{e}T - 0.36T^{2}10^{-3} + 0.99T^{-1}10^{5} + 31.28T$ cals/mole

$(T = 693 - 1181^{\circ}K)$

These two literature sources are of unknown reliability. Fortunately, however, there have been two recent direct determinations of the Zn-O_2 equilibrium. Kazenas[96] and co-workers, using a mass spectrometric technique, have studied the $Zn_{(g)} + \frac{1}{2}O_{2(g)}$ reaction at high temperatures. They calculate the standard free energy of formation of $ZnO_{(s)}$ to be

$\Delta G^{\circ}T = -119800 + 52.8T$ cals/mole $\quad (T = 1300 - 1450^{\circ}K)$

Wilder[95], employing a calcia stabilised zirconia solid electrolyte cell with the Ni/NiO system for reference, gives, for the $Zn_{(l)} + \frac{1}{2}O_{2(g)}$ reaction

$\Delta G^{\circ}T = -85080 + 25.7T$ cals/mole $\quad (T = 693 - 1181^{\circ}K)$

The four sets of data given above refer to two zinc standard states. The heat of vapourisation of $Zn_{(l)}$ as given by reference 3 is:

ΔH_{ev} = + 27.3 ± 0.4 k cals/mole

T_{ev} = 1180°K

thus

ΔS_{ev} = +23.13 cals/mole °K

Making the necessary adjustments due to the change in standard state, it is now possible to extrapolate reference 4 and reference 95 data to higher temperatures so that the four different sets of values may be simultaneously compared. Calculated $\Delta G^{\circ}T$ values, over the temperature range of interest, for the reaction $Zn_{(g)} + \frac{1}{2}O_{2(g)} = ZnO_{(s)}$ are given in the table below.

$\Delta G^{\circ}T$ cals/mole

Ref \ T°K	1000*	1050*	1100*	1150*	1200	1250	1300
(4)	-60640	-58070	-55500	-52940	-50370**	-47810**	-45250**
(96)	-67000**	-64360**	-61720**	-59080**	-56440**	-53800**	-51160
(3)	-64090**	-61750**	-59430**	-57110**	-54800	-52510	-50220
(95)	-63550	-61110	-58670	-56220	-53780**	-51340**	-48900**

TABLE L4 $ZnO_{(s)}$

Data due to Wicks and Block[4] is in considerable disagreement with the other three sources. Of the remaining comparable sets of values, reference 3 and reference 95 appear to be in best agreement; since the latter of these two is known to have been due to a direct determination it is possibly the more reliable.

L5 $ZnCl_2$

In 1950 Kellogg[29] and Villa[30] both published comprehensive compilations of the standard free energies of formation of many metal chlorides. Unfortunately at that time much fundamental data was either not available, or was quite inaccurate and consequently their data will not be reproduced here.

Three studies of the reaction

$Zn_{(l)} + Cl_{2(g)} = ZnCl_{2(l)}$

based upon electrochemical measurements will now be briefly reviewed.

Simple calculation* on the EMF values of Wachter and Hildebrand[98], obtained in the temperature range 773-848°K, gives

$\Delta G^{\circ}T = -97330 + 32.06T$ cals/mole

Lumsden[100], in reviewing fused salt data, reports the work of Markov, who measured

$\Delta G^{\circ}T = -97660 + 31.7T$ cals/mole

In more recent work, Markov et al[99] have apparently re-determined this standard free energy change; it is now given as

$\Delta G^{\circ}T = -88300 + 32.32T$ cals/mole $(T = 723 - 853^{\circ}K)$

Kubaschewski and co-workers[3] in their book on thermochemistry, reproduce the data of Villa[30] whilst Wicks and Block[4] rely upon extrapolations of low temperature data. These two sources are thus thought to be unreliable with regard to $ZnCl_2$. As Lumsden[101] has pointed out, electrochemical work was always assumed to be in error when compared with compiled $ZnCl_2$ data. However, once Cubicciotti and Eding[102] had shown that ΔS fusion $ZnCl_2$ was 4.2 ± 0.5 cals/mole°K instead of the previously erroneous value of about 10 cals/mole°K, the main error was then seen to be in the compiled data rather than the EMF measurements. ΔS° values for the three sets of $ZnCl_{2(l)}$ data given above are in good agreement. This is not the case for ΔH°.

A recent publication[103] gives the following thermochemical values for $ZnCl_2$:

$\Delta H^{\circ}298 = -99.2$ k cals/mole

$\Delta G^{\circ}298 = -88.3$ k cals/mole

$\Delta S^{\circ}298 = -36.58$ k cals/mole°K

These data are for solid Zn and $ZnCl_2$. These data could be extrapolated to higher temperatures, but ΔCp terms would have to be neglected. However, accounting for phase changes only (ΔH fusion Zn = 1.74 ± 0.03 k cals/mole - 420°C[3]), $\Delta H^{\circ}ZnCl_{2(l)}$ (formed from liquid Zn) becomes - 98.42 k cals/mole. The discrepancy between this value and that due to Markov and Volkov[99] is large and certainly outside the bounds of ΔCp errors. It is thus possible that Markov's earlier work (see Lumsden[100]) was more accurate.**

The enthalpy of evaporation of Zn at its boiling point of 1180°K is $+27.3 \pm 0.4$ k cals/mole[3]. The entropy change is therefore +23.14 cals/mole°K. For $ZnCl_2$ at its boiling point of 1005°K the corresponding constants are[3] $+28.5 \pm 3.0$ k cals/mole, and +28.36 cals/mole°K. By changing standard

---

* Using Nernst's equations

** It seems very probable that the results of Markov et al[99] have been misreported in the Chemical Abstracts, ΔH° being - 98300 and not 88300; however, before this explanation can be accepted the original work must be seen.

states and extrapolating the sets of measurements to higher temperatures, ΔG°_{T} values for the reaction

$Zn_{(g)} + Cl_{2(g)} = ZnCl_{2(g)}$

have been calculated. These are given in the table below.

ΔG°_{T} cals/mole

Ref \ $T^{\circ}K$	1000*	1050*	1100*	1150*	1200	1250	1300
(98)	-69290**	-67950**	-66610**	-65260**	-63920**	-62580**	-61240**
(100)	-69980**	-68660**	-67330**	-66000**	-64680**	-63360**	-62040**
(99)	-60000**	-58640**	-57290**	-55930**	-54580**	-53225**	-51870**
(103)	-65870**	-64300**	-62730**	-61160**	-59590**	-58010**	-56440**

TABLE L5 $ZnCl_{2(g)}$

Data from reference 103 is included (ΔCp neglected) since it is probably the best available 298°K compilation to date. ΔG°_{T} values derived from sources 98 and 100 are in good agreement; they are probably the most accurate in the table. As has already been stated, data from reference 99 is thought to be unreliable.

L6 $CdCl_2$

Only two electrochemical studies of the reaction

$Cd_{(l)} + Cl_{2(g)} = CdCl_{2(l)}$

could be found in literature. Lorenz and Velde[97] performed measurements in the temperature range 599°C to 771°C; their results can be expressed in the form of the equation below.

$\Delta G^{\circ}_{T} = -87210 + 29.02T$ cals/mole

Lantratov, whose work is reported by Lumsden[100] found

$\Delta G^{\circ}_{T} = -85020 + 26.7T$ cals/mole

Villa[30] and Kellogg[29] both give data compilations on $CdCl_2$ formation in all threee phases. Their high temperature data are, however, based upon extrapolations of low temperature measurements. These therefore include estimates for ΔCp effects, together with some not entirely reliable heats of fusion and evaporation. Recent values[103] for the relevant thermodynamic functions at 298°K are (for the reaction $Cd_{(s)} + Cl_{2(g)} = CdCl_{2(s)}$):

ΔH°_{298} = -93.57 Kcals/mole
ΔG°_{298} = -82.2 Kcals/mole
ΔS°_{298} = -38.15 cals/mole$^{\circ}$K

These figures are taken to be an improvement on those that were used in earlier reviews. Early compilations relied to some extent upon the work of Ishikawa[104] and co-workers, who reported

ΔH°_{298} = -92.15 Kcals/mole
ΔG°_{298} = -81.86 Kcals/mole
ΔS°_{298} = -34.53 cals/mole$^{\circ}$K

To extrapolate references 97, 100, and 103 values to higher temperatures (for the reaction $Cd_{(g)} + Cl_{2(g)} = CdCl_{2(g)}$) the following phase change data[3] may be used:

Cd ΔHfusion = +1.53 $\pm$ 0.04 k cals/mole(594°K)
ΔHevap. = +23.9 $\pm$ 0.3 k cals/mole(1038°K)

$CdCl_2$ ΔHfusion = +7.2 $\pm$ 0.2 k cals/mole(841°K)
ΔHevap. = +29.6 $\pm$ 0.8 k cals/mole(1234°K)

Calculated ΔG°_{T} values for the gas phase reaction are given in the table below.

ΔG°_{T} cals/mole

Ref \ T$^{\circ}$K	1000*	1050*	1100*	1150*	1200*	1250	1300
(97)	-53450**	-52050**	-50650**	-49240**	-47840**	-46440**	-45030**
(100)	-53580**	-52290**	-51000**	-49720**	-48430**	-47140**	-45860**
(103)	-51000**	-49440**	-47880**	-46320**	-44760**	-43200**	-41640**

TABLE L6 $CdCl_{2(g)}$

Agreements between values 97 and 100, although quite good, appear to be slightly better than they actually are. This is because the two ΔG°_{T} lines involved intersect just below the temperature range under consideration Reference 103 values, being based upon extrapolated 298°K data (without account of ΔCp) are least reliable.

L7 $CoCl_2$

The free energy of formation of $CoCl_2$ is less accurately established than is that of either $ZnCl_2$ or $CdCl_2$. In the literature there appear to be no reports on fused $CoCl_2$ electrochemical studies; neither do there appear to be reports on any other types of equilibrium determinations involving liquid or gaseous cobalt chloride. Phase transformation data is also in a state of uncertainty. The melting point of $CoCl_{2(s)}$ is variously given as 989°K[100], 997°K[4] and 1013°K[3]. Disagreement between ΔHfusion values is even greater with figures of 7.2[100], 7.4[4], 5.7[30] and 14.1[3] k cals/mole being reported. A similar situation exists for cobalt chloride evaporation. Here quoted data are 1298°K, + 37.6 Kcals/mole[3] and 1323°K, + 27.2 Kcals/mole[4] for the boiling point and heat of evaporation respectively. ΔH°_{298} $CoCl_{2(s)}$ is reported as being (in k cals/mole) - 77.8[4], -77.8[3], (reference 3 data is presumably taken from reference 4 although this is not in fact stated) -76.9[30] and most recently -74.7[103]. For ΔS°_{298}, the room temperature entropy of formation, two thermodata reviews give - 34.38 cals/mole°K[3] and -34.22 cals/mole°K[103]. Gee[106], using EMF cells, has investigated equilibria in the system.

$M,MCl_{2(s)} \;/\; BaCl_{2(s)} \;/\; M^1,M^1Cl_{2(s)}$

The metals studied were Cr, Mn, Fe, Co, Ni and Ag. For the reaction

$Co_{(s)} + Cl_{2(g)} = CoCl_{2(s)}$

calculated free energies of formation are

ΔG°_T = -72980 + 31.66T cals/mole (Ni/$NiCl_2$ reference)

ΔG°_T = -74420 + 33.08T cals/mole (Fe/$FeCl_2$ reference)

Gee[106] favours the measurements made with reference to Fe/$FeCl_2$ since this system is itself more accurately quantified than is the Ni/$NiCl_2$ system.

Egan[105], using an EMF cell, has studied the system

$\frac{1}{2}Co + AgCl$ (20 mole % in NaCl) = $\frac{1}{2}CoCl_2 + Ag$

his results indicate

$\Delta G^\circ_{673°K}$ = -52.73 k cals/mole

$\Delta G^\circ_{723°K}$ = -51.28 k cals/mole

for the free energy of formation of $CoCl_{2(s)}$

Gee's preferred equation gives

$\Delta G^\circ_{673°K}$ = -52.16 k cals/mole

$\Delta G^\circ_{723°K}$ = -50.50 k cals/mole

These two independent determinations are thus in quite good agreement.

Since the necessary high temperature data on cobalt chloride is not well known, it would be of little value to extend any of the EMF determinations up to temperatures at which $CoCl_2$ is gaseous. Under the given circumstances the best that can be done is to reproduce the data of previous authors. In the table below are given extrapolated ΔG°_T values for the reaction $Co_{(s)} + Cl_{2(g)} = CoCl_{2(g)}$

$\Delta G^\circ T$ cals/mole

Ref. \ $T^\circ K$	1100*	1150*	1200 *	1250*	1300*	1350
(30)	-36540**	-36490**	-36430**	-36350**	-36260**	-36170
(29)	-37660**	-37640**	-37620**	-37580**	-37530**	-37470
(3)	-38110**	-38100**	-38070**	-38030**	-37980**	-37910

TABLE L7 $CoCl_{2(g)}$

That the three sets of values above are in quite good agreement is mainly a result of many same data sources being used in each compilation.

APPENDIX M

X-RAY ANALYSIS OF ZnO/CoO AND ZnO/Co_3O_4 HEAT TREATED MIXTURES

M1 Sample preparation and heat treatment

The pure component oxides used in this investigation were a) ZnO as described in appendix D, b) Co_3O_4 (as used in appendix K) prepared by heating cobaltous oxide* for 24 hours at 850°C in pure oxygen and c) CoO prepared by holding part of this Co_3O_4 in a vacuum for 4 hours at 950°C. Before being weighed out the component oxides were dried at 150°C for about 30 minutes. Over 5 gms of each sample was prepared, the various compositions are estimated to have been accurate to within ±0.5% of the predetermined values. After weighing each sample was carefully mixed in a mortar and pestle for about 15 minutes. About half of each sample was heat treated. The Co_3O_4-ZnO mixtures were rapidly heated, in air, to 850°C, maintained at this temperature and then air cooled. To prevent oxidation the CoO-ZnO mixtures were contained in sealed silica tubes under about 0.3 atmospheres (at room temperature) of argon. The tubes were then rapidly heated to 1000°C, held at temperature and then air cooled. Once cooled, the samples, which tended to sinter into a single mass of porous oxide, were ground into fine powders in a mortar and pestle. Reacted** and unreacted cobalt oxide(s)/zinc oxide pellets were also ground into fine powders prior to X-ray examination.

M2 X-ray analysis

The X-ray analyses were performed using a) a Guinier type (manufacturers Nonius - Holland) focussing X-ray camera, b) an Elliot cobalt target tube and c) a Philips high voltage generator. With the Guinier camera a beam of polychromatic X-rays is simultaneously monochromated (Co-K_α) and focussed (at the surface of the camera drum) by a specially cut reflecting quartz crystal, adjusted by bending it under tension:

---

* British Drug Houses

** In each case about 20 reacted pellets from a variety of different chlorinatio runs were chosen so that the samples would be representative of the experiments as a whole.

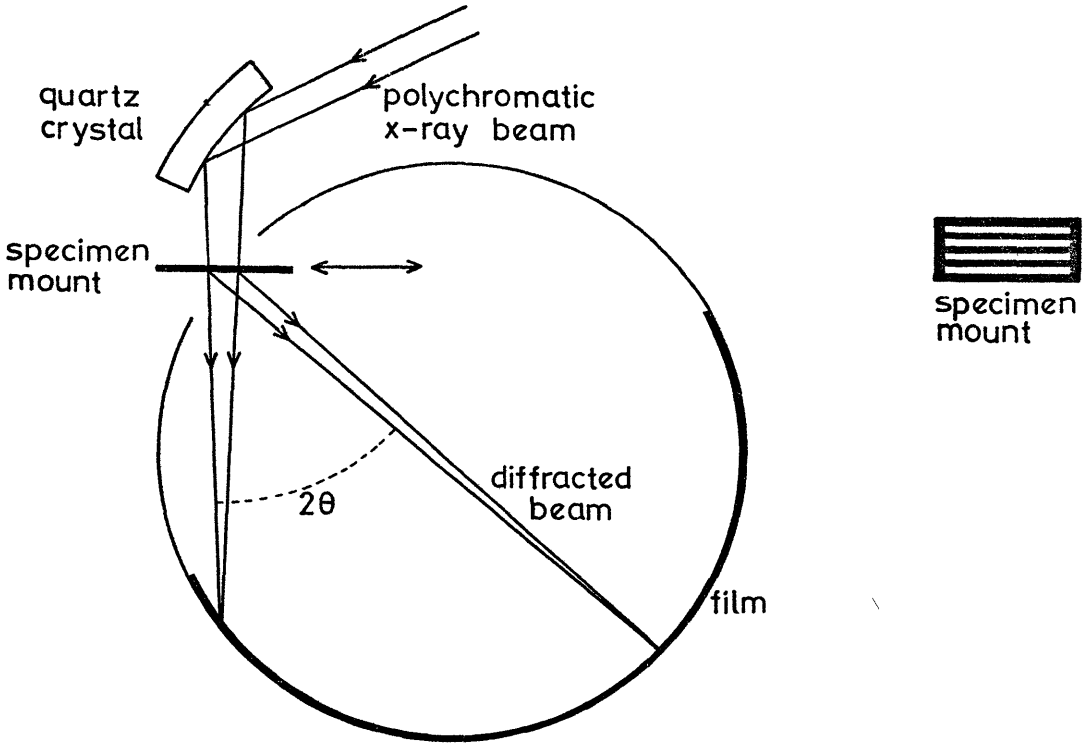

The powder samples, four of which can be examined at the same time, are mounted at the surface of the diffraction drum normal to the incident monochromatic X-ray bean. The powders are smeared onto 4 'cellotape' windows in a metal frame. Whilst being exposed the frame is slowly moved backwards and forwards across the beam. A diagram of the camera and sample mount is shown above. The effective diameter of the camera is 19 cms; the cobalt target was excited with 30 kV electrons; the cobalt Kα characteristic emission line has a wave length of 1.790 Å; the films were exposed for about $1\frac{1}{2}$ hours.

M3 Results

Twenty different X-ray diffraction photographs are shown on plate 13, the top five of which are standards. These standards are:

1. Pure CoO; this has an NaCl type cubic structure with a unit cell dimension of[139] 4.260 Å, the reflections from left to right (the undiffracted beam being on the extreme left of all the photographs) are from the 111, 200 and 220 planes respectively.
2. Pure Co_3O_4; this has a 2.3 type normal spinel structure with a unit cell dimension of[139] 8.084 Å, the reflections from left to right are from the 111, 220, 311, 222, 400, 422, 511 and 440 planes respectively.
3. Pure ZnO; this has a wurtzite hexagonal structure with a unit cell dimension of[139] 3.249 Å, the reflections from left to right are from the 100, 002, 101, 102, 110, 103, 200 and 112 planes respectively.
4. This film was obtained with an empty sample window.
5. This film was obtained with the sample window covered only with cellotape.

PLATE 13:

X-RAY DIFFRACTION PHOTOGRAPHS

The photographic process used for reproducing the exposures has reduced the contrast between the different reflections.

1. CoO, from the left: 111, 200 and 220
2. Co_3O_4, from the left: 111, 220, 311, 222, 400, 422, 511, and 440
3. ZnO, from the left: 100, 002, 101, 102, 110, 103, 200 and 112
4. No specimen or cellotape mount

5. cellotape mount only
6. Unreacted cobalt oxide(s)/zinc oxide pellets
7. Reacted Co_3O_4/ZnO pellets
8. Reacted CoO/ZnO pellets

9. 5 atom % Zn + 95 atom % Co (as Co_3O_4/ZnO) unheat-treated
10. 5 atom % Zn + 95 atom % CO (as Co_3O_4/ZnO) 6 hours - 851°C
11. 5 atom % Co + 95 atom % Zn (as Co_3O_4/ZnO) unheat-treated
12. 5 atom % Co + 95 atom % Zn (as Co_3O_4/ZnO) 6 hours - 851°C

13. 5 atom % Zn + 95 atom % Co (as Co_3O_4/ZnO) unheat-treated
14. 5 atom % Zn + 95 atom % Co (as Co_3O_4/ZnO) 3 hours - 850°C
15. 10 atom % Zn + 90 atom % Co (as Co_3O_4/ZnO) unheat-treated
16. 10 atom % Zn + 90 atom % Co (as Co_3O_4/ZnO) 3 hours - 850°C

17. 10 atom % Zn + 90 atom % Co (as CoO/ZnO) unheat -treated
18. 10 atom % Zn + 90 atom % Co (as CoO/ZnO) 3 hours - 1000°C
19. 10 atom % Co + 90 atom % Zn (as CoO/ZnO) unheat-treated
20. 10 atom % Co + 90 atom % Zn (as CoO/ZnO) 3 hours - 1000°C

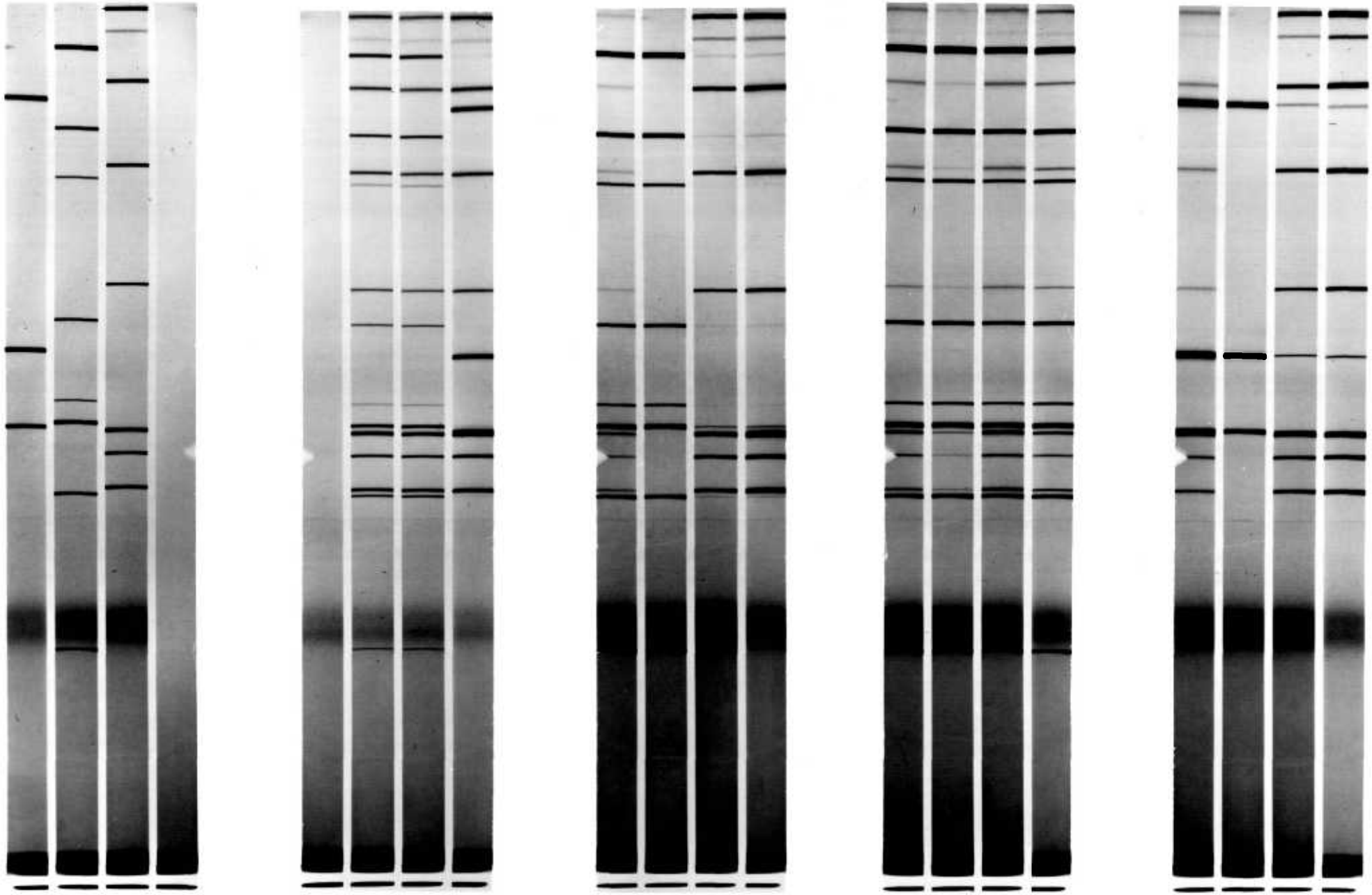

Comparison of exposures 4 and 5 shows that the cellotape produced a diffuse band on the left with a thin faint line immediately to its right. Some of the CoO, ZnO and Co_3O_4 lines are broad since in order to obtain reasonable exposures for the faint lines it was necessary to overexpose the intense lines. Exposures 6, 7 and 8 are of the unreacted as manufactured pellets, the pellets from the Co_3O_4/ZnO experiments and the pellets from the CoO/ZnO experiments respectively. These exposures show that the unreacted pellets and the pellets from the Co_3O_4/ZnO experiments did not contain CoO, whilst the pellets from the CoO/ZnO experiments did not contain Co_3O_4. No additional lines to those produced by the pure component oxides were produced by any of the oxide mixtures. Due to the closeness of the CoO 111 (d-spacing 2.460 Å)[139] and the ZnO 101 (d-spacing 2.476 Å)[139] lines, they tended to merge when overexposed (as in 8, also in 17, 18, 19 and 20).

Exposures 9-16 are of the various unheat-treated and heat treated Co_3O_4/ZnO mixtures; these are grouped in pairs with the unheat-treated sample being above the heat treated sample. 9 and 10 show that in 6 hours at 851°C the Co_3O_4 appeared to have completely dissolved 5 atom % Zn*. However, 13 and 14 show that after heat treating this same mixture for only 3 hours a small amount** of the 5 atom % Zn remained undissolved. This second result is in agreement with 15 and 16 where it can be seen that with a mixture containing 10 atom % Zn the majority remained undissolved after 3 hours' heating at 850°C. At the other end of the composition range exposures 11 and 12 show that a mixture containing 5 atom % Co appears to have been unchanged by 6 hours' heating at 851°C. These results indicate that with the Co_3O_4/ZnO experiments the rates of solution of Zn^{++} in Co_3O_4 and Co^{++} in ZnO were comparatively low.

Exposures 17-20 are of the two different composition CoO/ZnO mixtures. 17 and 18 show that after 3 hours at 1000°C the CoO appears to have completely dissolved 10 atom % Zn. However, 19 and 20 show that with this same heat

---

* With all the CoO/ZnO and Co_3O_4/ZnO mixtures the compositions are expressed in terms of atom % metal.

** Since it was not possible to control accurately how much oxide powder was smeared onto the cellotape, results deduced from comparisons of line intensities are only semi-quantitative.

treatment only a very small amount of Co dissolves in ZnO. (These last two exposures are interesting since they show that after heat treatment the 3 CoO lines are slightly displaced, due to dissolved zinc, from their initial positions.) The common feature between the Co_3O_4/ZnO and CoO/ZnO heat treatment tests is tha solution of Zn^{++} in both Co_3O_4 and CoO is more rapid than solution of Co^{++} in ZnO.

A P P E N D I X N

CALCULATION OF THE VISCOSITY OF MULTI-COMPONENT GAS MIXTURES

The viscosity of a pure gas can be calculated by using the Chapman-Enskog viscosity equation. This equation, developed from the same kinetic theory of gases as used to develop the Chapman-Enskog diffusivity equation given in section 8B3a is shown below.

$$\mu_i = 2.669 \times 10^{-5} \frac{\sqrt{M_i T}}{\sigma_i^2 \Omega_\mu}$$

μ_i = viscosity - gm/cm sec
T = temperature - ^oK
M_i = molecular weight of 'i'
σ_i = 'collision diameter' ('i' - 'i') - Å
Ω_μ = collision integral (dimensionless function of temperature and intermolecular potential field between two 'i' molecules: this collision integral is not equal to Ω_D the diffusivity collision integral).

Values for σ_i and Ω_μ can be determined by using similar methods as described in section 8B3a for determining the equivalent diffusivity parameters σ_{ij} and Ω_D. Data necessary for calculating gas viscosities are given by Hirschfelder et al[121] and Bird et al[62].

The viscosities of gas mixtures are often extremely non-linear with changing composition. An equation, obtained by making several approximations to the kinetic theory of gases, which predicts the viscosity of gas mixtures to within an average deviation of about ±2% is given by Wilke[138]. This equation is given below for an n component gas mixture.

$$\mu_m = \sum_{i=1}^{i=n} \left[\mu_i \left(1 + \frac{1}{N_i} \sum_{\substack{j=1 \\ j \neq 1}}^{j=n} N_j E_{ij} \right)^{-1} \right]$$

where:

$$E_{ij} = \left[1 + \left(\frac{\mu_i}{\mu_j}\right)^{\frac{1}{2}} \cdot \left(\frac{M_j}{M_i}\right)^{1/4} \right]^2 \cdot \frac{4}{\sqrt{2}} \left[1 + \frac{M_i}{M_j} \right]^{-\frac{1}{2}}$$

μ_i = viscosity of component 'i'
N_i = mole fraction of component 'i'
M_i = molecular weight of component 'i'

The Chapman-Enskog and Wilke equations given above are most accurate for non-polar gases at low density (eg 1 atmosphere).

A P P E N D I X O

COMPUTER PROGRAM LISTING AND SOLUTION OF EQUATIONS M1-M12

O1 Solution of equations M1-M12

Under a given set of conditions only one solution satisfies the simultaneous equations M1-M12. Solving these equations by a numerical method involves guessing the solution, testing this solution, modifying the guess and repeating the procedure until the guessed and test solution converge at the same value. The efficiency of this iterative process depends upon how rapidly the guessed and test values can be made to converge. A general method for solving the equations was required since they were to be used under a range of different conditions eg a) from the top to the bottom of each bed and b) for varying reaction parameters. Since it was found that the relationship between the guessed and test solutions was very complex, and also under certain conditions very sensitive, it was not possible to use an established (eg Newton-Raphson) iterative procedure. The procedure which was finally adopted, after a number of others had failed to guarantee convergence, required on average about 20-30 calculation loops to solve the surface chlorine partial pressure to within $\pm 0.0001\%$. Listed below is the calculation routine employed for solving equations M1-M12. The way in which the guessed surface chlorine partial pressure (step 1) was modified on the basis of the test surface chlorine partial pressure is explained after the list.

1. Guess surface chlorine partial pressure.
2. Calculate surface to bulk chlorine flux using equation M1.
3. Calculate surface to bulk oxygen flux using equation M8.
4. Calculate surface oxygen partial pressure using equation M2.
5. Calculate surface zinc chloride partial pressure using equation M11.
6. Calculate surface to bulk zinc chloride flux using equation M3.
7. Calculate surface to bulk cadmium chloride flux using eqation M7. If zero or negative return to 1 and use lower surface chlorine partial pressure value.
8. Calculate surface cadmium chloride partial pressure using equation M4.
9. If pellet radius = interface radius recalculate surface zinc chloride partial pressure using equation M12 and go to 15.

10. Calculate interface to surface cadmium chloride flux using equation M10.
11. Calculate interface cadmium chloride partial pressure using equation M6.
12. Calculate interface zinc chloride partial pressure using equation M12.
13. Calculate interface to surface zinc chloride flux using equation M9.
14. Re-calculate zinc chloride surface partial pressure using equation M5.
15. Re-calculate surface chlorine partial pressure (test value) using equation M11.
16. Compare guessed and test surface chlorine partial pressure values. If agreement is better than ±0.0001% solution is satisfactory; if not, return to 1 and use modified guessed value.

The method of obtaining convergence of the guessed and test surface chlorine partial pressure values relied upon the following two simple relationships: If the guessed value was greater than the correct solution then the test value was always smaller than the correct solution, and conversely if the guessed value was smaller than the correct solution then the test value was always greater than the correct solution. The way this behaviour was utilised is illustrated with the help of the diagram below:

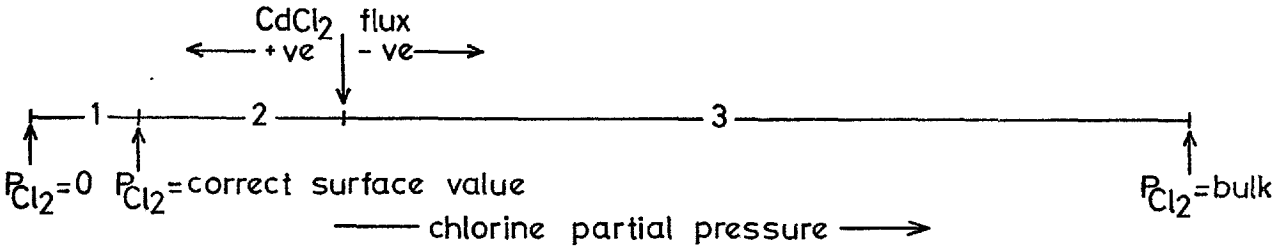

At the start of each calculation loop the guessed surface chlorine partial pressure was chosen to be equal to $\frac{1}{2}$(PPSMAX + PPSMIN); where PPSMAX = the current maximum surface chlorine partial pressure and PPSMIN = the current minimum surface chlorine partial pressure. For the first calculation loop PPSMIN = 0 and PPSMAX = the bulk chlorine partial pressure. If the guessed $_{s}P_{Cl_2}$ was high enough (ie in region 3 of the diagram above) to cause the $CdCl_2$ flux to be negative, PPSMAX was made equal to this guessed value and the calculation loop was repeated (in this way the calculation was repeated, PPSMAX being halved each time, until a positive $CdCl_2$ flux was obtained). When the $CdCl_2$ flux was positive the guessed $_{s}P_{Cl_2}$ value was tested to determine whether it was greater (ie region 2 above) or smaller (ie region 1 above) than the correct solution; if it was greater then PPSMAX was made equal to the guessed value, conversely if it was smaller then PPSMIN was made equal to the guessed value. The calculation loop was then repeated, the correct $_{s}P_{Cl_2}$ solution always being between the progressively converging PPSMAX and PPSMIN values, until the guessed and re-calculated values agreed to within ± 0.0001%.

02 Namelist

1. J = bed section (initially 50 later 100 in total).
2. TIM = time interval number.
3. M = counter for sections that are completely reacted.
4. I = species identification: 1 = $CdCl_2$, 2 = $ZnCl_2$, 3 = Cl_2, 4 = O_2 and 5 = N_2.
5. PPB(I,J), I = 1 to 5: bulk partial pressure entering section atmospheres.
6. PPS(I,J), I = 1 to 5: surface partial pressure in section atmospheres.
7. PPI(I,J), I = 1 and 2: interface partial pressure in section atmospheres.
8. F(I,J), I = 1 to 5: molar flow of species entering section gm-moles/sec.
9. FG(I,J), I = 1 to 4: flux of species through boundary layer per unit of pellet surface area gm-moles/sec cm^2.
10. FS(I,J), I = 1 and 2: flux through porous zinc oxide per unit of pellet surface area gm-moles/sec cm^2.
11. RP(J) = pellet radius cms.
12. RI(J) = interface radius cms.
13. DEFF(I), I = 1 and 2: effective diffusivity cm^2/sec.
14. RHOPZN, RHOPCD = ZnO and CdO molar densities respectively gm-moles/cm^3.
15. TNP, TNS = total number of pellets and sections respectively.
16. TNPS(L), L = 1 to 3: total number of pellets in the different sized sections.
17. DEPTH = bed depth cms.
18. DEEP(J), SUMDEP(J) = depth of section J and total bed depth to section J respectively.
19. GMTC(I), I = 1 to 4: boundary layer mass transfer coefficient cm/sec.
20. PRESS = total pressure atmospheres.
21. T = temperature ^oK.
22. R = gas constant atmos cm^3/gm-mole ^oK.
23. EQZN, EQZNCD = surface and interface equilibrium constants.
24. TIME = steady state reaction time interval seconds.
25. ANS, ANNS, ANSC = counters for subroutine ANSWER.
26. UTIL = chlorine utilisation %.
27. SUMTIM, TOTMIN = total time of reaction seconds and minutes respectively.
28. DEPLZN, DEPLCD = percentage ZnO and CdO depletion respectively.

```
JOB(UMCJ045,J10,CM30000,T300)                    D.T.CUMMINS.
MNF(D,T,R=0,P=5000)
'
      PROGRAM HALBED(INPUT,OUTPUT,TAPE5=INPUT,TAPE6=OUTPUT)
      INTEGER TIM
      COMMON/GPRESS/PPB(5,101),PPS(5,100),PPI(2,100)
      COMMON/GFLUX/F(5,101),FG(4,100),FS(2,100)
      COMMON/PELLET/RP(100),RI(100),RHOPZN,RHOPCD,DEFF(2),TNP,TNPS(3),
     1TNS
      COMMON/BED/DEEP(100),SUMDEP(100),DEPTH
      COMMON/GMT/GMTC(4)
      COMMON/UNSUB/PRESS,T,R,EQZN,EQZNCD,ANS,ANSC,TIME,SUMTIM,TOTMIN
     1,EQCD,SUMTCD,SUMTZN,SUMOLE,BEDTZN,BEDTCD,DEPLZN,DEPLCD,PELVOL,
     1UTIL,ANNS,TIMECD,TIMEZN
      COMMON/COUNT/ J,TIM,M
C
C     ******************************************************************
C     PROGRAM HALBED
C     THIS PROGRAM IS A MATHEMATICAL MODEL OF HIGH TEMPERATURE
C     CHLORINATION OF A PACKED BED OF PELLETS OF ZINC OXIDE AND CADMIUM
C     OXIDE MIXTURES. THE BED IS ASSUMED TO BE AT A UNIFORM TEMPERATURE
C     THROUGHOUT,ALL METAL CHLORIDES ARE GASEOUS AND CHEMICAL
C     EQUILIBRIUM IS ASSUMED AT THE PELLET SURFACE AND INTERFACE.
C     IT IS ASSUMED THAT NO CHLORINE PENETRATION OCCURS AND THAT ZINC
C     CHLORIDE IS THE CHLORINATING SPECIES FOR CADMIUM OXIDE.
C     THE MODEL IS A TRANSPORT CONTROL SYSTEM WITH A TOPOCHEMICAL
C     INTERFACE AND A SIMPLE GEOMETRIC REACTION MODE.
C     THE BED IS DIVIDED INTO 100 SECTIONS FOR THE CALCULATION.THE FIRST
C     40 SECTIONS CONTAIN 1/240 OF THE TOTAL PELLETS EACH THE NEXT 20
C     SECTIONS CONTAIN 1/120 OF THE TOTAL PELLETS EACH AND THE LAST
C     40 SECTIONS CONTAIN 1/60 OF THE TOTAL PELLETS EACH. THE EFFECTIVE
C     BULK GAS COMPOSITION IN EACH SECTION IS TAKEN TO BE THE SAME
C     AS THE ENTRY BULK GAS COMPOSITION
C     CONSTANT VOIDAGE IS ASSUMED THROUGHOUT THE BED DURING REACTION
C     ******************************************************************
C
C     RUN SK/  56 61   952 DEG C   10 MOLE PC.
C     ************ DECK C ************************************************
      NOLIST
C     ZERO ALL VARIABLES AND CONSTANTS
C
      DO 19 J=1,101
      DO 19 I=1,5
      F(I,J)=0.0
      PPB(I,J)=0.0
   19 CONTINUE
      DO 21 J=1,100
      DO 21 I=1,2
      PPI(I,J)=0.0
      FS(I,J)=0.0
   21 CONTINUE
      DO 22 J=1,100
      DO 22 I=1,4
      FG(I,J)=0.0
   22 CONTINUE
      DO 23 J=1,100
      RP(J)=0.0
      RI(J)=0.0
      DEEP(J)=0.0
      SUMDEP(J)=0.0
   23 CONTINUE
      DO 24 J=1,100
      DO 24 I=1,5
      PPS(I,J)=0.0
   24 CONTINUE
      GMTC(1)=0.0
      GMTC(2)=0.0
      GMTC(3)=0.0
```

```
      GMTC(4)=0.0
      RHOPZN=0.0
      RHOPCD=0.0
      DEFF(1)=0.0
      DEFF(2)=0.0
      TNP=0.0
      TNS=0.0
      PRESS=0.0
      T=0.0
      R=0.0
      EQZN=0.0
      EQZNCD=0.0
      EQCD=0.0
      ANS=0.0
      ANSC=0.0
      TIME=0.0
      SUMTIM=0.0
      TOTMIN=0.0
      SUMTZN=0.0
      SUMTCD=0.0
      SUMOLE=0.0
      BEDTZN=0.0
      BEDTCD=0.0
      DEPLZN=0.0
      DEPLCD=0.0
      PELVOL=0.0
      TIMECD=0.0
      TIMEZN=0.0
      DEPTH=0.0
C
C
C           MAIN PROGRAM
C
      CALL DATA
      DO 25 TIM =1,150
      DO 26 J=M,100
      CALL EQCALC
      CALL RESET
   26 CONTINUE
      CALL ANSWER
   25 CONTINUE
      STOP
      END
C
      SUBROUTINE DATA
      INTEGER TIM
      COMMON/GPRESS/PPB(5,101),PPS(5,100),PPI(2,100)
      COMMON/GFLUX/F(5,101),FG(4,100),FS(2,100)
      COMMON/PELLET/RP(100),RI(100),RHOPZN,RHOPCD,DEFF(2),TNP,TNPS(3),
     1TNS
      COMMON/BED/DEEP(100),SUMDEP(100),DEPTH
      COMMON/GMT/GMTC(4)
      COMMON/UNSUB/PRESS,T,R,EQZN,EQZNCD,ANS,ANSC,TIME,SUMTIM,TOTMIN
     1,EQCD,SUMTCD,SUMTZN,SUMOLE,BEDTZN,BEDTCD,DEPLZN,DEPLCD,PELVOL,
     1UTIL,ANNS,TIMECD,TIMEZN
      COMMON/COUNT/ J,TIM,M
C        DATA PACK UNITS      GMS CMS SECS
      DO 20 J=1,100
C        CM
      RP(J)=0.3146
      RI(J)=0.3146
   20 CONTINUE
C     SET BED SECTION DEPTHS
C     CMS
      DEPTH=10.0
      DO 30 J=1,40
      DEEP(J)=DEPTH/240.0
   30 CONTINUE
```

```
      DO 31 J=41,60
      DEEP(J)=DEPTH/120.0
   31 CONTINUE
      DO 32 J=61,100
      DEEP(J)=DEPTH/60.0
   32 CONTINUE
C        GM-MOL /CC
      RHOPZN=0.0451
      RHOPCD=0.00547
C        CM**2/SEC
      DEFF(1)=0.0009
      DEFF(2)=0.0009
C        CM /SEC
      GMTC(1)=6.0
      GMTC(2)=6.0
      GMTC(3)=9.0
      GMTC(4)=12.0
C         ATMOS
      PRESS=1.0065
      PPB(1,1)=0.0
      PPB(2,1)=0.0
      PPB(3,1)=0.04037
      PPB(4,1)=0.0
      PPB(5,1)=PRESS-(PPB(1,1)+PPB(2,1)+PPB(3,1)+PPB(4,1))
C        GM-MOL/SEC
      F(1,1)=0.0
      F(2,1)=0.0
      F(3,1)=0.00004053
      F(4,1)=0.0
      DO 27 J=1,101
      F(5,J)=0.0008792
   27 CONTINUE
C        ATMOS**.5
      EQZN=161.0
C        DIMENSIONLESS
      EQZNCD=29.4
      EQCD=EQZN*EQZNCD
C        DEG K
      T=1225.0
C        ATMOS-CC/MOL- DEG K
      R=82.057
C        SEC
      TIME=30.0
      TNS=100.0
      TNP=211.0
      ANS=1.0
      ANNS=0.0
      ANSC=0.0
C     DIVISION OF PELLETS INTO SEPARATE ZONES
      TNPS(1)=TNP/240.0
      TNPS(2)=TNP/120.0
      TNPS(3)=TNP/60.0
      PELVOL=TNP*3.14159*(4.0/3.0)*(RP(1)**3)
      BEDTZN=PELVOL*RHOPZN
      BEDTCD=PELVOL*RHOPCD
      M=1
C
C
      WRITE(6,115) (PPB(I,1),I=1,5)
  115 FORMAT(1X, 9HPPB(1,1)=,E15.8,2X, 9HPPB(2,1)=,E15.8,2X, 9HPPB(3,1)=
     1,F15.8,2X, 9HPPB(4,1)=,E15.8,2X, 9HPPB(5,1)=,E15.8)
      WRITE(6,116) (F(I,1),I=1,5)
  116 FORMAT(1X, 7HF(1,1)=,E15.8,2X, 7HF(2,1)=,E15.8,2X, 7HF(3,1)=,E15.8
     1,2X, 7HF(4,1)=,E15.8,2X, 7HF(5,1)=,E15.8)
      WRITE(6,117) (GMTC(J),J=1,4)
  117 FORMAT(1X,8HGMTC(1)=,E15.8,2X, 8HGMTC(2)=,E15.8,2X, 8HGMTC(3)=,E15
     1.8,2X, 8HGMTC(4)=,E15.8)
      WRITE(6,118)RP(1),RP(50),RI(1),RI(50)
```

```
  118 FORMAT(1X,6HRP(1)=,E15.8,2X, 7HRP(50)=,E15.8,2X, 6HRI(1)=,E15.8,2X
     1,  7HRI(50)=,E15.8)
      WRITE(6,119)RHOPZN,RHOPCD,DEFF(1),DEFF(2)
  119 FORMAT(1X, 7HRHOPZN=,E15.8,2X, 7HRHOPCD=,E15.8,2X, 8HDEFF(1)=,E15.
     18,2X,8HDEFF(2)=,E15.8)
      WRITE(6,121) EQZN,EQZNCD,T,R,ANS,ANSC,EQCD
  121 FORMAT(1X,5HEQZN=,F10.4,2X, 7HEQZNCD=,F10.4,2X, 2HT=,F10.4,2X,2HR=
     1,F10.4,2X, 4HANS=,F10.4,2X,5HANSC=, F10.4,2X,5HEQCD=,F10.4)
      WRITE(6,120) TNP,TNS,PRESS,TIME
  120 FORMAT(1X,4HTNP=,F6.1,2X,4HTNS=,F6.1,2X,6HPRESS=,F7.5,2X, 5HTIME=,
     1F6.1)
      WRITE(6,189) DEEP(1),DEEP(41),DEEP(61),DEPTH
  189 FORMAT(1X,8HDEEP(1)=,F10.6,3X,9HDEEP(41)=,F10.6,3X,9HDEEP(61)=,
     1F10.6,3X,6HDEPTH=,F10.6)
      WRITE(6,199) TNPS(1),TNPS(2),TNPS(3)
  199 FORMAT(1X,39HNUMBER OF PELLETS IN DIFFERENT SECTIONS,2X,8HTNPS(1)=
     1,F8.6,1X,8HTNPS(2)=,F8.6,1X,8HTNPS(3)=,F8.6 // )
      RETURN
      END
C
      SUBROUTINE EQCALC
      INTEGER TIM
      COMMON/GPRESS/PPB(5,101),PPS(5,100),PPI(2,100)
      COMMON/GFLUX/F(5,101),FG(4,100),FS(2,100)
      COMMON/PELLET/RP(100),RI(100),RHOPZN,RHOPCD,DEFF(2),TNP,TNPS(3),
     1TNS
      COMMON/BED/DEEP(100),SUMDEP(100),DEPTH
      COMMON/GMT/GMTC(4)
      COMMON/UNSUB/PRESS,T,R,EQZN,EQZNCD,ANS,ANSC,TIME,SUMTIM,TOTMIN
     1,FQCD,SUMTCD,SUMTZN,SUMOLE,BEDTZN,BEDTCD,DEPLZN,DEPLCD,PELVOL,
     1UTIL,ANNS,TIMECD,TIMEZN
      COMMON/COUNT/ J,TIM,M
C
      IF(M.GT.1) GO TO 216
      GO TO 11
  216 DO 217 I=1,5
      PPB(I,M)=PPB(I,1)
      PPS(I,M-1)=0.0
      F(I,M)=F(I,1)
  217 CONTINUE
      PPI(1,M-1)=0.0
      PPI(2,M-1)=0.0
      FG(1,M-1)=0.0
      FG(2,M-1)=0.0
      FG(3,M-1)=0.0
      FG(4,M-1)=0.0
      FS(1,M-1)=0.0
      FS(2,M-1)=0.0
C         START OF CALCULATION
C         INITIAL GUESS AT PPS CL2 TO BE HALF PPB CL2 ON FIRST CALC LOOP
   11 PPSMAX=PPB (3,J)
      PPSMIN=0.0
    7 PPS(3,J)=(PPSMIN+PPSMAX)/2.0
      GO TO 1
    2 PPSMAX=PPS(3,J)
      PPS(3,J)=(PPSMAX+PPSMIN)/2.0
C
C         CHLORINE FLUX BULK TO SURFACE
    1 FG(3,J)=-2.0*GMTC(3)*(PRESS/(R*T))*ALOG((1.0+0.5*(PPB(3,J)/PRESS
     1))/(1.0+0.5*(PPS(3,J)/PRESS)))
      FG(4,J)=-0.5*FG(3,J)
C         OXYGEN FLUX SURFACE TO BULK
      PPS(4,J)=PRESS*(1.0-((1.0-(PPB (4,J) /PRESS))/(EXP((R*T*FG(4,J))/(
     1GMTC(4)*PRESS)))))
C         SURFACE EQUILIBRIUM
      PPS(2,J)=(EQZN*PPS(3,J))/PPS(4,J)**0.5
C         ZNCL2 FLUX SURFACE TO BULK
      H=EXP((FG(4,J)*R*T)/(PRESS*GMTC(2)))
      FG(2,J)=((FG(4,J)/PRESS)*(PPB(2,J)-H*PPS(2,J)))/(1.0-H)
```

```
C          CDCL2 FLUX BY DIFFERENCE
      FG(1,J)=-(FG(3,J)+FG(2,J))
      IF(FG(1,J))2,2,3
CC         CALCULATION OF PPS CDCL2
    3 HA=EXP((FG(4,J)*R*T)/(PRESS*GMTC(1)))
      HB=(FG( 4,J))/(PRESS*FG(1,J))
      PPS(1,J)=(1.0-((1.0-PPB(1,J)*HB)/HA))/HB
C          TRANSPORT CDCL2 INTERFACE TO SURFACE
      IF(RP(J)-RI(J))4,4,5
    5 FS(1,J)=FG(1,J)
      PPI(1,J)=((FS(1,J)*R*T*(RP(J)-RI(J))*RP(J))/(DEFF(1)*RI(J)))
     1+PPS(1,J)
C          INTERFACE EQUILIBRIUM
      PPI(2,J)=PPI(1,J)/EQZNCD
C          ZNCL2 FLUX =CDCL2 FLUX
      FS(2,J)=-FS(1,J)
C          RECALCULATION OF PPS ZNCL2
      PPS(2,J)=-((FS(2,J)*R*T*(RP(J)-RI(J))*RP(J))/(DEFF(2)*RI(J)))
     1+PPI(2,J)
      GO TO 6
    4 PPS(2,J)=PPS(1,J)/EQZNCD
    6 TEST=((PPS(2,J))*(PPS(4,J)**0.5))/EQZN
      ATEST=TEST/PPS(3,J)
      IF(ATEST.GT.1.000001) GO TO 8
      IF(ATEST.LT.0.999999) GO TO 9
      GO TO 10
    8 PPSMIN=PPS(3,J)
      GO TO 7
    9 PPSMAX=PPS(3,J)
      GO TO 7
   10 PPS(5,J)=PRESS-(PPS(1,J)+PPS(2,J)+PPS(3,J)+PPS(4,J))
      RETURN
      END
C
      SUBROUTINE RESET
      INTEGER TIM
      COMMON/GPRESS/PPB(5,101),PPS(5,100),PPI(2,100)
      COMMON/GFLUX/F(5,101),FG(4,100),FS(2,100)
      COMMON/PELLET/RP(100),RI(100),RHOPZN,RHOPCD,DEFF(2),TNP,TNPS(3),
     1TNS
      COMMON/BED/DEEP(100),SUMDEP(100),DEPTH
      COMMON/GMT/GMTC(4)
      COMMON/UNSUB/PRESS,T,R,EQZN,EQZNCD,ANS,ANSC,TIME,SUMTIM,TOTMIN
     1,EQCD,SUMTCD,SUMTZN,SUMOLE,BEDTZN,BEDTCD,DEPLZN,DEPLCD,PELVOL,
     1UTIL,ANNS,TIMECD,TIMEZN
      COMMON/COUNT/ J,TIM,M
      TIMEZN=0.0
      TIMECD=0.0
      RPSAVE=RP(J)
      PA=4.0*3.14159*(RP(J)**2  )
      IJ=J+1
C          MASS BALANCE ON SECTION
      DO 11 I=1,4
      IF(J.LE.40) GO TO 198
      IF(J.LE.60) GO TO 197
      JZ=3
      GO TO 196
  198 JZ=1
      GO TO 196
  197 JZ=2
  196 F(I,IJ)=F(I,J)+FG(I,J)*PA*TNPS(JZ)
   11 CONTINUE
      FSUM=0.0
      DO 12 I=1,5
      FSUM=F(I,IJ)+FSUM
   12 CONTINUE
C          RESET BULK PARTIAL PRESSURES
      DO 191 I = 1,5
      PPB(I,IJ)=(F(I,IJ)*PRESS)/FSUM
```

```
      IF(PPB(I,IJ)) 190,190,191
  190 WRITE(6,195)
  195 FORMAT(1X,100H**********************************************************
     1**********************************************)
      WRITE(6,192)
  192 FORMAT(1X,20HHALBED ERROR MESSAGE)
      WRITE(6,194)
  194 FORMAT(1X,70HNEGATIVE PARTIAL PRESSURE PROBABLY DUE TO TOO HIGH GA
     1S PHASE M/T COEFF)
      WRITE(6,193)IJ,I,PPB(I,IJ)
  193 FORMAT(1X,8HSECTION=,I3,5X,11HSPECIES NO=,I3,5X,23HERROR PARTIAL P
     1RESSURE=,E12.5)
      STOP
  191 CONTINUE
C         RESET PELLET AND INTERFACE RADIUS
      Z=1.0/3.0
      RPTEST= RP(J)/RI(J)
      A=(RP(J))**3
      B=-((3.0*FG(3,J)*TIME*(RP(J)**2))/(RHOPZN+RHOPCD))
      C=(RI(J))**3
      D=((3.0*FG(1,J)*TIME*(RP(J)**2))/(RHOPCD))
      IF(A.LT.B) GO TO 207
      IF(C.LT.D) GO TO 207
      IF (RPTEST.LE.1.0) GO TO 201
      RP(J)=(A-B)**Z
      GO TO 202
  201 RP(J)=((RP(J)**3  )-((3.0*FG(2,J)*TIME*(RP(J)**2  ))/(RHOPZN)))**Z
  202 RI(J)=(C-D)**Z
      GO TO 208
  207 TIMEZN=-(((RP(J)**3)*(RHOPCD+RHOPZN))/(3.0*(RP(J)**2)*FG(3,J)))
      TIMECD= (((RI(J)**3)*(RHOPCD))/(3.0*(RP(J)**2)*FG(1,J)))
      IF(TIMEZN.LE.TIMECD) GO TO 209
      RI(J)=0.0
      RP(J)=((RP(J)**3)+((3.0*FG(3,J)*TIMECD*(RP(J)**2))/(RHOPCD+RHOPZN
     1)))**Z
      GO TO 210
  209 RP(J)=0.0
      RI(J)=((RI(J)**3)-((3.0*FG(1,J)*TIMEZN*(RP(J)**2))/(RHOPCD)))**Z
  210 M=J+1
      ZNLEFT=(133.333*3.14159*(RP(J)**3)*(RHOPCD+RHOPZN)*TNP)/(BEDTZN)
      CDLEFT=(133.333*3.14159*(RI(J)**3)*(RHOPCD)*(TNP))/(BEDTCD)
      WRITE(6,212)
  212 FORMAT(1X,50H**************************************************)
      WRITE(6,211)J ,TIM
  211 FORMAT(1X,7HSECTION,I3,44HPELLETS ALL VOLATILISED DURING TIME INTE
     1RVAL,I3)
      WRITE(6,213) TIMECD,TIMEZN
  213 FORMAT(1X,84HTIME TO REMOVE ALL REMAINING PELLET AT INITIAL CALCUL
     1ATED RATE OF REACTION--SECS CD=,F10.5,3HZN=,F10.5)
      WRITE(6,214) ZNLEFT,CDLEFT,RP(J),RI(J)
  214 FORMAT(1X,25HPERCENT INITIAL ZNO LEFT=,F10.7,25HPERCENT INITIAL CD
     10 LEFT=,F10.6,6HRP(J)=,F10.6,6HRI(J)=,F10.6)
      WRITE(6,212)
  208 BEZNCD=PPB(1,IJ)/PPB(2,IJ)
      BEQZN=(PPB(2,IJ)*(PPB(4,IJ)**0.5))/PPB(3,IJ)
      BEQCD=BEZNCD*BEQZN
      DEEP(J)=((RP(J)/RPSAVE)**3)*DEEP(J)
      IF(J.EQ.M) GO TO 974
      IF(J.EQ.1) GO TO 900
      GO TO 899
  900 SUMDEP(J)=0.0
      GO TO 973
  899 SUMDEP(J)=SUMDEP(J-1)+DEEP(J)
      GO TO 973
  974 DO 972 L=1,100
      SUMDEP(L)=0.0
  972 CONTINUE
      SUMDEP(J)=DEEP(J)
  973 IF(BEQCD.LT.0.99*EQCD) GO TO 982
```

```
      IF(IJ.EQ.101) GO TO 975
      K=IJ+1
      DO 965 L=IJ,100
      SUMDEP(L)=SUMDEP(L-1)+DEEP(L)
  965 CONTINUE
      DO 983 L=K,101
      DO 983 I=1,5
      PPB(I,L)=PPB(I,IJ)
      F(I,L)=F(I,IJ)
  983 CONTINUE
      DO 981 L=IJ,100
      DO 981 I=1,5
      PPS(I,L)=PPB(I,IJ)
  981 CONTINUE
      DO 980 L=IJ,100
      DO  980 I=1,2
      FS(I,L)=0.0
      RTEST=RP(L)/RI(L)
      IF(RTEST.LE.1.0) GO TO 977
      PPI(I,L)=PPB(I,IJ)
      GO TO 980
  977 PPI(I,L)=0.0
  980 CONTINUE
      DO 979 L=IJ,100
      DO 979 I=1,4
      FG(I,L)=0.0
  979 CONTINUE
  975 WRITE(6,978)J ,TIM
  978 FORMAT(1X,47HEQUILIB REACHED IN BED IN ALL SECTIONS AFTER NO,I3,14
     1HDURING TIM INT,I3)
      J=100
  982 RETURN
      END
C
      SUBROUTINE ANSWER
      INTEGER TIM
      COMMON/GPRESS/PPB(5,101),PPS(5,100),PPI(2,100)
      COMMON/GFLUX/F(5,101),FG(4,100),FS(2,100)
      COMMON/PELLET/RP(100),RI(100),RHOPZN,RHOPCD,DEFF(2),TNP,TNPS(3),
     1TNS
      COMMON/BED/DEEP(100),SUMDEP(100),DEPTH
      COMMON/GMT/GMTC(4)
      COMMON/UNSUB/PRESS,T,R,EQZN,EQZNCD,ANS,ANSC,TIME,SUMTIM,TOTMIN
     1,EQCD,SUMTCD,SUMTZN,SUMOLE,BEDTZN,BEDTCD,DEPLZN,DEPLCD,PELVOL,
     1UTIL,ANNS,TIMECD,TIMEZN
      COMMON/COUNT/ J,TIM,M
      IF(TIMEZN.GT.0.0.OR.TIMECD.GT.0.0) GO TO 219
      GO TO 219
  199 IF(TIMEZN.GT.TIMECD) GO TO 221
      SUMTIM =SUMTIM+TIMEZN
      GO TO 220
  221 SUMTIM=SUMTIM+TIMECD
      GO TO 220
  219 SUMTIM=SUMTIM+TIME
  220 TOTMIN=SUMTIM/60.0
      SUMTCD=SUMTCD+F(1,101)*TIME
      SUMTZN=SUMTZN+F(2,101)*TIME
      SUMOLE=SUMTCD+SUMTZN
      DEPLCD=SUMTCD*100.0/BEDTCD
      DEPLZN=SUMTZN*100.0/BEDTZN
      UTIL=(100.0*(F(1,101)+F(2,101)))/F(3,1)
      ANSC=ANSC+1.0
      IF(ANSC-ANS)203,204,203
  204 ANS=ANS+40.0
      WRITE(6,114) TIM
  114 FORMAT( 23H TIME INTERVAL NUMBER =,5X,I4 )
      WRITE (6,122) TOTMIN
  122 FORMAT(1X, 38H.....TOTAL TIME OF RUN=,F12.6,20H
     1MINUTES          //)
```

```
      WRITE(6,102)
  102 FORMAT( 52H BULK PARTIAL PRESSURES IN EACH SECTION OF BED*ATMOS)
      WRITE(6,103)
  103 FORMAT(99H SECTION        PPBCDCL2              PPBZNCL2
     1PPBCL2              PPB02              PPBN2)
      DO 14 J=1,101
      WRITE(6,100) J,(PPB(I,J),I=1,5)
  100 FORMAT(3X,I3,5(E15.8,5X))
   14 CONTINUE
      WRITE(6,125)
  125 FORMAT(47H GAS PHASE FLUXES FLOWING THROUGH BED-MOLES/SEC)
      WRITE (6,104)
  104 FORMAT(99H SECTION        CDCL2FLUX             ZNCL2FLUX
     1CL2FLUX             02FLUX             N2FLUX)
      DO 15 J=1,101
      WRITE(6,100) J,(F(I,J),I=1,5)
   15 CONTINUE
      WRITE(6,105)
  105 FORMAT(71H GAS PHASE FLUXES TO PELLET SURFACE FOR EACH BED SECTION
     1 MOLES/SQCM SEC)
      WRITE (6,106)
  106 FORMAT(100HSECTION        FGCDCL2               FGZNCL2
     1FGCL2               FG02          SUMDEPTH CMS)
      DO 16 J=1,100
      WRITE(6,123)      J,(FG(I,J),I=1,4),SUMDEP(J)
  123 FORMAT(1X,I3,6X,4(E14.6,5X),7X,F15.10)
   16 CONTINUE
C
      WRITE(6,124)
  124 FORMAT( 53H' PPS VALUES 1 TO 5  READING FROM LEFT TO RIGHT       )
      DO 17 J=1,100
      WRITE(6,100) J,(PPS(I,J),I=1,5)
   17 CONTINUE
      WRITE(6,107)
  107 FORMAT(117H PELLET SURFACE AND INTERFACE RADIUS INTERFACE PARTIAL
     1 PRESSURES AND GAS FLUXES IN PELLET CMS  ATMOS   MOLES/SQCMSEC)
      WRITE(6,108)
  108 FORMAT(97H SECTION    RP(J)          RI(J)          PPICDCL2
     1   PPIZNCL2        FSCDCL2          FSZNCL2)
      DO 18 J=1,100
      WRITE(6,101) J,RP(J),RI(J),PPI(1,J),PPI(2,J),FS(1,J),FS(2,J)
  101 FORMAT(1X,I3,3X,6(E14.6,2X))
   18 CONTINUE
  203 IF(ANSC-ANNS)205,206,206
  206 ANNS=ANNS+3.0
      WRITE(6,215) TOTMIN
  215 FORMAT(1X,35H**********RUN TIME MINS =,F10.5,20H*********
     1**********)
      WRITE(6,110) TIM,SUMOLE,SUMTCD,SUMTZN
  110 FORMAT(1X,8HTIME INT,I3,3X,61HSUM TOTALS==MOLES REMOVED FROM BED A
     1T END OF TIME INT  CD+ZN=,E12.6,1X,3HCD=,E12.6,1X,3HZN=,E12.6)
      WRITE(6,109) DEPLZN,DEPLCD,UTIL
  109 FORMAT(1X,29H PERCENT ZN DEPLETION OF BED=,F12.7,3X,28HPERCENT CD
     1DEPLETION OF BED=,F12.7,18H PERCENT CL2 USED=,F8.4)
      WRITE(6,112)(PPB(I,101),I=1,5)
  112 FORMAT(1X,29HBED EXIT PRESSURES  PPBCDCL2=,E11.5,9HPPBZNCL2=,E11.5
     1,7HPPBCL2=,E11.5,6HPPB02=,E11.5,6HPPBN2=,E11.5)
      WRITE(6,113)(F(I,101),I=1,5)
  113 FORMAT(1X,39HBED EXIT MOLAR FLOWS*MOLES/SEC  FCDCL2=,E11.5,7HFZNCL
     12=,E11.5,5HFCL2=,E11.5,4HF02=,E11.5,4HFN2=,E11.5 // )
  205 RETURN
      END
```

NUMBERED REFERENCE LIST

1. Handbook of nonferrous metallurgy - recovery of the metals
D.M. Liddell, McGraw Hill 1945

2. Investigations on the chlorination of non-ferrous metal ores
H. Hohn, G. Jangg, L. Putz, E. Schmiedl, International mineral dressing congress, Stockholm 1957

3. Metallurgical thermochemistry
Kubaschewski, Evans, Alcock, Fourth edition, 1967 Pergamon Press Ltd.

4. Thermodynamic properties of 65 elements, their oxides, halides, carbides and nitrides
C. Wicks, F. Block, US Bureau of Mines Bulletin 605, 1963

5. On the fluidising and selective chlorination roasting of pyrite cinder
K. Okajima, M. Inoue, K. Sano, Tetsu-to-Hagane Overseas Vol. 2 1962

6. Chloride sublimation of metals from cinders of pyrite concentrates
A.K. Orlov, I.M. Piskunov, Zap. Leningrad Gorn. Inst. 42(3) 110-120 1963

7. Process for chloride sublimation of cobalt from pyrite cinder concentrates
A.K. Orlov, I.M. Piskunov, Zap. Leningrad Gorn. Inst. 42(3) 102-109 1963

8. Effect of gaseous medium on the regularities of chloride sublimation
A.K. Orlov, Zap. Leningrad Gorn. Inst. 46(3) 41-46 1966

9. Recovery on non-ferrous metal impurities from iron ore pellets by chlorination (CV or LDK process)
K.K. Lippert, H.B. Pietsch, A. Roeder and H.W. Walden Trans. Sec. C Inst. Min. Met. Vol. 78 1969

10. The removal of impurities from pyrite cinders by a chloride volatilisation process
A. Yazawa, M. Kameda, Canadian Metallurgical Quarterly Vol. 6 no. 3 1967

11. Kowa Seiko pelletizing chlorination process - integral utilisation of iron pyrites
Y. Okubo, Journal of Metals, March 1968

12. Selective chlorination of iron from ilmenite with hydrochloric acid gas
C. Sanakaran, R.N. Misra, P.P. Bhatnagar, Advances in Extractive Metallurgy IMM Symposium, London April 1967

13. Upgrading of Egyptian ilmenite by partial chlorination
A. Rabie, M. Saada, S. Ezz, Advances in Extractive Metallurgy IMM Symposium, London, April 1967

14. Chemical beneficiation of chromite by selective chlorination in a fluidised bed
A.S. Athawale, V.A. Altekar, Transactions of the Indian Institute of Metals, Calcutta 22 No. 2, June 1969, 29-37

15. Study of the chlorination and beneficiation of Egyptian chromite ores
M.K. Hussein, K. El-Barawi, Metallurgical Transactions IMM, London, March 1971

16. Selective chlorination of iron ores containing chromium and nickel by fluidised roaster
A. Ohba, K. Gunji, R. Ishizuka, Proceedings memorial lecture 10th anniversary National Research Institute for Metals, Tokyo 1966

17. On selective chlorination of lateritic iron ores
T. Furvi, A. Suwa, Nippon Kogyo Kaishi 79(5) 7-12 1963

18. A study on the removal of nickel from laterite ore by selective chlorination
S. Yagi, K. Mitzoguchi, Kyushu Kozan Gakkai-Shi 32, 96-100 1964

19. Recovery of tin by chlorination in a fluidised bed
J.A.M. Nieuwenhuis, IMM Symposium, Advances in extractive metallurgy, April 1967

20. Development of chemical treatment of low-grade iron ores at Appleby-Frodingham
L. Reeve, Journal of the Iron and Steel Institute 181, 1955 26-40

21. Manganese recovery as chloride from ores and slags
A.A. Cochran, W.L. Falke, Journal of Metals, April 1967, 28-32

22. Separation of niobium and tantalum by chlorination
S. Hussain, P. Jena, Transactions Indian Institute of Metals 15 1962, 220-226

23. Extraction of tantalum and columbium from ores and concentrates by chlorination.
S. May, G. Engel, US Bureau of Mines, RI 6635 1965

24. Investigations into the recovery of niobium from the Mrima Hill deposit
P. Harris, D. Jackson, Trans. IMM Sec. C 75 1966

25. Treatment of refractory copper ores by the segregation process
E. Pinkney, N. Plint, Transactions Institute of Mining and Metallurgy Section C. June 1967

26. Extraction of tungsten from ore concentrates by chlorination
A. Henderson, R. Rhoads, R. Brown, US Bureau of Mines RI 6612 1965

27. A process for direct chlorination of rare earth ores at high temperatures on a production scale
W. Brugger, E. Greinacher, Journal of Metals, December 1967

28. Study on the separation of cobalt from nickel by means of blowing chlorine into the molten matte
Y. Shimagaya, Nippon Kogyo Kaishi 78 407-410 1962

29. Thermodynamic relationships in chlorine metallurgy
H. Kellogg, Journal of Metals, Transactions AIME, Vol. 188 June 1950

30. Thermodynamic data of the metallic chlorides
H. Villa, Journal Society Chemical Industry supplementary issue no. 1, 1950

31. Chlorination of zinc oxide at high temperature: equilibrium measurements
A. Orlov, J. Jeffes, IMM transactions section C 78 1969

32. Separation of nickel and zinc from a mixture of their oxides: Part 1 - chlorination
R. Sharma, P. Bhatnagar, T. Banerjee, Journal of Scientific and Industrial Research 15B July 1956, pp 378-382

33. Structural properties of packed beds - a review
D. Haughey, G. Beveridge, The Canadian Journal of Chemical Engineering vol. 47, April 1969, 130-140

34. Processing of solutions accruing in connection with chloridising volatilisation processes
H. Walden, Journal of metals, August 1969

35. Equilibrium pressures of solid copper halides
R. Shelton, Transactions, Faraday Society, 1961 57 2113

36. The thermodynamics of gaseous cuprous chloride, monomer and trimer
L. Brewer, N. Lofgren, Journal American Chemical Society 72 July 1950, 3038-3045

37. Mass spectrometric and thermodynamic study of gaseous transition metal (II) halides
R. Schoonmaker, A. Friedman, R. Porter, Journal of Chemical Physics 44 no. 6 1959, 1586

38. Thermodynamic properties of the vapour transport reactions in the Au-Cl system by a transpiration-mass spectrometric technique
J. Hager, R. Hill, Met. Trans. 1 October 1970, p 2723

39. Composition and properties of vapours over molten silver chloride
A. Visnapuv, J. Jensen, Journal of the Less-common Metals 20 1970, 141-148

40. The chemistry of molten salts
H. Bloom, W.A. Benjamin, Inc. 1967, New York, Amsterdam

41. Gaseous complexes formed between trichlorides ($AlCl_3$ and $FeCl_3$) and dichlorides
E. Dewing, Metallurgical transactions August 1970, 2169

42. Application of thermodynamics to the selection of vapour transport reactions
C. Alcock, J. Jeffes, Transactions section C. Institute of Mining and Metallurgy 76 1967 C246-C258

43. Vapourisation chemistry in extractive metallurgy
H. Kellogg, Metallurgical transactions AIME, May 1966 602-615

44. Chemical transport reactions
H. Schafer, Academic Press, New York-London 1964

45. The extraction of pure titanium from ferro-titanium
P. Gross, The Richardson Conference on physical chemistry of process metallurgy, Imperial College, London, 1973

46. On some equilibria involving aluminium monohalides
P. Gross, Discussions Faraday Society No. 4 1948, 206-215

47. Catalytic distillation of aluminium
P. Gross, Proceedings symposium on refining non-ferrous metals IMM 1950

48. Separation of chloride vapours during ilmenite chlorination
V. Nieberlein, US Bureau of Mines Report of Investigations 5602 1960

49. Chlorination of mangeniferrous iron ores
Y. Okahara, I. Iwasaki, Transactions Society of Mining Engineers of AIME Vol. 247 1 March 1970

50. Extraction of uranium from Elliot Lake ore by vapour-phase chlorination
R. Lapage, J. Marriage, IMM trans section C 82, 1973, pp 101-102

51. The rate of chlorination of metals and oxides: Part 3 - The rate of chlorination of Fe_2O_3 and NiO in Cl_2 and HCl
R. Fruehan, L. Martonik, United States Steel Corporation Research Centre, Monroeville, Pennsylvania, August 1972 (to be published in Met trans)

52. The rate of chlorination of metals and oxides: Part 1 - Fe, Ni and Sn in Cl_2
R. Fruehan, Metallurgical transactions 3 October 1972, 2585-2592

53. The rate of chlorination of metals and oxides: Part 2 - Iron and nickel in HCl
R. Fruehan, L. Martonik, United States Steel Corporation Research Centre, Monroeville, Pennsylvania, January 1972 (to be published in Met. trans)

54. Role of heat and mass transfer in gas-solid reactions involving two solid phases within sintered pellets
A. Hills, Heat and mass transfer in process metallurgy, Ed. A. Hills IMM London 1967

55. The mechanism of the thermal decomposition of calcium carbonate
A. Hills, Chemical engineering science, 23 1968 297-320

56. Reduction kinetics of hematite and the influence of gaseous diffusion
N. Warner, Transactions of the Metallurgical Society AIME 230 February 1964, 163-176

57. Rate phenomena in process metallurgy
J. Szekely, N. Themelis, John Wiley and Sons Inc. Wiley-Interscience 1971

58. The importance of macroscopic transport phenomena in gas-solid reactions
A. Hills, Heterogeneous kinetics at elevated temperatures Ed. G. Belton, Plenum Press 1970 449-501

59. Rate controlling factors in gas-solid reactions of metallurgical interest
A. Bradshaw, Met. trans Sec. C IMM 79 1970 C281-C294

60. A general structural model for non-catalytic gas solid reactions
J. Szekely, The Richardson Conference on physical chemistry of process metallurgy, Imperial College, London 1973

61. Heat and mass transfer from a single sphere to fluid flowing through an array
P. Rowe, K. Claxton, Transactions Institution of Chemical Engineers 43 1965 321-331

62. Transport phenomena
R. Bird, W. Stewart, E. Lightfoot, John Wiley and Sons Inc. New York and London 1960

63. Thermogravimetric investigation of the chlorination behaviours of some common metals and their oxides
R. Titi-Manyaka, I. Iwasaki, Transactions Society Mining Engineers AIME 252 No. 3 September 1972

64. A kinetic analysis of the TORCO copper segregation process
M. Brittan, R. Liebenberg, IMM September 1971, Trans. Sect. C 156-169

65. Catalytic effects in the chlorination of cassiterite
R. Lythe, A. Prosser, IMM 78 December 1969 Trans. Sect. C 206-213

66. Chlorination behaviours of some metal sulphides as investigated by thermogravimetric analysis
R. Titi-Manyaka, I. Iwasaki, Trans. Soc. Min. Eng. AIME 254 No. 1 March 1973

67. Kinetics of chlorination of metal sulphides
J. Gerlach, F. Pawlek, Trans. Met. Soc. AIME 239 October 1967 1557-1564

68. Phase diagrams for ceramists
E. Levin, C. Robbins, H. McMurdie, M. Reser editor, The American Ceramic Society 1964, Columbus Ohio

69. A microwave-induced argon plasma system suitable for trace analysis
K. Aldous, R. Dagnall, B. Sharp, T. West, Analytica Chimica Acta 54 1971 233-243

70. A simple low-power reduced-pressure microwave plasma source for emission spectroscopy
D. Hingle, G. Kirkbright, R. Bailey, Talanta 1969 16 1223-1225

71. Characteristics of low wattage microwave induced argon plasmas in metals excitation
J. Bunnels, J. Gibson, Analytical Chemistry 39 no. 12 October 1967 1398-1405

72. Atomic spectra and the vector model
C. Candler, 2nd Ed. Hilger and Watts Ltd., London 1964

73. Tables of spectral line intensities
US Dept. of Commerce, National Bureau of Standards, NBS Monograph 32, Pt. 1, December 1961

74. Constitution of binary alloys - second edition
M. Hansen, McGraw Hill 1958

75. Phase equilibria in the ferrite region of the system Fe-Co-O
B. Roiter, A. Paladino, Journal American Ceramic Society 1962 45 pp 128-133

76. Vapour pressures of $ZnCl_2$ and $ZnBr_2$
F. Keneshea, D. Cubicciotti, Journal of Chemical Physics 1964 40 p.191

77. The vapour pressure of cadmium and zinc chlorides
H. Bloom, A. Welch, Journal of Physical Chemistry 1958, 62 p.1594

78. Vapour pressure of cadmium chloride and thermodynamic data for $CdCl_2$ gas
F. Keneshea, D. Cubicciotti Journal of Chemical Physics 1964 40 1778-1779

79. Das gasformige Kobalt (III) - chorid und seine thermochemicschen Eigneschaften
H. Schafer, K. Krehl Z. anorg. allg. Chem., 1952 268 p.25

80. Physical chemistry for metallurgists
J. Mackowiak, George Allen and Unwin Ltd. 1966

81. Thermodynamics for chemists
S. Glasstone, D. Van Nostrand Co. Ltd. 1966

82. Thermochemical data of alloys
O. Kubaschewski, J. Catterall, Pergamon Press 1956

83. Constitution of binary alloys - First supplement
R. Elliot, McGraw-Hill 1965

84. Constitution of binary alloys - second supplement
F. Shunk, McGraw-Hill 1969

85. Cobalt monograph
Centre d'information du cobalt, Brussels 1960

86. Spectrophotometric study of the equilibrium formation of gaseous zinc (1) chloride
Corbett and Lynde, Inorg. Chem. 6(12), 2199-2204, 1967

87. Spectrophotometric study of the gaseous equilibrium of Cd and Cd(11) chloride
Buddy, Bruner and Corbett, Journal Physical Chemistry 68(5) 1115-1121 1964

88. Thermodynamic properties of solid solutions with spinel-type structure 1. The system Co_3O_4-Mn_3O_4
E. Aukrust, A Muan, Transactions Met. Soc. AIME 230 April 1964 pp 378-382

89. Phase equilibria ...summary for the system ZnO-CdO-P_2O_5
J. Brown, F. Hummel, Journal Electrochemical Society 111 no. 9 pp 1052-1057, 1964

90. Solid electrolyte galvanic cell studies: free energies of formation of CoO and Co_3O_4
W. Budgen, J. Pratt, Trans. Sec. C. Inst. Min. Met. 79 1970 C221-C225

91. Zur thermodynamik von spinellphasen
J. Tretjakow, H. Schmalzried Ber. Bunsenges. Phys. Chem. 69 1965 396-402

92. Thermodynamic study on the systems of metals and their oxides by EMF measurements using solid electrolytes
J. Moriyama, N. Sato, H. Asao, Mem. Fac. Eng. Kyoto Univ. 31 1969 253-267

93. The dissociation pressure of cadmium oxide
I. Gilbert, J. Kitchener, J. Chem. Soc. 3919 1956

94. Das Dissoziationsgleichgewicht $CdO_{(s)} = Cd_{(g)} + \frac{1}{2}O_{2(g)}$
O. Glemser, U. Stoecher Ber. Bunsenges Phys. Chem. 67 505 1963

95. Free energy of formation of zinc oxide for the temperature range 420 to 908°C , T. Wilder, Trans. Met. Soc. AIME 245 1969, p 1370

96. Thermodynamics of the sublimation and dissociation of zinc oxide
E. Kazenas, D. Chizhikov, Yu. Tsvetkov, Izv. Akad. Navk. SSSR Metal (1) 1969 150-153 (Russ) Chem. Abs. 70 1969 100333

97. Messung der EMK einiger Bildungsketten geschmolzener Salze
R. Lorenz, H. Velde, Z. anorg. allg. Chem. 183 1929 81-97

98. Thermodynamic properties of solutions of molten lead chloride and zinc chloride
A. Wachter, J. Hildebrand, J. and P. Am. Chem. Soc. 52 4655 1930

99. Free energy of formation of molten zinc chloride
B. Markov, S. Volkov, Ukr. Khim. Zh. 29 511-515 1963 (Russ) Chem. Abs. 59 12248

100. Thermodynamics of molten salt mixtures
J. Lumsden, Academic Press London 1966

101. Discussions and contributions
J. Lumsden, IMM Trans. Sec. C. 79 1970 C77-C76

102. Heat contents of molten zinc chloride and bromide and the molecular constants of the gases
D. Cubicciotti, H. Eding, J. Chem. Phys. 40 1964 978-982

103. NBS technical note 270-6
US Dept. of Commerce 1973

104. Thermodynamic data on zinc chloride and cadmium chloride
F. Ishikawa, G. Kimura, T. Murooka, Science Reps. Tohoku Imp. Univ. 1932 Series 1 21 455

105. Solid state electromotive force techniques. The free energy of formation of $NiCl_2$, $CoCl_2$ and several double salts of KCl
J. Egan, US Atomic Energy Commission BNL 9343 1965

106. R. Gee - PhD thesis, Metallurgy Dept. University of Manchester 1973

107. Ionic crystals, Lattice defects and nonstoichiometry
N. Greenwood, Butterworth and Co., London 1968

108. Recherches sur la constitution et la stabilite de quelques solutions solides a base d'oxyde de cobalt
J. Robin, Annales de chimie, May-June 1955 10 389-412

109. On the ferrimagnetism of some sulphides and oxides 3. Oxygen and sulphur spinels containing cobalt (MCo_2O_4 and MCo_2S_4)
F. Lotgering, Philips Research Reports 11
1956 337-350

110. The solubility of transition metal oxides in zinc oxide and the reflectance spectra of Mn^{++} and Fe^{++} in tetrahedral fields
C. Bates, W. White, R. Roy, Journal Inorganic and Nuclear Chemistry 1966 28 397-405

111. Activity-composition relations in the systems CoO-ZnO and NiO-ZnO at 1050°C
A. Navrotsky, A. Muan, J. Inorg. Nucl. Chem. 1971 33 35-47

112. Diffusion (in solids, liquids, gases)
W. Jost, Academic Press, New York 1960

113. Physical chemistry of metals
L. Darken, R. Gurry, McGraw-Hill 1953

114. Grundsatzliche Uberlegungen zur spinellbildung in Zunderschichten und zu den transporteigenschaften der spinelle
H. Schmalzried, Wekstoffe und Korrosion May 1971, 371-382

115. Nonstoichiometry, diffusion and electrical conductivity in binary metal oxides
P. Kofstad, John Wiley and Sons Inc. 1972

116. Adsorption, surface area and porosity
S. Gregg, K. Sing, Academic Press, London and New York, 1967

117. Mass transfer in heterogeneous catalysis
C. Satterfield, MIT Press 1970

118. Gaseous diffusion in porous solids and its role in gas/solid reactions
F. Campbell 1971, PhD. thesis, Metallurgy Dept., Imperial College, London

119. Handbook of Chemistry and Physics
54th edition 1974, Chemical Rubber Co., Cleveland Ohio

120. Non-catalytic heterogeneous solid fluid reaction models
C. Wen, Industrial and Engineering Chemistry 60 September 1968
pp 34-54

121. Molecular theory of gases and liquids
J. Hirschfelder, C. Curtiss, R. Bird, Hohn Wiley, New York 1954

122. Diffusional properties of multicomponent gases
C. Wilke, Chemical engineering progress 46 2 pp 95-104 1950

123. Molten salt handbook
G. Janz, Academic Press, New York 1967

124. Molten salt chemistry
M. Blander, New York Interscience 1964

125. Evaporation from drops
W. Rahz, W. Marshall, Chemical engineering progress 48 pp 141-146 1952

126. Chemical process principle charts
O. Hougen, K. Watson, R. Ragatz, John Wiley and Sons 1964

127. Surface and volume flow in porous media
R. Barrer pp 557-609, chapter 12, The gas-solid interface, Ed. E.A. Flood, Pub. E. Arnold, New York 1967

128. Diffusion of ideal gases in capillaries and porous solids
D. Scott, F. Dullien American Institute of Chemical Engineers' Journal 8 pp 113 1962

129. Diffusion in three-component gas mixtures in the transition region between Kundsen and molecular diffusion
R. Cunningham, C. Geankoplis, Industrial engineering chemistry fundamentals 7(3) pp 429-432 1968

130. Gaseous diffusion in porous media at uniform pressure
R. Evans, G. Watson, E. Mason, Journal Chemical Physics 35 pp 2076-2083 December 1961

131. Titanium minerals Pt. 1 and 2
Industrial Minerals pp 9-27 April 1971 and pp 9-27 May 1971

132. Sintering of ZnO: 1, densification and grain growth. 2, density decrease and pore growth during the final stage of the process.
T. Gupta, R. Coble, Journal of the American Ceramic Society 51 1968 pp 521-528

133. Non-stoichiometry of zinc oxide and its relation to sintering: Pt 2, sintering of zinc oxide in controlled atmospheres
J. Roberst, J. Hutchings, Transactions of the Faraday Society 55 5-8, 1959 pp 1394-1399

134. The pore sturcture of cadmium oxide
R. Mikhail, A. Kamel, Journal of Physical Chemistry 73, 6-7 1969 pp 2213-2216

135. Gaseous reduction of iron oxides: part 4. Mathematical analysis of partial internal reduction - diffusion control
R. Tien, E. Turkdogan. Met. Trans. 3 August 1972 2039-2048

136. Studies in gas-solid reactions: part 1. A structural model for the reaction of porous oxides with a reducing gas.
J. Szekely, J. Evans, Met. Trans. 2 June 1971 1691-1698

137. Chemical Engineering
J. Coulson, J. Richardson, Pergamon Press 1965

138. A viscosity equation for gas mixtures
C. Wilke, Journal of Chemical Physics 18 April 1950 pp 517-519

139. Powder diffraction file
Joint Committee on powder diffraction standards 1972 inorganic index

A C K N O W L E D G E M E N T S

It seems like a long time since I started work on this thesis. Over this period many people have played a part in the work. Unfortunately I am only able to record a few names since to acknowledge everyone would necessitate an additional appendix, or even chapter. First upon my honours list is my supervisor Bill Steen, whom I wish to thank for his tireless enthusiasm, his assistance and his friendship whilst performing this work. I am grateful to past and present members of the John Percy Group for their help and co-operation, and especially to Joe Herbertson, Ali Unal and Viruthiamparambath Rajakumar for the useful discussions we have had together. The work done by the JPG technicians has been much appreciated. Thanks go to the staff of the Metallurgy Department Workshop who have given invaluable assistance in manufacturing and repairing many different and unusual items. Thanks also go to the Photography Section for producing the photographs in this thesis. I am pleased to thank the Science Research Council for funding this project. The financial support received during the last part of this study has been greatly appreciated. A final word of thanks goes to Kathy Kelly who, despite thinking she might never see the end of the work, happily typed the thesis and modified most of the spelling.